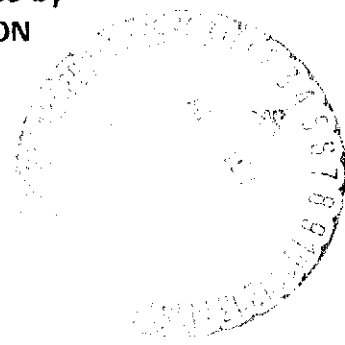


# STUDY OF THE ADAPTABILITY OF EXISTING HARDWARE DESIGNS TO A PIONEER SATURN/URANUS PROBE

## FINAL REPORT

OCTOBER 1973

Prepared under Contract No. NAS2-7488 by  
MARTIN MARIETTA CORPORATION  
Denver, Colorado 80201



For

AMES RESEARCH CENTER  
National Aeronautics and Space Administration

(NASA-CR-137650) STUDY OF THE ADAPTABILITY OF EXISTING HARDWARE DESIGNS TO A PIONEER SATURN/URANUS PROBE Final Report, 26 Mar. - 31 Oct. 1973 (Martin Marietta Corp.) 379 p HC \$10.25 N75-18287 Unclas 13643 CSCL 22B G3/15

FOREWORD

This document presents the results of Contract NAS2-7488, *Adaptability of Existing Hardware Designs to a Pioneer Saturn/Uranus Probe*, which was performed by Martin Marietta Corporation from March 26, 1973 through October 31, 1973.

PRECEDING PAGE BLANK NOT FILMED

CONTENTS

		<u>Page No.</u>
1.0	INTRODUCTION . . . . .	1.0-1 and 1.0-2
2.0	SUMMARY. . . . .	2.0-1
2.1	Science Design . . . . .	2.0-1
2.2	Mission Design . . . . .	2.0-4
2.3	System Design. . . . .	2.0-8
2.4	Electrical/Electronic Design . . . . .	2.0-8
2.5	Structural/Mechanical Design . . . . .	2.0-8
2.6	Hardware Availability. . . . .	2.0-8 thru 2.0-13
3.0	SPACECRAFT-TO-PROBE INTERFACE. . . . .	3.0-1
3.1	Mechanical Interface . . . . .	3.0-1
3.2	Thermal Interfaces . . . . .	3.0-1
3.3	Electrical/Electronic Interface. . . . .	3.0-2
3.4	Communications Interfaces. . . . .	3.0-2 thru 3.0-5
4.0	TECHNICAL STUDIES. . . . .	4.0-1
4.1	Hardware Availability Analysis . . . . .	4.1-1
4.1.1	Science Instruments. . . . .	4.1-1
4.1.2	Electrical and Electronic Subsystems . . . . .	4.1-4
4.1.2.1	Communications . . . . .	4.1-4
4.1.2.2	Data Handling Subsystem (DHS). . . . .	4.1-7
4.1.2.3	Power and Pyrotechnics Subsystem (PPS) . . . . .	4.1-8
4.1.3	Structural and Mechanical Subsystems . . . . .	4.1-8 and 4.1-9
4.2	Impact of Science Requirements on System Design. . . . .	4.2-1
4.2.1	Atmospheric Models . . . . .	4.2-1
4.2.2	Objectives, Measurements, and Performance Criteria . . . . .	4.2-5
4.2.3	Instruments and Measurement Techniques . . . . .	4.2-8
4.2.3.1	Temperature Gauge. . . . .	4.2-9
4.2.3.2	Pressure Gauge . . . . .	4.2-9
4.2.3.3	Accelerometers . . . . .	4.2-12
4.2.3.4	Nephelometer . . . . .	4.2-15
4.2.3.5	Neutral Mass Spectrometer (NMS). . . . .	4.2-17

4.2.4	Entry and Descent Science Analysis . . . . .	4.2-20
4.2.4.1	Science Sequence of Events . . . . .	4.2-20
4.2.4.2	Entry and Descent Science Mission Parameters . . . . .	4.2-21
4.2.5	Data Collection and Measurement Performance. . . . .	4.2-27
4.2.5.1	Data Collection for Final Configuration. . .	4.2-27
4.2.5.2	Descent Measurement Performance for Final Configuration. . . . .	4.2-32
4.2.5.3	Entry Accelerometer Performance for Final Configuration. . . . .	4.2-36
4.2.5.4	Dual Data Transmission . . . . .	4.2-38 thru 4.2-40
4.3	Impact of Mission Requirements on System Design. . . . .	4.3-1
4.3.1	Mission General Summary. . . . .	4.3-1
4.3.1.1	Launch and Interplanetary Trajectories . . .	4.3-1
4.3.1.2	Approach Orbit Determination and Dispersions. . . . .	4.3-1
4.3.1.3	Planetary Encounter. . . . .	4.3-2
4.3.1.4	Planetary Entry and Descent. . . . .	4.3-3
4.3.2	Mission Design Summary . . . . .	4.3-3
4.3.2.1	1979 Saturn Mission Definition . . . . .	4.3-3
4.3.2.2	Saturn/SU-80 Mission Definition. . . . .	4.3-8
4.3.2.3	Uranus/SU-80 Mission Definition. . . . .	4.3-12
4.3.3	Launch and Interplanetary Trajectories . . .	4.3-16
4.3.3.1	Launch Energy. . . . .	4.3-16
4.3.3.2	Launch Constraints . . . . .	4.3-17
4.3.4	Approach Orbit Determination and Dispersions. . . . .	4.3-20
4.3.4.1	Analytical Procedure and Ground Rules. . . .	4.3-20
4.3.4.2	Deflection Dispersion Trends . . . . .	4.3-23
4.3.5	Planetary Encounter. . . . .	4.3-27
4.3.6	Planetary Entry. . . . .	4.3-30
4.3.6.1	Selection of Entry Ballistic Coefficient . .	4.3-30
4.3.6.2	Entry Dynamics Analysis. . . . .	4.3-33 and 4.3-34
4.4	System Design and Integration. . . . .	4.4-1
4.4.1	Analyses and Tradeoffs . . . . .	4.4-1
4.4.1.1	Preentry Transmission Tradeoff . . . . .	4.4-1
4.4.1.2	Nose Cap Deployment Analysis . . . . .	4.4-1
4.4.1.3	Radiation Analysis . . . . .	4.4-3
4.4.1.4	Dual Data Return . . . . .	4.4-6

4.4.2	Baseline Configuration Definition . . . . .	4.4-7
4.4.2.1	Functional Sequence of Events . . . . .	4.4-7
4.4.2.2	Functional Block Diagram . . . . .	4.4-10
4.4.2.3	System Data Profile . . . . .	4.4-10
4.4.2.4	System Power Profile . . . . .	4.4-10
4.4.2.5	System Weight . . . . .	4.4-14
4.4.3	Alternate Configuration Definition . . . . .	4.4-14
4.4.3.1	Functional Sequence of Events . . . . .	4.4-14
4.4.3.2	Functional Block Diagram . . . . .	4.4-14
4.4.3.3	System Data Profile . . . . .	4.4-14
4.4.3.4	System Power Profile . . . . .	4.4-14
4.4.3.5	System Weight . . . . .	4.4-19
4.4.4	Configuration Comparison (Nominal Atmospheres) . . . . .	4.4-19
4.4.5	Updated Alternate Configuration (Nominal Atmospheres) . . . . .	4.4-19
4.4.6	Impact of the Worst-Case Atmospheres . . . . .	4.4-21
4.4.6.1	Functional Sequence of Events . . . . .	4.4-21
4.4.6.2	Functional Block Diagram . . . . .	4.4-21
4.4.6.3	System Data Profile . . . . .	4.4-21
4.4.6.4	System Power Profile . . . . .	4.4-25
4.4.6.5	System Weight . . . . .	4.4-25
4.4.6.6	System Environmental Requirements . . . . .	4.4-25 thru 4.4-28
4.5	Electrical and Electronic Design . . . . .	4.5-1
4.5.1	Analyses and Trade Studies . . . . .	4.5-1
4.5.1.1	Communications Subsystem . . . . .	4.5-1
4.5.1.2	Data Handling Subsystem (DHS) . . . . .	4.5-50
4.5.1.3	Power and Pyrotechnics Subsystem . . . . .	4.5-54
4.5.2	Baseline Configuration Definition . . . . .	4.5-61
4.5.2.1	Communication Subsystem . . . . .	4.5-62
4.5.2.2	Data Handling Subsystem . . . . .	4.5-71
4.5.2.3	Power and Pyrotechnic Subsystem (PPS) . . . . .	4.5-72
4.5.3	Alternate Configuration Definition . . . . .	4.5-72
4.5.3.1	Communication Subsystem . . . . .	4.5-74
4.5.3.2	Data Handling Subsystem . . . . .	4.5-79
4.5.3.3	Power and Pyrotechnics Subsystem . . . . .	4.5-79
4.5.4	Configuration Comparison . . . . .	4.5-80
4.5.4.1	Communication Subsystem . . . . .	4.5-80
4.5.4.2	Data Handling Subsystem . . . . .	4.5-80
4.5.4.3	Power and Pyrotechnics Subsystem . . . . .	4.5-80
4.5.5	Updated Alternate Configuration (Nominal Atmosphere) . . . . .	4.5-82
4.5.5.1	Communication Subsystem . . . . .	4.5-82

4.5.5.2	Data Handling Subsystem . . . . .	4.5-84
4.5.5.3	Power and Pyrotechnics Subsystem . . . . .	4.5-84
4.5.6	Impact of Worst-Case Atmosphere . . . . .	4.5-84
4.5.6.1	Communication Subsystem . . . . .	4.5-85
4.5.6.2	Data Handling Subsystem . . . . .	4.5-87
4.5.6.3	Power and Pyrotechnics Subsystem . . . . .	4.5-87
		thru
		4.5-92
4.6	Structural and Mechanical Designs . . . . .	4.6-1
4.6.1	Analysis and Tradeoff Studies . . . . .	4.6-1
4.6.1.1	Configuration Tradeoff Studies . . . . .	4.6-1
4.6.1.2	Structural Analysis . . . . .	4.6-2
4.6.1.3	Heat Shield Analysis and Tradeoff Studies . .	4.6-3
4.6.1.4	Thermal Control Subsystem . . . . .	4.6-6
4.6.2	Baseline Configuration Definition . . . . .	4.6-25
4.6.2.1	Configuration and General Arrangement . . . .	4.6-25
4.6.2.2	Structural Subsystems . . . . .	4.6-32
4.6.2.3	Mechanisms Subsystem . . . . .	4.6-33
4.6.2.4	Mass Properties . . . . .	4.6-33
4.6.2.5	Deceleration Subsystem . . . . .	4.6-34
4.6.2.6	Thermal Control Subsystem (Baseline Configuration) . . . . .	4.6-35
4.6.3	Alternate Configuration Definition . . . . .	4.6-35
4.6.3.1	Configuration and General Arrangement . . . .	4.6-36
4.6.3.2	Structural Subsystems . . . . .	4.6-41
4.6.3.3	Mechanisms Subsystem . . . . .	4.6-43
4.6.3.4	Mass Properties . . . . .	4.6-43
4.6.3.5	Deceleration Subsystem . . . . .	4.6-45
4.6.3.6	Thermal Control Subsystem (Alternate Configuration) . . . . .	4.6-47
4.6.4	Configuration Comparison (Nominal Atmosphere) . . . . .	4.6-47
4.6.5	Updated Alternate Configuration (Nominal Atmosphere) . . . . .	4.6-49
4.6.6	Final Configuration Definition (Worst-Case Atmosphere) . . . . .	4.6-49
4.6.6.1	Configuration and General Arrangement . . . .	4.6-53
4.6.6.2	Structural Subsystem . . . . .	4.6-54
4.6.6.3	Mechanisms Subsystem . . . . .	4.6-59
4.6.6.4	Mass Properties . . . . .	4.6-60
4.6.6.5	Deceleration Subsystem . . . . .	4.6-60
4.6.6.6	Thermal Control Subsystem (Final Configuration) . . . . .	4.6-62
		and
		4.6-63

5.0	CONCLUSIONS . . . . .	5.0-1 and 5.0-2
6.0	REFERENCES . . . . .	6.0-1 thru 6.0-4
	Appendix A -- Preliminary Stress Analysis . . . . .	A-1 thru A-24
	Appendix B -- Heat Shield Analysis . . . . .	B-1 thru B-16
	Appendix C -- Thermal Control Analysis . . . . .	C-1 thru C-18
	Appendix D -- ARC Mass Spectrometer and Instrument Data . . . . .	D-1

Figure

1.0-1	Study Flow Plan . . . . .	1.0-2
2.0-1	1979 Saturn Direct Mission Summary. . . . .	2.0-6
2.0-2	Uranus/SU-80 Mission Summary. . . . .	2.0-6
2.0-3	Pictorial Sequence of Events for the Final Configuration . . . . .	2.0-7
2.0-4	Data Profile for the Final Configuration. . . . .	2.0-9
2.0-5	Power Profile for Entry at Uranus . . . . .	2.0-9
2.0-6	Final Probe Configuration . . . . .	2.0-11
3.1-1	Pioneer SU Probe/Spacecraft Interface . . . . .	3.0-3
4.2-1	Monograph Model Atmospheres . . . . .	4.2-2
4.2-2	Model Atmospheres in the Probe Terminal Descent Region . . . . .	4.2-3
4.2-3	Temperature Gauge . . . . .	4.2-10
4.2-4	Pressure Gauge. . . . .	4.2-13
4.2-5	Probe Science Instrument Port . . . . .	4.2-14
4.2-6	Nephelometer Schematic. . . . .	4.2-16
4.2-7	Neutral Mass Spectrometer . . . . .	4.2-18
4.2-8	Entry Angle and Atmosphere Effects on Entry Accelerometer Measurement Time. . . . .	4.2-23
4.2-9	Baseline and Alternate Pressure Descent Profiles. . . . .	4.2-26
4.2-10	Total Descent Time vs Ballistic Coefficient . . . . .	4.2-26
4.2-11	Pressure Descent Profiles for Final Configuration . . . . .	4.2-29
4.2-12	Descent Performance for 24 Second Sampling Time - Saturn. . . . .	4.2-33
4.2-13	Descent Performance for 24 Second Sampling Time - Uranus. . . . .	4.2-34
4.2-14	Entry Accelerometer Measurement Performance . . . . .	4.2-39
4.3-1	Saturn 1979 Mission Definition. . . . .	4.3-4
4.3-2	Saturn/SU-80 Mission Definition . . . . .	4.3-11
4.3-3	Uranus/SU-80 Mission Definition . . . . .	4.3-13
4.3-4	Titan III E/Centaur/TE 364-4 Performance Data. . . . .	4.3-18
4.3-5	C <sub>3</sub> Launch Arrival Data Contours . . . . .	4.3-19
4.3-6	Peak Entry Deceleration, Uranus . . . . .	4.3-31
4.3-7	Peak Entry Deceleration, Saturn . . . . .	4.3-31
4.3-8	Saturn and Uranus Deployment Conditions . . . . .	4.3-32
4.3-9	Total Angle of Attack Envelope, Uranus Entry $\gamma_E = -0.61$ rad (-35 deg). . . . .	4.3-34



Figure

4.4-1	Probe Deceleration, Extreme Atmospheres . . . . .	4.4-4
4.4-2	Pictorial Sequence of Events, Baseline Configuration. . . . .	4.4-8
4.4-3	Simplified Block Diagram, Baseline Configuration . . . . .	4.4-11
4.4-4	Data Profile, Baseline Configuration. . . . .	4.4-12
4.4-5	Power Profile, Baseline Configuration . . . . .	4.4-13
4.4-6	Pictorial Sequence of Events, Alternate Configuration . . . . .	4.4-15
4.4-7	Data Profile, Alternate Configuration . . . . .	4.4-17
4.4-8	Power Profile, Alternate Configuration. . . . .	4.4-18
4.4-9	Pictorial Sequence of Events, Final Configuration . . . . .	4.4-22
4.4-10	Data Storage Comparison, Nominal and Worst-Case Atmospheres. . . . .	4.4-24
4.4-11	Power Profile, Uranus Extreme Atmospheres . . . . .	4.4-26
4.4-12	Power Profile, Saturn Extreme Atmospheres . . . . .	4.4-27
4.5-1	Probe Transmitter Power Required vs Frequency, Data Rate, and Periapsis Radius. . . . .	4.5-5
4.5-2	Communication Geometry vs Lead Time . . . . .	4.5-6
4.5-3	Computed Coding Advantage for the Viterbi Decoder . . . . .	4.5-10
4.5-4	FSK Modulation Performance. . . . .	4.5-11
4.5-5	Error Probability Performance as a Function of Bandpass Limiting . . . . .	4.5-13
4.5-6	Flowfield Regions and Plasma Properties for the Jovian Entry Probe. . . . .	4.5-16
4.5-7	Electron Density in the Near Wake During Saturn Entry. . . . .	4.5-18
4.5-8	Noise Components of the Spacecraft Receiver. . . . .	4.5-20
4.5-9	1970 State-of-the-Art Noise Figure for Microwave Receivers . . . . .	4.5-22
4.5-10	Thermal Noise Temperature of the Milky Way Galaxy. . . . .	4.5-24
4.5-11	Saturn/Uranus Geometries for Worst-Case Viewing Angle from the Spacecraft . . . . .	4.5-25
4.5-12	Receiving System Noise Temperature for Saturn with Split Axial Beam Antenna - All Configurations. . . . .	4.5-28

Figure

4.5-13	Receiving System Noise Temperature for Uranus with Split Axial Beam Antenna . . . .	4.5-29
4.5-14	Location of Clouds that Affect Microwave Absorption . . . . .	4.5-31
4.5-15	Zenith Absorption for the Saturn Nominal Atmosphere . . . . .	4.5-33
4.5-16	Zenith Absorption for the Saturn Cool Atmosphere. . . . .	4.5-34
4.5-17	Zenith Absorption for the Uranus Nominal Atmosphere . . . . .	4.5-35
4.5-18	Electron Number Density Models for Saturn and Uranus. . . . .	4.5-37
4.5-19	Radiation Patterns for a Turnstile/Cone Antenna. . . . .	4.5-40
4.5-20	Prototype Turnstile/Cone Antenna Mounted on Model Probe . . . . .	4.5-41
4.5-21	Probe Turnstile/Cone Antenna Design. . . . .	4.5-42
4.5-22	Functional Diagram for the Saturn/Uranus Probe Transmitter . . . . .	4.5-44
4.5-23	Required Spacecraft Antenna Pattern Coverage for the Final Configuration . . . .	4.5-45
4.5-24	Probe Receiver/Demodulator Characteristics and Interface Requirements . . . . .	4.5-48
4.5-25	Functional Diagram of the Binary FSK Receiver, Bit Synchronizer, and Symbol Detector. . . . .	4.5-49
4.5-26	Memory Configuration for Dual Data Transmission, Alternative No. 1 . . . . .	4.5-53
4.5-27	Memory Control Logic Changes for Dual Data Transmission, Alternative No. 2 . . . .	4.5-55
4.5-28	Updated Alternate Configuration Battery Subsystem Weights for the Atmosphere Models . . . . .	4.5-60
4.5-29	Probe-to-Spacecraft Communication Range for the Baseline Configuration . . . . .	4.5-63
4.5-30	Probe Aspect Angles for the Baseline Configuration. . . . .	4.5-64
4.5-31	Probe Angular Variations for the Baseline Configuration during Saturn Encounter. . . .	4.5-65
4.5-32	Probe Angular Variations for the Baseline Configuration during Uranus Encounter. . . .	4.5-66
4.5-33	Spacecraft Antenna Pattern Coverage Requirements for the Baseline Configuration. . . . .	4.5-68

Figure

4.5-34	Required Spacecraft Antenna Pattern Coverage for the Alternate Configuration. . . . .	4.5-76
4.5-35	Required Spacecraft Antenna Pattern Coverage for the Final Configuration . . . .	4.5-86
4.5-36	Required Probe RF Power for the Final Configuration. . . . .	4.5-90
4.5-37	Power Profile for the Final Configuration. . . . .	4.5-91
4.6-1	Descent Profiles at Saturn for Nominal Atmosphere, Baseline and Alternate Probe Configurations . . . . .	4.6-10
4.6-2	Descent Profiles at Uranus for Nominal Atmosphere, Baseline and Alternate Probe Configurations . . . . .	4.6-11
4.6-3	Descent Profiles at Saturn for Nominal and Worst-Case Atmospheres, Final Probe Configuration. . . . .	4.6-12
4.6-4	Descent Profiles at Uranus for Nominal and Worst-Case Atmospheres, Final Probe Configuration. . . . .	4.6-13
4.6-5	Probe Temperature Rise During Coast. . . . .	4.6-16
4.6-6	Probe/Spacecraft Cruise Configuration, Final Probe Configuration. . . . .	4.6-17
4.6-7	Probe Internal Temperature versus Heat Conducted Through Support Points During Cruise. . . . .	4.6-18
4.6-8	Component Temperatures During Descent in the Saturn/Uranus Cool Atmospheres, Final Probe Configuration. . . . .	4.6-21
4.6-9	Component Temperatures During Descent in the Saturn/Uranus Nominal Atmospheres, Final Probe Configuration. . . . .	4.6-22
4.6-10	Component Temperatures During Descent in the Saturn/Uranus Warm Atmospheres, Final Probe Configuration. . . . .	4.6-23
4.6-11	Component Temperatures During Descent in the Saturn Warm Atmospheres, Dual Data Transmission, Final Probe Configuration. . .	4.6-24
4.6-12	Pioneer S/U Probe Baseline Configuration . .	4.6-29
4.6-13	Baseline Configuration Separation and Deceleration System. . . . .	4.6-31

Figure

4.6-14	Pioneer S/U Probe Alternate Configuration . . . . .	4.6-37
4.6-15	Pitch Damping Coefficients. . . . .	4.6-42
4.6-16	Alternate and Final Configuration Nose Cap Jettisoning System . . . . .	4.6-44
4.6-17	Alternate and Final Configuration Nephelometer Cover Release System . . . . .	4.6-45
4.6-18	Alternate Configuration Deceleration System. . . . .	4.6-46
4.6-19	Pioneer S/U Probe Final Configuration . . .	4.6-55
4.6-20	Final Configuration Probe Deceleration System. . . . .	4.6-61
4.6-21	S/U Common Probe Thermal Control Subsystem Hardware. . . . .	4.6-63

Table

2.0-1	Study Constraints . . . . .	2.0-2
2.0-2	Science Measurements . . . . .	2.0-3
2.0-3	Instrument Characteristics for the Final Configuration . . . . .	2.0-3
2.0-4	Measurement Performance at the Cloud Tops . . . . .	2.0-5
2.0-5	Distribution of Mass Spectrometer Measurements . . . . .	2.0-5
2.0-6	Mission Design Summary . . . . .	2.0-7
2.0-7	Communication Subsystem Summary . . . . .	2.0-10
2.0-8	Power and Pyrotechnics Subsystem Summary . . . . .	2.0-10
2.0-9	Weight Statement for the Final Configuration . . . . .	2.0-11
2.0-10	Hardware Availability for Science Instruments . . . . .	2.0-12
2.0-11	Hardware Availability for Electrical/ Electronic Components . . . . .	2.0-12
2.0-12	Hardware Availability for Structural/ Mechanical Components . . . . .	2.0-13
4.0-1	Study Constraints . . . . .	4.0-1
4.1-1	Modifications Required to Pioneer Venus Instruments . . . . .	4.1-2
4.1-2	Probe Transmitter Hardware . . . . .	4.1-6
4.2-1	Model Atmosphere Compositions . . . . .	4.2-4
4.2-2	Relevant Measurements . . . . .	4.2-6
4.2-3	Instruments Related to Measurements . . . . .	4.2-6
4.2-4	Instruments Characteristics Summary . . . . .	4.2-11
4.2-5	Descent Science Mission Parameters - Baseline Configuration . . . . .	4.2-23
4.2-6	Descent Science Mission Parameters - Alternate Configuration . . . . .	4.2-24
4.2-7	Entry and Descent Science Mission Parameters - Final Configuration . . . . .	4.2-28
4.2-8	Minimum Sampling Requirements and Data Rate . . . . .	4.2-30
4.2-9	Data Construction for 32 bps - Final Configuration . . . . .	4.2-31
4.2-10	Measurement Performance Summary . . . . .	4.2-37
4.2-11	Distribution of Mass Spectrometer Measurements . . . . .	4.2-37
4.2-12	Data Construction for Dual Data Transmission at 51.2 bps . . . . .	4.2-40

Table

4.3-1	Saturn 1979 Mission Summary Data . . . . .	4.3-5
4.3-2	Saturn/SU-80 Mission Summary Data . . . . .	4.3-9
4.3-3	Uranus/SU-80 Mission Summary Data . . . . .	4.3-14
4.3-4	DSN Tracking Data Summary . . . . .	4.3-22
4.3-5	Planetary Ephemeris and Mass Uncertainties ( $1\sigma$ ) . . . . .	4.3-22
4.3-6	Entry Dispersions ( $3\sigma$ ) for Execution Error Levels of Saturn 1979 Mission . . . . .	4.3-24
4.3-7	Entry Dispersions ( $3\sigma$ ) as a Function of Entry Angle, Uranus Mission . . . . .	4.3-25
4.3-8	Comparison of Dispersions for JPL and Martin Marietta Orbit Determination Results . . . . .	4.3-26
4.3-9	Comparison of Martin Marietta and JPL Orbit Determination Results . . . . .	4.3-28
4.4-1	Alternate Probe Comparison With and Without Preentry Transmission . . . . .	4.4-2
4.4-2	Nose Cap Deployment Analysis . . . . .	4.4-5
4.4-3	Comparison of Single and Dual Data Return . . . . .	4.4-7
4.4-4	Detailed Sequence of Events, Baseline Configuration . . . . .	4.4-9
4.4-5	Detailed Sequence of Events, Alternate Configuration . . . . .	4.4-16
4.4-6	Comparison of Baseline and Alternate Configurations . . . . .	4.4-20
4.4-7	Detailed Sequence of Events, Final Configuration . . . . .	4.4-23
4.4-8	Probe System Environmental Requirements . . . . .	4.4-28
4.5-1	RF Link Frequency Trade Study Comparison . . . . .	4.5-2
4.5-2	Communication Subsystem Variables that Affect RF Power . . . . .	4.5-4
4.5-3	Composition of the Model Atmospheres by Volume . . . . .	4.5-15
4.5-4	Probe Descent Parameters . . . . .	4.5-15
4.5-5	Abundance of Ammonia in the Atmospheric Models . . . . .	4.5-32
4.5-6	Design Requirements for the Probe Receiving Antenna for the Final Configuration . . . . .	4.5-46
4.5-7	Receiver/Demodulator Performance Characteristics . . . . .	4.5-46

Table

4.5-8	Data Handling Subsystem Capability/ Requirements Comparison . . . . .	4.5-51
4.5-9	Battery Subsystem Comparisons for Single-Battery Systems. . . . .	4.5-57
4.5-10	Battery Subsystem Comparisons for Two-Battery Systems . . . . .	4.5-58
4.5-11	Power Subsystem Losses. . . . .	4.5-60
4.5-12	Probe Telemetry Link Design Table for the Baseline Configuration. . . . .	4.5-69
4.5-13	Telecommunication Subsystem for the Baseline Configuration. . . . .	4.5-70
4.5-14	Descent Battery Sizing for the Baseline Configuration. . . . .	4.5-73
4.5-15	Trajectory Communication Parameters for the Alternate Configuration . . . . .	4.5-75
4.5-16	Probe Telemetry Link Design Table for the Alternate Configuration . . . . .	4.5-77
4.5-17	Telecommunications Subsystem for the Alternate Configuration . . . . .	4.5-78
4.5-18	Descent Battery Sizing for the Alternate Configuration . . . . .	4.5-81
4.5-19	3-Sigma Dispersions for the Updated Alternate Configuration . . . . .	4.5-83
4.5-20	Trajectory Communication Parameters for the Final Configuration . . . . .	4.5-83
4.5-21	Probe Telemetry Link Design for the Final Configuration . . . . .	4.5-88
4.5-22	Telecommunication Subsystem for the Final Configuration . . . . .	4.5-89
4.5-23	Battery Calculations for the Final Design. . . . .	4.5-92
4.6-1	Configuration Comparisons . . . . .	4.6-1
4.6-2	Structural Margin of Safety Summary . . . . .	4.6-4
4.6-3	Preentry and Descent Times for Baseline, Alternate, and Final Configurations. . . . .	4.6-9
4.6-4	Temperature Limits, Saturn/Uranus Common Probe. . . . .	4.6-14
4.6-5	Predicted Equipment Operating Temperatures During Descent for Baseline and Alternate Configurations in Nominal Atmospheres. . . . .	4.6-20

Table

4.6-6	Baseline Configuration Weight Breakdown. . . . .	4.6-26
4.6-7	Alternate Configuration Weight Breakdown. . . . .	4.6-39
4.6-8	Nominal Atmosphere Configuration Comparisons. . . . .	4.6-48
4.6-9	Updated Alternate Configuration Weight Breakdown . . . . .	4.6-50
4.6-10	Updated Alternate and Final Configurations Comparisons . . . . .	4.6-52
4.6-11	Final Configuration Weight Breakdown. . . . .	4.6-57



## SYMBOLS AND ABBREVIATIONS

A/D	analog-to-digital
AFC	automatic gain control
AGC	automatic frequency control
AU	astronomical unit
B	plane perpendicular to incoming velocity vector and passing through the center of the planet; binary; ballistic coefficient; receiver noise bandwidth
BER	bit error rate
BFSK	binary frequency-shift keying modulation
bps	bit per second
BW	beamwidth
C	cool atmosphere
CA	cone angle
c.g.	center of gravity
CP	carbon phenolic
D	deuterium; diameter
d	day
DHS	data handling subsystem
DLA	declination angle
DSN	Deep Space Network
DTU	digital telemetry unit
E	entry ( $10^{-7}$ bar)
e	electron
EA	early arrival

$E_b$	energy per data bit
ENT	effective noise temperature
EOM	end of mission
FAB	convective blocking factor
FAR	radiative blocking factor
f	frequency
FSK	frequency-shift keying modulation
$G_1$	power gain ratio of RF amplifier
$G_2$	power gain ratio of IF amplifier
IF	intermediate frequency
K	constraint length
k	Boltzmann's constant ( $1.38 \times 10^{-23}$ W-s/ $^{\circ}$ K)
K.E.	kinetic energy
$kT_B$ S	total available noise power referred to the receiver output terminals
LA	late arrival
$L_F$	feedline power-loss ratio
M	Mach number
MFSK	multiple frequency shift keying
m	mass
MS	margin of safety
N	Nominal atmosphere; ratio of IF bandwidth to the data bit rate
n	neutron
$n_e$	electron density

NA	nominal arrival
NMS	neutral mass spectrometer
$N_o$	noise spectral density
P	pressure
p	proton
PAA	probe aspect angle
PCU	power control unit
PLL	phase lock loop
ppm	part per million
PPS	power and pyrotechnics subsystem
PSK	phase-shift keying
PV	Pioneer Venus
Q	quantizing level; total heat
$Q_{conv}$	total convective heat
$\dot{q}_{conv}$	convective heating rate
$Q_{rad}$	total radiative heat
$\dot{q}_{rad}$	radiation heating rate
QNP	quartz nitrile phenolic
R	range
r	roentgen
rad	radians; radiation unit
$R_B$	base radius
RCA	radius of closest approach

$R_{EJ}$	radius of ejection
RF	radio frequency
RFI	radio frequency interference
RHU	radioisotope heater unit
$R_N$	nose radius
ROM	read-only memory
$R_p$	periapsis radius
$R_S$	radius of Saturn
RTG	radioisotope thermoelectric generator
$R_U$	radius of Uranus
S	Saturn; separation
s	second
SC	Saturn cool atmosphere
sec	secant, second
SCU	signal conditioning unit
SMAA	semimajor axis
SMIA	semiminor axis
SN	Saturn nominal atmosphere
S/N	signal-to-noise ratio
SSB	single sideband
SU	Saturn/Uranus
SW	Saturn warm atmosphere
T	temperature

t	thickness
T <sub>A</sub>	antenna noise temperature
T <sub>BD</sub>	planet disk noise temperature
T <sub>BS</sub>	synchrotron noise temperature
T/C	thermal control
T <sub>F</sub>	antenna feedline noise temperature
T <sub>G</sub>	galactic noise temperature
T <sub>L</sub>	lead time
T <sub>R</sub>	receiver noise temperature
T <sub>S</sub>	system noise temperature
T <sub>1</sub>	RF amplifier noise temperature
T <sub>2</sub>	mixer noise temperature
T <sub>3</sub>	IF amplifier noise temperature
U	Uranus
UC	Uranus cool atmosphere
UHF	ultra high frequency (300 MHz to 3 GHz)
UN	Uranus nominal atmosphere
UW	Uranus warm atmosphere
v	velocity
v	inertial velocity
V <sub>HP</sub>	velocity of spacecraft relative to planet
W	warm atmosphere, watts
z	altitude

$\alpha$	angle of attack
$\beta$	dispersion ellipse orientation angle
$\gamma$	flight path angle
$\gamma_E$	entry flight path angle
$\Delta F$	frequency change
$\Delta V$	velocity change
$\epsilon$	emissivity
$\lambda$	wavelength
$\rho$	gas density
$\rho_\infty$	ambient density
$\psi$	probe aspect angle
$\Omega_A$	antenna pattern solid angle
$\Omega_p$	planet disk solid angle

## 1.0 Introduction

## 1.0 INTRODUCTION

The general objective of this study was to define a common Pioneer Saturn/Uranus probe, compatible with the required science objectives and the worst-case atmospheric models, and more specifically, to: (1) use designs based on existing hardware from the Pioneer Venus (PV) program; (2) to assess the effect of modifying the PV hardware designs to make the hardware compatible with mission objectives, and (3) to use designs from other sources whenever the first two of these efforts failed to provide suitable components.

Initially, the nominal atmospheric models for Saturn and Uranus were included in the design constraints that resulted in the baseline and alternate probe definitions. These two configurations were then evaluated and a recommended configuration was selected for the remainder of the study. The study was then expanded to include the cool, nominal, and warm atmospheric models for Saturn and Uranus in the design constraints. The impact of these extreme atmospheres on the previous configuration was assessed and a final probe system was defined to meet the "worst-case" atmospheres. The term "worst-case" is used because the Uranus cool atmosphere establishes one design factor, the Saturn warm atmosphere establishes a different factor, and so forth.

The relationship between these activities is shown in Figure 1.0-1.

The summary is presented in Section 2.0; probe-to-spacecraft interfaces are summarized in Section 3.0; the detailed technical study is summarized in Section 4.0; and the major conclusions are shown in Section 5.0. Section 4, which encompasses most of the volume, first covers probe hardware availability, and then each of the five major design disciplines: science design, mission design, system design, electronics design and mechanical design. The analyses and tradeoff studies for each discipline are followed by a discussion of the baseline configuration, a similar discussion for the alternate configuration, a trial comparison of the two configurations, and a short summary showing the impact of the "worst-case" atmosphere.

For your convenience, we have compiled our detailed design drawings for the final probe configuration into a separate bound volume, Martin Marietta report IR-73-2, and are submitting them along with this report.



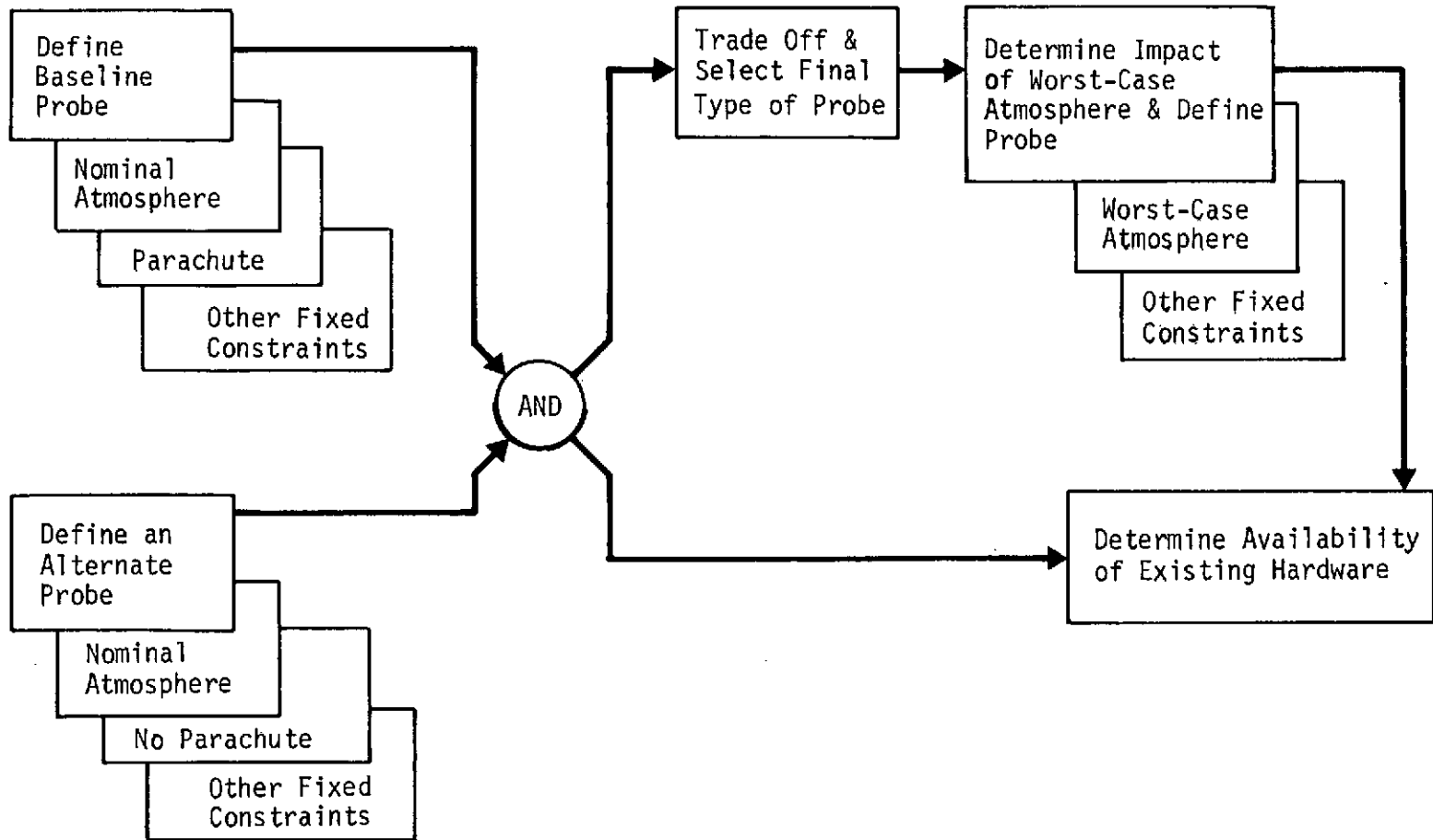


Figure 1.0-1 Study Flow Plan

## 2.0 Summary

## 2.0 SUMMARY

During the initial phase of the study we defined two different types of probe systems based on the nominal atmospheric models. The first of these is our baseline (parachute) configuration; and the second is an alternate (no parachute) configuration. Later in the study we made a number of modifications to the alternate configuration to update the science instruments and make it compatible with the worst-case atmospheric models. This updated version is referred to as the final configuration. The following sections of this summary emphasize the final configuration.

### 2.1 SCIENCE DESIGN

The science constraints and basic scientific objectives are shown in Table 2.0-1. Note that the science instruments required to meet these objectives are a temperature gauge, a pressure gauge, an accelerometer triad, a neutral mass spectrometer, and a nephelometer. The primary and secondary measurements performed by each of these instruments are shown in Table 2.0-2.

The major characteristics of the science instruments are shown in Table 2.0-3. Note that the science payload weighs a total of 11.46 kg (25.3 lb) and requires 18.5 watts of power, and that the real-time data rate for the science measurements during descent is 21.92 bps. The science data, the interleaved stored data, and other real-time engineering data all combine to account for the 32-bps transmitted data rate.

The wide extremes posed by the cool and warm atmospheric models caused a wide variation in many of the design parameters. The descent ballistic coefficients varied from 160 kg/m<sup>2</sup> to 162 kg/m<sup>2</sup>. In contrast, the entry coefficient remained constant at 142.6 kg/m<sup>2</sup>. The entry duration varied from 47 seconds to 98 seconds; the descent duration, from 27.3 minutes to 73.9 minutes; and the pressure at the beginning of the descent measurement, from  $3.9 \times 10^2$  to  $1.4 \times 10^3$  N/m<sup>2</sup> (39 to 114 mb).

Table 2.0-4 evaluates the measurement performance of the temperature gauge, pressure gauge, and turbulence accelerometers at the cloud tops.

Table 2.0-1 Study Constraints

Science Objectives

- Measure Atmospheric Structure & Composition Down to 10 bar
- Determine Location and Composition of Clouds
- Obtain Science & Engineering Data

Missions

- Saturn Direct 1979
- Saturn/SU - 1980
- Uranus/SU - 1980

Spacecraft Bus - Pioneer F/G

Launch Vehicle - Titan IIIE/Centaur/TE 364-4

Baseline Probe Requirements

- Science Advisory Groups,  
Exploratory Payload + Nephelometer
- Nominal Atmospheric Models for Baseline & Alternate Configurations
- Worst-Case Atmospheric Models for Final Configuration
- S/C Deflection Mode
- Present State-of-the-Art Heat Shield Material
- Sphere-Cone with Nose-to-Base Ratio of 0.4 to 0.6 and  
0.79 to 1.05-rad (45° to 60°) Half Cone Angle
- Maximum Diameter, 0.914 m (36 in.)
- Maximum Weight, 113.40 kg (250 lb)
- Relay Link Requiring No Despun S/C Antenna

Table 2.0-2 Science Measurements

Measurement	Instrument				
	Temperature Gauge	Pressure Gauge	Accelerometer Triad	Neutral Mass Spectrometer	Nephelometer
H/He Ratio in the Mixed Atmosphere	R	R	R	D	N
Isotopic Ratios (Primary Isotopes thru A)	N	N	N	D	N
Concentration Profiles for Minor Constituents	R	R	N	D	R
Temperature/Pressure Descent Profiles	D	D	R	R	N
Mean Molecular Weight of Mixed Atm.	R	R	R	R	R
Cloud Composition	R	R	N	D	N
Cloud Location	R	R	N	R	D
Indication of Magnitude of Turbulence	R	R	R	N	R

D = Direct measurement;  
R = Related measurement;  
N = Little or no relation.

Table 2.0-3 Instrument Characteristics for the Final Configuration

	Instrument				
	Temperature Gauge	Pressure Gauge	Accelerometers (3-axis)	Nephelometer	Neutral Mass Spectrometer
Weight, kg (lb)	0.32 (0.7)	0.45 (1.0)	1.13 (2.5)	0.49 (1.1)	9.07 (20)
Volume, cm <sup>3</sup>	98	115	656	524	9830
Power Required, W	0.5	0.5	2.3	1.2	14.0
Warmup Time, sec	300	30	30	10	300
Sampling Interval, sec	24	24	24	12	400
Data Bits per Sample	8	8	40	43	6400
Data Bit Rate, bps	0.33	0.33	1.67	3.58	16
Required Range	40°K to 450°K	10 <sup>3</sup> to 10 <sup>7</sup> N/m <sup>2</sup> (10 <sup>-2</sup> to 10 <sup>2</sup> bar)	0.098 to 5884 m/sec <sup>2</sup> (10 <sup>-2</sup> to 600 g)		1 to 40 amu
Output Signal Mode	Analog	Analog	Analog	Digital	Digital

ORIGINAL PAGE IS  
OF POOR QUALITY

The neutral mass spectrometer makes at least four full samples in the cool atmospheres and six in the other atmospheres prior to reaching 10 bars.

The distribution of the atmospheric samples from the mass spectrometer is shown in Table 2.0-5.

The entry accelerometers sample at two different rates-- 5 samples/sec and 2.5 samples/sec--to enable us to reconstruct the most severe entry deceleration in the cool atmospheres.

## 2.2 MISSION DESIGN

The 1979 Saturn direct mission is described in Figure 2.0-1 in terms of the interplanetary trajectory, launch analysis, deflection maneuver, and approach trajectories. The approach covers spacecraft and probe traces for a period ranging from preentry through spacecraft periapsis. The end of the mission varies from Entry + 28 minutes (for the cool atmosphere) to Entry + 63 minutes (for the warm atmosphere).

The Uranus/SU-80 mission is similarly depicted in Figure 2.0-2. For the Uranus mission, the end of the mission can vary from Entry + 29 minutes (for the cool atmosphere) to Entry + 74 minutes (for the warm atmosphere).

Table 2.0-6 compares the mission parameters for the Saturn direct, the Saturn/SU-80, and the Uranus/SU-80 missions. The boxed values are the controlling values for various portions of the system. For example, the range and the cone angles govern the design of the communication link, the entry time dispersion governs the size of the battery, and the entry angle of dispersion determines the maximum loads on the structure and represents the "worst-case" for heat shield design.

Table 2.0-4 Measurement Performance at the Cloud Tops

	Pressure & Temperature Gauges & Turbulence Accelerometer (24 sec)			Nephelometer (20 bits/6 sec)
	km/Meas	Cloud Top Pressure, $10^5$ N/m <sup>2</sup> (bar)	Meas/Scale Ht	km/Meas
Criterion:	≤5.0	--	≥5.0	≤1.0
Saturn Nominal	3.5	0.73	13	0.9
Uranus Nominal	2.4	0.49	12	0.6
Saturn Warm	5.7	0.27	11	1.4
Uranus Warm	5.6	0.12	7	1.3
Saturn Cool	1.7	3	21	0.4
Uranus Cool	1.3	1	13	0.3

Table 2.0-5 Distribution of Mass Spectrometer Measurements

NMS Measurement ( $\Delta t=400$ sec)	Time from Nose Cover Release, sec	Ambient Atmospheric Pressure, $10^5$ N/m <sup>2</sup> (bar)					
		Saturn Cool	Saturn Nominal	Saturn Warm	Uranus Cool	Uranus Nominal	Uranus Warm
1	51	0.21	0.15	0.10	0.12	0.08	0.06
2	451	1.61	1.00	0.58	1.16	0.64	0.41
3	851	4.02	2.18	1.32	2.96	1.63	1.02
4	1251	7.10	3.80	2.18	5.67	3.12	1.68
5	1651	10.57	5.57	3.17	9.45	4.71	2.51
6	2051	14.33	7.57	4.20	13.61	6.55	3.45

Boxed values are those measurements taken below the design pressure limit of 10 bar. However with systems designed for 74 minutes descent in the warm, the probe should survive past 10 bars (~29 minutes) in the cool.

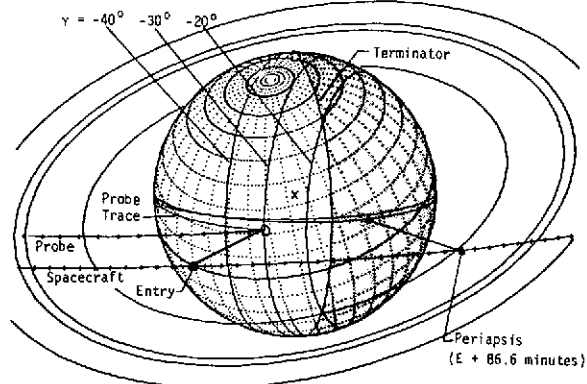
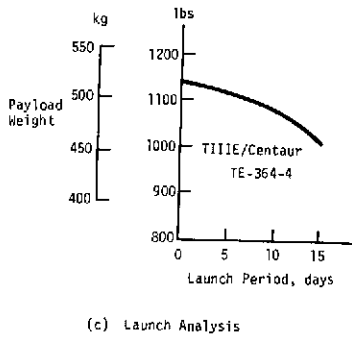
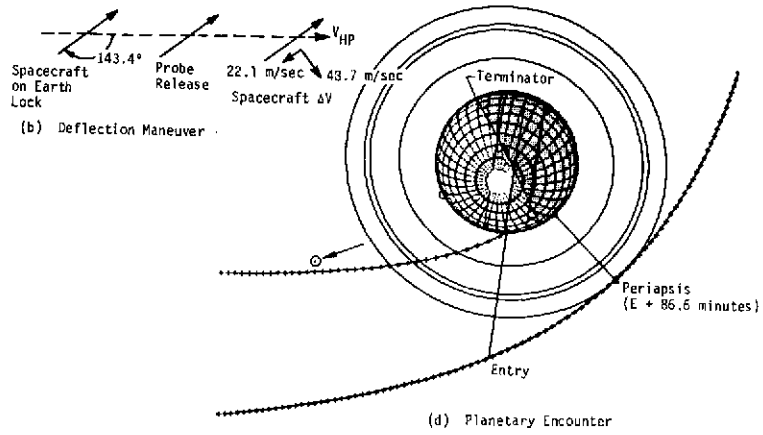
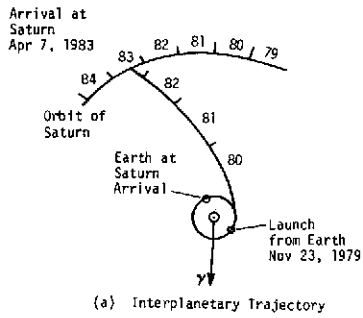


Figure 2.0-1 1979 Saturn Direct Mission Summary

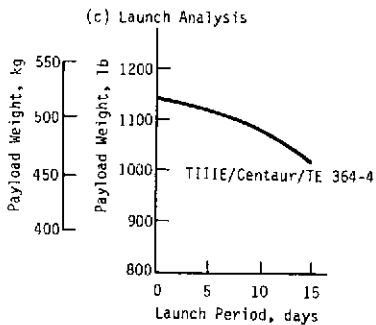
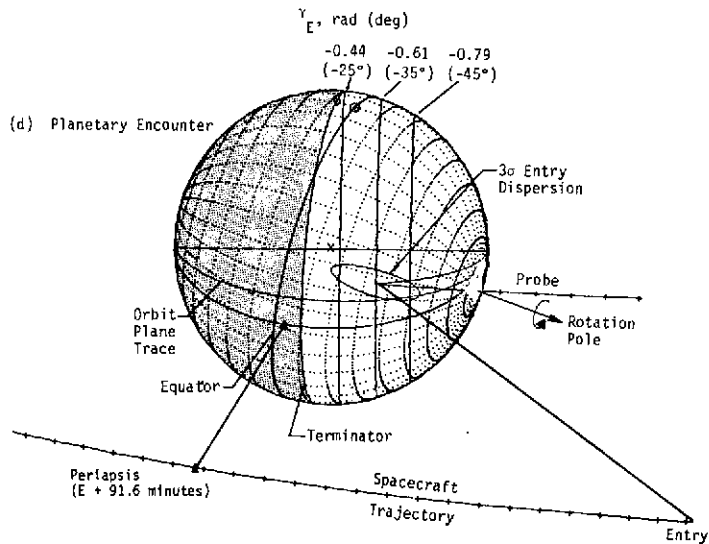
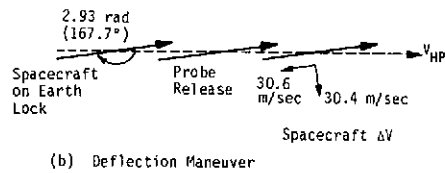
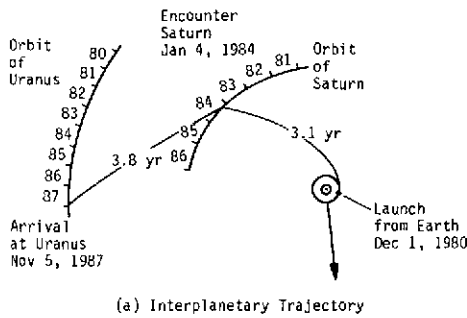


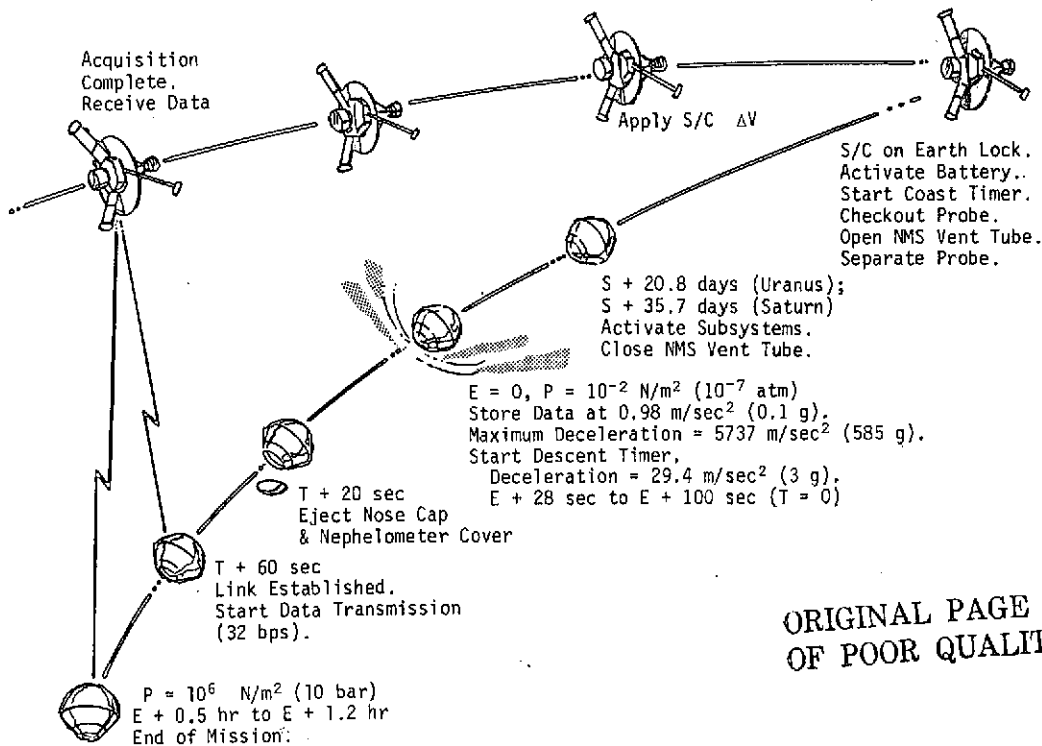
Figure 2.0-2 Uranus/SU-80 Mission Summary



Table 2.0-6 Mission Design Summary

Mission Parameter	Design Missions		
	Saturn -79	Saturn (SU-80)	Uranus (SU-80)
$V_{HP}$ , km/sec	9.18	10.6	13.8
Entry Angle, rad (deg)	-0.52 (-30)	-0.52 (-30)	-0.61 (-35)
Periapsis	2.3 $R_S$	23 $R_S$	3.0 $R_U$
Deflection Radius, $10^6$ km	30 (500 $R_S$ )	30 (500 $R_S$ )	25 (925 $R_U$ )
Coast Time, days	35.7	31.2	20.8
$\Delta V_{Earth}$ , m/sec	22.1	17.2	30.6
$\Delta V_{\perp}$ , m/sec	48.7	52.4	30.4
$\Delta V_{total}$ , m/sec	70.8	69.6	61.0
Angle of Attack, rad (deg)	0.15 (8.4)	0.24 (13.5)	0.13 (7.3)
Lead Time, sec	5200	4900	5500
Range at Entry, $10^5$ km	1.08	1.07	0.94
PAA* at Entry, rad (deg)	0.20 (11.4)	0.20 (11.6)	0.56 (31.9)
PAA at End of Mission, rad (deg)	0.24 (13.7)	0.27 (15.5)	0.62 (35.8)
CA† at Entry, rad (deg)	2.23 (127.7)	2.25 (128.7)	2.57 (147)
CA at End of Mission, rad (deg)	1.68 (96.4)	1.66 (95.0)	1.62 (93)
Entry Time Dispersion, minutes	4.01	3.3	27.95
Entry Angle Dispersion, rad (deg)	0.02 (1.2)	0.02 (1.18)	0.23 (13.2)
Angle of Attack Dispersion, rad (deg)	0.03 (1.7)	0.02 (1.17)	0.07 (4.2)

\* PAA = Probe aspect angle.  
 † CA = Cone angle.  
 □ = Design drivers.



ORIGINAL PAGE IS OF POOR QUALITY

Figure 2.0-3 Pictorial Sequence of Events for the Final Configuration

## 2.3 SYSTEM DESIGN

The sequence of events for the final configuration is shown in Figure 2.0-3. This sequence covers a period from approximately 40 days prior to separation until the end of the mission. A detailed discussion of this sequence is presented in Section 4.4.

The data profile is shown in Figure 2.0-4. The curves show the maximum storage capacity required and the amount of time required to empty the storage buffers in three different atmospheres. Note that the maximum amount of data transmitted to the spacecraft is 139K bits (278K symbols), which is sent at a rate of 32 bps.

The power profile for Uranus is presented in Figure 2.0-5. This profile represents the worst-case condition for sizing the battery. Note that different times are shown for late, nominal, and early arrival. Two different descent times represent the extremes for the cool and warm atmospheres. As shown, the maximum energy required is 562 kJ (156 W-h). The term "Late arrival" is defined as, "The probe arrives at the planet so late that the coast timer times out and starts the sequence before it is really needed."

## 2.4 ELECTRICAL/ELECTRONIC DESIGN

The communication requirements for the final configuration are defined in Table 2.0-7. Note that the required operating frequency, modulation, and RF power are 560 MHz, FSK, and 18 watts, respectively. The data symbols transmitted to the spacecraft as tones are demodulated on the spacecraft and must be stored until relayed to earth. Each of the 278,000 data symbols required a storage space of one bit. Therefore, the spacecraft memory must have 278K bits of storage capability. The power and pyrotechnics subsystem for the final configuration is defined in Table 2.0-8.

## 2.5 STRUCTURAL/MECHANICAL DESIGN

Figure 2.0-6 shows the internal components and their relative locations for the final probe configuration. The final weight breakdown for this configuration is summarized in Table 2.0-9. Note that the total entry weight and the weights shown at the bottom of the table incorporate a 15% margin.

## 2.6 HARDWARE AVAILABILITY

Tables 2.0-10 through 2.0-12 show the hardware availability for the science, electrical/electronic, and structural/mechanical designs. Emphasis is placed on using Pioneer Venus (PV) hardware and on identifying modifications that are required for SU missions.

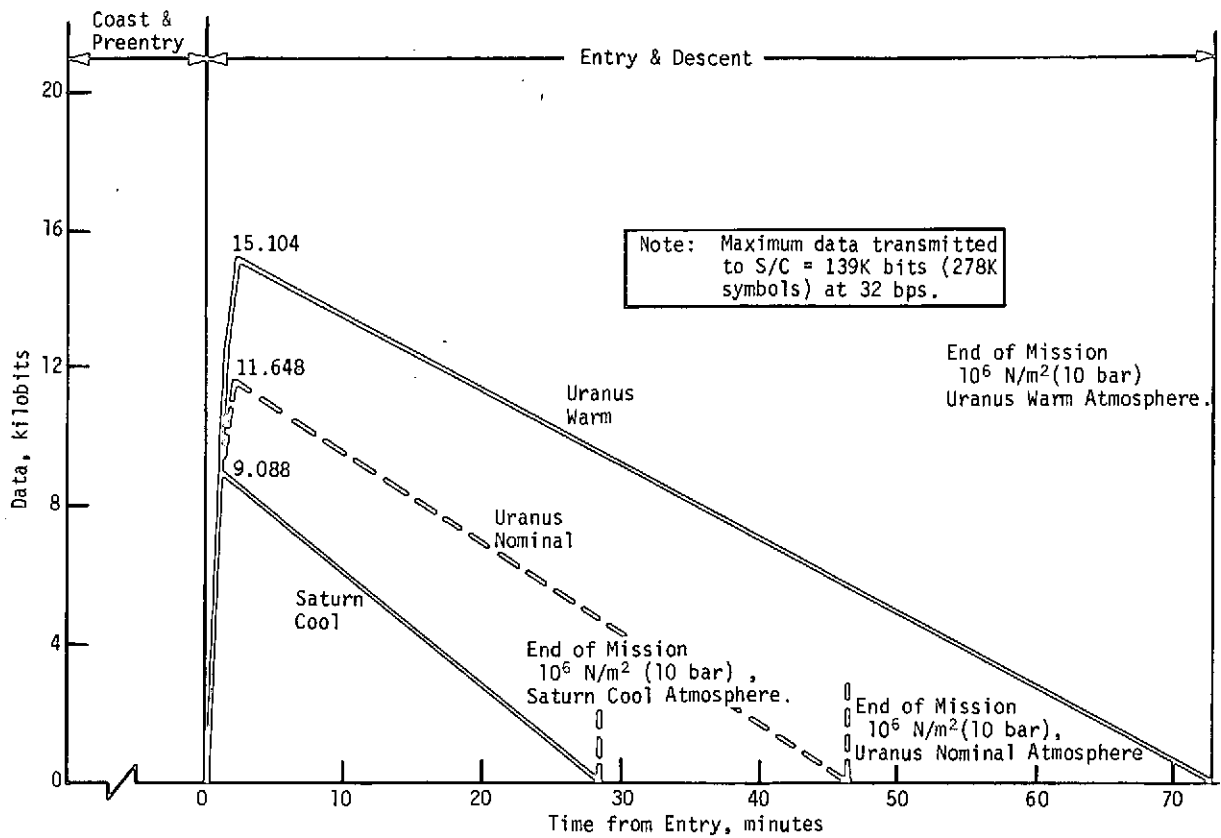


Figure 2.0-4 Data Profile for the Final Configuration

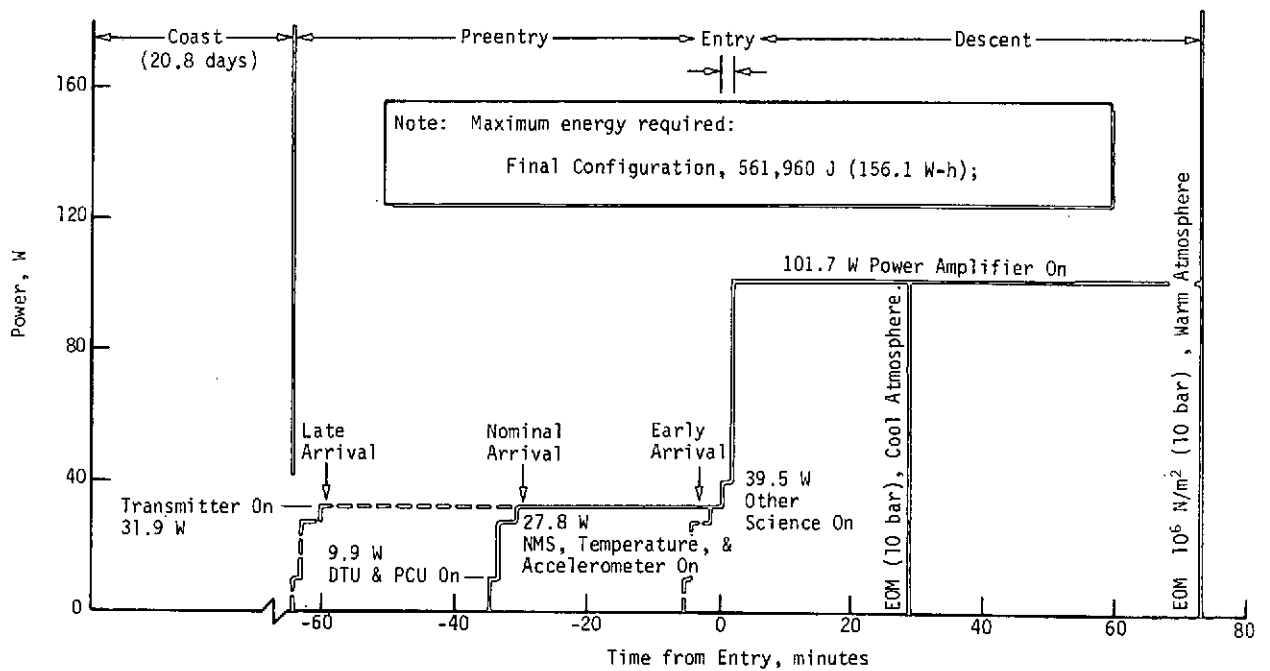


Figure 2.0-5 Power Profile for Entry at Uranus

Table 2.0-7 Communication Subsystem Summary

Parameter	Value	Comments
Frequency, MHz	560	Minimizes link losses.
Modulation	FSK + Tone	Most reliable.
Spacecraft Antenna		
Beamwidth, rad (deg)	0.96 (55)	Butterfly pattern with circular polarization.
Maximum Gain, dB	3.1	
Spacecraft Receiver		
Noise Figure, dB	2.6	Solid-state design.
S/N Ratio, dB	10	Minimum.
Oscillator Stability, ppm	10	Long-term.
Probe Antenna	Turnstile/cone	
Beamwidth, rad (deg)	1.75 (100)	Axial pattern with circular polarization.
Maximum Gain, dB	6.5	
Data Rate, bps	32	Single data transmission.
Transmitter Power, W	18	Uranus (entry), warm model.
Data Storage, K bits	15	Probe.
	278	Spacecraft.

Table 2.0-8 Power and Pyrotechnics Subsystem Summary

Subsystem	Description
Power Subsystem	<ul style="list-style-type: none"> <li>- Remotely activated Ag-Zn battery, activated prior to separation</li> <li>- 156 W-h, at 28 Vdc (Usable Energy)</li> </ul>
Pyrotechnics Subsystem	<ul style="list-style-type: none"> <li>- SCR direct fire</li> <li>- 24 firing circuits</li> <li>- Latching relay (safe/arm)</li> </ul>

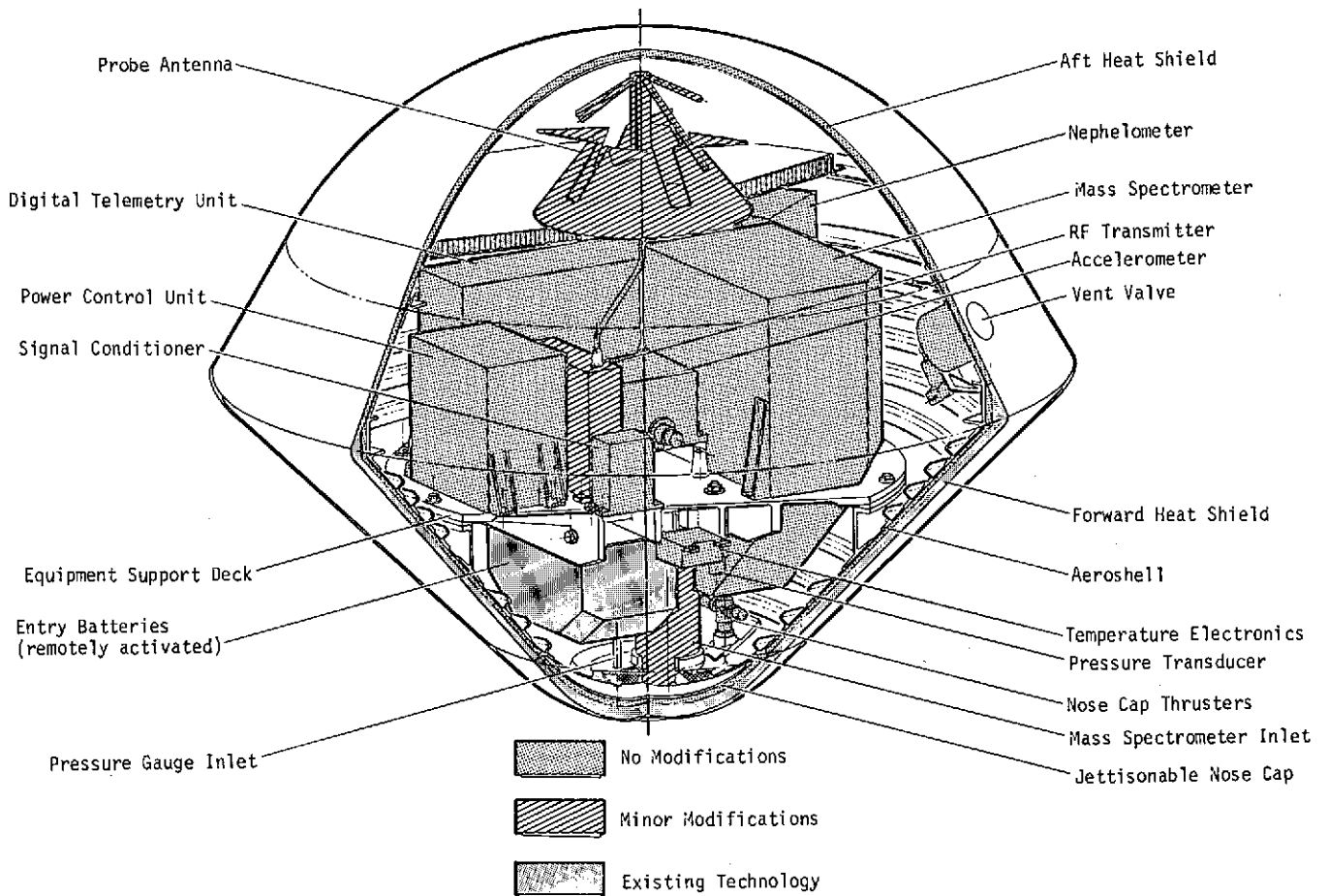


Figure 2.0-6 Final Probe Configuration

Table 2.0-9 Weight Statement for the Final Configuration

	Weight	
	kg	lb
Science	11.88	26.20
Power & Conditioning	10.09	22.25
Cabling	3.22	7.10
Data Handling	1.95	4.30
Communication	1.68	3.70
Structures & Heat Shield	44.89	98.96
Mechanisms	1.85	4.09
Thermal	4.24	9.34
Subtotal	79.90	176.14
Margin (15%)	11.98	26.42
Total Entry Weight	91.88	202.56
Postentry Weight (S)	73.65	162.38
Postentry Weight (U)	70.72	155.92
Descent Weight (S)	72.30	159.39
Descent Weight (U)	69.37	152.93

Table 2.0-10 Hardware Availability for Science Instruments

Science Instruments	PV Commonality or Other Source	Remarks
Nephelometer	PV, Either Probe	No modification.
Pressure Gauges	PV, Either Probe	No modification; excess range capability.
Accelerometers	PV, Large Probe	Modified for range.
Temperature Gauge	PV, Either Probe	Modified for range.
Neutral Mass Spectrometer	PV, Large Probe	Modified for mass range. Porous plug leaks replaced. Vent tube added for outgassing. Repackage to fit probe. Possible replacement of ion pump system for helium. Alternate sources possible.

Table 2.0-11 Hardware Availability for Electrical/Electronic Components

Electrical & Electronic Design	PV Commonality or Other Source	Remarks
<u>Data</u>		
DTU	PV, Either Probe	Minimal modification to replace two programmed ROMs
PCU	PV, Either Probe	Modify coast timer decoding logic. Replace 6 programmed ROMs.
Signal Conditioner	PV, Either Probe	No change.
<u>Power</u>		
PCU	PV, Either Probe	Update unijunction transistors. Modify wiring to add 29.4 m/sec <sup>2</sup> (3 g) switch.
Battery	New Design & Build	Existing technology.
<u>Communications</u>		
Transmitter	PV, Either Probe	Modified for frequency and modulation change.
Antenna	PV, Either Probe	Modified for frequency change.
<u>General</u>		
g Switches	PV, Either Probe	Change 49 m/sec <sup>2</sup> (5 g) switch to 0.98 m/sec <sup>2</sup> (0.1 g). Add 29.4 m/sec <sup>2</sup> (3 g) (decreasing) switch.

Table 2.0-12 Hardware Availability for Structural/  
Mechanical Components

Mechanical & Structural Design	PV Commonality or Other Source	Remarks
<u>Configuration</u>	PV, Small Probe	Use aeroshell tooling.
<u>Aerodecelerator &amp; Aerodynamics</u>	PV, Small Probe	Use aerodynamic test data.
<u>Heat Shield</u>	New Design & Build	Existing technology.
<u>Mechanisms</u>		
Pin Pullers	Viking, PV	No modification.
Ball-Lock Release Pins	TRW Programs, Minuteman	No modification.
Cable Cutter	PV, TRW Programs	No modification.
Pyro Thrusters	Hi Shear	No Modification
<u>Thermal Control</u>		
Isotope Heaters	Pioneer Spacecraft	No modification.
Thermal Blanket	Pioneer Spacecraft	No modification.
Foam Insulation	Saturn II	No modification.
Argon Gas Assembly	New Design & Build	Existing technology.
<u>Structure</u>		
Aeroshell	PV, Small Probe	Modified for larger diameter.
Remaining Structure	New Design & Build	Existing technology.

### 3.0 Spacecraft-to-Probe Interface



### 3.0 SPACECRAFT-TO-PROBE INTERFACE

This section discusses the characteristics of the spacecraft-to-probe interface for the final probe configuration before and after probe separation.

#### 3.1 MECHANICAL INTERFACE

The interface between the Saturn/Uranus probe and the Pioneer carrier spacecraft is shown in Figure 3.1-1. Note that the probe is mounted between the spacecraft and the launch vehicle, all of which have a common centerline. The probe is retained to and separated from the spacecraft by three gas-activated, ball-lock release mechanisms, which use integral springs to supply the required separation force between the probe and the spacecraft.

A 96.52-cm (38.00-in.) interstage adapter and a 37.21-cm (15.83-in.) probe/spacecraft support adapter attach the probe and spacecraft to the launch vehicle. The separation mechanisms and the cable cutter that severs the umbilical between the probe and the spacecraft are both integrated into the probe/spacecraft support adapter.

#### 3.2 THERMAL INTERFACES

The equilibrium temperature for the probe must be reduced during the cruise phase of the mission. Since probe heating is supplied exclusively by radioisotope heaters whose output cannot be changed, the probe support points on the spacecraft/probe interstage adapter were used to reject 4.2 watts of excess heater power during cruise. Although the design of the interstage adapter is not included in this study, we assumed that this 4.2 watts would be radiated to space from small fins on the adapter near the probe support points. These heat paths are disconnected at probe separation, which allows the probe to warm to the desired preentry temperature during the coast phase.

The temperature of the probe during cruise is also affected by the temperature of the spacecraft/probe interstage adapter. This adapter is radiatively coupled to the spacecraft's aft surface and louver system. Our preliminary analysis shows that this radiative coupling can be minimized by using a low-emissivity coating ( $\epsilon = 0.05$ ) on the outside of this adapter.

### 3.3 ELECTRICAL/ELECTRONIC INTERFACE

An inflight-disconnect umbilical provides power, command and data interfaces between the Pioneer spacecraft and the Saturn/Uranus probe systems until the probe is separated from the spacecraft. This interface is identical to that used in the Pioneer Venus spacecraft. All command data, command clock, execute, data clock, enable, and spacecraft power requirements are supplied to the probe by the spacecraft. Probe data are returned to the spacecraft under spacecraft control. The spacecraft must be able to buffer the data received from the probe, or transmit these data in real time, during the cruise and during the preseparation checkout periods.

The spacecraft will supply power for all probe activities that precede probe/spacecraft separation. Although the exact launch and cruise functions have not yet been defined, we expect that critical probe measurements such as internal temperature, pressure and vibration will be monitored periodically during launch and cruise without activating the probe subsystems.

The preseparation checkout entails powering up the probe subsystems and testing them under spacecraft control. The exact power level required from the spacecraft during this period depends on the DHS and each subsystem which is tested in the series in order to reduce the peak power demand on the spacecraft. The DHS provides the common interface with all other probe subsystems and is on for the duration of the preseparation checkout. Probe checkout is expected to require approximately 15 minutes, however, test results will be relayed to earth for review and new commands, if required, will be sent back to the spacecraft. This communication cycle is approximately 5.3 hours at Uranus and 2.7 hours at Saturn during which time the probe will be deactivated to reduce the power drain on the spacecraft.

The only critical timed event that must occur during the separation period is probe coast timer start. This timer which has a timing interval of approximately 40 days must time out 34 minutes and 40 seconds before entry (nominal arrival) at Uranus and at 9 minutes and 59 seconds before entry (nominal arrival) at Saturn.

### 3.4 COMMUNICATIONS INTERFACES

Specific communication requirements for the spacecraft receiver and demodulator interface and spacecraft antenna requirements are presented in Section 4.5.1.1. In addition to meeting

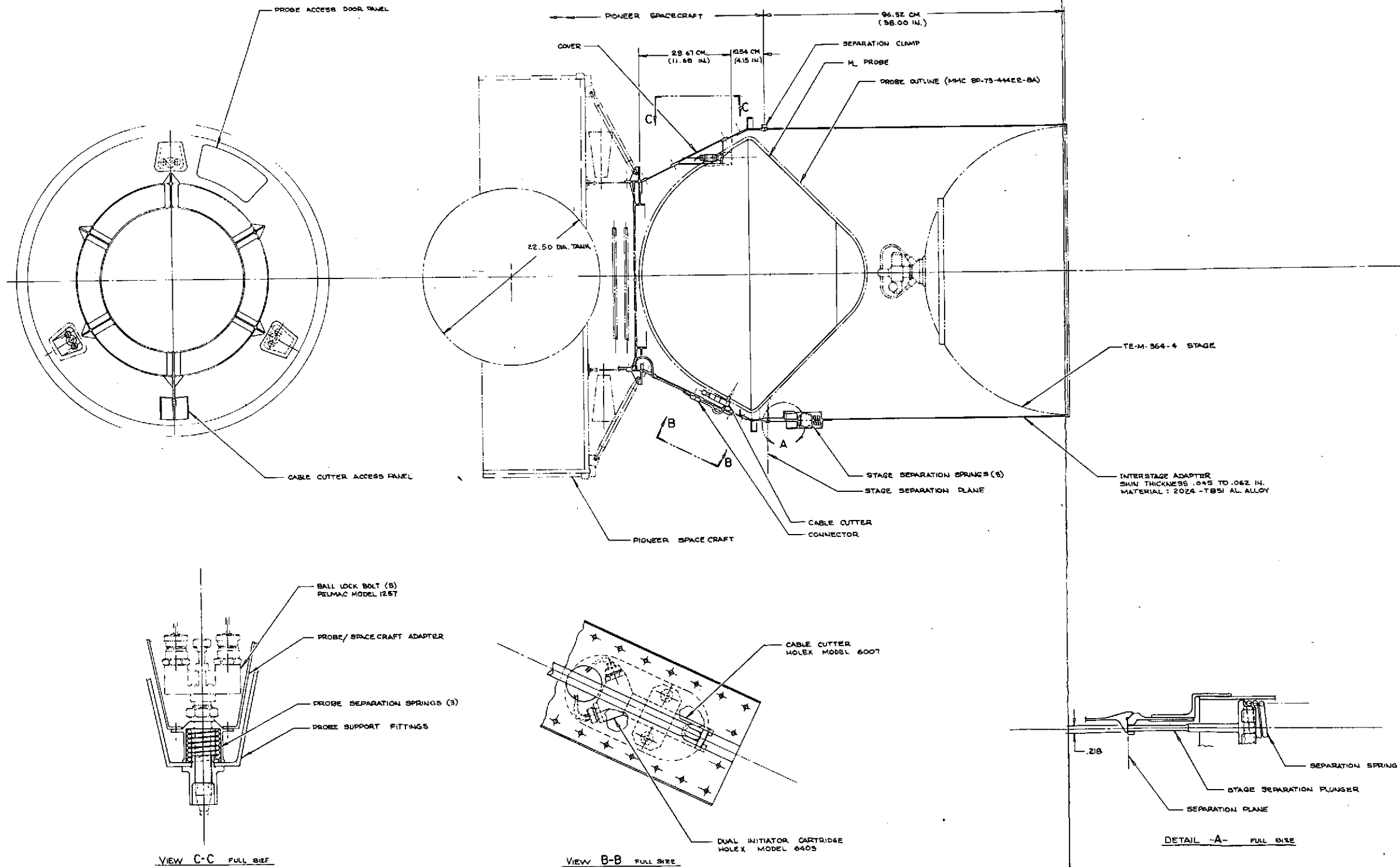


Figure 3.1-1 Pioneer SU Probe/Spacecraft Interface

Page 3.0-3 & 3.0-4

ORIGINAL PAGE IS  
OF POOR QUALITY

FOLDOUT FRAME

2

ORIGINAL PAGE IS  
OF POOR QUALITY

FOLDOUT FRAME

these requirements, the spacecraft must be able to transmit the probe entry and descent data in real time or have a buffer memory capable of holding the probe data for later transmissions. Delayed transmission requires a memory twice the size of transmitted data (139K bits), because the data are encoded in a rate 1/2 encoder. Therefore the number of symbols received by the spacecraft (278,000) is twice the number of probe data bits.

## 4.0 Technical Studies

## 4.0 TECHNICAL STUDIES

The study was begun with the constraints shown in Table 4.0-1, but was limited to the nominal atmospheric models. Later in the study, the extreme atmospheric models became controlling factors for the final configuration.

Table 4.0-1 Study Constraints

Science Objectives
- Measure Atmospheric Structure & Composition Down to 10 bar
- Determine Location and Composition of Clouds
- Obtain Science & Engineering Data
Missions
- Saturn Direct 1979
- Saturn/SU - 1980
- Uranus/SU - 1980
Spacecraft Bus - Pioneer F/G
Launch Vehicle - Titan IIIE/Centaur/TE 364-4
Baseline Probe Requirements
- Science Advisory Groups, Exploratory Payload + Nephelometer
- Nominal Atmospheric Models for Baseline & Alternate Configurations
- Worst-Case Atmospheric Models for Final Configuration
- S/C Deflection Mode
- Present State-of-the-Art Heat Shield Material
- Sphere-Cone with Nose-to-Base Ratio of 0.4 to 0.6 and 0.79 to 1.05-rad (45° to 60°) Half Cone Angle
- Maximum Diameter, 0.914 m (36 in.)
- Maximum Weight, 113.40 kg (250 lb)
- Relay Link Requiring No Despun S/C Antenna

## 4.1 Hardware Availability Analysis

## 4.1 HARDWARE AVAILABILITY ANALYSIS

This section describes the analysis made to determine whether the Pioneer Venus (PV) hardware would meet the requirements of the probe without modifying the study constraints. In areas where the PV hardware did not satisfy the requirements, we conducted additional studies to determine what constraints had to be revised for it to be used, and to determine what suitable hardware was available from other sources. For example, the PV S-band frequency requires several hundred watts of RF power if the constraints are not violated. However, using a spacecraft despun antenna and a different cone angle for each planet reduces the power requirement to 70 watts. A transmitter with this high an output is still beyond the state of the art, so lower frequencies were investigated.

Another example involves the PV battery, which is activated prior to launch. For the Pioneer Saturn/Uranus (SU) probe, the capacity of this battery is depleted after a cruise period of 7 years; therefore, a different approach was necessary.

### 4.1.1 Science Instruments

This hardware applicability study has determined that the PV science instruments can be used, with some modification, for the SU mission. Detailed descriptions and characteristics of these instruments are given in Section 4.2.3, and only those necessary modifications will be discussed here. Table 4.1-1 summarizes the modifications for the nominal-atmosphere and "worst-case" models.

No change is required for the pressure gauge or the nephelometer since the former must measure to  $10^7$  N/m<sup>2</sup> (100 bar) on Venus and the latter is concerned only with optical characteristics of the cloud particles, and not cloud composition. Both instruments are currently planned for both the large and small PV probes.

The major change from the PV temperature gauge, again for either probe, is in the range of the sensor. The present temperature gauge range for Venus is from 200°K to 850°K and is measured with a platinum resistance wire. However, the worst-case atmospheres on Saturn and Uranus require a range from 40°K to 450°K. This change involves recalibrating the resistance of the platinum wire or replacing it. The deployment mechanism can be the same as that for the PV-small probe.



Table 4.1-1 Modifications Required to Pioneer Venus Instruments

PV Instrument	Modifications Required for S/U Nominal Atmospheres	Additional Modifications Required for Worst-Case Atmospheres
Pressure Gauge 10 <sup>3</sup> to 10 <sup>7</sup> N/m <sup>2</sup> (10 <sup>-2</sup> to 10 <sup>2</sup> bar)	None Required	None Required
Temperature Gauge (200° to 850°K)	Modify Range to 50° to 350°K	Modify Range to 40° to 450°K
Accelerometers 0.098 to 3923 m/sec <sup>2</sup> (10 <sup>-2</sup> to 400 g)	None Required	Modify Range for Peak Deceleration in Cool Atmosphere (600 g)
Nephelometer	None Required	None Required
Mass Spectrometer (1 to 254 amu)	Modify Range to 1 to 40 amu  Replace Porous Plug Leaks in Inlet Tubes for Different Atm.  Add Chamber Vent Tube to Reduce Pressure from Long Outgassing Period  Repackage for Optimum Location  Possibly Replace Ion Pump System for Helium	Same as for Nominal Atmospheres  Recalibrate Inlet Leaks for Cool & Warm Atmospheres  Same as for Nominal Atmospheres  Same as for Nominal Atmospheres  Same as for Nominal Atmospheres

The PV large-probe accelerometers are triaxial instruments with a range of from  $0.098 \text{ m/sec}^2$  ( $10^{-2} \text{ g}$ ) to  $3923 \text{ m/sec}^2$  (400 g) in the probe's axial direction. These units are upgraded versions of the Bell Aerospace Model X accelerometer, which has a tested analog range of  $0.00098 \text{ m/sec}^2$  ( $10^{-4} \text{ g}$ ) to  $1962 \text{ m/sec}^2$  (200 g). For the nominal atmospheres of Saturn and Uranus, the PV range is satisfactory since the maximum deceleration is  $3776 \text{ m/sec}^2$  (385 g). However, the "worst-case" atmospheres involve loads up to  $5737 \text{ m/sec}^2$  (585 g), so an additional modification is required. Discussions with Bell Aerospace have indicated that upgrading the Model X accelerometer requires only increasing the flexure of the pendulous proofmass.

The neutral mass spectrometer is the primary instrument in the payload and also requires the most modification. The PV instruments range of 2 to 254 amu must be reduced to 1 to 40 amu, which requires an internal recalibration of the analyzer. The sintered porous plug inlet leaks will be changed from those used on PV because of the lower molecular weight, and lower ambient temperature and pressure of the SU atmospheres. The ion pump will have a lower efficiency at Saturn and Uranus than at Venus because of the large percentage of inert helium in the atmosphere, which will probably require adding a chemical gettering pump and increasing the voltage of the ion pump ionizer.

Another problem that may require additional apparatus is the longer time for outgassing in the mass spectrometer's analyzer chamber. During this time gettering materials would reach saturation and become inadequate. Therefore, this problem may be solved by venting the chamber to space vacuum at the times discussed in Section 4.2.3. Finally, the external shape of the mass spectrometer envelope will also require a modification from that used on PV to permit packaging it in the SU probe.

Since several changes are required to the PV neutral mass spectrometer, and since it is the largest and heaviest single instrument, other sources were investigated as possible replacements. Of the four instruments that were analyzed, only one is a possibility for improvement. This was a small quadrupole instrument built and tested by Teledyne Earth Sciences Company as an astronaut breath analyzer for NASA under Contract NAS 9-8371. This unit is currently available from Analog Technology Corporation, Pasadena, California (ref 4.1-1), and Martin Marietta has purchased one for laboratory use. Since its quadrupole rods are only 5.08 cm (2 in.) long, as compared with 12.7 cm (5 in.) for the proposed PV instrument, a weight and volume savings can be expected.

Estimates from Analog Technology Corp. (see Appendix D), show that the total weight of the mass spectrometer can be reduced from 9 kg (20 lb) to 2.5 kg (5.5 lb); its volume from 9800 cm<sup>3</sup> (600 in<sup>3</sup>) to 1500 cm<sup>3</sup> (92 in<sup>3</sup>); and its power consumption from 14 watts to about 5 watts. These reductions would result in considerable probe size and power savings; however, the total cost might not be much different since more development would be required. Essentially all the changes required for the PV instrument would also be required for the Analog Technology instrument, plus developing an inlet system. Also, although the analyzer itself is currently flight hardware, the electronics are not, and thus could involve considerable development costs. Despite these considerations, the astronaut breath analyzer is well suited for operation in the 1- to 40-amu range, and its physical benefits are so attractive that further investigations should be attempted.

#### 4.1.2 Electrical and Electronic Subsystems

The majority of the components used in the electrical and electronic subsystems have been obtained from configurations used in other programs. Our recommended approach is to make only those modifications that are required to meet SU mission requirements.

Existing PV hardware has been used to the maximum extent possible. When this was found to be unacceptable for SU, other existing hardware was surveyed to find whether it could be used with minor modifications. New hardware has been recommended only in those cases where no known existing hardware is suitable.

Note that the electrical and electronic hardware described in this section is based on a no-parachute configuration and the "worst-case" atmosphere models for each planet.

##### 4.1.2.1 Communications

###### Probe Antenna

The antenna design chosen to provide the required radiation pattern (see Section 4.5.1.1) consists of a pair of dipoles oriented into a turnstile over a truncated, slotted cone. This antenna operates at 560 MHz and is a modification to an antenna being used by Martin Marietta for the Viking lander radar altimeter. The Viking antenna uses dipoles of equal length without petals to provide linear polarization. It operates at a frequency of 1 GHz and has a beamwidth of 1.75 rad (100°).

The same basic design is also being used on PV for both probes. In this application, the antenna is circularly polarized and operates at 2.3 GHz. This provides a compact, light-weight design, highly efficient with minimum ground plane effects and good circularity. The Viking antenna is now undergoing final acceptance and environmental testing.

For the SU mission, minor modifications must be made to strengthen the dipoles and petals so that they can withstand a design load of  $7.16 \text{ km/sec}^2$  (730 g).

#### Probe Transmitter

Several suppliers of solid-state power amplifiers have been contacted regarding their capabilities and product line items in the UHF (0.5 to 1 GHz) range for RF power outputs between 15 and 30 watts. The results of the survey are shown in Table 4.1-2. Emphasis was placed on hardware that uses "hi-rel" parts that have been flight qualified for space programs. No off-the-shelf hardware was available at 560 MHz. However, the suppliers indicate that about 50% circuit modifications to existing hardware would be required. The primary modifications consist of changing from stripline to lumped parameters and using a different power transistor for the lower frequency. For an RF power output of 20-25 watts, the same case size and weight shown in the table for the first three suppliers could be maintained. Also, the size and weight of the RCA transmitter could also be reduced.

The power conversion efficiency of the probe transmitter also improves as the frequency is lowered. At 560 MHz, the efficiency is projected to be 30% with +10% regulation on the 28-Vdc bus supply, based on data furnished by Teledyne. The package will include solid-state hardware for the modulator, driver, and power amplifier. RF power levels up to 30 watts can be accommodated within the constraints of the Teledyne envelope (see Table 4.1-2).

#### Spacecraft Receiver

Seventeen suppliers were requested to furnish technical information on hardware that could be modified to meet the requirements for the SU probe. Only five suppliers gave us technical information indicating their experience with frequency shift key (FSK) receivers. Less space-qualified hardware exists due to the lack of noncoherent systems in Earth-orbiting satellites.

Table 4.1-2 Probe Transmitter Hardware

Supplier	Operating Frequency, MHz	Model/ Program	RF Power, W	Size, cm (in.)	Mass, kg (lb)	Efficiency %
Teledyne	1430	TR-2400	24	12.7 x 14 x 3.8 (5 x 5.5 x 1.5)	1.4 (3.0)	24
Motorola	2300	MTT-501	10	12.7 x 12.7 x 7.6 (5 x 5 x 3)	0.9 (2.0)	25
Philco-Ford	860	ATS F&G	55	15.2 x 15.2 x 7.6 (6 x 6 x 3)	2.0 (4.5)	40
RCA	381	Viking Lander	1, 10, & 30	25.4 x 15.2 x 5.1 (10 x 6 x 2)	4.5 (10)	26

Motorola, Philco-Ford, RCA, Airborne Electronics Laboratory & Radiation Incorporated, all have the capability to develop space-qualified FSK receivers. They all responded indicating a receiver could be built to our design requirements, using solid-state components.

Motorola is presently developing the orbiter relay receivers for Viking, which use FSK modulation at 381 MHz. This receiver is a fixed-frequency, low-noise, dual-conversion, superheterodyne unit with two FSK demodulators. Two simultaneous data outputs are provided: a 4-kbps or 16-kbps Manchester-coded bit stream. The Viking receiver uses modular construction, measures 15 by 17 by 11.4 cm (6 by 6.7 by 4.5 in.), and weighs 3.2 kg (7 lb), has a nominal noise figure of 3.4 dB with a stability of  $\pm 7$  ppm and a dynamic range of -70 dBm. The demodulator can be included in the receiver package.

#### 4.1.2.2 Data Handling Subsystem (DHS)

The Pioneer Venus DHS hardware is directly applicable for the SU probe missions. Modifications are minimal and could be made during the detail design and assembly of the PV hardware with no impact on their function.

##### Digital Telemetry Unit (DTU)

The PV DTU may be used with no hardware modification, except for part-for-part replacement of the read-only memories (ROMs) used to define the data format during the entry and descent phases of the probe mission.

##### Signal Conditioner Unit (SCU)

The PV SCU can be used for the mission without modification.

##### Power Control Unit (PCU), Data Handling Section

The data handling section of the PCU, contains the sequencer, coast timer, and memory functions. It will require a part-for-part replacement of the ROMs used for defining the sequence of events and controlling all discrete commands to the rest of the probe system. In addition, the decoding logic for the coast timer must be modified to provide a time delay in excess of 35.7 days. (The PV system has a delay of 27 days). This change can be implemented during PV design.

### g-Switches

The 49-m/sec<sup>2</sup> (5-g) switch will be replaced by a 0.98-m/sec<sup>2</sup> (0.1-g) switch and a 29.4-m/sec<sup>2</sup> (3-g) decreasing-deceleration switch will be added.

### 4.1.2.3 Power and Pyrotechnics Subsystem (PPS)

The PV hardware is directly applicable to the SU mission, except for the battery system.

#### Wiring and Connectors

The PV wire type, size and connectors can be used. However, new cables must be prepared, routed & clamped to resist the higher deceleration forces.

#### Power Control Unit, Power Section

The PV PCU can be used directly in the SU probes. The uni-junction transistors in the pyro firing circuits must be changed to a more radiation resistant variety.

#### Battery

A new battery subsystem must be developed to meet the SU requirements of a 7.2-year (including post-build and prelaunch time) shelf life followed by a 37-day wet stand. Our recommended subsystem is a Ag-Zn remotely activated battery that uses individual cell-activation mechanisms. The cells will be constructed using slow-activation, "heavy-duty" separators to provide the long wet-stand capability.

### 4.1.3 Structural and Mechanical Subsystems

The design of the structural outer fairing for the SU probe is similar to that for the PV small probe. The forebody aeroshell is a 0.79-rad (45°) half-angle conical surface 82 cm (32.4 inches) in diameter with a nose-to-base radius ratio of 0.43. The afterbody has a 0.52-rad (30°) half-angle truncated conical surface, faired by a spherical radome, which is generated by a radius about the probe's c.g. The entry configuration is aerodynamically coincident with the PV small probe, to allow common aerodynamic testing. The aeroshell and afterbody structure are correlated to the design of the PV small probe and the aeroshell for the Viking program. The structural design of the SU probe is a new design using state-of-the-art or existing technology.

The SU probe mechanical deployment systems for the nephelometer cover and the temperature sensor are the same as those in the PV small probe. The SU probe vent valve is similar to the one in the PV small probe, except it vents external pressure rather than internal pressure. The nose cap system is a new design using available pyrotechnic thrusters. The probe-to-spacecraft release system uses gas-activated ball-lock release pins common to the Minute Man Missile Program. Model 8003 G&H Technology nonexplosive pin pullers, used on the PV program, activate the temperature sensor, nephelometer cover, and vent valve release system. The cable cutter used to separate the umbilical between the probe and the spacecraft is a Horex Model 6007.

The forward heat shield materials consist of carbon phenolic, an existing material now being developed for planetary applications, on an insulator of SLA 220, a well-proven space material. The aft heat shield consists of ESA 3560 and teflon, and are common to the PV Program.

The thermal control system incorporates the Pioneer spacecraft 1-watt radioisotope heaters and the multilayer high-performance insulation. This insulation was also used on the Apollo programs. The internal foam insulation was developed for the Saturn II launch vehicle. The argon gas system is a new design based on existing technology.



## 4.2 Impact of Science Requirements on System Design

## 4.2 IMPACT OF SCIENCE REQUIREMENTS ON SYSTEM DESIGN

This section discusses the requirements placed on the various probe systems by the science instruments. The analyses included the location on the probe for optimum sampling, the necessary sampling times and bit requirements, the rate at which the probe must descend, and the site at which the probe enters. This section also presents the model atmospheres and shows how the variations between them affect mission design.

The atmospheres are discussed in Section 4.2.1. The science objectives and system design requirements due to the science measurements and performance criteria are presented in Section 4.2.2. The third subsection describes the instruments and the techniques used to make the measurements. Subsections 4.2.4 and 4.2.5 show entry and descent parametrics for the various configurations, the data collection and transmission details for each, and the resulting measurement performance.

### 4.2.1 Atmospheric Models

The atmospheric models used for this study are presented in NASA Monograph SP-8091 for Saturn and SP-8103 for Uranus (references 4.2-1 and 4.2-2). Each document contains a nominal model, a warm, expanded limiting model, and a cool, dense limiting model. The final configuration was designed to the worst-case atmosphere. Each of the six models was assumed to have an equal probability, so all components were designed to function satisfactorily in each atmosphere.

Figure 4.2-1 shows the pressure versus temperature profiles for the three Saturn and three Uranus model atmospheres. Figure 4.2-2(a) shows the pressure and temperature for the region of probe terminal velocity descent where the instruments are operating. Locations of the major modeled clouds are given with respect to pressure in Figure 4.2-2(b) identified by their condensible constituent. Note that the coldest temperatures occur in the isothermal upper atmosphere and reach 47°K in the Uranus cool atmosphere. The temperatures at  $10^6$  N/m<sup>2</sup> (10 bar) range from 191°K to 424°K at Saturn and from 114°K to 300°K at Uranus. As shown in Table 4.2-1, there is a progressive increase in helium composition in going from the warm to the cool atmospheres. The Uranus cool is dominated by helium which is not true of the Saturn cool. Another major difference between Saturn and Uranus is the higher abundance of methane in the Uranus models. This is a one and one-half order of magnitude increase over the amount shown for the

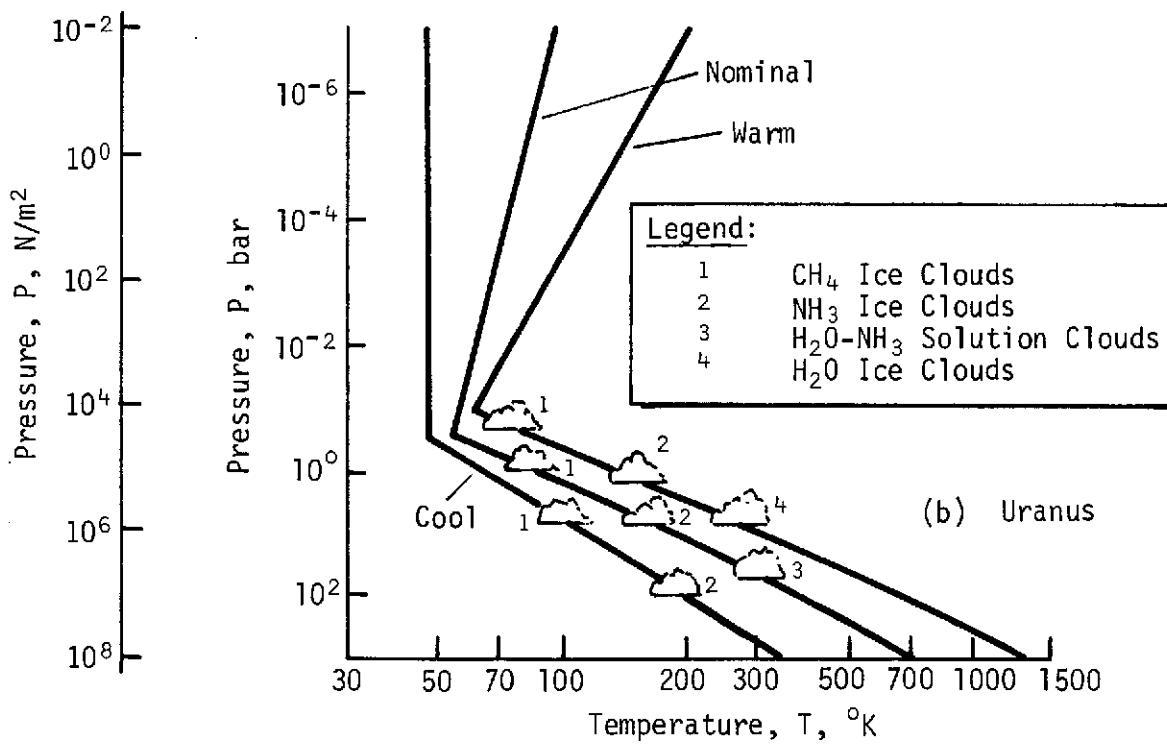
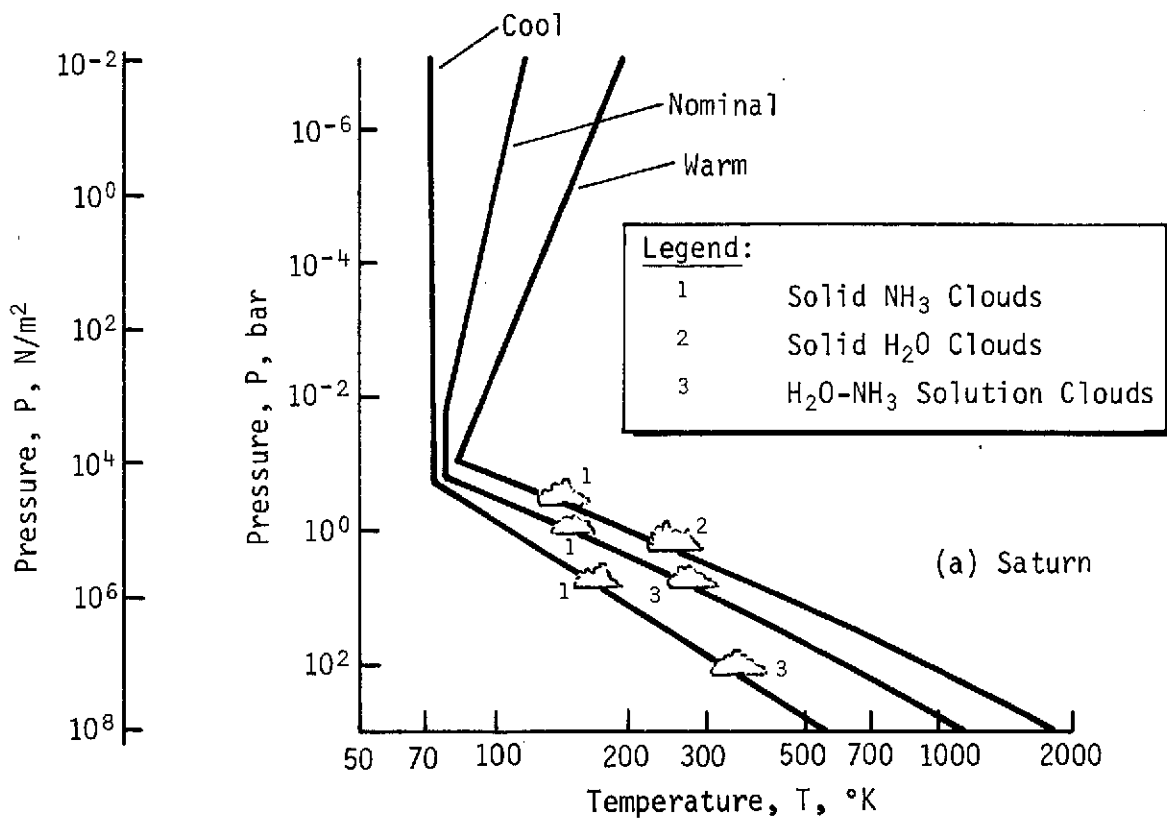
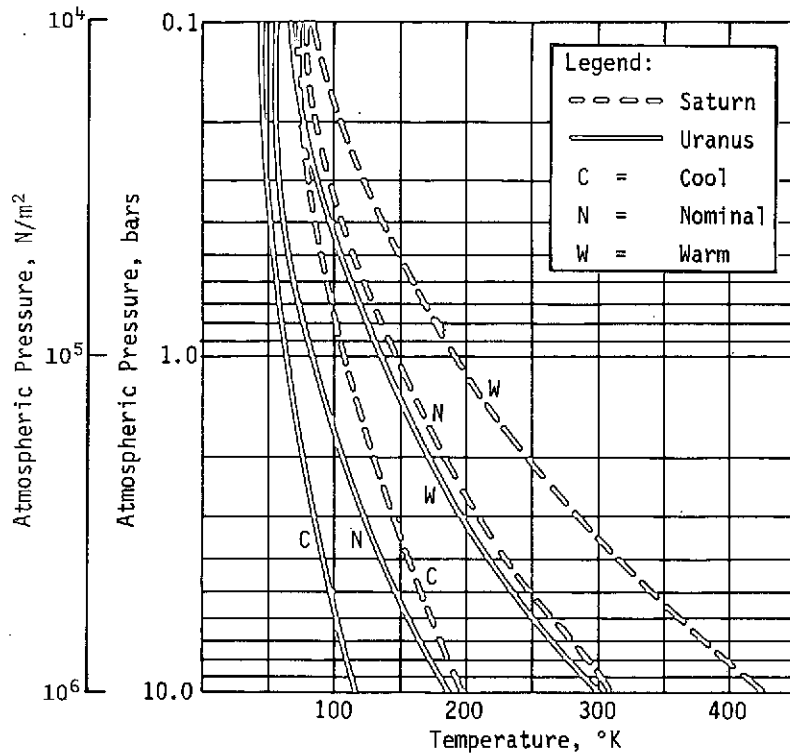
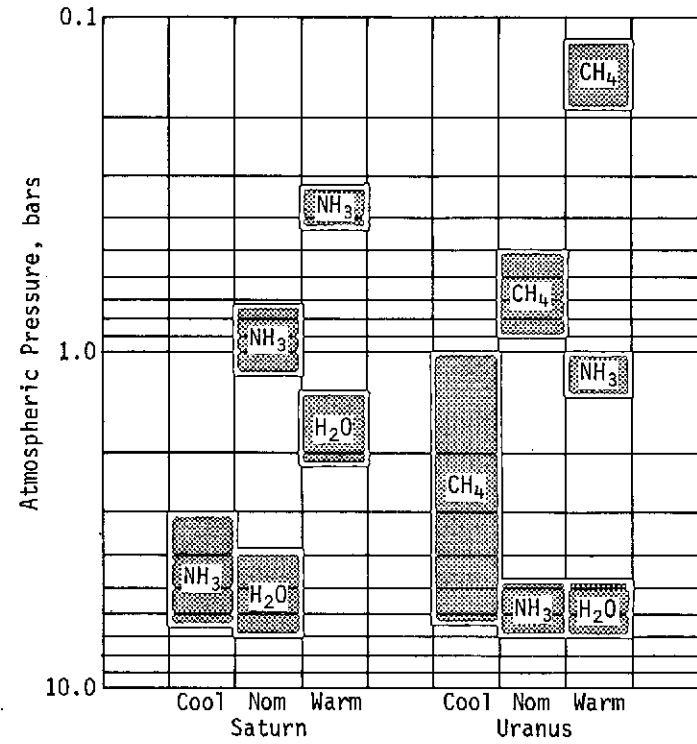


Figure 4.2-1 Monograph Model Atmospheres.



(a) Pressure vs Temperature



(b) Cloud Locations

Figure 4.2-2 Model Atmospheres in the Probe Terminal Descent Region.

Table 4.2-1 Model Atmosphere Compositions

Constituent	Percent Composition by Number					
	Saturn			Uranus		
	Warm	Nominal	Cool	Warm	Nominal	Cool
Hydrogen (H <sub>2</sub> )	94.68	88.57	73.00	95.29	85.85	30.56
Helium (He)	5.25	11.21	26.25	3.67	11.00	60.00
Methane (CH <sub>4</sub> )	0.02	0.06	0.22	1.00	3.00	9.00
Ammonia (NH <sub>3</sub> )	Trace	0.02	0.05	Trace	0.02	0.05
Water (H <sub>2</sub> O)	0.03	0.11	0.37	0.03	0.10	0.30

Saturn models. The high abundance of helium and methane combined in the Uranus cool atmosphere gives it a much higher mean molecular weight (4.55) than that of the other five models, which range from 2.1 to 2.7. Additional information concerning the atmospheric models can be obtained from the Monographs.

#### 4.2.2 Objectives, Measurements, and Performance Criteria

The statement of work for this contract listed basic scientific objectives of an exploratory atmospheric entry probe to Saturn and Uranus as:

- 1) Measure the structure and composition of the atmospheres to a depth corresponding to a pressure of at least 10 bars;
- 2) Determine location and composition of clouds;
- 3) Obtain science and engineering data to enhance future missions.

The statement of work also specified the SAG Exploratory Payload (pressure gauge, temperature gauge, accelerometer triad, and neutral mass spectrometer), as well as a nephelometer, for SU missions. Considering the above objectives and the instrument payload, we devised a list of specific measurements to satisfy these objectives. This list is shown in Table 4.2-2.

The first three measurements determine the abundance of elements, isotopes, and compounds, including cloud condensibles. A determination of the H/He ratio for both planets is essential for verification of formation theories of the solar system. The abundance ratios of isotopes up to mass 40 are also desirable since hydrogen and helium alone may not be representative of the planet's interiors. The next two measurements give data on the overall structure of the atmosphere that complement the composition measurements. The last two measurements determine detailed structure and composition with respect to the formation of cloud layers and general atmospheric turbulence. Together, these measurements provide a balanced approach to atmospheric investigation.

The instruments are shown in Table 4.2-3 in a matrix that relates them to the measurements they will accomplish. The coding indicates whether they perform a direct determination (D), a related or indirect determination (R), or are not related (N) to the specific measurement in question. All but two entries in

Table 4.2-2 Relevant Measurements

1. Determine the relative abundances of H and He in the lower atmosphere.
2. Determine the isotopic ratios H/D, He<sup>3</sup>/He<sup>4</sup>, Ne<sup>20</sup>/Ne<sup>23</sup>, C<sup>12</sup>/C<sup>13</sup>, A<sup>36</sup>/A<sup>40</sup> in the lower atmosphere.
3. Determine the concentration profiles of the minor atmospheric constituents, particularly Ne, A, N<sub>2</sub>, CH<sub>3</sub>, CH<sub>4</sub>, NH<sub>3</sub>, and H<sub>2</sub>O, down to 10<sup>6</sup> N/m<sup>2</sup> (10 bar).
4. Determine the temperature vs pressure and temperature vs time profiles from above the cloud tops down to 10<sup>6</sup> N/m<sup>2</sup> (10 bar).
5. Determine the mean molecular weight of the atmosphere and identify the major contributing gases.
6. Determine the vertical distribution of the cloud layers with respect to pressure and temperature, and the chemical composition of each layer.
7. Obtain an indication of the magnitude of any atmospheric turbulence from above the cloud tops down to 10<sup>6</sup> N/m<sup>2</sup> (10 bar).

Table 4.2-3 Instruments Related to Measurements

Measurement	Instrument				
	Temperature Gauge	Pressure Gauge	Accelerometer Triad	Neutral Mass Spectrometer	Nephelometer
H/He Ratio in the Mixed Atmosphere	R	R	R	D	N
Isotopic Ratios (Primary Isotopes thru A)	N	N	N	D	N
Concentration Profiles for Minor Constituents	R	R	N	D	R
Temperature/Pressure Descent Profiles	D	D	R	R	N
Mean Molecular Weight of Mixed Atm.	R	R	R	R	R
Cloud Composition	R	R	N	D	N
Cloud Location	R	R	N	R	D
Indication of Magnitude of Turbulence	R	R	R	N	R

D = Direct measurement;  
R = Related measurement;  
N = Little or no relation.

the matrix have at least one applicable direct measurement. The composition measurements are the direct responsibility of the neutral mass spectrometer. The overall structure and cloud locations will be determined by the pressure and temperature gauges and the nephelometer. The mean molecular weight of the atmosphere can be determined primarily from the composition measurements, and can be refined using pressure and temperature lapse rates. The descent accelerometers will directly measure large-scale turbulence, but data from other instruments will be necessary to infer the complex structure of this turbulence.

To satisfy the basic science objectives, measurement performance criteria must be established to evaluate the instruments' data sampling for a particular design. The neutral mass spectrometer, which is based on the Pioneer Venus (PV) design, has a fixed number of inlet tubes (currently six), and thus makes a fixed number of samples during descent. The sampling time is then controlled by the descent time, and the only requirement for measurement performance is to separate the measurements as far apart in atmospheric pressure as possible.

For the other instruments, the sampling rates were based on two sets of measurement performance evaluation criteria. One was the list of kilometers per measurement for each instrument, which was supplied as a part of the August 1972 Saturn/Uranus Probe RFP (reference 4.2-3). Although this did not become a part of the current contract, it did represent an initial estimate of the required measurement intervals for Saturn and Uranus. This document showed the minimum required performance as 5 km per measurement for the temperature and pressure gauges and the turbulence accelerometers. A more stringent requirement of 1 km per 20-bit measurement was given for the nephelometer.

The second source of evaluation criteria was a panel of science consultants, consisting of Dr. Richard Goody, Dr. Donald Hunten, Dr. John Lewis, Dr. Michael McElroy, Dr. Gordon Pettengill, Dr. Harold Masursky, Dr. Rochus Vogt, Mr. Harvey Allen, and Dr. George Wetherill. These consultants recommended a minimum of 5 to 10 measurements per scale height for sampling pressure and temperature and similar requirements for the turbulence accelerometers, depending on the type of turbulence measurement and the amount of onboard processing. They also recommended that nephelometer readings be taken at least as frequently as the temperature measurements, and in the vicinity of the cloud bases, twice as often. Both these criteria will be compared to



the performance of the sample missions in a subsequent section of this report.

In addition to meeting specific performance criteria during descent, the entry accelerometers must measure the deceleration loads sufficiently to enable reconstruction of the entry g curve and to accurately define the magnitude and time of the peak entry load. In general, the entry measurements should continue until the probe has slowed enough to deploy the descent science instruments. Therefore, the entry and aeroshell parameters should be designed to allow the descent measurements to begin as high in the atmosphere as possible. Ideally, the measurements should begin at altitudes above  $10^4$  N/m<sup>2</sup> (100 mb) of pressure, if possible, to permit cross-correlation with spacecraft radio occultation data, which can be obtained down to a few hundred millibars.

Planetary targeting considerations are also influenced by the scientific objectives. For a first-generation entry probe, the entry site should be selected so that it is both relevant to the desired objectives and typical of the planet as a whole. This would allow extrapolation of the data to other locations on the planet. The lack of solar or ionospheric instruments in the payload simplifies site selection by making lightside or darkside entries essentially equivalent. Other conditions then govern the particular entry site.

Uranus is inclined 1.71 rad (98°) to its orbital plane with its north pole pointing in the general direction of the sun (for at least 15 years), and all of the solar energy has been deposited into its northern hemisphere. This means that a large gradient in atmospheric conditions probably exists between lightside and darkside, so entry sites on the lightside and at least 0.35 rad (20°) from the terminator are desirable. For Saturn it would be unacceptable to enter on the terminator because atmospheric processes that occur there may cause variations that the instruments could not separate from normal conditions. Some Saturn entry sites may be unattainable, as the rings must be avoided by both spacecraft and probe.

#### 4.2.3 Instruments and Measurement Techniques

Five specific instruments have been identified for the Saturn/Uranus (SU) common probe. During the initial portion of this study we determined that the Pioneer Venus (PV) instruments could be used for the SU mission with minimum modification. As a result, our

primary data source for the science instruments was Reference 4.2-4, the Supplementary Requirements Document for the Pioneer Venus RFP. Additional data were available from several of the original instrument proposals submitted by the principal investigators. Caution was exercised using this information due to the competitive nature of some of the experiments. Additional information on the instruments and measurement techniques from the Viking and PAET programs was considered. These data were available from the JPL Contract 953311, Outer Planet Entry Probe System Study (Reference 4.2-5 Volumes II and IV).

#### 4.2.3.1 Temperature Gauge

The temperature sensing system consists of a platinum resistance thermometer sensor and an electronics package. The sensor is enclosed in a protective shield and oriented parallel to the flow and beyond the boundary layer. It is deployed through the heat shield on the side of the cone, near the maximum diameter. The electronics provide incoming power regulation, signal conditioning, and sensor range switching and are mounted on the equipment deck. Figure 4.2-3 shows the component design and dimensions for the final probe configuration. The characteristics of the instrument for the SU application are given in the first column of Table 4.2-4.

The major change from the PV instrument is in the range capability of the sensor. The present range for Venus application is from 200°K to 850°K. The nominal SU atmospheres requires a range from 50°K to 350°K, and the worst-case atmospheres requires a range of 40°K to 450°K. This involves recalibrating the platinum resistance wire. The location and deployment mechanism are the same as those in the PV small probe. In both, a plug is ejected from the aeroshell to allow the sensor element to extend into the flow stream.

The single 8-bit analog temperature measurement must be taken at least once every 24 seconds to satisfy the measurement criteria; this uses less than one-half bit per second of the total data bit rate. An electronics temperature word must also be transmitted as science subcommutated data (see Section 4.2.5).

#### 4.2.3.2 Pressure Gauge

The pressure sensing system consists of a set of five silicon strain-gauge pressure transducers with different full-scale ranges,

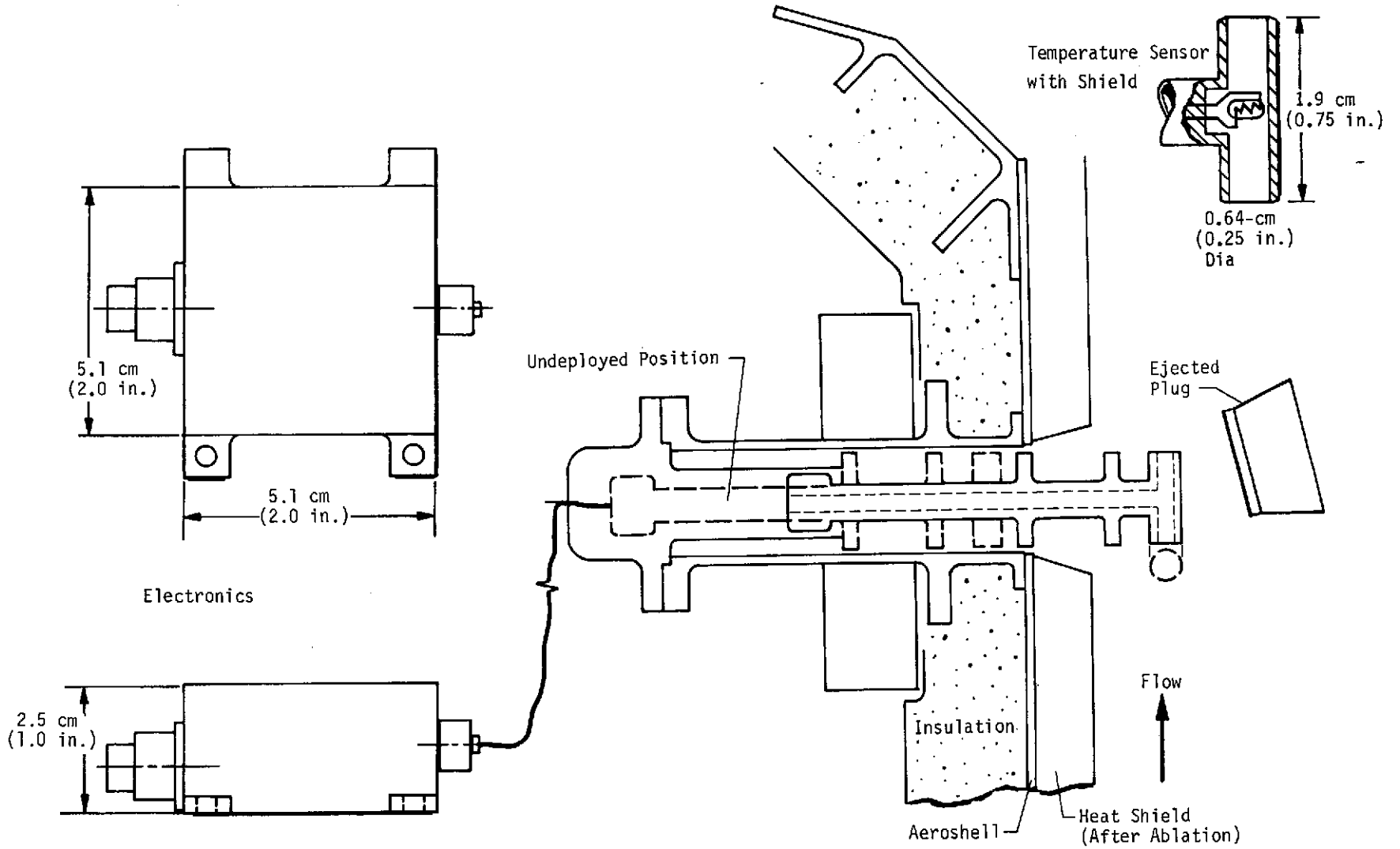


Figure 4.2-3 Temperature Gauge

Table 4.2-4 Instruments Characteristics Summary

	Instrument				
	Temperature Gauge	Pressure Gauge	Accelerometers (3-axis)	Nephelometer	Neutral Mass Spectrometer
Weight, kg (lb)	0.32 (0.7)	0.45 (1.0)	1.13 (2.5)	0.49 (1.1)	9.07 (20.0)
Volume, cm <sup>3</sup>	98	115	656	524	9830
Dimensions, cm	Sensor: 0.64 Dia x 1.9 Electronics: 5.1 x 5.1 x 2.5	7.6 x 5.1 x 2.5 + Inlet Tube	8.9 x 8.9 x 7.6	Window Holder: 4.7 Dia x 2.0 Electronics: 10 x 6.5 x 7.5	Inlet: 7 Dia x 16 Electronics: 33.8 x 25.4 x 15.2
Power Required, W	0.5	0.5	2.3	1.2	14.0
Warmup Time, sec	300	30	30	10	300
Sampling Interval, sec	18 to 24	18 to 24	18 to 24	10 to 15	400
Data Bits per Sample	8	8	40	43	4800 or 6400
Data Bit Rate, bps	0.3 to 0.5	0.3 to 0.5	1.7 to 2.1	2.9 to 4.3	12 or 16
Temperature Limits, °K	233 to 363	253 to 353	233 to 363	243 to 339	255 to 339
Onboard Processing Required	No	No	Possible	Possible	Possible
Required Range	40 <sup>0</sup> K to 450 <sup>0</sup> K	10 <sup>3</sup> to 10 <sup>7</sup> N/m <sup>2</sup> (10 <sup>-2</sup> to 10 <sup>2</sup> bar)	0.098 to 5884 m/sec <sup>2</sup> (10 <sup>-2</sup> to 600 g)		1 to 40 amu
Output Signal Mode	Analog	Analog	Analog	Digital	Digital

an electronics package, a pressure manifold, and an inlet tube. The sensors, manifold, and electronics are contained in a single package (see Figure 4.2-4). An inlet tube connects the manifold to the ambient atmosphere at the nose of the vehicle (Figure 4.2-5). The pressure gauge electronics provide input power regulation, signal conditioning, and sensor range switching. Instrument characteristics are given in Table 4.2-4.

No changes are required to the PV instrument as it is required to measure to  $10^7$  N/m<sup>2</sup> (100 bar) at Venus. Since the SU probe is only required to go to  $10^6$  N/m<sup>2</sup> (10 bar), the highest-ranged sensor could be eliminated, but would not be cost-effective. As in the PV mission, the SU pressure data will be in the form of one 8-bit word at least every 24 seconds, transmitted along with a subcommutated electronics temperature word every 192 seconds. Both signals are analog.

#### 4.2.3.3 Accelerometers

The three-axis analog accelerometer system consists of a primary axial accelerometer, a backup axial accelerometer, and two lateral, orthogonally mounted accelerometers. All are single-axis, pendulous-proofmass, force rebalancing transducers that use a capacitive bridge pickoff to detect acceleration forces acting on the spring-supported proofmass. Rebalancing the proofmass is accomplished by surrounding it with a magnetic field and passing an accurately measured current through a coil wound around the proofmass. Reference 4.2-6 discusses the Bell Aerospace Co. Model IX and X accelerometers, which are precursors for the ones to be used on the SU mission. The characteristics of the SU accelerometers are shown in Table 4.2-4. Note that the primary and backup axial instruments must be mounted on the probe's center of gravity with their axes aligned with the centerline of the probe.

The major modification from PV will be in the range of the sensors. The present Model X accelerometer has a tested analog range of  $9.8 \times 10^{-4}$  to  $1961 \text{ m/sec}^2$  ( $10^{-4}$  g to 200 g). Venus entries require a range of 0.098 to  $3920 \text{ m/sec}^2$  ( $10^{-2}$  to 400 g), and for SU applications, a maximum range of  $5880 \text{ m/sec}^2$  (600 g) will be required to accurately measure peak decelerations in the worst-case atmospheres. Discussions with Bell Aerospace indicate that this change will only require modifying the flexure of the pendulous proofmass.

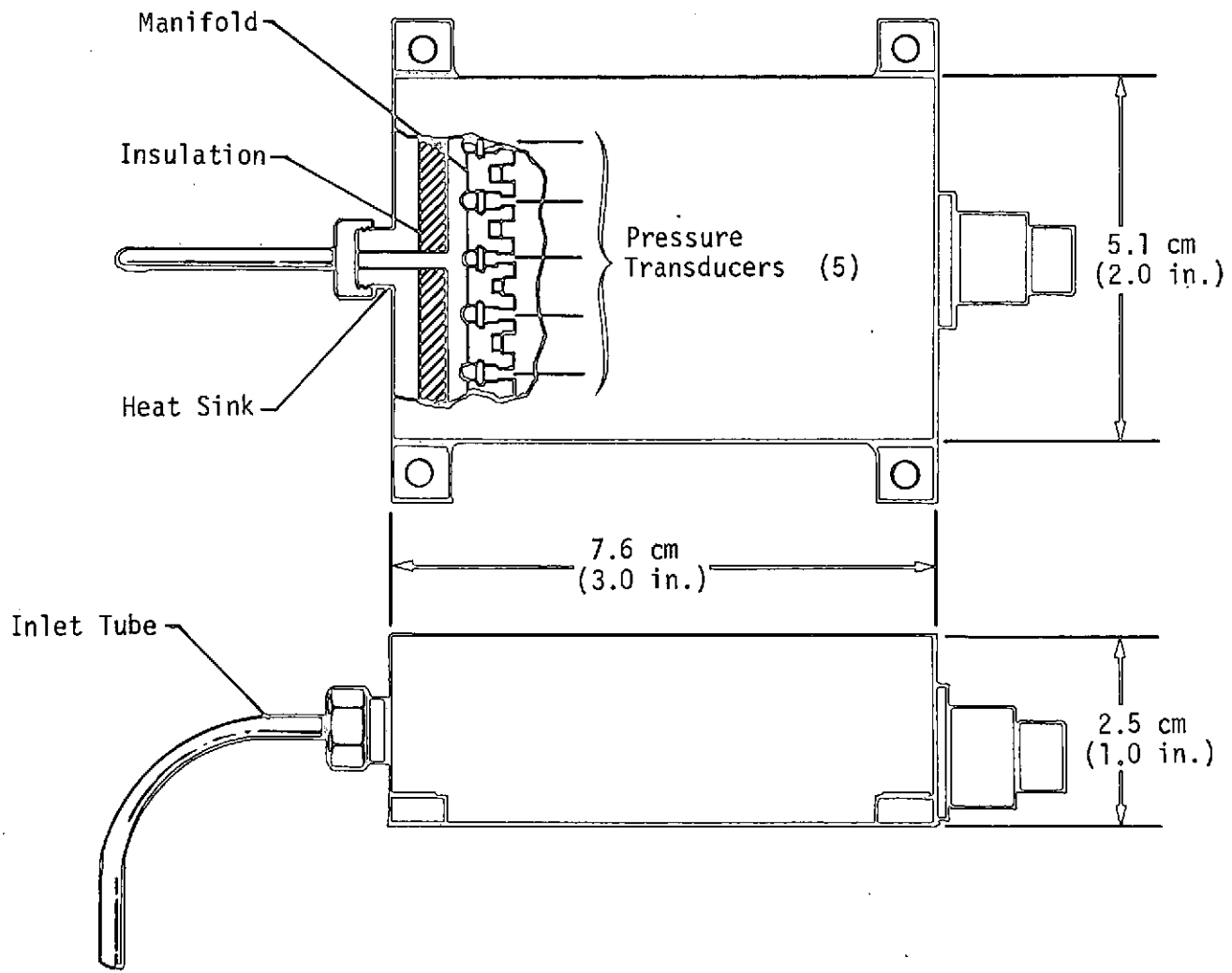


Figure 4.2-4 Pressure Gauge

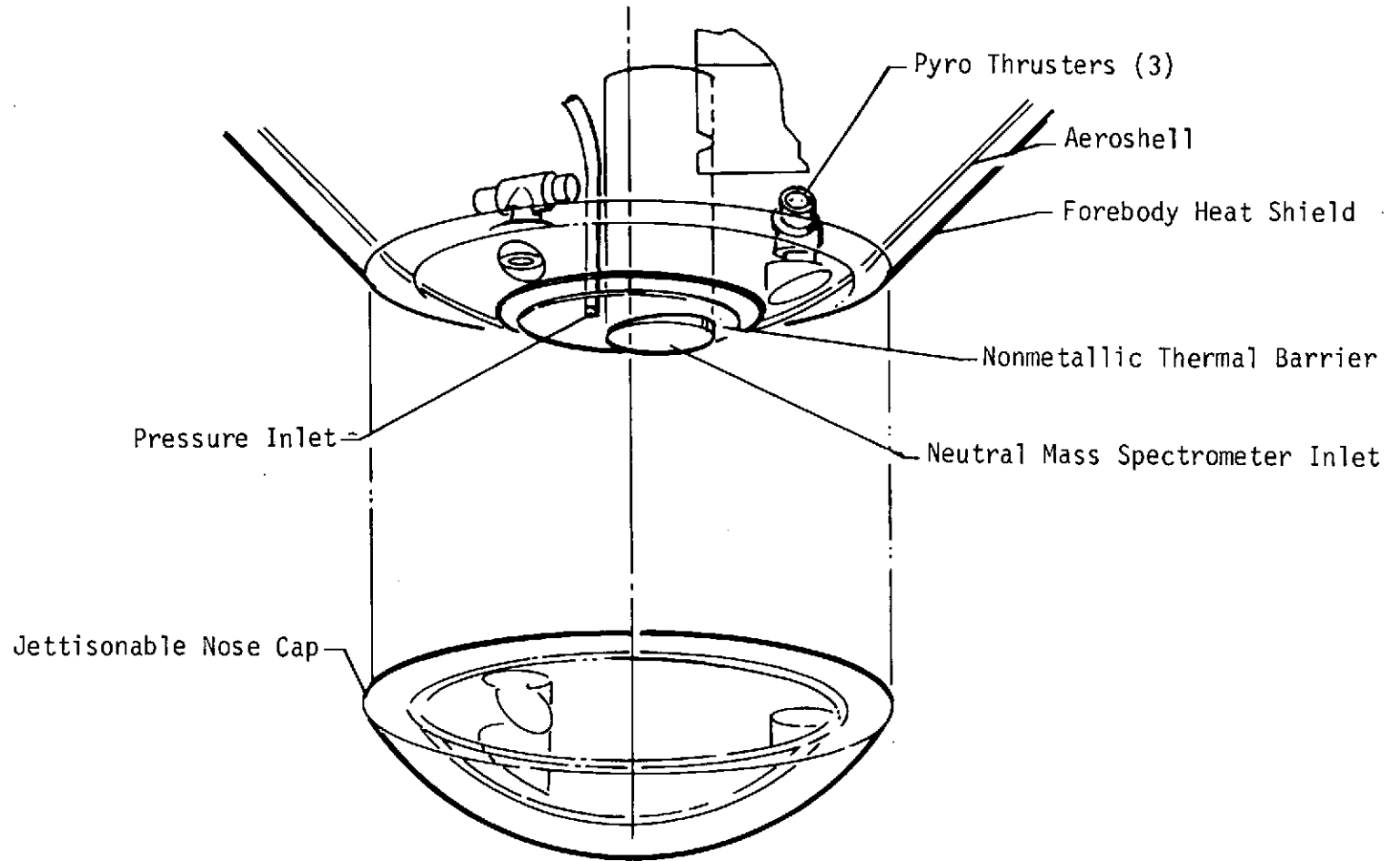


Figure 4.2-5 Probe Science Instrument Port

During the entry phase of the mission; which is between 47 and 98 seconds duration, the accelerometers must measure the decelerations with sufficient frequency and accuracy to reconstruct the time versus deceleration curve, especially at the peak g point. Subsequently this data will be used to determine the atmospheric structure. This requires 5 samples/sec from the primary axial instrument and half this rate from each of the lateral instruments. The backup axial unit can also measure at 2.5 samples/sec. Since these analog signals will be converted to 8-bit words, the total collection data rate from all four sensors is 100 bps. The unit continues to measure during the communication blackout, so all of the data gathered during the blackout is stored and interleaved with real-time data during terminal descent.

The accelerometers begin to store data on receiving a signal from a  $0.98\text{-m/sec}^2$  (0.1-g) sensor and continue to store until 20 seconds after sensing  $29.4\text{ m/sec}^2$  (3 g) decreasing. At this time, the nose cap of the probe is ejected and the accelerometer mode is switched to sensing atmospheric turbulence. This requires a sampling time increase for descent to between 18 and 24 seconds per sample. The resultant data rate during descent is  $\sim 2$  bps. The methods of interleaving the stored and real-time data and the specific measurement performance values are discussed in Section 4.2.5.

#### 4.2.3.4 Nephelometer

This instrument is the single addition to the SAG-recommended Exploratory Payload and is included to better define the location and density of aerosol cloud formations. The nephelometer consists of a pulsed GaAs laser light source that illuminates a region outside the probe, and photodiode detectors with spectral filters that observe reflected radiation from the illuminated region. The instrument will also measure the background scattered sunlight.

Figure 4.2-6 shows a schematic of the nephelometer inside the envelope dimensions provided from reference 4.2-4. No change to the unit is required for SU missions from that currently defined for PV. It is located on the side of the afterbody heat shield about 9 cm behind the maximum diameter, and has a horizontal field of view. At the same time the nose cap is ejected, a plug is ejected from the heat shield of the probe and the nephelometer begins measuring. Window heaters are provided during descent to maintain the temperature of the external window above that of the ambient atmosphere to prevent condensation from forming and distorting the signal. Less than 5 W of power are required for these, compared to 11 W for PV. Connecting the PV heaters in series with the 28 V source, rather than in parallel, would yield an adequate 5.5 W.



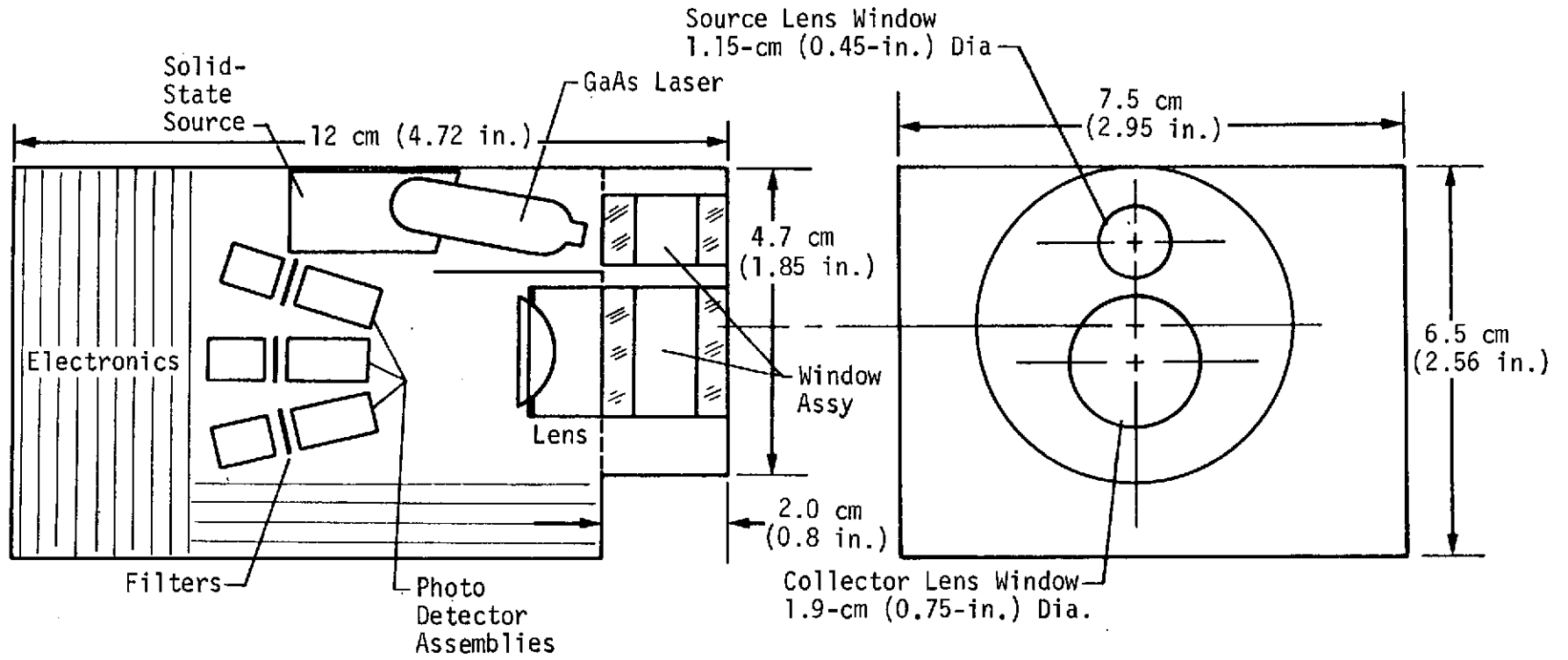


Figure 4.2-6 Nephelometer Schematic

The signals from the detectors will be amplified and converted from analog to a digital bit stream by the nephelometer. The data for one measurement consist of four 10-bit words that represent cloud light reflection measurements and background determinations, along with a 3-bit monitoring word. There are also some nephelometer subcommutated words for calibration and electronics temperatures.

According to our panel of science consultants, the sampling time should be about half that for the temperature and pressure gauges, so we considered a range of 10 to 15 seconds per sample. At 12 seconds sampling time the bit rate is 3.6 bps.

#### 4.2.3.5 Neutral Mass Spectrometer (NMS)

The NMS is the primary instrument in the payload and makes direct measurements of the planet's atmospheric and cloud composition. The instrument consists of an inlet system, an ion source, a mass analyzer, which may be either a quadrupole or magnetic sector, ion pumps, and related electronics. Except for the inlet system, all components are contained within a single volume. The basic dimensions and performance characteristics of the NMS are given in Table 4.2-4.

The inlet is located at the nose of the descent probe, behind the cover (see Figure 4.2-5) and consists of six inlet tubes in a cylindrical housing. Pyrotechnically actuated valves open and close the tubes sequentially during descent, allowing six discrete atmospheric samples to be collected. Gases from an inlet tube are passed through a porous plug leak and into the ionizer, accelerated, and measured.

The same inlet system can be used for either quadrupole or magnetic sector analyzer. Figure 4.2-7 (b) is a detail drawing of the inlet system showing the method used for collecting the six gas samples without mutual contamination. Not shown, but necessary, is a heater to prevent condensation in the inlet tubes and subsequent blockage. Two to three watts of the NMS power allocation has been assigned for this heater, which is similar to the PV requirement.

Figure 4.2-7 (a) shows a quadrupole analyzer packaged inside the PV envelope and gives the relative locations of the various components. The magnetic sector instrument could also fit within this envelope. The external shape of the NMS envelope must be modified slightly from that used for PV to allow adequate packaging in the SU probe.

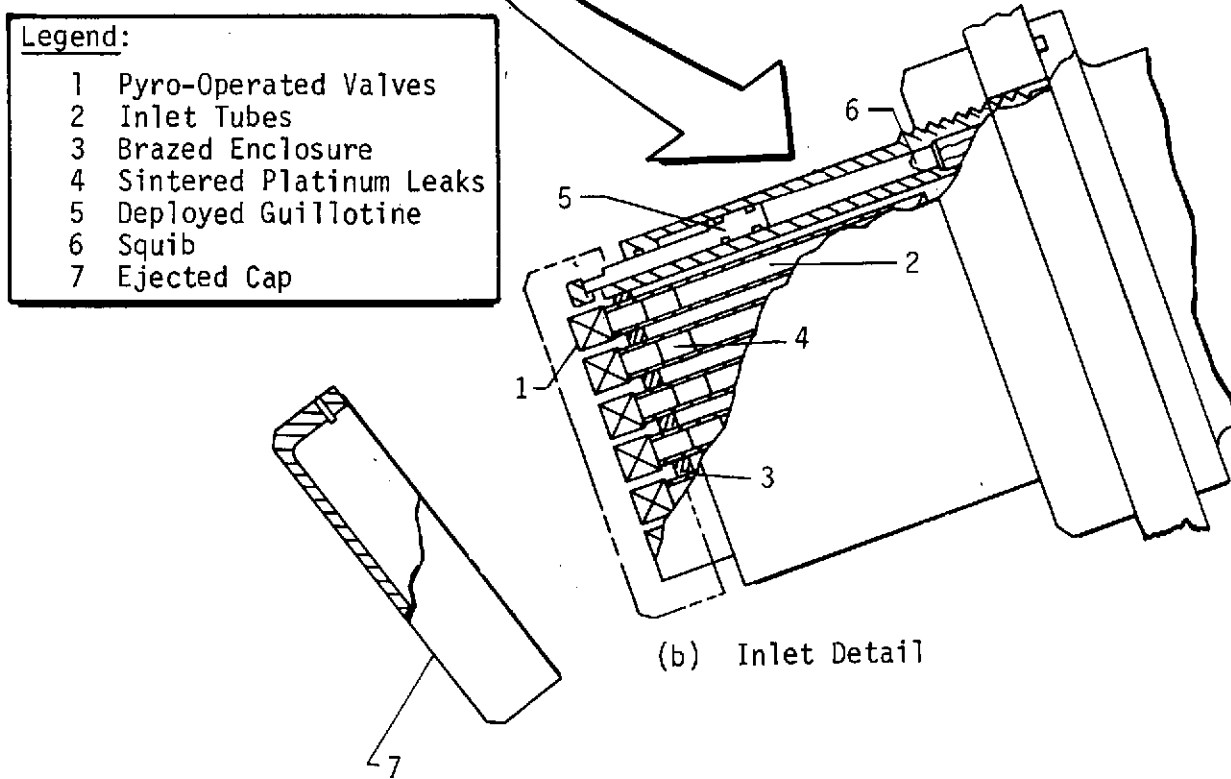
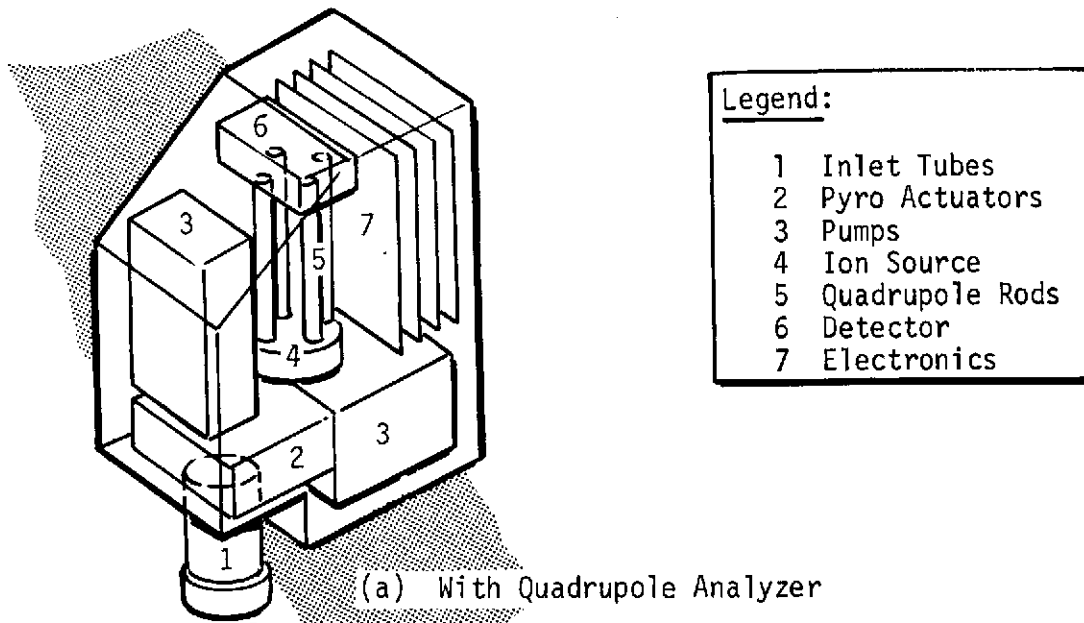


Figure 4.2-7 Neutral Mass Spectrometer

The PV NMS will have a mass range on the order of 2 to 254 amu. For SU, this range can be reduced to between 1 and 40 amu. This is adequate to measure the constituents of the SU atmospheres, which are sufficiently abundant to be within the dynamic range of the instrument. Second, the sintered porous plug inlet leaks may also have to be changed from those used on the PV instrument. This is due to the lower molecular weight of the constituent gases in the SU atmospheres and the lower ambient temperatures and pressures. Finally, because of the high percentage of inert helium in the SU atmospheres, the ion pump will not have the same pumping efficiency as for Venus. This may require using a chemical gettering pump to remove some of the active gases before they can reach the ion pump, and then increasing the voltage on the ion pump ionizer.

Another problem unique to outer-planet missions is the longer flight time for outgassing from materials within the mass spectrometer analyzer chamber. If the outgassing rate for a typical baked system is taken as  $10^{-11}$  torr-ℓ/sec-cm<sup>2</sup>, it requires only a few hours for the pressure in the analyzer to reach  $10^{-5}$  torr, where the ion pump will not start. On PV this problem was solved by using chemical gettering materials that last for the few months involved in the flight, but this method is inadequate for longer missions since the gettering material would quickly become saturated. Our recommended solution is to provide a vent from the analyzer chamber to space vacuum. This vent will be opened at probe separation; allowed to remain open during coast; and then be closed using redundant pyro-actuated valves before entry. The ion pump will then be turned on for a warmup period after the vent valves are closed, maintaining the vacuum.

The NMS provides its own analog-to-digital conversion using 10-bit words. The six inlet tubes in the inlet system each allow six sample volumes of atmospheric gas to be measured. In PV, three complete independent scans will be made of each sample. If three 1- to 40-amu scans of each sample are used for SU, and if four voltage and RF field settings are made at each mass number, then the total number of bits collected for each sample of gas is 4800 bits, as shown below:

$$\frac{3 \text{ spectrum scans}}{\text{measurement}} \times \frac{40 \text{ amu}}{\text{scan}} \times \frac{4 \text{ voltage steps}}{\text{amu}} \times \frac{10 \text{ bits}}{\text{voltage step}}$$

Note that since three complete scans are made of each gas sample, the total number of mass spectra for the mission is 18, and the

total number of data bits from the NMS is 28,800. For some of the SU missions considered in this study, the PV data handling hardware gave an excess data rate capability. This was allocated to the NMS allowing it to make four scans per gas sample, yielding 6400 bits/sample. This gives 38,400 total bits from 24 scans. This is the case for the final recommended configuration.

Since the number of samples is fixed at six for a given descent, and the objective is to obtain them as far apart in the atmosphere as possible, each measurement must be performed in one-sixth of the descent time. Using the nominal atmospheres, the time interval between measurements is then 400 seconds. The gas sample is collected in the first 48 seconds and then analyzed and digitized. The analyzer chamber must be pumped out in preparation for the next sample. Using 4800 bits per sample gives a required data rate of 12 bps; if the data amount to 6400 bits per sample, then the data rate must be increased to 16 bps.

Other information pertaining to mass spectrometers for outer-planet missions--particularly comparisons of quadrupole versus magnetic sector instruments and a list of possible compounds to be measured--can be found in Volume II, Chapter III, of Reference 4.2-5.

#### 4.2.4 Entry and Descent Science Analysis

##### 4.2.4.1 Science Sequence of Events

Two basic configurations were investigated during this study. A configuration that used a parachute to remove the descent capsule from the aeroshell was analyzed before the midterm review. A stable descent body with its own aeroshell and without a parachute was analyzed during and after the midterm. Detailed sequences of events for all configurations are given in Section 4.4. This section discusses only the events that influence the science measurements to compare the parachute and no-parachute designs.

The accelerometers, temperature gauge, and mass spectrometer are turned on to be warmed up at least five minutes before entry. An additional time is added to this to account for trajectory uncertainties. The warmup period for the nephelometer and pressure gauge begins at entry, and the accelerometers begin storing high-speed deceleration data at a level of  $0.98 \text{ m/sec}^2$  (0.1 g) increasing. Depending on the model atmosphere, entry may last from 47 to 121 seconds.

In the baseline (parachute) configuration, where only the nominal atmospheres were considered, the parachute is deployed 20 seconds after the probe decelerates to a decreasing level of  $49 \text{ m/sec}^2$  (5 g). The descent capsule is then pulled from the aeroshell, the instruments are deployed, and the science measurements begin at an atmospheric pressure of 4700 to 6200  $\text{N/m}^2$  (47 to 62 mb). The probe remains on the parachute for 20 additional seconds and is then released.

In the no-parachute configuration, a nose cap is ejected, revealing the instrument ports (see Figure 4.2-5). For the worst-case atmospheres, this cap is ejected 20 seconds after the deceleration reaches  $29.4 \text{ m/sec}^2$  (3 g) and the pressure at the first measurement varies from 4000  $\text{N/m}^2$  (40 mb) for the Uranus warm atmosphere to 11400  $\text{N/m}^2$  (114 mb) for the Saturn cool atmosphere. As the nose cap is ejected, pyrotechnic devices simultaneously remove the nephelometer cover. After a 3-second delay to allow the covers to leave the vicinity of the probe, the temperature sensor is deployed through the aeroshell and the accelerometers are switched to the low-speed turbulence sampling mode. All above events must be preprogrammed because the spacecraft has not yet acquired the probe.

The descent to  $10^6 \text{ N/m}^2$  (10 bar) requires about the same time for Saturn as for Uranus when the ballistic coefficients are identical. We then fixed the descent time at 44.5 minutes for the baseline configuration in the nominal atmospheres. This makes the end-of-mission (EOM) pressure  $1.07 \times 10^6 \text{ N/m}^2$  (10.7 bar) at Saturn and  $10^6 \text{ N/m}^2$  (10.0 bar) at Uranus, making the descent sequence after parachute deployment identical for both planets. A subsequent analysis of the descent sequence showed that a constant time could not be used for the worst-case atmospheres because of the wide range of times (27 to 74 minutes) involved in reaching  $10^6 \text{ N/m}^2$  (10 bar). Thus, the EOM occurs at  $10^6 \text{ N/m}^2$  (10 bar) for each of the six descents. Data transmission occurs in real time from acquisition to EOM and includes the interleaved stored data. Acquisition occurs at  $49 \text{ m/sec}^2$  (5 g) plus 60 seconds in the baseline configuration and at  $29.4 \text{ m/sec}^2$  (3 g) plus 60 seconds for all others.

#### 4.2.4.2 Entry and Descent Science Mission Parameters

The entry phase parameters depend on the model atmosphere, entry angle, and ballistic coefficient, although the effects of the latter are minimal. Section 4.3.5 details the effects of these factors on such parameters as the peak deceleration and

dynamic pressure. Their only direct effect on science performance is to vary the times at which the accelerometers must make high-rate entry deceleration measurements. Since the accelerometers sample at a constant rate during entry, longer times for sampling require a larger data storage capability.

Figure 4.2-8 shows this variation for Uranus as a function of the atmosphere and entry angle. Note that warm-atmosphere entries will establish the storage requirements and that low entry angles increase the number of bits collected.

The descent phase parameters are a function of the ballistic coefficient of the descent body, the velocity at the beginning of descent, and the model atmosphere. Detailed parametric analyses of pressure versus descent time as a function of atmosphere and ballistic coefficient were performed in a previous study and are fully documented in Volume II of Reference 4.2-5. The only pressure-descent profiles shown in the report will be those for the three configurations studied.

The baseline configuration consists of an entry shape and a descent shape separated by a parachute. Once the aeroshell is released, the ballistic coefficient during descent is governed by the shape and weight of the descent capsule. Selection of this coefficient is relatively flexible. Choice of a particular value is influenced by equipment packaging requirements as well as by the maximum descent times allowed by available data transmission power. Our selected value of  $170 \text{ kg/m}^2$  results in the science mission parameters shown in Table 4.2-5. Note that parachute deployment occurs at subsonic speeds and prior to  $10^4 \text{ N/m}^2$  (100 mb), above the depth to which spacecraft occultation data can penetrate. This provides some data for cross correlation. In order to use the same descent sequence timer, we fixed the time to EOM, resulting in a slightly higher EOM pressure at Saturn than the  $10^6 \text{ N/m}^2$  (10 bar) reached at Uranus.

The alternate configuration (without a parachute) uses the same basic shape for entry and descent. The descent ballistic coefficient is then determined by the size and shape of the ablated aeroshell and by the descent weight. In addition, each planet ablates the heat shield differently, so the resulting ballistic coefficients are different. Science mission parameters for both planets and for two different aeroshell cone angles are shown in Table 4.2-6.

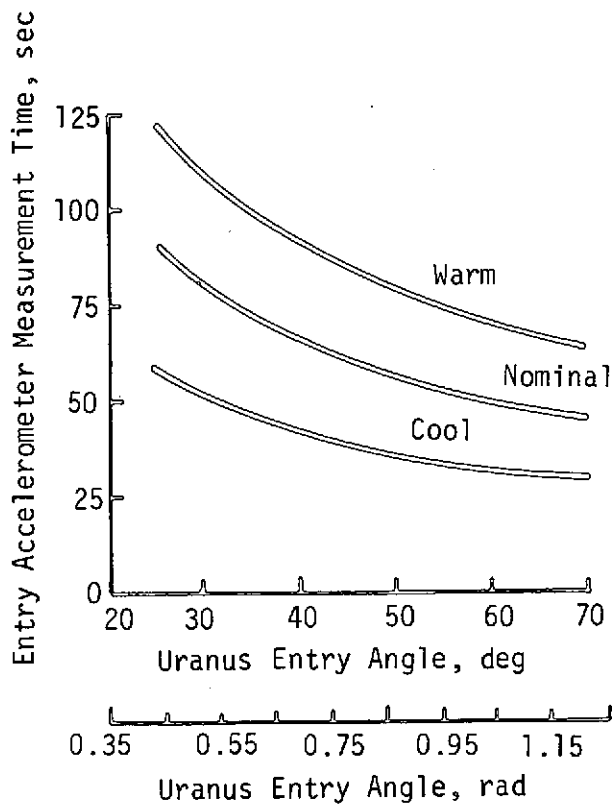


Figure 4.2-8 Entry Angle and Atmosphere Effects on Entry Accelerometer Measurement Time

Table 4.2-5 Descent Science Mission Parameters Baseline Configurations

	Saturn*	Uranus*
Descent Ballistic Coefficient, kg/m <sup>2</sup> (slug/ft <sup>2</sup> )	170 (1.083)	170 (1.083)
Time to Parachute Deployment, sec	63	65
Mach Number at Parachute Deployment	0.67	0.75
Parachute Deployment Pressure, 10 <sup>2</sup> N/m <sup>2</sup> (mb)	62	47
Parachute Release Time, sec	83	85
Time to End of Mission, minutes	44.5	44.5
Pressure at End of Mission, 10 <sup>5</sup> N/m <sup>2</sup> (bar)	10.7	10.0
Descent Measurement Time, sec	2605	2603

\* Nominal atmosphere. Entry Angle is -30° for Saturn; -45° for Uranus



Table 4.2-6 Descent Science Mission Parameters - Alternate Configuration\*

	Aeroshell Cone Angle	0.79-rad (45°) Half-Angle Cone		0.96-rad (55°) Half-Angle Cone	
	Nominal Atmospheres	Saturn	Uranus	Saturn	Uranus
Descent Ballistic Coefficient, kg/m <sup>2</sup>		131.8	138.8	147.4	154.6
Time to Mach 1.0, sec		48.5	53.5	50.5	56.0
Time to Terminal Velocity, sec		104.6	178.1	112.3	184.8
Instrument Uncovering or Deployment					
Time to 49 m/sec <sup>2</sup> + 20 sec (5 g + 20 sec), sec		63	65	63	65
Deceleration, m/sec <sup>2</sup>		16	14	17	15
Mach Number		0.67	0.75	0.71	0.80
Pressure, 10 <sup>2</sup> N/m <sup>2</sup> (mb)		61	46	63	47
Altitude, km		94.5	83.7	93.7	83.2
Time to End of Mission, minutes		49.2	49.2	46.7	46.7
Pressure at End of Mission, 10 <sup>5</sup> N/m <sup>2</sup> (bar)		10.5	10.0	10.5	10.0
Descent Measurement Time, sec		2889	2887	2736	2734

\* Entry Angle is -30° for Saturn; -45° for Uranus

Actually, the 0.79-rad ( $45^\circ$ ) half-angle cone is considered the alternate configuration; the data for the 0.96-rad ( $55^\circ$ ) half-angle cone aeroshell are given in the above table for reference since this was the value used for early designs. The entry ballistic coefficient for both cone angles is  $102 \text{ kg/m}^2$ . For the alternate configuration the instruments can be uncovered and deployed at the same time used for the parachute in the baseline configuration. There is less than  $19.6 \text{ m/sec}^2$  (2 g) of deceleration force on the sensors. Again, the first measurement can be made much less than  $10^4 \text{ N/m}^2$  (100 mb). The time to reach  $10^6 \text{ N/m}^2$  (10 bar) at Uranus is longer for the smaller cone angle, and both descent times for the alternate configuration are larger than those for the baseline configuration because of the large probe diameters. The EOM pressure at Saturn is  $5 \times 10^4 \text{ N/m}^2$  (0.5 bar) greater than at Uranus.

Figure 4.2-9 gives the pressure descent profile for the baseline and alternate missions for the descent regime of  $10^4$  to  $10^7 \text{ N/m}^2$  (100 mb to 10 bar). Despite the fact that the descents are into different planets and that the ballistic coefficients for a planet differ by more than  $30 \text{ kg/m}^2$ , the profiles are quite similar. Figure 4.2-10 plots the time to  $10^6 \text{ N/m}^2$  (10 bar) in the nominal atmospheres for a range of ballistic coefficients that includes those for the design missions. Note that the difference is only 2 minutes out of 37 at  $230 \text{ kg/m}^2$  (5.4%) or 3 minutes out of 54 at  $110 \text{ kg/m}^2$  (5.5%). This allows a commonality of design in the descent events. More detailed descent parametrics are given in References 4.2-5 and 4.2-7.

The final configuration is basically the alternate configuration modified to perform satisfactorily in all three atmospheres. Several significant changes had to be made to accomplish this. First, the entry angle at Uranus was reduced from 0.79 rad ( $45^\circ$ ) to 0.61 rad ( $35^\circ$ ) in order to reduce the high entry heating imposed on the heat shield by the cool atmosphere. Next the entry ballistic coefficient was increased to reflect increases in the mass of the heat shield for the cool atmospheres. This resulted in a corresponding increase in the descent ballistic coefficient, which shortened the descent time. Then, both the entry time for collecting acceleration data and the descent time were subjected to a range of values that increased the data storage requirements and changed the required data bit rates during descent. The point at which the nose cover is removed and measurements begin also depends on the atmosphere.

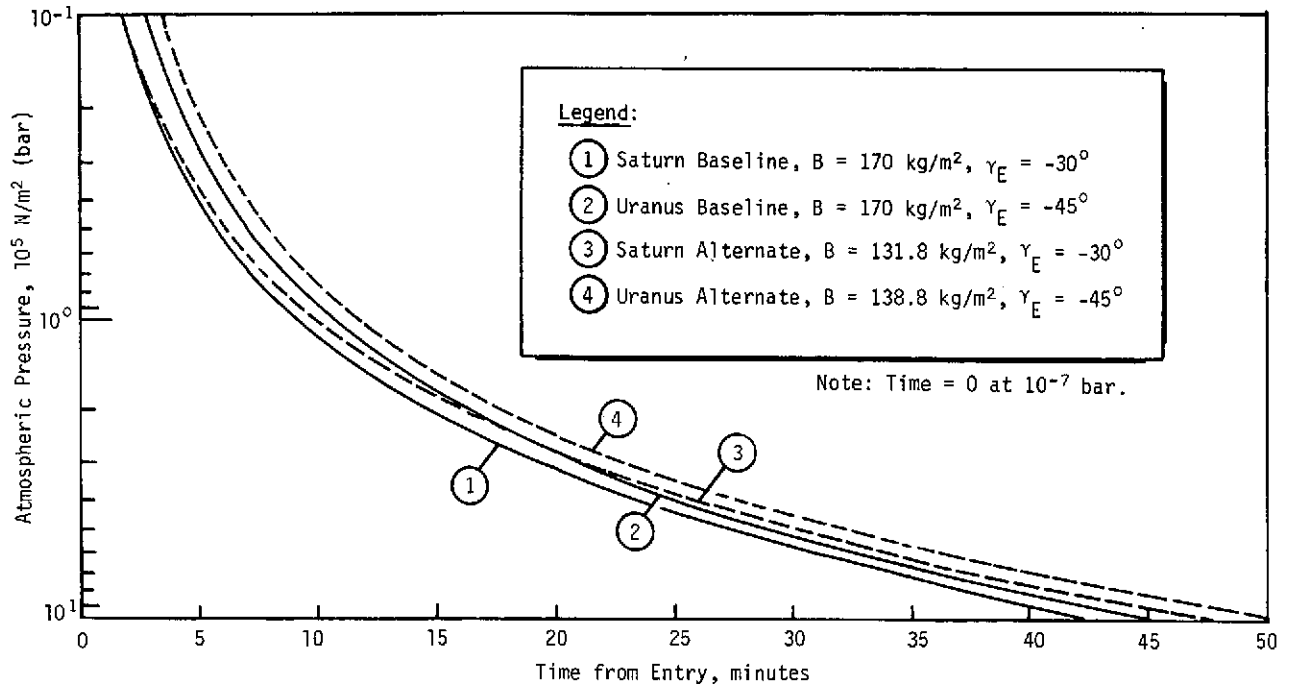


Figure 4.2-9 Baseline and Alternate Pressure Descent Profiles

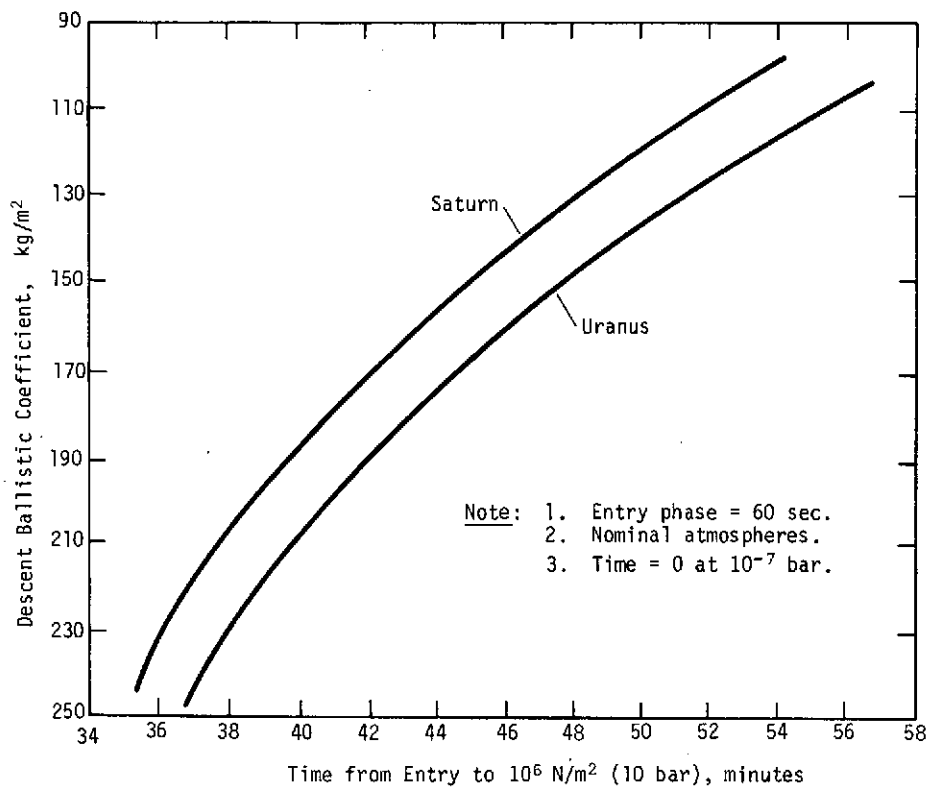


Figure 4.2-10 Total Descent Time vs Ballistic Coefficient

Table 4.2-7 lists the values of some critical parameters for all six atmospheres and the final configuration. Values of specific entry parameters used in the mission analysis are given in Table 4.3-2(d). Note that the ballistic coefficients during descent are almost equal.

The long times required for entry into the warm atmospheres result in the need to store a large amount of accelerometer data. Similarly, long descent times present problems in establishing an acceptable communication link for transmitting the data. The values for the peak deceleration in the cool atmospheres are within 3% of each other for both Saturn and Uranus, so differences in heating rates are due to composition and other factors. The pressure at the first descent measurement is highest for Saturn's cool atmosphere but only slightly higher than  $10^4$  N/m<sup>2</sup> (100 mb).

The pressure descent profiles for all six atmospheres are shown in Figure 4.2-11. Note that the difference between planets for a given atmosphere is less significant than the difference between models for a single planet. Therefore, since each atmosphere is considered in this study to be separate and equally possible, the probe commonality design is for six independent planetary atmospheres. The resultant design is thus more conservative than that if the nominal atmospheres were considered most probable and the cool and warm models were limiting (thus improbable) extremes.

#### 4.2.5 Data Collection and Measurement Performance

##### 4.2.5.1 Data Collection for Final Configuration

To fully utilize the PV data handling hardware in the SU probe with only minor modification, the data transmission rate during descent must be a binary multiple of 8 bps. Also the data words from the instruments must fit within a frame of 768 bits to be time coordinated with the bit rates. The bit rate for the five instruments required to satisfy the basic objectives and criteria (see Section 4.2.2) is about 25 bps. Thus, analyses were performed for descent bit rates of 16, 32, and 64 bps. (The high-speed entry accelerometer collects data at a rate of 128 bps, and stores it for transmission during descent.)

A descent value of 16 bps requires a significant reduction in collected data, particularly that from the mass spectrometer and accelerometer. The 64-bps value requires excessive power and returns excess data. The additional data from using a rate of 32 bps and the benefits from making minimum modifications to existing hardware far outweigh the small penalty in weight and power, and 32 bps was therefore adopted for all configurations.

Table 4.2-7 Entry and Descent Science Mission Parameters - Final Configuration

Parameter	Warm Atmosphere		Nominal Atmosphere		Cool Atmosphere	
	Saturn	Uranus	Saturn	Uranus	Saturn	Uranus
Entry Angle, deg	-30	-35	Same	Same	Same	Same
Entry Ballistic Coefficient, kg/m <sup>2</sup>	142.6	142.6	Same	Same	Same	Same
Descent Ballistic Coefficient, kg/m <sup>2</sup>	161.3	160.0	Same	Same	Same	Same
Entry Time [0.98 m/sec <sup>2</sup> to 29.4 m/sec <sup>2</sup> + 20 sec (0.1 g to 3 g + 20 sec)], sec	82	98	66	71	51	47
Peak Deceleration, m/sec <sup>2</sup> (g)	2275 (232)	1451 (148)	3776 (385)	2354 (240)	5737 (585)	5590 (570)
Time to Maximum Deceleration, sec	41	62	23	29	12	10
Instrument Deployment						
Time from Entry, sec	96	121	71	78	53.5	48.5
Mach Number	0.71	0.86	0.58	0.76	0.49	0.60
Deceleration, m/sec <sup>2</sup>	15	14	13	13	13	10
Altitude, km	156	152	86	84	46	37
Pressure, ·10 <sup>2</sup> N/m <sup>2</sup> (mb)	63	39	85	46	114	59
Time to Terminal Velocity, sec	137	282	100	249	72	150
Pressure at Terminal Velocity, ·10 <sup>2</sup> N/m <sup>2</sup> (mb)	91	132	118	196	145	193
Time to 10 <sup>6</sup> N/m <sup>2</sup> (10 bar), minutes	62.9	73.9	42.6	46.6	27.3	29.2

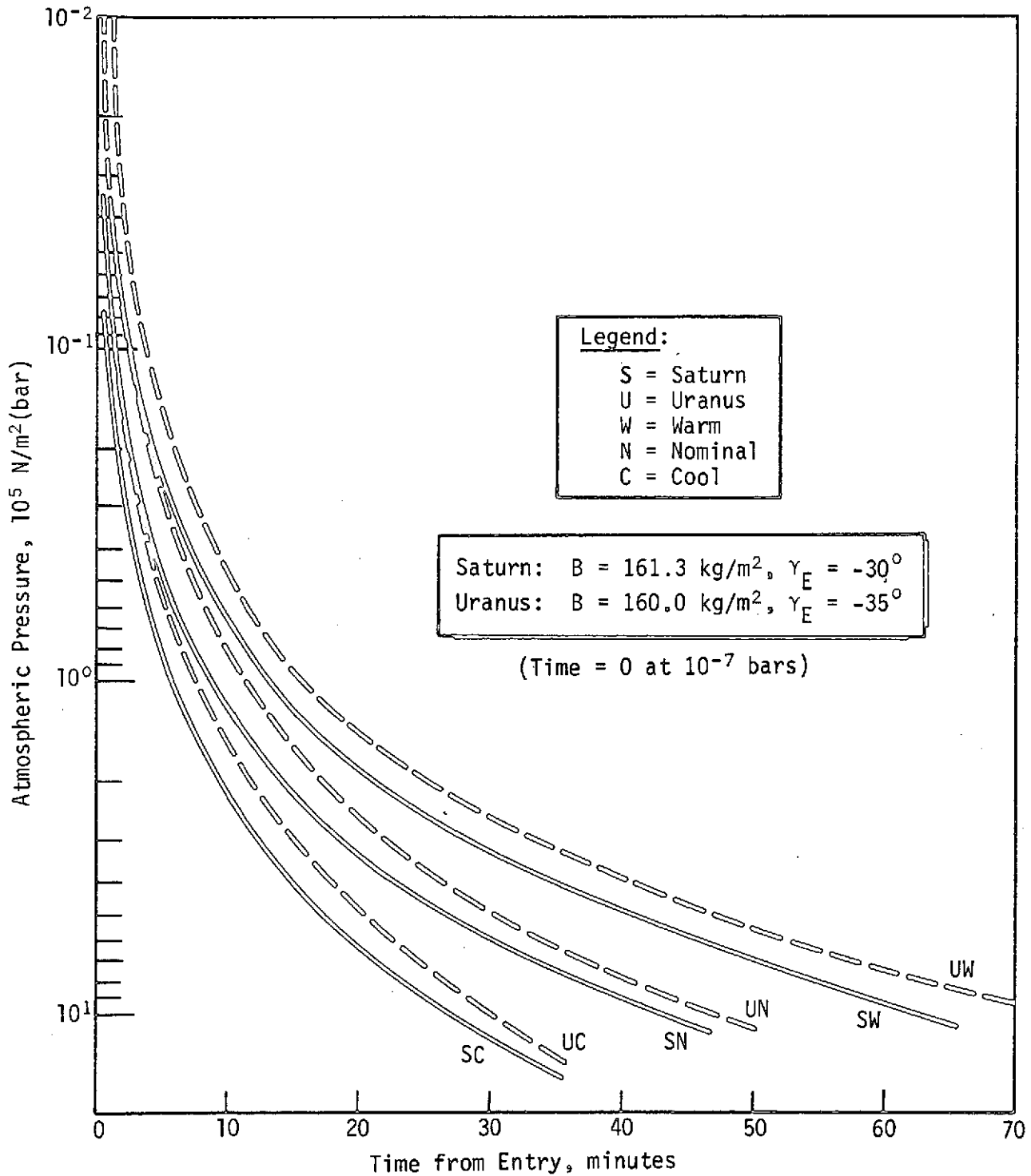


Figure 4.2-11 Pressure Descent Profiles for Final Configuration

Table 4.2-8 gives the minimum required data rate based on acceptable minimum sampling. The entry data storage is calculated for the worst-case atmosphere with the shortest descent time (Saturn cool) which determines the highest playback rate. Spacecraft acquisition is assumed to occur at the nominal time of 3 g plus 60 seconds.

Table 4.2-8 Minimum Sampling Requirements and Data Rate

Data Source	Bits/Sample	sec/Sample	Bits/sec
Pressure Gauge	8	25	0.32
Temperature Gauge	8	25	0.32
Nephelometer	43	12.5	3.44
Accelerometers	40	25	1.60
Mass Spectrometer	4800	400	12.00
Stored Data Playback	8128	1541	5.27
Subcom/Housekeeping	64	24	2.67
Total =			25.62 bps

Table 4.2-9 shows the details of the selected 32 bps for each instrument and the actual data composition values used for the final configuration.

Part of the excess capability from using 32 bps is removed when the data frame is organized. The pressure, temperature, and turbulence accelerometer measurements are transmitted without buffer storage, and thus must occur at equal intervals within and between frames. This requires an even number of measurements per frame, and generally (as in the PV system), requires using a binary-based number of measurements per frame to ensure a smooth data flow. Additional excess bit rate is removed by using an entry data storage unit that is larger than the minimum storage required because it is a multiple of the basic PV unit with 2560 bits/unit, and because the data must be formatted with a fixed number of bits per frame.

Table 4.2-9 Data Construction for 32 bps - Final Configuration

Data Source	Bits/Sample	sec/Sample	Bits/sec	Bits/Frame <sup>*</sup>
Pressure Gauge	8	24	0.33	8
Temperature Gauge	8	24	0.33	8
Nephelometer	43	12	3.58	86
Accelerometers	40	24	1.67	40
Mass Spectrometer <sup>†</sup>	6400	400	16.00	384
Stored Data Playback <sup>§</sup>	9118	1541	5.92	142
Subcom/Housekeeping	64	24	2.67	64
Spare			<u>1.50</u>	<u>36</u>
			32.00	768

<sup>\*</sup> 24 sec/frame transmitted.  
<sup>†</sup> 3 measurements/50 frames.  
<sup>§</sup> Maximum storage in Uranus Warm atmosphere = 15,200 bits at 128 bps.  
Maximum playback rate in Saturn Cool atmosphere is shown here.



The remainder of the data transmission capability can then be used to make a more detailed mass spectrum, or an additional spectrum from a given gas sample which was done for the final configuration. This is further explained in the mass spectrometer part of Section 4.2.3. Note from Table 4.2-9 that 1.5 bps (36 bits/frame) remain as spare capacity. Each frame requires 24 seconds for transmission, and thus one temperature and pressure determination are telemetered in each frame. Each mass spectrometer measurement requires 16.7 frames. A partial frame is possible since the NMS measurements are in a digital bit stream from the instrument.

The subcom/housekeeping entry in Table 4.2-9 is explained in detail as follows: Word formatting and data frame identifiers occupy 42 bits per frame. The remaining 22 bits per frame comprise two 6-bit housekeeping engineering words and one 10-bit science engineering word. Each various type of engineering measurement is repeated every 192 seconds, which is every eighth data frame. This gives a capability for 16 housekeeping measurements and 8 science engineering measurements, used as follows:

Housekeeping Engineering	No. of Words
Transmitter power	1
Transmitter crystal temperature	1
Antenna voltage standing wave ratio	1
Power amplifier temperature	1
Battery voltage/current	1
Battery temperature	1
Instrument electronics temperatures	4
Internal equipment temperatures	4
Internal structure strain gauges	1
Spare	<u>1</u>
	16
Science Engineering	
Instrument sensor temperatures	4
Mass spectrometer voltage/current	2
Nephelometer window temperature	1
Spare	<u>1</u>
	8

#### 4.2.5.2 Descent Measurement Performance for Final Configuration

The measurement performance of the science instruments was evaluated using the descent profiles for the final configuration and the sampling times given in Table 4.2-9. Figures 4.2-12 and 4.2-13 show the descent performance of the pressure and temperature

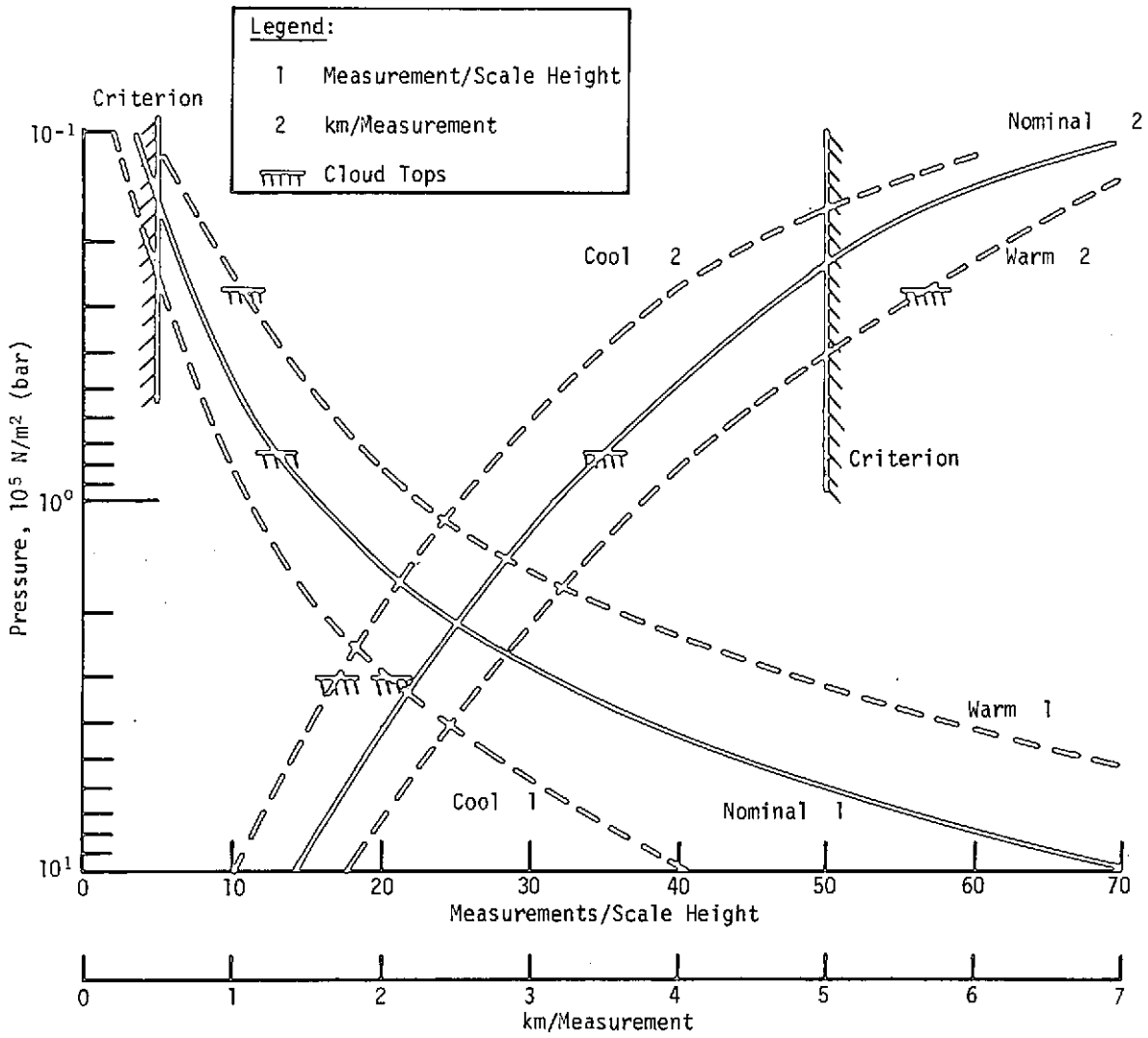


Figure 4.2-12 Descent Performance for 24 Second Sampling Time - Saturn (Final Configuration)

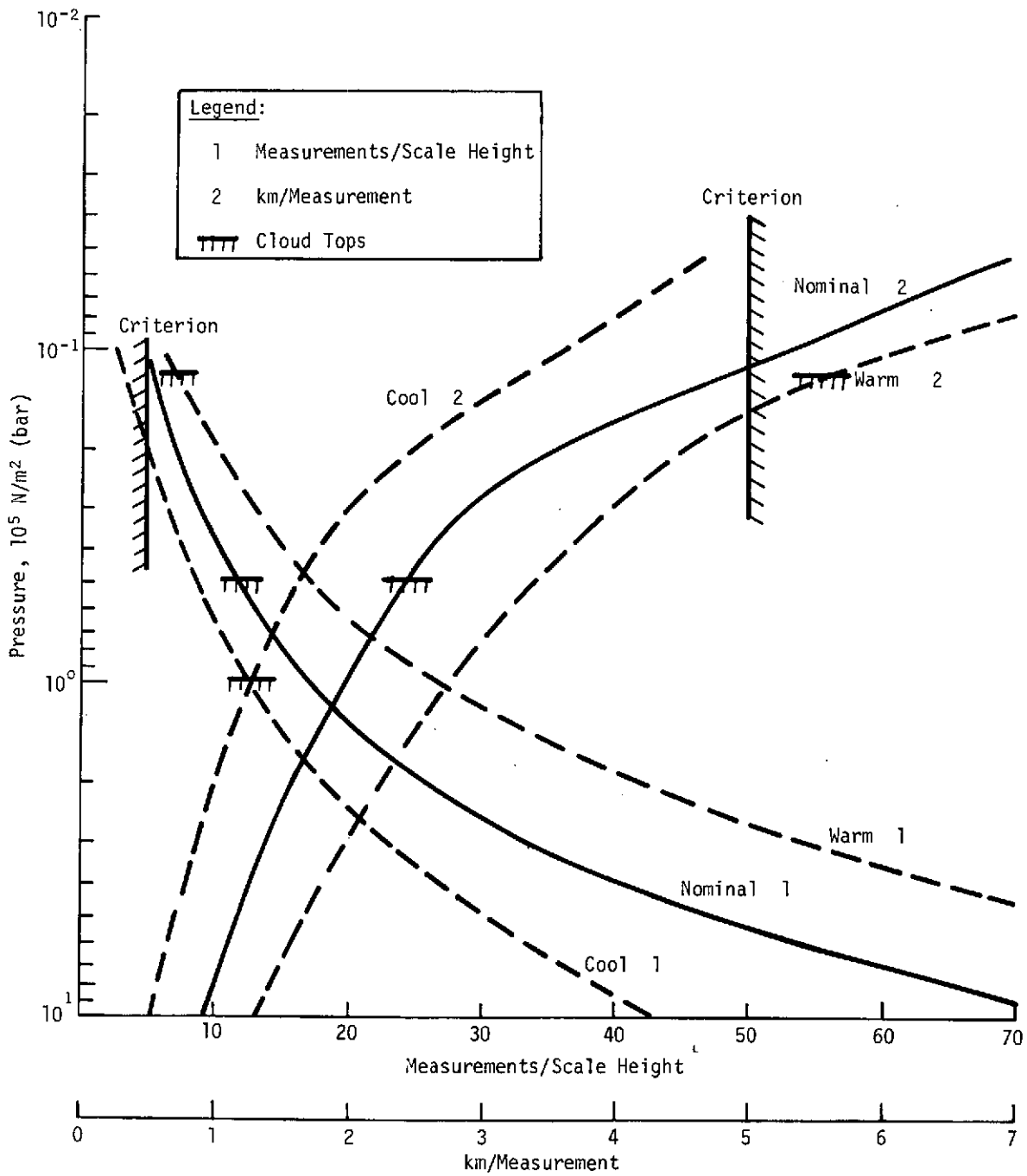


Figure 4.2-13 Descent Performance for 24 Second Sampling Time - Uranus (Final Configuration)

gauges and turbulence accelerometers for Saturn and Uranus respectively. Performance is indicated in terms of the number of measurements per scale height and kilometers per measurement. Note the cloud top locations for each of the model atmospheres. Entry and descent conditions were given in Table 4.2-7.

To evaluate the performance of the nephelometer, the four 10-bit words constituting the measurement will be assumed to be composed of two laser reflections and two solar backgrounds, giving 20 bits for a single determination. (Note that the criterion of 1 km per measurement was based on 20-bit measurements in Reference 4.2-3). The effective sampling time for cloud locating measurements is then half that given in Table 4.2-9, or 6 seconds. The axes of Figures 4.2-12 and 4.2-13 can then be interpreted as four measurements per scale height and kilometers per four measurements for the effective sampling time of 6 seconds.

Table 4.2-10 summarizes the performance of the science instruments by comparing the criteria from Section 4.2.2 with data at specific points in the descent. The top half of the table gives the pressure at which a level of 5 km per measurement is first reached and shows the resulting number of measurements per scale height for all six atmospheres. Note that the two methods of evaluating performance are compatible. The point labeled "undefined" in the Uranus cool atmosphere is reached prior to nose cap deployment. The lower half of the table shows the performance at the cloud tops in each atmosphere, with the cloud top pressure as defined by the monographs. As shown in the table, all values satisfy the performance criteria except for the kilometers per measurement in the warm atmospheres, and even they are probably within the accuracy of the calculation techniques. Note that all performance values improve with time, as the probe slows during descent.

Since the mass spectrometer makes a fixed number of measurements during descent, if the sampling time is designed for the cool atmospheres so that all six can be made prior to  $10^6 \text{ N/m}^2$  (10 bar), then the last measurement is made at  $3.7 \times 10^5 \text{ N/m}^2$  (3.7 bar) in the nominal atmosphere and only  $2 \times 10^5 \text{ N/m}^2$  (2 bar) in the warm atmosphere. On the other hand, if the design is for the nominal atmosphere then only four measurements can be made prior to  $10^6 \text{ N/m}^2$  (10 bar) in the cool, but the measurements are better distributed in pressure, and the required bit rate for mass spectrometer data is 36% lower.

This second method is our recommended method for the final configuration. The resultant sampling time is ideally 405 seconds, but by reducing this to 400 seconds and extending the Saturn cool mission time by 66 seconds we ensure four full mass spectrometer samples in both cool atmospheres prior to 10 bars. Table 4.2-11 lists the times and the ambient atmospheric pressures at the closing of each of the six inlet tubes for each of the six model atmospheres. This indicates the distribution in the atmosphere obtained by the instrument.

Taking six mass spectrometer measurements requires collecting and transmitting 100 total frames of data at 24 sec/frame. Since the descent times to  $10^6 \text{ N/m}^2$  (10 bar) vary between atmospheres, the total number of frames transmitted also varies, as shown below:

	<u>Warm</u>	<u>Nominal</u>	<u>Cool</u>
Saturn	151	102	67
Uranus	178	111	69

Four mass spectrometer measurements can be sent in 67 frames. However, since the communication link, battery power, thermal control, and other critical subsystems are designed for descent times in warm atmospheres (74 minutes maximum compared to 29.2 minutes required in the cool) there is high probability that the probe will survive long enough to make all six mass spectrometer measurements in the cool atmospheres.

#### 4.2.5.3 Entry Accelerometer Performance for Final Configuration

The entry accelerometers consist of a primary axial sensor sampling at a rate of 5 samples per second and backup axial, x-lateral, and y-lateral sensors, each sampling at 2.5 samples per second. With 8-bit analog words, this yields 40 bps from the primary axial unit, 20 bps from the backup axial unit, and 20 bps from each lateral sensor, for a total data rate of 100 bps. The remainder of the allowed 128 bps consists of formatting and house-keeping data and spare capacity.

The primary function of the accelerometer triad is to collect the entry g-load information with sufficient accuracy to be able to reproduce the g-curve, and in particular, the sharp maximum point on the curve. This can be used to reconstruct the atmosphere, as described in Reference 4.2-5. However, since the g-load may go from 10% of its peak value through peak and back to 10% in only a few seconds, we conducted an analysis using a sampling rate of 5 samples per second to ensure that the axial accelerometer would

Table 4.2-10 Measurement Performance Summary

	Pressure & Temperature Gauges & Turbulence Accelerometer (24 sec)			Nephelometer (20 bits/6 sec)
	km/Meas	Pressure, $10^2 \text{ N/m}^2$ (mb)	Meas/Scale Ht	km/Meas
Criterion:	≤5.0	≤400	≥5.0	≤1.0
<u>Atmosphere</u>				
Saturn Nominal	5	236	7.0	1.2
Uranus Nominal	5	111	5.1	1.2
Saturn Warm	5	400	14.0	1.2
Uranus Warm	5	150	8.7	1.2
Saturn Cool	5	162	4.2	1.2
Uranus Cool	5	46	Undefined	1.2
Uranus Cool	2.5	200	5.0	0.6
	km/Meas	Cloud Top Pressure, $10^5 \text{ N/m}^2$ (bar)	Meas/Scale Ht	km/Meas
Saturn Nominal	3.5	0.73	13	0.9
Uranus Nominal	2.4	0.49	12	0.6
Saturn Warm	5.7	0.27	11	1.4
Uranus Warm	5.6	0.12	7	1.3
Saturn Cool	1.7	3	21	0.4
Uranus Cool	1.3	1	13	0.3

Table 4.2-11 Distribution of Mass Spectrometer Measurements

NMS Measurement ( $\Delta t=400$ sec)	Time from Nose Cover Release, sec	Ambient Atmospheric Pressure, $10^5 \text{ N/m}^2$ (bar)					
		Saturn Cool	Saturn Nominal	Saturn Warm	Uranus Cool	Uranus Nominal	Uranus Warm
1	51	0.21	0.15	0.10	0.12	0.08	0.06
2	451	1.61	1.00	0.58	1.16	0.64	0.41
3	851	4.02	2.18	1.32	2.96	1.63	1.02
4	1251	7.10	3.80	2.18	5.67	3.12	1.68
5	1651	10.57	5.57	3.17	9.45	4.71	2.51
6	2051	14.33	7.57	4.20	13.61	6.55	3.45

Boxed values are those measurements taken below the design pressure limit of 10 bar. However with systems designed for 74 minutes descent in the warm, the probe should survive past 10 bars (~29 minutes) in the cool.

give enough points along the curve to allow us to reproduce the steep slope.

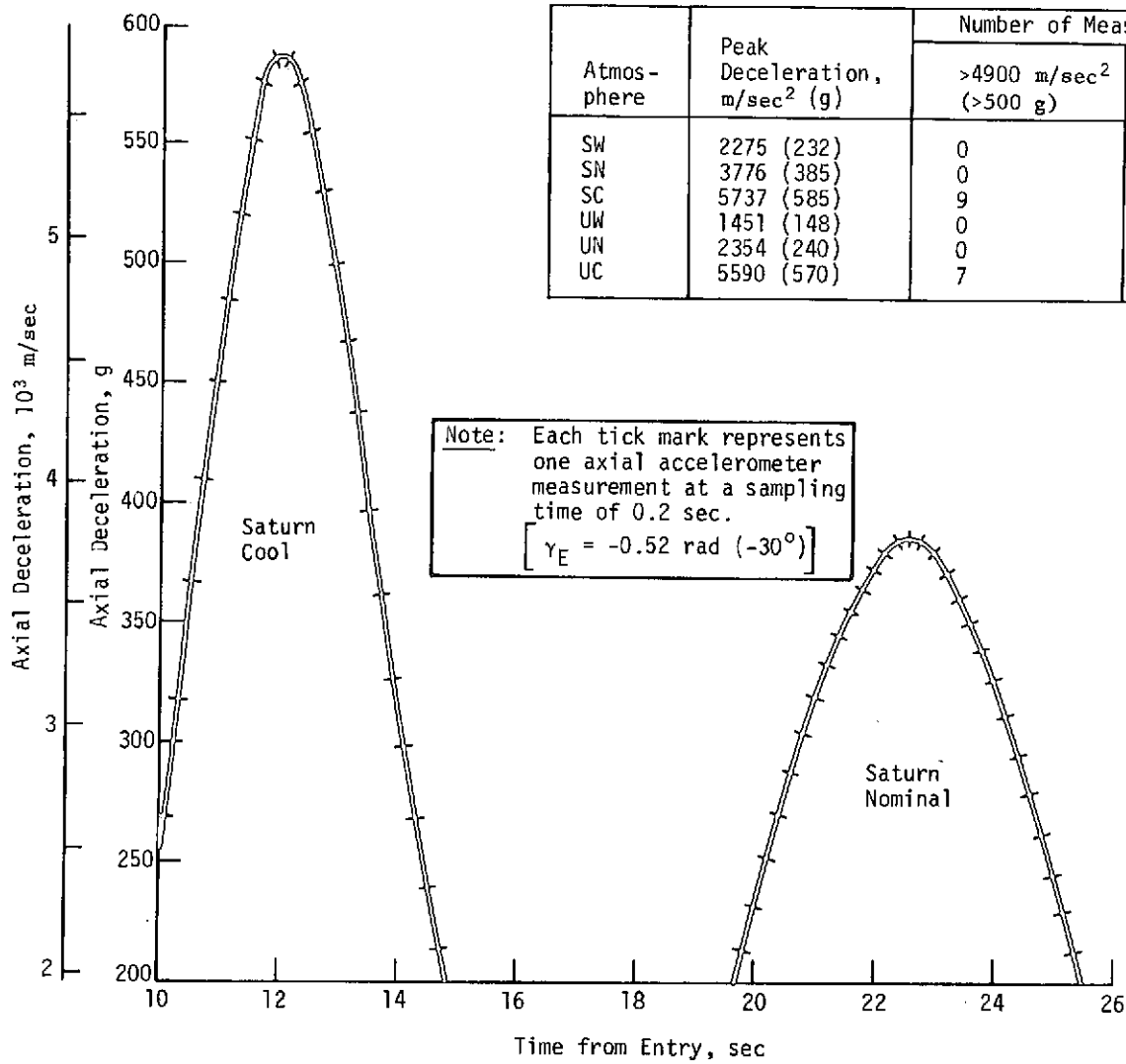
Figure 4.2-14 shows the expected g-load curves based on the Saturn cool and nominal atmospheres calculated by an entry dynamics computer program. Superimposed on this are marks that represent individual axial accelerometer measurements 0.2 seconds apart. In addition, the table lists the number of measurements made by the axial accelerometer in each of the six model atmospheres and above three different g-levels to indicate the data taken near each peak. The maximum lateral decelerations expected are within the sensor range capability of  $\pm 343 \text{ m/sec}^2$  ( $\pm 35 \text{ g}$ ).

#### 4.2.5.4 Dual Data Transmission

We conducted a separate investigation of the requirements and effects of transmitting all of the data from the probe twice, using buffers to delay the second transmission. The details for implementing the method and on how the PV hardware must be modified to accomplish this are discussed in Section 4.5.1.2.

The detail construction of the data collection is shown in Table 4.2-12. The results of our analysis show that the data collection rate during descent is 20.48 bps, which is divided among the instruments as shown in the table. Note that the mass spectrometer is back to the required 4800 bits per measurement and that the sampling times of the other instruments are changed to be compatible with the 37.5-second transmission time per frame. This allows improved performance since the times are shorter. The sampling time for the nephelometer increased by 0.5 second, which does not significantly affect performance. Through buffering and interleaving the memory data, the transmission bit rate is 51.2 bps. Dumping memory data takes one-fifth of this, or 10.24 bps, but the worst-case Saturn cool atmosphere requires only 9.44 bps, so a margin of safety is inherent. Only 12K bits are collected during entry, in contrast to 15K bits from Table 4.2-9 because the collection rate is 102.4 bps instead of 128 bps. However, the 12K bits must be transmitted twice.

Note that less total data are obtained using this method. In addition, the additional required changes from PV hardware tend to negate the benefit of redundant transmission.



Atmos- phere	Peak Deceleration, m/sec <sup>2</sup> (g)	Number of Measurements at		
		>4900 m/sec <sup>2</sup> (>500 g)	>2940 m/sec <sup>2</sup> (>300 g)	>980 m/sec <sup>2</sup> (>100 g)
SW	2275 (232)	0	0	57
SN	3776 (385)	0	18	46
SC	5737 (585)	9	19	38
UW	1451 (148)	0	0	45
UN	2354 (240)	0	0	48
UC	5590 (570)	7	17	33

Note: Each tick mark represents one axial accelerometer measurement at a sampling time of 0.2 sec.  
 $\gamma_E = -0.52 \text{ rad } (-30^\circ)$

Figure 4.2-14 Entry Accelerometer Measurement Performance.



Table 4.2-12 Data Construction for Dual Data Transmission at 51.2 bps

Data Source	Bits/Sample	sec/Sample	Bits/sec	Bits/Frame <sup>*</sup>
Pressure Gauge	8	18.75	0.43	16
Temperature Gauge	8	18.75	0.43	16
Nephelometer	43	12.50	3.44	129
Accelerometers	40	18.75	2.13	80
Mass Spectrometer <sup>†</sup>	4800	400	12.00	450
Subcom/Housekeeping	64	37.5	1.71	64
Spare			<u>0.34</u>	<u>13</u>
			20.48	768
			Dual Transmission =	40.96
			Stored Data <sup>§</sup> =	<u>10.24</u>
			Total =	51.2
<sup>*</sup> 37.5 sec/frame collected; 15 sec/frame transmitted. <sup>†</sup> 3 measurements/50 frames. <sup>§</sup> Maximum storage required = 12,000 bits at 102.4 bps.				

## 4.3 Impact of Mission Requirements on System Design

## 4.3 IMPACT OF MISSION REQUIREMENTS ON SYSTEM DESIGN

### 4.3.1 Mission General Summary

#### 4.3.1.1 Launch and Interplanetary Trajectories

Launch analysis can be conveniently divided into three categories: launch energy or payload analysis, launch constraints, and arrival constraints. Neither the launch nor arrival constraints have a significant system impact. In most cases they are simply checked and verified to be either acceptable or unacceptable. On the other hand, launch energy requirements have a significant impact on system design.

The payload weight is a direct function of the launch energy and increases as the launch energy decreases. Once the maximum payload capability is determined, the total weight of the spacecraft and all subsystems is also determined.

For the missions and launch vehicle considered in this study, the payload capability is approximately 476.3 kg (1050 lb), assuming a 15-day launch period. At present, these are the baseline numbers; a small increase in payload capability could be realized by accepting longer flight times to Saturn and Uranus. The launch and interplanetary phases of the mission have for the most part, minimal impact on the design of the probe subsystems. Near the earth the probe is protected by a thermal control blanket, and there is no problem with thermal loads on the probe during interplanetary cruise.

#### 4.3.1.2 Approach Orbit Determination and Dispersions

The approach orbit determination and resultant dispersions are most significant at Uranus. Radio-only navigation can resolve the one-sigma B-plane uncertainty to no better than the ephemeris error, or approximately 10,000 km. The resultant dispersions imply that:

- 1) Radio navigation must be supplemented with optical measurements; or
- 2) A high entry angle [ $\gamma \sim 1.40$  rad ( $80^\circ$ )] is required.

Since the mission has tight weight constraints and the weight of the probe heat shield is highly sensitive to the entry angle, an optical V-slit scanner is the preferred choice for reducing dispersions. An additional benefit of using an optical guidance sensor is that this reduces the  $\Delta V$  magnitude of the post-Saturn midcourse maneuver.

Ideally, the entry angle is selected to minimize structural and thermal loads during entry, while simultaneously satisfying science constraints. Uniform sampling of the atmosphere by the science instruments is a primary science objective that requires a lightside entry and descent. At Uranus, with a retrograde approach, the entry site is approximately 0.44 rad (25°) from the terminator when  $\gamma = -0.61$  rad (-35°). The semimajor axis (SMAA) of the entry footprint is then 0.31 rad (18°) aligned in the downtrack direction, which leaves a 0.12-rad (7°) margin between the terminator and the tip of the entry footprint. In comparison, using an entry angle of -0.52 rad (-30°) leaves no margin, whereas an entry angle of -0.79 rad (-45°) places excessive demands on the design of the heat shield.

Based on the relationship between the entry angle, the entry dispersions, and the resultant structural/thermal impact we set the nominal entry angle at Uranus equal to -0.61 rad (-35°).

At Saturn, the entry footprint of 0.028 rad by 0.09 rad (1.6° by 2.2°) does not set any significant bounds on the nominal entry site selection. By way of comparison the entry footprint at Uranus is 0.31 rad by 0.09 rad (18° by 5°).

The selection of the deflection radii at both Saturn and Uranus significantly affects the deflection  $\Delta V$  budgets of the spacecraft bus. From an orbit determination standpoint, the deflection radius should be as small as possible to allow for improved tracking efficiency. The spacecraft bus, however, has a deflection  $\Delta V$  budget of 70 m/sec. Primarily with this constraint in mind, we set the deflection radius as  $30 \times 10^6$  km ( $500 R_S$ ) at Saturn and  $25 \times 10^6$  km ( $925 R_U$ ) for Uranus.

#### 4.3.1.3 Planetary Encounter

Planetary encounter includes the deflection event, coast, entry, and descent. During the critical entry and descent phases, the *in situ* measurements are made and the corresponding data are sent back to Earth with the spacecraft acting as a relay link. Accordingly, the successful operation of the communication link is of primary importance. As a result, we conducted an extensive series of encounter mission tradeoff studies at both Saturn and Uranus to optimize the performance of this link. Of particular importance is obtaining a uniformity in spacecraft cone angles at Saturn and Uranus while simultaneously minimizing range. Our strategy was to have a broadbeam

probe antenna and a narrow beam spacecraft antenna, hence, minimizing the range of cone angles (CA) becomes more important than insuring small probe aspect angles (PAAs). Range is always important since the space loss increases as the range squared. Since range for all missions is maximum at entry and decreases during descent, our strategy was to bias the main lobe of the spacecraft antenna toward entry to maximize the antenna gain when the range is maximum. Similarly, by balancing the various factors contributing to the efficiency of the communication link during descent, we were able to obtain improved link performance for both planets.

#### 4.3.1.4 Planetary Entry and Descent

During entry the probe experiences the most hostile aerothermodynamic environment. The structural and heating loads are both at a maximum at this time and are inversely proportional to the entry angle. Our rationale for selecting the entry angle at Uranus has already been discussed.

For entry into Saturn and Uranus, the cool-atmosphere model yields the worst-case aerothermodynamic environment and the probe structure and heat shield were designed accordingly. The maximum descent time, which results in worst-case communication link geometry, occurs with the warm atmosphere model; and the communication link has been designed to accommodate this worst-case atmosphere. The science requirements governing the number of samples per kilometer or equivalent samples per scale height are discussed in Section 4.2.

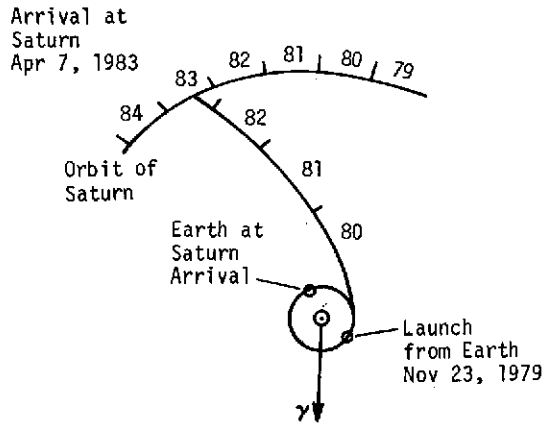
#### 4.3.2 Mission Design Summary

##### 4.3.2.1 1979 Saturn Mission Definition

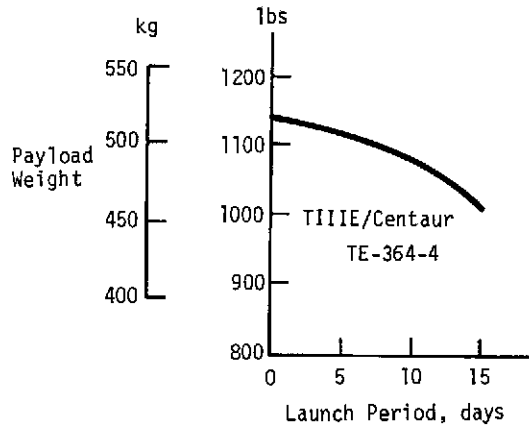
The Saturn Direct 1979 mission is shown in Figure 4.3-1 and Table 4.3-1. Important mission design results are summarized below.

##### Interplanetary Trajectory Selection

The Type I interplanetary trajectory from Earth to Saturn is shown in Figure 4.3-1 (a) with 1 year intervals noted. The launch date of November 23, 1979 and a Saturn arrival date of April 7, 1983 results in a total trip time of 3.4 years.



(a) Interplanetary Trajectory



(c) Launch Analysis

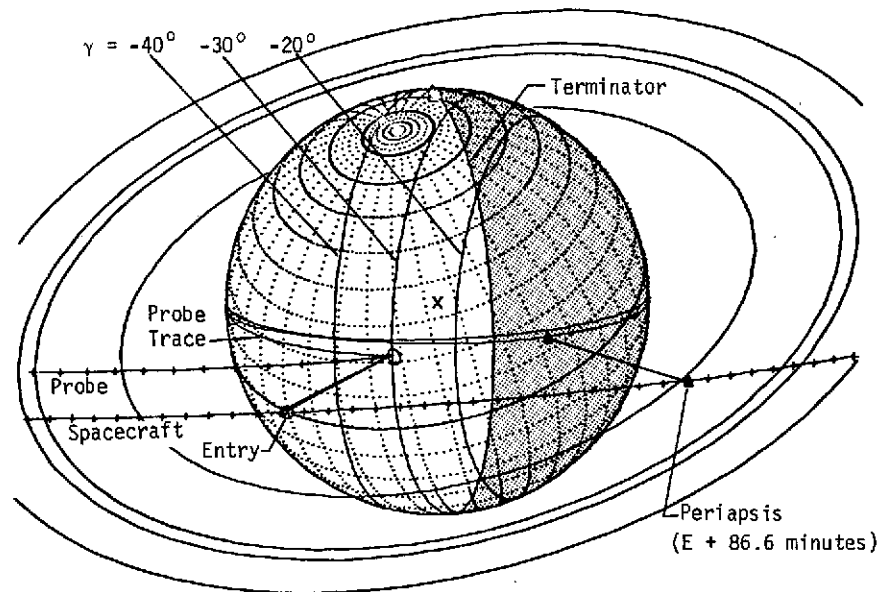
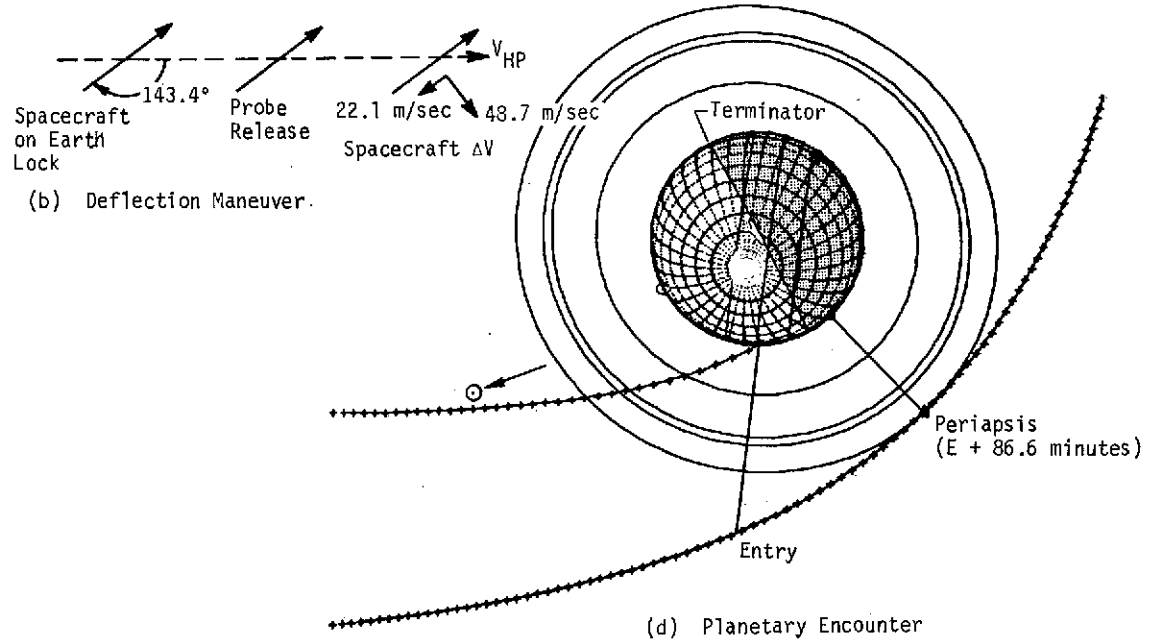


Figure 4.3-1 Saturn 1979 Mission Definition

Table 4.3-1 Saturn 1979 Mission Summary Data

(a) Conic Trajectory Data

Interplanetary Trajectory	Launch Trajectory	Arrival Trajectory
Launch Date: 11/23/79 (2444200.5)  Arrival Date: 4/7/83 (2445431.5)  Flight Time: 1231 days 3.4 yr	Nominal $C_3$ : 134.7 km <sup>2</sup> /sec <sup>2</sup> Nominal DLA: 0.56 rad (31.9°)  $C_3$ (5-day): 135 km <sup>2</sup> /sec <sup>2</sup> $C_3$ (10-day): 138 km <sup>2</sup> /cm <sup>2</sup> $C_3$ (15-day): 143 km <sup>2</sup> /sec <sup>2</sup>	$V_{HP}$ : 9.18 km/sec $RA$ :* 0.0059 rad (0.34°)  $DEC$ :* 3.058 rad (175.2°) $ZAE$ : 2.501 rad (143.4°) $ZAP$ : 2.529 rad (144.9°)  $R_p$ : 2.3 $R_S$ 137,554 km
*Ecliptic equinox system.		

(b) Deflection Maneuver and Probe Conic

Deflection Maneuver	Probe Conic Definition
Deflection Mode: Spacecraft Deflection Radius: 30 x 10 <sup>6</sup> km Coast Time: 35.7 days $\Delta V_{Earth}$ : 22.1 m/sec $\Delta V_{\perp}$ : 48.9 m/sec  $\Delta V_{Total}$ : 70.8 m/sec	Entry Angle: -0.52 rad (-30°) Entry Latitude:* 0.380 rad (21.8°) Entry Longitude:* 1.168 rad (66.9°) Lead Time: 5200 sec Probe Spacecraft Range (entry): 1.08 x 10 <sup>5</sup> km Cone Angle (entry): 2.229 rad (127.7°) Cone Angle (EOM): 1.682 rad (96.4°) Probe Aspect Angle (entry): 0.199 rad (11.4°) Probe Aspect Angle (EOM): 0.539 rad (13.7°) Angle of Attack: 0.147 rad (8.4°)
*Planet equator - Sun.	

Table 4.3-1 Continued

(c) Dispersion Analysis Summary

Navigation Uncertainties ( $1\sigma$ )	Execution Errors ( $3\sigma$ )	Dispersions ( $3\sigma$ )
Tracking: Range/Doppler 40-day Arc SMAA: 1840 km SMIA: 812 km $\beta$ : 1.634 rad (93.6°) TOF: 80.2 sec	$\Delta V_{\perp}$ Proportionality: 1% $\Delta V_{\perp}$ Pointing: 0.017 rad (1°) Probe Tipoff Error: 0.017 rad (1°)	Entry Angle: 0.021 rad (1.2°) Angle of Attack: 0.030 rad (1.7°) Downrange: 3384 km Crossrange: 4436 km Range: 3745 km Range Rate: 0.85 km/sec Probe Aspect Angle: 0.050 rad (2.85°) Cone Angle: 0.048 rad (2.76°)

(d) Entry and Descent Summary

	Atmosphere Model		
	Warm	Nominal	Cool
Entry Parameters			
Entry Velocity, km/sec	36.57	36.67	36.66
Entry Altitude, km	968.5	536	297.0
Entry B, kg/m <sup>2</sup>	142.6	142.6	142.6
Maximum Deceleration, m/sec <sup>2</sup> (g)	2275 (232)	3776 (385)	5737 (585)
Maximum Dynamic Pressure, N/m <sup>2</sup>	2.9 x 10 <sup>5</sup>	4.6 x 10 <sup>5</sup>	7.3 x 10 <sup>5</sup>
EOM Pressure, N/m <sup>2</sup> (bar)	10 <sup>6</sup> (10)	10 <sup>6</sup> (10)	10 <sup>6</sup> (10)
Descent B, kg/m <sup>2</sup>	161.3	161.3	161.3
Critical Entry Events			
0.98 m/sec <sup>2</sup> (0.1 g) Increasing, sec	14.0	6.0	2.0
4.90 m/sec <sup>2</sup> (50 g) Increasing, sec	34.0	17.0	8.0
29.4 m/sec <sup>2</sup> (3 g) Descending, sec	76.0	49.0	33.0
Maximum Deceleration, sec	41.0	23.0	12.0
Mach = 0.7, sec	96.0	61.0	38.0
EOM Time, minutes	63.0	42.6	27.3

C-2



### Launch Analysis

The launch analysis is provided in Figure 4.3-1 (a). Available payload is plotted against launch period for the Titan IIIE/Centaur/TE364-4 launch vehicle. The nominal launch window and parking-orbit coast times were both checked and found to be satisfactory.

### Approach Trajectories

The probe and spacecraft trajectories are phased to yield an entry geometry similar to that for Saturn/SU-80 and Uranus/SU-80, and are based on a nominal entry angle of  $\gamma = -0.52$  rad ( $-30^\circ$ ). The resulting approach trajectory is shown in Figure 4.3-1 (d) and summarized in Table 4.3-1 (b).

Since Saturn is the terminal planet for this mission, the spacecraft periapsis radius was selected to be  $2.3 R_S$  to avoid encountering the rings. The probe aspect angle at the start of the warm atmosphere descent phase is  $0.190$  rad ( $10.9^\circ$ ) and increases to  $0.239$  rad ( $13.7^\circ$ ) at the end-of-mission 63 minutes later.

### Deflection Maneuver

The spacecraft deflection maneuver is performed with the spacecraft in an Earth-pointing attitude at a deflection radius of 30 million km. This makes the coast time 35.7 days. The deflection  $\Delta V$  is supplied by the radial and axial thrusters; a  $\Delta V$  of 22.1 m/sec is applied along the Earth-line direction and 48.7 m/sec is applied orthogonally. The deflection sequence is pictured in Figure 4.3-1 (b).

### Dispersion Analysis Summary

The results of the navigation and dispersion analysis are given in Table 4.3-1 (c) for standard 40-day radio only tracking. The B-plane uncertainty ellipse is characterized by a SMAA which is approximately the magnitude of the Saturn ephemeris uncertainty. Execution errors associated with the deflection event are combined with the navigation uncertainties in determining communication and entry dispersions. Analysis indicates that the magnitudes of the resultant dispersions are decreased by approximately 50% when execution errors are not considered.

## Entry and Descent Trajectories

Table 4.3-1 (d) summarizes the entry and descent phases of the mission. The maximum deceleration load of  $5737 \text{ m/sec}^2$  (585 g) is encountered when entering the cool atmosphere.

Since the EOM pressure is assumed to be  $10^6 \text{ N/m}^2$  (10 bar), the descent time is governed by the ballistic coefficient during descent and the model atmosphere. For a fixed ballistic coefficient ( $B_E = 142.6 \text{ kg/m}^2$ ) the time to descent to 10 bars in the cool, nominal and warm atmospheres is 27.3, 42.6 and 63 minutes respectively.

### 4.3.2.2 Saturn/SU-80 Mission Definition

The Saturn/SU-80 mission is shown in Figure 4.3-2 and detailed in Table 4.3-2. The important mission design results are summarized below.

#### Interplanetary Trajectory Selection

The 1980 Saturn trajectory is similar to the 1979 Saturn trajectory. Note that the trip time has been decreased slightly, and now requires 3.1 years [see Figure 4.3-2 (a)].

#### Launch Analysis

The launch analysis for the Saturn/SU-80 mission is provided in Figure 4.3-2 (b). Assuming a 10-day launch period the payload capability of the Titan IIIE/Centaur/TE 364-4 launch vehicle is 490.0 kg (1080 lb). The nominal launch window and parking orbit were both checked and found satisfactory.

#### Approach Trajectories

The most notable difference between the S-79 and SU-80 Saturn approach trajectories is in the nominal angle of attack, which increased from 0.147 rad ( $8.4^\circ$ ) for 1979 mission to 0.236 rad ( $13.5^\circ$ ) for the 1980 mission. The other parameters for the two Saturn missions vary by less than 10%. The nominal entry angle,  $\gamma_E$ , is  $-0.52 \text{ rad}$  ( $-30^\circ$ ).

#### Deflection Maneuver

The spacecraft deflection maneuver is performed 30 million km from entry and results in a coast time of 31.2 days. The

Table 4.3-2 Saturn/SU-80 Mission Summary Data

(a) Conic Trajectory Data

Interplanetary Trajectory	Launch Trajectory	Arrival Trajectory
Launch Date: 12/1/80 (2444574.5)  Arrival Date: 1/4/83 (2445703.5)  Flight Time: 1129 days 3.1 yr	Nominal $C_3$ : 138 km <sup>2</sup> /sec <sup>2</sup> Nominal DLA: 0.436 rad (25.0°)  $C_3$ (5-day): 139.3 km <sup>2</sup> /sec <sup>2</sup> $C_3$ (10-day): 141 km <sup>2</sup> /sec <sup>2</sup> $C_3$ (15-day): 145 km <sup>2</sup> /sec <sup>2</sup>	$V_{HP}$ : 10.6 km/sec $RA$ : 0.017 rad (1.0°)  $DEC$ : 3.310 rad (189.6°) $ZAE$ : 2.543 rad (145.7°) $R_p$ : 2.3 $R_S$
* Ecliptic equinox system.		

(b) Deflection Maneuver and Probe Conic

Deflection Maneuver	Probe Conic Definition
Deflection Mode: Spacecraft Deflection Radius: 30 x 10 <sup>6</sup> km Coast Time: 31.2 days $\Delta V_{Earth}$ : 17.2 m/sec $\Delta V_{\perp}$ : 52.4 m/sec $\Delta V_{Total}$ : 69.6 m/sec	Entry Angle: -0.52 rad (-30°) Entry Latitude: * 0.436 rad (19.8°) Entry Longitude: * 1.234 rad (70.7°) Lead Time: 4900 sec Probe Spacecraft Range (entry): 1.07 x 10 <sup>5</sup> km Cone Angle (entry): 2.246 rad (128.7°) Cone Angle (EOM): 1.66 rad (95.0°) Probe Aspect Angle (entry): 0.202 rad (11.6°) Probe Aspect Angle (EOM): 0.271 rad (15.5°) Angle of Attack: 0.236 rad (13.5°)
* Planet equator - Sun.	

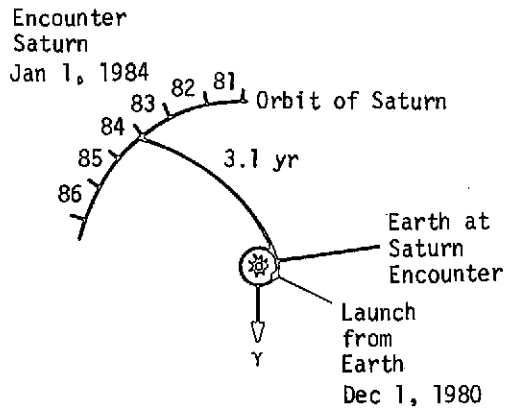
Table 4.3-2 Continued

(c) Dispersion Analysis Summary

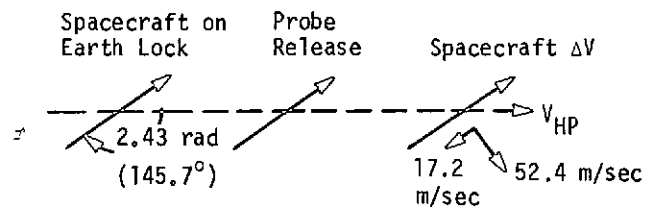
Navigation Uncertainties (1σ)	Execution Errors (3σ)	Dispersions (3σ)
Tracking: Range/Doppler SMAA: 1766 km SMIA: 827 km β: 1.633 rad (93.6°) TOF: 66.2 sec	ΔV <sub>⊥</sub> Proportionality: 1% ΔV <sub>⊥</sub> Pointing: 0.017 rad (1°) Probe Tipoff Error: 0.017 rad (1°)	Entry Angle: 0.020 rad (1.18°) Angle of Attack: 0.020 rad (1.17°) Downrange: 3384 km Crossrange: 4436 km Range: 3745 km Range Rate: 0.855 km/sec Probe Aspect Angle: 0.050 rad (2.85°) Cone Angle: 0.048 rad (2.76°)

(d) Entry and Descent Summary

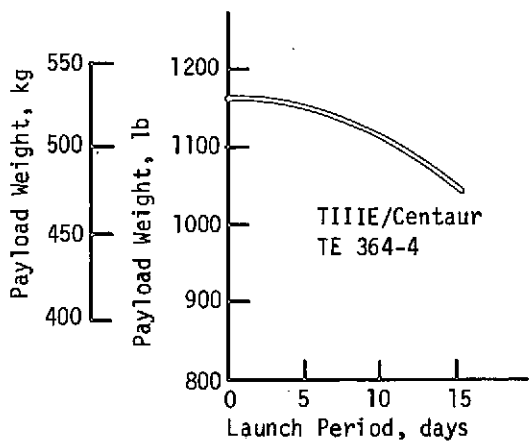
	Atmosphere Model		
	Warm	Nominal	Cool
Entry Parameters			
Entry Velocity, km/sec	36.89	36.99	37.045
Entry Altitude, km	968.5	536	297.0
Entry B, kg/m <sup>2</sup>	142.6	142.6	142.6
Maximum Deceleration, m/sec (g)	2275 (232)	3776 (385)	5737 (585)
Maximum Dynamic Pressure, N/m <sup>2</sup>	2.9 x 10 <sup>5</sup>	4.6 x 10 <sup>5</sup>	7.3 x 10 <sup>5</sup>
EOM Pressure, N/m <sup>2</sup> (bar)	10 <sup>6</sup> (10)	10 <sup>6</sup> (10)	10 <sup>6</sup> (10)
Descent B, kg/m <sup>2</sup>	161.3	161.3	161.3
Critical Entry Events			
0.98 m/sec <sup>2</sup> (0.1 g) Increasing, sec	14.0	6.0	2.0
490 m/sec <sup>2</sup> (50 g) Increasing, sec	34.0	17.0	8.0
29.4 m/sec <sup>2</sup> (3 g) Descending, sec	76.0	49.0	33.0
Maximum Deceleration, sec	41.0	23.0	12.0
Mach = 0.7, sec	96.0	61.0	38.0
EOM Time, minutes	63.0	42.6	27.3



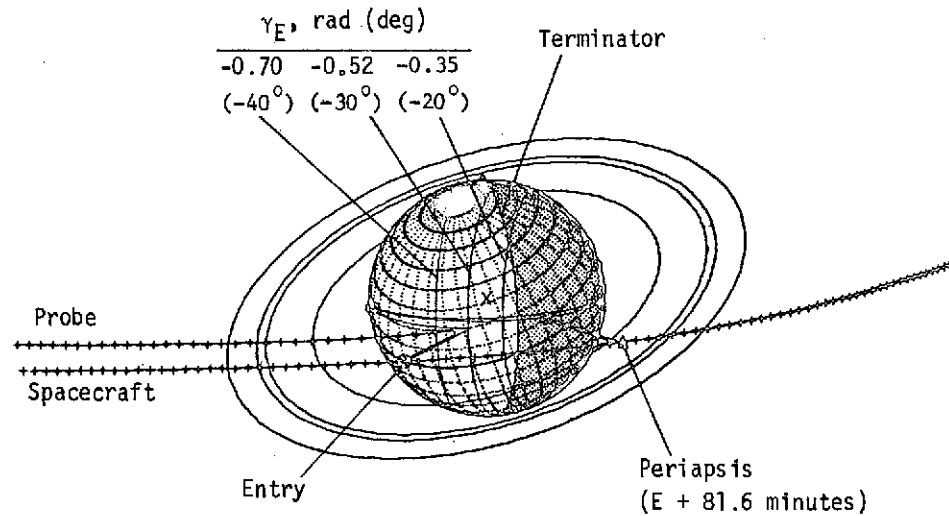
(a) Interplanetary Trajectory



(b) Deflection Maneuver



(c) Launch Analysis



(d) Planetary Encounter

4.3-11

Figure 4.3-2 Saturn/SU-80 Mission Definition

deflection  $\Delta V$  is applied in two components--one acting along the Earth line and the other perpendicular. A total  $\Delta V$  of 69.2 m/sec is required for the deflection maneuver, of which 52.4 m/sec is applied perpendicular to the Earth line.

#### Dispersion Analysis Summary and Entry and Descent Trajectories

Tables 4.3-2 (c) and 4.3-2 (d) summarize the dispersion analysis and entry and descent trajectories, respectively. The results are similar to those for the Saturn 1979 mission.

#### 4.3.2.3 Uranus/SU-80 Mission Definition

The 1980 Saturn/Uranus mission is shown in Figure 4.3-3 and detailed in Table 4.3-3.

#### Interplanetary Trajectory Selection

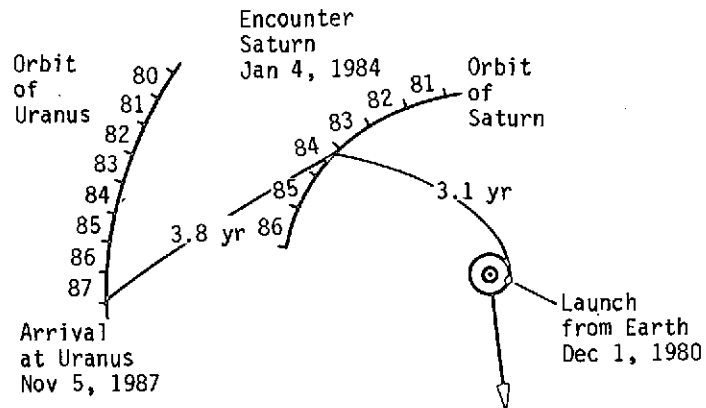
The 1980 Saturn/Uranus trajectory is a continuation of the 1980 Saturn trajectory [see Figure 4.3-3 (a)]. The total trip time from Earth to Uranus is 6.9 years.

#### Launch Analysis

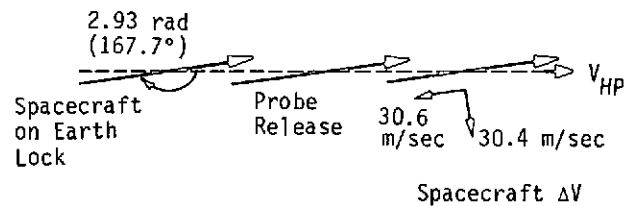
The launch analysis and results for the Uranus/SU-80 mission is shown in Figure 4.3-3 (b) and is identical to that for the Saturn/SU-80 mission.

#### Approach Trajectories

Uranus offers an intriguing target since its axis of rotation is nearly in the ecliptic plane. A retrograde approach trajectory was selected to reduce the entry angle of attack. The nominal entry angle of  $-0.61$  rad ( $-35^\circ$ ) resulted from a tradeoff between dispersions and peak deceleration. The resulting approach trajectory is shown in Figure 4.3-3 (d) and detailed in Table 4.3.3 (b). Note that a spacecraft periapsis radius of  $3 R_U$  results in an acceptable spacecraft-to-probe range at entry. The probe aspect angle, although relatively large [ $0.557$  rad ( $31.9^\circ$ )] at entry, increases to only  $0.625$  rad ( $35.8^\circ$ ) at EOM. The maximum and minimum cone angles occur at entry and EOM respectively, and vary from  $2.57$  rad to  $1.62$  rad ( $147^\circ$  to  $93^\circ$ ).



(a) Interplanetary Trajectory



(b) Deflection Maneuver

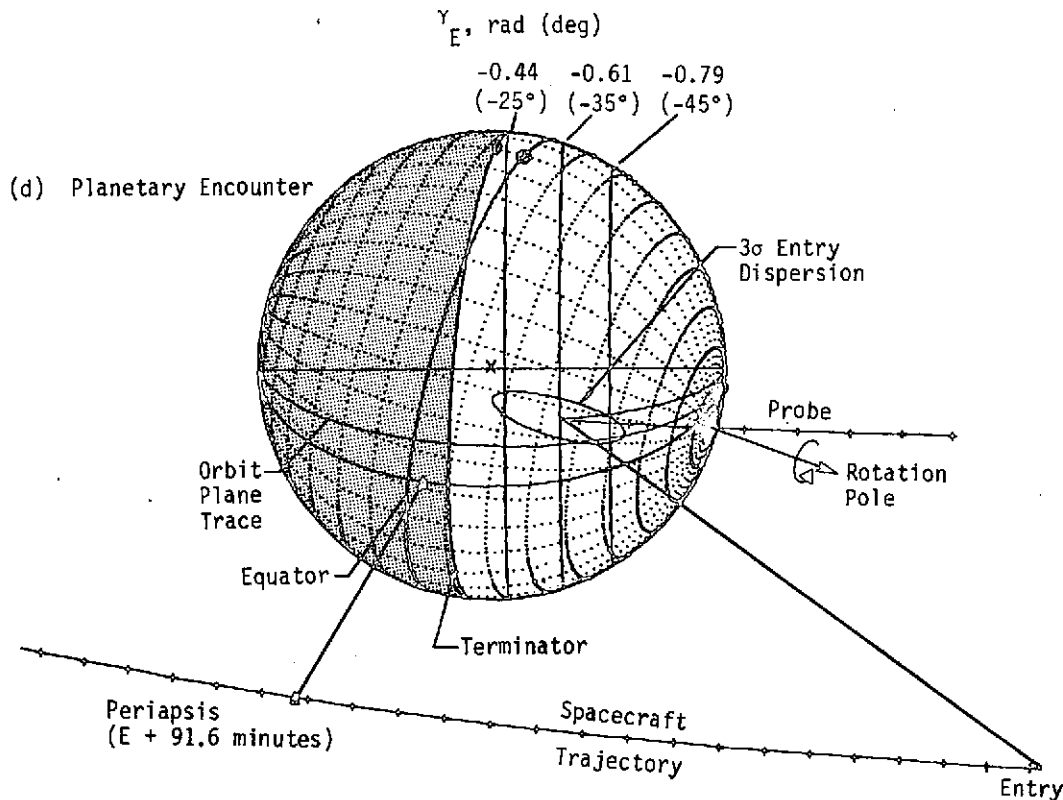


Figure 4.3-3 Uranus/SU 1980 Mission Definition

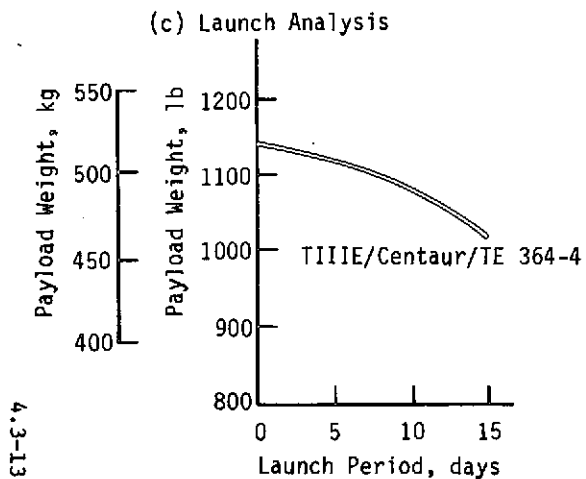


Table 4.3-3 Uranus/SU-80 Mission Summary

(a) Conic Trajectory Data

Interplanetary Trajectory	Launch Trajectory	Arrival Trajectory
Launch Date: 12/1/80 (2444574.5)  Arrival Date: 11/5/87 (2447105.5)  Flight Time: 2529 days 6.9 yr	Nominal $C_3$ : 138 km <sup>2</sup> /sec <sup>2</sup> Nominal DLA: 0.436 rad (25.0°)  $C_3$ (5-day): 139.3 km <sup>2</sup> /sec <sup>2</sup> $C_3$ (10-day): 141 km <sup>2</sup> /sec <sup>2</sup> $C_3$ (15-day): 145 km <sup>2</sup> /sec <sup>2</sup>	$V_{HP}$ : 13.8 km/sec RA: * -0.037 rad (-2.1°)  DEC: * 4.817 rad (276°) ZAE: 2.927 rad (167.7°) ZAP: 2.962 rad (169.7°)  $R_p$ : 3.0 $R_U$
* Ecliptic equinox system.		

(b) Deflection Maneuver and Probe Conic

Deflection Maneuver	Probe Conic Definition
Deflection Mode: Spacecraft Deflection Radius: 25 x 10 <sup>6</sup> km Coast Time: 20.8 days $\Delta V_{Earth}$ : 30.6 m/sec $\Delta V_{\perp}$ : 30.4 m/sec  $\Delta V_{Total}$ : 61 m/sec	Entry Angle: -0.61 rad (-35°) Entry Latitude: * 0.614 rad (35.2°) Entry Longitude: * 2.178 rad (124.8°) Lead Time: 5500 sec Probe/Spacecraft Range (entry): 94 x 10 <sup>3</sup> km Cone Angle (entry): 2.57 rad (147°) Cone Angle (EOM): 1.62 rad (93°) Probe Aspect Angle (entry): 0.557 rad (31.9°) Probe Aspect Angle (EOM): 0.624 rad (35.8°) Angle of Attack: 0.127 rad (7.3°)
* Planet equator - Sun.	



Table 4.3-3 Continued

(c) Dispersion Analysis Summary

Navigation Uncertainties ( $1\sigma$ )	Execution Errors ( $3\sigma$ )	Dispersions ( $3\sigma$ )
Tracking: Radio + Optical	$\Delta V_{\perp}$ Proportionality: 1%	Entry Angle: 0.230 rad (13.2°)
SMAA: 2088 km	$\Delta V_{\perp}$ Pointing: 0.017 rad (1°)	Angle of Attack: 0.072 rad (4.2°)
SMIA: 897 km	Probe Tipoff Error: 0.017 rad (1°)	Downrange: 3300 km
$\beta$ : 0.37 rad (21°)		Crossrange: 1650 km
TOF: 559 sec		Range: 2540 km
		Range Rate: 0.89 km/sec
		Probe Aspect Angle: 0.241 rad (13.8°)
		Cone Angle: 0.057 rad (3.3°)

(d) Entry and Descent Summary

	Atmosphere Model		
	Warm	Nominal	Cool
Entry Parameters			
Entry Velocity, km/sec	24.88	24.88	24.88
Entry Altitude, km	1073.8	532	200
Entry $B$ , kg/m <sup>2</sup>	142.6	142.6	142.6
Maximum Deceleration, m/sec <sup>2</sup> (g)	1451 (148)	2354 (240)	5590 (570)
Maximum Dynamic Pressure, N/m <sup>2</sup>	$1.8 \times 10^5$	$2.9 \times 10^5$	$7.07 \times 10^5$
EOM Pressure, N/m <sup>2</sup> (bar)	$10^6$ (10)	$10^6$ (10)	$10^6$ (10)
Descent $B$ , kg/m <sup>2</sup>	160	160	160
Critical Entry Events			
0.98 m/sec <sup>2</sup> (0.1 g) Increasing, sec	23.0	7.0	1.0
490 m/sec <sup>2</sup> (50 g) Increasing, sec	54.0	23.0	6.5
29.4 m/sec <sup>2</sup> (3 g) Descending, sec	101.0	58.0	27.5
Maximum Deceleration, sec	62.0	29.0	10.0
Mach = 0.7, sec	141.0	84.0	40.5
EOM Time, minutes	74.0	46.6	29.2

### Deflection Maneuvers

The deflection maneuver is performed at a radius of 25 million km ( $926 R_U$ ) from Uranus and results in a coast time of 20.8 days. The deflection  $\Delta V$ , (61 m/sec) is split almost equally between the radial and axial thrusters. This deflection sequence is shown in Figure 4.3-3 (b).

### Navigation and Dispersions

For the Uranus/SU-80 mission, optical tracking is required to supplement the standard Earth-based tracking. The optical instrument modeled in the software is an approximation of the V-slit scanner, which is presently the proposed approach guidance sensor. Note that the navigation results presented in Table 4.3-3 (c) are approximately equivalent to the radio-only results for Saturn and that the one-sigma time-of-flight error at Uranus is 9.3 minutes.

### Entry and Descent Trajectories

Table 4.3-3 (d) summarizes the entry and descent phases of the mission. Both entry and descent were simulated using all three atmospheric models. The descent time varies from 74 minutes in the warm atmosphere to 29 minutes in the cool atmosphere. The worst-case environment occurs 10 seconds after entry into the cool atmosphere. The maximum deceleration at this time is  $5590 \text{ m/sec}^2$  (570 g).

### 4.3.3 Launch and Interplanetary Trajectories

Opportunities for an Earth-to-Saturn transfer occur about every 12.3 months. These transfers can be divided into two types: (1) Type I transfers, which have central angles of less than  $3.14 \text{ rad}$  ( $180^\circ$ ), and (2) Type II transfers, which have central angles of greater than  $3.14 \text{ rad}$  ( $180^\circ$ ) and involve longer flight times. This study was limited to Type I transfers to Saturn in the 1979 and 1980 time frame.

#### 4.3.3.1 Launch Energy

Fixing the launch and arrival dates essentially determines the conic trajectory from Earth to Saturn. In the case of a swingby mission to Uranus, it also determines the arrival date at Uranus. Given these dates, the heliocentric position vectors of Earth at launch and Saturn at arrival are determined by Lambert's theorem. The energy (per unit mass) is a constant

on any given conic section and may be represented by the equation

$$E = \frac{V^2}{2} - \frac{\mu}{4} = \frac{V^2}{2} = \text{Constant.}$$

This leads to a common term in defining interplanetary trajectories,

$$C_3 = 2E = V_{HE}^2,$$

which represents twice the energy per unit mass of the spacecraft.

For a given launch vehicle, the payload that can be injected into an interplanetary trajectory is a function of the launch energy: the smaller the required energy, the larger the possible payload.

Figure 4.3-4 illustrates the payload capability of the launch vehicle considered in this study---the Titan IIIE/Centaur/TE 364-4. The data shown in the figure were taken from Reference 4.3-1, and were modified by subtracting 25.4 kg (56 lb), the weight of the spacecraft adapter.

Figure 4.3-5 shows the  $C_3$  contours for the launch years 1979, 1980, 1981, and 1982. Note that the required launch energy decreases progressively. In addition, note that the periapsis radius at Saturn required to take the spacecraft on to an encounter at Uranus increases progressively with the launch year. Using the data, reasonable selections of the launch date and arrival date can be made. The 1979 and the 1980 reference missions are indicated by a  $\odot$  on the respective launch date/arrival date contours.

#### 4.3.3.2 Launch Constraints

Other requirements in addition to launch energy must be considered in selecting the launch and arrival dates. A primary consideration involves the range safety constraint. Given a particular launch site the launch azimuth essentially determines the ground trace of the trajectory. The standard launch profile includes azimuths from 1.57 to 2.01 rad ( $90^\circ$  to  $115^\circ$ ). Because Cape Kennedy is at  $28.5^\circ$  N. Latitude, the maximum declination angle (DLA) for the launch asymptote would be 0.497 rad ( $28.5^\circ$ ) for a 1.57-rad ( $90^\circ$ ) launch azimuth and 0.63 rad ( $36^\circ$ ) for a 2.01-rad ( $115^\circ$ ) launch azimuth. Contours for  $DLA = 0.63$  rad ( $36^\circ$ )

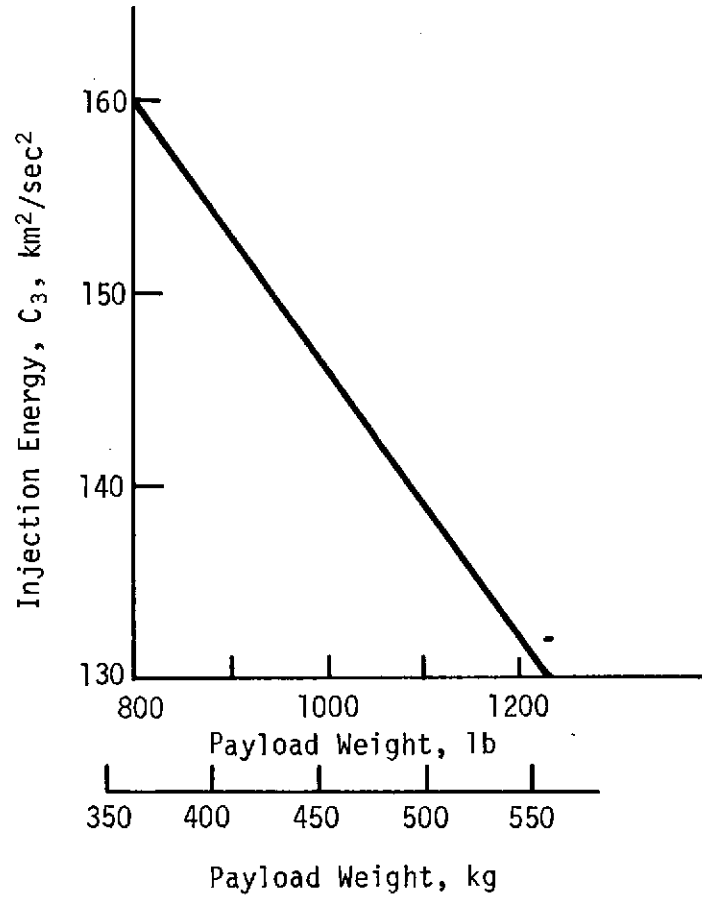
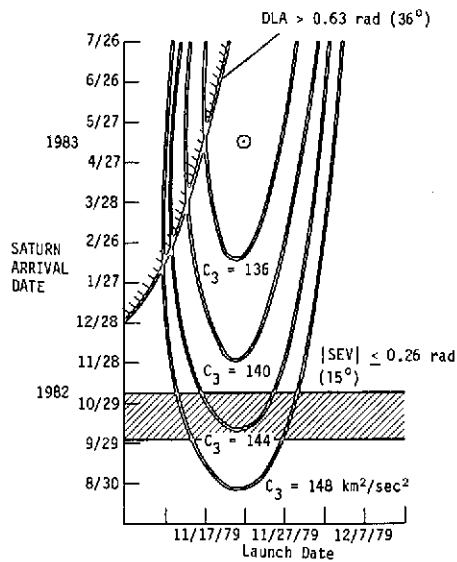
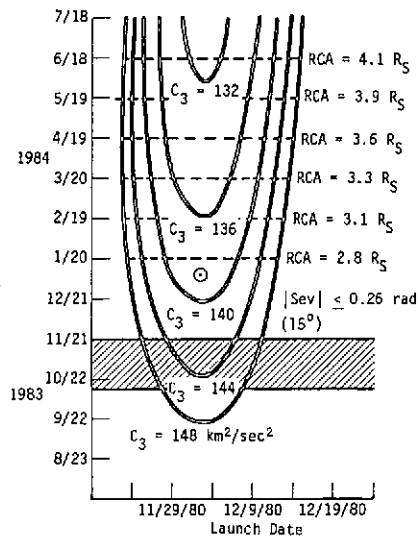


Figure 4.3-4 Titan IIIE/Centaur/TE 364-4 Performance Data



a) S-79 Launch Energy Contours



b) SU-80 Launch Energy Contours

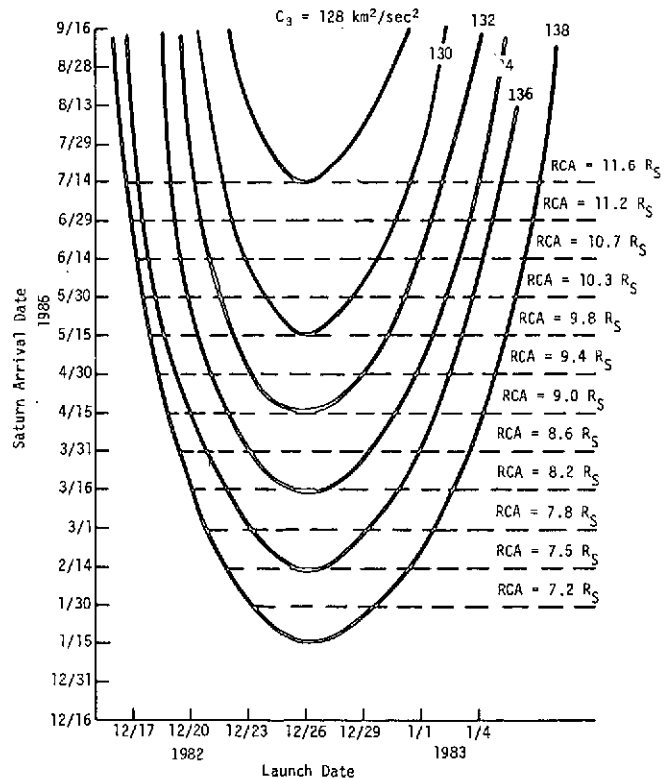
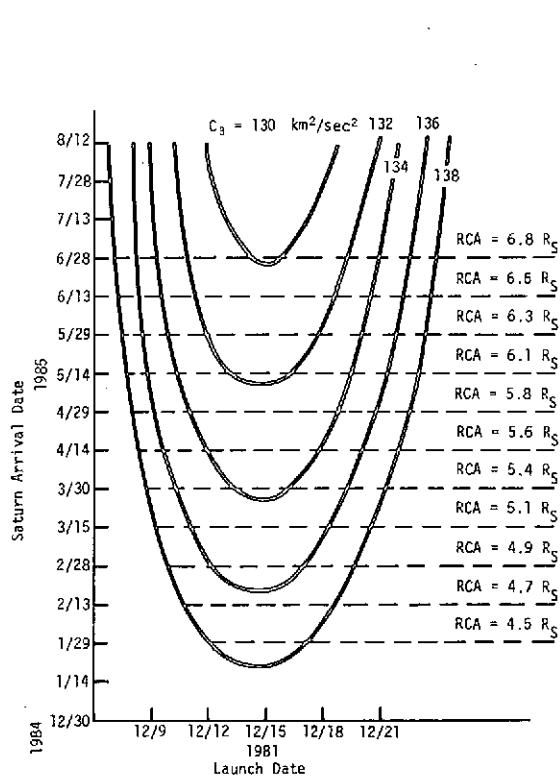


Figure 4.3-5 C<sub>3</sub> Launch Arrival Data Contours

are indicated on Figure 4.3-5. As shown, the constraint is most restrictive for the 1979 launch; after that it is of little consequence.

A second launch constraint is frequently imposed on the DLA to avoid navigation problems for the first midcourse maneuver. The uncertainty in the declination of the spacecraft has a singularity for DLAs in the vicinity of zero. Thus, the navigation process is degraded when the spacecraft's trajectory is near a declination of zero. The spacecraft will be on the launch asymptote 2 or 3 days after launch, and will therefore have the declination of the asymptote at that time. Since the declination is near zero, the critical tracking for the first midcourse will be impaired. To avoid this we have imposed a navigation constraint such that

$$|\text{DLA}| > 0.035 \text{ rad } (2^\circ)$$

The daily launch window defined by launches over azimuths from 1.57 to 2.01 rad (90° to 115°) must be at least 1 hour. The coast time in the parking orbit must be less than 1 hour, and hopefully, will be less than 30 minutes. Our evaluation shows that these constraints have not been violated.

#### 4.3.4 Approach Orbit Determination and Dispersions

The purpose of the approach orbit determination was to estimate the knowledge and control uncertainties at the probe deflection point. The dispersion analysis was conducted using Monte Carlo simulation and involved sampling from the control covariance, adding the effects of execution errors, propagating the trajectory through entry and descent, and tabulating the results. Parameters whose dispersions are most critical fall into two classes--entry parameters and communication parameters. Entry parameters refer to such variables as entry site, flight path angle, etc. Dispersions in these parameters can effect the science return of the mission. Communication parameters are quantities that describe the communication link between the probe and the spacecraft, such as the probe aspect angle, communication range, etc. Dispersions in the communication parameters must be accounted for in designing the telemetry link to ensure that the science data can be returned to Earth.

##### 4.3.4.1 Analytical Procedure and Ground Rules

The approach sequence used in the orbit-determination studies for the missions can be summarized as follows:

tracking is performed up to the point 5 days before the deflection event, at which time the thrusters are fired for the final mid-course maneuver. Mapping the knowledge plus execution error covariance forward to the probe deflection time determines the control covariance, and continuing to track the spacecraft up to the probe deflection maneuver results in the knowledge covariance.

The optical navigation analysis at Uranus assumed optical tracking for the full duration (40 days) of the tracking arc. In reality this is somewhat idealized since the V-slit scanner does not acquire Titanca (the largest satellite of Uranus) until E-25 days and hence termination of tracking should be delayed as long as possible. JPL's analysis differs from ours in this respect, however, the resultant B-plane error for both analyses is in close agreement.

For the missions considered in this study, the additional tracking does not greatly reduce the covariance, therefore the data will be presented only in terms of control uncertainties. In all cases, radio tracking is assumed to be performed by the Deep Space Network (DSN). Our navigation analyses concentrated on the 1979 Saturn direct and on Uranus/SU-80 missions. The coordinate system used was the ecliptic equinox system.

The principal variables that affect the navigation and guidance analysis are tracking station location uncertainties, tracking station measurement noise, and planetary mass and ephemeris uncertainties. The DSN tracking data used in this study are shown in Table 4.3-4, and the ephemeris and mass uncertainties are shown in Table 4.3-5. The equivalent station location errors are a compromise between the "loose" constraints of  $\sigma_{RS} = 1$  m,  $\sigma_{\Delta\lambda} = 2$  m and the "tight" constraints of  $\sigma_{RS} = 3$  m,  $\sigma = 5$  m used by JPL in their analysis of the missions (Reference JPL 760-88, "Navigation Analysis for Advanced Pioneer Outer Planet Probe Missions", C. K. Paul and R. K. Russell).

At Uranus, ground-based tracking stations are unable to observe any significant gravitational effect of the planet on the trajectory until the spacecraft is quite near the planet. Therefore, an onboard optical tracker is necessary at Uranus to reduce the navigation uncertainties to a reasonable level. The optical tracker simulated in our analysis is an approximation of the V-slit scanner. The V-slit scanner was modeled as a star planet angle with error sources including bias and noise, which we assumed to be on the order of 0.0029 rad (10 arc-sec) ( $1\sigma$ ).

Table 4.3-4 DSN Tracking Data Summary

Tracking Station	Equivalent $1\sigma$ Station Location Errors	
Madrid	Distance from Earth's Spin Axis, m	1.5
Canberra	Longitudinal Distance, m	3.0
Goldstone	Distance Parallel to Spin Axis, m	10.0
	Longitudinal Correlation of Station, deg	0.97
<p>* Doppler noise = 0.5 m, <math>5 \times 10^4</math> sec count time = 0.3 mm/sec for 1-minute count time.</p> <p>Range noise: 150 m.</p>		

Table 4.3-5 Planetary Ephemeris and Mass Uncertainties ( $1\sigma$ )

Error	Saturn	Uranus
In-Orbit Track, km	750	10,000
Radial, km	750	10,000
Out-of-Plane, km	250	2,000
Mass	$1.13 \times 10^{-4} M_S$	$3.7 \times 10^{-3} M_U$



#### 4.3.4.2 Deflection Dispersion Trends

##### Execution Error Levels

The errors in executing the deflection maneuver are assumed to apply only to the component of  $\Delta V$  perpendicular to the Earth-line vector and arise from three sources:

- 1)  $\Delta V$  proportionality error - This is the error in measuring the magnitude of the delivered deflection,  $\Delta V$ . Normally, the  $3\sigma$  uncertainty for this error is about 1%;
- 2)  $\Delta V$  pointing error - This is the error between the direction of the net delivered  $\Delta V$  and the commanded direction;
- 3) Probe orientation error - This is the error in measuring the orientation of the probe as it is deflected from the spacecraft.

##### Navigation Uncertainties versus Execution Errors

Entry dispersions are produced both by errors in measuring the position and orientation of the spacecraft at deflection (which are caused by navigation uncertainties) and errors on the delivering the proper deflection  $\Delta V$  (which are caused primarily by implementation errors). Table 4.3-6 compares the relative contribution of these two error sources for the Saturn 1979 mission. The Uranus mission is not shown since the dispersions at Uranus are almost totally caused by navigation uncertainties, and the execution errors have little effect.

Table 4.3-6 shows that navigation and execution errors have about an equal effect on the dispersions. In addition, note that the magnitude of the execution error has a significant effect on the dispersions.

##### Entry Angle

The variations in dispersions are illustrated in Table 4.3-7 as a function of the entry angle. The table is based on assumed execution errors of 1% in proportionality, 0.017 rad ( $1^\circ$ ) in orientation. All dispersion analyses were conducted assuming optical tracking and a deflection radius of  $25 \times 10^6$  km for entry angles of  $-0.52$  rad ( $-30^\circ$ ),  $-0.61$  rad ( $-35^\circ$ ),  $-0.79$  rad ( $-45^\circ$ ), and  $-1.05$  rad ( $-60^\circ$ ).

Table 4.3-6 Entry Dispersions ( $3\sigma$ ) for Execution Error Levels of Saturn 1979 Mission

$\Delta V$ Pointing Error ( $3\sigma$ ), rad (deg)	Range, km	Range Rate, km/sec	Probe Aspect Angle, rad (deg)	Spacecraft Probe Look Angle	
				CA, rad (deg)	CLA rad (deg)
No Errors	1,304	0.46	0.0369 (2.12)	0.0138 (0.79)	0.022 (1.28)
0.0174 (1.0)	3,745	0.855	0.0498 (2.85)	0.094 (5.4)	0.0428 (2.4)
0.0349 (2.0)	7,345	1.429	0.075 (4.31)	0.17 (9.6)	0.054 (3.11)
0.0524 (3.0)	10,988	2.1	0.105 (6.0)	0.25 (14.4)	0.098 (5.6)

The general trend of the data is predictable: the shallower the entry angle, the larger the dispersion in the entry parameter. Note that of all the parameters considered, the entry time is least affected by variations in the entry angle. On the contrary, the range and entry footprint are most affected. The relatively large dispersions in these parameters is a direct result of the degraded navigation at Uranus.

#### Navigation Types

For Saturn and Uranus missions, navigation uncertainties play an important role in generating entry dispersions. Table 4.3-8 compares the dispersions resulting from three different tracking assumptions. The first two columns show the dispersions resulting from the JPL-generated covariances. Martin Marietta's orbit determination assumptions are detailed in Table 4.3-4.

Table 4.3-7 Entry Dispersions ( $3\sigma$ ) as a Function of Entry Angle, Uranus Mission

Mission	Entry Angle, rad (deg)	Entry Time, minutes	Entry Angle, rad (deg)	Angle of Attack, rad (deg)	Entry Site		Spacecraft Probe Direction		Range, km	Range Rate, km/sec	Probe Aspect Angle, rad (deg)
					SMAA, rad (deg)	SMIA, rad (deg)	CA, rad (deg)	CLA, rad (deg)			
Uranus SU-80	-0.52 (-30)	29.15	0.267 (15.3)	0.087 (5.0)	0.37 (21.2)	0.077 (4.4)	0.02 (1.16)	0.08 (4.8)	3121	1.13	0.28 (16.0)
	-0.61 (-35)	28.65	0.23 (13.2)	0.073 (4.2)	0.32 (18.2)	0.084 (4.8)	0.005 (0.31)	0.06 (3.34)	2539	0.89	0.24 (13.8)
	-0.78 (-45)	28.09	0.19 (10.8)	0.078 (4.5)	0.26 (14.8)	0.108 (6.2)	0.006 (0.34)	0.04 (2.4)	1978	0.73	0.21 (12.1)
	-1.04 (-60)	27.14	0.12 (6.9)	0.038 (2.2)	0.24 (13.5)	0.103 (5.9)	0.007 (0.42)	0.03 (1.6)	1161	0.33	0.09 (5.3)

Table 4.3-8 Comparison of Dispersions for JPL and Martin Marietta Orbit Determination Results

3 $\sigma$ Dispersion	1979 Saturn Direct		
	"Tight" *	"Loose" *	Martin Marietta *
Entry Angle, rad (deg)	0.03 (1.7)	0.05 (2.98)	0.02 (1.18)
Angle of Attack, rad (deg)	0.02 (1.3)	0.03 (1.74)	0.02 (1.17)
Probe Aspect Angle, rad (deg)	0.05 (3.03)	0.06 (3.4)	0.05 (2.85)
Flight Time, minutes	3.65	7.02	4.56
Range, km	3811	4998	3745
Range Rate, km/sec	1.06	1.64	0.855
Entry Footprint			
Downrange Angle, rad (deg)	0.02 (1.2)	0.03 (1.5)	0.03 (1.58)
Downrange Distance, km	1256	1545	1661
Crossrange Angle, rad (deg)	0.06 (3.2)	0.1 (5.8)	0.04 (2.2)
Crossrange Distance, km	3372	6075	2293

\*Station location error assumptions:

"Tight" corresponds to  $\sigma_{RS} = 1$  m,  $\sigma_{\Delta\lambda} = 2$  m.

"Loose" corresponds to  $\sigma_{RS} = 3$  m,  $\sigma_{\Delta\lambda} = 5$  m.

Martin Marietta corresponds to  $\sigma_{RS} = 1.5$  m,  $\sigma_{\Delta\lambda} = 3$  m.

In all cases, execution errors amount to 1% in proportionality, 0.017 rad ( $1^\circ$ ) in  $\Delta V$  pointing, and 0.017 rad ( $1^\circ$ ) in probe orientation. The deflection radius is  $30 \times 10^6$  km and the nominal entry angle is  $-0.52$  rad ( $-30^\circ$ ). Note how the dispersions depend on the station location errors. This is particularly true for the flight time and range dispersions. In our baseline design, the Martin Marietta-generated navigation dispersions were used in sizing the respective subsystems. As shown in Table 4.3.9, our results are not significantly different from those generated by JPL.

#### 4.3.5 Planetary Encounter

The planetary encounter phase of the mission encompasses the deflection maneuver, acquisition, entry, and descent. The primary problems associated with planetary encounter include designing the communication relay link, selecting the approach trajectory, and the deflection maneuver. The primary emphasis of our approach was on selecting a common approach geometry at Saturn and Uranus.

The key parameters associated with the analysis of the relay link are the cone angle, probe aspect angle, range, and range rate. During preentry, the probe is assumed to move on a conic trajectory in an attitude coincident with the spacecraft-to-Earth vector at deflection. For this attitude, the probe generally enters with a nonzero angle of attack. Then, during the entry phase, the probe rotates so its axis is radial relative to the center of the planet. During descent, the probe descends along a radius vector as that vector rotates about the center of the planet at the angular rotation rate of the planet.

Ideally, the distance between the probe and the spacecraft should be as small as possible since the relay link power increases in direct proportion to the square of the range. The most significant orbital parameter that affects the communication range is the spacecraft's periapsis radius. For this reason, we set the minimum spacecraft periapsis radius equal to  $2.3 R_S$  at Saturn. For Uranus, we set the periapsis radius at  $3.0 R_U$  as a compromise between a reasonable range and a tolerable spread in cone angles for entry and EOM.

Table 4.3-9 Comparison of Martin Marietta and JPL Orbit Determination Results

Planet Model <sup>*</sup>	Control Uncertainty (1 $\sigma$ )		
	SMAA, km	SMIA, km	TOF, sec
Saturn <sup>†</sup>			
Martin Marietta	1839	812	80.2
"tight"	1805	1077	54.1
"Loose"	3195	1170	99.5
Saturn <sup>§</sup>			
Martin Marietta	1766	827	66.2
"tight"	1776	1115	46.9
"Loose"	3249	1189	86.5
Uranus <sup>¶</sup> (radio + optical)	2088	897	559
<p><sup>*</sup>Station location error assumptions:  "tight" corresponds to <math>\sigma_{RS} = 1</math> m, <math>\sigma_{\Delta\lambda} = 2</math> m;  "Loose" corresponds to <math>\sigma_{RS} = 3</math> m, <math>\sigma_{\Delta\lambda} = 5</math> m;  Martin Marietta Corresponds to <math>\sigma_{RS} = 1.5</math> m, <math>\sigma_{\Delta\lambda} = 3.0</math> m.</p> <p>Deflection radius, km</p> $\left. \begin{array}{l} \text{† Saturn 1979} \\ \text{§ Saturn 1980} \end{array} \right\} 30 \times 10^6 \text{ km}$ $\text{¶ Uranus SU/1980} \quad 25 \times 10^6 \text{ km}$			

The PAA is the angle between the longitudinal axis of the probe and the probe-to-spacecraft vector. The importance of obtaining small PAAs during the descent phase of the mission is very dependent on the beamwidth of the probe antenna. Our strategy is to accept a reasonably broadband probe antenna and concentrate on reducing the beamwidth of the spacecraft antenna. For our design the beamwidth of the probe antenna is 1.75 rad (100°) and PAAs less than 0.70 rad (40°) result in reasonable antenna gains.

The lead time is defined as the time from entry to spacecraft periapsis. It is primarily a mission analysis targeting parameter and can be effectively used to vary the communication range and the cone angle at entry. Increasing the lead time has the effect of increasing both the range and the cone angle.

The cone angle is the angle subtended by the spacecraft-to-Earth and the spacecraft-to-probe vectors. Both the magnitude and variation of the cone angle are important factors in determining the characteristics of the spacecraft's relay link antenna.

The final communication geometry at both Saturn and Uranus resulted from an iterative procedure that began with the spacecraft directly over the probe midway through descent. From this point, the lead time was parametrically varied to yield cone angles at Saturn and Uranus that were compatible with the beamwidth and orientation of the spacecraft antenna. This resulted in a small, but acceptable, increase in range.

The resulting planetary encounter characteristics for the Saturn 1979, Saturn/SU-80, and Uranus/SU-80 missions are summarized in Section 4.3.1. Note that for entry and descent at Saturn, there is a possibility that the probe may rotate past the terminator. A descent to  $10^6 \text{ N/m}^2$  (10 bar) in the warm atmosphere requires 63 minutes. During this time, the planet rotates 0.63 rad (36°), placing the probe approximately at the terminator at EOM. If this poses a serious problem, either the probe can be targeted to a higher latitude or a higher [ $< -9.52 \text{ rad}$  ( $< -30^\circ$ )] entry angle could be used to displace the entry site further from the terminator. Of these two solutions, targeting the probe to a higher latitude has the least impact on the system.

#### 4.3.6 Planetary Entry

The key mission design parameters associated with the probe entry phase are the ballistic coefficient (B), entry flight path angle, ( $\gamma_E$ ), entry angle of attack ( $\alpha_E$ ), and probe science deployment time.

Figures 4.3-6 and 4.3-7 show the peak deceleration in Earth g's during entry, both as a function of  $\gamma_E$  and the model atmosphere, at Saturn and Uranus, respectively. Note that using the nominal  $\gamma_E$  of  $-0.52$  rad ( $-30^\circ$ ) at Saturn results in a peak deceleration of  $5742$  m/sec<sup>2</sup> (585 g), whereas the peak deceleration levels reach  $5590$  m/sec<sup>2</sup> (570 g) for the nominal  $\gamma_E$  of  $-0.61$  rad ( $-35^\circ$ ) at Uranus. In each case, the highest deceleration loads are experienced for entries into the cool atmosphere.

A particularly interesting item is the large variation in the expected decelerations at Uranus. For the nominal entry angle [ $\gamma_E = -0.61$  rad ( $-35^\circ$ )], the possible spread in peak deceleration ranges from  $1452$  to  $5590$  m/sec<sup>2</sup> (148 to 570 g).

##### 4.3.6.1 Selection of the Entry Ballistic Coefficient

The primary considerations in selecting the entry ballistic coefficient were to make the deployment conditions compatible with technology requirements and science objectives. The aeroshell nose cap is deployed 20 seconds after the probe senses a decreasing level of  $29.4$  m/sec<sup>2</sup> (3 g), and the mass spectrometer measurements then begin. For the purpose of correlating spacecraft occultation data with probe measurements, it is desirable to begin the science measurements above the  $1 \times 10^4$  N/m<sup>2</sup> (100 mb) pressure level.

Aerodynamic considerations dictate that the nose cap be deployed at subsonic velocity. During the contract we performed a parametric study to investigate the effect of entry angle, ballistic coefficients, and model atmospheres on the conditions at nose cap deployment. The results of our study are shown in Figure 4.3-8. Note that the staging altitude is most sensitive to variations in the entry ballistic coefficient for the warm-atmosphere model. Also note that there is a strong similarity in the staging altitudes for Saturn and Uranus. The most stringent mission--in terms of satisfying the science requirement of deploying the nose cap at an altitude above  $1 \times 10^4$  N/m<sup>2</sup> (100 mb)--is for an entry into the Saturn cool atmosphere, where the nose cap is deployed at 114 mb. For this mission deploying the nose cap 14 mb late has virtually no impact on the science return during descent.



Note:  $B = 142.6 \text{ kg/m}^2$   
 $(0.908 \text{ slug/ft}^2)$

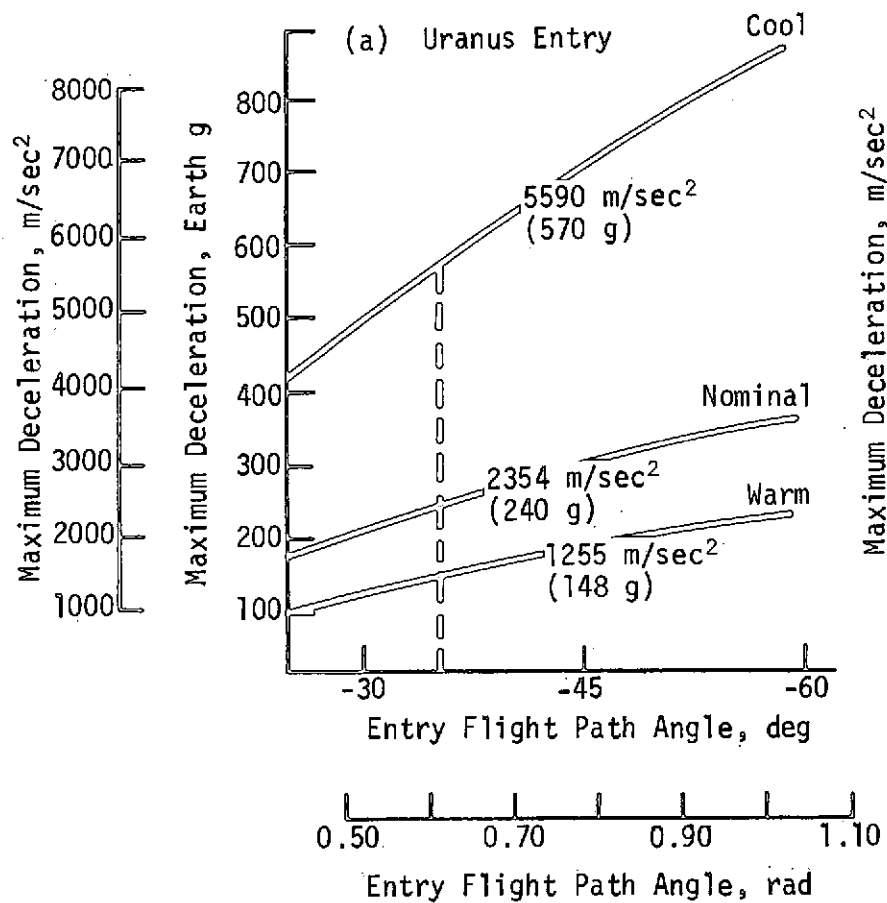


Figure 4.3-6 Peak Entry Deceleration, Uranus

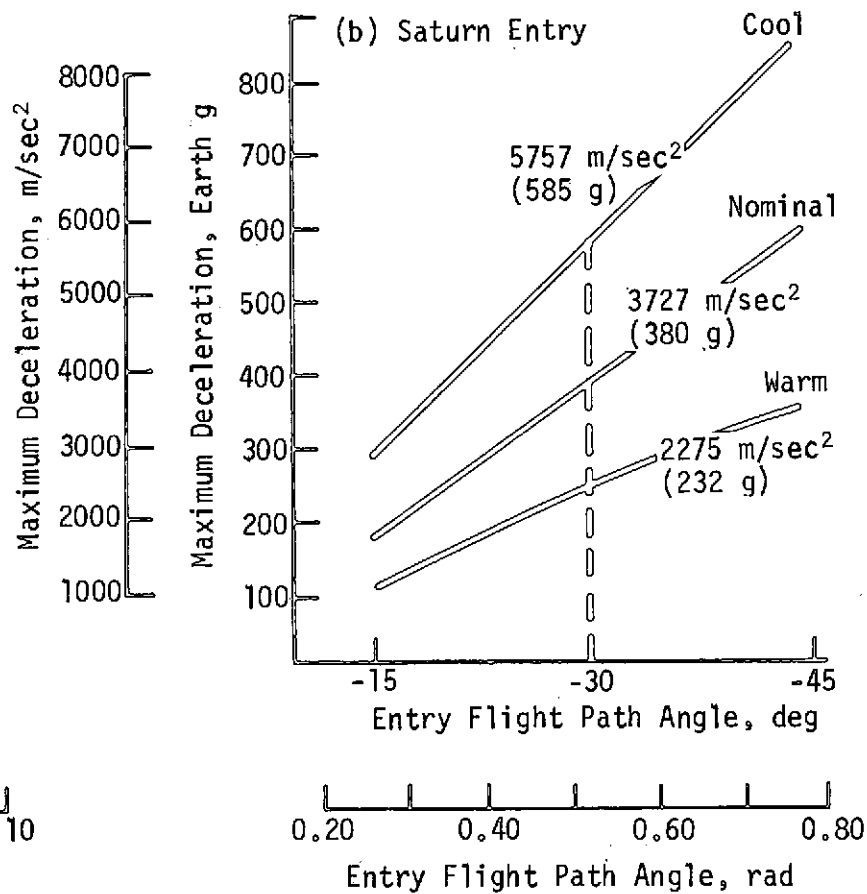


Figure 4.3-7 Peak Entry Deceleration, Saturn

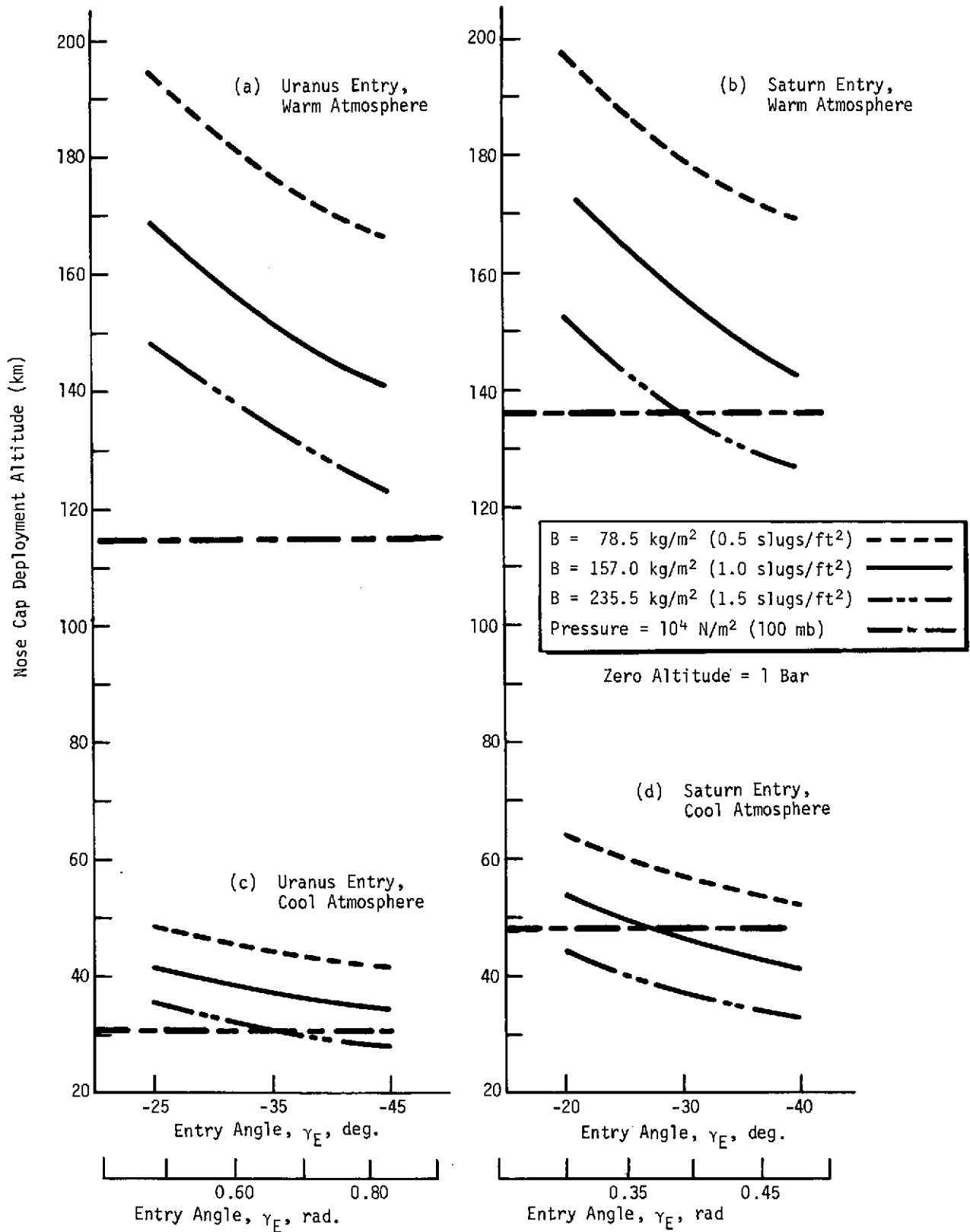


Figure 4.3-8 Saturn and Uranus Deployment Conditions

Ideally, it is desirable to select as large an entry ballistic coefficient as possible to reduce mission time; however, for the Saturn cool-atmosphere mission, the maximum value that can be attained while simultaneously satisfying the science constraints is  $B = 157 \text{ kg/m}^2$  ( $1.0 \text{ slug/ft}^2$ ). The entry ballistic coefficient used for the baseline probe configuration was accordingly chosen as  $B = 142.5 \text{ kg/m}^2$  ( $0.908 \text{ slug/ft}^2$ ). This value resulted from packaging constraints arrived at from mechanical design considerations.

#### 4.3.6.2 Entry Dynamics Analysis

The dynamic characteristics of the probe during entry were evaluated to define the probe's mass control requirements and to determine the subsystem design requirements imposed by the entry environment. A number of dynamic analyses were conducted, primarily at Uranus, using the cool-atmosphere model. All entries were made using a flight path angle of  $-0.61 \text{ rad}$  ( $-35^\circ$ ). The high dynamic pressure gradient built up for the Uranus entry results in excellent angle-of-attack convergence between entry and maximum dynamic pressure. These results can be misleading in terms of subsystem design environments. As a result, a subsequent analysis was performed to investigate the impact of an imperfect mass balance and high entry angles-of-attack on the probe's dynamic characteristics. The total-angle-of-attack envelopes are summarized in Figure 4.3-9 for values of  $\alpha_E$  ranging from  $0.17$  to  $0.44 \text{ rad}$  ( $10^\circ$  to  $25^\circ$ ).

The key factor in Figure 4.3-9 is that with no lateral center of gravity (c.g.) offset ( $Z_{c.g.}$ ), the angle of attack converges to a few tenths of a degree at maximum dynamic pressure ( $q_{max}$ ). Introducing a lateral c.g. offset--i.e., moving the actual c.g. off the geometric centerline a distance of  $0.25 \text{ cm}$ --made  $\alpha_{trim}$  approximately  $0.0140 \text{ rad}$  ( $0.8^\circ$ ). For the high- $\alpha_E$  case, the change in the rate of decay of  $\alpha_{total}$  is due to gyroscopic effects that occur early in the entry.

In addition to studying the convergence of the angle of attack, we also studied the effects of lateral accelerations and changes in the spin rate. For models with virtually no c.g. offset, the lateral loads are low and symmetrical [less than  $19.6 \text{ m/sec}^2$  ( $2 \text{ g}$ )]. Introducing a c.g. offset results in unsymmetrical loading and increases the lateral loads at

the c.g. to  $118 \text{ m/sec}^2$  (12 g). These lateral loads are imposed at a frequency of approximately 20 cycles per second. Since they are small compared to the maximum longitudinal load of  $5590 \text{ m/sec}^2$  (570 g), they should not create a design problem.

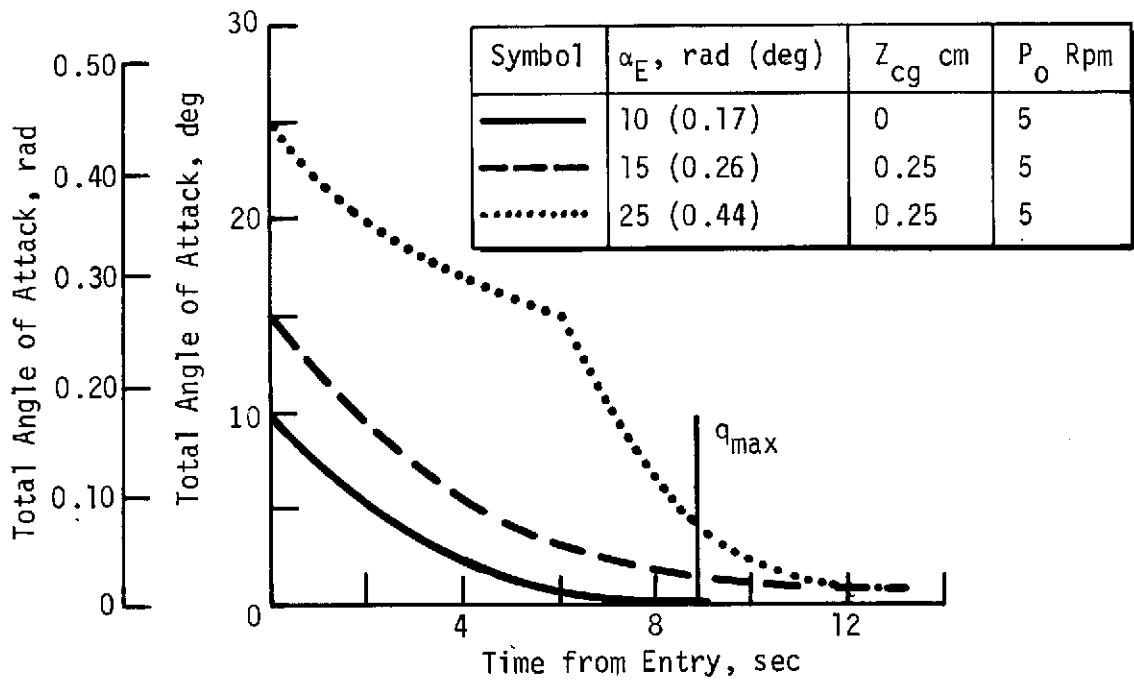


Figure 4.3-9 Total Angle of Attack Envelope, Uranus Entry  
 $\gamma_E = -0.61 \text{ rad} (-35 \text{ deg})$

## 4.4 System Design and Integration

## 4.4 SYSTEM DESIGN AND INTEGRATION

### 4.4.1 Analyses and Tradeoffs

The following sections describe the system-level analyses and tradeoff studies conducted to evaluate preentry data transmission, various nose cap deployment times, radiation levels and dual versus single data return.

#### 4.4.1.1 Preentry Transmission Tradeoff

For the SU mission the baseline and alternate configurations collect preentry engineering data and transmit the data, in real time, to the spacecraft at a rate of 2 bps for approximately 1 minute after the probe has been acquired. The RF power amplifier is then turned off until after entry, during which time communications are blacked out.

The intent of this preentry transmission was to determine the status of the probe subsystems and science instruments just prior to entry. The entry arrival uncertainty, however, stops the transmission of status data as early as 68.6 minutes before entry for Uranus, and as early as 19.4 minutes before entry for Saturn. Transmitting until the probe deceleration increases to 0.1 g would give status data up to entry, but would require extra power. Therefore, using the mission sequence and power profile for the alternate configuration and making the sequence similar to that for the final configuration simplifies the probe (see Table 4.4-1). Based on these data, preentry transmission has not been included in our definition of the final configuration. Preentry transmission is further discussed in Section 4.5.

#### 4.4.1.2 Nose Cap Deployment Analysis

The nose cap on the alternate and final probes must be removed before the neutral mass spectrometer and pressure gauges can start making measurements. Two constraints determine when the nose cap is deployed:

- 1) The science measurements should start at pressures of  $10^4$  N/m<sup>2</sup> (100 mb) or less so that these data can be correlated with the spacecraft occultation data;
- 2) The nose cap should be deployed at subsonic velocities to simplify the design of the deployment device at a lower dynamic pressure.

Table 4.4-1 Alternate Probe Comparison with and without Preentry Transmission

Advantages of Preentry Transmission	Disadvantages of Preentry Transmission
<p>Preentry Condition Established:</p> <p>Uranus - As late as E - 21 sec                      As early as E - 68.6 minutes</p> <p>Saturn - As late as E - 21 sec                      As early as E - 19.4 minutes</p> <p>Acceptable Communication Geometry            Obtained without Added Targeting            Constraint</p>	<p>4% Battery Capacity Increase Required</p> <p>1% Battery Weight Increase Required</p> <p>DTU &amp; S/C Receiver Modifications needed            for Low Data Rate</p>

This analysis was made primarily for the final configuration. As can be seen from Figure 4.4-1, this analysis is needed because of the large variation of the six curves. Table 4.4-2 shows the various (decreasing) g-levels and timing intervals that were investigated. Based on the results of the analysis, three g-levels-- 98, 49 and 26.4 m/sec<sup>2</sup> (10, 5 and 3 g)--were selected, along with a subsonic velocity of M = 0.95.

Note that the Uranus warm atmospheric model establishes the highest Mach number, the Saturn cool determines the highest pressure, and that the lowest g-level best meets the design constraints. Since a value of 3 g (decreasing) was considered the lowest limit for reliable performance, the deployment time was chosen as 29.4 m/sec<sup>2</sup> + 20 seconds (3 g + 20 sec) to better assure a subsonic velocity. The deployment devices will be designed to meet the highest dynamic pressure, 2230 N/cm<sup>2</sup>.

#### 4.4.1.3 Radiation Analysis

A radiation analysis was conducted on the final probe configuration to determine the environment to which the materials and component piece-parts could be subjected. Reference 4.4-1 gives the radiation environment in the spacecraft electronic equipment compartment due to the two spacecraft radioisotope thermoelectric generators (RTGs) and the Saturnian radiation belts as follows:

<u>Source</u>	<u>Environment</u>
RTGs	$7 \times 10^{10}$ neutrons/cm <sup>2</sup> (1 to 5 MeV Energy)
Saturnian Radiation Belts	$1.5 \times 10^{11}$ electrons/cm <sup>2</sup> (1 to 10 MeV Energy)
	$3 \times 10^{10}$ protons/cm <sup>2</sup> (2 to 100 MeV Energy)

Calculations by Mr. A. Wilbur of NASA-ARC, using the plutonium now available, reduces the RTG environment to  $1 \times 10^{10}$  n/cm<sup>2</sup>. Since the probe is aft of the plane passing through the spacecraft RTGs and the spacecraft electronics compartment, the probe radiation due to the RTGs is less than  $1 \times 10^{10}$  n/cm<sup>2</sup> using the plutonium now available.

The probe also includes ten 1-W radioisotope heater units (RHUs) for thermal control. The gamma and neutron fluxes for each RHU are 0.7 mr/hr at a distance of 100 cm and 8.68 n/cm<sup>2</sup>-sec at the same distance. A point on the outside of the digital telemetry unit (DTU) nearest the RHUs, and in the plane of the RHUs, was selected for the analysis. The distance to the RHUs varied from 10.4 cm to 55 cm, with an average of 36.6 cm. Based on a mission lasting 61,320 hours ( $2.2 \times 10^8$  sec), the RHUs contribute a total of  $0.4 \times 10^{10}$  n/cm<sup>2</sup> and  $0.75 \times 10^3$  rad to the probe environment due to the use of plutonium which is presently available.



4.4-4

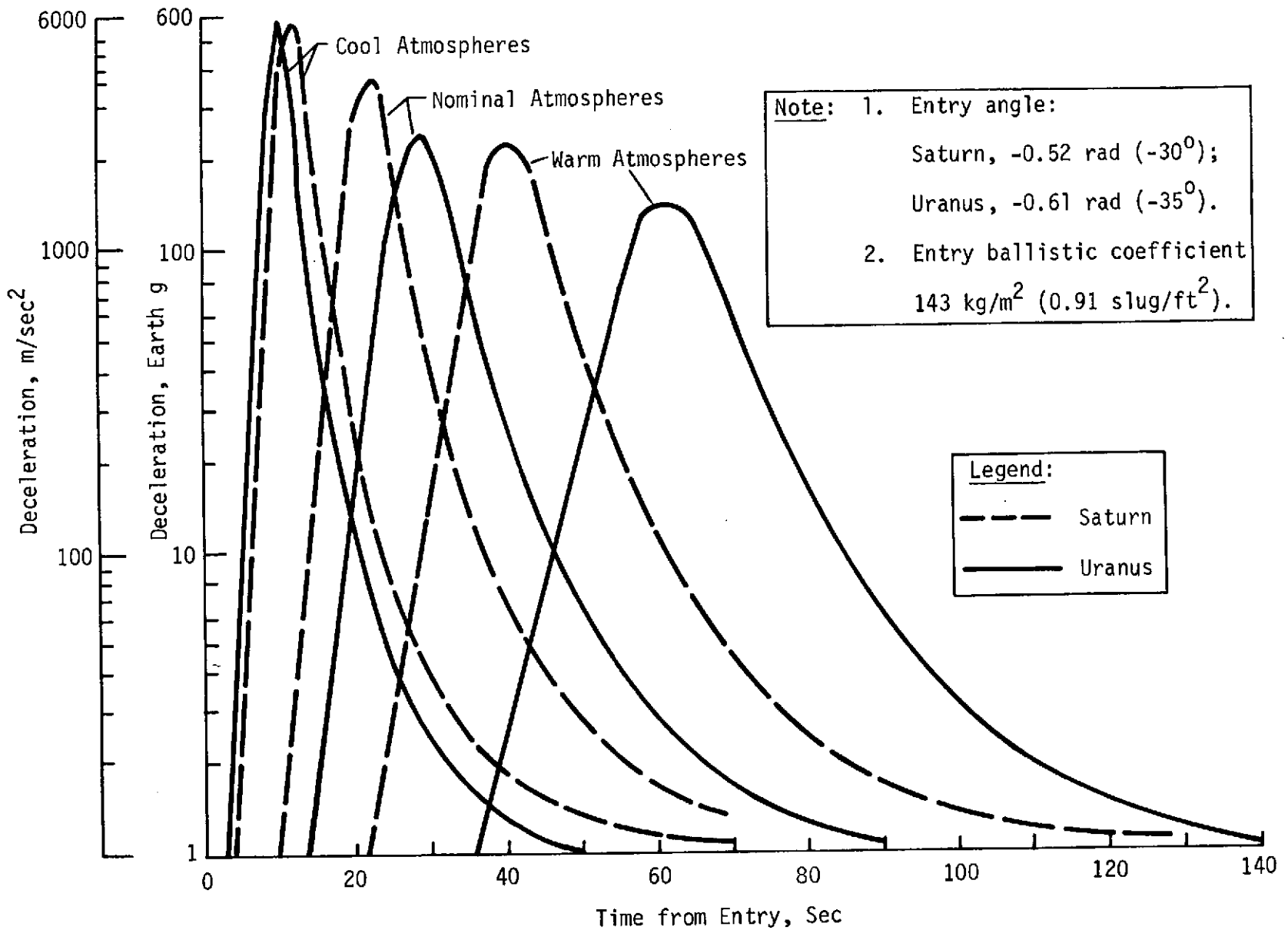


Figure 4.4-1 Probe Deceleration, Extreme Atmospheres

Table 4.4-2 Nose Cap Deployment Analysis

	Saturn			Uranus		
	Cool	Nominal	Warm	Cool	Nominal	Warm
10g + 30 sec	E + 55 sec	E + 68 sec	E + 92 sec	E + 51 sec	E + 76 sec	E + 115 sec
Mach No.	0.48	0.61	0.75	0.57	0.78	(0.95)
Pressure, mb	(117.3)	82.0	60.4	61.6	45.3	36.1
5g + 22 sec	E + 51 sec	E + 65 sec	E + 90 sec	E + 46.5 sec	E + 74 sec	E + 115 sec
Mach No.	0.51	0.64	0.77	0.62	0.81	(0.95)
Pressure, mb	(111.0)	79.0	59.2	57.6	44.2	36.1
3g + 15 sec	E + 48 sec	E + 64 sec	E + 91 sec	E + 43 sec	E + 73 sec	E + 115 sec
Mach No.	0.54	0.65	0.76	0.66	0.81	(0.95)
Pressure, mb	(106.3)	78.0	59.8	54.6	43.7	36.1
3g + 20 sec	E + 53 sec	E + 69 sec	E + 96 sec	E + 48 sec	E + 78 sec	E + 120 sec
Mach No.	0.49	0.60	0.71	0.60	0.76	(0.88)
Pressure, mb	(114.1)	83.1	62.9	58.9	46.4	38.1
Dynamic Pressure, N/m <sup>2</sup>	2026	2174	(2230)	1608	1889	2084

\* Legend: ○ = Analysis Comparisons; □ = Design Points.

The Saturnian radiation belt environment denoted above applies to a periapsis radius,  $R_p$  of  $\geq 2.3 R_S$ , therefore the probe receives only half the spacecraft<sup>p</sup> exposure. This is because the probe is released half way through the spacecraft exposure and the probe enters the planet's atmosphere which is  $< 2.3 R_S$ . Therefore the probe environment from the radiation belts is  $0.75 \times 10^{11} \text{ e/cm}^2$  and  $1.5 \times 10^{10} \text{ p/cm}^2$ . Conversion of protons to equivalent neutrons is as follows:

$$1.5 \times 10^{10} \text{ p/cm}^2 (2-100 \text{ MeV}) \times 1.34 \frac{20 \text{ MeV Eq.}}{2-100 \text{ MeV}} \times \frac{33 \text{ n}}{\text{p}} (1-5 \text{ MeV}) = 6.6 \times 10^{11} \text{ n/cm}^2 (1-5 \text{ MeV})$$

The total radiation environment at the probe DTU due to the three above sources, assuming use of plutonium now available and that no shielding is provided within the probe, is as follows:

RTGs	$0.1 \times 10^{11} \text{ n/cm}^2$
RHUs	$0.04 \times 10^{11} \text{ n/cm}^2$ and $0.75 \times 10^3 \text{ rad}$
Saturnian Radiation Belts	$6.6 \times 10^{11} \text{ n/cm}^2$
Total	* $6.7 \times 10^{11} \text{ n/cm}^2$ and $0.75 \times 10^3 \text{ rad}$

The impact of this environment on the probe design is discussed in Sections 4.5 and 4.6.

#### 4.4.1.4 Dual Data Return

A tradeoff study was conducted on the final configuration to assess the impact of transmitting the probe data twice instead of only once. In case there was a short interruption of the communication link, the data would have a second chance of being received by the spacecraft.

The dual data return requires an additional 67 kJ (18.5 W-h) over that required for a single data return. This energy difference comes from the fact that 18 watts of RF power are required for a single data return at 32 bps, but 25 watts are needed for a dual data return at 51 bps. This subject is discussed further in Sections 4.2 and 4.5. The salient features of the tradeoff are summarized in Table 4.4-3.

\* Conversion factors are as follows:  $1 \text{ n} = 0.03 \text{ p} = 3000 \text{ e}$ , and  $1 \text{ r} = 0.83 \text{ R}$ ;  $1.34$  (20 MeV equivalent energy) protons = 1 (2 to 100 MeV energy) proton.

Table 4.4-3 Comparison of Single and Dual Data Return

Factor	Single Data Return	Dual Data Return
Science Objectives	Exceeds Minimum Requirements	Meets Minimum Requirements
DTU & PCU Modifications	Minimal	Significant
Maximum Data Stored Real-Time Transmission Rate	15K bits 32 bps	12K bits 51 bps
Maximum Data Transmitted to S/C	139K bits (278K symbols)	222K bits (444K symbols)
RF Power Required	18 W	25 W
Maximum Battery Energy Required	562 KJ (156 W-H)	629 KJ (175 W-H)

#### 4.4.2 Baseline Configuration Definition

##### 4.4.2.1 Functional Sequence of Events

Figure 4.4-2 depicts the major probe and spacecraft events from before probe separation until mission completion. Note that the major emphasis is placed on probe activity.

As shown, the coast time (time from probe separation until entry) is 35.7 days for Saturn missions and 8.3 days for Uranus. This coast time for Uranus requires a spacecraft  $\Delta V$  that exceeds the spacecraft's capability. As a result, we increased the coast time for Uranus to 20.8 days for the final probe configuration. Table 4.4-4 shows the detailed sequence of events for this

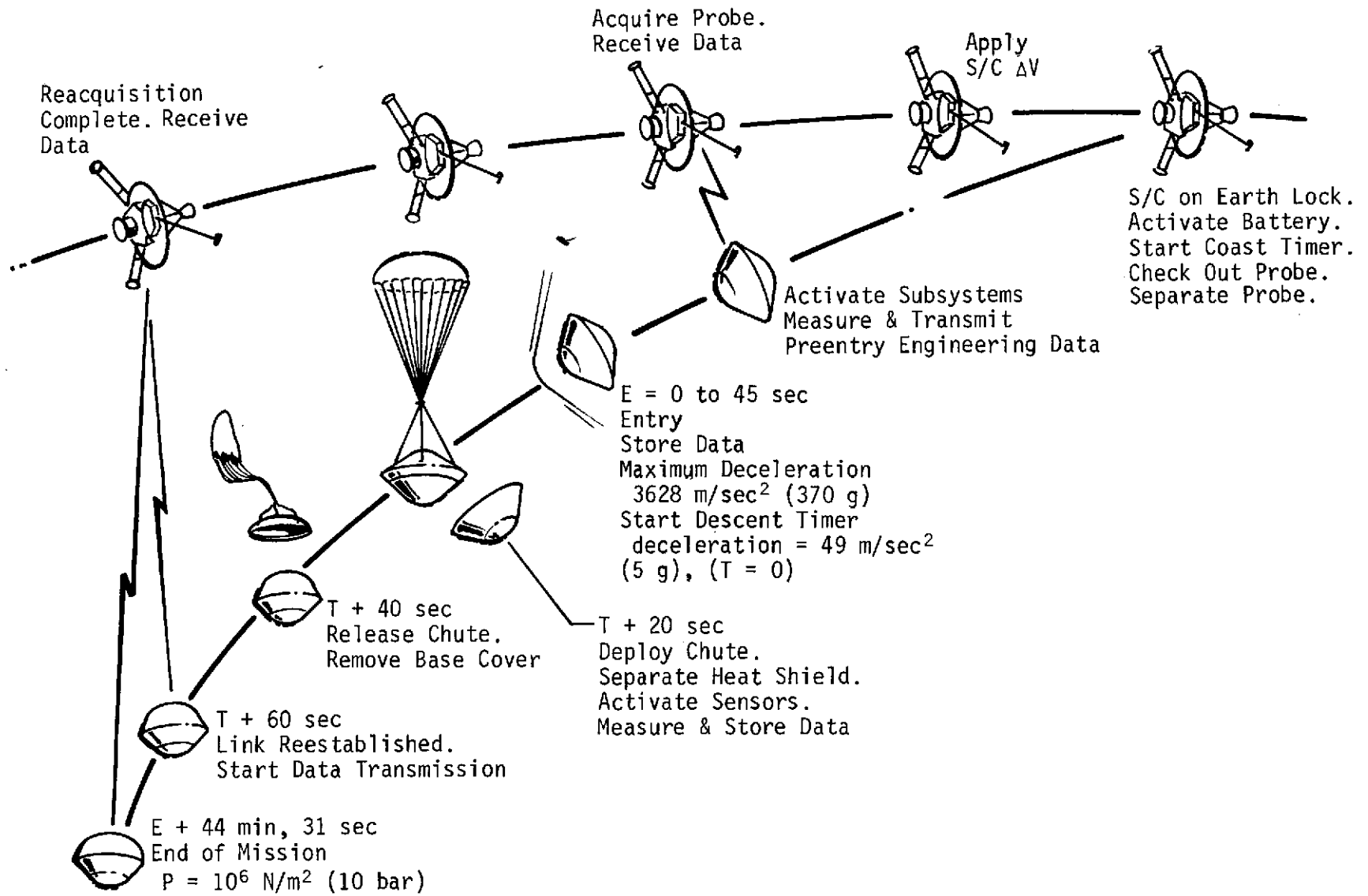


Figure 4.4-2 Pictorial Sequence of Events, Baseline Configuration

Table 4.4-4 Detailed Sequence of Events, Baseline Configuration

Time (Saturn)*	Event	Time (Uranus)*
E - 14m, 23s (S + 35.7d)	Turn Power On to DTU & PCU	E - 38m, 59s (S + 8.3d)
E - 13m, 23s	Turn Science, Transmitter, & RF Power Amplifier On (warmup period)	E - 37m, 59s
E - 11m, 53s	Start Probe Acquisition & Data Transmission (2 bps)	E - 36m, 29s
E - 10m, 53s	Probe Acquisition Complete (ref)	E - 35m, 29s
E - 9m, 53s	Turn RF Power Amplifier Off: Start Data Storage	E - 34m, 29s
E = 0	Entry $P = 1.01 \times 10^{-2} \text{ N/m}^2$ ( $10^{-7} \text{ atm}$ )	E = 0
E + 5s	Deceleration = $0.98 \text{ m/sec}^2$ (0.1 g) & Increasing (ref)	E + 5s
E + 9s	Start Blackout (ref)	(Saturn Controls)
E + 16.3s	Enable $49\text{-m/sec}^2$ (5 g) Sensor. Turn Backup Power On sense deceleration = $490 \text{ m/sec}^2$ (50 g) & increasing	E + 17.7s
E + 30s	End Blackout (ref)	(Saturn Controls)
E + 43s (T = 0)	Start Descent Program deceleration = $49 \text{ m/sec}^2$ (5 g) & decreasing Activate T/C Environment Tanks & Vent Door. Start Acquisition. Turn RF Power Amplifier On	E + 45s (T = 0)
T + 17s	Operate Aeroshell Pin Pullers	T + 17s
T + 20s	Deploy Chute. Separate Aeroshell	T + 20s
T + 23s	Deploy Temperature Gauge. Open NMS Tube 1. Start Temperature, Pressure, & NMS Measurements. Switch Acceleration Mode	T + 23s
T + 40s	Release Chute	T + 40s
T + 60s	Acquisition Complete. Start Data Transmission (32 bps)	T + 60s
T + 71s	Close NMS Tube 1	T + 71s
T + 207s	Open NMS Tube 2	T + 207s
T + 255s	Close NMS Tube 2†	T + 255s
E + 44m, 31s (T + 2628s)	End of Mission $P = 1.07 \times 10^6 \text{ N/m}^2$ (10.7 bar) (S); $10^6 \text{ N/m}^2$ (10 bar) (U)	E + 44m, 31s (T + 2626s)

\* Entry arrival uncertainty: 4.4 minutes (S); 29 minutes (U); Coast timer error: 308 sec (S) or (U).  
Battery activated before separation. Entry  $B = 102 \text{ kg/m}^2$  (0.65 slug/ft<sup>2</sup>) for both planets.  
Descent  $B = 170 \text{ kg/m}^2$  (1.08 slug/ft<sup>2</sup>).

† 10 Tubes. 255 sec between tube openings. Turn...open for...48 sec. Tube 10 left open.

baseline configuration, which is designed for the nominal atmospheres. The preentry activities for each planet are functionally identical and differ only with regard to the entry arrival uncertainty, which amounts to 29 minutes for Uranus and 4.4 minutes for Saturn.

Because the science instruments require a 5-minute warmup period and the transmitter oscillator requires a 1.5-minute warmup, both are turned on during the preentry phase. The nominal environment is so similar for Saturn and Uranus that a single entry and descent time of 44.5 minutes satisfies the science objectives.

#### 4.4.2.2 Functional Block Diagram

Figure 4.4-3 is a simplified functional block diagram showing the functional relationship between the probe's internal subsystems and the probe-to-spacecraft interface before and after separation.

#### 4.4.2.3 System Data Profile

Figure 4.4-4 shows the system data profile as a function of the mission time during coast, preentry, entry, and descent.

During the coast phase, the probe is dormant and collects no data. During the preentry phase, the probe science and subsystems are on. Engineering data are collected and transmitted in real time to the spacecraft at a rate of 2 bps for approximately 1 minute (see Section 4.4.2.1). During the entry phase accelerometer data are collected at 128 bps and stored. After the parachute is deployed, descent data are collected and stored until the spacecraft acquires the probe. Then the 10,000 bits of stored data are interleaved with real-time data and transmitted to the spacecraft at a rate of 32 bps. The total amount of data transmitted is 82,000 bits.

#### 4.4.2.4 System Power Profile

Figure 4.4-5 shows the system power required versus mission time for the same four probe mission phases. During the coast phase, the only power used is 1.0 mW, for the coast timer. Here the Uranus preentry is shown because its arrival uncertainties are more severe. Late arrival requires the maximum amount of energy from the battery. This condition exists when the probe arrives so late that the timer times out too soon and starts the preentry

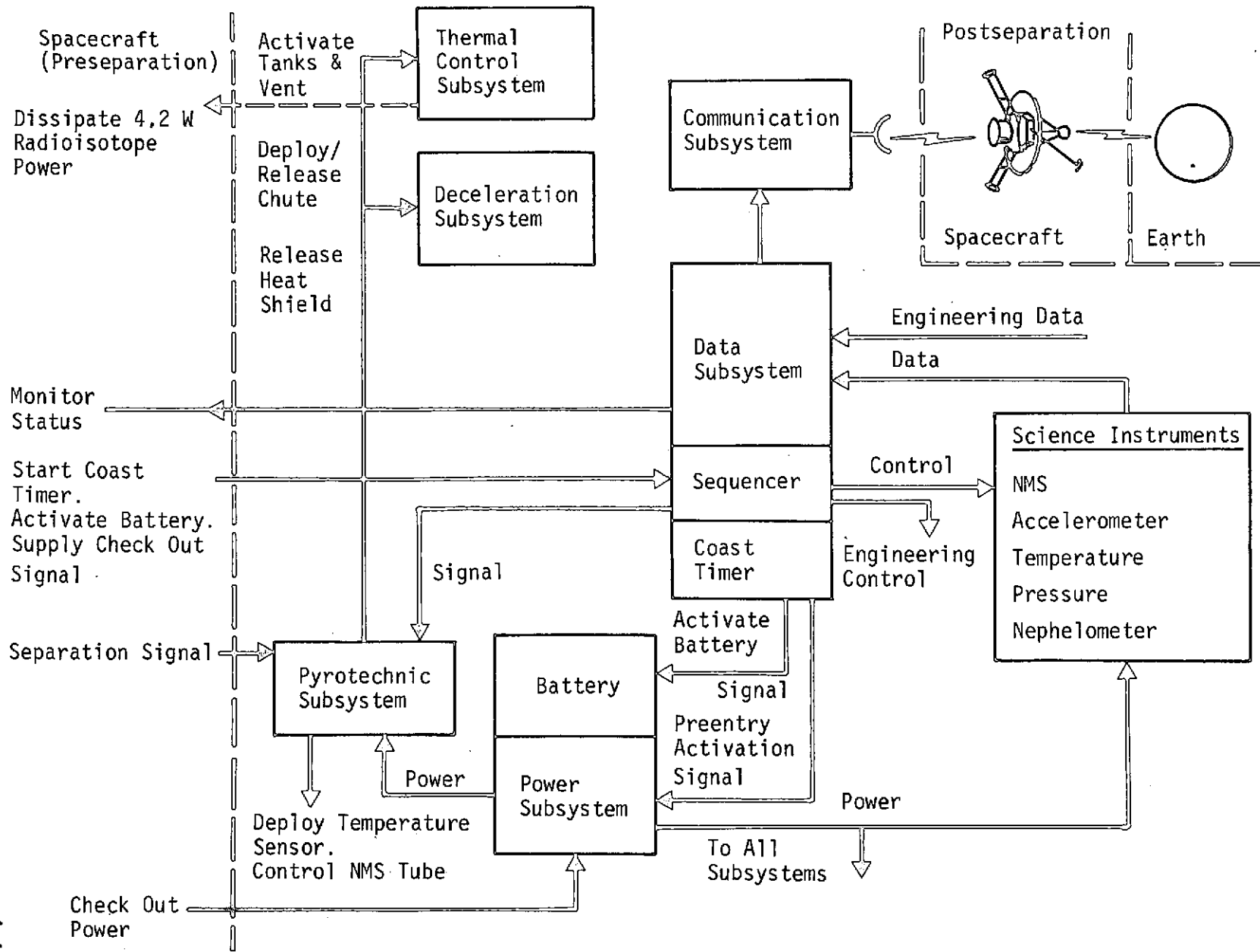


Figure 4.4-3 Simplified Block Diagram, Baseline Configuration



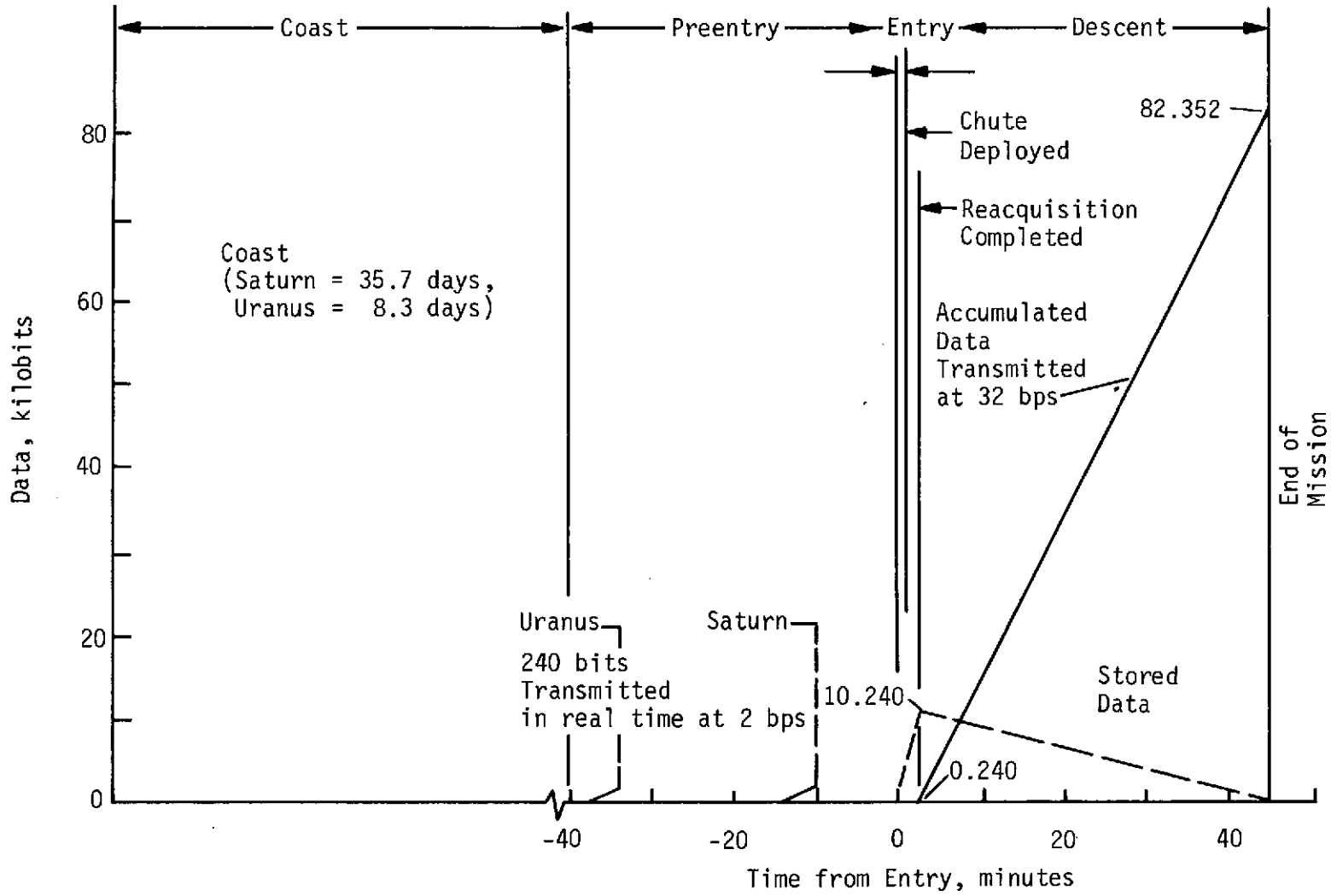


Figure 4.4-4 Data Profile, Baseline Configuration

Note: Maximum energy required for late arrival = 487,440 J (135.4 W-H).

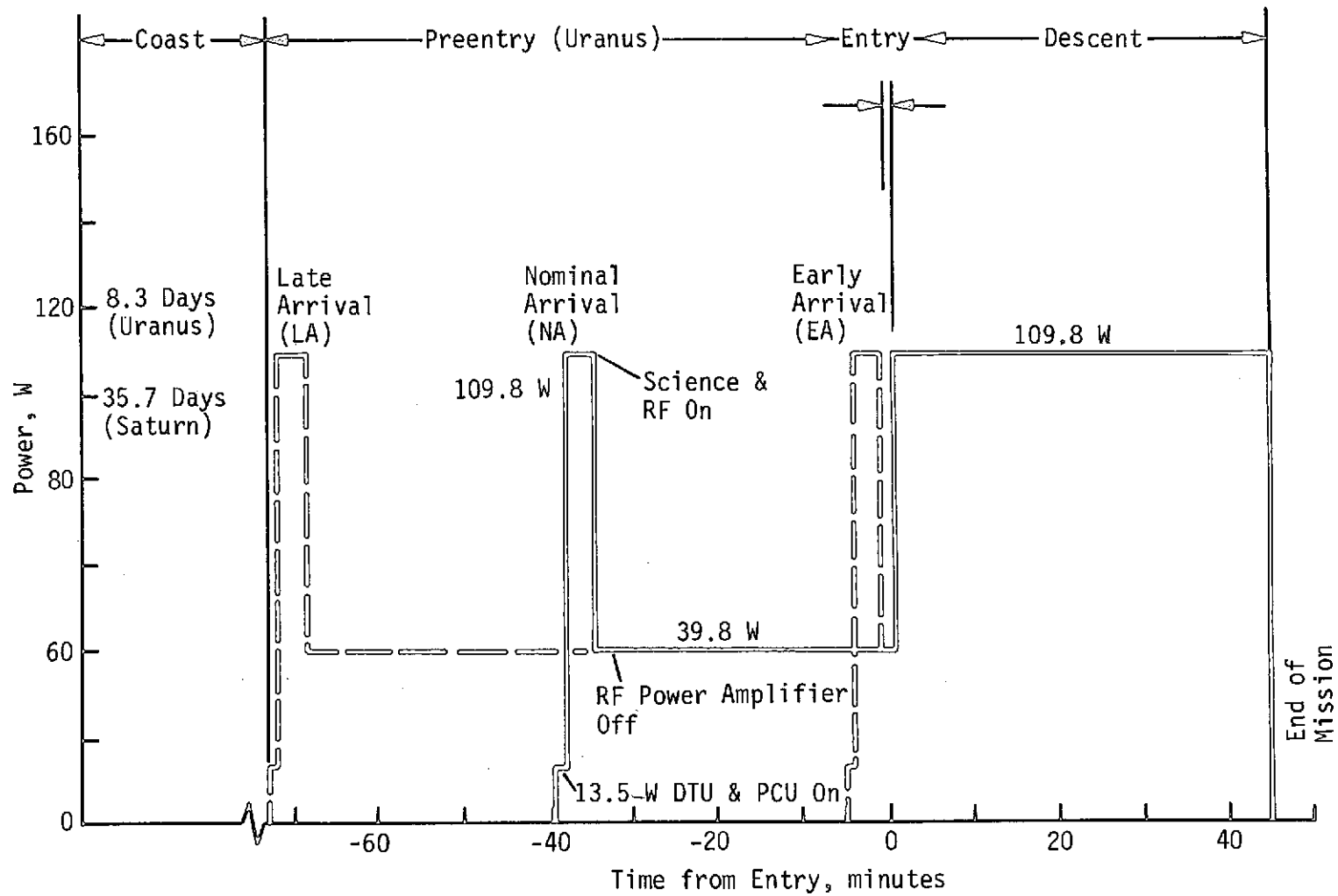


Figure 4.4-5 Power Profile, Baseline Configuration

sequence early. Note that the maximum energy required from the battery is 487 kJ (135 W-h).

#### 4.4.2.5 System Weight

The weight of the probe at entry is 71.73 kg (158.15 lb). During entry, ablation losses reduce this value to 63.03 kg (138.97 lb), and the weight of the descent probe after the parachute has been ejected is 45.50 kg (100.32 lb).

#### 4.4.3 Alternate Configuration Definition

##### 4.4.3.1 Functional Sequence of Events

A pictorial sequence of events for the alternate configuration is shown in Figure 4.4-6 and presented in more detail in Table 4.4-5. The primary difference between this and the baseline configuration is that the parachute has been deleted. The sequence of events is similar for both configurations. A nose cap ejection event for this configuration replaces the parachute deployment and ejection in the baseline configuration. Another difference is that the mission for this alternate configuration lasts approximately 5 minutes longer, due to the use of a different descent ballistic coefficient.

##### 4.4.3.2 Functional Block Diagram

The functional block diagram for the baseline configuration (Figure 4.4-3) also applies to this configuration. The deceleration functions related to parachute deployment and heat shield release were replaced with the nose-cap ejection functions.

##### 4.4.3.3 Systems Data Profile

Figure 4.4-7 shows the data profile for the alternate configuration. The only difference between this and the baseline configuration is due to the five-minute longer descent. The alternate probe sends 91,000 bits of data to the spacecraft, compared with only 82,000 for the baseline configuration.

##### 4.4.3.4 System Power Profile

Figure 4.4-8 shows the system power required versus the time for the four major probe mission phases. Except for the minor difference in the length of the descent phase, the only significant difference between the two power profiles is that the alternate probe uses only 67 watts of power during data transmission compared with 110 watts for the baseline probe. This lower

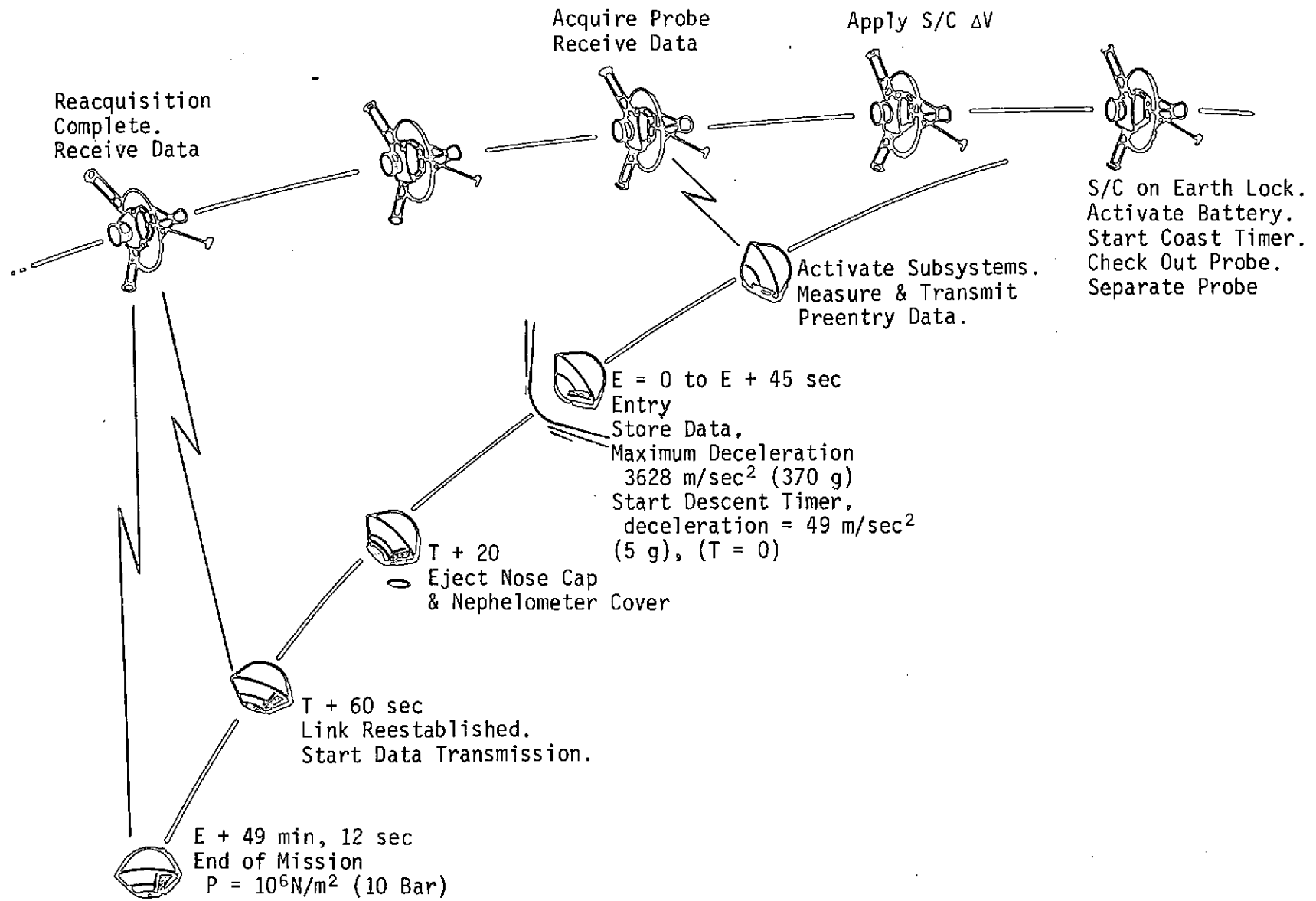


Figure 4.4-6 Pictorial Sequence of Events, Alternate Configuration

Table 4.4-5 Detailed Sequence of Events, Alternate Configuration

4.4-16

Time (Saturn)*	Event	Time (Uranus)*
E - 14m, 23s (S + 35.7d)	Turn Power On to DTU & PCU	E - 38m, 59s (S + 8.3d)
E - 13m, 23s	Turn Science, Transmitter, & RF Power Amplifier On (warmup period)	E - 37m, 59s
E - 11m, 53s	Start Probe Acquisition, Data Transmission (2bps)	E - 36m, 29s
E - 10m, 53s	Probe Acquisition Complete (ref)	E - 35m, 29s
E - 9m, 53s	Turn RF Power Amplifier Off, Start Data Storage	E - 34m, 29s
E = 0	Entry [ $P = 1.01 \times 10^{-2} \text{ N/m}^2$ ( $10^{-7} \text{ atm}$ )]	E = 0
E + 5s	Deceleration = $0.98 \text{ m/sec}^2$ (0.1 g) & Increasing (ref)	E + 5s
E + 9s	Start Blackout (ref)	(Saturn Controls)
E + 16.3s	Enable $49\text{-m/sec}^2$ (5-g) Sensor, Turn Backup Power On sense deceleration = $490 \text{ m/sec}^2$ (50 g) & increasing	E + 17.7s
E + 30s	End Blackout (ref)	(Saturn Controls)
E + 43s (T = 0)	Start Descent Program deceleration = $49 \text{ m/sec}^2$ (5 g) & decreasing; Activate Environmental Tanks & Vent Door; Start Acquisition; Turn RF Power Amplifier On	E + 45s (T = 0)
T + 20s	Eject Nose Cap & Nephelometer Cover	T + 20s
T + 23s	Open NMS Tube 1, Deploy Temperature Sensor, Start Temperature, Pressure & NMS Measurements. Switch Acceleration Mode	T + 23s
T + 60s	Acquisition Complete, Start Data Transmission (32 bps)	T + 60s
T + 71s	Close NMS Tube 1	T + 71s
T + 311s	Open NMS Tube 2	T + 311s
T + 359s	Close NMS Tube 2 <sup>†</sup>	T + 359s
E + 49m, 12s (T + 2909s)	End of Mission [ $P = 1.05 \times 10^6 \text{ N/m}^2$ (10.5 bar) (S); $10^6 \text{ N/m}^2$ (10 bar) (U)]	E + 49m, 12s (T + 2907s)

\*Entry arrival uncertainty: 4.4 minutes (S); 29 minutes (U). Coast timer error: 308 sec (S) or (U).  
Batt activated before Separation. Entry B =  $102 \text{ kg/m}^2$  ( $0.65 \text{ slug/ft}^2$ ) for both planets. Descent B =  $131.8 \text{ kg/m}^2$  ( $0.839 \text{ slug/ft}^2$ ) (S) and  $138.8 \text{ kg/m}^2$  ( $0.884 \text{ slug/ft}^2$ ) (U).

<sup>†</sup>10 tubes. 288 sec between tube openings. Tube open for 48 sec. Tube 10 left open.

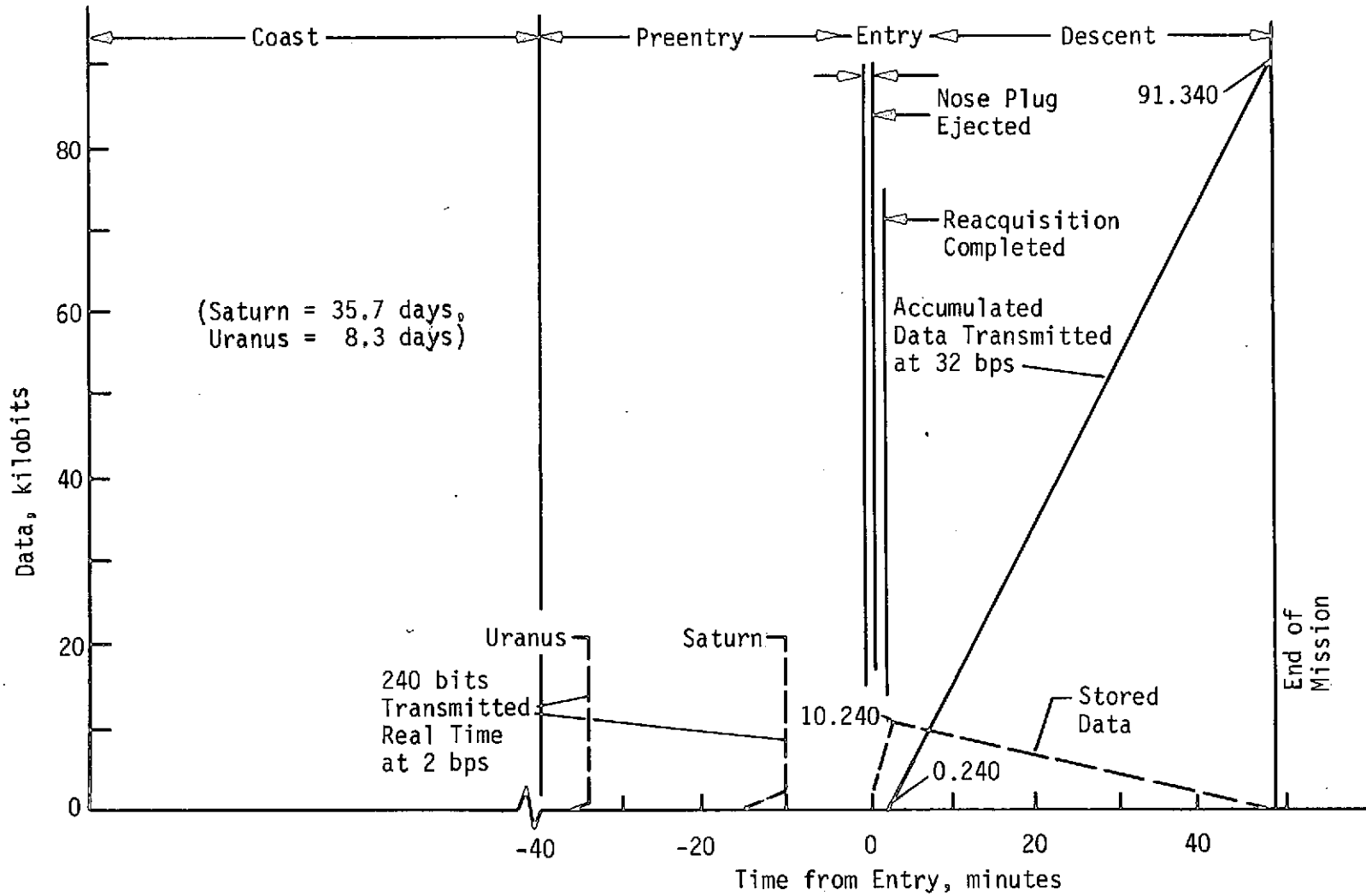


Figure 4.4-7 Data Profile, Alternate Configuration

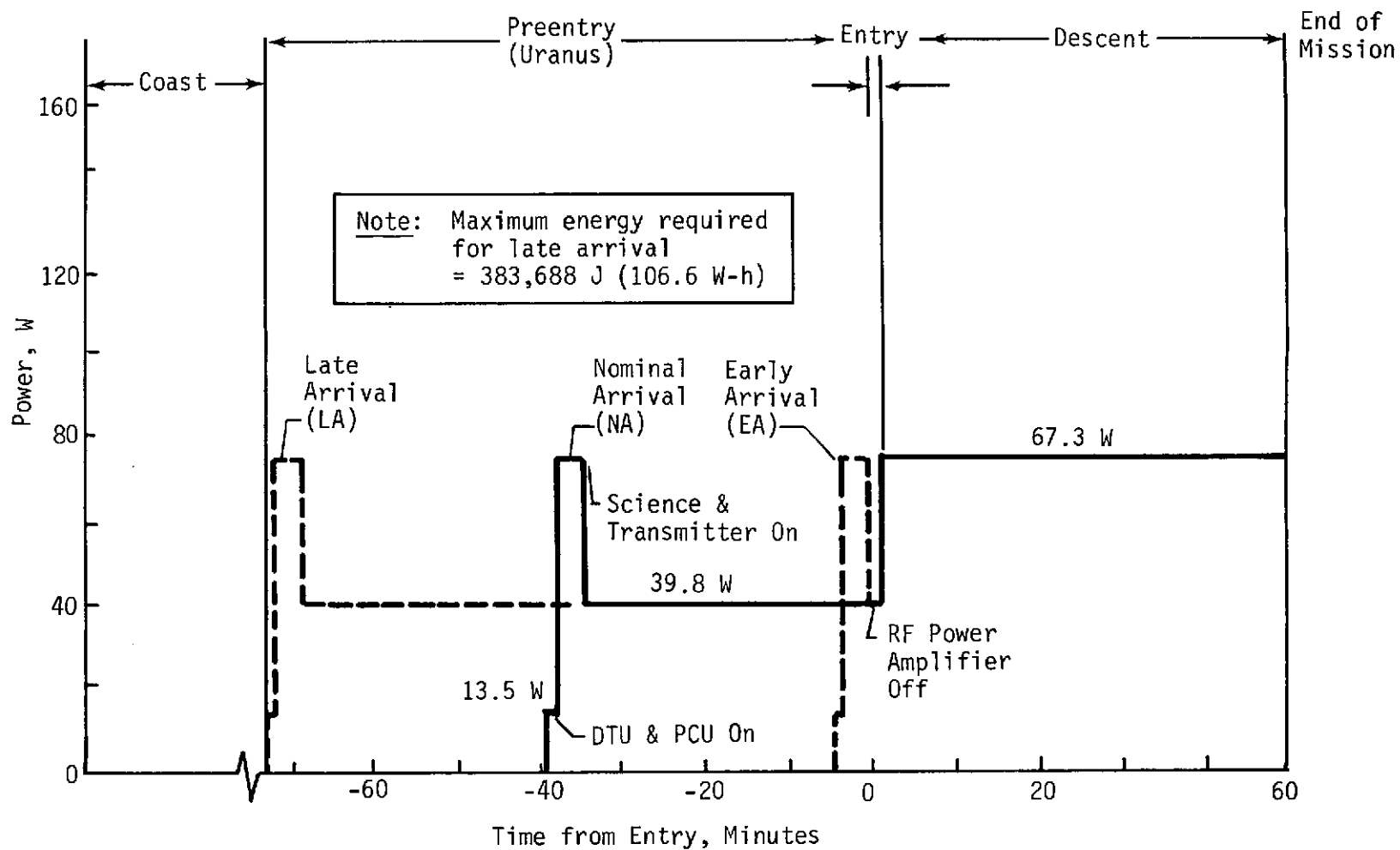


Figure 4.4-8 Power Profile, Alternate Configuration

power requirement results from using a radio frequency of 560 MHz. At this frequency, the transmitter output power is only 11 watts for a posigrade Uranus mission. In contrast, the baseline configuration operates at a frequency of 800 MHz and uses 28 watts. A probe antenna could not be accommodated for this lower frequency in the baseline configuration because of the space taken up by the parachute.

#### 4.4.3.5 System Weight

The system weight at entry is 59.27 kg (130.67 lb). The weight just after entry is 51.92 kg (114.48 lb) and the descent weight is 50.33 kg (110.97 lb).

#### 4.4.4 Configuration Comparison (Nominal Atmospheres)

Both configurations were analyzed using nominal atmospheric models, with other constraints held constant throughout the study. The characteristics of these two configurations are summarized in Table 4.4-6.

Compared with the baseline probe, the alternate configuration is smaller and lighter at entry, simpler, and expected to be less expensive due to no parachute development. Therefore, we decided to use the alternate configuration to assess the impact of the "worst-case" atmospheres.

Both configurations used early versions of Pioneer Venus (PV) subsystems and an operational mode to be changed for the final configuration. To make the alternate configuration comparable with the final configuration, it was updated as discussed below.

#### 4.4.5 Updated Alternate Configuration (Nominal Atmospheres)

The alternate configuration was updated to: (1) use the most recently defined PV components; (2) delete preentry transmission as discussed in Section 4.4.1; (3) use a Uranus retrograde instead of a Uranus posigrade mission; and (4) use discrete, remotely activated Ag-Zn battery cells. This was done so that we could assess the impact of the "worst-case" atmosphere and configure the probe to withstand the extreme atmospheres.

The entry weight of the updated alternate configuration is 63.94 kg (140.96 lb). This new configuration also uses 22 kJ (6.2 W-h) less energy than it did before updating.



Table 4.4-6 Comparison of Baseline and Alternate Configurations

Comparison Factor	Baseline Configuration (Heat Shield Ejected)	Alternate Configuration (Integrated Heat Shield)
Ejected Weight, kg (lb)	71.74 (158.15)	59.33 (130.67)
Post Entry Weight, kg (lb)	63.04 (138.97)	51.93 (114.48)
Descent Weight, kg (lb)	45.50 (100.32)	50.34 (110.97)
Entry Diameter, cm (in.)	90.4 (35.6)	82.3 (32.4)
Descent Diameter, cm (in.)	67.56 (26.6)	80.77 (31.8)
c.g. Location at Entry, % Forward of Maximum Diameter	9.6	9.3
Descent c.g. Location, % Forward of Maximum Diameter	5.3	8.9
Probe Frequency, MHz	800	560
RF Power Required, W	28	11
Power Energy Requirements, kJ (W-H)	487 (135)	384 (107)
Data Transmitted to S/C, 10 <sup>3</sup> bits	82	91
Descent B, kg/m <sup>2</sup> (slug/ft <sup>2</sup> )	170 (1.08)	131.8 (0.839) for Saturn 138.8 (0.884) for Uranus
Parachute Development	Required	Not Required

#### 4.4.6 Impact of the Worst-Case Atmospheres

This section discusses the impact of the extreme atmospheres on the updated alternate configuration and defines the final configuration that satisfies these atmospheric conditions.

##### 4.4.6.1 Functional Sequence of Events

Figure 4.4-9 and Table 4.4-7 show the sequence of events for the final probe configuration. Compared with the updated alternate configuration, the basic difference in this sequence is that it uses a range of times to define an event. For example,  $0.98 \text{ m/sec}^2$  ( $0.1 \text{ g}$ ) can occur from entry + 1 sec to entry + 23 sec,  $29.4 \text{ m/sec}^2$  ( $3 \text{ g}$ ) now ranges from entry + 28 sec to entry + 100 sec, and the end of the mission can occur anywhere from entry + 0.5 hr to entry + 1.2 hr.

The nose cap deployment time for the nominal probe was at  $49 \text{ m/sec}^2 + 20 \text{ seconds}$  ( $5 \text{ g} + 20 \text{ sec}$ ). However, in accordance with the analysis discussed in Section 4.4.1, this time was changed to  $29.7 \text{ m/sec}^2 + 20 \text{ seconds}$  ( $3\text{g} + 20 \text{ sec}$ ) to make the mission sequence compatible for the extreme atmospheres.

##### 4.4.6.2 Functional Block Diagram

The functional block diagram discussed in Section 4.4.2 (see Figure 4.4-3) can be adapted to the final configuration by replacing the deceleration functions related to parachutes and heat shield release with nose-cap ejection functions. All other functions are the same.

##### 4.4.6.3 System Data Profile

Figure 4.4-10 shows the varying amount of data stored and the times for playback in the warm and cool atmospheres. For example, the Uranus warm-atmosphere mission requires 15K bits of storage, which must be interleaved with real-time data in approximately 70 minutes. The Saturn cool-atmosphere mission is the other extreme condition. This mission requires 9K bits of storage, which must be emptied in approximately 27 minutes. The data storage requirement for the nominal atmospheric model are between the two extremes. Since data are transmitted to the spacecraft at a rate of 32 bps, the maximum amount of data transmitted is equal to 139K bits.

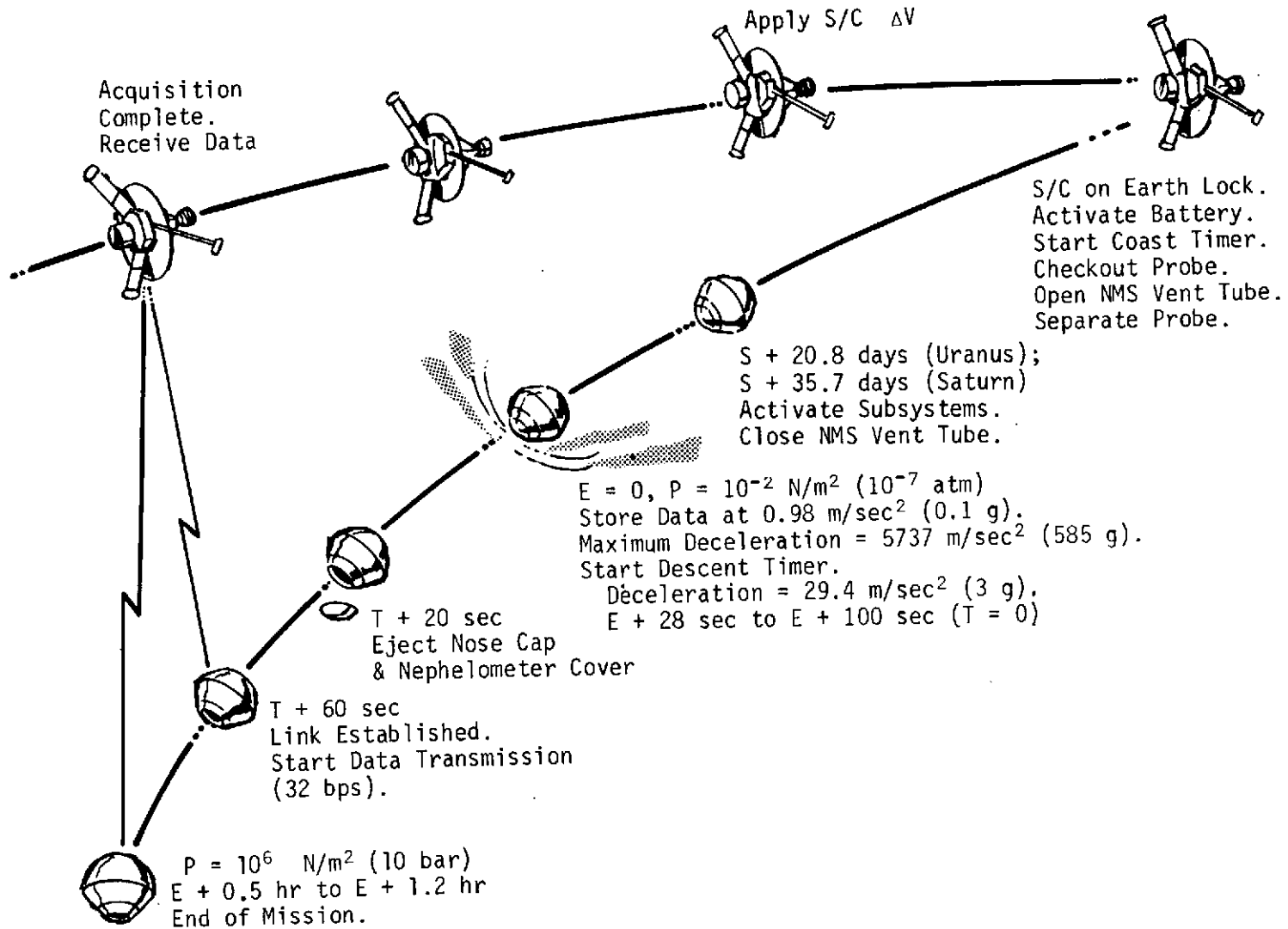


Figure 4.4-9 Pictorial Sequence of Events, Final Configuration

Table 4.4-7 Detailed Sequence of Events, Final Configuration

Time (Saturn)*	Events	Time (Uranus)*
E - 9m, 59s (S + 35.7d)	Switch Power On to DTU & PCU. Close NMS Vent Tube	E - 34m, 40s (S + 20.8d)
E - 8m, 59s	Switch NMS, Temperature & Accelerometer On (warmup period). Start NMS Pump	E - 33m, 40s
E - 5m, 52s	Switch Transmitter On (warmup period) (Power Amplifier off)	E - 30m, 33s
E = 0	Entry [ $P = 1.01 \times 10^{-2} \text{ N/m}^2$ ( $10^{-7} \text{ atm}$ )](Ref)	E = 0
E + 0m, 2s (C) <sup>†</sup>	Deceleration = 0.98 m/sec (0.1 g) & Increasing (ref). Switch Nephelometer, Window Heater, Pressure, & Engineering Instrument On. Start Deceleration Measurement & Storage	{ E + 0m, 1s (C) E + 0m, 23s (W)
E + 0m, 14s (W)		
E + 0m, 8s (C)	Enable 29.4-m/sec <sup>2</sup> (3 g) Sensor. Switch Backup Power On, Deceleration = 490 m/sec <sup>2</sup> (50 g) & Increasing	E + 0m, 6.5s (C)
E + 1m, 16s (W) <sup>‡</sup>	Start Descent Program. Deceleration = 29.4 m/sec <sup>2</sup> (3 g) & Decreasing (T = 0). Switch RF Power Amplifier On, Start Acquisition. Activate T/C Tanks and Vent Door.	{ E + 1m, 40s (W) E + 0m, 28s (C)
E + 0m, 33s (C)		
T + 20s	Eject Nose Cap & Nephelometer Cover	T + 20s
T + 23s	Open NMS Tube 1. Deploy Temperature Sensor. Start Temperature, Pressure, & NMS Measurements. Switch Acceleration Mode	T + 23s
T + 60s	Acquisition Complete. Start data transmission (32 bps)	T + 60s
T + 71s	Close NMS Tube 1	T + 71s
T + 423s	Open NMS Tube 2	T + 423s
T + 471s	Close NMS Tube 2 <sup>¶</sup>	T + 471s
E + 1h, 2m, 54s (W) <sup>‡</sup>	End of Mission [ $P = 10^6 \text{ N/m}^2$ (10 bar)]	{ E + 1h, 13m, 56s (W) E + 0h, 29m, 12s (C)
E + 0h, 28m, 24s (C)		

\*Entry arrival uncertainty = 4.4 minutes (S); 29 minutes (U), coast timer error = 31 sec.  
<sup>†</sup>W = Warm atmosphere; C = Cool atmosphere; S = Saturn or separation; U = Uranus.  
<sup>‡</sup>6 tubes: 400 sec between tube openings. Tubes open for 48 sec. Tube 6 left open. Battery activated prior to probe S/C separation. Entry B = 143 kg/m<sup>2</sup> (0.91 slug/ft<sup>2</sup>). NMS vent tube opened approximately 10 days before probe separation.

ORIGINAL PAGE IS OF POOR QUALITY

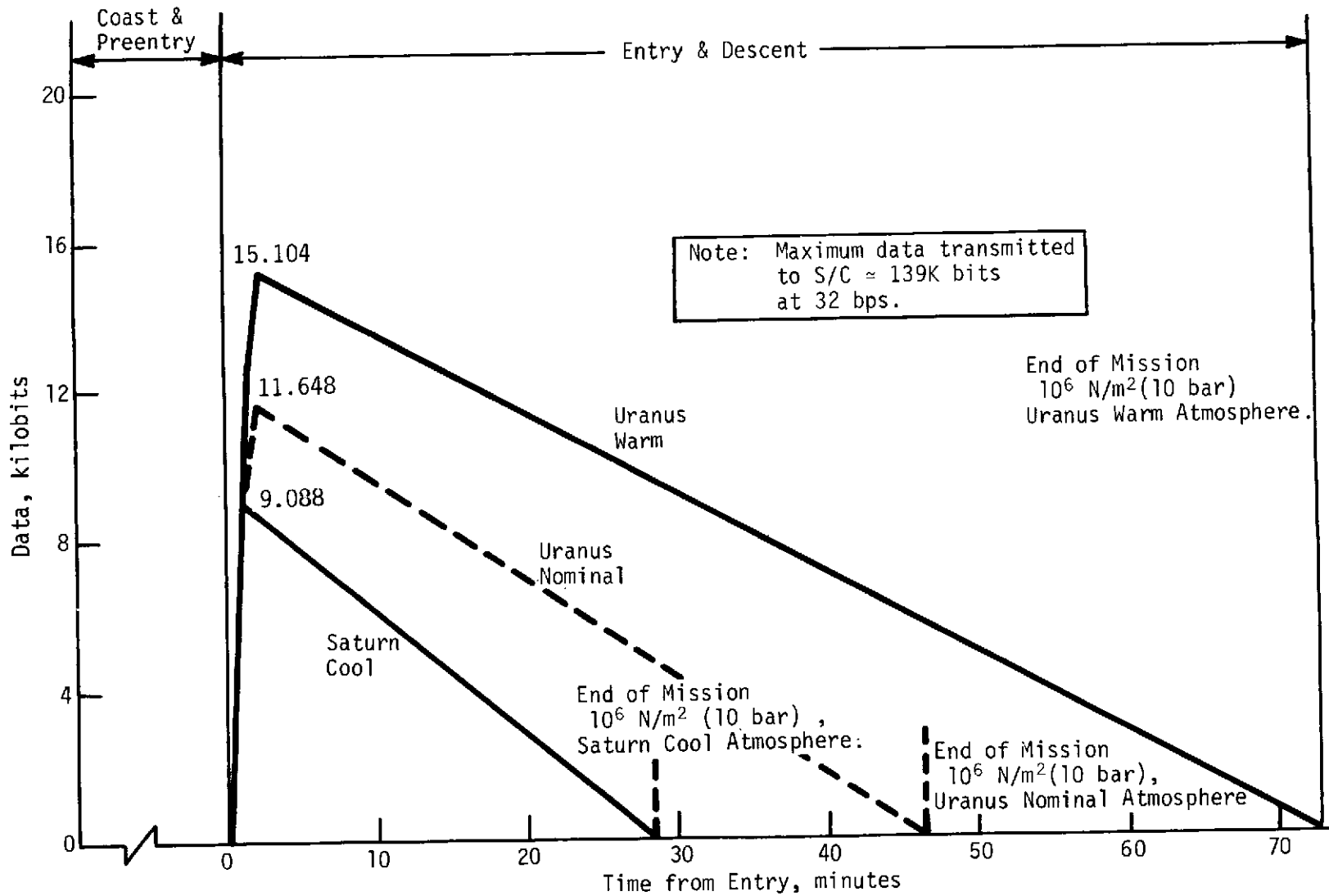


Figure 4.4-10 Data Storage Comparison, Nominal and Worst-Case Atmospheres

#### 4.4.6.4 System Power Profile

Figure 4.4-11 shows the power profile for Uranus in terms of the power required versus time for coast, preentry, entry and descent. Preentry power requirements are shown for late, nominal and early arrivals. Descent requirements are shown for the cool and warm atmospheres. For comparison, the figure also shows the descent power required for the updated alternate configuration. At preentry, the power requirements are identical for both these configurations. The maximum energy required is 562 kJ (156 W-h) for the final configuration and 286 kJ (80 W-h) for the updated alternate configuration.

Figure 4.4-12 shows similar data for Saturn. Saturn entries do not determine the size of the battery but are useful in setting minimum requirements for the thermal control analysis.

#### 4.4.6.5 System Weight

The updated alternate and final configuration weights at entry are 63.94 kg (140.96 lb) and 91.88 kg (202.56 lb), respectively. The extra structural and heat shield materials required to withstand the higher entry deceleration and higher heat pulses from the cool-atmosphere models account for most of the difference.

#### 4.4.6.6 System Environmental Requirements

The most significant system environmental requirements are presented in Table 4.4-8. These requirements apply only to the final configuration.

Note: Maximum energy required:  
 Final Configuration, 561,960 J (156.1 W-h);  
 Updated Alternate Configuration, 286,200 J (79.5 W-h).

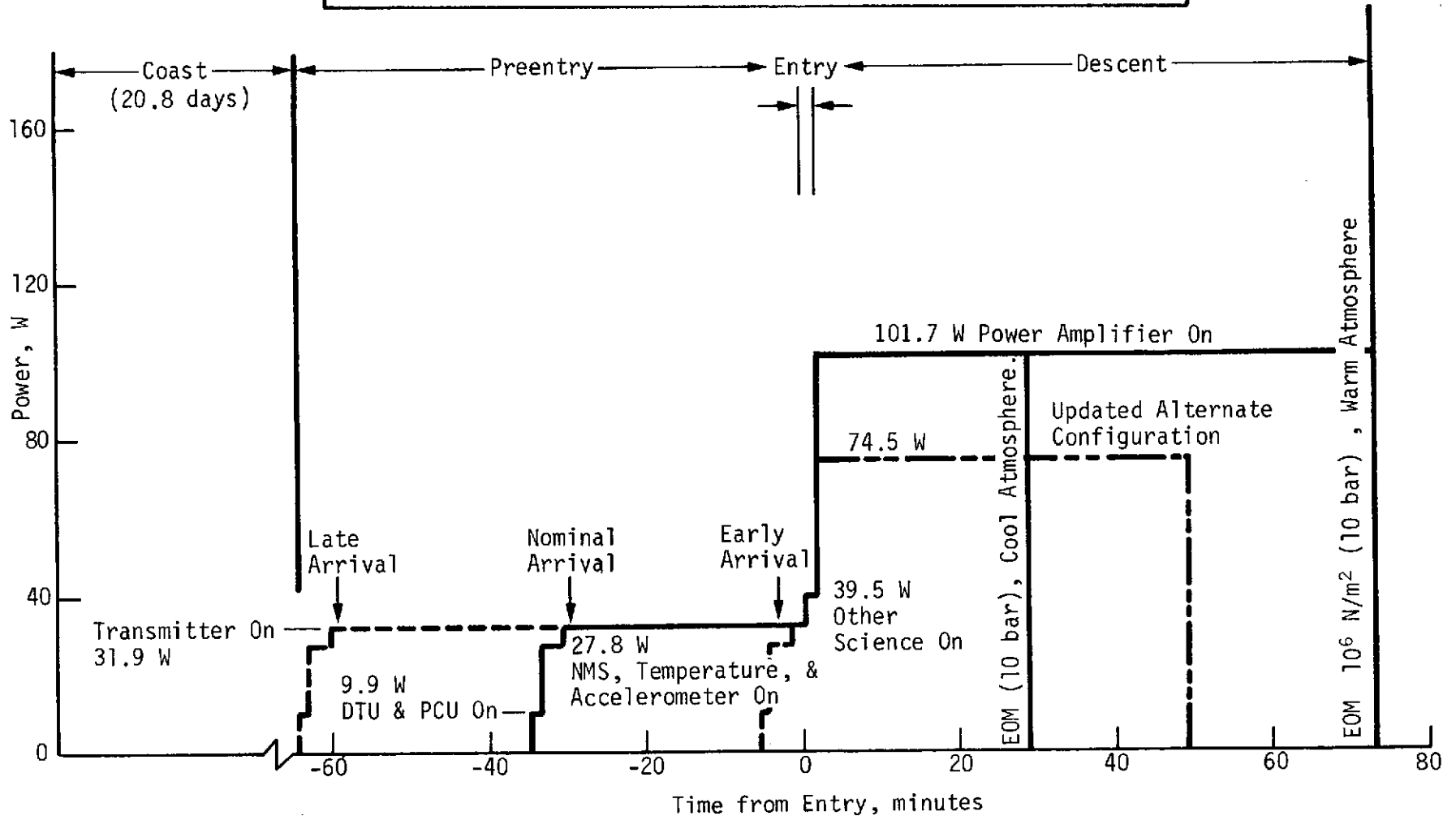


Figure 4.4-11 Power Profile, Uranus Extreme Atmospheres

Note: Maximum energy required:  
 Final Configuration, 406,440 J (112.9 W-h);  
 Updated Alternate Configuration, 245,520 J (68.2 W-h).

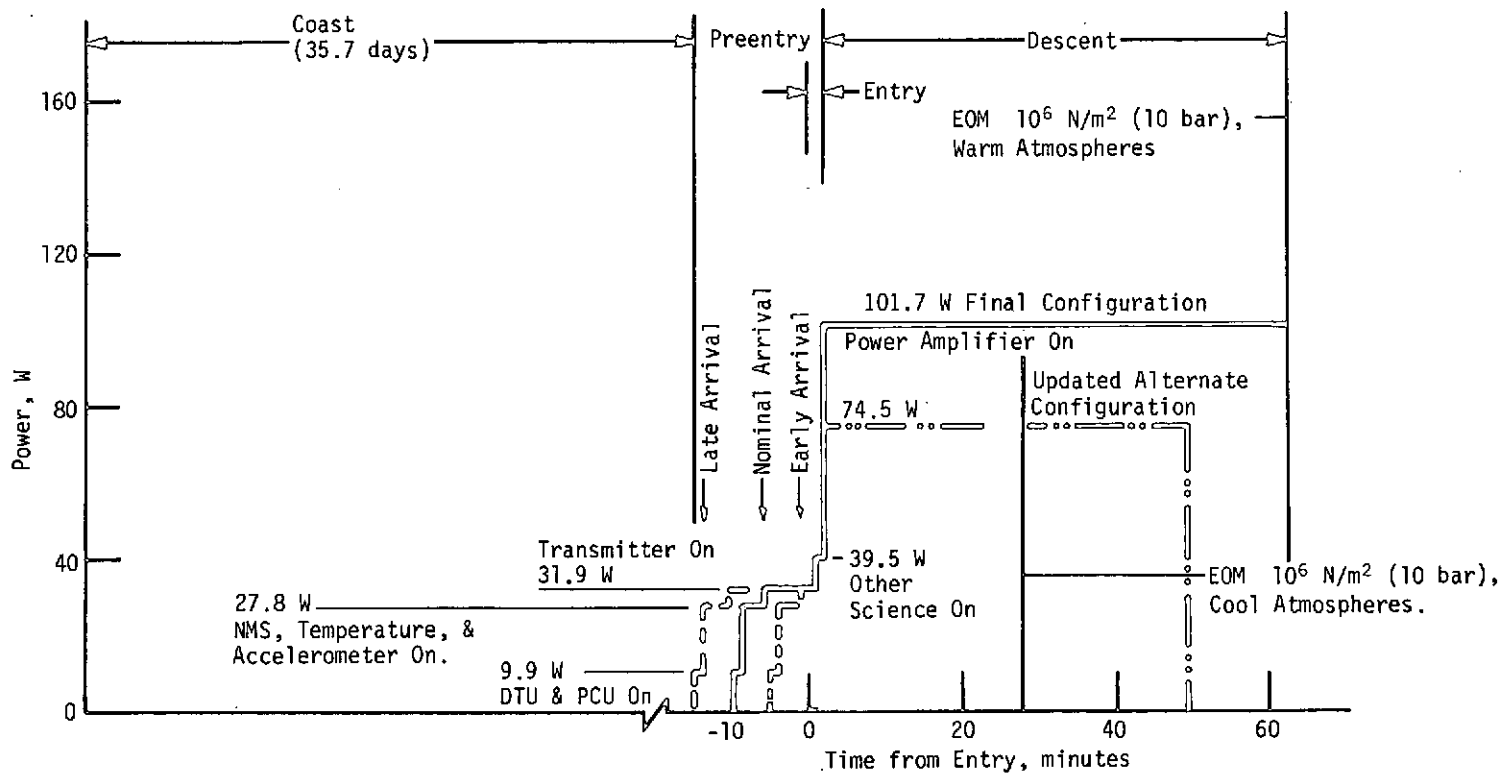


Figure 4.4-12 Power Profile, Saturn Extreme Atmospheres



Table 4.4-8 Probe System Environmental Requirements

4.4-28

	Saturn			Uranus		
	Cool	Nominal	Warm	Cool	Nominal	Warm
TEMPERATURE						
1. Entry & Descent Ambient						
Upper Limit, °K (°F)	190.8 (-116.2)	309.9 (98.2)	424.1 (303.7)	114.0 (-454.5)	185.3 (-126.2)	299.4 (79.8)
Lower Limit, °K (°F)	72.0 (-330.1)	77.0 (-321.1)	82.0 (-312.1)	47.0 (-375.1)	54.0 (-362.5)	-60.0 (-351.7)
2. Internal Temperature (except battery & power amplifier)						
Cruise thru Coast (nonoperating), °K (°F)	233.2 to 338.7 (-40 to 150)					
Preentry thru Descent (operating), °K (°F)	255.4 to 338.7 (0 to 150)					
Battery						
Cruise (nonoperating), °K (°F)	253.2 to 303.1 (-4 to 86)					
Coast thru Descent (operating), °K (°F)	283.1 to 322.0 (50 to 120)					
RF Power Amplifier						
Cruise thru Entry (nonoperating), °K (°F)	255.4 to 338.7 (0 to 150)					
Descent (operating), °K (°F)	348.1 (167) maximum					
3. Aeroshell (operating), °K (°F)	477.6 (400) maximum					
Pressure, N/cm <sup>2</sup> (bar)	1 x 10 <sup>6</sup> (10) minimum					
Deceleration, *m/sec <sup>2</sup> (g)	7180 (731.25)					
Internal Radiation Fluence (based on 7-yr mission)						
1. Neutrons, n/cm <sup>2</sup>	6.7 x 10 <sup>11</sup>					
2. Gammas, R	0.75 x 10 <sup>3</sup>					

\*Includes 25% margin

## 4.5 Electrical and Electronic Design

## 4.5 ELECTRICAL AND ELECTRONIC DESIGN

### 4.5.1 Analyses and Trade Studies

All the electrical and electronics subsystems proposed for the PV design have been analyzed in terms of their applicability to the SU missions. Where possible, each subsystem has been used as is, or modified to conform to the SU requirements and design constraints. In Cases where the PV subsystem was not compatible with the SU mission, an alternate existing design has been proposed.

#### 4.5.1.1 Communications Subsystem

##### Operating Frequency Selection

Making the telemetry operating frequency of the SU and PV probes compatible was highly desirable in order to achieve maximum utilization of existing hardware. Data transmission on PV is via an S-band (2.29-GHz) direct link to Earth. During our evaluation of the PV operating frequency we performed a study to determine whether S-band direct and/or relay links could be used and, if not, what would be a desirable frequency band for data transmission.

In selecting an acceptable operating frequency band, we established two baseline criteria: (1) the chosen frequency must result in transmitter power levels of 50 watts or less, based on RF corona and breakdown considerations, the thermal control requirements of the power amplifier, and the availability of existing space-qualified RF power amplifiers; and (2) the antenna and transmitter hardware must fit in the available space on the SU probe.

Complete compatibility with PV would exist if a direct S-band RF link were feasible for the SU probes. Our analysis indicated that the high amount of space loss for a Uranus probe (19 AU) required approximately 29 kW of transmitter power, using a low-gain probe antenna. A high-gain phased array still requires approximately 400 watts as seen in Table 4.5-1 under Configuration A. The analysis indicated that a direct S-band communication link from the SU probe to Earth is not feasible.

The second best configuration is an S-band relay link. Probe hardware would be common to PV, but a receiver would be necessary on the Pioneer spacecraft. This is shown as Configuration B in Table 4.5-1. A split-axial (butterfly) S/C antenna pattern was used in this configuration since it is less costly and does not use a despun spacecraft

Table 4.5-1 RF Link Frequency Trade Study Comparisons

Parameter	Frequency Trade Off Configuration					
	A	B	C	D	E	F
Type of Link	Direct			Relay		
Frequency, GHz			2.3			0.86
Modulation	PSK			BFSK		
Data Rate, bps			24.4			
Probe Antenna Beamwidth, rad (deg) Maximum Gain, dB	0.23 (13) 22	2.09 (120) 5.6	2.09 (120) 5.6	2.09 (120) 5.6	2.09 (120) 5.6	1.75 (100) 6.5
S/C Antenna Type Beamwidth, rad (deg) Maximum Gain, dB	DSN 0.0026 (0.15) 61.7	Split Axial 0.47 (45) 3.1	← 0.52 (30) 15	Dish 0.61 (35) 14	→ 0.70 (40) 12.3	Split Axial 0.79 (45) 3.1
Planet/Time	Uranus/EOM			Saturn/EOM		
Condition	Use DSN, Direct Link	S-Band Relay without Despun S/C Antenna	S-Band with Despun Dish on S/C, Common Cone Angle	S-Band with Despun Dish on S/C and 2 Cone Angles	S-Band with Dish on S/C, Off Earth Lock	UHF with Butterfly S/C Antenna
Total RF Power, W	400	527	80	71	112	27
RF Power Level	High	High	Lower	Lower	High	Good

receiving antenna. The worst case communications geometry occurs at the end of the mission (EOM) for the Saturn encounter and requires 527 watts of RF power. Note that the significant decrease in space loss is overshadowed by the drastic reduction in the gain of the receiving antenna.

At this point, an extensive study was launched into the variables affecting RF power in order to determine if reasonable power levels could be achieved using an S-band relay link. Table 4.5-2 lists the variables that affect RF power in decreasing order of importance. These variables are generally classified as geometrical or electrical. The communication range is primarily affected by the periapsis radius of spacecraft flyby and, to a lesser extent, by entry flight path angle. The RF power required at the EOM for Saturn is shown as a function of the periapsis radius in Figure 4.5-1 for various data rates and frequencies. As seen in this figure the periapsis radius directly affects the communication range and, therefore, the RF power. We also considered several other geometries that minimize the range, probe aspect angle (PAA), and spacecraft cone angles, but the results did not significantly reduce the RF link power required at S-band frequencies. Instead, the depth-of-descent effects were offset by the shorter range at EOM. Figure 4.5-2 shows that the lead time also affects the range, PAA, and cone angle variations. In conclusion, the range and frequency are too high for an effective relay link at S-band using a spacecraft receiving antenna with omnidirection in the roll plane. Even if the periapsis radius is decreased below  $2.3 R_S$ , over 100 watts of RF power is still required.

The third emphasis was then placed on increasing the gain in the RF link by having a higher gain for the spacecraft receiving antenna. This can only be accomplished by concentrating more energy in the direction of the probe which requires missions using a directional antenna. The antenna must either be despun or be placed parallel to the spacecraft's roll axis and used in conjunction with an off-Earth-lock geometry. These two possibilities were investigated even though the design philosophy for the Pioneer SU probe mission has ruled out using a despun spacecraft antenna and going off Earth lock.

There are several problems in incorporating a mechanically despun antenna on the spin-stabilized Pioneer F spacecraft. First, the cost impact would be major to the spacecraft. Second, although the antenna feed could be fixed by using a despun reflector or an electronically despun array, neither system is presently developed for space vehicle applications.

Table 4.5-2 Communication Subsystem Variables that Affect RF Power

Variable	Comment
<p>Communication Geometry</p> <p>Range, R</p> <p>Probe Aspect Angle, PAA</p> <p>S/C Cone Angle, CA</p> <p>Descent Time</p> <p>PAA and CA Dispersions</p> <p>Depth of Descent, h</p> <p>Lead Time, <math>T_L</math></p>	<p>Space loss varies as <math>R^2</math></p> <p>Determines probe antenna beamwidth and 3-<math>\sigma</math> uncertainty.</p> <p>Determines S/C antenna beamwidth.</p> <p>Determines spread in cone angle coverage from entry to EOM and affects S/C antenna beamwidth.</p> <p>Depend on 3-<math>\sigma</math> error ellipses and descent time. Affects both antenna beamwidths.</p> <p>Affects atmospheric attenuation, which varies with PAA, <math>f^2</math>, and h.</p> <p>Affects maximum range, PAA, and CA.</p>
<p>Communication Parameters</p> <p>Frequency, f</p> <p>Modulation</p> <p>Coding</p> <p>Energy/bit, <math>E_b/N_0</math></p> <p>Data Rate</p>	<p>Space loss varies as <math>f^2</math>.</p> <p>Saturn Doppler rates are too high for PSK.</p> <p>Reduces RF power required.</p> <p>Depends on coding and bit error rate.</p> <p>Affects data power.</p>

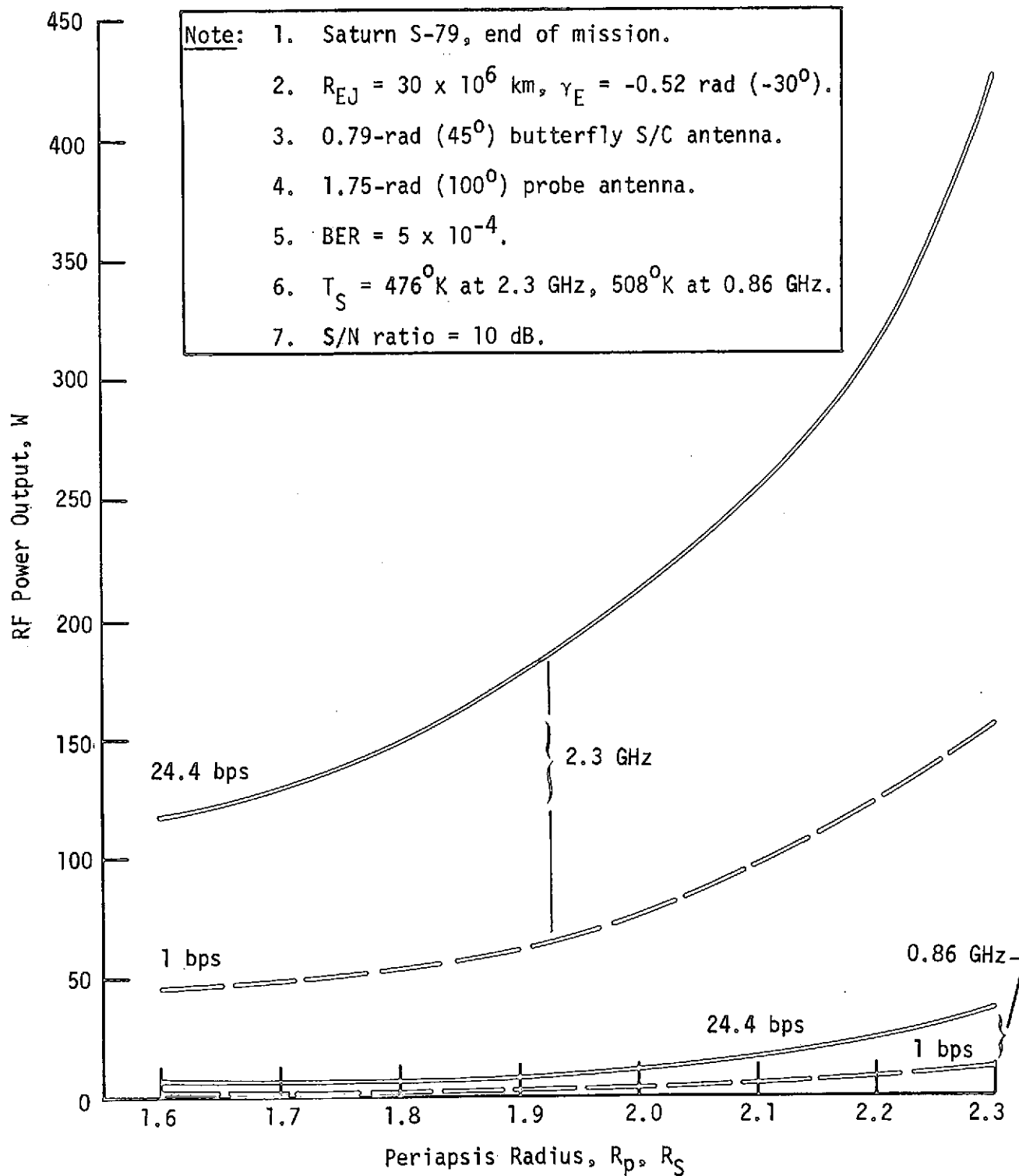
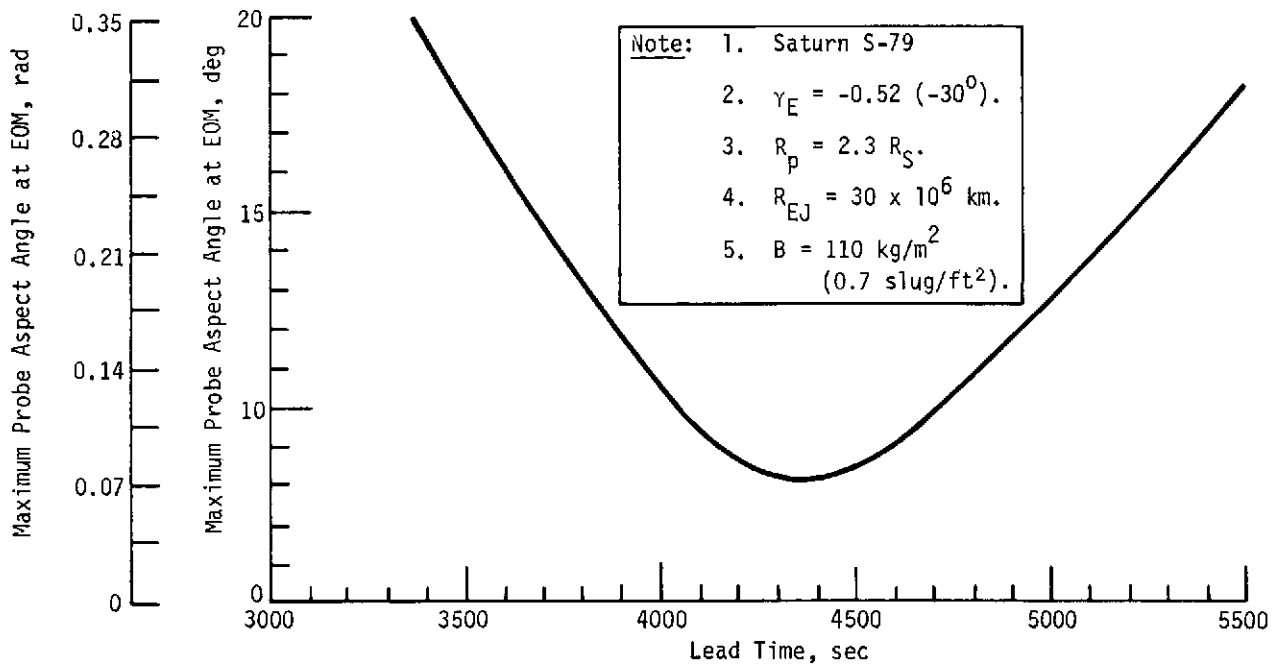
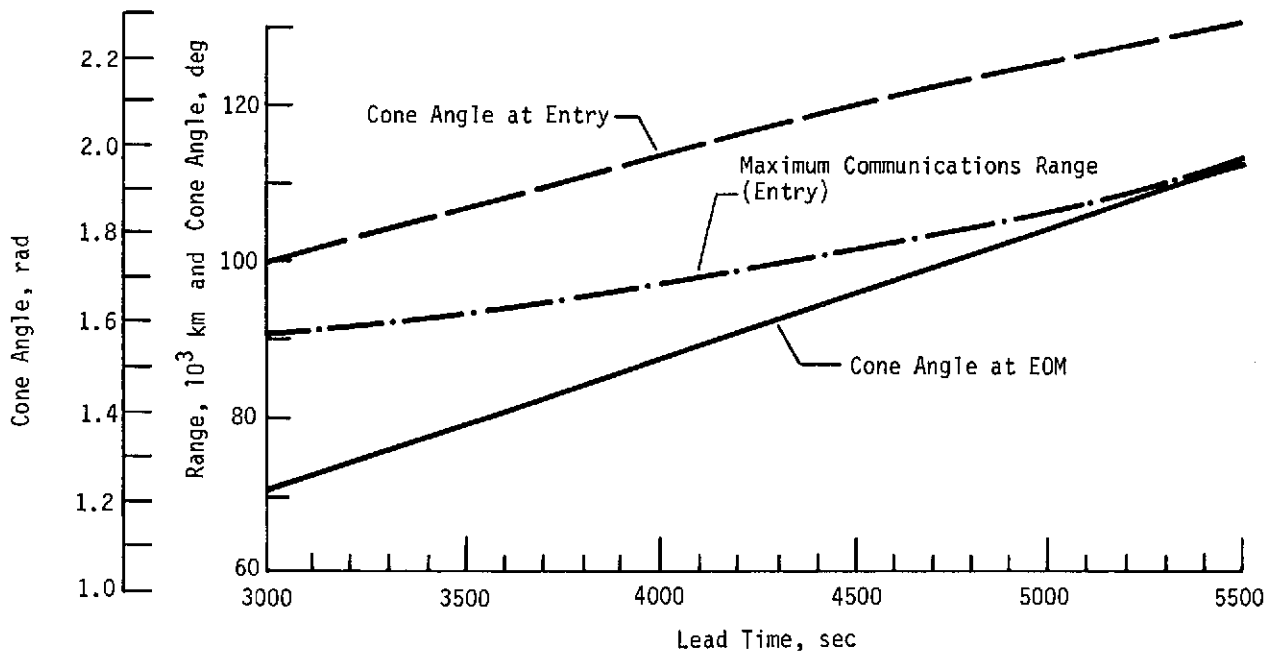


Figure 4.5-1 Probe Transmitter Power Required vs. Frequency, Data Rate, and Periapsis Radius



(a) Probe Aspect Angle



(b) Range and Cone Angles

Figure 4.5-2 Communication Geometry vs Lead Time



Configuration C in Table 4.5-1 lists the details of a despun dish antenna on the spacecraft that still requires 80 watts of RF power. A high-gain 20 dB, electronically steerable array on the spacecraft was not considered cost-effective even though it would reduce the RF power to below 50 watts at S-band. Configuration C was targeted for a common range of spacecraft-to-probe cone angles. The next step was to consider two despun beam positions - one to optimize each planet encounter. This is shown in Table 4.5-1 as Configuration D. The optimum cone angle for Saturn is 1.6 rad ( $90^\circ$ ), but a larger spacecraft antenna beamwidth was necessary to include probe dispersions. The net result is to decrease the required RF power to 71 watts.

Another configuration that was evaluated involved locating the spacecraft antenna on the spin axis and moving from an Earth-pointing to a probe pointing attitude during the probe mission; i.e., moving off Earth lock by 1.31 rad ( $75^\circ$ ). This is shown as Configuration E in Table 4.5-1, here the spacecraft antenna does not have to be despun since it is circularly polarized and located parallel to the spin axis. The offset does not introduce any significant signal modulations. This option has the additional advantages of accommodating different cone angles at the two planets and of optimizing the link geometry for each planet. The major disadvantage is that during the critical entry and descent phase of the mission, communication with Earth from the spacecraft is not possible. In our analysis, the spacecraft was moved off Earth lock a minimum amount since a pointing error results that is 5% of the angle turned. To account for the accumulated pointing error the beamwidth of the spacecraft antenna was increased to 0.7 rad ( $40^\circ$ ). The resultant RF power required was 112 watts.

As seen in Table 4.5-1, five attempts at designing an S-band link proved unsuccessful. The excessive space loss, and atmospheric attenuation cannot be overcome by adjusting the antenna gain and communication geometry to provide transmitter power levels of less than 50 watts. Therefore, we concluded that a viable S-band relay link is not economically feasible.

Lowering the operating frequency relieves the space loss and atmospheric attenuation problems and reduces the criticality of the communication geometry. Configuration F in Table 4.5-1 depicts the major parameters of a link at 860 MHz that uses a split-axial beam antenna and requires 27 watts. From the standpoint of spacecraft antenna complexity, lowering the operating frequency relieves the design problems considerably. Therefore, UHF is considered the preferred band of operation for SU probes. The lower frequency limit

is determined by whether an antenna can be accommodated on the probe and/or on the spacecraft to operate at that frequency. There is not an "optimum" frequency from the standpoint of all the variables listed in Table 4.5-2. The lower the frequency, the lower the required transmitter power, but the size of the probe antenna and RF power amplifier increases. The decision as to which RF frequency to use then depends on whether or not the hardware can be packaged into the probe. Another consideration is that the selected frequency, or its harmonics, should not interfere with the spacecraft downlink.

In conclusion, an S-band (2.3-GHz) direct or relay link is not practical for SU probe missions. Any frequency below 1 GHz will result in transmitter power levels of 50 watts or less using a probe antenna with hemispherical coverage and a spacecraft antenna with a split-axial pattern. As the frequency is lowered, the transmitter power is reduced, and the minimum practical frequency depends on whether the antenna can be packaged into the probe.

#### Modulation and Coding

The principal problems in designing the probe communication link are: (1) Doppler rates and accelerations due to relative motion between the descending probe and the orbiting spacecraft; (2) fading, as a result of turbulence effects in a dense atmosphere; (3) planet multi-path scattering and (4) short-term oscillator instabilities in the transmitter. The most suitable candidates for modulation techniques are binary frequency shift keying (FSK) and phase shift keying (PSK). The choice between these two should be made on the basis of the above considerations. The complexity of multiple frequency shift keying (MFSK) makes it undesirable.

At the present time uncertainty exists as to the amount of fading that will be present on the SU relay links and its effect on a coherent receiver. The Doppler rates expected (3 to 15 Hz/sec) would create high stress on a moderate-bandwidth, standard second-order phase lock loop (PLL). Wide bandwidths require inefficient power allocation between the data and carrier to maintain sufficient signal-to-noise (S/N) ratios in the loop. With a third-order loop, acquisition is difficult. As a result, PSK modulation has not been chosen at this time. However, we are presently conducting a study to establish the performance of a coherent receiver in the presence of fading due to turbulence (reference 4.5-1). If the results of study are favorable and a second-order tracking loop provides satisfactory tracking performance then PSK modulation would be recommended. This would result in less modification to the PV hardware.

Binary FSK with a pilot tracking tone has been recommended even though a power penalty exists as a result of adding the tone (reference 4.5-2, Vol III, Appendix C). The pilot tracking tone is used since no method of frequency tracking using only the data has been established to track the high Doppler rates expected. Cycle slipping effects are not catastrophic in terms of data loss in binary FSK, and this was an additional reason for its choice over PSK.

The baseline/alternate subsystem includes convolutional encoding and viterbi decoding using a constraint length 8, rate 1/2 code with soft decisions and 8 quantization levels. A strong alternative is to use a constraint length 6, rate 1/2 code since storage and computational complexity are proportional to  $2^K$ , where K is the constraint length (reference 4.5-3). Further investigation as to the hardware impact of this alternative must be made. For the alternative code, the performance curves, such as those shown in Figure 4.5-3, must be degraded by 0.5 dB (reference 4.5-4). The baseline choice provides a 4.3-dB coding gain when used with FSK on the additive Gaussian white-noise channel with ideal synchronization.

To compute the performance of the coded FSK system, the effects of using wideband FSK to allow for frequency uncertainties and fading effects due to turbulence and planetary multipath distortion must be included. These effects cannot be assessed until the channel parameters have been established. Once the fading parameters, the fading depth and time response, have been established, Reference 4.5-1 can then be used to predict system performance.

There are no data available on the coding gain for binary FSK modulation when using a Viterbi algorithm. Consequently, our approach was to estimate the required threshold energy per data bit ( $E_b/N_o$ ) for a desired bit error rate (BER) of 5 parts in  $10^4$ . The maximum error rate for PV probes is one part in  $10^3$ . The lower BER was chosen to be certain that the required level was achieved.

The first step was to determine the performance of an ideal non-coherent FSK system. Reference 4.5-5 was used to plot this relationship. The ideal FSK curve without any coding gain is shown in Figure 4.5-4 for  $N = 1$ .  $N$  is the ratio of the IF bandwidth to the data bit rate. For an error rate of  $5 \times 10^{-4}$ ,  $E_b/N_o = 11.4$  dB for uncoded ideal FSK.

The coding gain for BFSK is assumed to be as good as that for PSK if both use Viterbi coding with  $V = 2$  (rate 1/2), a constraint length (K) of 8, and a quantizing level (Q) of 8. The coding gain is taken from Reference 4.5-6. Figure 4.5-3 shows curves for un-

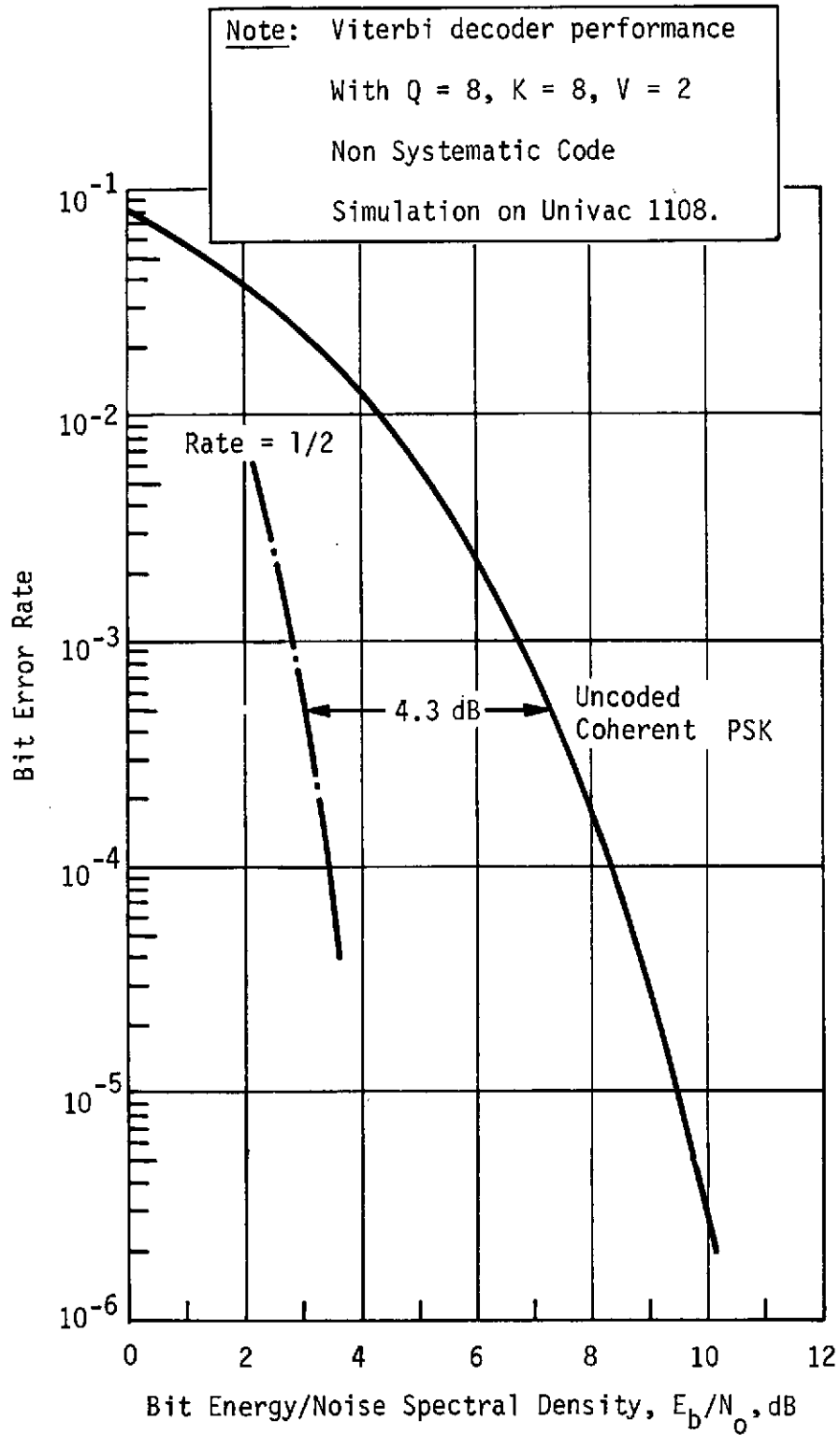


Figure 4.5-3 Computed Coding Advantage for the Viterbi Decoder

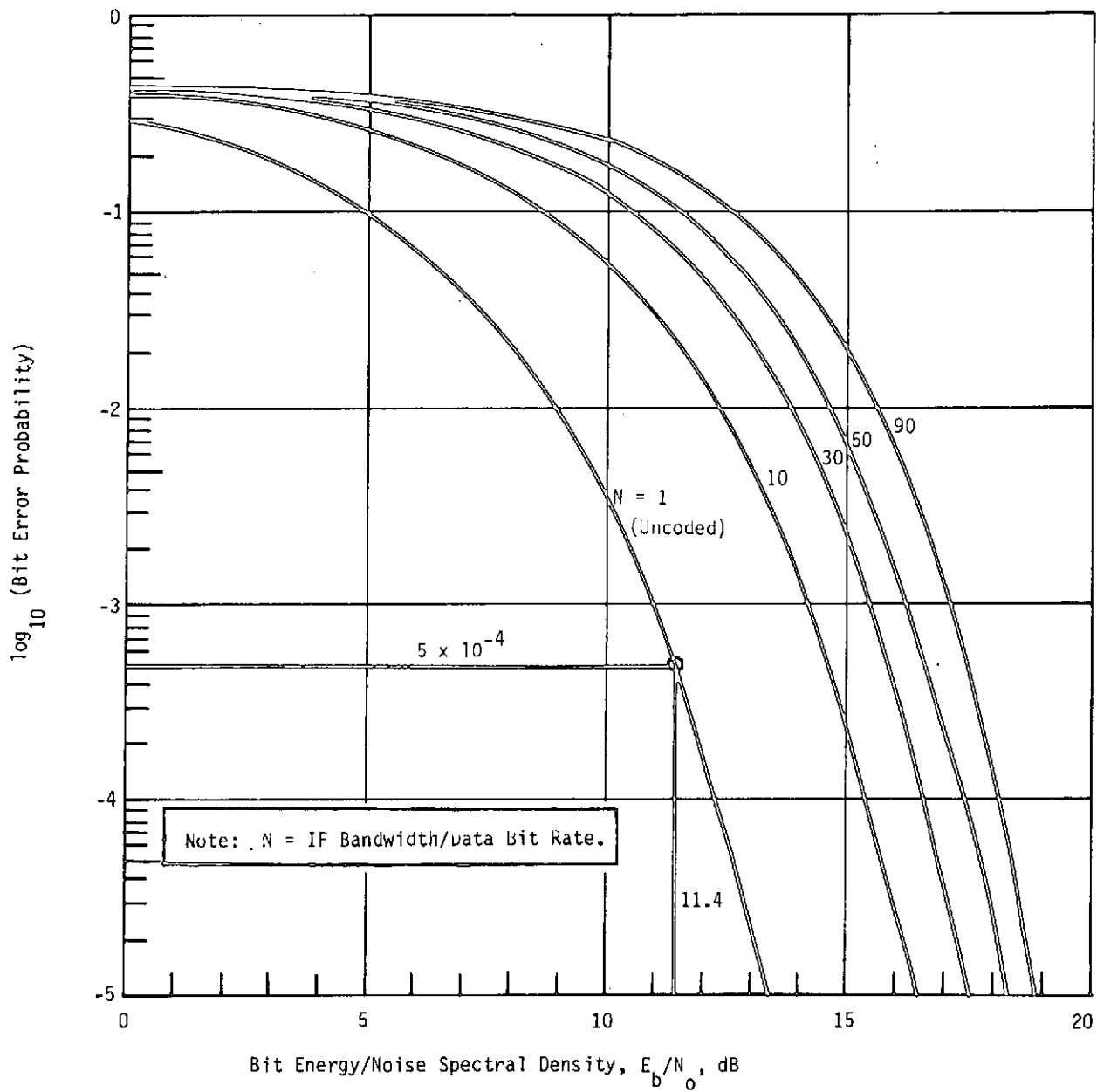


Figure 4.5-4 FSK Modulation Performance

coded coherent PSK and for rate 1/2 Viterbi decoding. For a BER of  $5 \times 10^{-4}$ , the coding gain is 4.3 dB. This reduces the  $E_b/N_0$  to  $11.4 - 4.3 = 7.1$  dB. An additional processing loss of  $1 \text{ dB}$  is also assumed, bringing the value up to 8.1 dB. This is the value used for noncoherent binary FSK modulation with a tracking tone, convolutional encoding, rate 1/2 Viterbi decoding for a bit error rate of 5 parts in  $10^4$ , and a constraint length of 8.

Although the probe communication subsystem does not include a bandpass limiter preceding the predetection bandpass filter, further investigation may indicate a requirement for bandpass limiting. Figure 4.5-5 shows the bit error rate with and without bandpass limiting. Note that for wideband FSK (i.e.,  $N > 1$ ) using bandpass limiting degrades the performance of the system.

Four basic design approaches for a relay link have been considered: (1) FSK using a pilot tone for tracking, (2) FSK with data tracking, (3) coherent PSK modulation and, (4) PSK modulation using data-aided tracking loops. The first approach is the most inefficient with respect to usage of available transmitter power. However, this option was chosen on the basis of channel uncertainties and represents the most conservative approach. The areas requiring additional investigation are:

- 1) Fading effects due to atmospheric turbulence;
- 2) Tracking performance with respect to Doppler rate, loop bandwidth, and S/N ratio;
- 3) Acquisition time.

Future research should be concentrated on approaches 2, 3, and 4 from the viewpoint of efficient power usage. Further analyses, computer simulation, and hardware breadboarding will be necessary to select a preferred configuration. Results concerning the fading effects of a turbulent atmosphere on a standard, second-order tracking loop and a convolutionally coded system are forthcoming in Reference 4.5-1. Additional details on promising FSK and PSK systems that use data tracking are also included in this reference.

#### Entry Blackout

The SU probe enters the planet's atmosphere at a high relative velocity. Interactions with the atmosphere result in thermal ionization, with an attendant RF blackout. The extent of the RF blackout must be established to determine when communication from the probe can be expected after entry. During the RF blackout, science and engineering data are stored in memory circuits on the probe. The probe transmitter is turned on when a g-switch senses a value of  $49 \text{ m/sec}^2$  ( $5 \text{ g}$ ) decreasing in the nominal atmosphere. At this time, the probe is

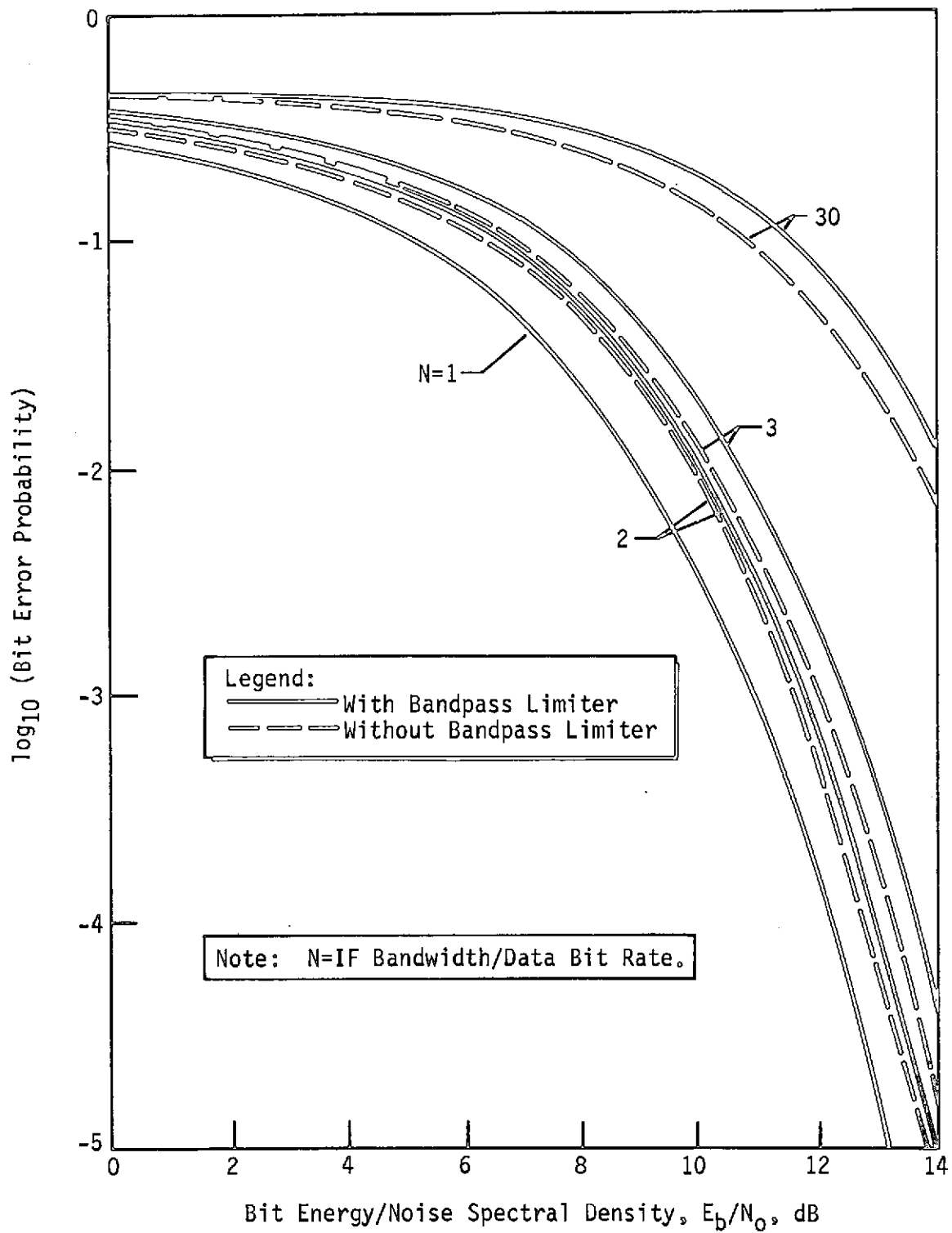


Figure 4.5-5 Error Probability Performance as a Function of Bandpass Limiting

descending at a velocity less than supersonic. An analysis was performed to verify that RF blackout was over when the transmitter was energized.

Saturn has the highest atmospheric density of the two planets, and the higher entry velocity and will create the longest RF blackout. Equilibrium chemistry is applicable for low altitudes where

$$\rho_{\infty} D > 10^{-7} \text{ g/cm}^2, \quad (4.5-1)$$

$\rho_{\infty}$  = ambient density, g/cm<sup>3</sup>

D = diameter of the conical entry probe and heat shield, cm.

Nonequilibrium chemistry is applicable when Equation (4.5-1) is less than  $10^{-7}$  g/cm<sup>2</sup>, which occurs at the higher altitudes.

Data are not available on electron density profiles in a hydrogen/helium atmosphere for a conical entry geometry. Work was done for the atmosphere of Jupiter 60 km below the turbopause where  $\rho_{\infty}$  was  $4.3 \times 10^{-10}$  g/cm<sup>3</sup> with a velocity of 50 km/s and ambient temperature of 95°K. The atmospheric composition is 89% hydrogen and 11% helium by volume (reference 4.5-7). The composition of the Jovian atmosphere is almost the same as that for the nominal Saturn and Uranus models, as shown in Table 4.5-3. Therefore, for the nonequilibrium region, the Jupiter turbopause probe calculation was used to determine the stagnation electron density. The flow regimes and plasma properties are shown in Figure 4.5-6. The probe antenna is located on the aft bulkhead in the near wake.

A kinetic energy ratio was set up for the conditions at Saturn:

$$\text{kinetic energy (K.E.)} = 1/2 \rho v^3. \quad (4.5-2)$$

The electron density was then proportioned in accordance with the kinetic energy available.

As seen from Equation (4.5-2), the electron density,  $n_e$ , becomes a function of the inertial velocity (v) and gas density ( $\rho$ ). Thus, the electron density at any point in the nonequilibrium region can be interpolated from the Jupiter calculation at the stagnation point (see Figure 4.5-6) using the equation

$$n_e = \frac{\rho v^3}{\rho' v'^3} n_e' \quad (4.5-3)$$



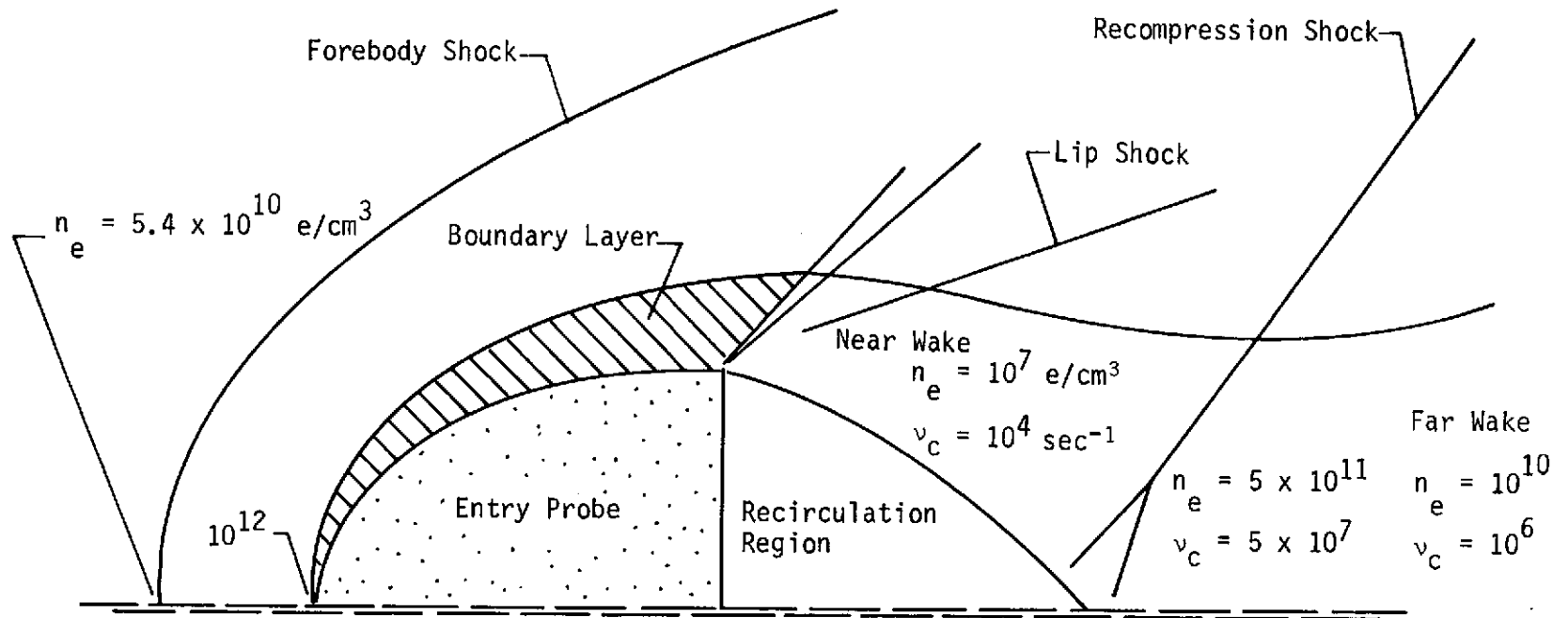
Table 4.5-3 Composition of the Model Atmospheres by Volume

Parameter	Saturn, %			Uranus, %		
	Cool	Nominal	Warm	Cool	Nominal	Warm
Hydrogen	73	88	95	30	86	95
Helium	26	11	5	60	11	4
Water	0.4	0.1		0.3	0.1	
Methane	0.2			9	3	1

Table 4.5-4 Probe Descent Parameters

Atmosphere Model	Time before Mach 10 (E + time), sec	Velocity at Mach 10, km/sec	Time before, 49 m/sec <sup>2</sup> (5 g), sec
Saturn			
Cool	15	5.5	29
Nominal	26	6.2	44
Warm	47	6.9	69
Uranus			
Cool	16	3.5	21
Nominal	40	5.0	45
Warm	80	6.3	78

\*Conditions: 1. 0.79 rad (45°) half-angle conical shape.  
 2.  $\gamma_E = -0.52$  rad (-30°)  
 3. B = 125.6 kg/m<sup>2</sup> (0.8 slug/ft<sup>2</sup>).



**Note:** 1. Atmospheric composition = 89%  $\text{H}_2$ , 11% He (by volume).  
 2. Conditions 60.0 km below turbopause:  
 $v_\infty = 50 \text{ km/sec}$ ;  
 $T_\infty = 95.5^\circ\text{K}$ ;  
 $\rho_\infty = 4.3 \times 10^{-10} \text{ g/cm}^3$ .

Figure 4.5-6 Flowfield Regions and Plasma Properties for the Jovian Entry Probe

where the primed terms represent Jupiter values. Using the values from Figure 4.5-6 in Equation (4.5-3), yields the following relationship for Saturn:

$$\frac{n_e}{\rho v^3} = \frac{10^{12}}{4 \times 1.25 \times 10^{-5}} = 2 \times 10^{16}. \quad (4.5-4)$$

The density profile for the nominal Saturn atmosphere indicates that Equation (4.5-1) is satisfied until approximately 20 seconds after entry, at which time equilibrium flow begins to take place.

At the lower elevations, where the gas density is increasing and equilibrium chemistry prevails, the electron density decays with the Mach number and the temperature behind the shock. For a ratio of specific heats of 1.3 for the hydrogen/helium mixture, electron densities...

below  $10^8$  begin to occur at Mach numbers below 10. The probe operating frequency of 560 MHz, when used for the critical plasma frequency, corresponds to a critical electron density of  $3 \times 10^9$  electrons/cm<sup>3</sup>. Any density below this value will not create RF blackout at the operating frequency. Therefore, we conclude that the probe will be out of the RF blackout when it reaches a Mach number of 10 and lower.

For the Saturn encounter, Mach 10 occurs 47 seconds after entry with a relative velocity of 7 km/sec in the warm atmosphere model as seen in Table 4.5-4. The electron density in the near wake during Saturn entry is shown in Figure 4.5-7. This curve is based on the Jupiter electron density data extrapolated to the entry conditions at Saturn. The shape of the curve is not exact, but the peak electron density agrees quite well with the Jupiter entry calculations. The value calculated at 45 seconds after entry is based on equilibrium chemistry that exists at the lower elevations as the probe velocity decreases. Entry is defined as the pressure [ $10^{-2}$  N/m<sup>2</sup> ( $10^{-7}$  bar)] where aerodynamic effects are present and represents the boundary of the turbo-pause.

A heat shield is affixed to the forebody of the probe. This is made of quartz nitrile phenolic for the nominal atmospheres and carbon phenolic for the worst-case atmosphere. For either case, the material is a charring ablator that is very low in free electron sources. The exact level of additional electrons added to the flow field during entry is not known but would only slightly increase the peak density shown in Figure 4.5-7. The heat shield materials are inherently low in alkali metal impurities (sodium and potassium) and should not be a significant source of electrons that would enhance the ionized plasma entry sheath.

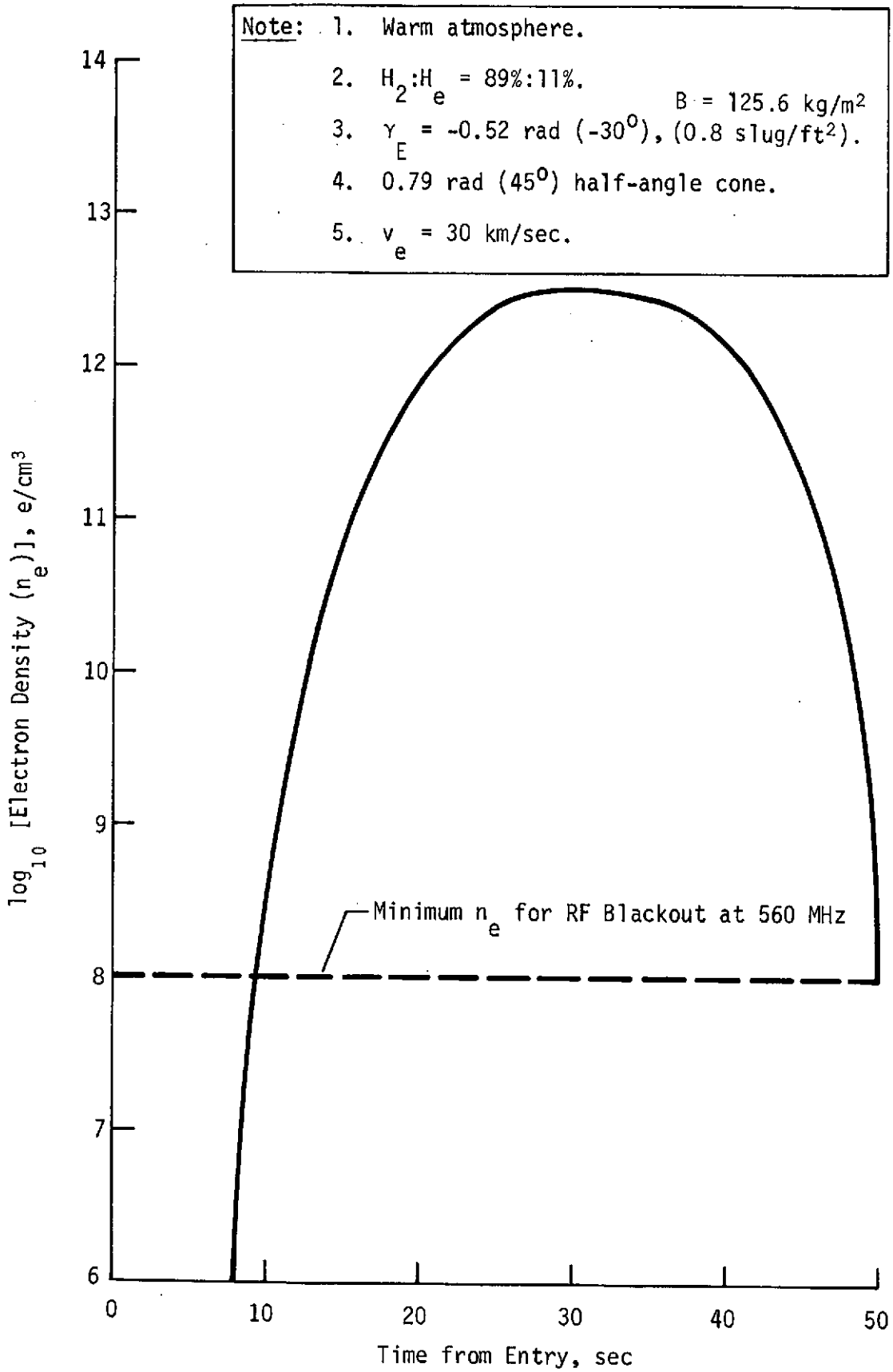


Figure 4.5-7 Electron Density in the Near Wake During Saturn Entry

In conclusion, the RF power amplifier portion of the probe transmitter should not be turned on during entry to obviate the possibility of an antenna RF breakdown due to corona effects. Hypersonic entry ionization is sufficient to cause RF blackout at 560 MHz, approximately 8 seconds after entry and lasting until 50 seconds after entry (see Figure 4.5-7).

Mach 10 occurs at different times for the three atmosphere models and also depends on the size and weight of the probe. The mission sequence is scheduled to turn the RF power amplifier portion of the probe transmitter on at  $49 \text{ m/sec}^2$  (5 g) decreasing for the nominal atmosphere and at  $29.4 \text{ m/sec}^2$  (3 g) for the worst-case atmospheres. The latter will result in a probe velocity even lower than that shown in the last column of Table 4.5-4. This is sufficient time to ensure that the RF blackout is over for any atmosphere model since the transmitter turn-on times exceed the Mach-10 times.

#### Receiver System Noise Temperature

The noise present in the communication subsystem is a disturbing factor and places a limit on the minimum detectable signal. The various effects of noise are not constant during a probe mission and change with the relative geometry. This adds to the complexity and requires a worst-case analysis to determine the system noise temperature. Internal noise sources include feedline loss and the electronic circuitry of the receiver. External noise sources, such as the galaxy, stars, magnetospheres, planets, and atmospheres can also be significant contributors through the receiving antenna on the spacecraft (references 4.5-8 and 4.5-9).

In general, the internal noise increases and the external noise decreases as the frequency increases. Noise power may be evaluated in terms of an absolute temperature and may be summed to determine the total receiver system noise temperature, which relates to the system noise level. The noise performance of a receiver is also related by a noise figure (reference 4.5-10). The following paragraphs summarize an analysis described in Reference 4.5-11. This reference should be consulted for a complete description of the approach.

The total noise power in the receiving system may be represented by a system noise temperature,  $T_s$ , such that the total available noise power referred to the receiver's output terminals is  $kT_s B$ , where  $B$  is the receiver noise bandwidth and  $k$  is Boltzmann's constant. Generally,

$T_S$  may be regarded as the sum of three components: (1) the contribution of the antenna due to reception of noise from external radiating sources; (2) the thermal noise generated due to dissipative losses in the receiving transmission line system; and (3) the noise from sources within the receiver itself. The division of the receiving system into three components is shown in Figure 4.5-8.

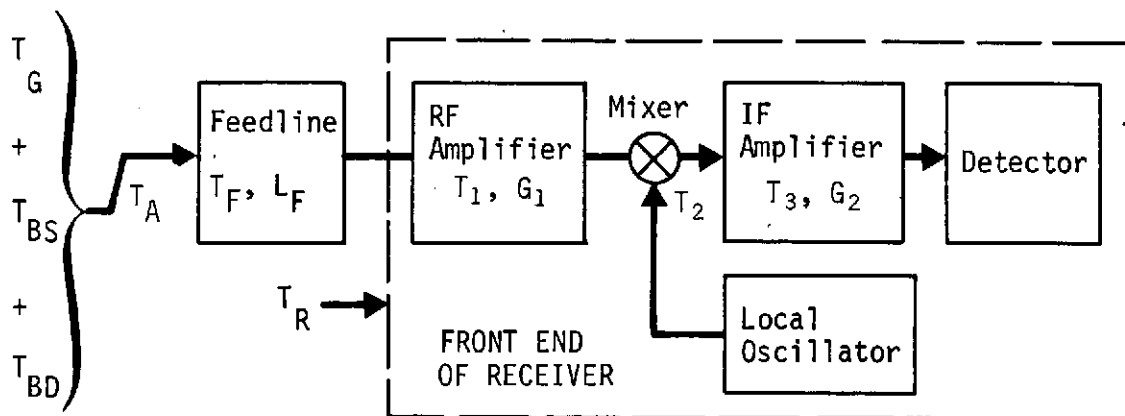


Figure 4.5-3 Noise Components of the Spacecraft Receiver

The system noise temperature is used in all receiver sensitivity considerations and in calculating the total effective noise power density per modulation bandwidth (reference 4.5-12). System noise temperature is defined as

$$T_S = T_A + T_F + L_F T_R, \quad (4.5-5)$$

- where  $T_S$  = receiving system noise temperature,  $^{\circ}\text{K}$   
 $T_A$  = antenna noise temperature,  $T_G + T_{BS} + T_{BD}$  as applicable,  $^{\circ}\text{K}$   
 $T_G$  = galactic noise temperature,  $^{\circ}\text{K}$   
 $T_{BS}$  = synchrotron noise temperature,  $^{\circ}\text{K}$   
 $T_{BD}$  = planet disk noise temperature,  $^{\circ}\text{K}$   
 $T_F$  = antenna feedline noise temperature,  $^{\circ}\text{K}$   
 $T_R$  = receiver noise temperature,  $^{\circ}\text{K}$   
 $L_F$  = feedline power loss ratio.

As seen in Equation (4.5-5), the feedline loss affects the noise temperature of the receiver. The feedline temperature in °K is expressed by

$$T_F = 290^\circ (L_F - 1). \quad (4.5-6)$$

The loss in 0.91 meter (3 ft) of coaxial cable (from antenna feed to receiver) is 0.6 dB at 560 MHz. The two connectors add 0.4 dB, for a total loss of 1 dB (power ratio = 1.26). From Equation (4.5-6), then,  $T_F = 75^\circ\text{K}$ . It is important to have the receiving antenna close to the receiver and minimize the length of the feedline cable. Low-loss cable and connectors should be used on the spacecraft to keep the reflected noise temperature to a minimum.

The receiver consists of an amplifier and mixer (see Figure 4.5-8) that feed a detector. The receiver noise temperature of a typical superheterodyne receiver, with an RF amplifier and a mixer down-converter to IF frequencies, is given by the relationship

$$T_R = T_1 + \frac{T_2}{G_1} + \frac{T_3}{G_1 G_2}, \quad (4.5-7)$$

where T represents the noise temperatures of the various amplifier stages and G represents the power gain ratio of the RF and IF amplifier stages. For a typical RF amplifier and mixer package, as shown in Figure 4.5-8, where  $T_1 = 289^\circ\text{K}$  ( $N_F = 3\text{ dB}$ ),  $T_2 = 600^\circ\text{K}$ ,  $T_3 = 3000^\circ\text{K}$ ,  $G_1 = 30\text{ dB}$  (ratio = 1000), and  $G_2 = 13\text{ dB}$  (ratio = 20), the receiver noise temperature from Equation (4.5-7) is  $289.75^\circ\text{K}$ . As can be seen, the noise temperature of this receiver is controlled by the RF amplifier noise ( $T_1$ ). The other high-gain stages in the receiver add less than one degree of noise.

The effective noise temperature (ENT) of solid-state receivers for the frequency range of interest is shown in Figure 4.5-9. The curves depict the noise temperature,  $T_R$ , and the noise figure for tunnel diodes and transistor receivers based on the 1970 state-of-the-art (reference 4.5-13). Noise figures have not improved significantly since that year (reference 4.5-14). Consequently, we constructed an average curve 1 dB above the minimum curve and used the average curve in the study. The curves shown in the figure are averages for several suppliers and represent the state-of-the-art for solid-state microwave receivers. The slope of the curves indicate that the average ENT is increasing with increasing frequency.

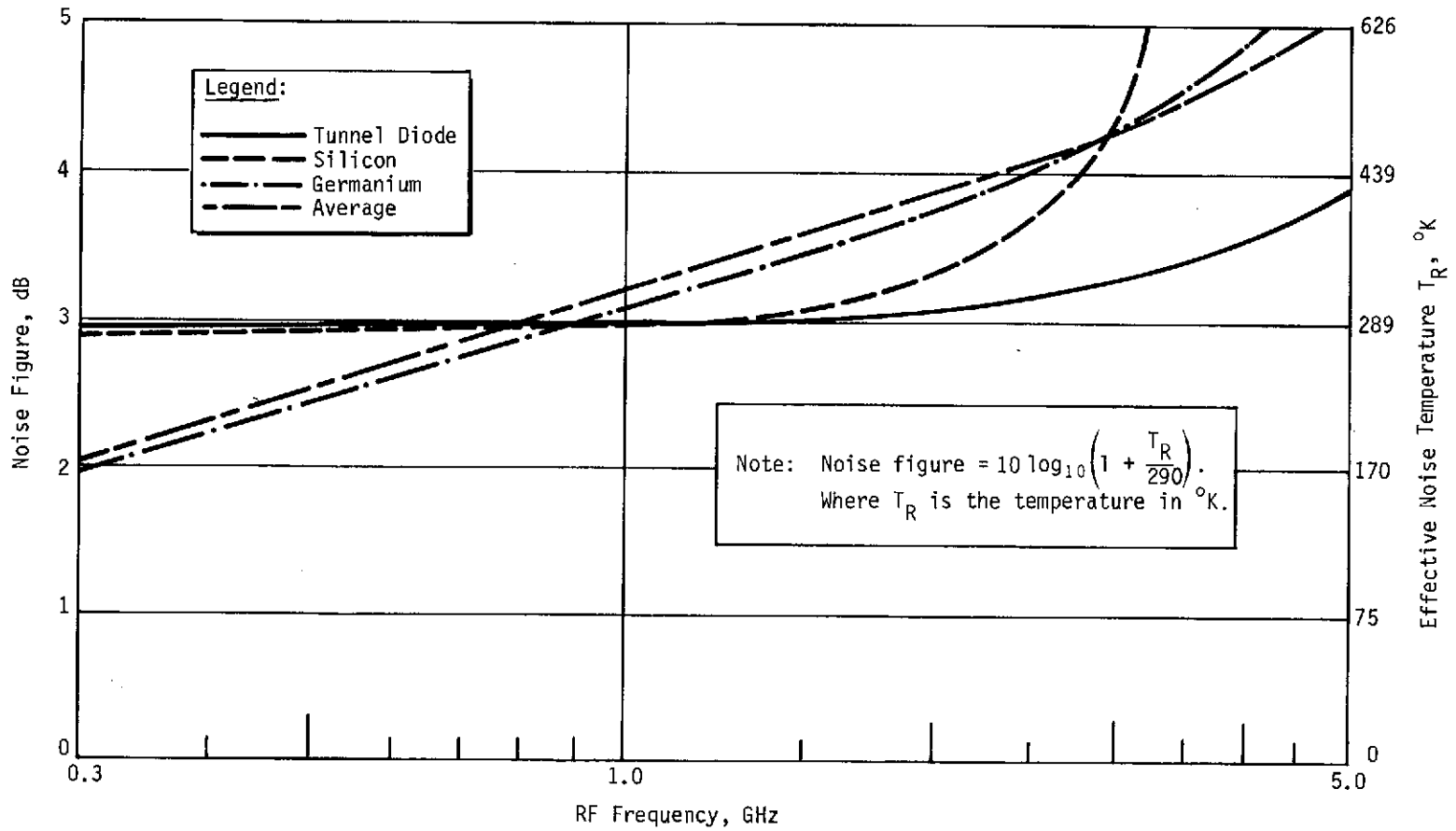


Figure 4.5-9 1970 State-of-the-Art Noise Figure for Microwave Receivers



In Equation (4.5-5),  $T_A$  is the only quantity not determinable by measuring components of the radio receiving system in the laboratory. It is basically determined by the environment rather than the system. Thus the antenna ENT is the composite result of the radiating noise sources within the total pattern of the antenna. In the case of the probe receiving antenna on the Pioneer spacecraft, the antenna is exposed to noise sources that vary with the probe mission time. For the link analysis, the geometry resulting in the worst-case conditions was chosen to provide a degree of conservatism in the RF link.

A probe receiving antenna with a split axial (butterfly) radiation pattern is required for the spin-stabilized Pioneer spacecraft. The planet disk occupies only a small portion of the total antenna radiation envelope in the roll plane. For Saturn and Uranus, a thermal noise source emanates from the planet disk in the form of black-body radiation. References 4.5-15 (pp 15-19) and 4.5-16 (pp 20-22) contain measured data and upper-limit curves that indicate the magnitude of decimetric (UHF) radiation in terms of the brightness temperatures,  $T_{BD}$ .

Saturn has a second source of noise that emanates in the form of nonthermal UHF radiation from the magnetosphere surrounding the planet. The radiation belt of Saturn is weaker than Jupiter's, and Uranus does not have any evidence of synchrotron (relativistic) radiation. A model does not presently exist that defines the extent of the magnetosphere. The rings probably interfere with the formation of a uniform belt interior to  $2.3 R_S$ . Therefore, it was assumed that synchrotron noise also originates from the planet disk. The Saturn monograph gives an equation for the upper limit synchrotron temperature,  $T_{BS}$ , as a function of the wavelength,  $\lambda$ , in cm:

$$T_{BS} = 0.4 \lambda^2. \quad (4.5-8)$$

Depending on the spacecraft-planet geometry, a third source of thermal noise may be present in the form of galactic noise. Background cosmic noise from the Milky Way galaxy is shown in Figure 4.5-10 (reference 4.5-17). As seen from the figure, the orientation of the antenna pattern toward or away from the galactic center significantly affects the value chosen. The position of the galactic center relative to the antenna look direction depends on the planet of interest, the arrival date, and the spacecraft-to-probe geometry.

The relative geometries for the two missions are shown in Figure 4.5-11. As seen in Figure 4.5-11(a) for Saturn, whenever the axial beamwidth is greater than  $0.87$  rad ( $50^\circ$ ) galactic noise will be present, in addition to planet disk and synchrotron noise. At Uranus

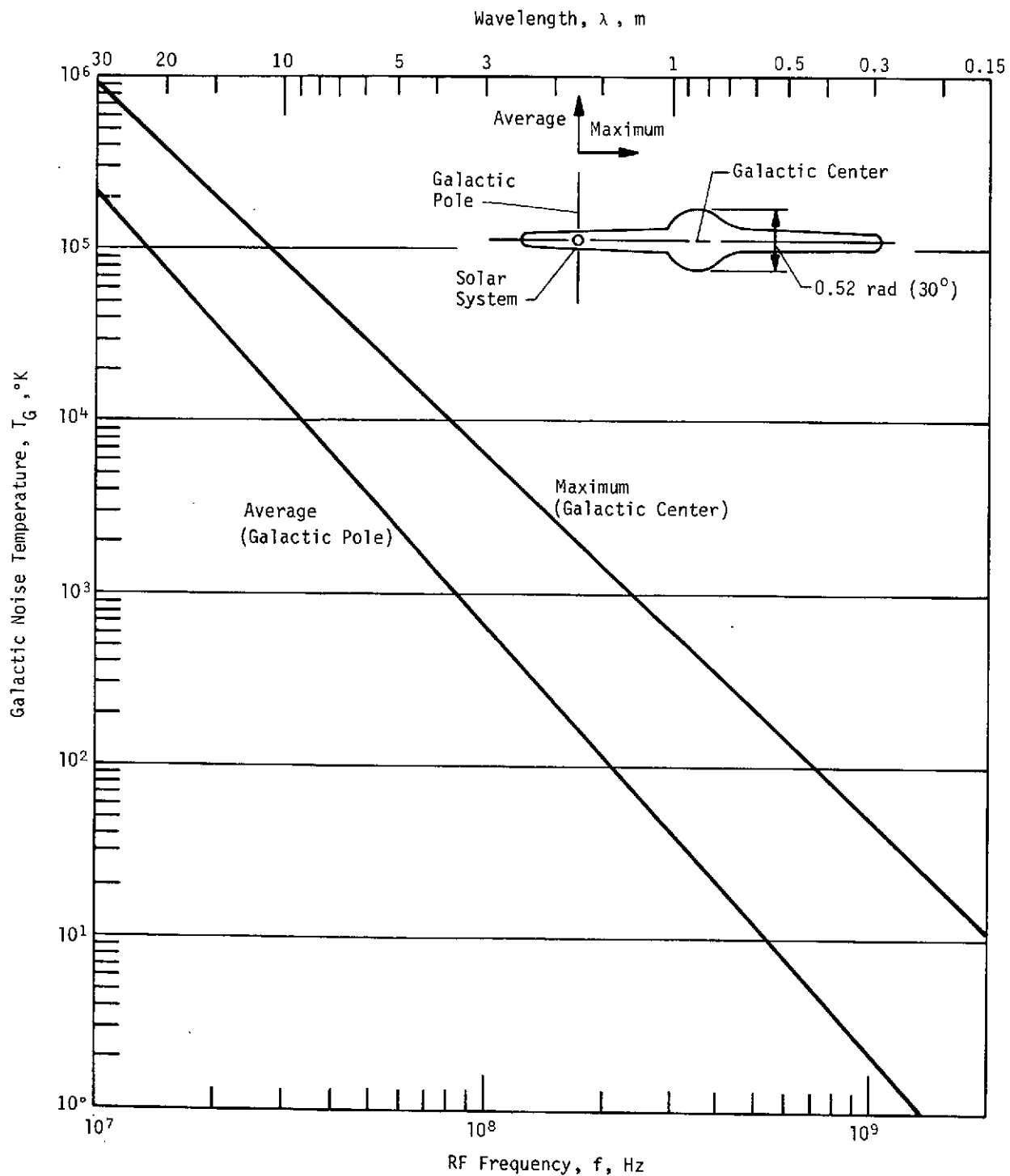


Figure 4.5-10 Thermal Noise Temperature of the Milky Way Galaxy

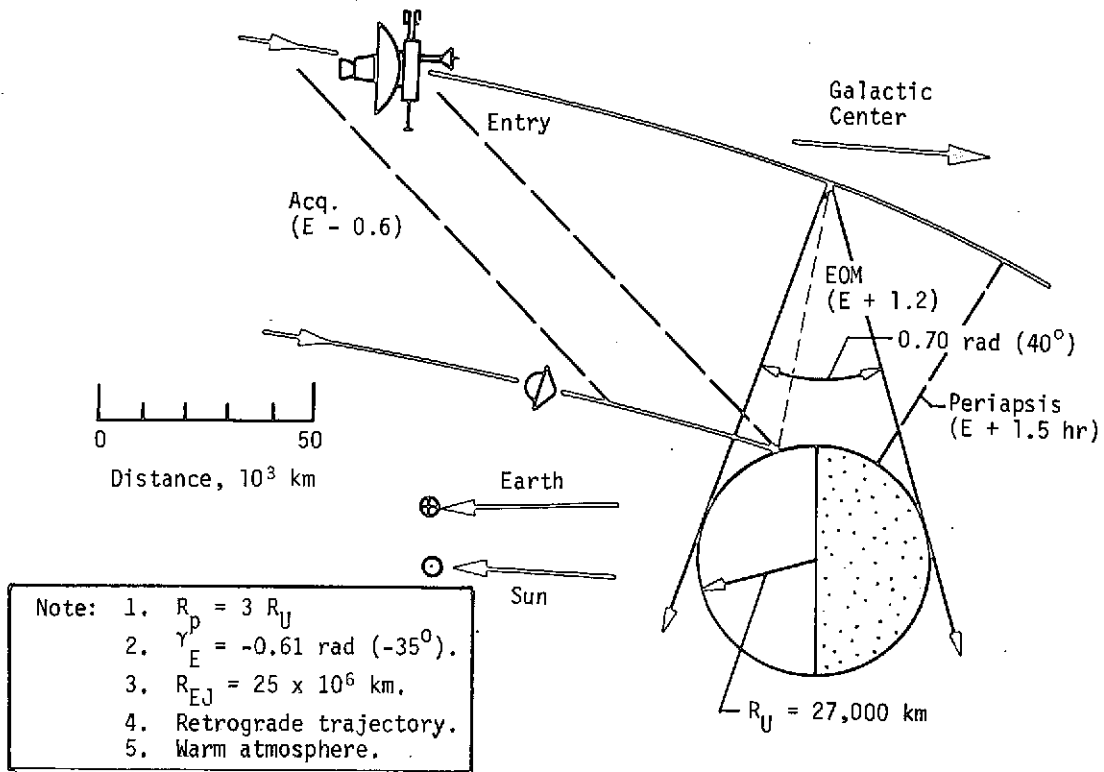
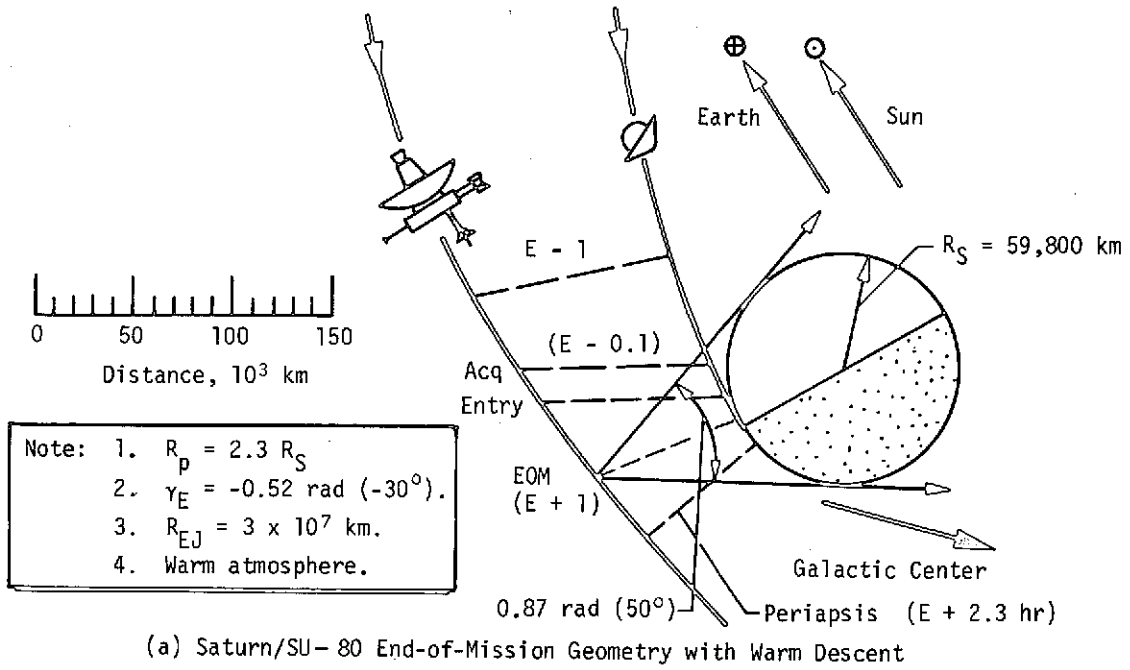
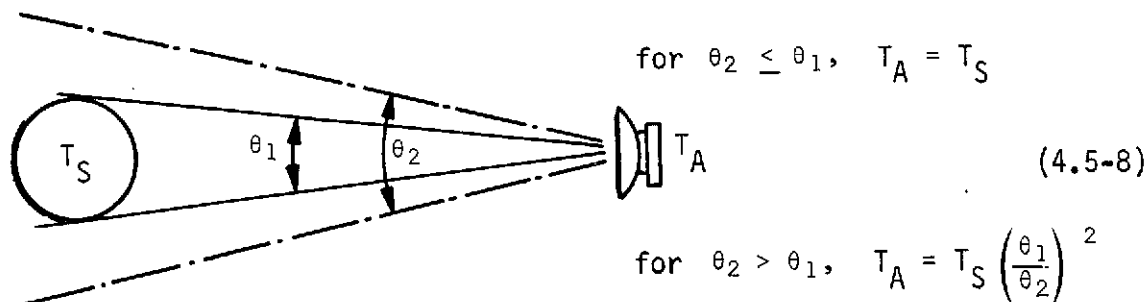


Figure 4.5-11 Saturn/Uranus Geometries for Worst-Case Viewing Angle from the Spacecraft

[Figure 4.5-11(b)] for beamwidths greater than 0.70 rad ( $40^\circ$ ), galactic noise is present. The average values, shown in Figure 4.5-10, are used as a result of the direction to the galactic center at Uranus.

In our analysis, equations for the antenna noise temperature at the two planets were developed using the encounter geometries for the SU-80 mission. As seen in Figure 4.5-11, minimizing the communication range causes the included angle of the planet disk to be a maximum, which occurs at the end of the mission. This condition gives the highest noise temperature and is the worst-case geometry. The spacecraft antenna noise temperature is constantly changing during the probe mission. Before probe acquisition, the antenna noise is relatively low and is essentially made up of contributions from stellar, cosmic, and galactic sources. As the planet disk comes into the antenna pattern, the noise level increases and peaks as the full disk occupies the background of the antenna pattern.

When a noise source is located within the antenna pattern, the planar relationships are expressed by Equation (4.5-8), where  $\theta_2$  is the planar angle subtended:



Using a split axial beam on the spacecraft with discrete noise sources within the beam requires a mathematical integration to determine the area of the antenna pattern and the ratio between the areas of the noise source and that of the antenna pattern. The antenna noise temperature is then the sum of the external noise sources, weighted in accordance with the solid angle ratios for each of the sources to the pattern area (references 4.5-18 and 4.5-19). Galactic noise is present throughout the beam as a fairly uniform source. In addition, the planet noise must be added in the proper proportion, dependent on the maximum included angle (see Figure 4.5-11). The

total antenna noise temperature then becomes a function of the ratios of the solid angles of the planet disk and antenna pattern, or

$$T_A = T_G + (T_P - T_G) \frac{\Omega_P}{\Omega_A}. \quad (4.5-9)$$

The SU-80 geometries result in spacecraft cone angles centered at  $S = 1.05$  rad ( $60^\circ$ ) to cover both planet missions with a beamwidth of  $0.96$  rad ( $55^\circ$ ) for the final configuration. The antenna beam area,  $\Omega_A$  is then  $5$  sr.

The solid angle intercepted by the planet,  $\Omega_P$ , is a function of the planet's size and the relative geometry between the spacecraft and the planet during flyby (see Figure 4.5-11). Using the geometry for Saturn shown in the figure, the worst-case included angle of the planet disk is  $0.87$  rad ( $50^\circ$ ), which occurs at mission completion;  $\Omega_P$  is  $0.6$  sr; and  $\Omega_P/\Omega_A$  is  $0.12$ . Applying the two noise sources to Equation (4.5-9), the antenna noise temperature for Saturn becomes

$$T_A = T_G + 0.12 (T_{BS} + T_{BD} - T_G). \quad (4.5-10)$$

The values used for  $T_G$  for Saturn are taken midway between the curves in Figure 4.5-10 as a result of the relative direction to the galactic center.

For a Uranus flyby using the same butterfly beam discussed previously for Saturn, since a common spacecraft antenna must be used,  $\Omega_A$  is  $5$  sr. In this case, Figure 4.5-11 (b) shows that the worst-case included angle of the planet disk is  $0.7$  rad ( $40^\circ$ ), occurring at mission completion,  $\Omega_P$  is  $0.38$  sr, and  $\Omega_P/\Omega_A$  is  $0.06$ . Since Uranus has only one noise source, the planet disk, Equation (4.5-9) then becomes

$$T_A = T_G + 0.06 (T_{BD} - T_G). \quad (4.5-11)$$

Note that the galactic noise temperature used in Equation (4.5-11) for Uranus is the average curve shown in Figure 4.5-10 since the galactic center is in the sidelobe region of the beam [see Figure 4.5-11 (b)].

Figures 4.5-12 and 4.5-13 depict the noise temperatures of the antenna and receiving system for Saturn and Uranus with a split axial receiving antenna on the spacecraft. Note that in all the system noise curves, a constant feedline loss of  $1$  dB was used

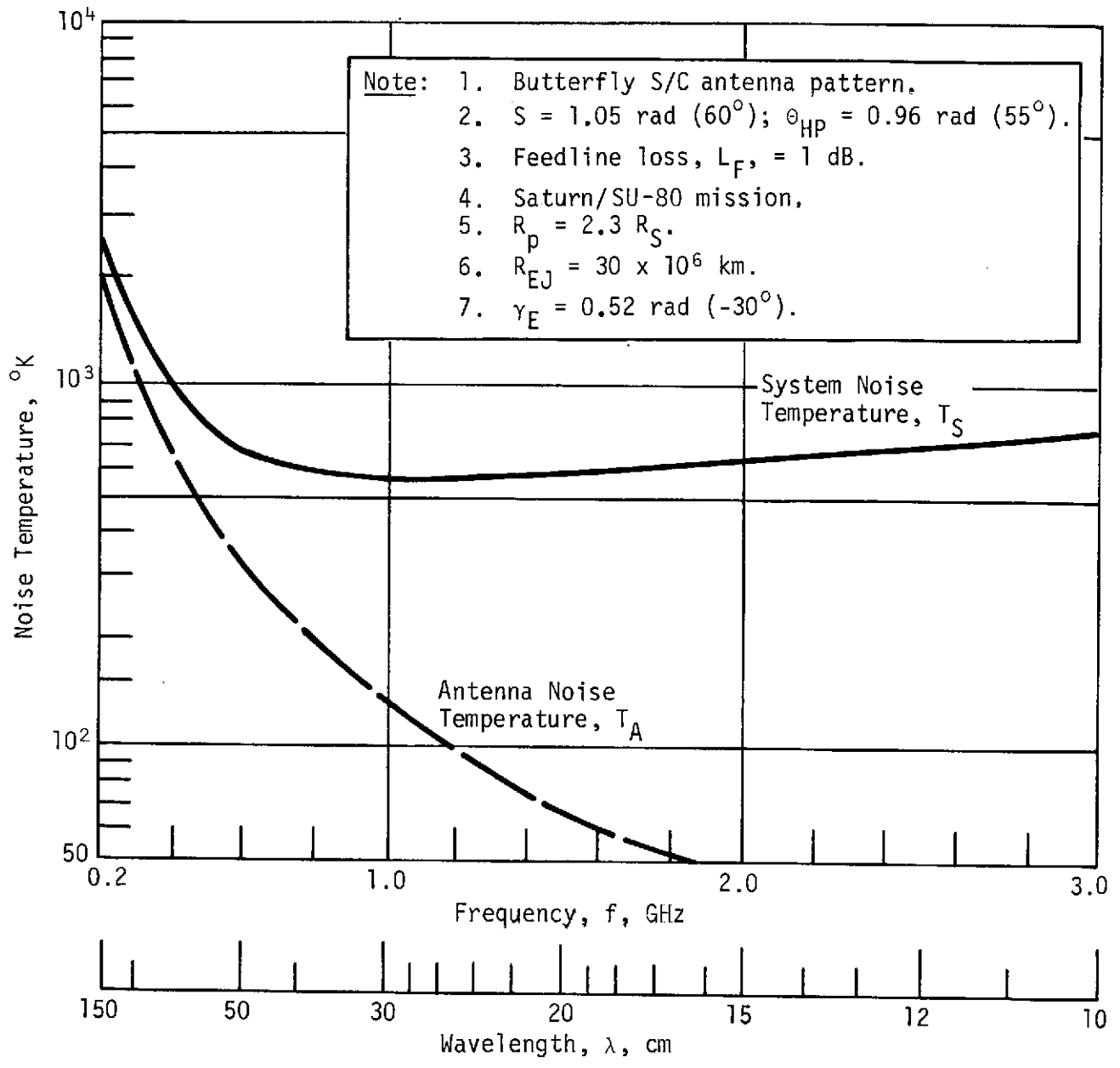


Figure 4.5-12 Receiving System Noise Temperature for Saturn with Split Axial Beam Antenna - All Configurations

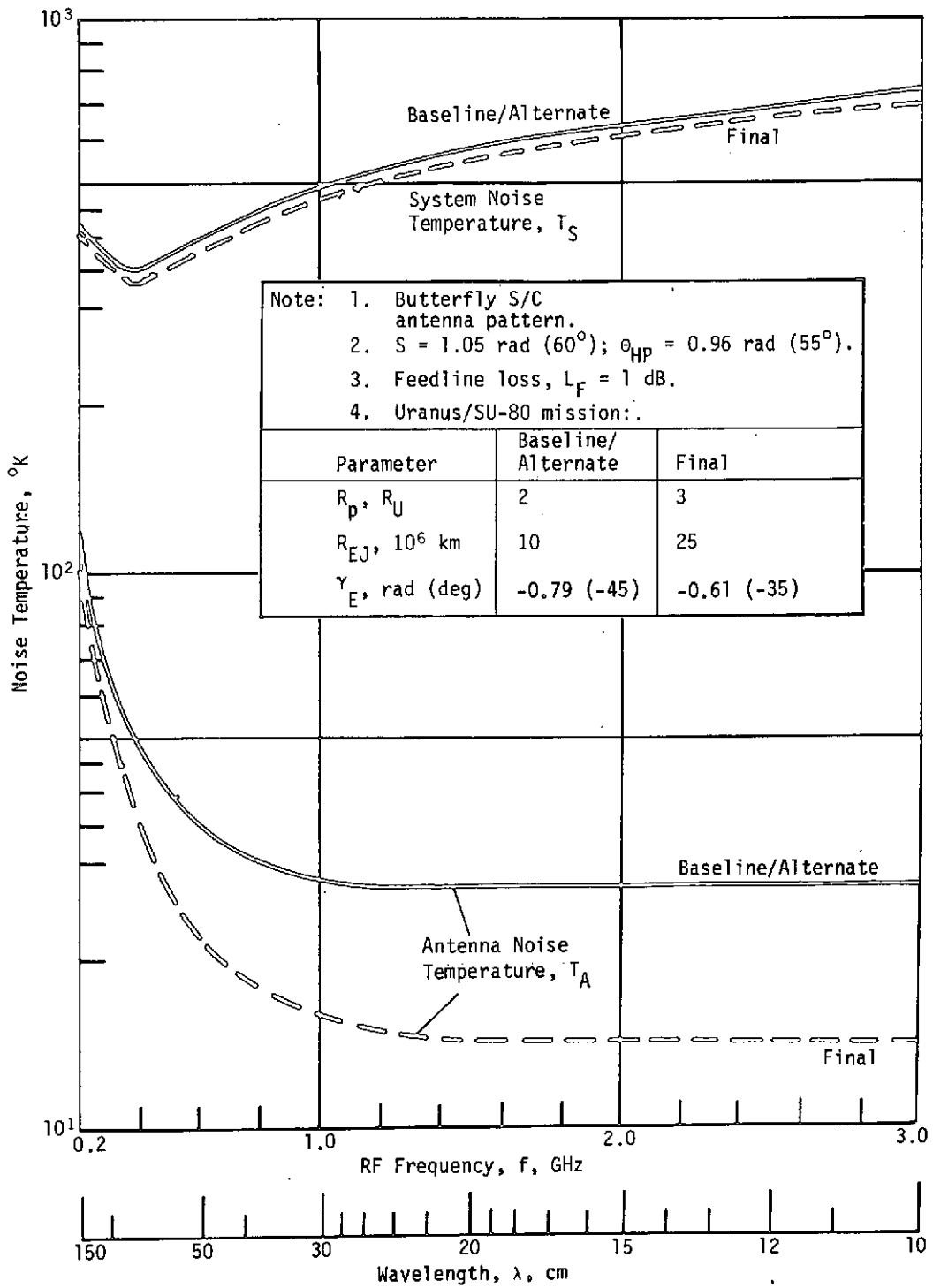


Figure 4.5-13 Receiving System Noise Temperature for Uranus with Split Axial Beam Antenna

since the variation in coaxial cable and connector attenuation over the frequency range of interest is very small. These figures describe the worst-case system noise temperature as a function of frequency. This relationship can then be used in the RF link analysis when calculating the noise power spectral density,  $N_o = kT_S$ , of the receiver. Note that two curves for Uranus are shown in Figure 4.5-13 since the trajectory changed for the final design configuration. Final configuration geometries are shown in Figure 4.5-11(b).

#### Atmospheric Microwave Losses

The basic method of computing absorption and defocusing losses in the planetary atmosphere is described in Reference 4.5-2, Vol III Appendix A and Vol IV pp III-63 thru III-70. Detailed results for the Saturn and Uranus nominal-atmosphere models are given in Vol III of the reference, and those for the worst-case atmospheres are presented in Vol IV. The basic method is summarized below.

For atmospheres such as those found on Saturn and Uranus, the principal source of microwave absorption is gaseous ammonia. Water vapor and liquid water/ammonia solution clouds also contribute to absorption losses. Absorption in solidified ammonia or water clouds is negligible. During descent, the probe encounters solid ammonia clouds before reaching the water/ammonia solution clouds as seen in Figure 4.5-14. In general, the atmosphere model with the highest ammonia concentration will result in the greatest microwave absorption if the probe penetrates to the ammonia saturation level. However, for the descent into the cool Uranus atmosphere, this does not hold true because the probe fails to reach the saturation level as seen in the figure. In comparison, the saturation level for the nominal Uranus atmosphere occurs at -80 km and the probe descends to approximately 120 km at mission completion. Ammonia abundances for Saturn and Uranus are shown in Table 4.5-5. The values shown for Saturn were taken from Reference 4.5-15, p 43, and those for Uranus, from Reference 4.5-16, p 33. The warm models for both planets are very low in ammonia and were not investigated because their microwave absorption will be smaller than that for the nominal or cool models. Methane clouds were also excluded from our analysis since their microwave absorption is negligible. The nominal atmospheric models used in our analysis are based on work completed by D. A. De Wolf of RCA (Reference 4.5-20). Data on the atmosphere models were taken from the two monographs (References 4.5-15 and 4.5-16).



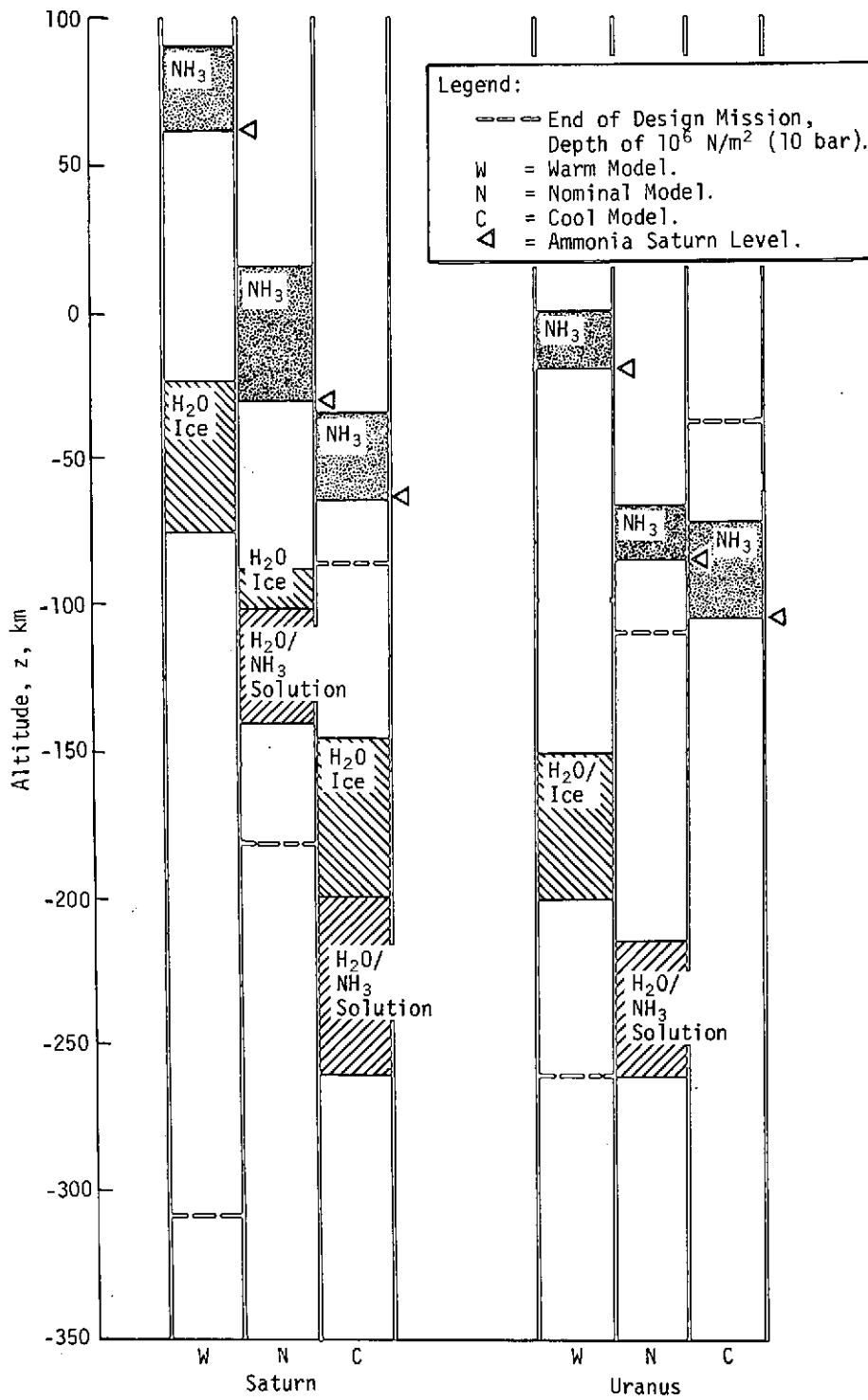


Figure 4.5-14 Location of Clouds That Affect Microwave Absorption

Table 4.5-5 Abundance of Ammonia in the Atmospheric Models

	Saturn Atmosphere			Uranus Atmosphere		
	Warm	Nominal	Cool	Warm	Nominal	Cool
Ammonia Mass Fraction, %	0.037	0.113	0.34	0.038	0.095	0.168

The zenith microwave absorptions for the nominal and cool Saturn models and for the Uranus nominal model are shown in Figures 4.5-15 thru 4.5-17. Each model depicts absorption as a function of altitude and pressure at several selected frequencies. Note that the zenith absorption is equal to the total microwave attenuation since the defocusing losses are zero at zenith. The defocusing losses for the two planets are similar to those shown in Figures A-8 and A-9 of Vol III, Appendix A of Reference 4.5-2, and are less than 0.1 dB for the altitudes and aspect angles encountered during the missions. For small departures from zenith, the attenuation due to atmospheric absorption increases as  $\sec \psi$ , where  $\psi$  is the probe aspect angle. For larger values of  $\psi$ , ray-bending effects must be considered, but the diffraction error is quite small out to about 1.05 rad ( $60^\circ$ ) off zenith.

A recent change in the atmospheric analysis consisted of calculating the variable abundances of ammonia and water in the saturated region in and above the clouds, rather than setting the abundances equal to zero above the saturation elevation. Absorption in this region is very low compared to that below the saturation elevation. Therefore, it can be neglected for probe missions that penetrate any distance below the ammonia saturation elevations, which are represented by triangles in Figure 4.5-14. The necessity of adding this computation arose from an examination of the cool Uranus model. Since the ammonia saturation level occurs at a pressure of  $8.07 \times 10^6 \text{ N/m}^2$  (80.7 bar), a  $10^6 \text{ N/m}^2$  (10-bar) mission would be flown completely in the saturated region of the atmosphere. The equation used to compute the ammonia abundance was taken from Reference 4.5-21 and a similar expression was also used for the water abundance.

Computation of the microwave absorption loss in the cool Uranus model indicates that this loss is completely negligible due to the very low ammonia abundance in the saturation region and the fact that the mission is over before the probe reaches the ammonia cloud

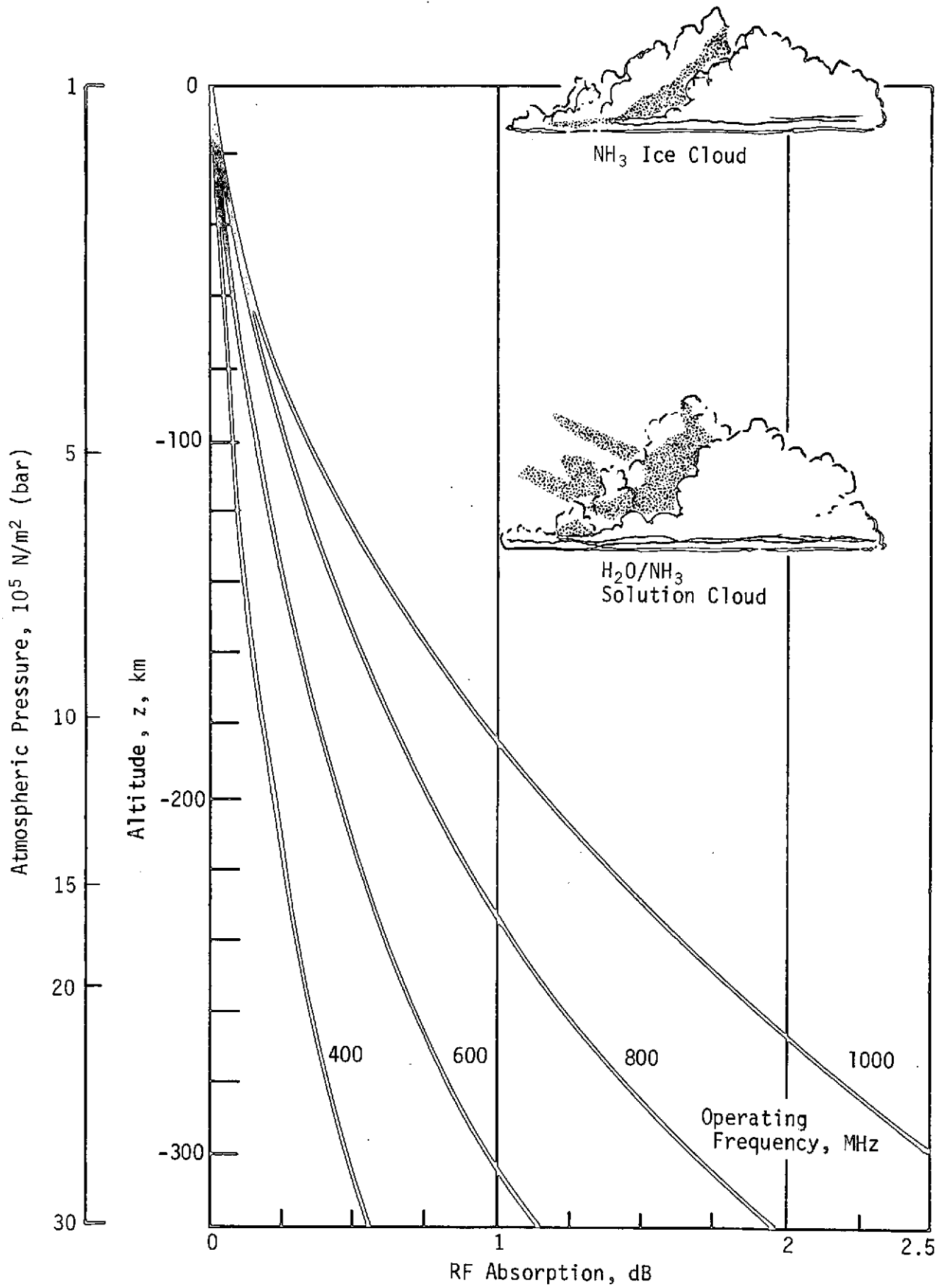


Figure 4.5-15 Zenith Absorption for the Saturn Nominal Atmosphere

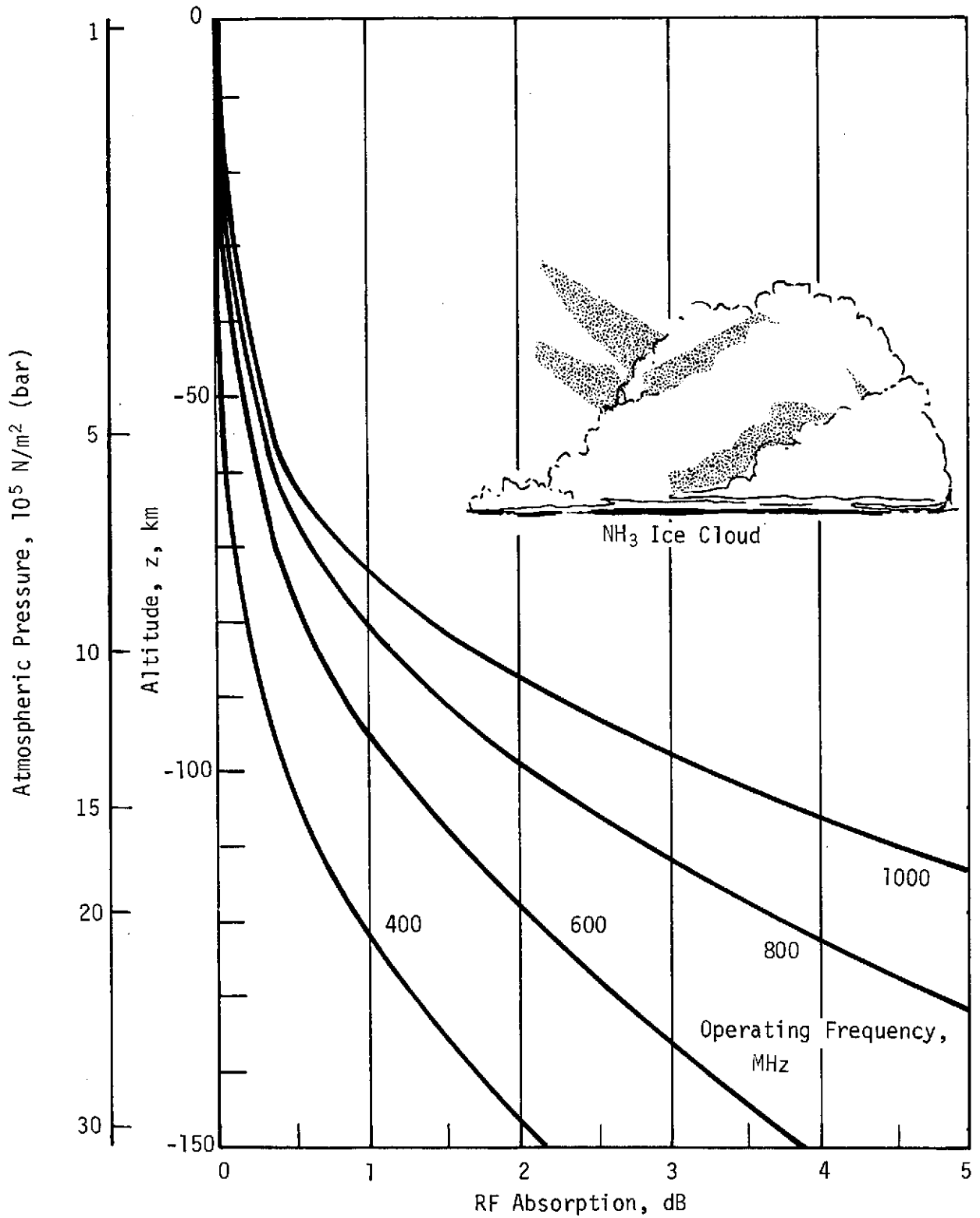


Figure 4.5-16 Zenith Absorption for the Saturn Cool Atmosphere

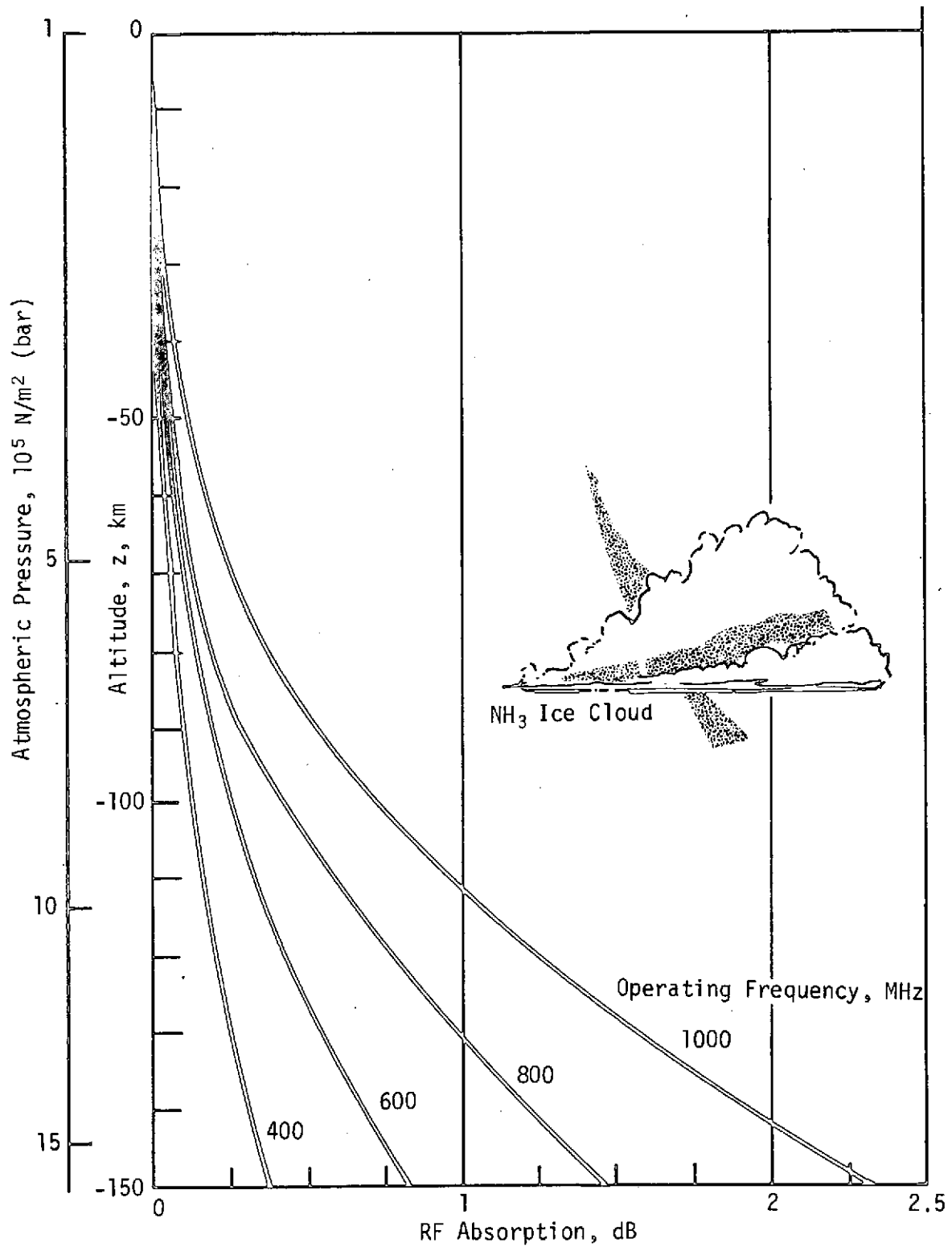


Figure 4.5-17 Zenith Absorption for the Uranus Nominal Atmosphere

level (see Figure 4.5-14). The zenith absorption at 1 GHz and a depth of  $2.8 \times 10^6$  N/m<sup>2</sup>(bar) was only 0.007 dB. Consequently, no absorption curve for the cool Uranus atmosphere was plotted because the absorption is essentially zero to  $3 \times 10^6$  N/m<sup>2</sup> (30 bar). The nominal Uranus atmosphere and cool Saturn atmosphere are the two worst-case atmospheres; and the cool Saturn model provides the greatest microwave absorption, as seen in Figure 4.5-16.

No data observed for Saturn or Uranus have been related to the characteristics of their ionospheres. Theories pertaining to Jupiter's ionosphere have been published but the conclusions have not been applied to Saturn. The peak electron and proton densities of  $10^7$  cm<sup>-3</sup> derived for Jupiter may, however, be representative for Saturn and Uranus. The ionospheric descriptions adopted for the two planets in the NASA monographs have a temperature of  $150 \pm 50$  °K and equal electron and proton concentrations given by

$$n_e = 10^6 \pm 1 \exp\left(-\frac{z - z_1}{250}\right) \text{ cm}^{-3}, \quad (4.5-12)$$

where  $z$  is the altitude in km (reference 4.5-15, p 38, and 4.5-16, p 30). The lower limit of the ionosphere is bounded by a reference altitude ( $z_1$ ), and  $n_e$  is zero for altitudes less than  $z_1$ . Equation (4.5-12) is valid for the following altitudes for the two planets:

- 1) Saturn,  $z > z_1 = 450 \pm 200$  km;
- 2) Uranus,  $z > z_1 = 300 \pm 200$  km.

The range of values for  $z_1$  is large enough to include different ionospheric layers of local maximum electron density, a situation analogous to the D, E, and F layers of the Earth's ionosphere.

The physical and chemical processes that affect the equilibrium distribution of ionization in the atmospheres of the outer planets are fairly well known. M. B. McElroy and other members of the Science Advisory Group are presently reviewing the ionospheric models to provide more comprehensive data. The relevant absorption and ionization cross-sections of electrons produced from the photoionization of H<sub>2</sub>, He, and H have been determined. In general, the electron density varies as the square root of the proton production rate. Computed densities are shown in Figure 4.5-18 for Saturn and Uranus.

The models used to generate the densities assumed that photochemical equilibrium applies (reference 4.5-22). The predicted electron

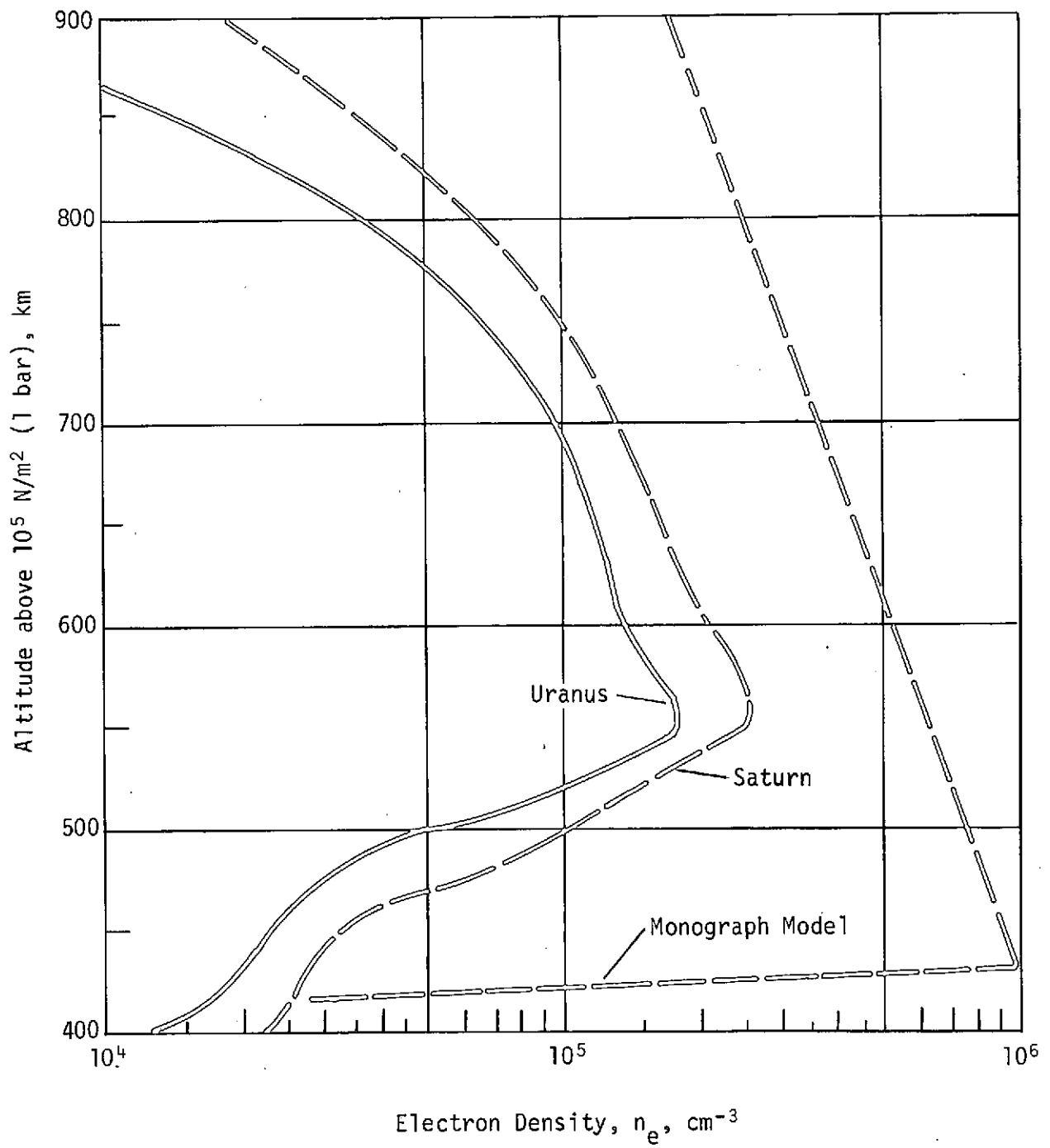


Figure 4.5-18 Electron Number Density Models for Saturn and Uranus

densities determined by McElroy are below the monograph upper limit given by Equation (4.5-12). Almost the same curves are generated for both planets for the nominal atmosphere model since the turbo-pause for each planet is located within 4 km of the same altitude (532 km).

The diffusion and recombination time constants for the electron production models were predicted by assuming the electron and proton densities were essentially equal. Transport processes were also found to be important above 300 km. The ionospheres for Saturn and Uranus were computed using a chemical and kinetic analysis of the atmospheric structures and represent the first definitive work published for the two planets.

To determine the effect of the ionospheres of Saturn and Uranus on probe-to-spacecraft communications, we performed a comparative analysis using the Earth's ionosphere as a reference. The Earth's ionosphere is well known, and absorption and refractions can be accurately predicted for any operating frequency, location, and sunspot activity. The highest electron density occurs in the F-region at an average altitude of 300 km, and has a value of  $6 \times 10^5 \text{ cm}^{-3}$  (reference 4.5-23). The RF characteristic of the ionosphere depend on the time of day, sunspot cycle, latitude, and month of the year. The values discussed in this section are typical or average values and are presented to relate a mean level of parameters. The average electron-neutral collision rate is  $1.2 \times 10^4 \text{ sec}^{-1}$  (reference 4.5-24). Diurnal variations of the lowest useful frequency indicate that the optimum working frequency is approximately 20 MHz (reference 4.5-25). Other investigators indicate that ionospheric attenuation effects become essentially negligible above, roughly, 100 MHz for normal conditions (reference 4.5-26).

By making the basic assumption that the ionospheres of Saturn and Uranus are comparable to that of Earth, and by using analytical and extensive rocket test data about the F-region, we have concluded that the ionospheres of the two outer planets will not attenuate RF signals for operating frequencies above 100 MHz. More precisely, ionospheric absorptions will be 0.1 dB or less at 100 MHz, and will decrease as the frequency increases. During periods of high sunspot activity, ionospheric absorption could increase by an order of magnitude and be extended upward in frequency. The extent of this increase can only be estimated at this time until actual data are available from future flyby spacecraft. The only other information on signal strength degradation comes from scintillations, which are amplitude and phase variations of signals transmitted through the ionosphere. The most common source of these is cosmic



noise from outer space. Because of the probe/spacecraft geometry, a large amount of cosmic noise that has traveled through the ionosphere of the planet is not expected to be present at the probe receiving antenna during entry.

### Probe Antenna

The variations and dispersions of the probe aspect angle during descent can be accommodated by using an antenna with a 3-dB beamwidth of 1.75 rad ( $100^\circ$ ). This beamwidth is defined as the sum of three angles: (1) the maximum probe aspect angle during descent, which occurs at EOM; (2) the 3- $\sigma$  dispersion of the aspect angle; and (3) lateral wind shear and turbulence effects. Circular polarization is required since the spacecraft is spin-stabilized and the probe can rotate about its longitudinal axis. Several antenna designs will satisfy the radiation pattern requirements. A turnstile/cone antenna provides the best efficiency, while at the same time minimizes ground-plane effects. In addition, the design is compact and lightweight and has already been selected by Martin Marietta as the antenna for the Viking lander radar altimeter. Its measured radiation and polarization patterns are shown in Figure 4.5-19. All the patterns shown in the figure were measured with the antenna mounted on a hemisphere 61 cm (24 in.) in diameter (see Figure 4.5-20). The radiation pattern of the main beam is uniform and symmetrical in both the E- and H- planes. The on-axis polarization ratio is 1.8 dB, and 2.8 dB at the 3-dB points. High circularity and low backlobe levels have been achieved as the result of an improved feed and ground-plane design. The basic design of the probe antenna is shown in Figure 4.5-21. This antenna is designed for an operating frequency of 560 MHz with circular polarization. A stress analysis of the design shows that this antenna can be made to withstand a design load of  $7.16 \text{ km/sec}^2$  (730 g) by using thin-walled tubing for the dipoles welded at the attachment point. The petals must also be welded to the cone. Calculated safety margins are shown in the figure.

A Teflon/fiberglass radome is located over the probe antenna to provide aerodynamic control during entry and descent and to provide thermal control to the interior of the probe. RF attenuation through the radome is negligible. The radome configuration is essentially a hemisphere with an unobstructed field of view of 2.97 rad ( $170^\circ$ ). The parachute canister for the baseline configuration was constructed of fiberglass. Metal eyelets must not be used in constructing the parachute because of the need to avoid reflective objects for the propagated signal.

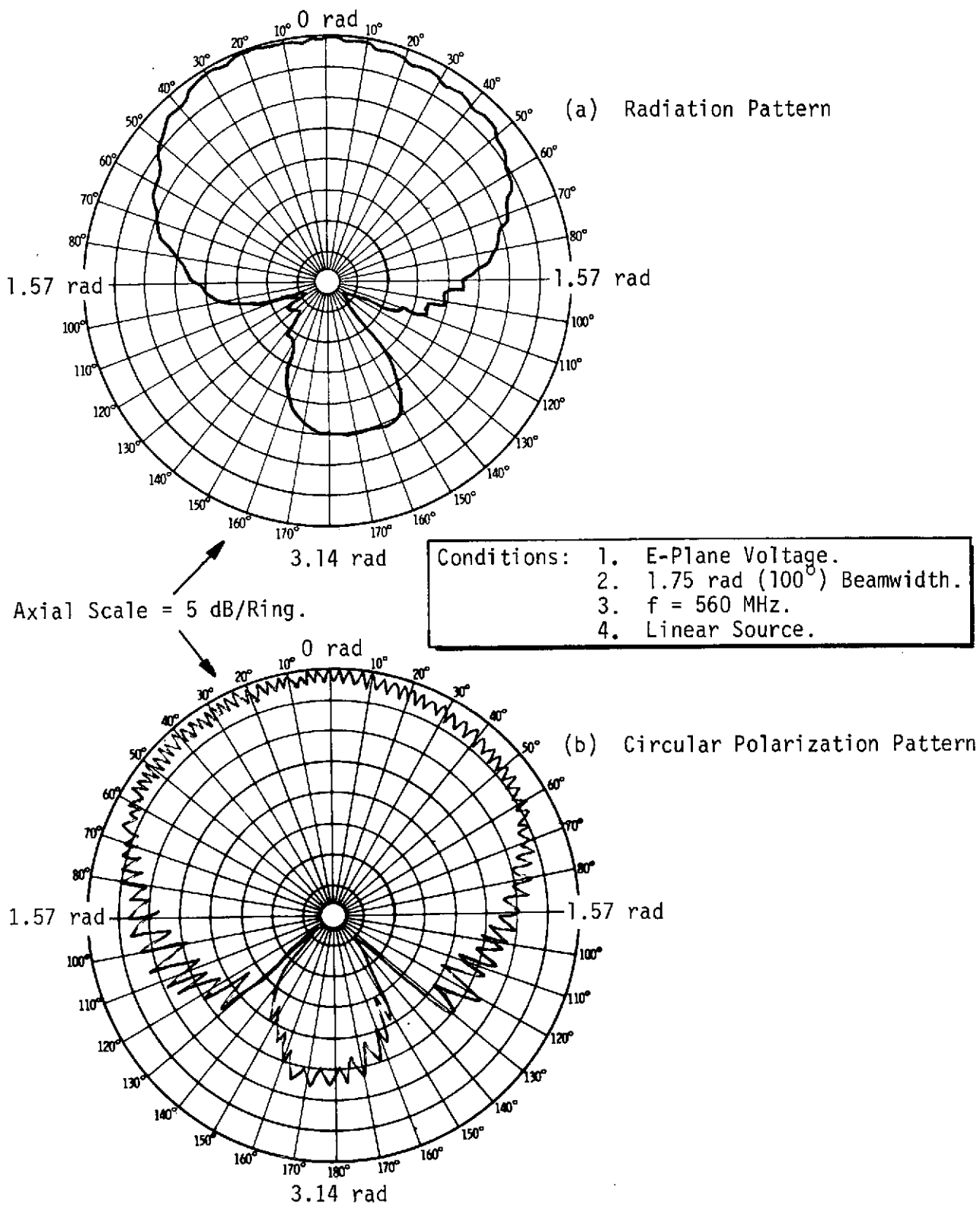


Figure 4.5-19 Radiation Patterns for a Turnstile/Cone Antenna

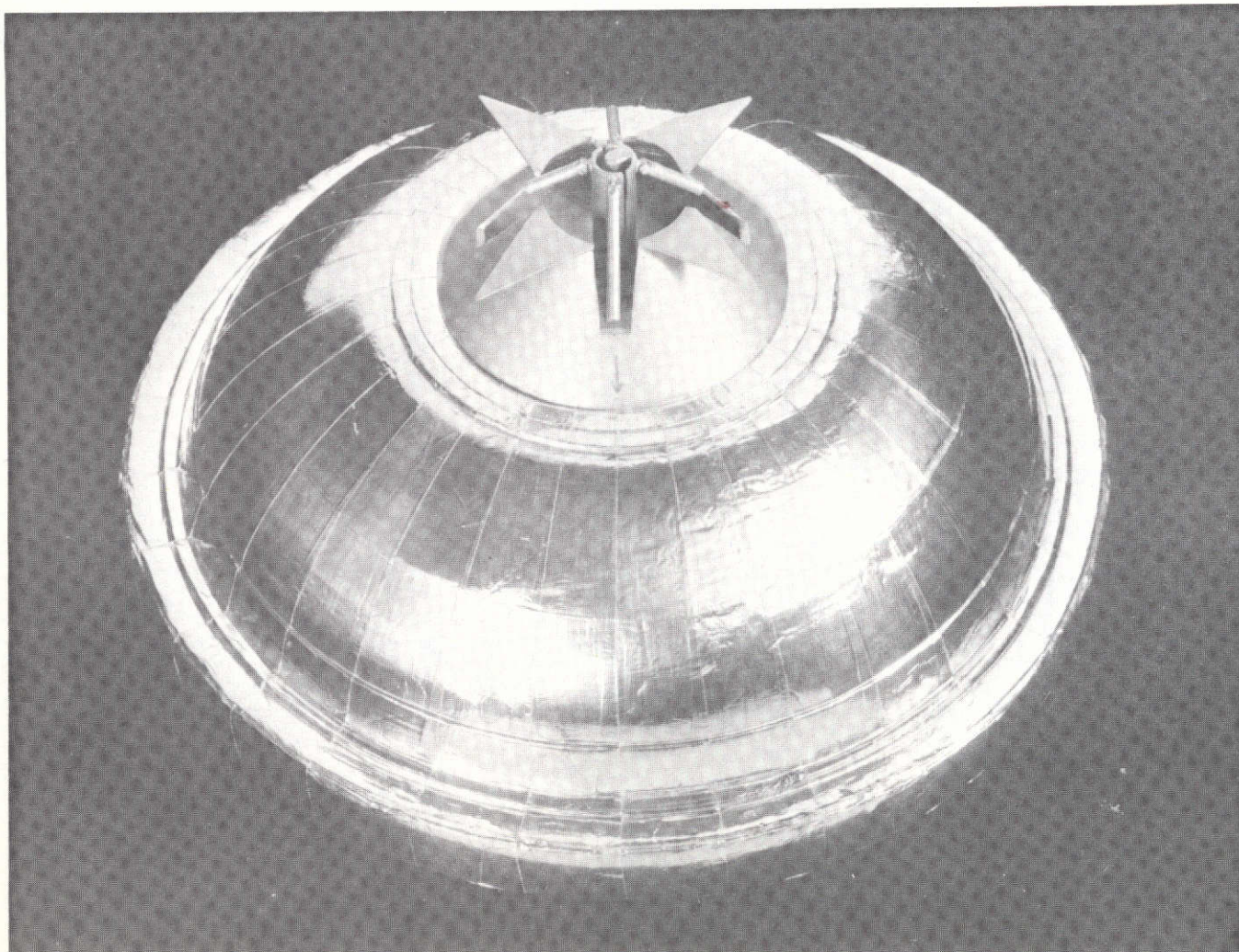


Figure 4.5-20 Prototype Turnstile/Cone Antenna Mounted on Model Probe

ORIGINAL PAGE IS  
OF POOR QUALITY

4.5-41

3

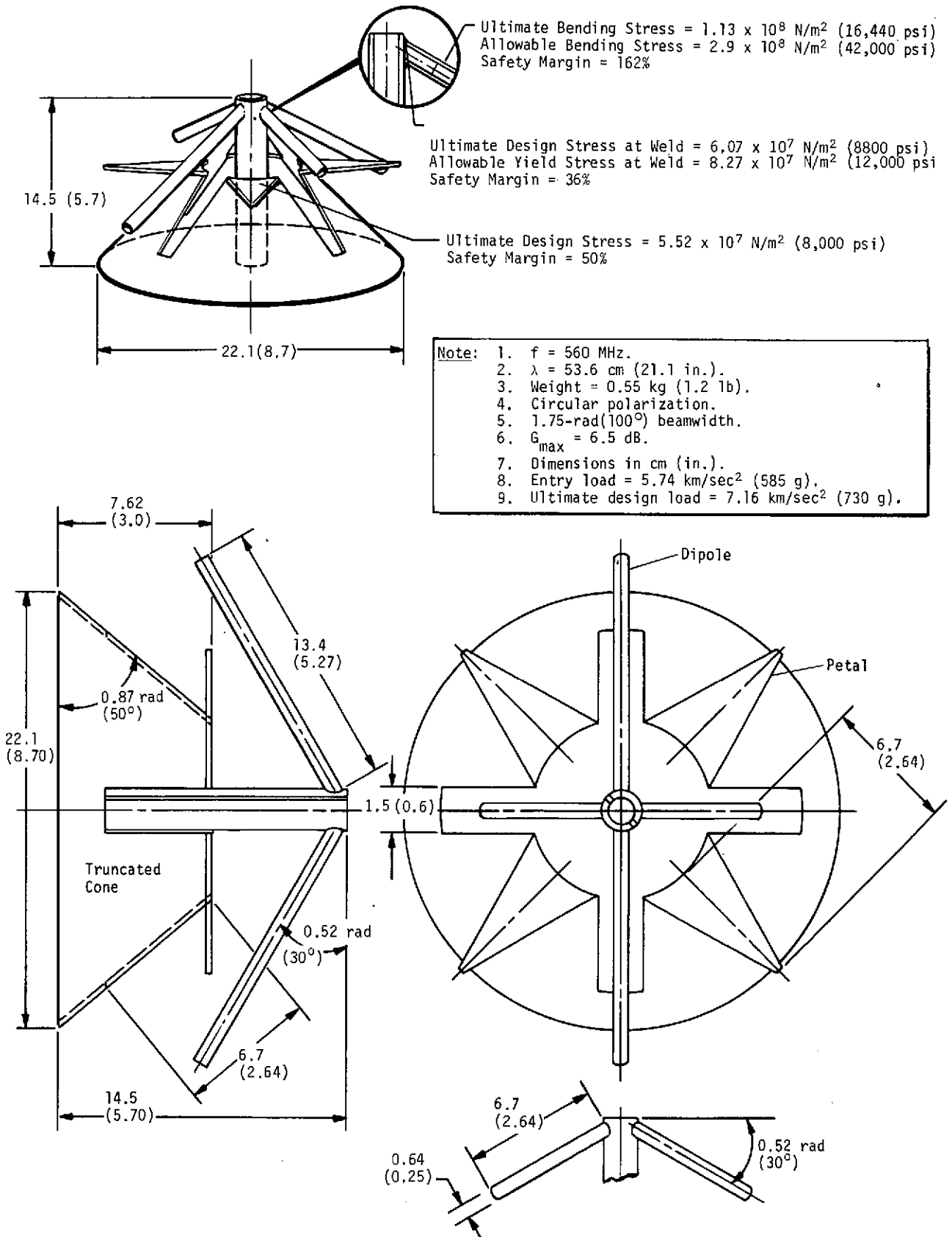


Figure 4.5-21 Probe Turnstile/Cone Antenna Design

As shown in Figure 4.5-19(b), the turnstile/cone design has a low axial ratio. A value of 3 dB was used for the probe antenna, whereas 1.5 dB was used for the probe receiving antenna on the spacecraft. The equation and curve that determine the polarization loss due to pattern ellipticity are given in Reference 4.5-2, Vol IV, pp III-72 and III-76. For the two axial ratios selected, and for the antenna oriented in a worst-case orthogonal relationship, the resulting polarization loss is calculated to be 0.3 dB. This value was used in all RF link calculations.

#### Probe Transmitter

The problem of acquiring and tracking a probe signal was evaluated during previous studies and data tracking was discarded. This was due to the low data S/N ratio available in the type of filter bandwidth needed to pass coded data (reference 4.5-2, Vol III, Appendix C). The power penalty for adding a tracking tone was offset by the higher gain resulting from coding.

One method of generating FSK with a pilot tone is shown in Figure 4.5-22. This method uses single sideband (SSB) modulation with the lower sideband being suppressed for an encoded data bit of 1 and the upper sideband suppressed for an encoded data bit of 0. The sideband suppression results from performing a  $3.14 \text{ rad}$  ( $180^\circ$ ) phase shift on a sine wave subcarrier at 32.77 kHz. A square-wave frequency of 32.77 kHz is available from the probe DTU and is used for the modulation frequency after being filtered to provide a sine wave. A frequency synthesizer is used to generate the RF frequency,  $f_o$ , with a stability of 10 ppm. The output of the SSB modulator is fed into a power combiner where it is added to the pilot tone. The signal is then amplified to the required power level by the solid-state RF power amplifier.

As discussed in Section 4.1.2.1, the transmitter design is not currently available as space-qualified hardware. However, existing hardware can be modified to provide FSK with a tone and the required RF output power. The operating frequency for the relay link also requires equipment modifications in the form of changing the output transistors and associated circuitry to operate at UHF.

#### Spacecraft Antenna Requirements

The required radiation pattern for the probe receiving antenna on the spacecraft is based on the RF link analysis and trajectory geometry. Both the Saturn and Uranus missions were targeted to have a common range of spacecraft cone angles, as shown in Figure 4.5-23. The spacecraft antenna pattern must have the radiation pattern

depicted in this figure. Design requirements for the spacecraft antenna are listed in Table 4.5-6. Several antenna designs will provide the efficiency necessary to give the peak gain and beam-width shown in the table. Circular polarization is required for the spin-stabilized spacecraft.

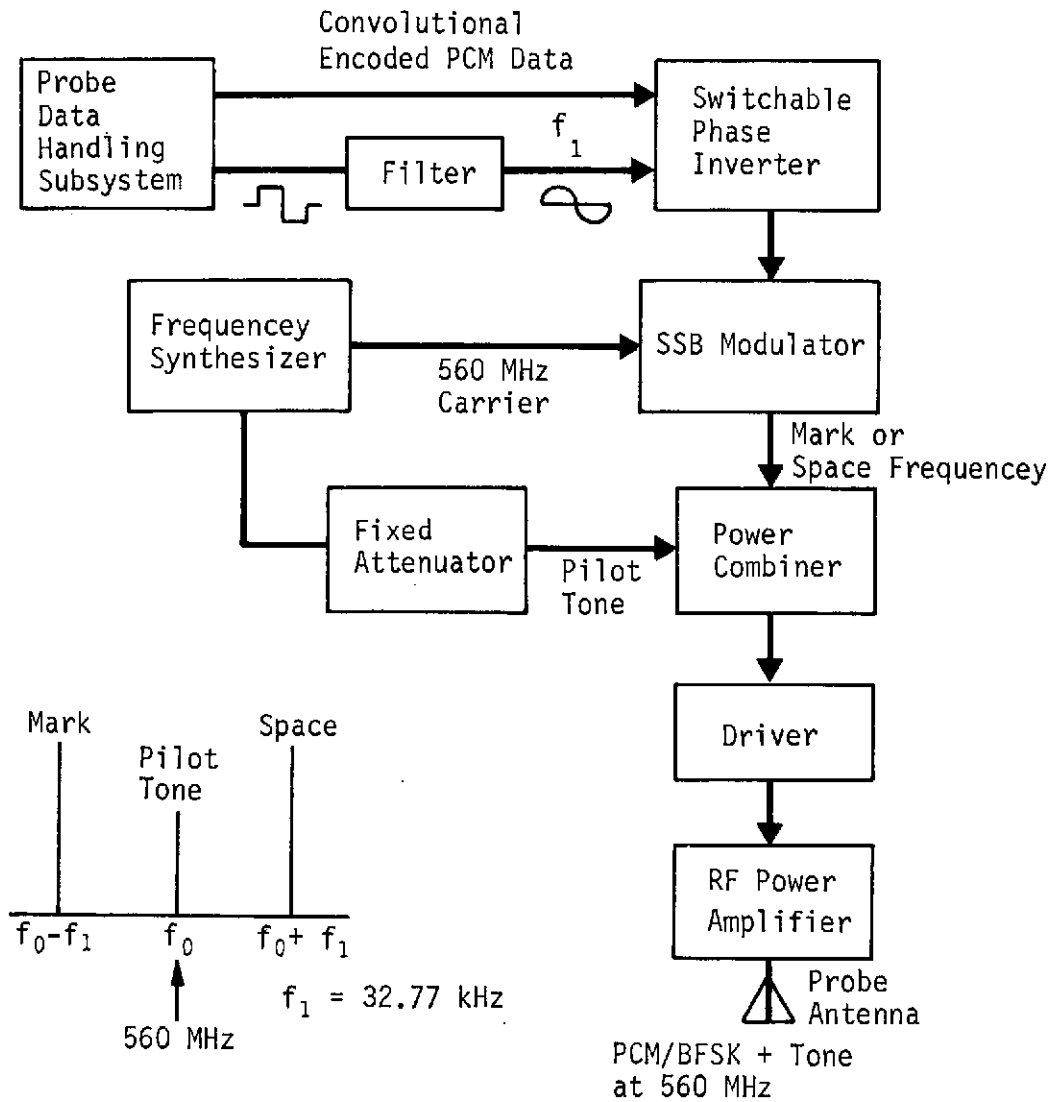

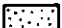


Figure 4.5-22 Functional Diagram for the Saturn Uranus Probe Transmitter

- Notes:
1. Saturn-79 and Saturn/SU-80 missions
  2. Uranus/SU-80 (retrograde) mission.
  3.  $3\text{-}\sigma$  cone angle uncertainties. included in the design.
  4. Atmosphere models:
    -  Cool
    -  Warm

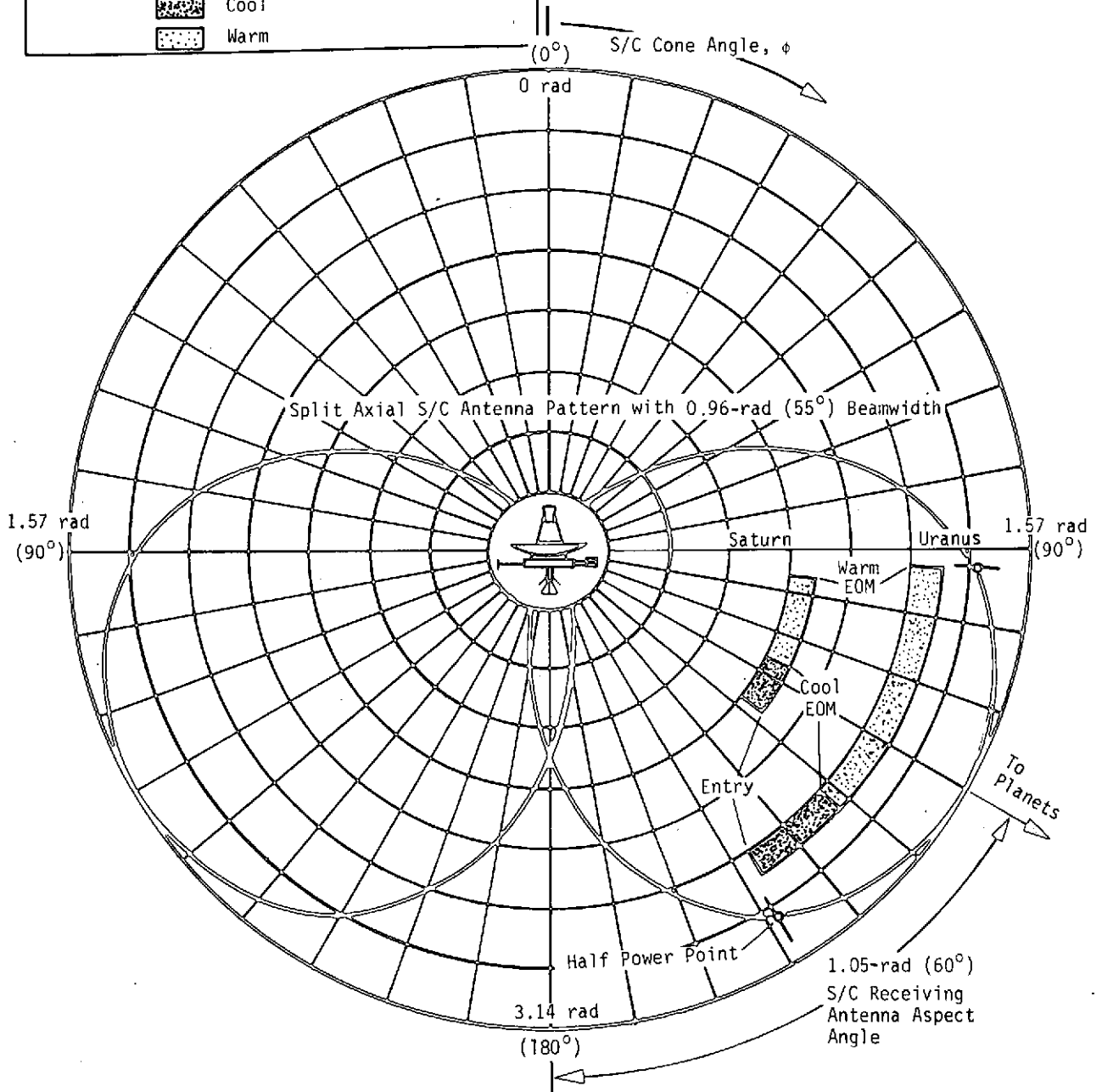


Figure 4.5-23 Required Spacecraft Antenna Pattern Coverage for the Final Configuration

Table 4.5-6 Design Requirements for the Probe Receiving Antenna for the Final Configuration

Parameter	Value
Beamwidth, rad (deg)	0.96 (55)
Aspect Angle for Maximum Gain, rad (deg)	1.05 (60)
Maximum Gain, dB	3.1
Polarization	Right-Hand Circular
Axial Ratio, dB	1.5 at Half-Power Points
Frequency, MHz	560
Bandwidth, %	10
Operating Temperature, °K (°F)	171 to 316 (-150 to 110)

Table 4.5-7 Receiver/Demodulator Performance Characteristics

Parameter	Value
Nominal Operating Frequency, MHz	560
Intermediate Frequency	Double Superheterodyne
Automatic Frequency Control	Search, Acquire, and Frequency-Track the Pilot Tone
Search and Tracking Range, kHz	<u>+40</u>
Maximum Search Rate, Hz/sec	400
Maximum Static and Dynamic Frequency Tracking Errors, Hz	<u>+5</u>
Noise Figure, dB	2.5
Image Rejection, dB	80 (Minimum)
Spurious Noise Rejection, dB	60 (Minimum)
Local Oscillator Stability, ppm	<u>+10</u> (long term) <u>±0.5</u> (short term)
Dynamic Range, dB	50 (Minimum)
Maximum Doppler Tracking Rate, Hz/sec	20
Maximum Channel Error Rate for $E_b/N_o = 7.3$ dB	$5 \times 10^{-4}$
Symbol Error Rate for $E_b/N_o = 7.3$ dB	$3 \times 10^{-2}$

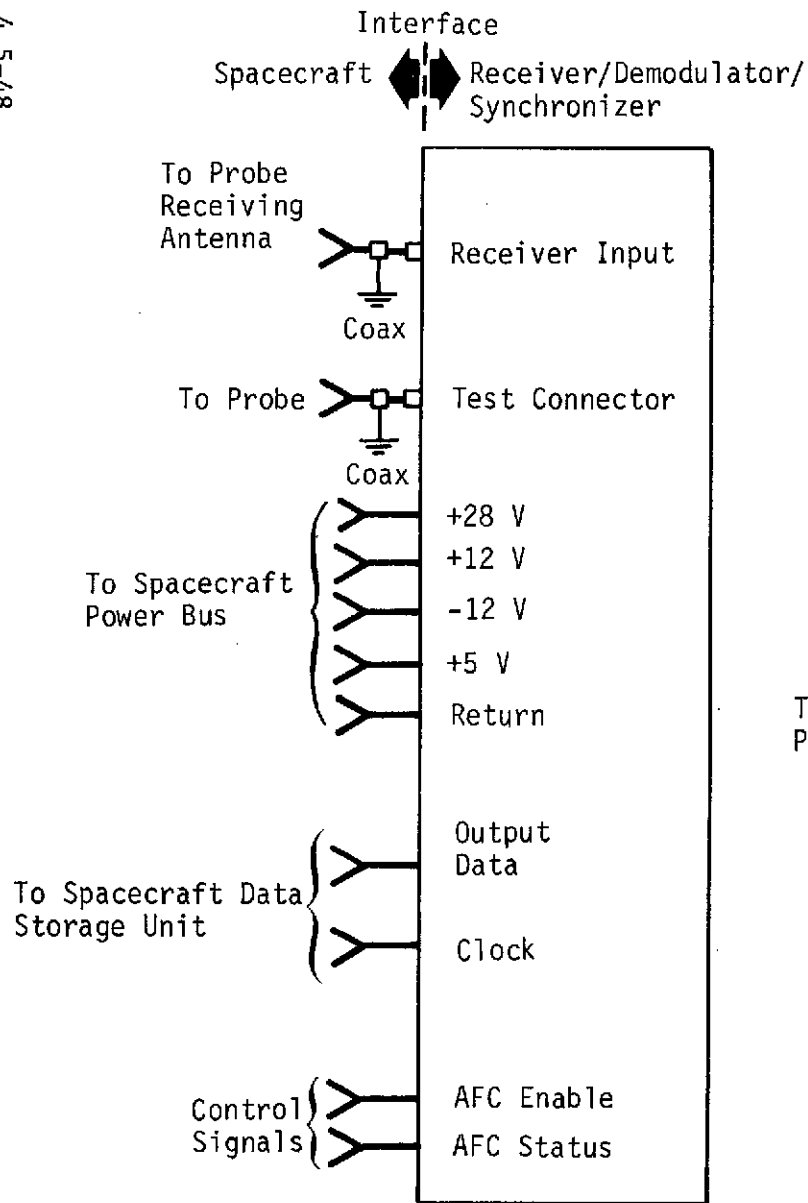


### Spacecraft Receiver/Demodulator

The spacecraft receiver/demodulator acquires and demodulates the signal transmitted from the probe, establishes symbol timing and digitizes the data for subsequent buffering by the spacecraft data handling subsystem. The unit receives a binary FSK-modulated signal at 560 MHz from the probe receiving antenna mounted on the spacecraft and converts the signal to encoded PCM data to be fed to the spacecraft data handling subsystem. The principal interface characteristics of the receiver/demodulator are shown in Figure 4.5-24. The basic design of the receiver is shown in Figure 4.5-25. Principal performance characteristics for the receiver/demodulator are given in Table 4.5-7 for the final configuration.

The receiver/symbol detector can be configured to provide hard decision symbol outputs ( $Q = 2$ ) or soft quantized outputs ( $Q > 2$ ) for use in decoding onboard the spacecraft or by the Deep Space Network (DSN). Using 8-level quantized symbol outputs and decoding at the DSN, the amount of data to be transmitted over the spacecraft/DSN link is three times greater than when hard decisions are used. Sequential decoding is required when all the decoding is done at the DSN.

The modulation and coding analysis discussed in the preceding paragraphs was based on Viterbi decoding with  $K = 8$ . This coding method was used for the baseline/alternate configurations since it provides a greater degree of protection from loss of data during atmospheric fading than does sequential decoding. The subject was discussed with the customer and they indicate that the spacecraft contractor will process the probe data without decoding on the spacecraft. Since decoding on the spacecraft is no longer of prime concern, sequential decoding with  $K = 32$  was used for the final design to minimize modifications to the probe data handling subsystem which is derived from the PV program.



Note: 1. Total volume = 1967 cm<sup>3</sup> (120 in.<sup>3</sup>).  
 2. Weight of Unit = 1.9 kg (4.2 lb).  
 3. Weight of cable = 0.136 kg (0.3 lb).  
 4. DC power required = 8 W at 28 V.

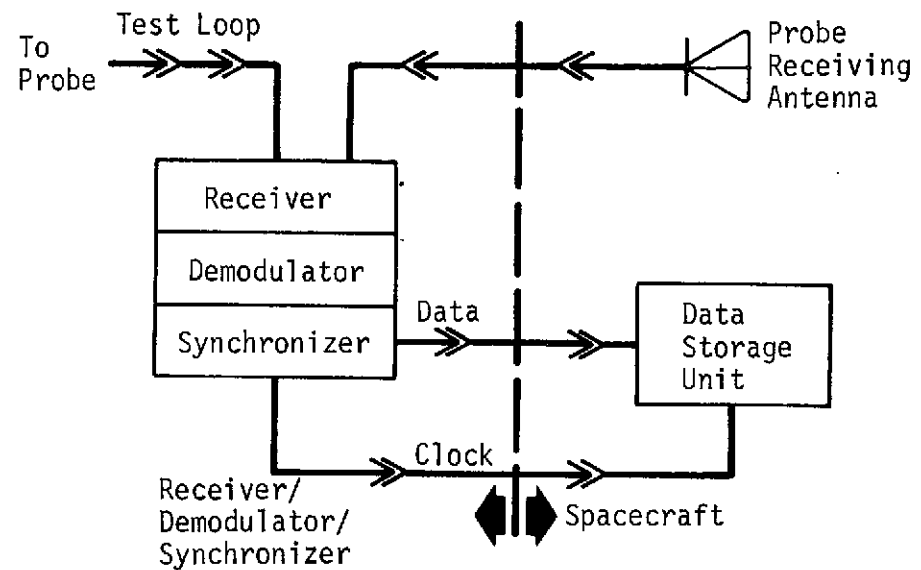
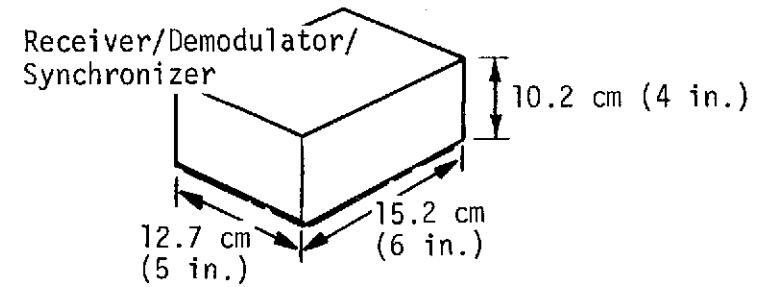


Figure 4.5-24 Probe Receiver/Demodulator Characteristics and Interface Requirements

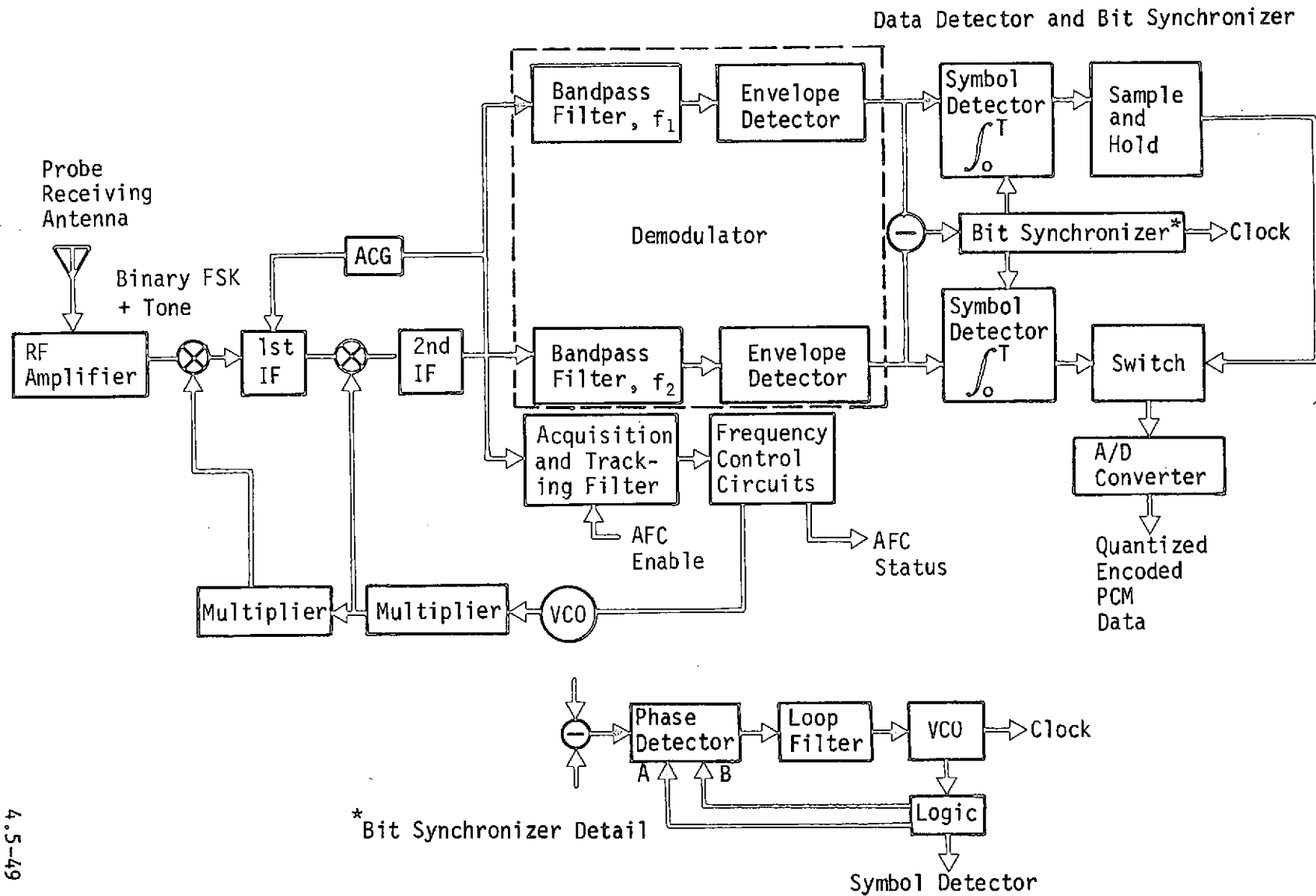


Figure 4.5-25 Functional Diagram of the Binary FSK Receiver, Bit Synchronizer and Symbol Detector

#### 4.5.1.2 Data Handling Subsystem (DHS)

The DHS defined for use in the PV probes has been selected for the SU mission. As various system configurations were identified, the required modifications to the PV DHS were also determined. Both the type of modification and the preferred method of implementing it were defined. Table 4.5-8 compares the capabilities of the PV DHS with SU requirements for four different configurations. The parameter requiring a hardware modification is noted to indicate the minor impact of this modification on the system.

Note that as the configurations change, the number of required hardware modifications decreases. Modifications that require only part-for-part replacement (effectively a paper work change), such as the read-only memories (ROMs) (see Section 4.1.2.2) are not shown since they do not involve changing the mechanical layout. The impacts of the changes noted in Table 4.5-8 are discussed below.

##### 2-bps Data Rate

The baseline and alternate configurations involved a requirement for preentry data transmission. Because of the communication link limitations prior to entry, a maximum data rate of 2 bps was possible within the power limitation. The minimum data rate of the PV system is 8 bits per second. Two ways of reducing the minimum data rate were considered: reduce the frequency of the oscillator by a factor of 4, or insert a divide-by-four counter in the countdown circuit. Changing the oscillator frequency appeared to be only a part change, except that the lower-frequency crystal was found to break under shock and vibration in the Viking build and test cycle, and is therefore not recommended. As a result, a decision was made to add an integrated circuit to the countdown circuit. The 2-bps clock is not used in the updated alternate or final configurations and this problem does not exist.

##### Pyro Firing Circuit Shortage

To accommodate the extra pyro circuits required, an unused board of relays was replaced with a second pyro firing circuit board identical to the one in the PV design.

##### Memory Capacity

Two 2.54-cm-square flat packs had to be added to the baseline configuration to supply the required storage capacity. As the PV design became final, the memory capacity was increased to 25,600 bits. This memory now meets all requirements for the SU configurations.

Table 4.5-8 Data Handling Subsystem Capability/Requirements Comparison

Function	Pioneer Venus Capability	Baseline Configuration (Nominal atmosphere)	Alternate Configuration (nominal atmosphere)	Updated Alternate Configuration (nominal atmosphere)	Final Configuration (worst-case atmosphere)
Basic Clock Frequency, MHz	4.194304 Stability = 0.0002 %/year	Same	Same	Same	Same
Type of Data & Modulation	PCM	Same	Same	Same	Same
Bit Rates, bps	2048 1024 256 128 64 32 16 8	128 64 32 <span style="border: 1px solid black; padding: 2px;">2</span>	128 64 32 <span style="border: 1px solid black; padding: 2px;">2</span>	128 64 32	128 32
Data Input Channels					
Main Frame	Analog = 16 Digital = 32 Bilevel = 0	Analog = 6 Digital = 3 Bilevel = 0	Same as Baseline	Same as Baseline	Same as Baseline
Subframe	Analog = 95 Digital = 55 Bilevel = 92	Analog = 24 Digital = 0 Bilevel = 10	Same as Baseline	Same as Baseline	Same as Baseline
Input Voltage Range	0 to 5 V Analog, Digital & Bilevel Comparator Threshold = 2.0 V	Same	Same	Same	Same
A/D Resolution, bits	8	Same	Same	Same	Same
Data Output	Biphase Modulated, NRZ-L	Same	Same	Same	Same
Data Coding	Convolutional Rate 1/2, K = 32	<span style="border: 1px solid black; padding: 2px;">K = 8</span>	<span style="border: 1px solid black; padding: 2px;">K = 8</span>	K = 32	K = 32
Operating Modes	1. Real Time 2. Telemetry Storage 3. Real Time with Memory Readout	Same	Same	Same	Same
Data Formats	12, ROM-Programmable	4	4	3	2
Frame Size					
Main Frame	768 bits	Same	Same	Same	Same
Engineering Subcom	64 Addresses of two 6-bit Words per Frame	54 Two-Word Addresses	Same as Baseline	Same as Baseline	Same as Baseline
Science Subcom	64 Addresses of one 6-bit Words per Frame	32 Addresses	Same as Baseline	Same as Baseline	Same as Baseline
Frame Counter	Identifies up to 4096 Frames	<1000	<1000	<800	<800
No. of Pyro Firing Circuits	24	<span style="border: 1px solid black; padding: 2px;">38</span>	<span style="border: 1px solid black; padding: 2px;">34</span>	24	24
No. of Discrete Commands	75	<40	<40	<40	<40
Data Bits in Memory	5K (early version) 25.6K (late version)	<span style="border: 1px solid black; padding: 2px;">10K</span>	10K	10K	15.8K
Coast Timer Output, days	27	<span style="border: 1px solid black; padding: 2px;">&gt;35.7</span>	<span style="border: 1px solid black; padding: 2px;">&gt;35.7</span>	<span style="border: 1px solid black; padding: 2px;">&gt;35.7</span>	<span style="border: 1px solid black; padding: 2px;">&gt;35.7</span>
Usable Energy (battery energy after all derating)	N/A	<span style="border: 1px solid black; padding: 2px;">132.7 W-h</span>	<span style="border: 1px solid black; padding: 2px;">112.6 W-h</span>	<span style="border: 1px solid black; padding: 2px;">106.4 W-h</span>	<span style="border: 1px solid black; padding: 2px;">156.1 W-h</span>
g Switches	49 m/sec <sup>2</sup> (5 g) (increasing); 490 m/sec <sup>2</sup> (50 g) (increasing)	<span style="border: 1px solid black; padding: 2px;">490 m/sec<sup>2</sup> (50 g) (increasing); 49 m/sec<sup>2</sup> (5 g) (decreasing)</span>	<span style="border: 1px solid black; padding: 2px;">490 m/sec<sup>2</sup> (50 g) (increasing); 49 m/sec<sup>2</sup> (5 g) (decreasing)</span>	<span style="border: 1px solid black; padding: 2px;">490 m/sec<sup>2</sup> (50 g) (increasing); 49 m/sec<sup>2</sup> (5 g) (decreasing)</span>	<span style="border: 1px solid black; padding: 2px;">0.98 m/sec<sup>2</sup> (0.1 g) (increasing); 490 m/sec<sup>2</sup> (50 g) (increasing); 29.4 m/sec<sup>2</sup> (3 g) (decreasing)</span>

   Areas requiring modification to PV hardware

ORIGINAL PAGE IS  
OF POOR QUALITY

### Coast Timer Output

A minor change to the decoding circuitry is required to provide the SU timing signal. The PV hardware could be designed to use a different jumper wire or a programmable, command-controlled output with little impact.

### Sequencer

The flexibility in the sequencer portion of the power control unit (PCU) precludes any need to change that circuitry. Only the program designed into the ROM parts needs to be changed.

### g-Switches

The g-switch selections were based on a required entry detection level of  $0.98 \text{ m/sec}^2$  (0.1 g) and on a required time reference that could be made common to all missions. Switches that sensed an increase in deceleration were unusable for the time reference because of the great variation in entry times. A  $29.4 \text{ m/sec}^2$  (3-g) decreasing deceleration switch was selected to provide the optimum point reference. A  $490 \text{ m/sec}^2$  (50-g) switch is still used as a backup to the coast timer.

### Dual Data Return Trade Studies

An action item was accepted during the August interface meeting, to determine the impact of transmitting all data at least twice before reaching a  $10^6 \text{-N/m}^2$  (10-bar) pressure level. Two methods of implementing this capability were considered--a buffer system and a system requiring two format changes.

To buffer the data for a second transmission, a circuit block must be inserted between the data combiner and the convolutional encoder in the digital telemetry unit (DTU). A block diagram of the required circuitry is shown in Figure 4.5-26.

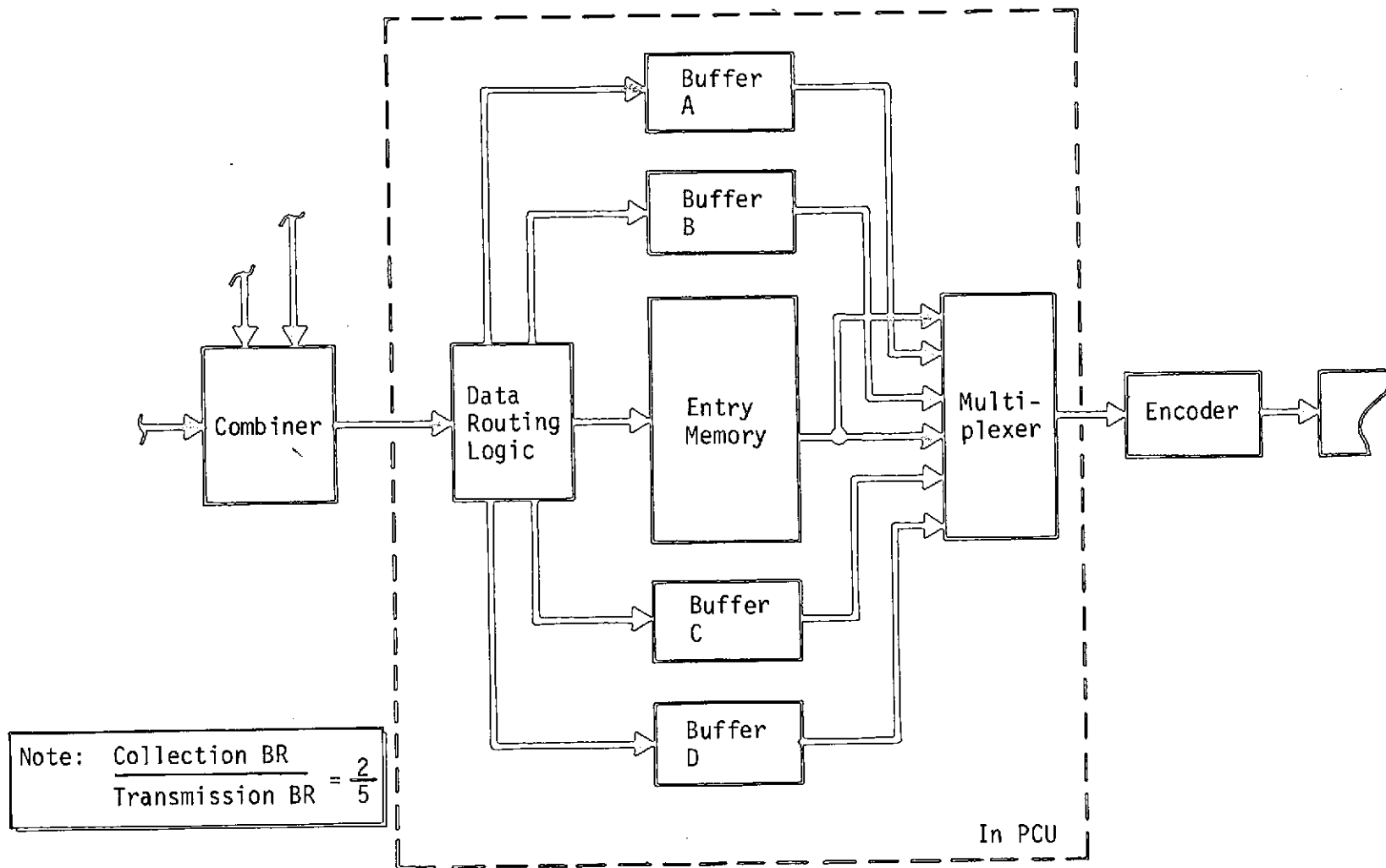


Figure 4.5-26 Memory Configuration for Dual Data Transmission, Alternative No. 1

For a single cycle, each buffer is filled once and emptied twice, and two frames of data are taken from memory. This circuitry would be located in the PCU--a new component on PV--to minimize changes to the DTU boards.

To implement the buffer system, the clock going to the output logic board, which is now twice the collection bit rate, must be changed to five times the data bit rate. This requires putting a divide-by-five counter between the "2 x bit-rate" output and the clock input to the multiplexers and instruments.

Dual data transmission can also be implemented by changing the data format, once at E + 15 minutes and again at a pressure of  $10^6$  N/m<sup>2</sup> (10 bar). However, this extends the time required to complete the second dump of the blackout data until 150 seconds after the entry pressure reaches  $10^6$  N/m<sup>2</sup> (10 bar). On the other hand, it helps by taking the buffers out of the direct transmission bit stream and reduces the complexity of the hardware change. Although the control logic for the memory system must still be changed, this change is relatively minor (see Figure 4.5-27). The reliability tradeoff then becomes one of relating the reliability of the buffers to the probability of surviving the increased pressure during the 150 seconds following the time when a pressure of  $10^6$  N/m<sup>2</sup> (10 bar) is reached.

The latter is our recommended approach since, in all cases, the data are transmitted at least once before reaching  $10^6$  N/m<sup>2</sup> (10 bar), and twice for every atmosphere except the Saturn cool,

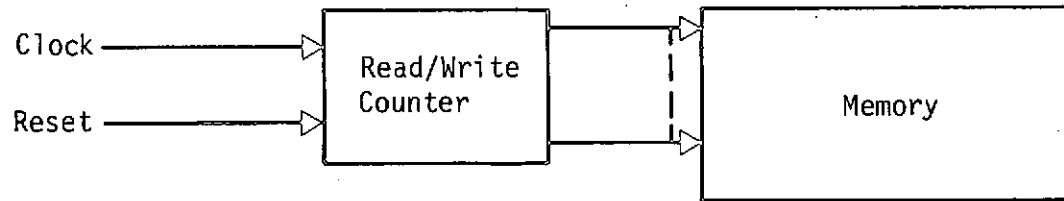
#### 4.5.1.3 Power and Pyrotechnics Subsystem

The cabling and connectors for the PV probe system meet all requirements for the SU mission. Our concern about the higher deceleration stresses on the cable mounting system is reflected in the structural drawing shown in Martin Marietta Report IR-73-2. A new harness is required for SU but the same wire and connectors used for PV can be used.

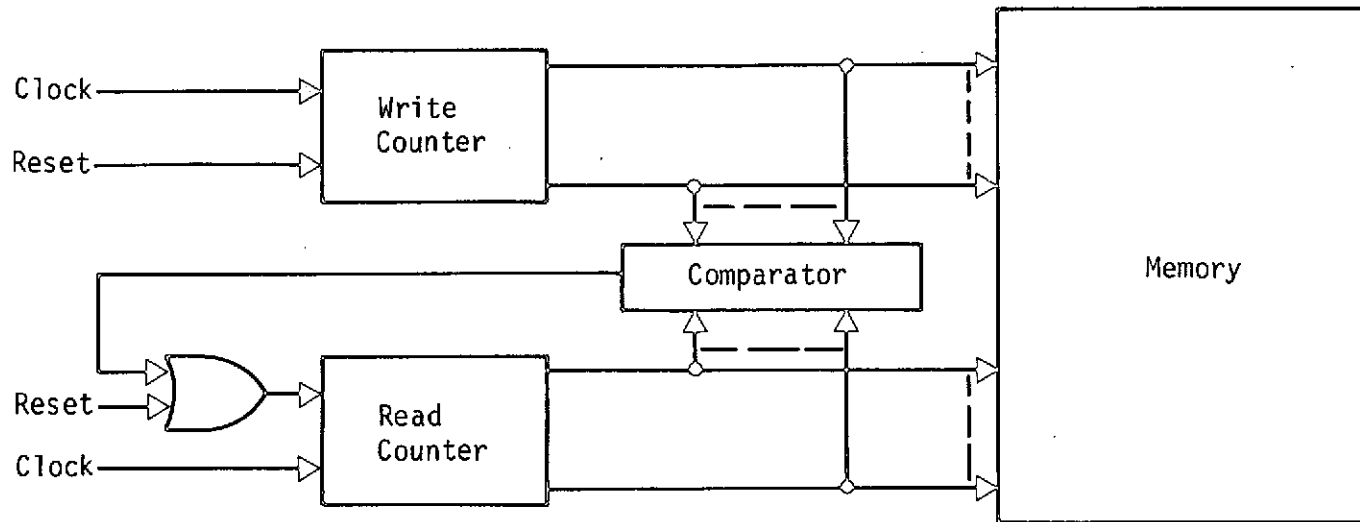
The pyro firing circuits designed for PV are directly applicable for SU both in kind and quantity. No circuit or board changes are anticipated except for a possible part replacement of the unijunction transistors to avoid radiation degradation if the PV design does not use planar design unijunctions.

The dc-to-dc converter requires no change for use in the SU system. Some analysis will be required if the probe requires sterilization since we have assumed that the PV filter capacitors may not be capable of surviving an extended, high-temperature bakeout.





(a) Pioneer Venus Memory Control



(b) Saturn/Uranus Memory Control - Double Transmission

Figure 4.5-27 Memory Control Logic Changes for Dual Data Transmission, Alternative No. 2

may not be capable of surviving an extended, high-temperature bakeout.

The power transfer relays have the proper rating for SU and enough spares are available to allow parallel redundancy for all uses.

The PV battery cannot be used in its present design configuration. The unit is a manually activated, Ag-Zn secondary battery design with a wet-stand life of less than 1 year.

Several batteries have been considered and compared in terms of their capability to perform mission requirements, stay within the weight/volume constraints, and still have an acceptable reliability. Tables 4.5-9 and 4.5-10 compare several of the candidate battery systems.

Table 4.5-9 compares the estimated characteristics of single-battery systems and lists their good and bad points. Table 4.5-10 compares two-battery systems.

During the selection process, the following organizations and personnel were consulted:

- 1) Eagle Picher  
- Pete Carr, Jeff Wilson, and Bill Long;
- 2) Yardney  
- Sandy Seidmas;
- 3) Electro-Storage Battery  
- Al Jordan and Art Samia;
- 4) Power Sources  
- Vern York;
- 5) Goddard Space Flight Center  
- Tom Hennigan, Floyd Ford, and Ed Tanciuttl;
- 6) Lewis Research Center  
- John Bozek and Bill Robertson;
- 7) Power Conversion  
- Bruce Jagid;
- 8) Stanford Research Institute  
- Dr. J. S. Smatko.

Table 4.5-9 Battery Subsystem Comparisons for Single-Battery Systems

Parameter	Subsystem Configuration				
	Ni-Cd	Ag-Zn (Dry Stand)	Ag-Zn (Wet Stand discharged)	Ag-Zn/ Converter (dry stand)	Li/ Regulator
Weight, kg (lbs)	13.6 to 18.1 (30 to 40)	7.3 to 9.1 (16 to 20)	5.0 to 5.9 (11 to 13)	8.6 to 9.5 (19 to 21)	1.8 to 2.3 (4 to 5)
Volume, cm <sup>3</sup> (in. <sup>3</sup> )	3770 (230)	2131 (130)	1393 (85)	7048 (430)	1311 (80)
Test Data, yr	7	10	2	10	1 to 2
Available Cell Design	Yes	Yes	Yes	Yes	Yes
Cell in Production	Custom	Custom	No	Custom	Custom
Available Battery System Design Exists	No	No	No	No	No
Problems	Deceleration Data, Weight, Volume, Charge Rate, Charge Stand	Activation System, Plate Information, Effect of Vacuum	Life Data	Volume, Activation System, Plate Information, Effect of Vacuum, Converter Design	Life Test Data, Regulator, Heat at Discharge
Advantages	Simple	Weight, Volume	Weight, Volume, Simplicity	Known Technology	Volume, Weight

Table 4.5-10 Battery Subsystem Comparisons for Two-Battery Systems

Parameter	Subsystem Configuration	
	Hg-Cd/ Ag-Zn (dry stand)	Ni-Cd/ Ag-Zn (dry stand)
Weight, kg (lbs)	7.3 to 9.1 (16 to 20)	7.3 to 9.1 (16 to 20)
Volume, cm <sup>3</sup> (in. <sup>3</sup> )	2950 (180)	2950 (180)
Test Data, yr	4 to 10	7 to 10
Available Cell Design	Yes	Yes
Cell in Production	Custom	Custom
Available Battery System Design Exists	No	No
Problems	Life Data, Limited Current from Hg-Cd, Charger	Deceleration Data, Volume, Charger
Advantages	Little Development	Little Development

The preferred system, of those considered, is the Ag-Zn, dry-charged, single-battery system described in the third column of Table 4.5-9. This design uses individual-cell remote activation. It is activated before spacecraft separation and can withstand a greater than 37-day wet stand with minimum discharge. The system does not presently exist, but is considered within the state-of-the-art technology.

Remotely activated Ag-Zn batteries, as presently designed, have only a few hours' wet stand capability. Their major failure modes tend to be cell- to cell-shorts through the activation manifold and separator failures. The manifold shorting path will be eliminated by individually activating each cell. Separator designs are available with a wet-stand capability in excess of 1 year.

Previous designs of remotely activated batteries required that the batteries be used almost instantaneously. This precluded the use of the type of separators which require slow filling and long soak periods for activation. Since several hours, or even days, are available for battery activation during the SU mission, this should not be a problem.

The activation system is projected to weigh about one-half that of the packaged battery cells. With this criterion, and assuming the degradation shown in Table 4.5-11, several battery weights were calculated for different mission constraints. These results are shown in Figure 4.5-28.

The excessive weight and volume of the Ni-Cd and Ag-Zn plus converter battery systems (Table 4.5-9) eliminates them from further consideration. Of the remaining candidates, the lithium battery and regulator would be very desirable from a weight and volume standpoint, but the heat generated during discharge is catastrophic to the thermal control system.

The Ag-Zn, wet-stand battery that is designed to be discharged during cruise looks attractive, but requires putting a battery charger in the spacecraft. Furthermore, only minimal data are available on its shelf-life capability. The available data shows that failures have occurred in less than 2 years, so this battery cannot be recommended without making further tests and, probably, some design changes.

Table 4.5-11 Power Subsystem Losses

Parameter	Assumed Loss, %*
Diode/Line Losses	4
Contingency (one cell out)	5
7-yr Dry Stand at 278 K	5
37-day Wet Stand at 298 K	5
Monovalent Operation	25

\* Net efficiency =  $0.96 \times 0.95 \times 0.95 \times 0.95 \times 0.75 = 0.58$ .

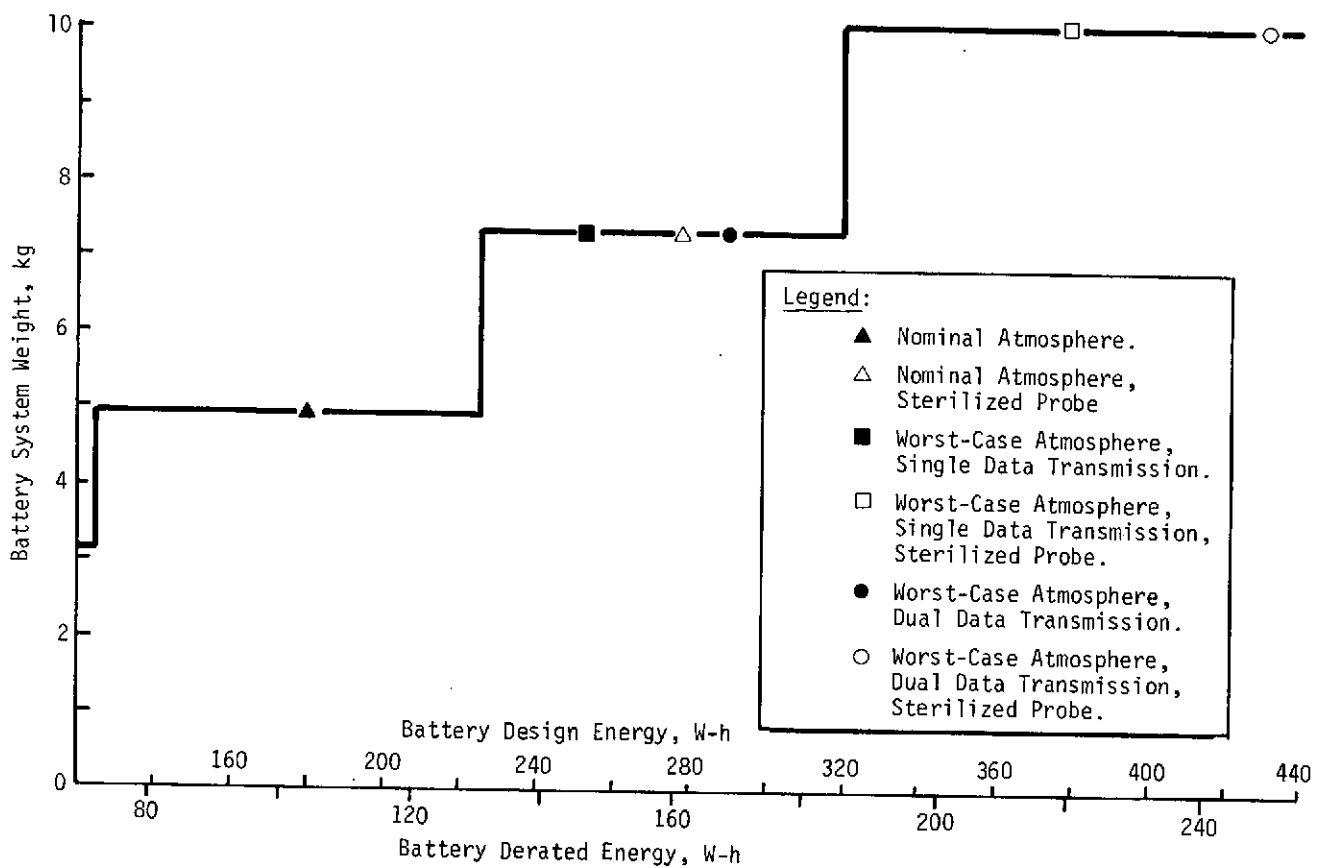


Figure 4.5-28 Updated Alternate Configuration Battery Subsystem Weights for the Atmosphere Models

The two-battery systems use small, single-cell batteries to activate a Ag-Zn battery just prior to entry. Possible problems are associated with the weak separators typically used in remotely activated batteries, especially when considering a 7-year shelf life, and the costs related to designing and qualifying the two types of batteries. They are feasible systems, however, and should not be discarded until the Ag-Zn, dry-charged, remotely activated single-battery system is completely proven.

#### Dual Data Return and Sterilization Trade Studies

During the August interface meeting, we were asked to consider the effects on the power subsystem of transmitting the data twice and the effects of sterilization on the battery.

Dual transmission necessitates a 15% to 20% increase in usable battery energy to accommodate the increased data rate. No other effect is apparent.

A number of Ag-Zn batteries have been designed to withstand sterilization at 125°C to 135°C, and some of these systems could probably be used for the SU probe. However, the sterilization requirement poses some serious problems from a battery standpoint. Many of these problems have involved seal leaks and wet separator problems (see reference 4.5-27).

It would seem that a remotely activated battery system would be even more reliable than a conventional system, but no data have yet been found to indicate that such a system has ever been sterilized and tested. Despite this, most of the battery experts we contacted during the study held the opinion that the maximum loss due to sterilization can be expected to be about 25%.

#### 4.5.2 Baseline Configuration Definition

The parachute version of the SU probe was defined as a baseline for all subsequent configurations. The following sections define the electrical and electronic subsystem modifications required to implement the parachute version of the SU probe.

#### 4.5.2.1 Communication Subsystem

The Saturn encounter generates the worst-case communication geometry, mainly due to the large range of  $10^5$  km at entry. The Saturn encounter for either the Saturn-79 or Saturn/Uranus-80 trajectory is equally bad. Atmospheric effects are minimal for the nominal atmosphere models at UHF.

The communication frequency selected was based on the space available on the aft bulkhead of the probe for mounting the antenna. The descent parachute canister occupies a large portion of the available space. A turnstile/cone probe antenna operating at 800 MHz will fit into the available space and does not require a ground plane. This is the lowest frequency (largest antenna) that can be accommodated on the baseline probe.

The maximum included angle for the SU mission is 0.87 rad ( $50^\circ$ ) at EOM for Saturn [see Figure 4.5-11 (a)]. In the azimuth plane of the spacecraft antenna, the ratio of noise from the planet to total noise is 50/360, or 0.14. The corresponding maximum antenna noise temperature was calculated to be  $200^\circ\text{K}$ . A receiver front-end noise figure of 2.85 dB ( $275^\circ\text{K}$ ) at 800 MHz was used with a feedline noise temperature of  $75^\circ\text{K}$  for a 1-dB loss in 91.5 cm (3 ft) of coaxial cable. The resulting system noise temperature based on these inputs is  $620^\circ\text{K}$ , which is a worst-case (Saturn EOM) value.

Trajectory adjustments were made to optimize the communication geometry for Saturn encounter and, at the same time, develop common trajectories for both planets. Figure 4.5-29 shows the probe-to-spacecraft communication range and mission geometry for the Saturn mission, which is the worst case. The probe aspect angle is shown as a function of mission time in Figure 4.5-30.

Note that a probe antenna beamwidth of 1.75 rad ( $100^\circ$ ) adequately covers the maximum probe aspect angle, the 3-sigma dispersions, and the 0.35 rad ( $\pm 20^\circ$ ) parachute swing due to lateral wind turbulence during the descent to  $10^6$  N/m<sup>2</sup> (10 bar). The antenna is covered by a fiberglass radome to protect it from extreme entry heating.

Relative probe positions for the two encounters are shown in Figures 4.5-31 and 4.5-32. The ellipses account for the navigational uncertainties and execution errors and the triangles denote the positions of the probe. Note that the ellipses are rotated to a different relative position for Uranus in Figure 4.5-32, since the planet's rotation is orthogonal to the orbital



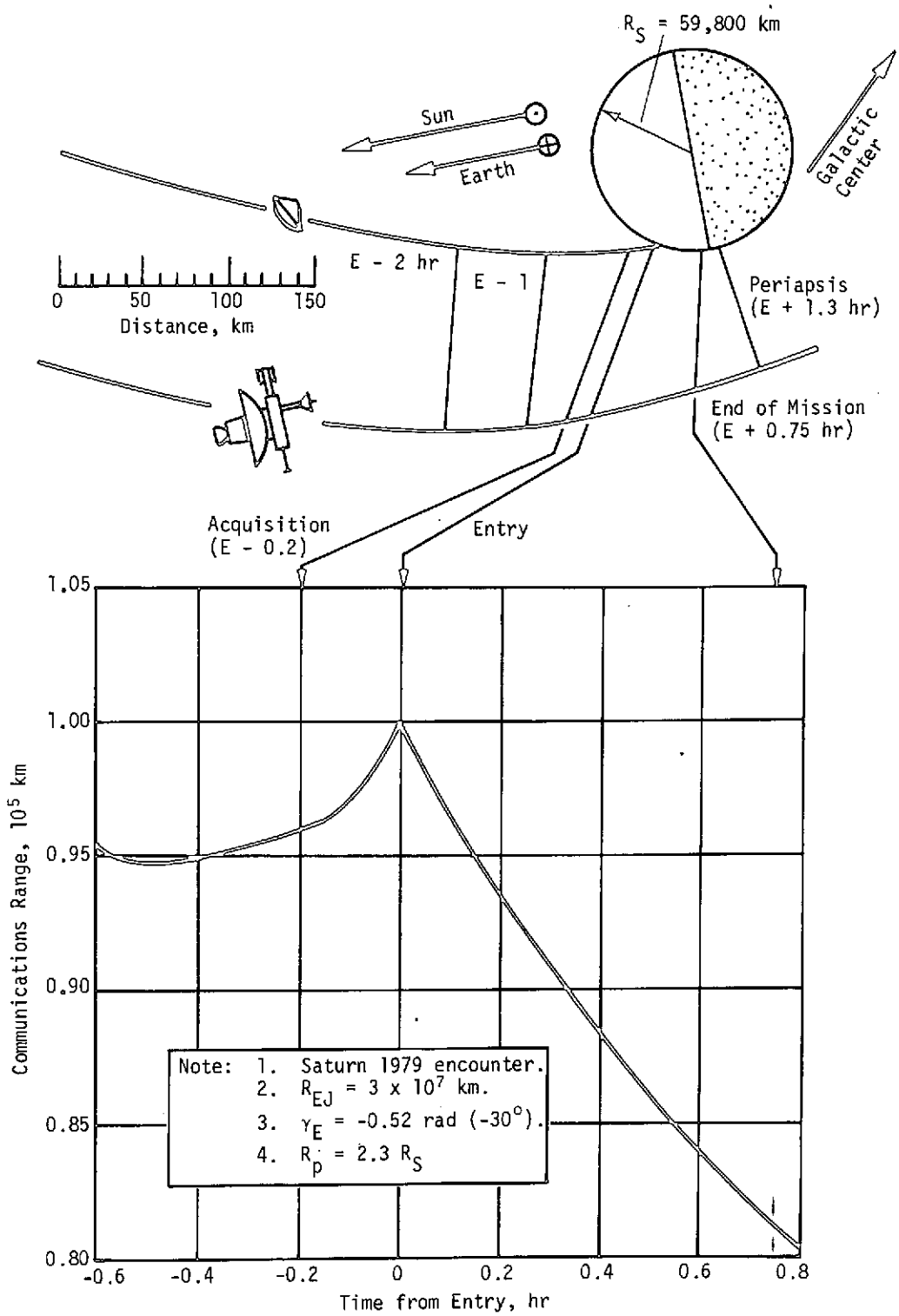
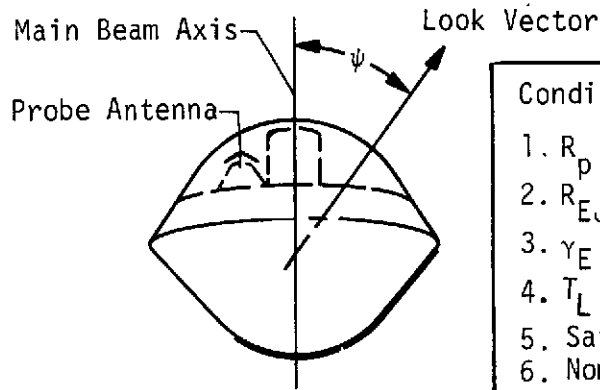


Figure 4.5-29 Probe-to-Spacecraft Communication Range for the Baseline Configuration



- Conditions:
1.  $R_p = 2.3 R_S$ .
  2.  $R_{EJ} = 3 \times 10^7$  km.
  3.  $\gamma_E = -0.52$  rad ( $-30^\circ$ ).
  4.  $T_L = 4700$  sec (1.3 hr).
  5. Saturn-79 mission.
  6. Nominal atmosphere.

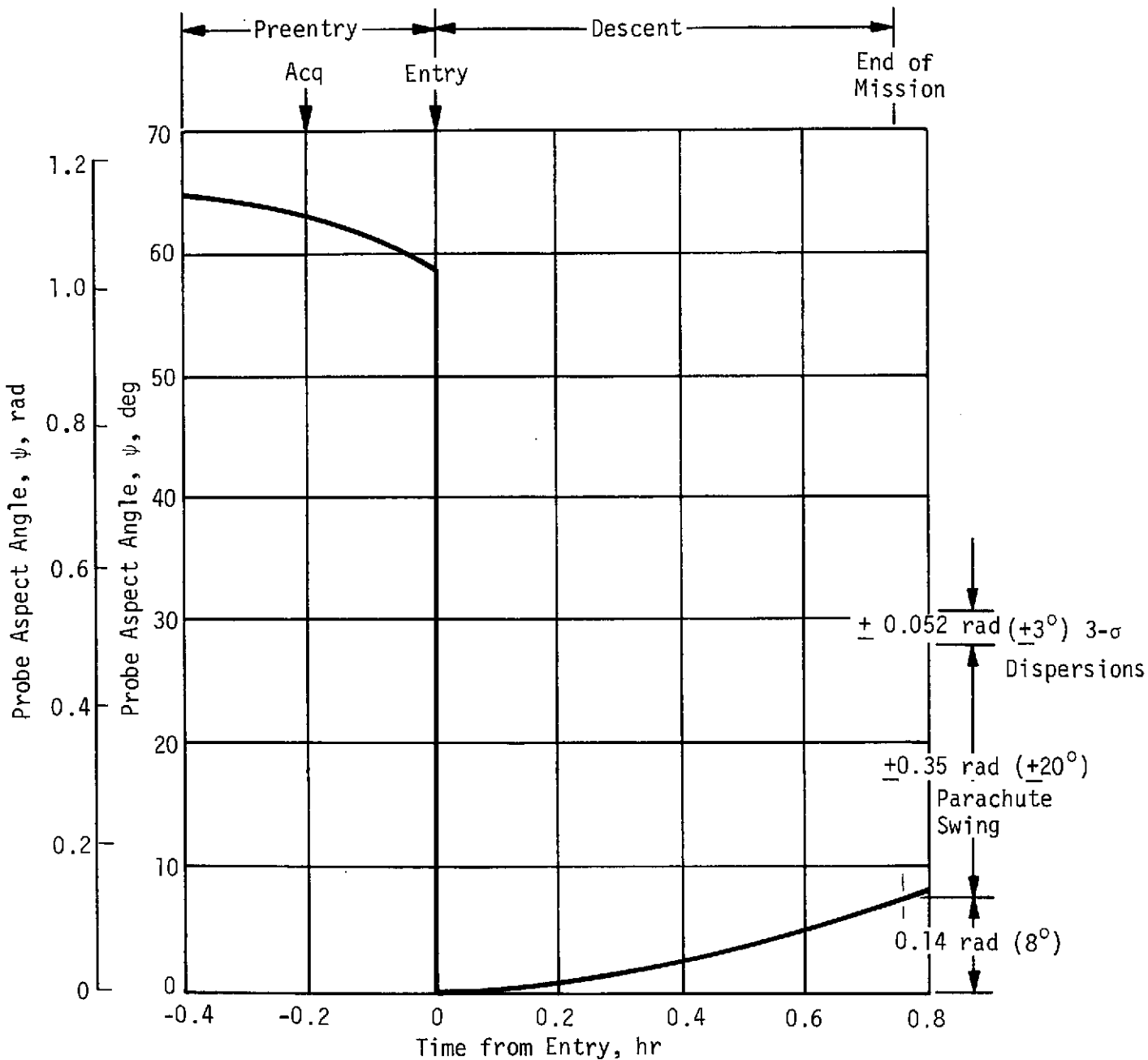


Figure 4.5-30 Probe Aspect Angles for the Baseline Configuration

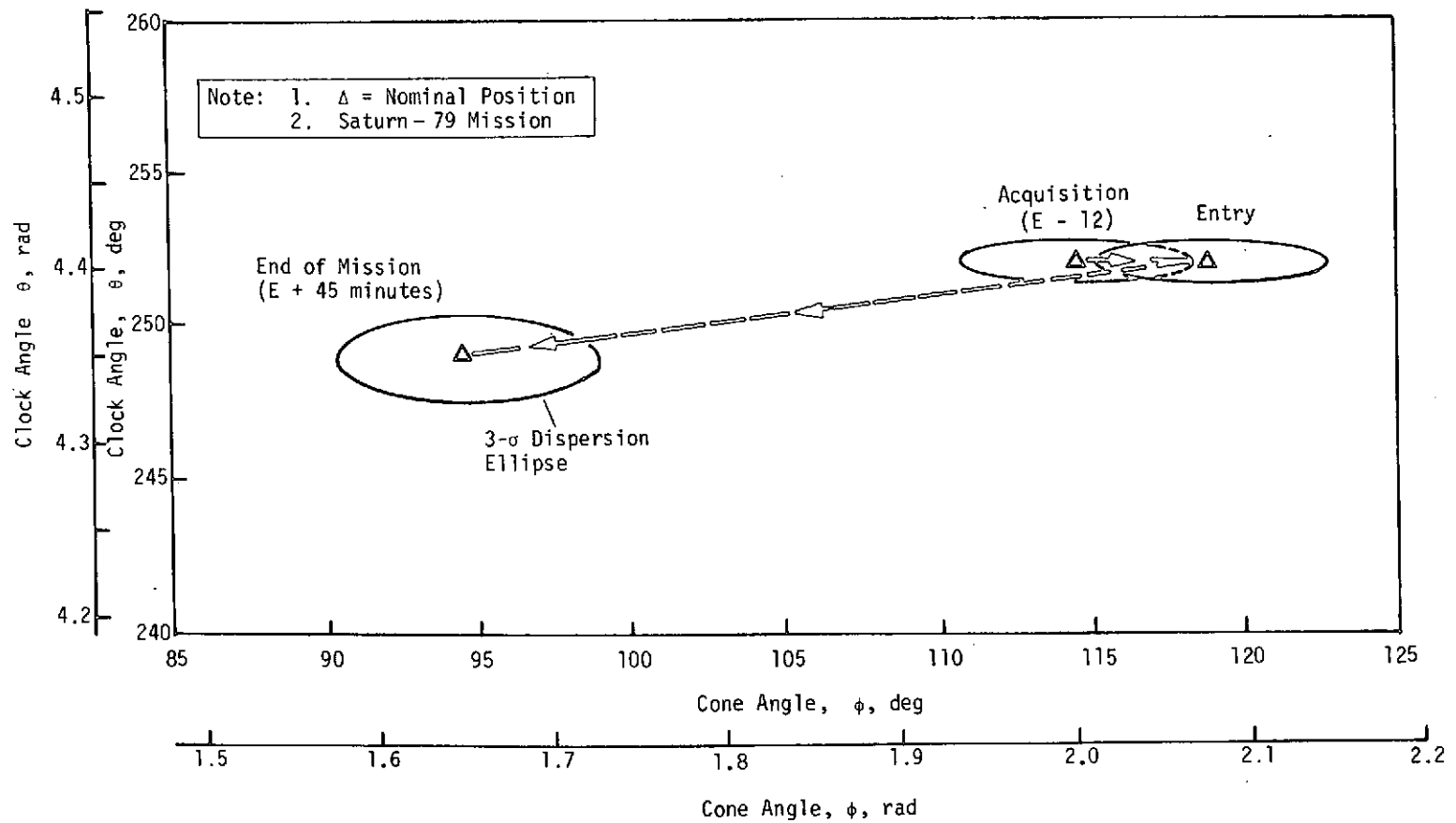


Figure 4.5-31 Probe Angular Variations for the Baseline Configuration during Saturn Encounter

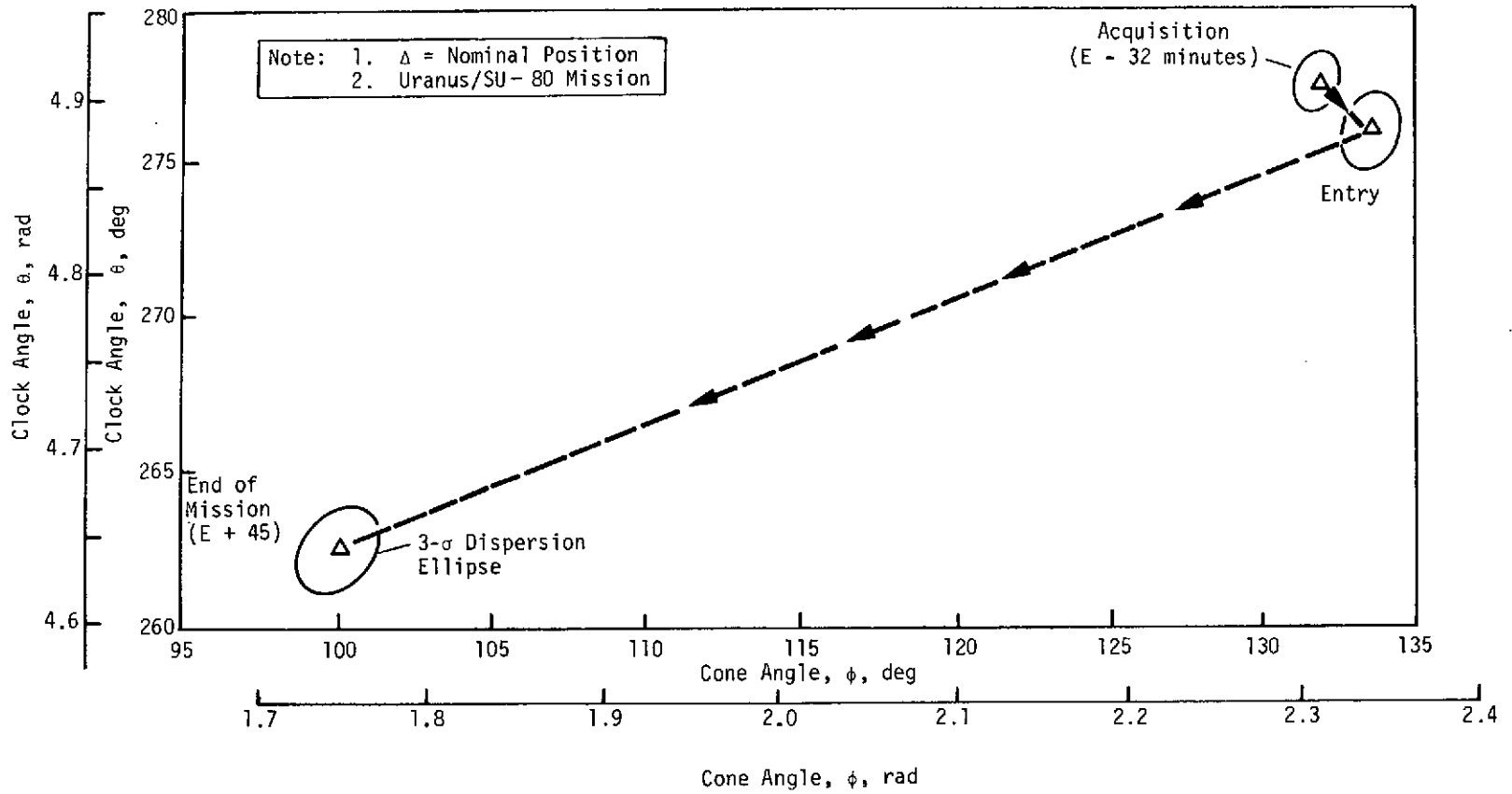


Figure 4.5-32 Probe Angular Variations for the Baseline Configuration during Uranus Encounter

plane. The dispersions differ in magnitude since optical navigation is necessary at Uranus and the encounter geometries are also different since Saturn encounter occurs closer to periapsis than Uranus encounter. The decreasing cone angles during descent result as the spacecraft pulls ahead of the descending probe.

Figure 4.5-33 shows spread in nominal cone angles for the two planets. A split-axial (butterfly) antenna pattern is required on the spacecraft since the pioneer spacecraft rotates about its spin axis at 4.8 rpm to maintain attitude stability in inertial space. For this reason relative clock angle positions are not important since the spacecraft antenna pattern has 3.14-rad (360°) coverage in that plane (⊙). The position of the main beam and the 3-dB beamwidth of the antenna are determined by the spread in cone angle for the various trajectories. This antenna pattern centered at a cone angle of 2.01 rad (115°) with a beamwidth of 0.79 rad (45°) is required to provide maximum gain for the Saturn encounter, which represents the worst case.

The parameters of the RF link shown in Table 4.5-12 for the worst-case condition, which determines the probe transmitter power output. A maximum RF power output of 28 watts is required at 800 MHz using binary FSK modulation with a tracking tone. Maximum power is required at Saturn EOM.

Table 4.5-13 describes the design characteristics of the RF components for the baseline telecommunication subsystem. The transmitter is based on PV hardware, which uses a solid-state microwave integrated circuit power amplifier. The modulator/driver is in a separate package and also uses solid-state design.

This configuration proposed preentry data transmission, as discussed in Section 4.4.1. The trajectories are designed so that the range (Figure 4.5-29), probe aspect angle (Figure 4.5-30), and cone angles (Figures 4.5-31 and 4.5-32) are not critical during acquisition. The data rate is 2 bps and 20 watts of RF power are required. The major impact is in designing the probe receiver to receive and track signals at such a low data rate.

- Note:
1. Saturn-79 and Saturn/SU-80 missions
  2. Uranus/SU-80 (retrograde) mission.
  3.  $3\text{-}\sigma$  cone angle uncertainties included in the design.
  4. Nominal atmosphere models.

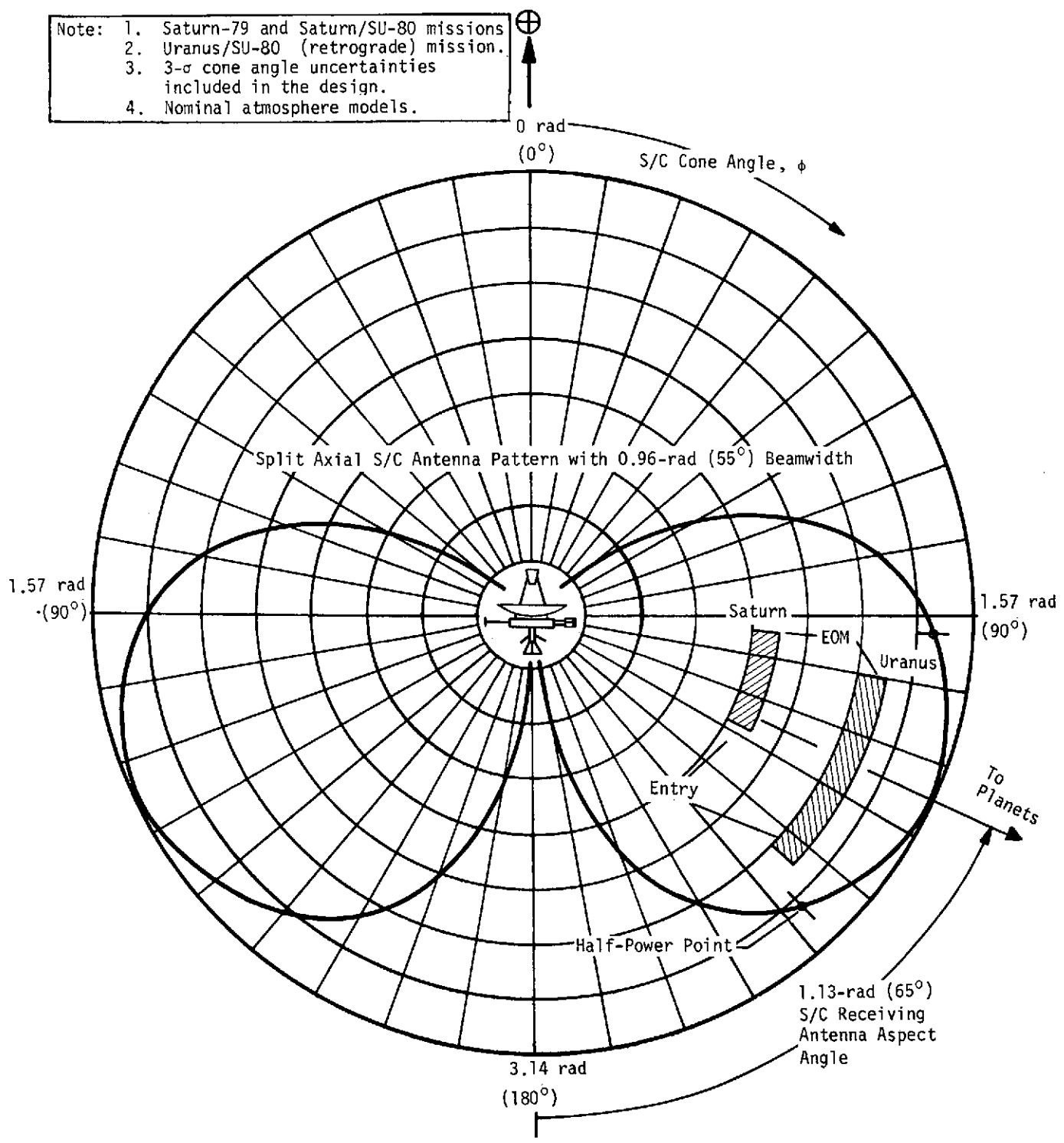


Figure 4.5-33 Spacecraft Antenna Pattern Coverage Requirements for the Baseline Configuration

Table 4.5-12 Probe Telemetry Link Design Table for the Baseline Configuration

Parameter	Nominal Value	Adverse Tolerance	Remarks
1. Total Transmitter Power, dBW	14.4	0	27.8 W at 800 MHz.
2. Transmitting Circuit Loss, dB	-0.8	0.1	61-cm (2-ft) RF coax.
3. Transmitting Antenna Gain, dB	6.5	1.1	1.75 rad (100°) beamwidth.
4. Communications Range Loss, dB	-188.8	0.5	$8.2 \times 10^4$ km at EOM.
5. Planetary Atmosphere & Defocusing Loss, dB	-0.6	0.1	Nominal atmosphere.
6. Polarization Loss, dB	-0.3	0	3 dB, 1.5 dB axial ratios.
7. Antenna Pattern Ripple Loss, dB	0	0.2	
8. Receiving Antenna Gain, dB	0.8	1.4	0.79 rad (45°) butterfly
9. Receiving Circuit Loss, dB	-1.0	0.1	92.4-cm (3-ft) RF coax.
10. Net Circuit Loss, $\Sigma$ (2 → 9), dB	-184.2	3.5	
11. Total Received Power (1 + 10), dBW	-169.8	3.5	
12. Receiver Noise Spectral Density, dBW/Hz	-200.7	0.4	$T_S = 620^\circ\text{K}$ , $NF_S = 5$ dB.
Tracking Tone			
13. Tone Power/Total Power, dB	-4.5	0	$P_C = 9.7$ W.
14. Received Tone Power, (11 + 13), dBW	-174.3	3.5	
15. Tracking Threshold Bandwidth, dB	12.4	0	17.5-Hz bandwidth.
16. Threshold SNR, dB	10.0	0	
17. Threshold Tracking Power (12 + 15 + 16), dBW	-178.3	0.4	
18. Tracking Performance Margin (14 - 17), dB	4.0	3.9	
Data Channel			
19. Data Power/Total Power, dB	-1.8	0	$P_d = 18.1$ W.
20. Radio System Processing Loss, dB	-1.0	0	
21. Fading Loss, dB	-1.0	0	
22. Received Data Power (11 + 19 + 20 + 21), dBW	-173.6	3.5	
23. Data Bit Rate, dB	15.0	0	32 bps.
24. Threshold $E_b/N_0$ , dB	8.1	0	
25. Threshold Data Power (12 + 23 + 24), dBW	-177.6	0.4	
26. Performance Margin (22 - 25), dB	4.0	3.9	
Conditions: 1. Saturn-79 mission at EOM. 2. $R_p = 2.3 R_S$ , $R_{EJ} = 30 \times 10^6$ km, $\gamma_E = -0.52$ rad (-30°), $T_L = 4700$ sec. 3. Convolutional encoder: $M = 2$ , $V = 2$ , $Q = 8$ , $K = 8$ code. 4. BER = $5 \times 10^{-4}$ for binary FSK with a tracking tone. 5. Rate 1/2 Viterbi decoder. 6. $B = 170$ kg/m <sup>2</sup> (1.083 slug/ft <sup>2</sup> ) on parachute. 7. $T_R = 275^\circ\text{K}$ (NF = 2.9 dB), $T_A = 200^\circ\text{K}$ , $T_F = 75^\circ\text{K}$ .			

Table 4.5-13 Telecommunication Subsystem for the Baseline Configuration

Component	Characteristic	Value
Power Amplifier	RF Frequency, $\lambda = 37.5$ cm (14.76 in.) , MHz	800
	RF Power Out, W	28
	Efficiency, %	40
	DC Power in at 28 V, W	70
	Weight Without Heat Sink, kg (lb)	0.9 (2.0)
	Volume, cm <sup>3</sup> (in. <sup>3</sup> )	737 (45)
	Size, cm (in.)	12.7 x 7.6 x 7.6 (5 x 3 x 3)
Transmitter Modulator/Driver	Modulation	BFSK + Tone
	Encoding	Convolutional
	DC Power In at 28 V, W	4
	Weight, kg (lb)	0.64 (1.4)
	Volume, cm (in. <sup>3</sup> )	490 (30)
Probe Antenna	Size, cm (in.)	12.7 x 7.6 x 5.1 (5 x 3 x 2)
	Type	Turnstile/Cone
	Polarization	RHC
	Main Beam Aspect Angle, rad (deg)	0 (0)
	3-dB Beamwidth, rad (deg)	1.75 (100)
	Maximum Gain (on-axis), dB	6.5
	Size (diameter x height), cm (in.)	17.8 x 10.1 (7 x 4)
Weight, kg (lb)	0.45 (1.0)	
S/C Antenna	Type	Split-Axial Pattern
	Polarization	RHC
	Main Beam Cone Angle, rad (deg)	1.13 (65)
	3-dB Beamwidth, rad (deg)	0.79 (45)
	Maximum Gain (on-axis), dB	3.35
	Size (diameter x height), cm (in.)	15.2 x 22.9 (6 x 9)
	Weight, kg (lb)	0.9 (2.0)
S/C Receiver/ Demodulator	Noise Temperature, °K	289
	Noise Figure, dB	3.0
	Frequency Acquisition, sec	60
	DC Power In at 28 V, W	3
	Weight, kg (lb)	0.9 (2.0)



#### 4.5.2.2 Data Handling Subsystem

The DHS defined for the baseline configuration contained the PV DHS, as it was then defined, in its entirety, but required some modification to all components except the signal conditioning units (SCUs). The modifications required and the reasons for these modifications are described below.

##### Digital Telemetry Unit

The mission definition called for a preentry data transmission, which was limited to 2 bps by the communication link. The minimum data rate can be reduced to 2 bps by changing the frequency of the oscillator or inserting a divide-by-4 circuit in the countdown circuitry. The latter was selected, as explained in Section 4.5.1.2.

The internal programs for the format ROMs must be changed for any SU mission configuration.

##### Power Control Unit, Data Handling Section

The PV configuration at the time the baseline was defined contained 5120 bits of memory capacity. The SU system required approximately 10,000 bits, so added memory elements and related counter modifications were necessary.

In addition, the decoding logic for the PV coast timer must be modified to provide an output at approximately 37 days. In comparison, the PV output is set at 27 days.

The sequencer ROMs require new internal programs for any SU configurations.

##### Signal Conditioner

No change from PV is required.

##### g Switches

The sensors selected were a  $490\text{-m/sec}^2$  (50-g) (increasing) sensor and a  $49.0\text{-m/sec}^2$  (5-g) (decreasing) sensor. The first unit is a backup to the coast timer and the second is a reference for the descent mission.

#### 4.5.2.3 Power and Pyrotechnics Subsystem (PPS)

The PPS defined for the baseline configuration uses the PV PCU (with some modification), the same type of cables and connectors, and a new battery design. The modifications to the PV unit and the selected battery description are presented below.

##### Wiring and Connectors

New cables are required to match the probe layout, but the PV wiring and connectors are satisfactory.

##### Power Control Unit, Power Section

The parachute (baseline) configuration required 38 pyro firing circuits, whereas the PV unit contained only 24. Space for the extra 14 circuits was made available by removing 8 unused relays and related switching circuits that took up an entire printed wiring board. No other PCU changes were required.

##### Battery

The PV battery was not usable for SU. Instead, we proposed to use a remotely activated Ag-Zn battery that incorporated the PV battery cells and modifications to accept a remote activation manifold. Electrolyte transfer tubes were to be longer than 9 cm (3.54 in.) to reduce the possibility of intercell shorts. The reservoir was packaged separately from the battery to allow flexibility in the probe layout. The power requirements summary and size derivation for this new battery are shown in Table 4.5-14. The battery losses shown in this table were based on the data available at that time.

#### 4.5.3 Alternate Configuration Definition

The alternate configuration probe system is a no-parachute version. This section discusses the impact on the electrical and electronic subsystems of changing the baseline to this new configuration. The design changes needed to effect this change are minor, but they do present some advantages over the baseline configuration.

Table 4.5-14 Descent Battery Sizing for the Baseline Configuration

Sequence (Uranus)	Time, T, h/m/s	Accumulative Time, hr	$\Delta T$ , hr	Load Energy, W-h	Bus Power, W	Loads, W					
						DTU	Transmitter	Power Control Unit	Transducer	Science	
DTU & PCU On	-0/38/59	0	}	0.23	13.5	5.3	0	6.2	2	0	
Science & RF Power Amplifier On	-0/37/59	0.017		6.15	109.8	5.3	74	6.2	2	22.3	
RF Power Amplifier Off	-0/34/38	0.073		}	46.12	39.8	5.3	4	6.2	2	22.3
Timer & Uranus Uncertainty (0.569 hr)					0.590						
RF Power Amplifier On (40% efficient)	+0/0/45	0.663		0.730	80.15	109.8	5.3	74	6.2	2	22.3
EOM	+0/44/31	1.393									
TOTAL = 132.65 W-h											

Battery Weight Calculation:

- Battery Power = Bus power  $\times \frac{1}{0.95} = 132.65/0.95 = 139.5$  W-h
- Add 12% for  $3\sigma$  low.  
Capacity prior to degradation =  $139.5$  W-h  $\times 1.12 = 156$  W-h
- Degradation:  
81% capacity due to 7-yr dry stand at  $273^{\circ}\text{K}$  ( $32^{\circ}\text{F}$ ).  
88% capacity due to 35-day wet stand at  $300^{\circ}\text{K}$  ( $80.5^{\circ}\text{F}$ ).  
100% capacity due to 2.3-day wet stand at  $290^{\circ}\text{K}$  ( $62.5^{\circ}\text{F}$ ).  
Capacity =  $156 \times \frac{1}{0.81} \times \frac{1}{0.88} = 219$  W-h or 7.8 A-h at 28 V.
- Cell size (20 required) =  $0.95 \times 4.75 \times 8.15$  cm ( $0.76 \times 1.87 \times 3.21$  in.).
- Activator size =  $1065$  cm<sup>3</sup> (65 in.<sup>3</sup>).
- Total battery weight =  $219$  W-h/ $20$  W-h/lb = 5.0 kg (11 lb).

#### 4.5.3.1 Communication Subsystem

The alternate configuration allows more room on the aft bulkhead of the probe for a larger antenna since the parachute was deleted. This enabled the operating frequency to be lowered to 560 MHz, which was established by the size of the turnstile/cone antenna design. 560 MHz is approximately a fourth subharmonic of 2.29 GHz, which is the operating frequency of the PV S-band transmitter.

From the standpoint of frequency interference, 560 MHz is within the frequency range for channel 29 for UHF television. The video carrier operates at 561.25 MHz, so interference is not expected during the mission. RFI precautions may be required during ground checkout at the launch site due to local interference problems.

The Saturn encounter generates the worst-case communication geometry. For the alternate configuration, we used a retrograde trajectory at Uranus to reduce the angle of attack and provide more dynamic stability to the probe. The trajectory parameters are shown in Table 4.5-15.

Using a retrograde trajectory at Uranus produces a larger spread in the cone angles than existed for the baseline configuration. This, in turn, results in a larger spacecraft antenna beamwidth (see Figure 4.5-34). The probe antenna beamwidth of 1.75 rad (100°) adequately covers the maximum probe aspect angle (see Table 4.5-15), the 3-sigma dispersions of 0.052 rad (3°), and the  $\pm 0.18$  rad ( $\pm 10^\circ$ ) dispersion due to wind shear during descent. Thermal control for the antenna is provided by using a Teflon/fiberglass radome.

Table 4.5-16 lists the characteristics of the RF link for the worst-case condition, which sizes the probe transmitter. An RF power output of 12 watts is required at 560 MHz using binary FSK modulation with a tracking tone. Note that the maximum power is required at Saturn EOM, but that this is matched well with the power required at entry.

Table 4.5-17 describes the design characteristics of the RF components that comprise the telecommunications subsystem for the alternate configuration. The transmitter is based on PV hardware considerations that use a separately packaged power amplifier from Microwave Semiconductor Corp. and a solid-state modulator/driver.

The alternate configuration is also based on an assumption of preentry data transmission, which is discussed in Section 4.4.1. As seen in Table 4.5-15, the large probe aspect angle during acquisition results in low probe antenna gain and sets the required power at 11 watts for a 2-bps transmission rate. The cone angle during acquisition is slightly less than that at entry and thus is within the spacecraft antenna beamwidth. The total frequency search time during acquisition will not exceed 60 seconds.

Table 4.5-15 Trajectory Communication Parameters for the Alternate Configuration

Parameter	Saturn-79			Uranus/SU-80		
	Acq	Entry	EOM	Acq	Entry	EOM
Range, 10 <sup>4</sup> km	9.6	10	8.1	5.5	6.3	3.5
Cone Angle, rad (deg)	1.99 (114)	2.07 (118.5)	1.61 (92)	2.51 (144)	2.58 (148)	1.57 (90)
Probe Aspect Angle, rad (deg)	1.10 (63)	0 (0)	0.16 (9)	0.61 (35)	0.34 (19.7)	0.73 (42)
Probe Antenna Gain, dB	1.7	6.5	6.4	5.1	6.1	4.4
S/C Antenna Gain, dB	2.9	2.8	0.7	-0.7	-1.8	0.4
Total RF Power for 560 MHz, W at 2 bps at 32 bps	11	10.1	12	2.4	8.3	2.5
General Constraints:	Saturn			Uranus		
Type of Trajectory	Posigrade			Retrograde		
Atmosphere Model	Nominal			Nominal		
Periapsis Radius	2.3 R <sub>S</sub>			2.0 R <sub>U</sub>		
Ejection Radius, 10 <sup>6</sup> km	30			10		
Entry Flight Path Angle, rad (deg)	-0.52 (-30)			-0.79 (-45)		
Lead Time, sec	4700			4200		
Acquisition Time (E - time), minutes	12			36.5		
End of Mission Time (E + time), minutes	49			49		
End of Mission Pressure, N/m <sup>2</sup> (bar)	1.05 x 10 <sup>6</sup> (10.5)			10 <sup>6</sup> (10)		
Descent Ballistic Coefficient, kg/m <sup>2</sup> (slug/ft <sup>2</sup> )	132 (0.84)			140 (0.89)		

- Note:
1. Saturn-79 and Saturn/SU-80 missions.
  2. Uranus/SU-80 (posigrade) mission.
  3.  $3\text{-}\sigma$  cone angle uncertainties included in the design.
  4. Nominal atmosphere models.

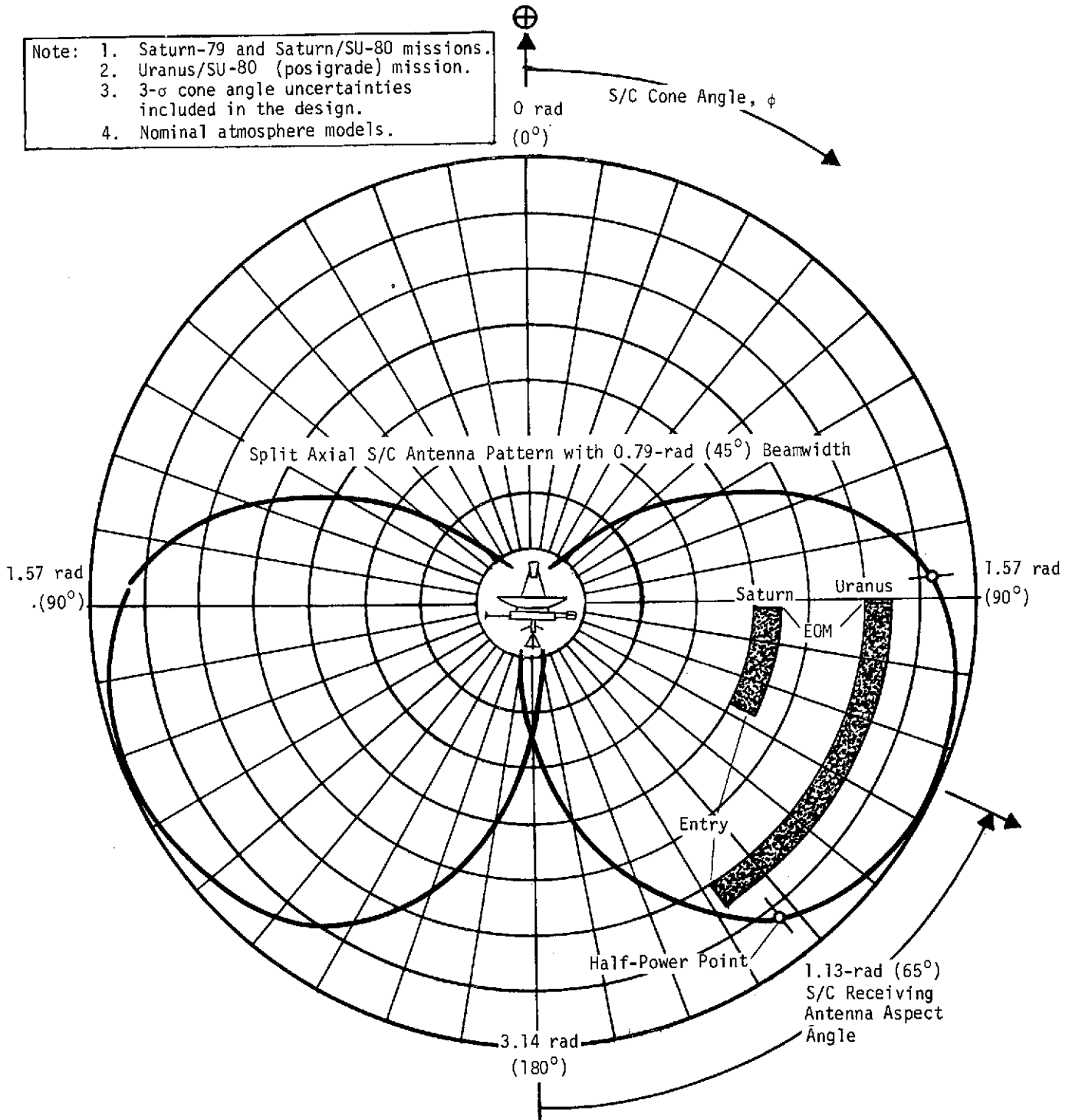


Figure 4.5-34 Required Spacecraft Antenna Pattern Coverage for the Alternate Configuration

Table 4.5-16 Probe Telemetry Link Design Table for the Alternate Configuration

Parameter	Nominal Value	Adverse Tolerance	Remarks
1. Total Transmitter Power, dBW	10.8	0	12 W at 560 MHz.
2. Transmitting Circuit Loss, dB	-1.0	0.1	Coax & radome.
3. Transmitting Antenna Gain, dB	6.4	0.5	1.75-rad (100°) beamwidth.
4. Communications Range Loss, dB	-185.6	0.5	8.1 x 10 <sup>4</sup> km.
5. Planetary Atmosphere & Defocusing Loss, dB	-0.3	0.1	Nominal atmosphere.
6. Polarization Loss, dB	-0.3	0	3 dB & 1.5 dB axial ratios
7. Antenna Pattern Ripple Loss, dB	0	0.2	
8. Receiving Antenna Gain, dB	0.7	1.0	0.96-rad (55°) butterfly.
9. Receiving Circuit Loss, dB	-1.0	0.1	91.4-cm (3-ft) RF coax.
10. Net Circuit Loss, $\Sigma$ (2-9), dB	-181.1	2.5	
11. Total Received Power (1 + 10), dBW	-170.3	2.5	
12. Receiver Noise Spectral Density, dBW/Hz	-200.1	0.4	$T_S = 702^{\circ}\text{K}$ , $NF_S = 5.33$ dB.
Tracking Tone			
13. Tone Power/Total Power, dB	-4.6	0	$P_c = 4.2$ W,
14. Received Tone Power (11 + 13), dBW	-174.9	2.5	
15. Tracking Threshold Bandwidth, dB	12.4	0	17.5-Hz bandwidth.
16. Threshold SNR, dB	10.0	0	
17. Threshold Tracking Power (12 + 15 + 16), dBW	-177.7	0.4	
18. Tracking Performance Margin (14 - 17), dB	2.8	2.9	
Data Channel			
19. Data Power/Total Power, dB	-1.9	0	$P_d = 7.8$ W.
20. Radio System Processing Loss, dB	-1.0	0	
21. Fading Loss, dB	-1.0	0	
22. Received Data Power (11 + 19 + 20 + 21), dBW	-174.2	2.5	
23. Data Bit Rate, dB	15.0	0	32 bps.
24. Threshold $E_b/N_o$ , dB	8.1	0	
25. Threshold Data Power (12 + 23 + 24), dBW	-177.0	0.4	
26. Performance Margin (22 - 25), dB	2.8	2.9	
Conditions: 1. Saturn-79 mission at EOM. 2. Convolutional encoder: $M = 2$ , $V = 2$ , $Q = 8$ , $K = 8$ code. 3. BER = $5 \times 10^{-4}$ for binary FSK with a tracking tone. 4. Rate 1/2 Viterbi decoder. 5. $T_R = 238^{\circ}\text{K}$ ( $NF = 2.6$ dB), $T_A = 327^{\circ}\text{K}$ , $T_F = 75^{\circ}\text{K}$ .			

Table 4.5-17 Telecommunications Subsystem for the Alternate Configuration

Component	Characteristic	Value
Power Amplifier	RF Frequency $\lambda = 53.6$ cm (21.1 in.) , MHz	560
	RF Power Out, W	12
	Efficiency, %	40
	DC Power In at 28 V, W	30
	Weight, kg (lb)	0.9 (2.0)
	Volume, cm <sup>3</sup> (in. <sup>3</sup> )	737 (45)
	Size, cm (in.)	12.7 x 7.6 x 7.6 (5 x 3 x 3)
Transmitter Modulator/Driver	Modulation	BFSK + Tone
	Encoding	Convolutional
	DC Power In at 28 V, W	4
	Weight, kg (lb)	0.64 (1.4)
	Volume, cm <sup>3</sup> (in. <sup>3</sup> )	490 (30)
Probe Antenna	Size, cm (in.)	12.7 x 7.6 x 5.1 (5 x 3 x 2)
	Type	Turnstile/Cone
	Polarization	RHC
	Main Beam Angle, rad (deg)	0 (0)
	3-dB Beamwidth, rad (deg)	1.75 (100)
	Maximum Gain (on-axis), dB	6.5
	Size (diameter x height), cm (in.)	22.8 x 25.2 (9 x 6)
	Weight, kg (lb)	0.45 (1.0)
S/C Antenna	Type	Split-Axial Pattern
	Polarization	RHC
	Main Beam Cone Angle, rad (deg)	1.13 (65)
	3-dB Beamwidth, rad (deg)	0.96 (55)
	Maximum Gain (on-axis), dB	2.9
	Size (diameter x height), cm (in.)	35.5 x 30.4 (14 x 12)
	Weight (including coaxial cable), kg (lb)	2.0 (4.5)
S/C Receiver/ Demodulator	Noise Temperature, °K	238
	Noise Figure, dB	2.6
	Frequency Acquisition, sec	60
	DC Power In at 28 V, W	8
	Weight, kg (lb)	2.0 (4.5)
	Volume, cm <sup>3</sup> (in. <sup>3</sup> )	1960 (120)
	Size, cm (in.)	15.2 x 12.7 x 10.2 (6 x 5 x 4)



#### 4.5.3.2 Data Handling Subsystem

The DHS defined for the alternate (no-parachute) configuration is similar to that for the baseline configuration in that it uses PV hardware, but the modifications involved are slightly different.

##### Digital Telemetry Unit

The modifications to the PV DTU for the alternate configuration are the same as those required for the baseline configuration (see Section 4.5.2.2).

##### Power Control Unit, Data Handling Section

By the time the alternate configuration was defined the memory capacity of the PV PCU had already been increased to 25,600 bits, which eliminated the need for additional memory. The coast timer and sequencer ROMs require the same changes defined for the baseline configuration.

##### Signal Conditioner

No change is required from the PV hardware.

##### g-Switches

The same changes are required as in the baseline configuration.

#### 4.5.3.3 Power and Pyrotechnics Subsystem

As in the baseline configuration, the SU PPS uses modified PV hardware in all cases except for the battery.

##### Cables and Connectors

These are the same as in the baseline configuration.

##### Power Control Unit, Power Section

By selecting the alternate configuration the number of required pyros and nonexplosive initiators reduced to 34. However, since this number still exceeded the PV capability (24), the same modification is required.

## Battery

Although the battery design concept had not changed from the baseline configuration, the size of the battery changes slightly due to the new mission loads. Table 4.5-18 shows the battery size derivation for the alternate configuration. Note that no packing factor has been included. There is no significant difference from using either a prograde or retrograde approach.

### 4.5.4 Configuration Comparison

#### 4.5.4.1 Communication Subsystem

The baseline and alternate communication subsystems have been discussed in Sections 4.5.2.1 and 4.5.3.1, respectively. The basic difference between the two is their operating frequency, which was determined by the largest probe antenna that can be mounted in the rear portion of the probe. Due to the space loss relationship, the corresponding RF power required was higher for the higher-frequency (baseline) configuration. The modulation, coding, data rate, and other major elements of the RF link are identical for both configurations. Lowering the operating frequency relieves the space loss and atmospheric attenuation problems and reduces the criticality of the communication geometry and data rate. Regardless of which frequency is selected, approximately 50% modification to the PV probe transmitter is required. Therefore, from the standpoint of the communication subsystem, the alternate configuration, operating at 560 MHz, is preferred since it requires less RF power. The probe antenna uses basically the same design as that used for PV, but must be modified to operate at a lower frequency.

#### 4.5.4.2 Data Handling Subsystem

Since the memory capacity of the PV DHS was increased after the baseline configuration had been defined, the difference in memory size is purely academic. No significant differences exist between the baseline and alternate configurations as far as the DHS is concerned.

#### 4.5.4.3 Power and Pyrotechnics Subsystem

The alternate configuration requires fewer pyro firing circuits, but still exceeds the capability of the PV subsystem. The same modification is required for the SU alternate configuration as for the SU baseline configuration.

Table 4.5-18 Descent Battery Sizing for the Alternate Configuration

Sequence (Uranus)	Time, T, h/m/s	Accumu- lative Time, hr	ΔT, hr	Battery Energy, W-h	Battery Power, W†	Bus Power, W	Load, W						
							DTU	Trans- <sup>s</sup> mitter	Power Control Unit	Trans- ducer	Science		
DTU & PCU On	-0/38/59	0	} 0.017	0.24 (0.24)*	14.2	13.5	4	0	7.5	2	0		
Transmitter & Science On	-0/37/59	0.017		} 0.058	4.28 (4.52)	74	70	4	34	7.5	2	22.3	
Transmitter & Power Ampli- fier Off	-0/34/29	0.075			} 1.156	48.4 (52.9)	41.8	39.8	4	4	7.5	2	22.3
Uranus & Timer Uncertainty	(0.569 hr)			} 0.81		59.7 (112.6)	74	70	4	34	7.5	2	22.3
Transmitter On	+0/0/45	1.231				2.04							
EOM	+0/49/12	2.04											

\* Accumulative

† Battery Power = Bus Power ×  $\frac{1}{0.95}$

<sup>s</sup> Transmitter Power = RF output ×  $\frac{1}{0.40}$  + 4 W (driver).

Battery Weight Calculation:

- Capacity prior to degradation = (Add 12% for 3σ low) = 112.6 W-h × 1.12 = 123 W-h
- Degradation:  
 81% capacity due to 7 yr dry stand at 273°K (32°F).  
 88% capacity due to 3.5 days wet stand at 300°K (80.5°F).  
 Capacity =  $123 \times \frac{1}{0.81} \times \frac{1}{0.88} = 173 \text{ W-h or } 6.2 \text{ A-h at } 28 \text{ V.}$
- Cell Size (20 required) = 1.68 × 4.21 × 7.37 cm (0.66 × 1.66 × 2.9 in.).
- Activator size = 70% × 20 each × 52 cm<sup>3</sup> (3.2 in.<sup>3</sup>) = 734 cm<sup>3</sup> (44.8 in.<sup>3</sup>).
- Total battery weight = 173 W-h ÷ 20 W-h/lb = 3.9 kg (8.6 lb) (wet)

The battery selection and design problems are similar to those for the baseline PPS, but the alternate configuration requires less usable energy (112.6 W-h versus 132.7 W-h) and is therefore the recommended system.

#### 4.5.5 Updated Alternate Configuration (Nominal Atmosphere)

During our analysis and tradeoff studies, we updated the alternate configuration and used this updated version with worst-case atmospheres so that the atmospheric effects could be defined. This section discusses design changes made to the alternate configuration that are *not* a result of the worst-case atmospheres, but rather of nominal atmosphere design iterations.

##### 4.5.5.1 Communication Subsystem

The alternate subsystem was updated as a result of the latest PV design and the mid-term review. Six changes occurred in the communication subsystem: (1) preentry data transmission was eliminated; (2) the bandwidth of the tracking loop was increased to 20 Hz; (3) the 3-sigma dispersions for both planets were reevaluated; (4) the transmitter/driver/modulator on the probe was packaged into a single case; (5) the efficiency of the transmitter was decreased to 30%; and (6) sequential decoding, with a constraint length of 32, was included in the design.

Deleting the requirement for preentry communications did not alter the link design since the mission geometry is such that preentry conditions do not govern the size of the probe transmitter. The only effects are in the areas of receiver design and battery capacity (see Section 4.4.1). The bandwidth of the filter for the tracking tone was increased from 17.5 to 20 Hz to accommodate the Doppler rates at Saturn. This will increase the tone power by 0.6 dB. A Monte Carlo analysis was performed on the latest trajectories for the two planets to update the 3-sigma dispersions used for the range, probe aspect angle, and cone angle. The new dispersions are shown in Table 4.5-19,

Additional data from transmitter suppliers indicate that a modified design can be packaged into a single unit. The preferred design is Teledyne's Model TR-2400, which is described in Table 4.1-2. The modified version, designed to operate at 560 MHz with FSK modulation, can be packaged into the same envelope and same resultant weight. A single unit simplifies circuit design, environmental testing, and packaging into the probe. Supplier data also indicated that the dc power conversion

Table 4.5-19 3-Sigma Dispersions for the Updated Alternate Configuration

Parameter	Planet	
	Saturn	Uranus
Range, km	3745	2539
Range Rate, km/sec	0.85	0.89
Cone Angle, $\pm$ rad ( $\pm$ deg)	0.047 (2.7)	0.028 (1.6)
Probe Aspect Angle, rad (deg)	0.051 (2.9)	0.241 (13.8)

Table 4.5-20 Trajectory Communication Parameters for the Final Configuration

Parameter	Saturn-79		Uranus/SU-80	
	Entry	EOM	Entry	EOM
Range, $10^4$ km	10.8	8.17	9.4	5.7
Cone Angle, rad (deg)	2.23 (128)	1.68 (96.5)	2.57 (147)	1.62 (93)
Probe Aspect Angle, rad (deg)	0.19 (11)	0.24 (14)	0.56 (32)	0.63 (36)
Probe Antenna Gain, dB	6.4	6.3	5.34	5.0
S/C Antenna Gain, dB	2.8	0.9	0.14	0.16
Total RF Power, for 560 MHz and 32 bps, W	13.3	13.2	18.3	7.9
General Constraints:				
Type of Trajectory	Prograde		Retrograde	
Atmosphere Model	Warm		Warm	
Periapsis Radius	$2.3 R_S$		$3.0 R_U$	
Ejection Radius, $10^6$ km	30		25	
Entry Flight Path Angle, rad (deg)	-0.52 (-30)		-0.61 (-35)	
Lead Time, sec	5200		5500	
End of Mission Time (E + time), minutes	63		74	
End of Mission Pressure, N/m <sup>2</sup> (bar)	$10^6$ (10)		$10^6$ (10)	
Descent Ballistic Coefficient, kg/m <sup>2</sup> (slug/ft <sup>2</sup> )	161.3 (1.03)		160 (1.01)	

efficiency of 40% used for solid-state UHF transmitter in the baseline/alternate designs was too high. Using an efficiency of 30% is more realistic (see Table 4.1-2) and has a minor effect on the size of the probe battery.

The PV DHS has a constraint length of 32 with sequential decoding at the DSN site. Both the baseline and alternate configurations for SU use Viterbi decoding with a constraint length (K) of 8 since it was uncertain early in the study whether the data would be decoded on the spacecraft and Viterbi decoding is less susceptible to high data loss due to atmospheric fading. To be able to use the PV DHS without modifying the constraint length, we choose sequential decoding with K=32. This gives a larger coding gain over Viterbi but the fading loss is greater (see Reference 4.5-1). The net result is that  $E_b/N_o$  is 7.3 dB for sequential decoding, but 0.8 dB is included to account for the fading loss. The effect on the link design table is nil since the corrections are compensatory. The advantage is in PV hardware compatibility.

#### 4.5.5.2 Data Handling Subsystem

The elimination of preentry transmission eliminated the need for a 2-bps clock and its associated modification.

#### 4.5.5.3 Power and Pyrotechnics Subsystem

Reducing the number of pyros and nonexplosive initiators to 24 eliminated the need for providing more pyro circuits and modifying the system to accommodate them.

Further refinements to the battery configuration have evolved as more data have been collected from experts in the industry and from a literature search. As a result, we decided to use individual cell activators to avoid shorts between the cells and to avoid relying on long electrolyte paths to solve the problem. This creates a need for a further development program, but is considered the most cost-effective solution. The battery size was reduced to 79.5 W-h by the elimination of the preentry transmission and changes in other mission parameters (see Section 4.4.5).

#### 4.5.6 Impact of Worst Case Atmosphere

A final configuration has been defined to accommodate the worst-case atmospheres for Saturn and Uranus. The impact on the electronics is minimal and is described in the following paragraphs. All modifications are based on the updated alternate configuration discussed in Section 4.5.5.

#### 4.5.6.1 Communication Subsystem

Considering the warm and cool atmosphere models for Saturn and Uranus affects the probe communications subsystem from the standpoint of adjusting the encounter geometry to maintain common cone angles. The warm atmosphere models also require a longer descent time to  $10^6 \text{ N/m}^2$  (10 bar), which widens the range of cone angles at Uranus. The worst-case conditions occur during the Uranus encounter with the warm atmosphere model. To improve the encounter geometry, we increased the periapsis radius to  $3 R_U$  but this increased the communication range. For a frequency of 560 MHz, using binary FSK modulation with a pilot tone and a data rate of 32 bps, 18 watts of RF power are required. The trajectory parameters for the worst-case atmosphere probes are shown in Table 4.5-20.

A Uranus retrograde trajectory with a periapsis radius of  $2 R_U$  and a warm atmosphere descent results in unacceptable cone angles [i.e., less than  $1.57 \text{ rad}$  ( $90^\circ$ )]. The spread in cone angles was too large to allow an efficient design for a spacecraft receiving antenna. To solve this problem, we chose a periapsis radius of  $3 R_U$ . The resulting cone angles are shown in Figure 4.5-35.

The lead time at Saturn was also adjusted from 4700 seconds, as shown in Table 4.5-15, to 5200 seconds (see Table 4.5-20) to move the spread in cone angles for Saturn toward the center of the range of angles for Uranus. No other adjustments were made in the Saturn mission. The butterfly pattern of the spacecraft receiving antenna was then positioned at an aspect angle of  $1.05 \text{ rad}$  ( $60^\circ$ ). As seen in Table 4.5-20, the RF power requirements at Saturn are well balanced between entry and EOM conditions. The RF power requirements at Saturn for the cool atmosphere model are 13.3 watts at entry and 10 watts at EOM [ $1.05 \times 10^6 \text{ N/m}^2$  (10.5 bar) at E+28 minutes]. A probe antenna with a beamwidth of  $1.75 \text{ rad}$  ( $100^\circ$ ) adequately covers the maximum probe aspect angle (see Table 4.5-20), the 3-sigma dispersions of  $0.24 \text{ rad}$  ( $14^\circ$ ) (see Table 4.5-19), and  $\pm 0.18 \text{ rad}$  ( $\pm 10^\circ$ ) dispersion due to horizontal wind shear during descent.

The antenna is enclosed in a Teflon/fiberglass radome for thermal and aerodynamic control at the rear of the probe. There is negligible RF attenuation through the two materials. The fiberglass is 0.1 cm (0.040 in.) thick and the Teflon layer is 0.76 cm (0.3 in.) thick. The Teflon is put on the outside of the radome and sublimates during entry heating.

- Notes:
1. Saturn-79 and Saturn/SU-80 missions
  2. Uranus/SU-80 (retrograde) mission.
  3.  $3\text{-}\sigma$  cone angle uncertainties. included in the design.
  4. Atmosphere models:

 Cool  
 Warm

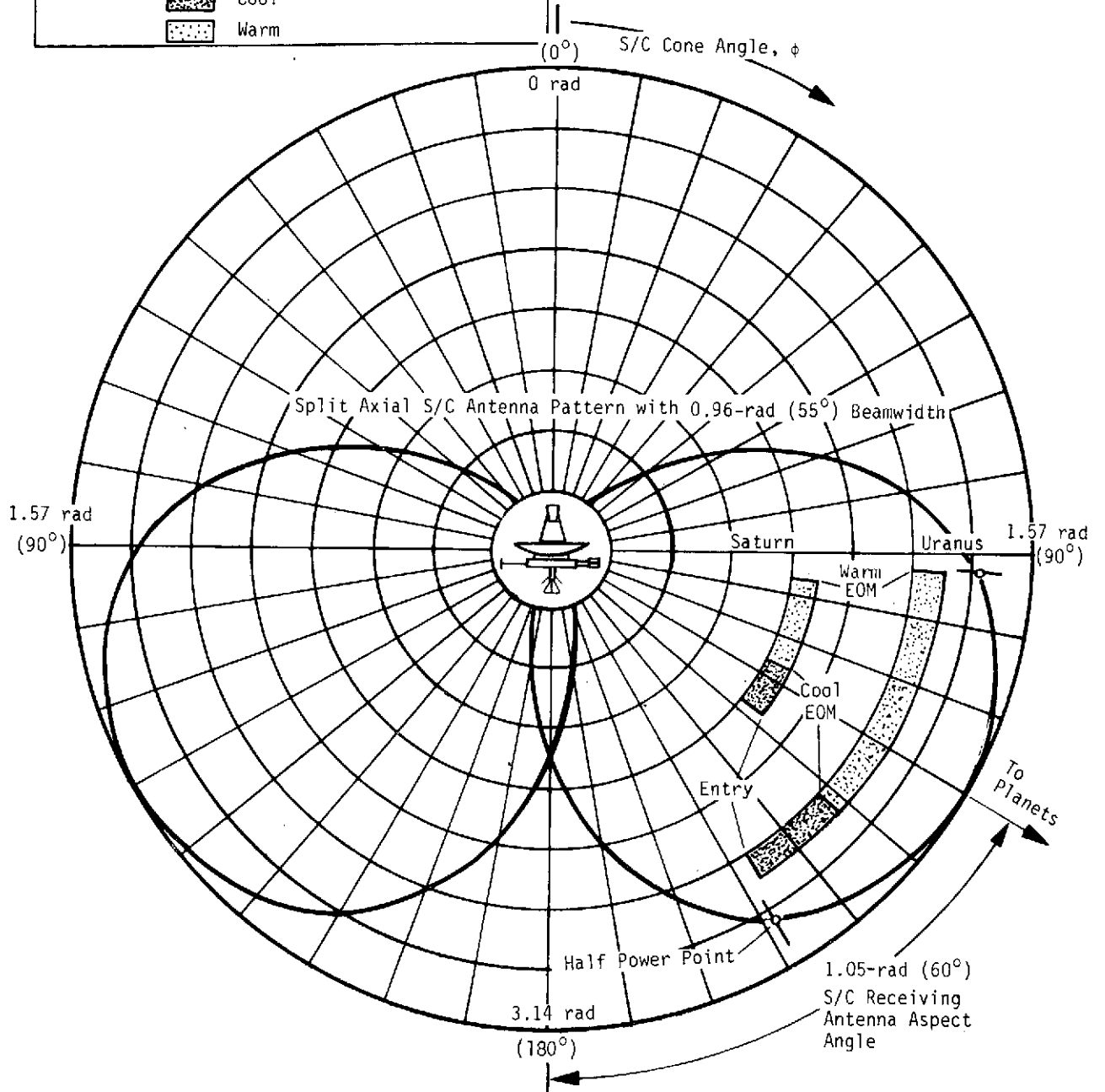


Figure 4.5-35 Required Spacecraft Antenna Pattern Coverage for the Final Configuration



The parameters for the RF link in the final configuration are shown in Table 4.5-21. This table applies for the worst-case condition (Uranus entry), which sizes the probe transmitter. The maximum RF power required for entry at Uranus is 18.3 watts, as shown in Table 4.5-20. The communication range is the major link loss that has to be overcome by the RF power level. The RF link was designed using the latest change discussed in Section 4.5.5.1. The dispersions used to establish the adverse tolerances are given in Table 4.5-19. Increasing the periapsis radius at Uranus to  $3 R_U$  reduced the antenna noise temperature from 36°K to 22°K since the maximum included angle shown in Figure 4.5-11(b) is reduced from 0.79 rad (45°) to 0.7 rad (40°). Equation (4.5-11) in Section 4.5.1.1 applies to the final design conditions. The RF power requirements are shown in Figure 4.5-36 as a function of mission time for three selected frequencies.

Table 4.5-22 lists the design characteristics of the RF components that comprise the telecommunication subsystem for the final configuration. The transmitter is based on the latest PV hardware considerations and the modulator, driver, and RF power amplifier are housed in a single solid-state package. The weight of the probe antenna has been increased from 0.45 kg (1 lb) to 0.55 kg (1.2 lb) as a result of a stress analysis (see Section 4.5.1.1) to ensure that this design will withstand the high entry deceleration, and additional welds have been added to critical areas.

#### 4.5.6.2 Data Handling Subsystem

The only changes in the DHS required to accommodate the worst-case atmospheres involve the need for a different sequence, different storage formats for the ROMs, and a different g-switch. The existing 32-bps data rate is sufficient to empty the entry data stored in memory even with the shortest descent time, so no additional bit rate capability is required. A 29.4-M/sec<sup>2</sup> (3-g) (decreasing) switch was used in place of the 49-m/sec<sup>2</sup> (5-g) switch to obtain a more common time reference for the six different SU atmosphere models.

#### 4.5.6.3 Power and Pyrotechnics Subsystem

No changes to the PPS are required for the final configuration, except for the battery. The long descent time and higher power rate require a significant increase in battery size. Figure 4.5-37 compares the nominal and worst-case power requirements for the Uranus warm atmosphere, which has the most severe impact on the battery.

Table 4.5-21 Probe Telemetry Link Design for the Final Configuration

Parameter	Nominal Value	Adverse Tolerance	Remarks
1. Total Transmitter Power, dBW	12,6	0	18,3 W at 560 MHz,
2. Transmitting Circuit Loss, dB	-1,0	0,1	Coax and radome,
3. Transmitting Antenna Gain, dB	5,3	2,9	1,75-rad (100°) Beamwidth
4. Communications Range Loss, dB	-186,9	0,3	9,4 x 10 <sup>4</sup> km,
5. Planetary Atmosphere & Defocusing Loss, dB	0	0,1	Entry
6. Polarization loss, dB	-0,3	0	3 dB & 1,5 dB axial ratios
7. Antenna Pattern Ripple Loss, dB	0	0,2	
8. Receiving Antenna Gain, dB	0,1	0,3	0,96-rad (55°) Butterfly,
9. Receiving Circuit Loss, dB	-1,0	0,1	91,4-cm (3-ft) RF coax,
10. Net Circuit Loss, $\Sigma$ (2 → 9), dB	-183,8	4,0	
11. Total Received Power (1 + 10), dBW	-171,2	4,0	
12. Receiver Noise Spectral Density, dBW/Hz	-202,9	0,4	T <sub>S</sub> = 374°K, NF <sub>S</sub> = 3,6 dB.
Tracking Tone			
13. Tone Power/Total Power, dB	-4,2	0	P <sub>C</sub> = 6,8 W.
14. Received Tone Power (11 + 13), dBW	-175,4	4,0	
15. Tracking Threshold Bandwidth, dB	13,0	0	20-Hz Bandwidth,
16. Threshold SNR, dB	10,0	0	
17. Threshold Tracking Power (12 + 15 + 16), dBW	-179,9	0,4	
18. Tracking Performance Margin (14 - 17), dB	4,5	4,4	
Data Channel			
19. Data Power/Total Power, dB	-2,1	0	P <sub>d</sub> = 11,2 W.
20. Radio System Processing Loss, dB	-1,0	0	
21. Fading Loss, dB	-1,8	0	
22. Received Data Power (11 + 19 + 20 + 21), dBW	-176,1	4,0	
23. Data Bit Rate, dB	15,0	0	32 bps,
24. Threshold E <sub>b</sub> /N <sub>0</sub> , dB	7,3	0	
25. Threshold Data Power (12 + 23 + 24), dBW	-180,6	0,4	
26. Performance Margin (22 - 25), dB	4,5	4,4	
Conditions: 1. Uranus/SU-80 mission at entry, 2. Convolutional encoder: M = 2, V = 2, Q = 8, 3. BER = 5 x 10 <sup>-4</sup> for binary FSK with a tracking tone. 4. Rate 1/2 sequential decoding, K = 32. 5. T <sub>R</sub> = 238°K (NF = 2,6 dB), T <sub>A</sub> = 22°K, T <sub>F</sub> = 75°K.			

Table 4.5-22 Telecommunication Subsystem for the Final Configuration

Component	Characteristic	Value
Power Amplifier/ Modulator/Driver	Modulation Encoding RF Frequency, $\lambda = 53.6$ cm (21.1 in.), MHz RF Power Out, W Power Amplifier Efficiency, % Total DC Power in at 28 V, W Weight, kg (lb) Volume, cm <sup>3</sup> (in. <sup>3</sup> ) Size, cm (in.)	BFSK + Tone Convolutional 560 18.3 30 64 1.36 (3.0) 675 (41) 14 x 12.7 x 3.8 (5.5 x 5 x 1.5)
Probe Antenna	Type Polarization Main Beam Angle, rad (deg) 3-dB Beamwidth, rad (deg) Maximum Gain, dB Size (diameter x height), cm (in.)  Weight, kg (lb)	Turnstile/Cone RHC 0 (0) 1.75 (100) 6.5 22.8 x 25.2 (9 x 6) 0.55 (1.2)
S/C Antenna	Type Polarization Main Beam Cone Angle, rad (deg) 3-dB Beamwidth, rad (deg) Maximum Gain (on-axis), dB Size (diameter x height), cm (in.)  Weight (including coax cable), kg (lb)	Split-Axial Pattern RHC 1.05 (60) 0.96 (55) 3.1 35.5 x 30.4 (14 x 12) 2.0 (4.5)
S/C Receiver	Noise Temperature, °K Noise Figure, dB Frequency Acquisition, sec DC Power in at 28 V, W Weight, kg (lb) Volume, cm <sup>3</sup> (in. <sup>3</sup> ) Size, cm (in.)	238 2.6 60 8 2.04 (4.5) 1967 (120) 12.7 x 15.2 x 10.2 (5 x 6 x 4)

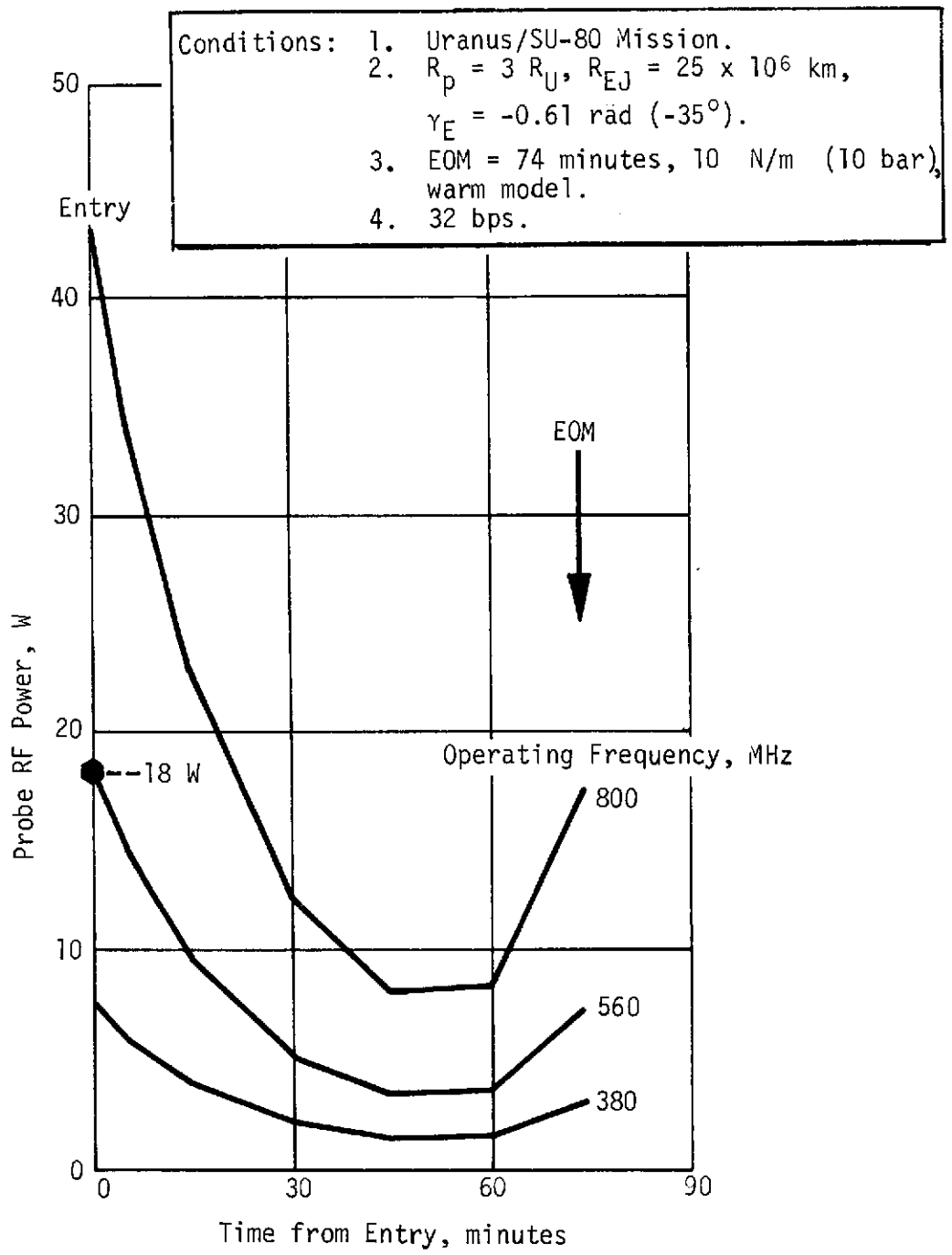


Figure 4.5-36 Required Probe RF Power for the Final Configuration

Note: Maximum energy required:

Final Configuration, 561,960 J (156.1 W-h);

Updated Alternate Configuration, 286,200 J (79.5 W-h).

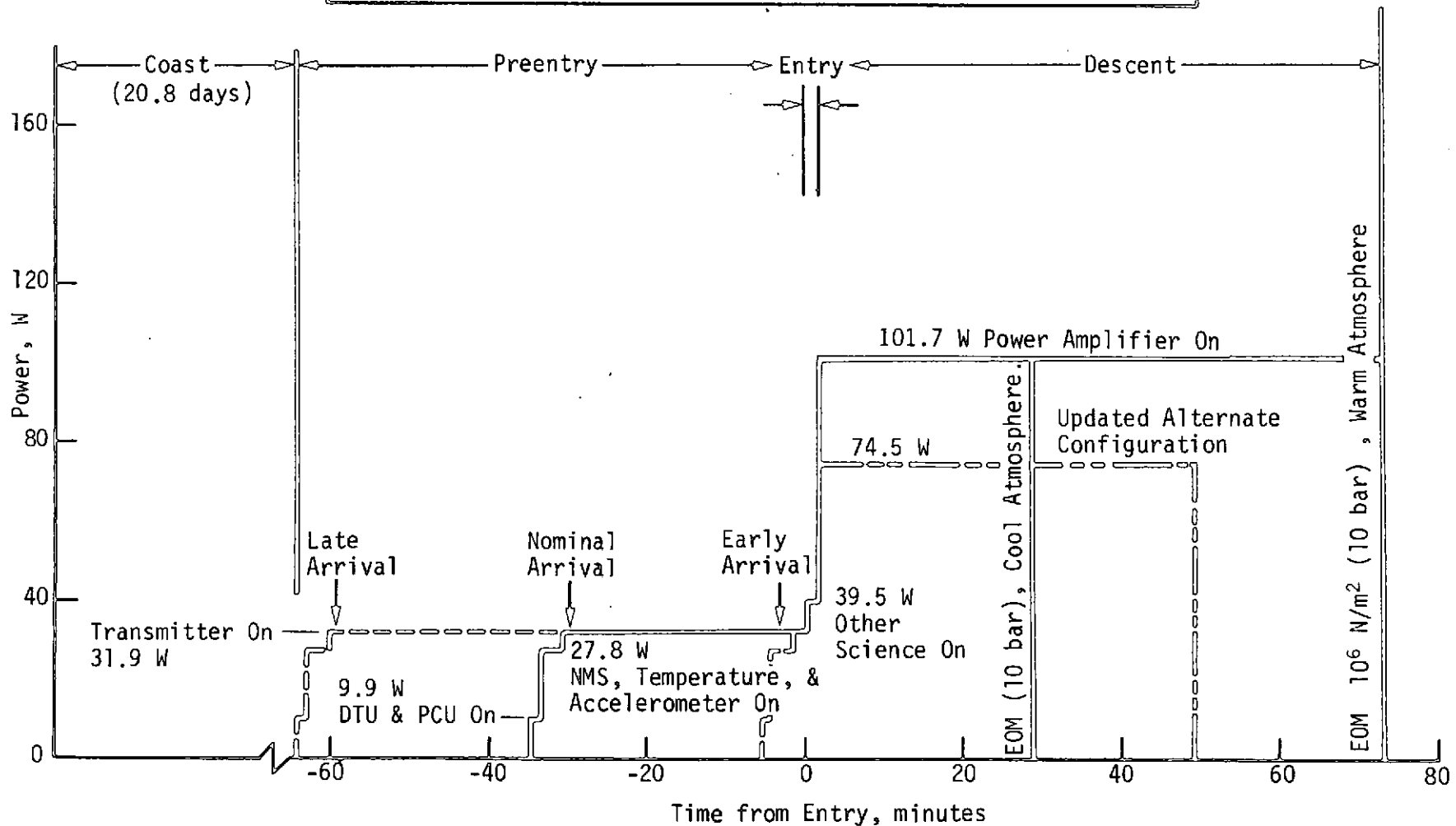


Figure 4.5-37 Power Profile for the Final Configuration

The battery size for the worst-case atmosphere was calculated using the best derating numbers available and a 1.4 form factor for packaging. The calculations and results are shown in Table 4.5-23.

Table 4.5-23 Battery Calculations for the Final Design

1. Required Probe Energy	= 156.1 W-h.
2. The following conditions are imposed:	
Battery Voltage	= $28 \pm 10\%$
Cruise Time + Prelaunch Shelf Life	= 7.2 yr
Coast Time	= 37 days
Cruise Temperature	= 278°K (5°C).
Coast Temperature	= 298°K (25°C).
3. Type of battery = Ag-Zn, remotely activated with heavy-duty separators and individual cell activators.	
4. Number of cells	= 20.
5. Power system losses:	
Diode/line loss	= 4%
Contingency (cell out)	= 5%
7-yr dry storage at 278°K (5°C)	= 5%
37-day wet stand at 298°K (25°C)	= 5%
Monovalent operation	= 25%
6. Efficiency = $0.96 \times 0.95 \times 0.95 \times 0.95 \times 0.75 = 0.58$ .	
7. Energy required = $156.1/0.58 = 270$ W-h = $270/28.6 = 9.4$ A-h.	
8. Next cell size = 11.2 A-h.	
9. Battery weight = $\frac{6.1 \text{ oz/cell} \times 20 \text{ cells} \times 1.4 \text{ packing factor}}{16 \text{ oz/lb}} = 10.7$ lb.	
10. Activation system = $0.5 \times$ battery weight = 5.4 lb.	
11. Total battery system weight = 16.1 lb = 7.3 kg.	

## 4.6 Structural and Mechanical Designs

## 4.6 STRUCTURAL AND MECHANICAL DESIGNS

### 4.6.1 Analysis and Tradeoff Studies

#### 4.6.1.1 Configuration Tradeoff Study

A tradeoff study was conducted to determine the most stable shape for the aeroshell. The statement of work placed emphases on the use of a 1.0-rad ( $60^\circ$ ) half-angle cone. Aerodynamic test data from the Pioneer Venus (PV) small probe showed that using a smaller, i.e., 0.79-rad ( $45^\circ$ ) half-angle conical forebody improved a probe's aerodynamic stability. The tradeoff study was performed on the baseline configuration to determine the effect of 1.05, 0.96, and 0.79-rad ( $60^\circ$ ,  $55^\circ$ , and  $45^\circ$ ) half-angle aeroshells on the probe's size, weight, and aerodynamic stability. The results of this study are depicted in Table 4.6-1. Note that as the half angle decreased, the c.g. moved forward, increasing the probe's aerodynamic stability. In the table a positive c.g. is defined as being forward of the probe's maximum diameter, and a negative c.g. is aft of the maximum diameter.

Table 4.6-1 Configuration Comparisons

	Aeroshell Half Cone Angle		
	1.05 rad ( $60^\circ$ )	0.96 rad ( $55^\circ$ )	0.79 rad ( $45^\circ$ )
Entry Probe c.g., % of Maximum Diameter	-6.0%	0.3%	9.6%
Descent Probe c.g., % of Maximum Diameter	-7.7%	-3.5%	5.3%
Weight of Entry Probe, kg	62.1	65.2	71.7
Diameter of Entry Probe, cm	71.1	76.6	90.4
Weight of Descent Probe, kg	43.2	43.8	45.5
Diameter of Descent Probe, cm	60.2	62.0	67.6
Weight of Forebody Heat Shield, kg	11.7	12.4	13.2



The probe diameter and weight increased slightly as the forebody half-angle decreased, but the probe's improved stability far outweighs the size and weight penalties incurred. These penalties still do not exceed the limitations given in the statement of work.

Our tradeoff study on the separable heat shield/aeroshell versus an integral heat shield/aeroshell is discussed in Section 4.6.4. To facilitate designing the jettisonable nose cap, we varied the  $R_N/R_B$  ratio of 0.5 given in the statement of work. Our values for the final design are 0.425 for entry, and 0.49 after the nose cap is jettisoned. The aerodynamic effect of this change on the drag and stability of the probe is negligible.

#### 4.6.1.2 Structural Analysis

A preliminary stress analysis was conducted to size the major structural elements and confirm the feasibility and integrity of the structure. The critical loading conditions considered in this analysis were the maximum aerodynamic pressure loads at entry, the resulting inertia load due to deceleration, and the differential internal/external pressure of  $+10^5$  N/m<sup>2</sup> (1 bar). Booster load levels are not critical for the probe except at the local interface support structure. An ultimate factor of safety of 1.25 was used in the analysis.

Another analysis was done on the aeroshell forebody to establish the size of the ring frame, the skin gauge, and the frame spacing. This served to check the general stability of the skin/frame structure, flange crippling, and skin buckling between the frames. The critical condition was at the maximum entry pressure, which occurs before aerodynamic heating significantly increases the structural temperatures.

The structure for the equipment support deck was sized to carry the inertia loads from entry deceleration. This structure is an integrally machined, aluminum-beam grid structure whose beams are designed to minimize deflections and prevent load coupling with the booster system. The top plate of the support platform is designed to be nonbuckling.

The mechanical joint between the equipment deck and the deck support ring attenuates both shock and thermal requirements. Additional

analyses and/or tests would be needed to determine the shock levels. No allowable levels for the equipment and no shock levels at the source were determined in this study, and further evaluation would be required for the final design.

The equipment support deck is supported by an aluminum monocoque cylinder attached to the conic aeroshell. The design of this cylinder is dictated by the compression load resulting from the equipment inertia load during the maximum entry deceleration. The cylinder thickness is increased locally at the ends of the equipment support beams, where the loads are concentrated. The ring is designed to distribute these inertia loads uniformly to the aeroshell forebody.

The aluminum materials selected for structural elements were high-strength aluminum alloys. Note that the environments are not anticipated to provide high susceptibility to stress corrosion. If environments and residual stress levels exceed the threshold levels for stress corrosion, then the materials will be painted or aged to reduce its susceptibility.

The aft bulkhead reacts to the  $10^5$  N/m<sup>2</sup> (1 bar) atmospheric collapse pressure during descent and the inertia load of the antenna during the entry deceleration. Since the pressure load is the most critical, we based our design on a PH 15-7 Mo steel honeycomb structure with a bulkhead thickness of 1.9 cm (0.750 in.). The deflection of this bulkhead is calculated to be 0.71 cm (0.28 in.) at the ultimate pressure with 0.038-cm (0.015 in.) thick face sheets, and a 0.0064-cm (0.0025 in.) thick core with a cell size of 0.635-cm (0.25 in.). The *Stresskin* design allowables manual, SDAM-100, was used in designing the panel.

The edge member flexes radically to prevent significant loads from temperature or pressure environments. This enables it to take the axial loads due to pressure loading. The "Z"-ring edge member carries the loads from the pressure bulkhead to the probe structure. Table 4.6-2 summarizes the margins of safety for the major structural elements. The detailed stress analysis is shown in Appendix A.

#### 4.6.1.3 Heat Shield Analysis and Tradeoff Studies

The heat shield analysis was conducted using the Martin Marietta Thermal Chemical Ablation Program. The input to this program consists of temperature-dependent material, atmospheric properties and time-dependent environmental conditions.

Heating data used in the analysis were derived from cold-wall unblown radiant and convective heat fluxes provided by Aerotherm

Table 4.6-2 Structural Margin of Safety Summary

Part Name	Critical Condition	Failure Mode	M. S.
Aeroshell Forebody	Maximum Entry	General Instability	1.22
Aeroshell Frame	↓	Flange Crippling	0.44
Aeroshell Skin	↓	Buckling Between Fr.	0.09
Base Cover Cone	Collapse Pressure	Buckling of Cone	0.10
Aft Bulkhead	↓		
Honeycomb Core	↓	Shear	0.49
Face Sheet	↓	Comparison Buckling	1.20*
Support Ring	↓	Flange Bonding	0.14
Equipment Support Ribs	Maximum Entry	Rib Bonding	0 <sup>†</sup>
Antenna Array	↓	Bonding (weld)	0.36
Antenna Petal	↓	Bonding (weld)	0.50
*Designed by deflection.			
†Many ribs analyzed and sized for 0 margin at $4.14 \times 10^8$ N/m <sup>2</sup> (60,000 psi).			

Acurex Corporation. In all cases the Aerotherm data were for trajectories somewhat different than those considered in this study and had to be modified. Details of such are in Appendix B.

The models we analyzed were one-dimensional models that consisted of elements representing the ablative material, insulator (if used), and the aeroshell structure. The structural design criteria were as follows:

- 1) Peak structural temperature =  $422^{\circ}\text{K}$ ;
- 2) Maximum weight = 13.6 kg (29.9 lbs);
- 3) Use PV materials if possible.

The use of the PV material was modified almost immediately because of excessive recession during entry.

The heat shield requirements for the baseline and alternate configurations were defined by the Saturn nominal atmospheric entry environment. The resultant heat shield consisted of 0.794-cm (0.3125 in.) thick quartz nitrile phenolic (QNP) bonded to a 0.457-cm (0.180 in.) thick honeycomb-reinforced SLA-220, which is bonded to the probe aeroshell.

The heat shield requirements for the final configuration were defined by both the Uranus cool atmosphere, because of the high heat pulse, and by the Saturn warm atmosphere, because of the thermal soakback to the aeroshell. The resulting heat shield consists of 1.27-cm (0.50 in.) of carbon phenolic and 0.794-cm (0.3125 in.) phenolic honeycomb-reinforced SLA-220. Details of the heat shield analysis are given in Appendix B.

Tradeoff studies were conducted to select the ablative materials used for the various configurations. The materials considered were the PV quartz nitrile phenolic, a modified quartz nitrile phenolic that has better recession characteristics than the PV material, and carbon phenolic. From this study we selected the modified QNP for the baseline and alternate configurations. Due to the excessive heat pulse encountered at worst-case atmospheric entry, unacceptable recession of QNP was experienced. Therefore carbon phenolic was selected for the final configuration.

A separate tradeoff study was conducted in which we introduced a layer of insulation between the ablative material and the probe aeroshell. Based on the results of this study, we have used SLA-220 as an insulator in all heat shield configurations, to reduce weight.

#### 4.6.1.4 Thermal Control Subsystem

The thermal control subsystem for a Saturn/Uranus (SU) common probe must keep the equipment and structures within specified temperature limits during each phase of the mission. These phases cover widely varying environments and timelines in which the probe thermal control hardware must function.

##### Mission Phase Requirements

*Cruise on Spacecraft* - The probe is carried in a cone-shaped adapter on the aft end of the spacecraft with the probe forebody viewing deep space. No direct solar fluxes will be incident on the probe because the aft of the spacecraft is always pointed directly away from the Sun. Nevertheless, a spacecraft maneuver near Earth might possibly point the probe at the Sun for a period of up to 5 hours.

The thermal control interface between the probe and spacecraft requires that the spacecraft receives no energy from the probe. To maintain the probe cruise temperature at 277°K (40°F), some energy must be dissipated within the probe. The probe is covered with multilayer insulation to minimize this heating requirement.

The probe heaters are sized by the insulation losses during the postseparation coast to the planet. This coast period represents a colder environment than the cruise mode. Consequently, some of the excess heater power available during the cruise phase must be conducted through the probe/adapter support points and then be radiated overboard by small fins. The successful operation of this heat rejection mode--in parallel with the probe's multilayer insulation--is the crux of our thermal control approach for the cruise phase of the mission.

*Coast to Planet* - After a 3.4-year cruise to Saturn, or a 6.9-year cruise to Uranus, the probe is separated from the spacecraft to begin the final approach to the planet. Temperatures in the probe will begin slowly rising because the entry temperature is higher than the cruise temperature. The energy previously conducted through the mounting points drives the temperature up, but the rise is slow due to the colder effective sink (deep space) to which the probe is now completely exposed. Direct solar radiation is incident on the probe's aft surfaces during the coast phase, but its intensity is too low to affect probe temperatures.

The thermal control design for this phase of the mission must ensure that probe temperatures are within an allowable specified range on arriving at the target planet. Since the coast times to Saturn and Uranus differ by 15 days, the transient heating rate of the

probe must be sized so that the desired band of entry temperatures will be reached at either planet. The coast thermal analysis in Appendix C contains a detailed evaluation of the probe heating requirements.

*Preentry Activation* - The probe's science and communication subsystems are warmed up a few minutes before entry into the planetary atmosphere. This warmup period affects the design of the thermal control subsystem because it can vary from 7 minutes to 69 minutes depending on the arrival uncertainties. These uncertainties arise from unknowns in determining the precise location of the spacecraft relative to the planet when releasing the probe.

When analyzing the probe's temperatures during its descent through the worst-case atmospheres, the preentry heating times are stacked to produce the extremes of the probe's final temperature. Thus, the hottest temperatures result when the longest preentry heating period is followed by a descent into the warmest atmosphere. In contrast the coldest probe temperatures occur when the shortest preentry heating is followed by a cold atmosphere descent.

*Atmospheric Entry* - During atmospheric entry, the probe's thermal balance is affected as heat from the entry heating pulse soaks back into the structure of the descent capsule. For the baseline configuration this effect is minimal because the heat shield is ejected from the probe immediately after entry; however, for the alternate and final configurations, the ablated heat shield remains on the probe and transfers heat to the structure of the aeroshell.

*Atmospheric Descent* - The probe falls ballistically through the gaseous hydrogen-helium mixture of the Saturn or Uranus atmosphere for periods ranging from 27 minutes in the Saturn cool atmosphere to 74 minutes in the Uranus warm atmosphere. In all atmospheric models, the end-of-mission (EOM) point is considered to be at absolute pressure of  $10^6$  N/m<sup>2</sup> (10 bar). The probe is vented to the atmosphere through a relief valve system which is sized to prevent the entry of atmospheric gases from entering the probe to an atmospheric pressure of 2.5 N/m<sup>2</sup> (2.5 bar). The probe's interior is pressurized with a low conductivity gas from tanks which are opened after entry.

Our thermal control approach for this phase of the mission consists of insulating the probe structure internally to uncouple the payload from the temperature extremes of the planetary atmospheres. These extremes range from 47°K (-375°F) at upper altitudes in the Uranus cool model to 424°K (304°F) at  $10^6$  N/m<sup>2</sup> (10 bar) in the Saturn warm atmosphere. The incoming atmospheric

gas degrades the performance of the probe's foam insulation because the conductivity of the insulation closely follows that of the gas filling the insulation. For the worst-case atmospheres, this degradation can be postponed by charging the probe with a low-conductivity gas immediately after entry to delay the time at which the atmospheric gas is vented into the probe.

This thermal control approach was evaluated for three different probe configurations. These configurations, and the atmospheres for which they were evaluated, are as follows:

- 1) Baseline Configuration - Heat shield jettisoned after entry, parachute deployed during descent. Evaluated in nominal model atmospheres;
- 2) Alternate Configuration - Heat shield remains on probe after entry; no parachute phase. Evaluated in nominal model atmospheres;
- 3) Final Configuration - Heat shield remains on probe after entry; no parachute phase. Evaluated in the nominal and worst-case atmospheres.

The thermal control analyses for these three configurations during descent are discussed in detail in Appendix C.

#### Mission Times and Atmospheric Descent Profiles

The missions that were specifically considered in this study are the following:

- 1) Saturn direct, 1979 launch, 3.4 years to Saturn;
- 2) Saturn-Uranus, 1980 launch, 3.1 years to Saturn;
- 3) Saturn swingby, 1980 launch, 6.9 years to Uranus.

These long cruise times highlight the need for a passive thermal control scheme that will reliably maintain probe temperatures within their specified limits. The time required for the probe to coast to Saturn is 35.7 days; the coast time to Uranus is 20.7 days. Table 4.6-3 lists the preentry activation times and atmospheric descent times for the three configurations that were evaluated in this study. Figures 4.6-1 thru 4.6-4 show the atmospheric temperature and pressure profiles during descent for the three probe configurations.

Table 4.6-3 Preentry and Descent Times for Baseline, Alternate, and Final Probe Configurations

Mission Phase	Time, minutes		
	Baseline Configuration	Alternate Configuration	Final Configuration
Preentry			
Saturn Early Arrival	10.0	4.4	6.6
Saturn Late Arrival	18.8	23.9	14.3
Uranus Early Arrival	10.0	4.4	6.6
Uranus Late Arrival	68.0	73.1	69.1
Atmospheric Descent*			
Saturn Nominal	43.4	48.2	41.4
Saturn Cool			26.4
Saturn Warm			61.3
Uranus Nominal	43.4	48.2	45.3
Uranus Cool			28.4
Uranus Warm			71.9

\* Atmospheric descent time is defined as the interval from instrument deployment (chute release time for the baseline configuration) to the end of mission (probe at  $10^6$  N/m<sup>2</sup> 10 bar).

Equipment Temperature Limits

Table 4.6-4 shows the temperature limits for probe equipment during operation (descent) and storage (cruise). Note that the temperature limits of the battery during cruise [253°K to 303°K (-4°F to 86°F)] define the allowable range of temperatures for the probe during the cruise and coast portions of the mission. A midrange temperature of 277°K (40°F) was chosen as the steady-state design point for the thermal control system during cruise. If cruise temperatures stabilize outside this range on the hot side, the charge on the battery plates will be degraded, and the storage capacity will fall off; for temperatures below the lower limit, the electrolyte will become slushy or frozen, making it



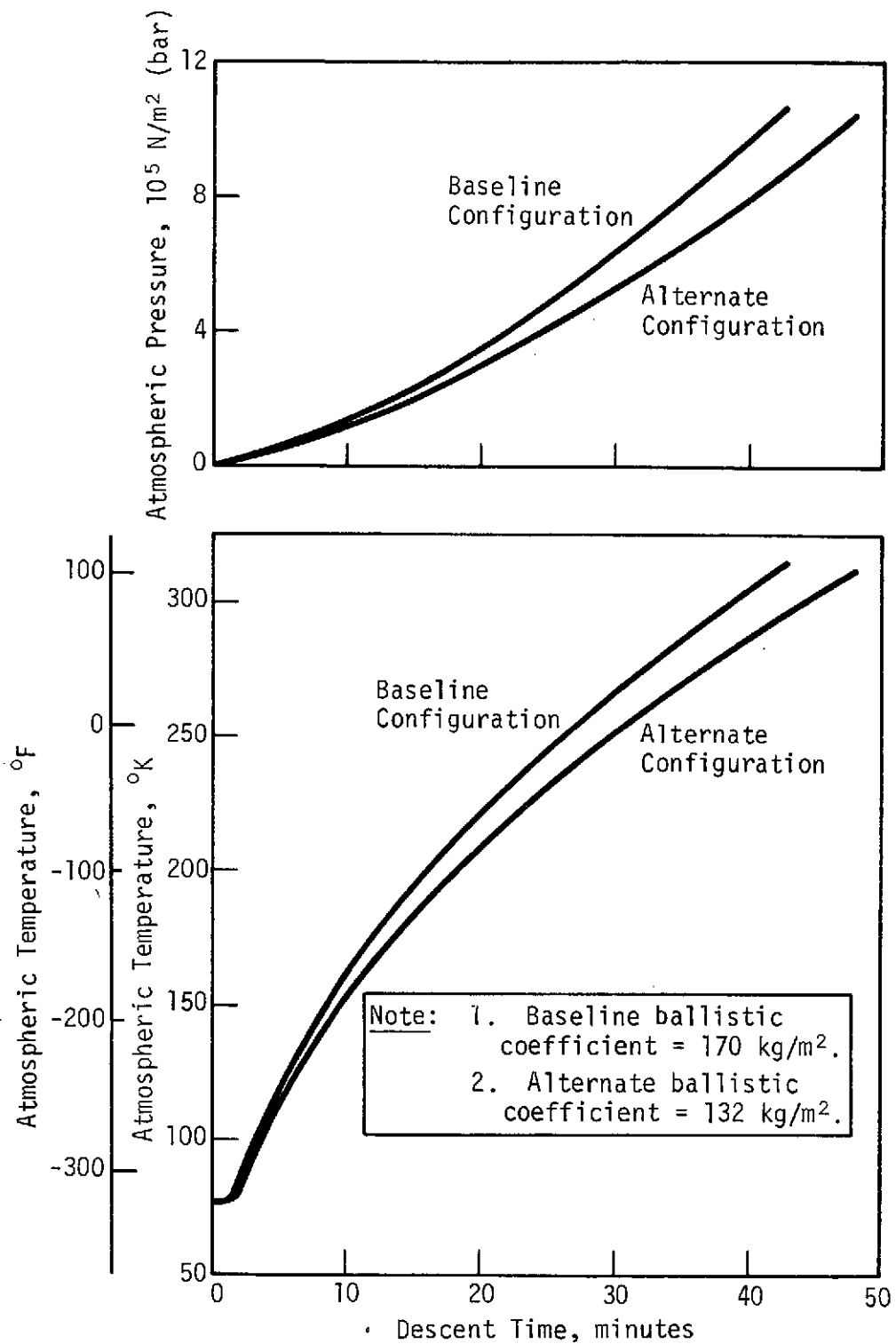


Figure 4.6-1 Descent Profiles at Saturn for Nominal Atmosphere, Baseline and Alternate Probe Configurations

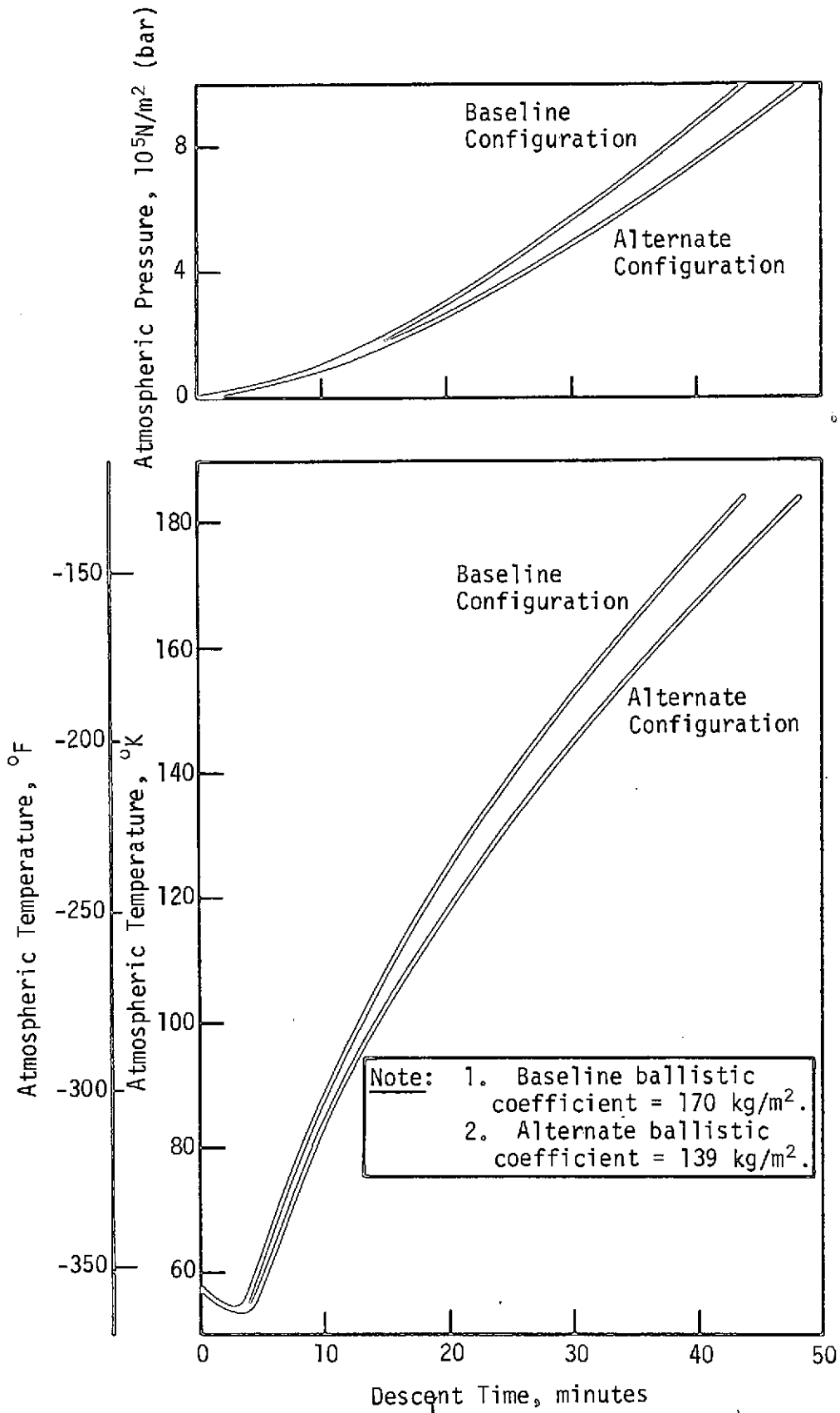


Figure 4.6-2 Descent Profiles at Uranus for Nominal Atmosphere, Baseline and Alternate Probe Configurations

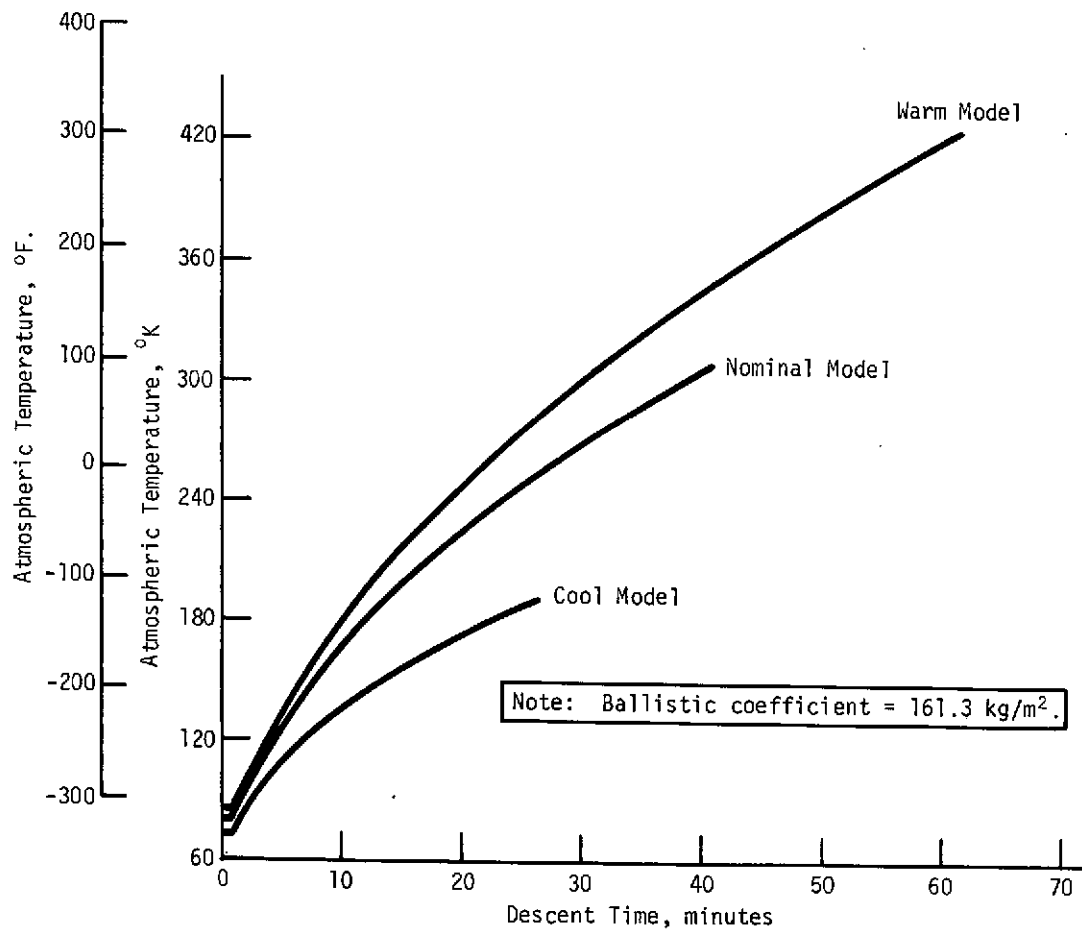
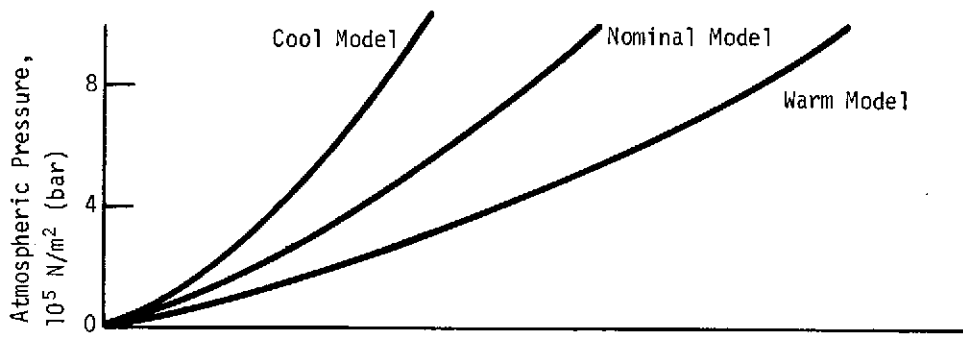


Figure 4.6-3 Descent Profiles at Saturn for Nominal and Worst-Case Atmosphere, Final Probe Configuration

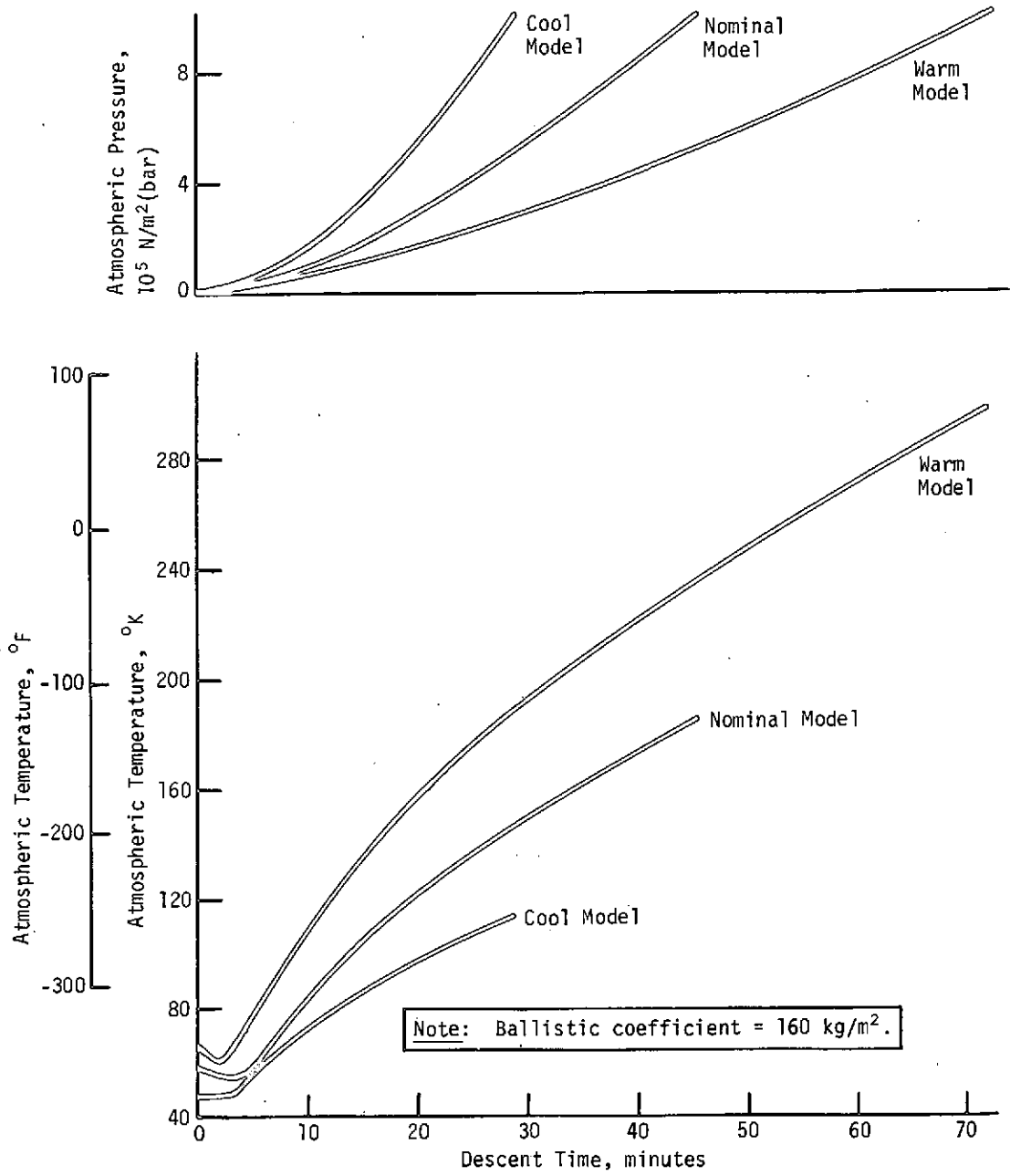


Figure 4.6-4 Descent Profiles at Uranus for Nominal and Worst-Case Atmospheres, Final Probe Configuration

Table 4.6-4 Temperature Limits, Saturn/Uranus Common Probe

	Operating Limits, °K	Nonoperating Limits, °K
<u>Internal Components</u>		
Temperature Electronics	233 to 363	233 to 363
Pressure Gauges & Electronics	253 to 353	253 to 353
Nephelometer	243 to 339	243 to 339
Accelerometer	233 to 363	233 to 363
Neutral Mass Spectrometer	255 to 339	233 to 339
Battery	283 to 322	253 to 303
Transmitter	255 to 348	228 to 339
Electrical Harness Assembly	255 to 339	228 to 339
RF Cabling	255 to 552	228 to 339
DTU	255 to 343	228 to 367
g Switch	233 to 367	233 to 367
Engineering Instrumentation	255 to 339	228 to 367
Power Control Unit	255 to 339	228 to 367
Nonexplosive Pin Pullers	200 to 367	200 to 367
<u>External Components</u>		
Forebody Heat Shield		228 to 367
Afterbody Heat Shield		172 to 367
Antenna Radome		228 to 367
Temperature Sensor	40 to 450	40 to 450
Antenna	200 to 388	200 to 388
Nephelometer Windows (2)	40 to 450*	40 to 450

\* Windows must be heated 10 °K above the local atmosphere temperature during descent.

impossible to activate the battery. Once the battery is activated (just before the probe is released from the spacecraft) it must be warmed to above 283°K (50°F) to provide the required conditions for discharge. This heating occurs slowly during the 20- or 35-day coast to the target planet.

The lower temperature limit of the antenna radome was set at 228°K (-50°F) because we were concerned that the radome might be

structurally degraded during the long cold soak on a cruise to Saturn or Uranus. The radome is a composite structure made by bonding and mechanically fastening Teflon to a fiberglass shell. During the cruise phase, the temperature of the radome tends to drop because the radome is thermally uncoupled from the probe; this could result in cracking and spalling of the Teflon from differential expansion if the radome temperature were allowed to reach equilibrium in an uninsulated condition.

#### Thermal Control Analytical Results

*Coast Phase* - Our analysis has shown that 10 watts of radioisotope heater power will be required to warm the probe to 297°K (75°F) for entry at Saturn and to 294.8°K (71°F) for entry at Uranus. This power offsets losses through the probe's multilayer insulation penetrations. Such losses include:

- 1) Losses through the fabrication ties, seams, and joints of the insulation blanket;
- 2) Losses through the electrical umbilical, which was severed in separating the probe from the spacecraft;
- 3) Losses at exposed support points that had been used to attach the probe to the spacecraft.

In our analysis, we set the effective emittance of the multilayer insulation at 0.01. This probe insulation also encloses the radome, which should be maintained above 228°K (-50°F) to ensure the structural integrity of the Teflon-coated fiberglass heat shield.

The temperature rise of the probe after its release from the spacecraft is shown in Figure 4.6-5.

*Cruise Phase* - The objective of the cruise thermal analysis was to verify that the thermal control subsystem could maintain the probe at a nominal temperature of 277.6°K (40°F) during this phase of the mission. As part of this analysis we made a parametric study to investigate the sensitivity of the steady-state design point to environmental factors. Figure 4.6-6 is a sketch of the probe stowed on the Pioneer spacecraft during the cruise phase. The probe is shut down while on the spacecraft but 10 watts is constantly being dissipated within the probe by the radioisotope heater units (RHUs). These units heat the probe to the desired entry temperature of 297°K (75°F) during the coast phase. The thermal control subsystem rejects 4.2 watts of this RHU power to space during the cruise to maintain the probe temperature at

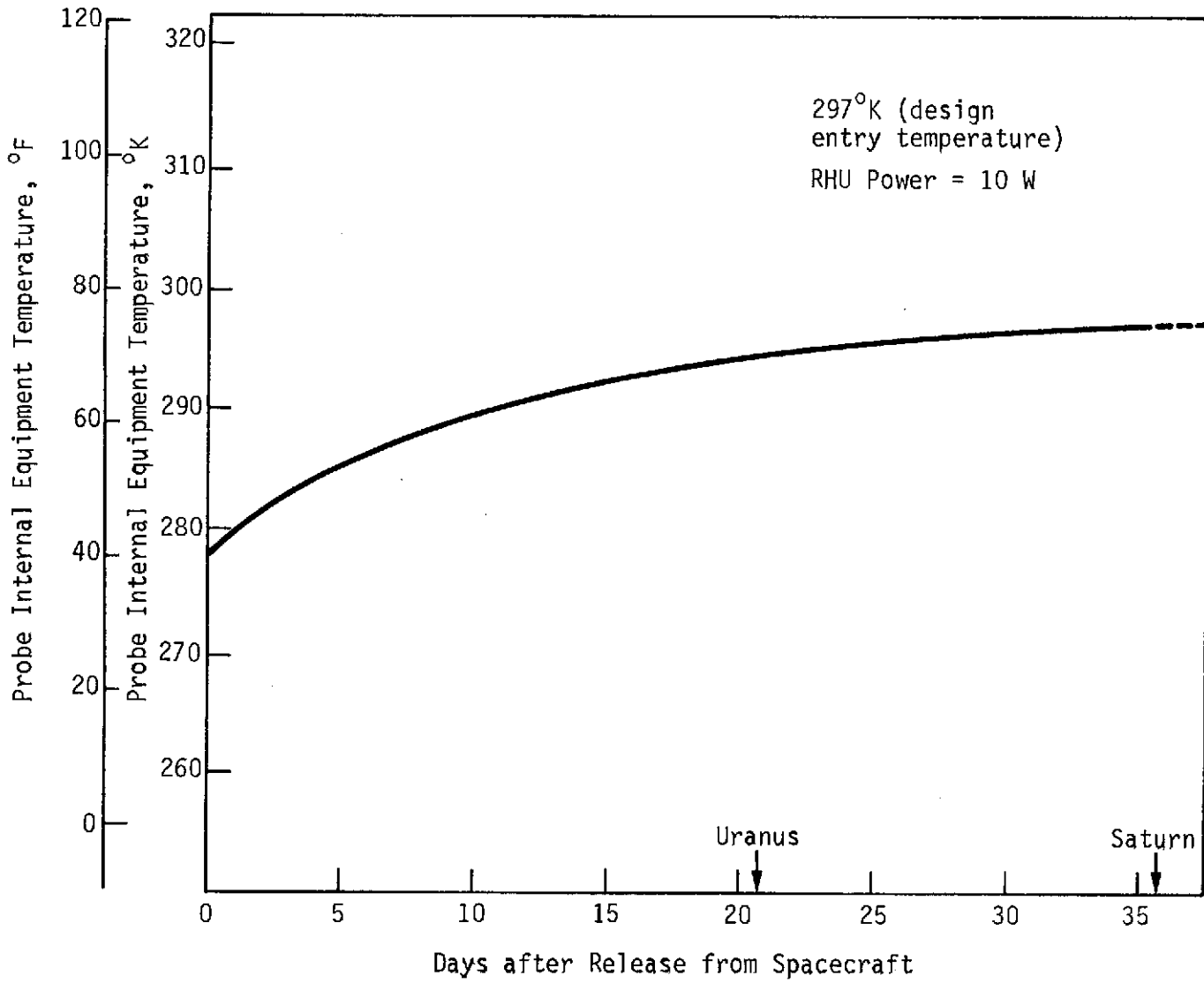


Figure 4.6-5 Probe Temperature Rise During Coast

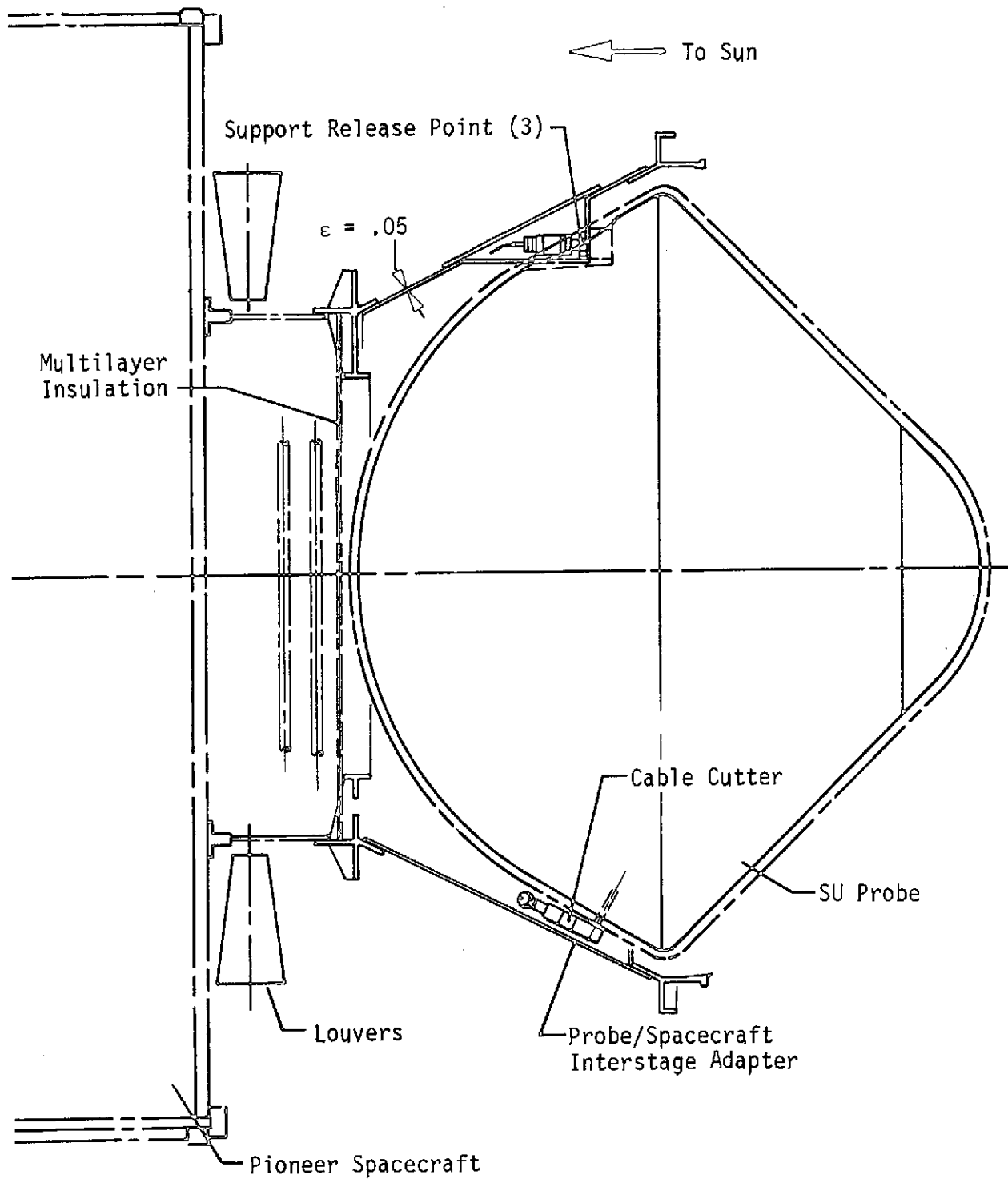


Figure 4.6-6 Probe/Spacecraft Cruise Configuration, Final Probe Configuration



277.6°K (49°F). The heat-transfer path for rejecting this energy is through the three probe support points to the spacecraft/probe interstage adapter cone; a small radiator fin approximately 6.5 cm<sup>2</sup> at each support point then radiates the energy to space.

Figure 4.6-7 shows the sensitivity of the probe temperatures to the heat transferred through the probe support points. Note the effect of having the spacecraft louver system operate between 255.4°K (0°F) and 305.4°K (90°F).

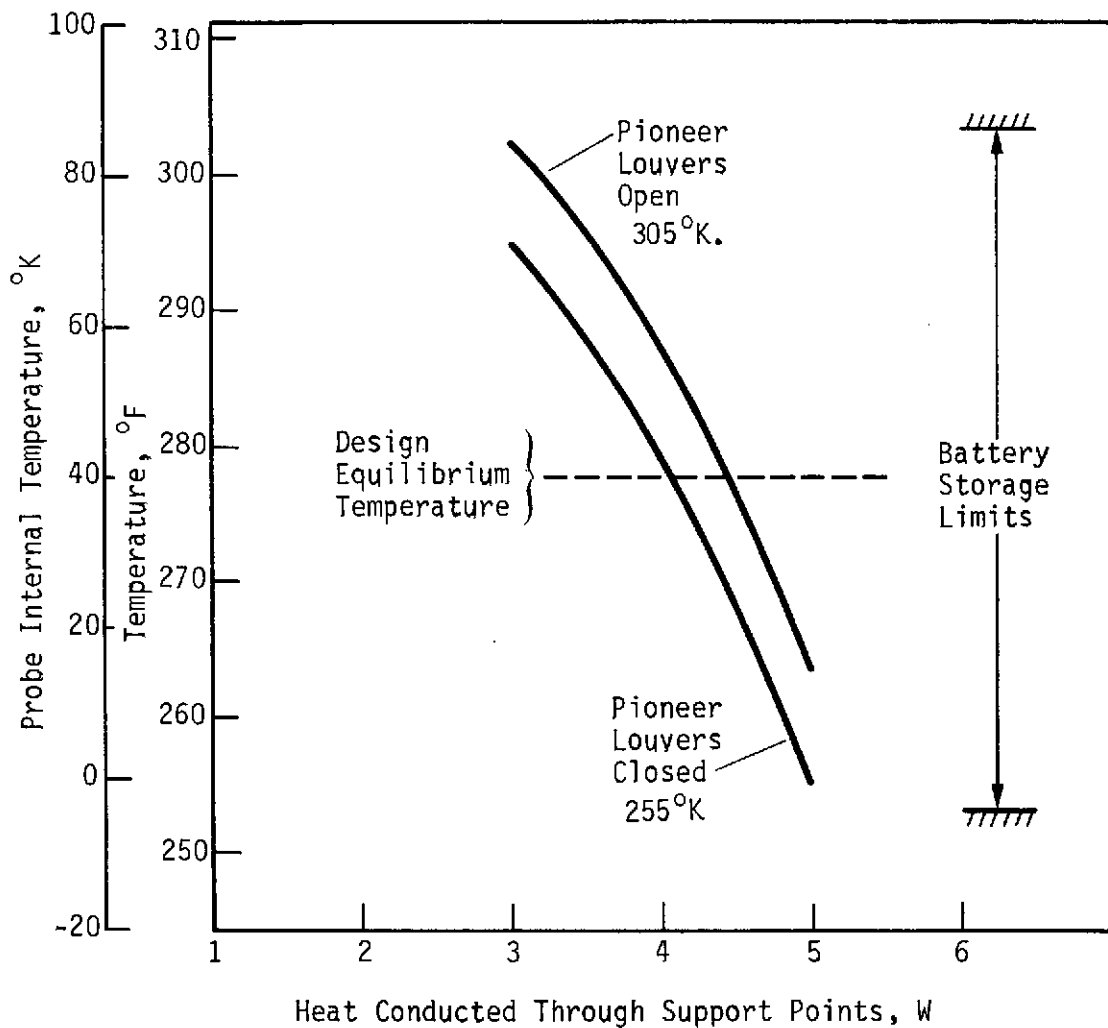


Figure 4.6-7 Probe Internal Temperature Versus Heat Conducted Through Support Points During Cruise

*Atmospheric Descent* - The thermal control approach for the atmospheric descent portion of the mission utilizes the thermal inertia of the probe and a slightly elevated equilibrium temperature at entry to enable the probe to survive cold-descent environments to  $10^6$  N/m<sup>2</sup> (10 bar) in the nominal atmospheres. A low-density foam insulation was required inside the probe to isolate the payload from the cold outer structure. All penetrations through this insulation were designed to minimize conduction losses. The effectiveness of the foam insulation is seriously degraded by the incoming atmospheric gas (a mixture of hydrogen and helium), because the thermal conductivity of the insulation is essentially the same as that of the permeating gas (see Appendix C). This degradation can be slowed by filling the probe with a low-conductivity gas like argon or neon to delay the entry of atmospheric gas into the probe.

Table 4.6-5 summarizes the predicted equipment operating temperatures during descent for the baseline and alternate probe configurations. The entry temperature for these cases was 297°K (75°F). The maximum and minimum temperatures shown in the table were predicted by considering early and late probe arrivals at the planets; these arrival times were given in Table 4.6-3. The descent temperatures for the final probe configuration are shown in Figures 4.6-8, 4.6-9, and 4.6-10 for the cool, nominal, and warm atmospheres, respectively. These data were generated using the single-data-transmission power profile. The thermal control features considered in these analyses were 2.5 cm of internal foam insulation, 1 cm of foam insulation around the battery, and an argon gas system sized to prevent atmospheric gas from entering into the probe until the atmospheric pressure reached  $2.5 \times 10^5$  N/m<sup>2</sup> (2.5 bar). The entry temperature for all analyses was 297°K (75°F).

Arrival uncertainties were used to generate the maximum or minimum probe temperatures, depending on the type of atmosphere encountered. Late arrivals (maximum probe preentry heating) were considered with warm atmospheres, and early arrivals (minimum probe preentry heating) were considered with the nominal and cold atmospheres. The descent in the nominal atmospheres resulted in lower probe temperatures because the descent times were long enough to significantly cool the probe. Figure 4.6-11 shows the temperature profiles of the battery, transmitter, and lumped equipment during descent with dual data transmission at Saturn. Note that the final probe configuration has some warmside thermal margin for the worst-case (Saturn warm atmosphere) encounter; at EOM the equipment is still 23°K (41.3°F) below its upper temperature limit and the transmitter is 18°K (32.4°F) below its upper limit.

Table 4.6-5 Predicted Equipment Operating Temperatures During Descent for Baseline and Alternate Probe Configurations in Nominal Atmospheres

Component	Allowable Temperature Range, °K	Temperature for Baseline Probe, °K*		Temperature for Alternate Probe, °K†	
		Saturn	Uranus	Saturn	Uranus
Battery	283 to 322	296 to 298	293 to 300	298 to 303	297 to 307
Transmitter	255 to 348	301 to 323	302 to 326	299 to 308	289 to 312
Internal Equipment	255 to 339	292 to 299	279 to 303	294 to 301	281 to 304
<p>* Baseline probe: neon gas system, 2 cm internal foam insulation, 1 cm battery foam insulation.</p> <p>† Alternate probe: argon gas system, 2.5 cm foam insulation, 1 cm battery foam insulation.</p>					

Entry Temperature = 297°K (75°F)

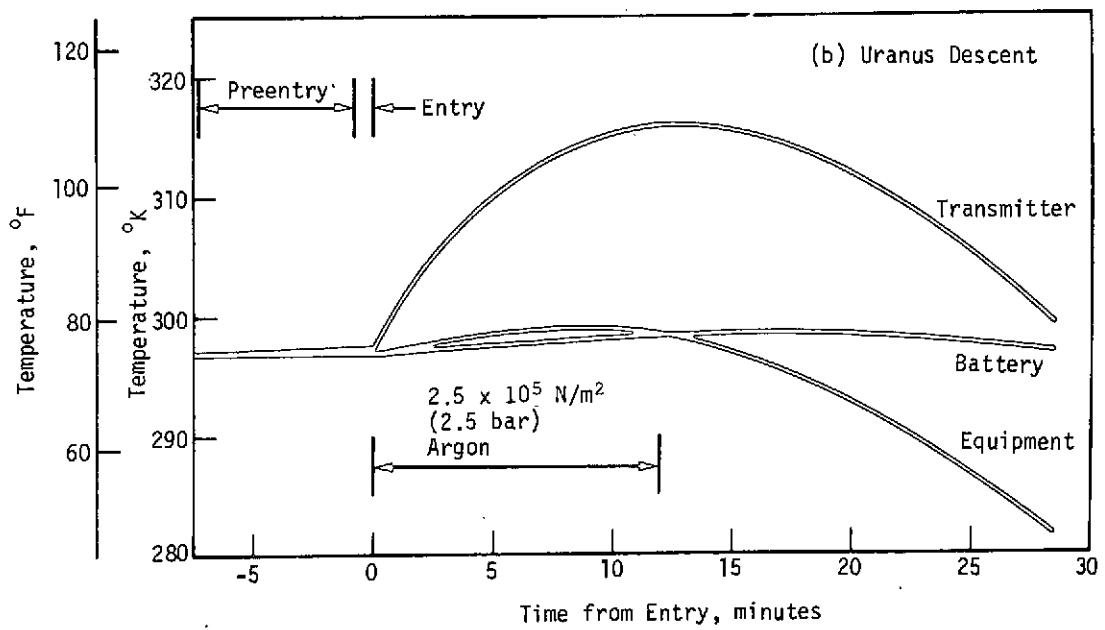
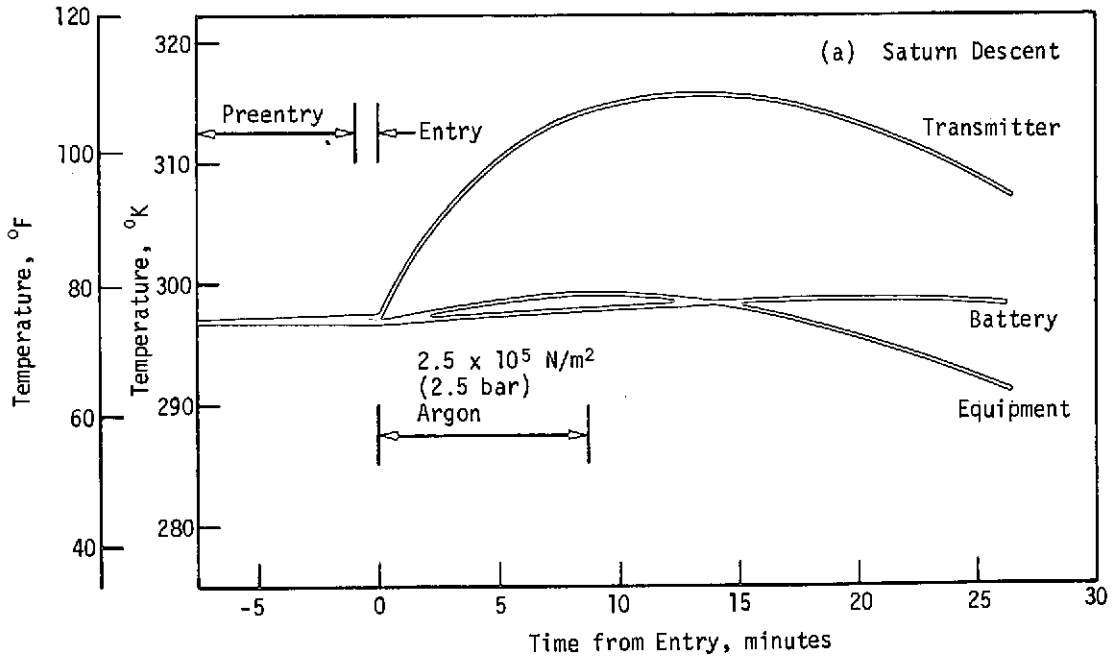


Figure 4.6-8 Component Temperatures During Descent in the Saturn and Uranus Cool Atmospheres, Final Probe Configuration

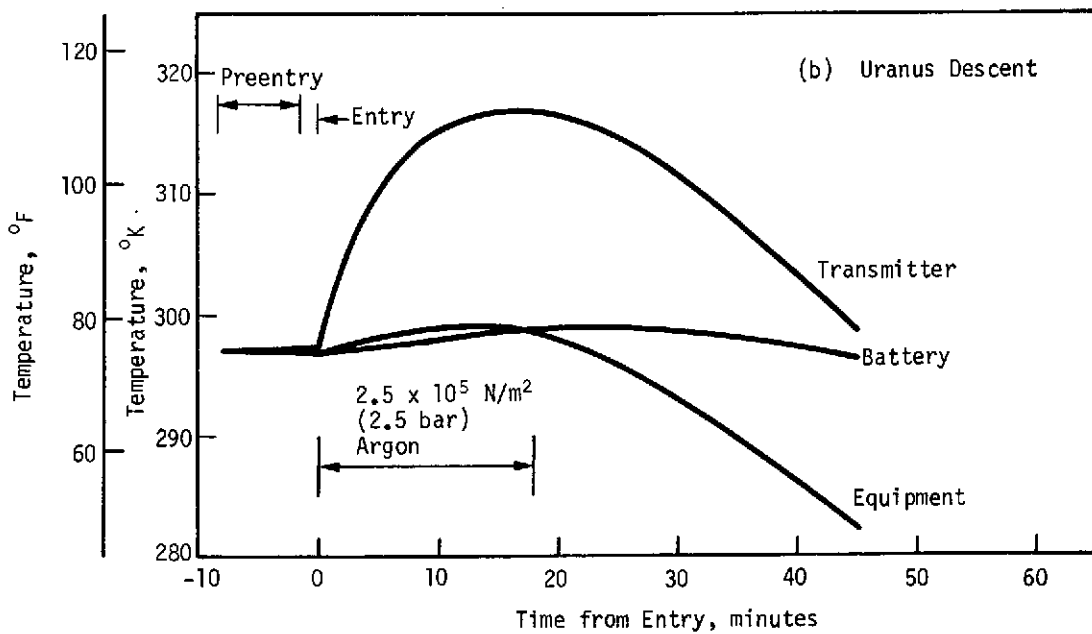
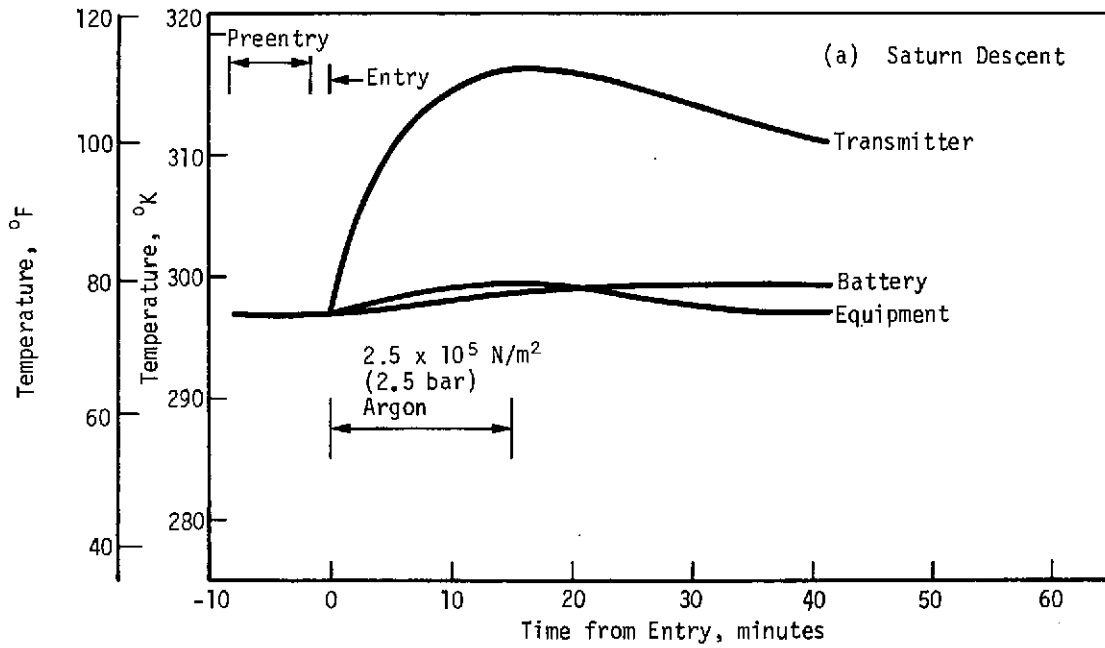


Figure 4.6-9 Component Temperatures During Descent in the Saturn and Uranus Nominal Atmospheres, Final Probe Configuration

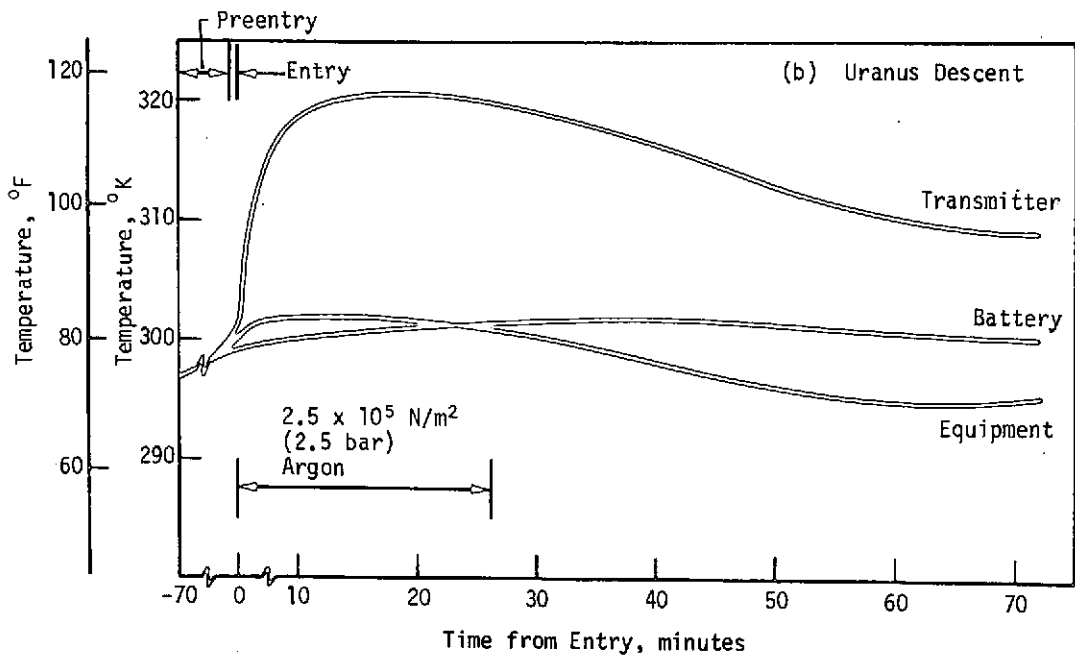
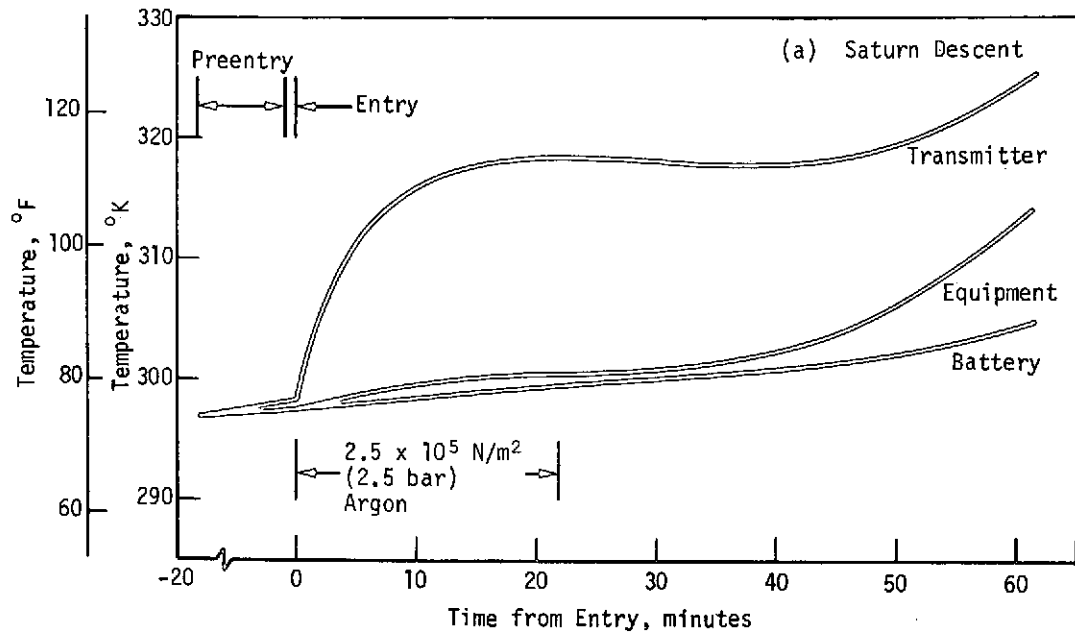


Figure 4.6-10 Component Temperatures During Descent in the Saturn and Uranus Warm Atmospheres, Final Probe Configuration

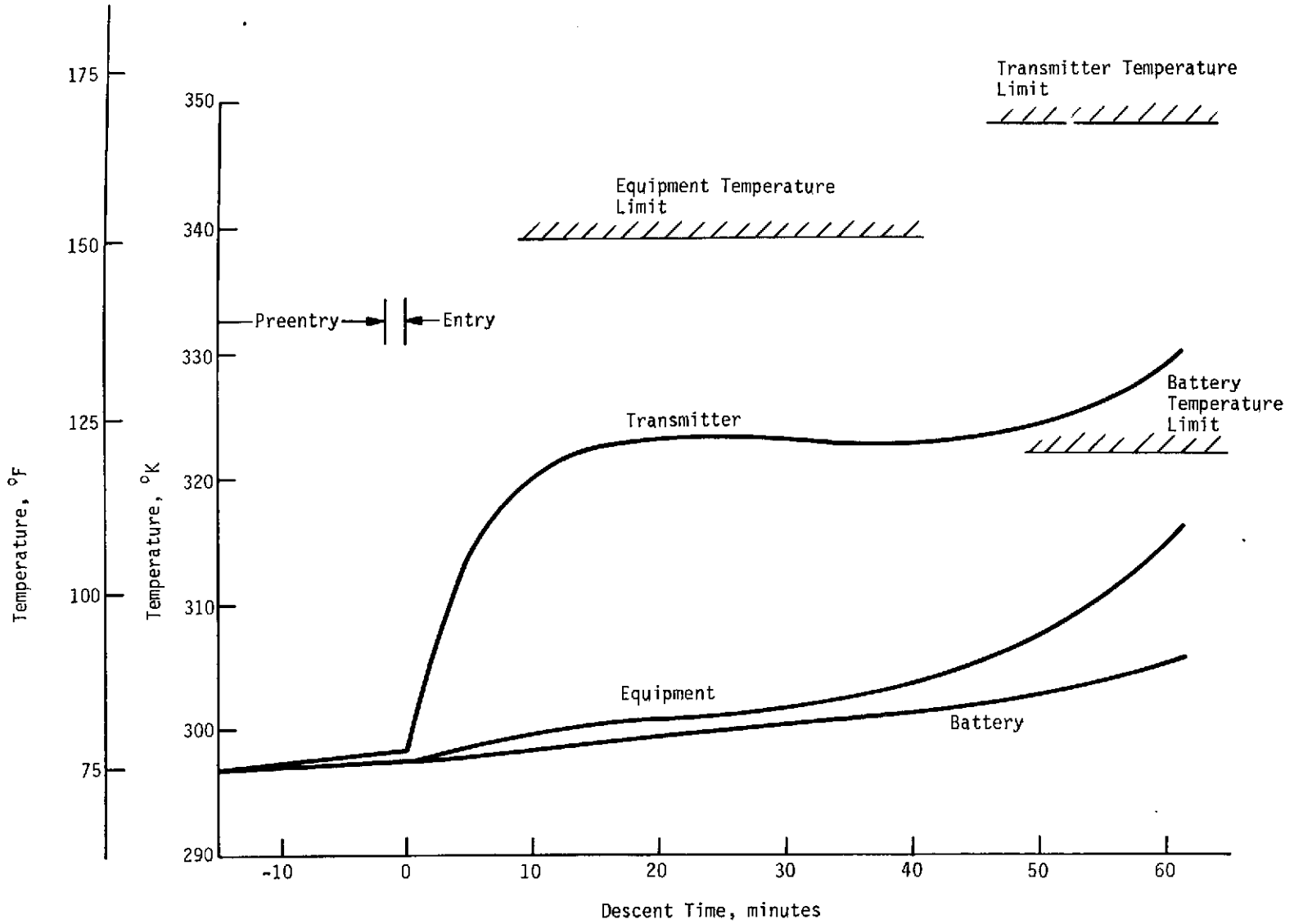


Figure 4.6-11 Component Temperatures During Descent in the Saturn Warm Atmosphere, Dual Data Transmission, Final Probe Configuration

*Nephelometer Window Heater* - In evaluating the requirements for the thermal control subsystem we also calculated the amount of power required to heat the nephelometer windows  $10^{\circ}\text{K}$  above the local atmospheric temperature during planetary descent. The Saturn warm atmosphere represents the worst-case environment. Maximum heater power is required to maintain this  $10^{\circ}\text{K}$  temperature difference at the end of the mission. At this point, the atmospheric temperature is  $424^{\circ}\text{K}$  ( $304^{\circ}\text{F}$ ). Our analysis showed that the conduction losses in the metallic tube holding the window govern the required heater power. For the nephelometer in the final probe configuration, a power level of 5.0 watts will satisfy the delta temperature requirements. See Appendix C for further details.

#### 4.6.2 Baseline Configuration Definition

The design of the structural and mechanical subsystems for the SU baseline probe is based on a spacecraft-deflection mode for the trajectory deflection maneuver. The probe uses an aeroshell/heat shield structure to withstand the high heating rates from planetary entry and to provide an entry ballistic coefficient that satisfies science mission requirements. The aeroshell structure and the heat shield are jettisoned after entry, and before beginning the atmospheric descent phase. This approach rids the descent probe of the heat shield and its absorbed heat load, and prevents the apertures of the mass spectrometer from being contaminated by elements that originate from the heat shield ablation. The descent probe is separated from the aeroshell and base cover after entry by means of a separation parachute. It then descends ballistically through the planetary atmosphere to accomplish the science objectives.

The entire probe is designed to withstand the entry loads encountered at Saturn and Uranus. For the selected missions, the entry heating and structural loads are most severe for the Saturn entry. The structural and mechanical design for the common probe is described in the following paragraphs.

##### 4.6.2.1 Configuration and General Arrangement

The common SU probe is a dual configuration that uses one configuration for the cruise, coast, and entry phases of flight and a second configuration for the descent into the planetary atmospheres. (See Figure 4.6-12). The weight breakdown for the probe before entry and the weights at various stages during entry and descent are shown on Table 4.6-6. The descent probe contains all the scientific instrumentation plus the supporting electrical and electronic components necessary to complete the science mission. Probe equipment required prior to entry, but not during descent,



Table 4.6-6 Baseline Configuration Weight Breakdown

	Weight	
	kg	lb
<u>Science</u>		
Temperature Gauge	0.318	0.70
Pressure Transducer	0.454	1.00
Accelerometer	1.134	2.50
Neutral Mass Spectrometer Analyzer	6.350	14.00
Nephelometer	0.499	1.10
	<u>8.755</u>	<u>19.30</u>
<u>Power &amp; Power Conditioning</u>		
Power Control Unit	2.835	6.25
Entry Batteries	5.625	12.40
Remote Activation Reservoir	0.816	1.80
	<u>9.276</u>	<u>20.45</u>
<u>Cabling</u>		
Inner Probe	2.676	5.90
<u>Data Handling</u>		
Digital Telemetry Unit	1.814	4.00
<u>Communications</u>		
Probe Antenna	0.454	1.00
RF Transmitter	0.635	1.40
Power Amplifier	0.907	2.00
	<u>1.996</u>	<u>4.40</u>
<u>Pyrotechnics Subsystem</u>		
Pyro Squibs	0.272	0.60
<u>Structures &amp; Heat Shields</u>		
Descent Probe Structures	7.262	16.01
Equipment Support Deck	3.084	6.80
Radome/Heat Shield (SLA-220)	0.839	1.85
Aeroshell	2.558	5.64
Forward Heat Shield 6.90 kg (15.20 lb) ablated during entry)	13.222	29.15
Aft Heat Shield ESA 3560 at 1.37 kg/m <sup>2</sup> (0.28 lb/ft <sup>2</sup> )	0.562	1.24
Base Cover	2.186	4.82
	<u>29.713</u>	<u>65.51</u>
<u>Mechanisms</u>		
Pin Puller (parachute/radome release)	0.499	1.10
Vent Valve	0.699	1.54
Separation Parachute Diameter = 2.50 m (8.6 ft)	3.148	6.94
Pin Puller (aeroshell release)	0.499	1.10
	<u>4.845</u>	<u>10.68</u>
<u>Thermal</u>		
External Insulation Blanket (forward heat shield)	0.671	1.48
External Insulation Blanket (base cover)		
Probe Hull Insulation (internal)	0.680	1.50
Isotope Heaters	1.134	2.50
Environmental Tank & Neon	0.544	1.20
	<u>3.029</u>	<u>6.68</u>
<u>TOTAL</u>	62.376	137.52
15% Contingency	9.357	20.63
	<u>71.733</u>	<u>158.15</u>

ORIGINAL PAGE IS  
OF POOR QUALITY

Table 4.6-6 Concluded

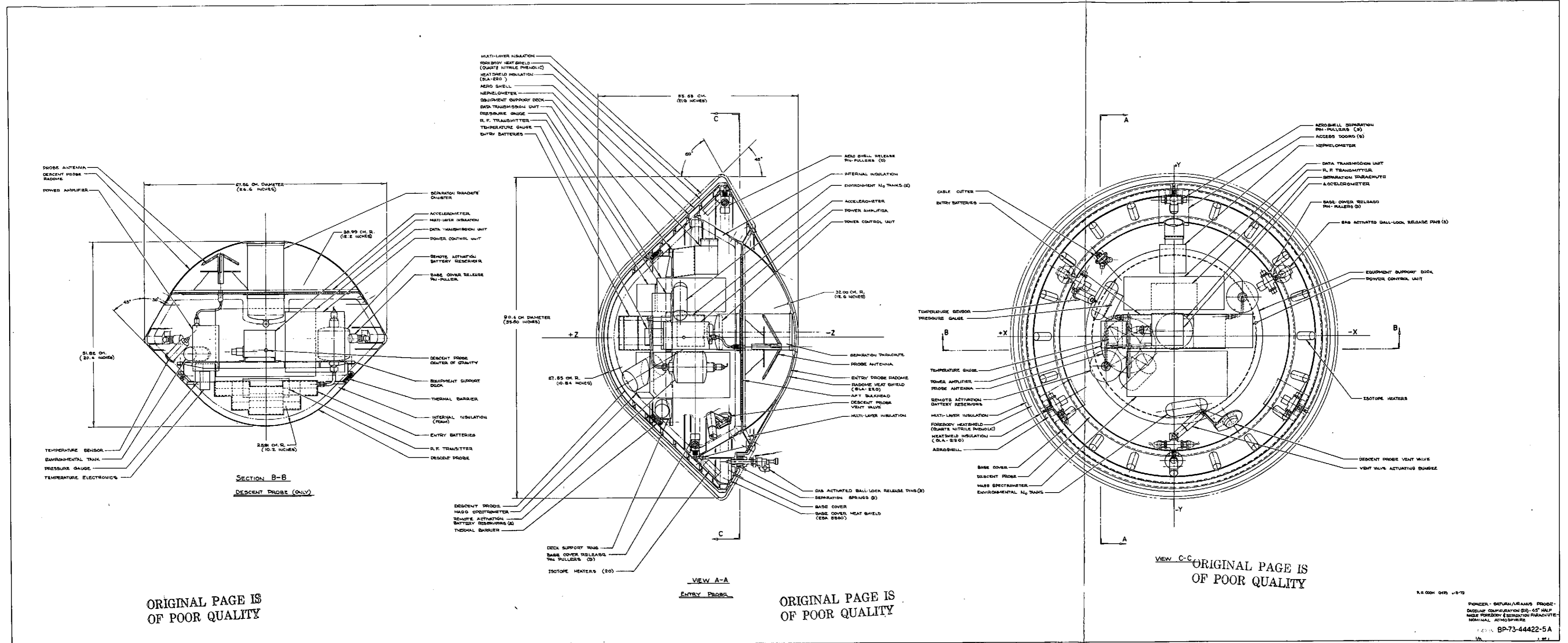
	Weight	
	kg	lb
<u>Postentry Weight</u>		
Forward Heat Shield (ablated)	-6.895	-15.20
Aft Heat Shield		
Forward Insulation Blanket	<u>-0.671</u>	<u>- 1.48</u>
Aft Insulation Blanket	-7.566	-16.68
15% Contingency	<u>-1.135</u>	<u>- 2.50</u>
Subtotal	-8.701	-19.18
TOTAL		
71.733 - 8.701 = 63.032 kg		
(158.15 - 19.18 = 138.97 lb)		
<u>Weight on Parachute at Separation</u>		
Aeroshell	-2.558	- 5.64
Forward Heat Shield (not ablated)	<u>-6.328</u>	<u>-13.95</u>
	-8.886	-19.59
15% Contingency	<u>-1.333</u>	<u>- 2.94</u>
Subtotal	-10.219	-22.53
TOTAL		
63.032 - 10.219 = 52.813 kg		
(138.97 - 22.53 = 116.44 lb)		
<u>Descent Weight</u>		
Radome	-0.517	-1.14
Radome Ablator	-0.322	-0.71
Isotope Heaters	-1.157	-2.55
Separation Chute, Bridel, Swivel	-1.175	-2.59
Aft Heat Shield	-0.562	-1.24
Base Cover	-2.127	-4.69
Pin Pullers	<u>-0.499</u>	<u>-1.10</u>
	-6.359	-14.02
15% Contingency	<u>-0.954</u>	<u>-2.10</u>
Subtotal	-7.313	-16.12
TOTAL		
52.813 - 7.313 = 45.500 kg		
(116.44 - 16.12 = 100.32 lb)		

is located within the aeroshell/heat shield structural assembly. The descent probe has a diameter of 67.6 cm (26.60 in.), weighs 45.6 kg (100.32 lbm). The equipment within the descent probe is protected from the hostile cold environment after entry by a layer of low-density foam insulation. The insulation is bonded to the interior of the descent probe's shell structure. The equipment support deck is thermally isolated from the outer structure by a nonmetallic thermal barrier ring located between the deck support ring and the outer structure.

The mass spectrometer inlet is exposed to the incoming uncontaminated atmosphere approximately 0.61 rad ( $35^{\circ}$ ) off the stagnation point. The temperature sensor, located on the outer portion of the forebody, is extended from the shell after separation. The pressure port for the pressure instrument is at the stagnation point and is continuously open. The descent antenna and a parachute system for separating the descent probe from the aeroshell are located on the aft bulkhead of the descent probe and are protected by the descent probe radome.

The entry probe consists of descent probe that is contained and encapsulated in the aeroshell/heat shield, base-cover entry structure. The forebody of the entry probe consists of a conical shape with a  $0.79$  rad ( $45^{\circ}$ ) half angle, capped with a spherical segment that has a nose radius-to-cone base radius ( $R_N/R_B$ ) of 0.62. The base cover of the entry probe is a truncated cone with a spherical radome. The entry probe has a maximum diameter of 90.40 cm (35.6 in.) and a weight of 71.8 kg (158.15 lbm). The ballistic coefficients of the entry probe is  $102 \text{ kg/m}^2$  ( $0.65 \text{ slug/ft}^2$ ) and the descent probe ballistic coefficient is  $170 \text{ kg/m}^2$  ( $1.083 \text{ slug/ft}^2$ ) meeting the mission science requirements.

A quartz nitrile phenolic forebody heat shield with an SLA-220 heat shield insulator protects the aeroshell and the descent probe during planetary entry heating. An ESA 3560 ablator protects the after-body structure, and a layer of SLA 220 protects the radome for the entry heating. The entire aeroshell/heat shield is jettisoned by activating pin-pullers and deploying the separation parachute. After a sufficient separation between the aeroshell and the descent probe has been obtained, the descent probe release pin-pullers are activated to jettison the base cover and the parachute from the descent probe (see Figure 4.6-13). Ballistically then the descent probe penetrates the atmosphere to a depth of  $10^6 \text{ N/m}^2$  (10 bar). All parts of the probe except the radome are completely enclosed within a blanket of multilayer high-performance insulation to assist in controlling the temperature of the probe and its components during the cruise and coast phases of flight. Only the probe attachments to the carrier spacecraft penetrate the insulation. In the proposed design, the in-



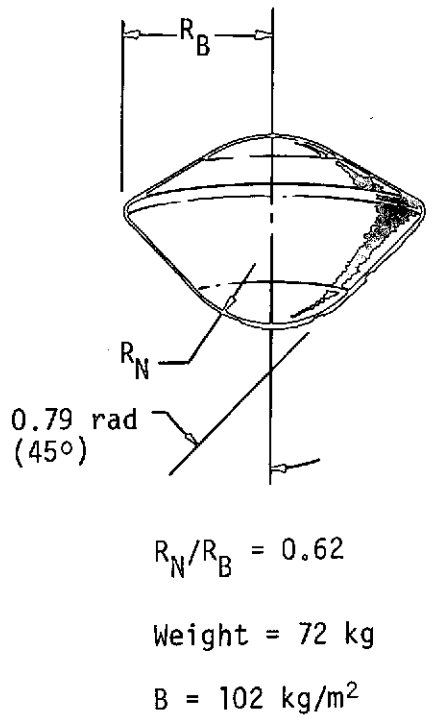
FOLDOUT FRAME

FOLDOUT FRAME

FOLDOUT FRAME

Figure 4.6-12 Pioneer SU Probe Baseline Configuration.

BP-73-44422-5A



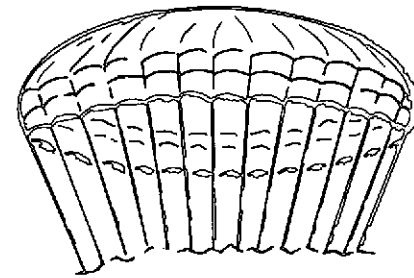
ENTRY PROBE

Disc-Gap-Band Parachute.  
 Diameter = 250 cm

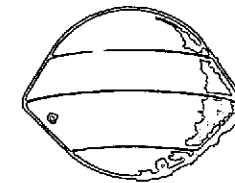
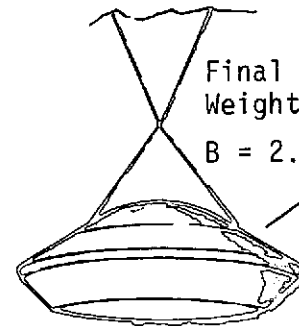
Separation  
 Weight = 52.8 kg  
 $B = 15 \text{ kg/m}^2$

Weight of Spent Aeroshell = 10.2 kg  
 $B = 18 \text{ kg/m}^2$

PROBE SEPARATION



Final Separation  
 Weight = 7.32 kg  
 $B = 2.2 \text{ kg/m}^2$



Weight = 45.6 kg.  
 $B = 170 \text{ kg/m}^2$

DESCENT PROBE

Figure 4.6-13 Baseline Configuration Separation and Deceleration System.

sulation is allowed to remain on the probe through entry, and should ablate away without causing excessive asymmetrical drag.

The aerodynamic stability of the probes is a function of their aerodynamic shape and the c.g. location in relation to the probe's maximum diameter. For the entry probe, the c.g. is 9.6% of the maximum diameter forward of the maximum diameter; for the descent probe, the c.g. is 5.3% forward of the maximum diameter.

#### 4.6.2.2 Structural Subsystem

The structural design of the SU common probe is conventional in most respects. Both the entry and descent probes are vented, obviating the need for making the structures capable of withstanding the external atmospheric pressures with the consequent weight penalties. The structure of the entire probe is designed for entry at Saturn, which represents the most severe environment. For an entry angle of  $-0.52$  rad ( $-30^\circ$ ), the peak deceleration is  $3590$  m/sec<sup>2</sup> (366 g) which allows for a  $0.09$  rad ( $5^\circ$ ) dispersion in the entry angle. The corresponding dynamic pressure on the aeroshell is  $3.59 \times 10^5$  N/m<sup>2</sup> (7,530 psf) at peak load.

The descent probe is designed entirely of aluminum alloy. The structural design of the probe is shown in Figure 4.6-12. Note that the equipment support deck is an integral-rib-stiffened disc that is machined from a solid plate. All components, with minor exceptions, are mounted on or suspended from this deck. The deck, in turn, rests directly on a circumferential deck-support ring that is attached to the conical forebody fairing of the descent probe. This support ring matches with the aeroshell payload ring, transferring the deceleration loads between the descent probe and the aeroshell. A conical forebody, a truncated conical base cover with a flat honeycomb aft bulkhead, and a spherical radome fair the afterbody into a conical spherical aerodynamic shape, completing the descent probe structure.

Even though the descent probe is vented during planetary atmospheric descent, it is temporarily pressurized to a level of approximately  $2.5 \times 10^5$  N/m<sup>2</sup> (2.5 bar) just at entry to delay the entry of planetary gases that degrade the thermal control insulation. The descent probe structure can accept this pressure load with a negligible penalty in weight.

The entry aeroshell configuration is a ring frame-stiffened monocoque structure with a peripheral ring frame and a payload ring frame at approximately the mid-diameter of the conical surface to accept descent probe loads. The structure has been designed of aluminum for this study.

The radome is a 32-cm (12.6 in.) radius spherical segment of nonmetallic laminates that is an integral part of the base cover. After entry the radome is jettisoned with the parachute by three pyrotechnic-activated pin pullers.

#### 4.6.2.3 Mechanisms Subsystem

The primary mechanisms in the probe are the spacecraft/probe support and separation mechanism, the descent probe release mechanism, the parachute deployment system, the parachute and the radome release system, and the probe vent system.

The spacecraft/probe separation mechanism is a three-point-support, gas-actuated, ball-lock pin release system that has concentrically located coil separation springs on each pin to provide a positive separation velocity of .1 m/sec (.3 fps).

The descent-probe release mechanism consists of the separation parachute and three pyro-activated pin-pullers that hold the descent probe to the base cover of the entry probe. Activating the pin-pullers jettisons the base cover and separation parachute from the descent probe.

The separation parachute is approximately in the center of the radome and is deployed by a mortar system. The separation parachute bridle is attached to the base cover radome assembly at the probe/spacecraft interface support fittings.

The aeroshell release mechanism consists of three pyro-activated pin-pullers, on and when activated, the aeroshell is released and the separation force is supplied by the separation parachute. These pin-pullers are mounted on the maximum diameter of the base cover and protrude into the edge member of the aeroshell.

The vent valve system is based on two simple spring loaded poppet valves designed to maintain the probe's internal/external differential pressure to within  $\pm 10^5$  N/m<sup>2</sup> (1 bar). One of these valves vent the excess internal pressure, and the other vents the external pressure. They are located in the aft honeycomb bulkhead and vent to and from the radome cavity which is vented to the atmosphere.

#### 4.6.2.4 Mass Properties

The weight breakdown for the probe is presented in Table 4.6-6. The last portion of the table reduces the weight sequentially, in keeping with the normal mission sequence of events, to indicate the weight at various phases of the mission.

#### 4.6.2.5 Deceleration Subsystem

##### Parachute System

The separation parachute is large enough to ensure prompt separation of the descent probe from the entry probe. The aeroshell/heat shield assembly weighs 10.2 kg (22.5 lbm) after entry and has a ballistic coefficient of approximately 18.0 kg/m<sup>2</sup> (0.116 slug/ft<sup>2</sup>) at Mach 0.7. To assure separation of the descent probe, the parachute was sized to give the descent probe a ballistic coefficient of 15.0 kg/m<sup>2</sup> (0.098 slug/ft<sup>2</sup>). The resulting parachute for a 45.6 kg (100.32 lbm) descent probe has a diameter of 250 cm (8.2 ft) in a disc-gap-band parachute configuration and weighs 3.5 kg (6.74 lbm). The parachute is exposed to dynamic pressures between 1770 and 2362 N/m<sup>2</sup> (36.8 to 49.2 psf) at a Mach level of approximately 0.7, depending on the planet and the atmospheric model at entry. After separation, the descent probe is decelerating at a rate of 19.6 m/sec<sup>2</sup> (2.0 g) relative to the spent aeroshell.

The parachute is deployed by a pyrotechnic mortar that ejects the entire parachute canopy using a sabot. The parachute is jettisoned along with the base cover and the radome by pyrotechnic pin-pullers located between the descent probe and the base cover. The parachute is stowed in fiberglass canisters to make it RF-transparent to the probe antenna. The parachute is designed of Dacron fabric and is maintained at "room" temperature until deployment. It appears that the Dacron material, which has been tested to the temperature of liquid nitrogen (77°K), will suffice in spite of the extreme low temperature. However, sufficient doubt exists to warrant testing the material at some time in the future.

##### Heat Shield

Based on the analyses and tradeoffs discussed in Section 4.3.1.3, the heat shield for the baseline configurations was sized by the entry environment for the Saturn nominal atmosphere.

The primary heat shield consists of 0.794 cm (0.3125 in.) layer of quartz nitrile phenolic bonded to 0.457 cm (0.180 in.) thick honeycomb-reinforced SLA-220, which in turn, is bonded to the probe aeroshell. The heat shield has a constant thickness over the aeroshell.

The heat shield on the aft cover consists of a 0.635 cm (0.25 in.) layer of SLA-220 over the radome and an equally thick layer of ESA-3560 over the remainder of the aft cover.



#### 4.6.2.6 Thermal Control Subsystem (Baseline Configuration)

The thermal control subsystem maintains the temperature within the probe at 278°K (40°F) during the cruise phase by using 10 one watt radioisotope heater units (RHUs). The probe is covered with a multilayer insulation blanket consisting of 21 layers of 1/4-mil, singly-aluminized mylar whose aluminized surfaces face the probe. During the cruise phase, 4.2 watts of excess heater power is conducted from the probe through the three support points to the probe/spacecraft interstage cone. After the probe is released from the spacecraft, this excess energy warms the probe to the required entry temperature at the target planet.

A 2-cm thick layer of low-density foam insulation (NOPCO BX-250, density = 0.034 g/cm<sup>3</sup>), was applied to the internal surfaces of the probe to isolate the payload from the aeroshell, which is rapidly cooled by the atmosphere. The battery is also insulated using 1 cm of this foam to prevent the incoming atmospheric gases from cooling the cells due to free convection.

A neon gas bottle was vented inside the probe immediately after entry to prevent atmospheric gases from entering the probe until reaching an ambient pressure of  $2.5 \times 10^5$  N/m<sup>2</sup> (2.5 bar). The neon gas enhances the performance of the foam because the conductivity of the foam will track the conductivity of the gas filling its structure. The thermal conductivity for neon is an order of magnitude lower than that for the atmospheric mixture of hydrogen and helium.

#### 4.6.3 Alternate Configuration Definition

The structural and mechanical subsystem for the alternate probe uses an aeroshell/heat shield structure to counteract the high heat loads from entry. It provides entry ballistic coefficients compatible with the science requirements for initiation of the atmospheric descent. The aeroshell, base cover, and radome are designed as integral parts of the descent probe. This reduces the total structural weight of the entry probe and eliminates the need for a separation parachute. The forward spherical part of the heat shield is a jettisonable cap that protects the inlet tubes for the mass spectrometer and the pressure sensing aperture. After entry three pyrotechnic thrusters are fired to jettison the nose cap exposing the mass spectrometer inlet to the uncontaminated atmosphere and uncover the aperture pressure of the gauge. The other science instruments, such as the temperature sensor and the nephelometer, are either deployed or uncovered after entry by mechanical systems. The probe, with its scientific sensors exposed, then makes a ballistic descent through the planetary atmosphere to accomplish the science objectives.

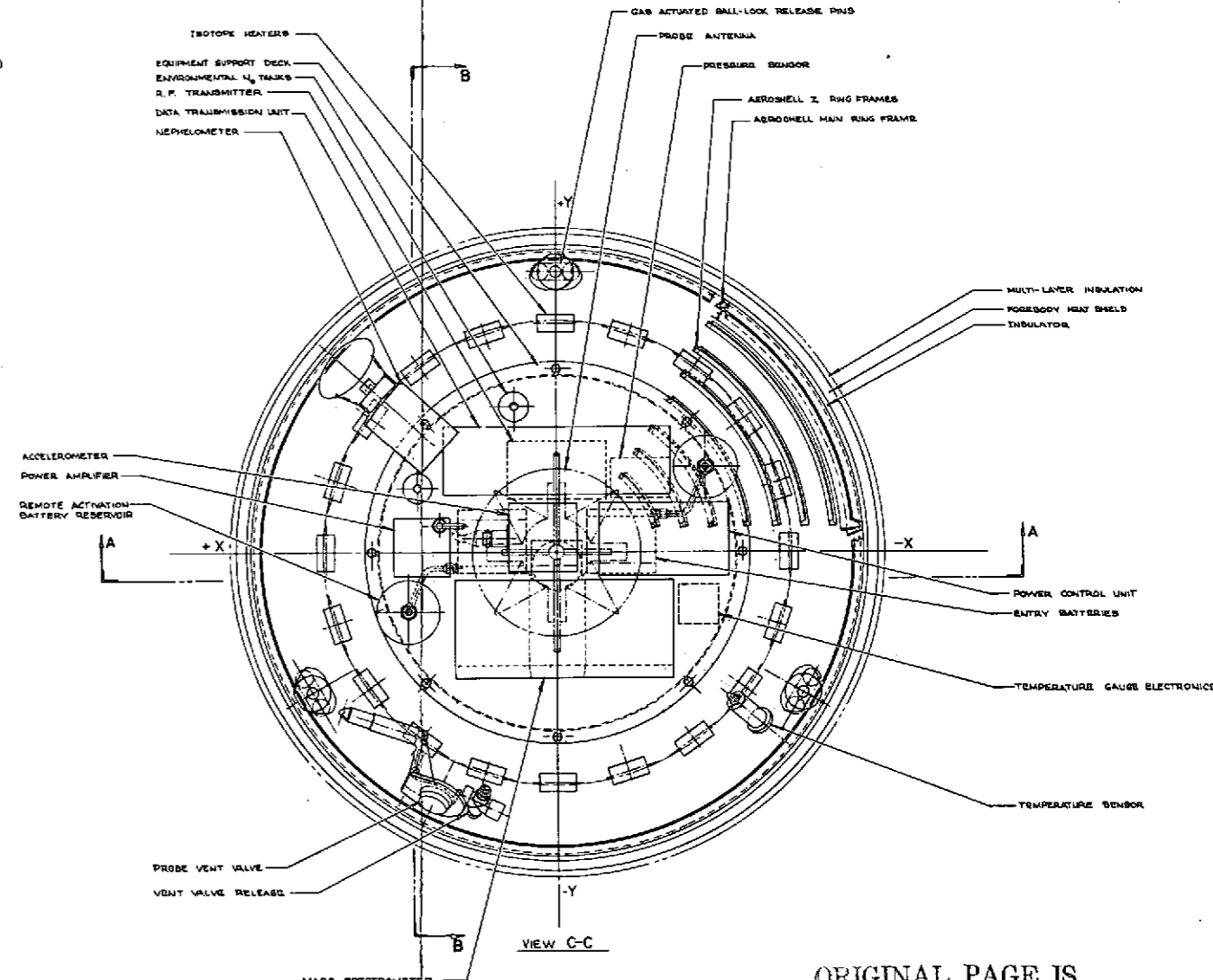
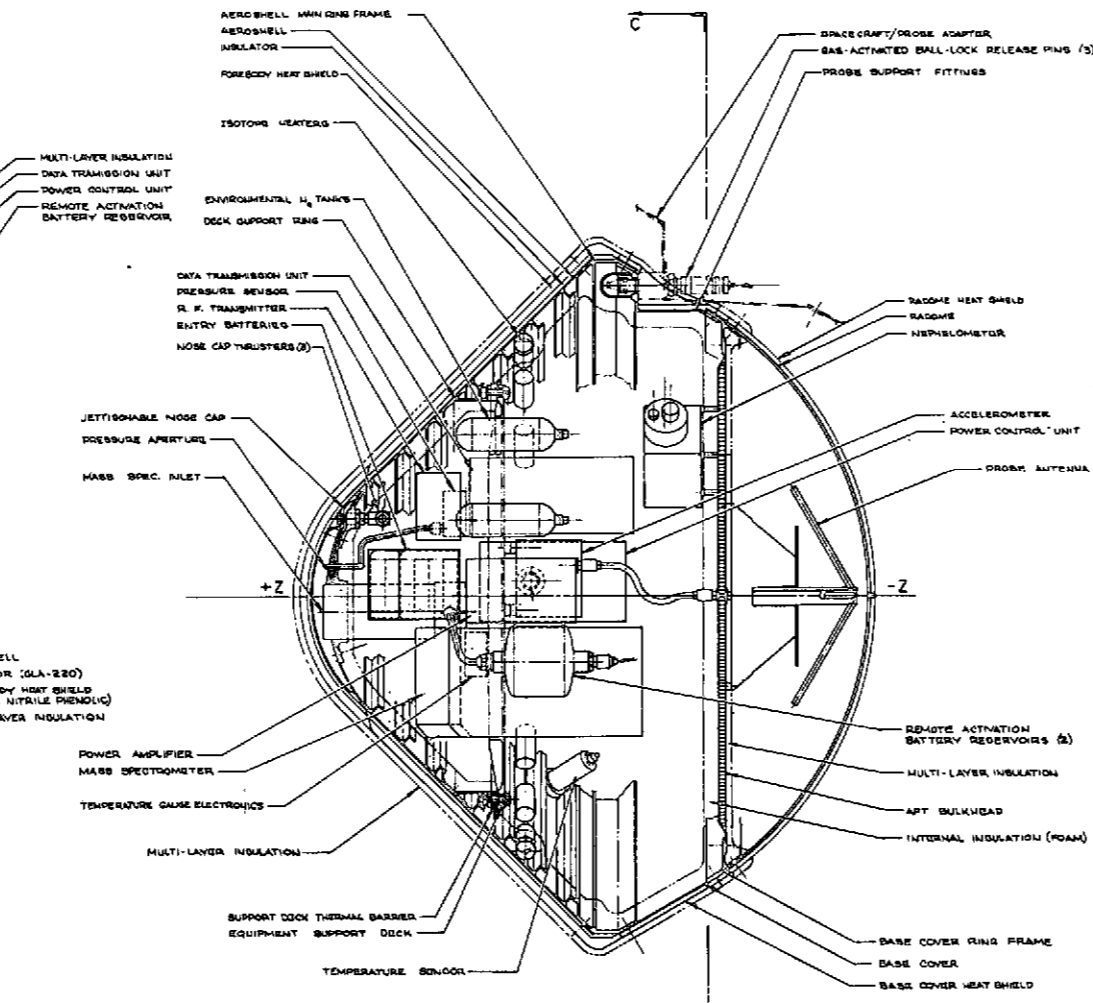
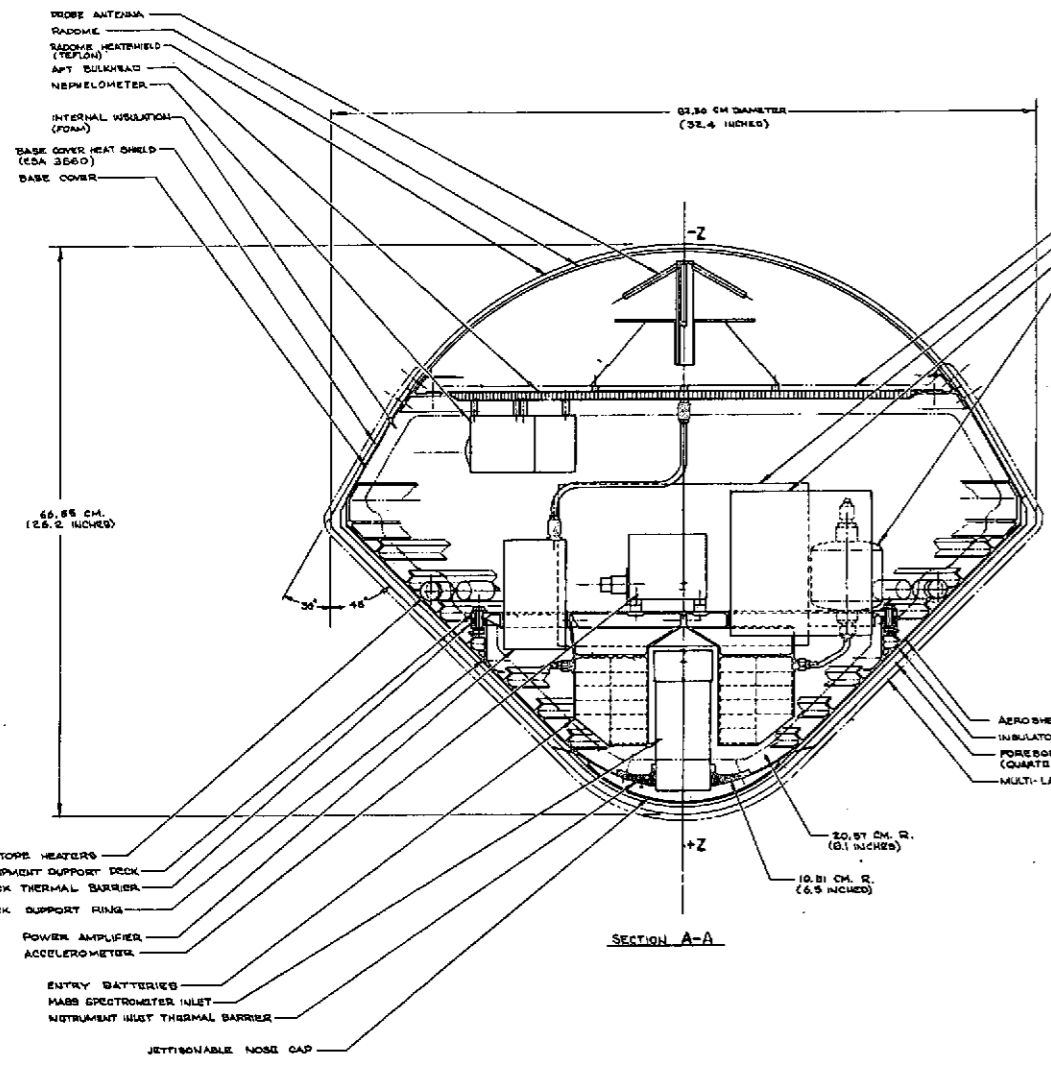
The entire probe is designed to withstand the entry loads. For the selected missions considered in this study, the entry heating and structural loads are most severe for a Saturn entry. Structural and mechanical details for the probe are described in the following sections.

#### 4.6.3.1 Configuration and General Arrangement

The probe configuration is shown in Figure 4.6-14. The probe contains all the scientific instruments and supporting electrical and electronic components required to successfully complete the science mission. A weight breakdown for the entire probe at various phases in the mission is in Table 4.6-7.

Prior to entry, the probe is 82.30 cm (32.4 in.) in diameter and has a nose radius-to-cone base radius ( $R_N/R_B$ ) of 0.43. The forebody of the probe is a 0.79 rad ( $45^\circ$ ) half-angle conical surface, and the afterbody is a 0.52 rad ( $30^\circ$ ) half-angle truncated cone with a spherical radome. At entry, the probe weighs 59.33 kg (130.68 lb) and has ballistic coefficient of  $102.0 \text{ kg/m}^2$  ( $0.65 \text{ slug/ft}^2$ ). The maximum diameter of the descent probe is only 80.77 cm (31.8 in.), which gives some idea as to the recession of the heat shield during entry. Note that the ratio of the nose radius to the base radius changes to 0.51 because of the aeroshell nose radius under the jettisonable nose cap. During atmospheric descent, the probe weighs 50.38 kg (110.97 lb) and has a ballistic coefficient of  $131.8 \text{ kg/m}^2$  ( $0.839 \text{ slug/ft}^2$ ) for Saturn, and  $138.8 \text{ kg/m}^2$  ( $0.884 \text{ slug/ft}^2$ ) for Uranus.

The equipment within the probe is protected from the hostile cold environment after entry by a layer of low-density foam insulation bonded to the interior of the probe shell structure. In addition, the equipment support deck is thermally isolated from the cold outer structure by a nonmetallic thermal barrier ring located between the equipment deck and the deck support ring. The inlet of the mass spectrometer and the aperture of the pressure gauge are both located at the stagnation point of the aeroshell and are protected during entry by a 25.4 cm (10 in.) diameter nose cap. This nose cap is then jettisoned, exposing the mass spectrometer inlet to the incoming, uncontaminated atmosphere of the planet. The mass spectrometer inlet and the pressure gauge aperture both penetrate the aeroshell through a nonmetallic thermal barrier to reduce the thermal effect of entry heating on the science instruments. These penetrations are also sealed to the thermal barrier to prevent argon gases from flowing into the mass spectrometer inlet and to prevent the planetary atmosphere from reaching



ORIGINAL PAGE IS  
OF POOR QUALITY

ORIGINAL PAGE IS  
OF POOR QUALITY

ORIGINAL PAGE IS  
OF POOR QUALITY

FOLDOUT FRAME  
1

FOLDOUT FRAME  
2

FOLDOUT FRAME  
3

FIGURE 4.6-14  
PIONEER SATURN/ARABUS PROBE -  
ALTERNATE CONFIGURATION (SA-43) HALF  
SCALE FOREBODY-NOMINAL STRIKE POSURE  
ORIENTED ORBIT/VELOCITY POS. PLAN  
DATE: BP-73-44422-6  
1871

Figure 4.6-14 Pioneer SU Probe Alternate Configuration

4.6-37 and 4.6-38

Table 4.6-7 Alternate Configuration Weight Breakdown

	Weight	
	kg	lb
<u>Science</u>		
Temperature Gauge	0.318	0.70
Pressure Transducer	0.454	1.00
Accelerometer	1.134	2.50
Neutral Mass Spectrometer Analyzer	6.350	14.00
Nephelometer	0.500	1.10
	<u>8.756</u>	<u>19.30</u>
<u>Power &amp; Power Conditioning</u>		
Power Control Unit	2.835	6.25
Entry Batteries	3.402	7.50
Remote Activation Reservoir	0.680	1.50
	<u>6.917</u>	<u>15.25</u>
<u>Cabling</u>		
Inner Probe	2.676	5.90
<u>Data Handling</u>		
Digital Telemetry Unit	1.814	4.00
<u>Communications</u>		
Probe Antenna	0.454	1.00
RF Transmitter	0.635	1.40
Power Amplifier	0.907	2.00
	<u>1.996</u>	<u>4.40</u>
<u>Pyrotechnics Subsystem</u>		
Pyro Squibs	0.272	0.60
<u>Structures &amp; Heat Shields</u>		
Probe Structure	8.437	18.60
Equipment Support Deck	3.084	6.80
Radome/Heat Shield (SLA-220)	0.839	1.85
Forward Heat Shield 5.72 kg (12.61 lb) ablated during entry	11.009	24.27
Aft Heat Shield ESA 3560 at 1.37 kg/m <sup>2</sup> (0.28 lb/ft <sup>2</sup> )	0.562	1.24
	<u>23.931</u>	<u>52.76</u>
<u>Mechanisms</u>		
Nose Cap Thrusters	0.499	1.10
Vent Valve	0.699	1.54
Nephelometer Cover	0.635	1.40
	<u>1.833</u>	<u>4.04</u>
<u>Thermal</u>		
External Insulation Blanket (forward heat shield)	0.671	1.48
External Insulation Blanket (base Cover)	0.998	2.20
Probe Hull Insulation (internal)	1.134	2.50
Isotope Heaters	0.544	1.20
Environmental Tank & Argon	3.347	7.38
TOTAL	51.541	113.63
15% Contingency	<u>7.731</u>	<u>17.04</u>
	<u>59.272</u>	<u>130.67</u>

Table 4.6-7 Concluded

	Weight	
	kg	lb
<u>Postentry Weight</u>		
Forward Heat Shield (ablated)	-5.720	-12.61
Aft Heat Shield		
Forward Insulation Blanket	-0.671	- 1.48
Aft Insulation Blanket		
	<u>-6.391</u>	<u>-14.09</u>
15% Contingency	-0.959	- 2.11
Subtotal	<u>-7.350</u>	<u>-16.20</u>
TOTAL		
$59.272 - 7.35 = 51.922 \text{ kg}$		
$(130.68 - 16.20 = 114.48 \text{ lb})$		
<u>Descent Weight</u>		
Nose Cap & Thrusters	-0.816	-1.80
Nephelometer Cover	-0.567	-1.25
	<u>-1.383</u>	<u>-3.05</u>
15% Contingency	-0.208	-0.46
Subtotal	<u>-1.591</u>	<u>-3.51</u>
TOTAL		
$51.922 - 1.591 = 50.331 \text{ kg}$		
$(114.48 - 3.51 = 110.97 \text{ lb})$		

the probe's interior cavity. The nephelometer is also isolated from the afterbody structure by using a nonmetallic viewing port to minimize internal heat losses. The temperature sensor is located on the outer edge of the aeroshell near the maximum diameter, and is extended through the forward heat shield after entry. The probe antenna is located inside the radome and mounted on the aft bulkhead on the probe's center-line.

The forebody heat shield is composed of quartz nitrile phenolic ablator on an SLA-220 insulator to reduce the entry heat on the aluminum aeroshell structure. The afterbody heat shield material is ESA-3560 bonded on the conical portion and SLA-220 on the radome to provide transparency to RF transmission and protect the fiberglass radome from entry heating. For the cruise, coast, and entry phases of the mission, the probe is completely enclosed within a blanket of high-performance multilayer insulation to help thermally control the probe and its components. Only the electrical umbilical and probe attachments to the carrier spacecraft penetrate the insulation. In our proposed design, the insulation blanket is allowed to remain on the probe during the entry phase, at which time it should ablate away without causing an excessive asymmetrical drag.

The aerodynamic stability of the probe depends on its aerodynamic shape and the relationship of the c.g. to the maximum diameter. During entry, the c.g. of the probe is approximately 9.3% of the maximum diameter forward of the maximum diameter, and the c.g. during descent is about 8.9% forward of the maximum diameter. Figure 4.6-15 shows the results of tests made on the probe's aerodynamic shape at the Langley Vertical Spin Tunnel and at the Ames Ballistic Range. These tests were conducted using an aerodynamic model of the PV small probe. In this model the c.g. was only 4% of the maximum diameter forward, compared to the 8% and 9% forward for the SU probe. The PV small probe and the SU probe have essentially the same aerodynamic shape.

#### 4.6.3.2 Structural Subsystem

The structural design of the probe is conventional in most aspects. The probe is vented, obviating the need for making the structure heavy enough to withstand the external atmospheric pressures. In addition, the probe will be temporarily pressurized to approximately  $10^5$  N/m<sup>2</sup> (1 bar) with argon gas at entry to further delay the entry of the planetary gases.

The overall structure is designed for entry at Saturn, which represents the most severe environment. For the selected entry angle of  $-0.52$  rad ( $-30^\circ$ ), the peak deceleration is  $3590$  m/sec<sup>2</sup> (366 g), which includes a  $0.09$  rad ( $5^\circ$ ) dispersion in the entry

Symbol	$\alpha$	c.g. % d	Facility
●	10-35	3.2	Spin Tunnel
■	6.8 (rms)	4	ARC PBR
○	15.2-19.5 (rms)	4	
○	15.2-19.5 (rms)	4	
△	44.3 (rms)	4	

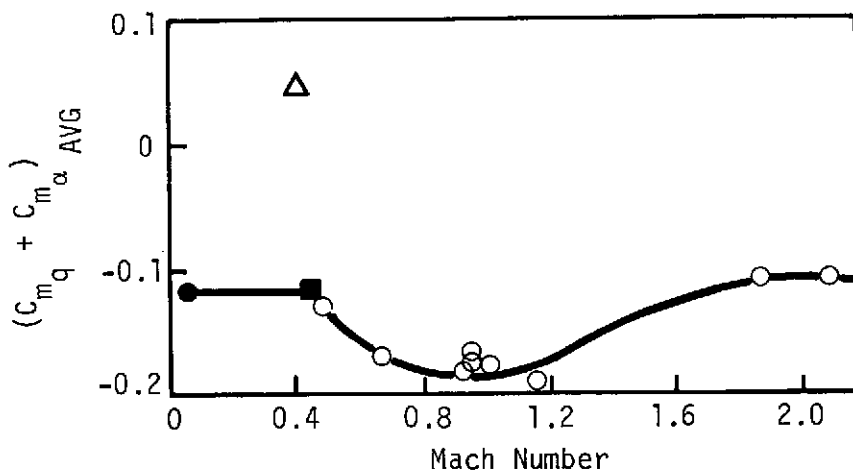


Figure 4.6-15 Pitch Damping Coefficients

angle. The corresponding dynamic pressure acting on the aeroshell is  $3.59 \times 10^5 \text{ N/m}^2$  (7530 psf) at peak load. The probe structure, which is shown in Figure 4.6-14, is made entirely of aluminum alloy. The equipment support deck is an integral rib-stiffened disc, machined from a solid plate. All components, with minor exceptions, are mounted on or suspended from this deck, which in turn, rests directly on the circumferential deck support ring attached to the probe aeroshell. The support ring transfers the deceleration loads to the aeroshell.

The conical aeroshell, the truncated conical afterbody with its flat honeycomb aft bulkhead, and the spherical radome, fair the afterbody into a conical/spherical aerodynamic shape that completes the probe structure. The aeroshell is configured as a Z-ring frame-stiffened monocoque structure with a machined peripheral ring frame, and the deck support ring frame is located at approximately the mid-diameter of conical surface to transfer the equipment loads to the aeroshell. The radome is a 39.37-cm (15.5-in.) radius spherical segment made from nonmetallic laminates. The entire area enclosed by the radome is vented to ambient atmosphere.

#### 4.6.3.3 Mechanisms Subsystem

The primary mechanisms in the probe are the probe/spacecraft support and separation mechanisms, the nose cap jettisoning system, the nephelometer cover and the temperature sensor deployment system, and the probe venting system.

The probe separation mechanism is a three-point-support, gas-activated; ball-lock, pin release system that uses concentrically located coil separation springs on each pin to provide a positive separation velocity of .1 m/sec (.3 fps). These pins are common to the Minute Man Program.

The nose cap jettisoning system is held in place by three pyro thrusters that are unsymmetrically located around the nose cap. When the pyros are activated, they release the nose cap with a separation force approximately 3178 kg (7000 lb), as shown in Figure 4.6-16.

The nephelometer cover is released by a G&H technology model 8003 nonexplosive pin-puller. The preloaded coil spring forces the cover assembly, together with the separation spring and the retention link, from the probe (see Figure 4.6-17).

The temperature sensor is also activated by a Model 8003 non-explosive pin-puller that permits a preloaded coil spring to extend the sensor into the airstream beyond the probe's boundary layer. The heat shield plug covering the temperature sensor is released and jettisoned when the sensor is deployed. (See figure 4.2-3).

The vent valve system is designed to maintain the differential pressure across the probe structure within  $\pm 10^5 \text{ N/m}^2$  (1 bar). The design consists of two valves. The external pressure vent valve is locked closed until after entry, then is permitted to open when the external pressure exceeds the internal pressure by  $10^5 \text{ N/m}^2$  (1 bar). The internal pressure vent valve is a simple poppet valve mounted in the aft bulkhead and activated by an excess internal pressure of  $10^5 \text{ N/m}^2$  (1 bar) over the atmospheric pressure. This valve vents into the vented radome cavity.

#### 4.6.3.4 Mass Properties

The weight breakdown for the probe is presented in Table 4.6-7. Note that the weights of each subsystem are first shown separately then summed to establish the total weight. The last portion of the table reduces the weight sequentially, in keeping with the nominal mission sequence of events, to indicate the weight of the probe at various phases during the mission.



104

4.6-44

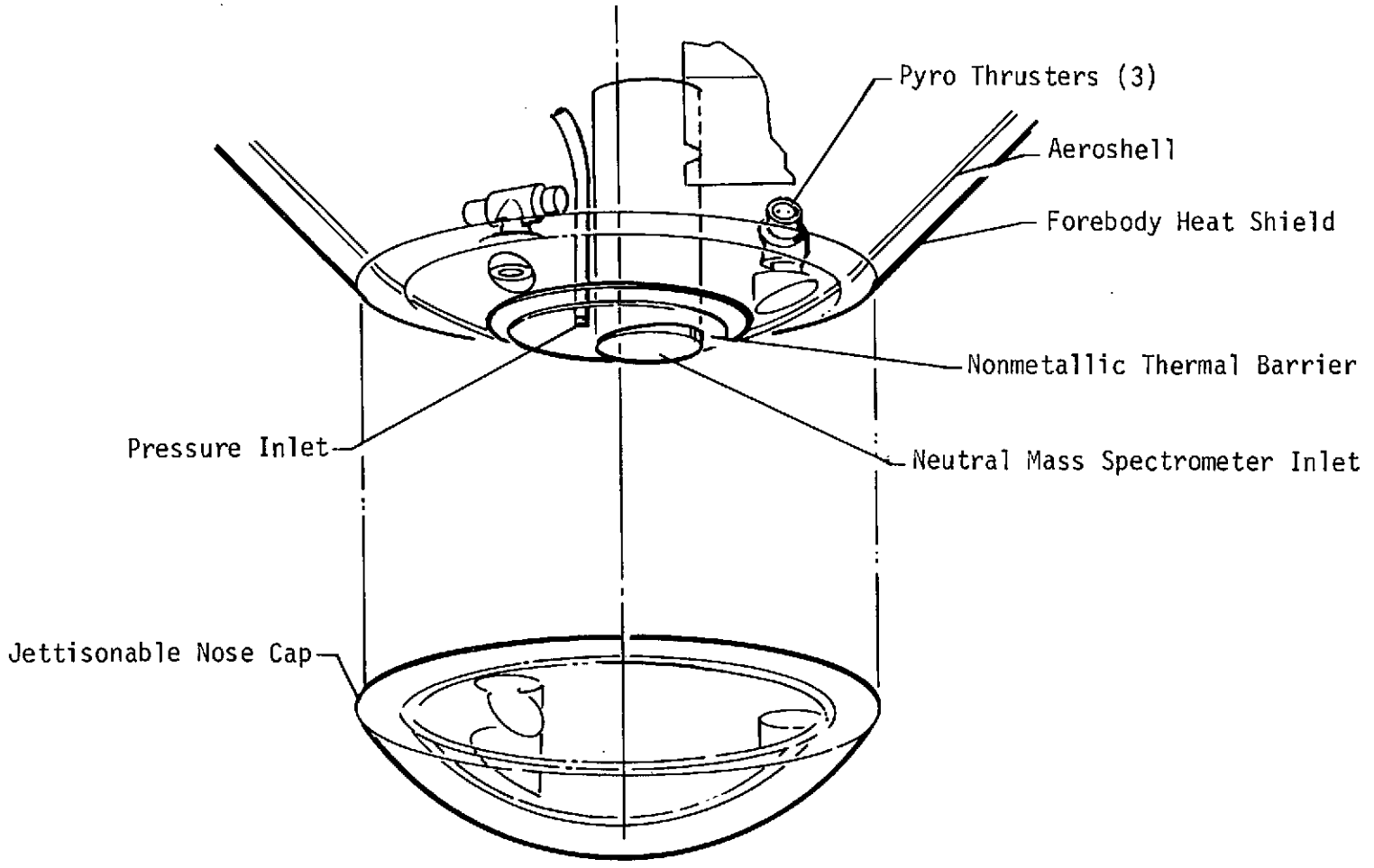


Figure 4.6-16 Alternate and Final Configuration Nose Cap Jettisoning System

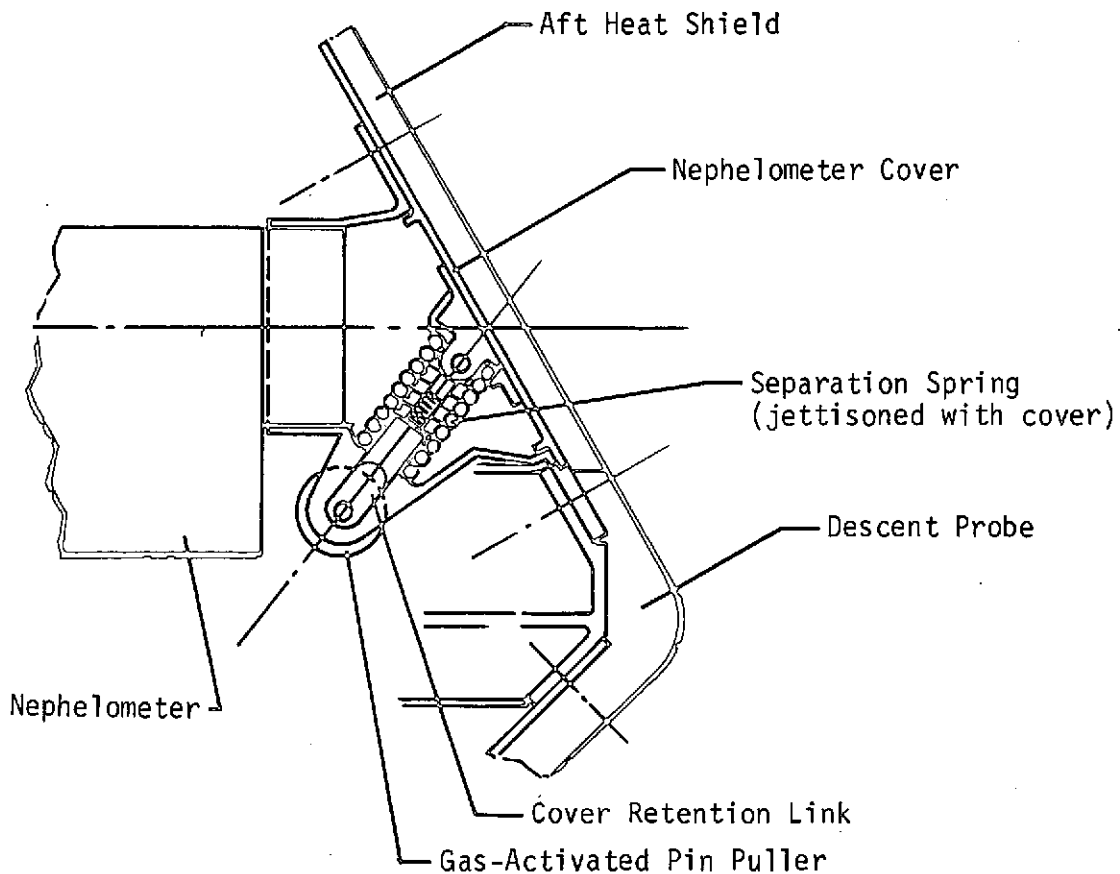


Figure 4.6-17 Alternate and Final Configuration Nephelometer Cover Release System

#### 4.6.3.5 Deceleration Subsystem

The deceleration system for the probe is based on the probe's aerodynamic drag and ballistic coefficients. As shown in Figure 4.6-18, no drag devices are deployed to maintain aerodynamic stability during entry or descent. The design, size, and c.g. location make the probe inherently stable and give it enough drag to effectively control the descent rate.

The heat shield for the alternate configuration is identical to that for the baseline configuration. For the baseline configuration, the temperatures through the heat shield had peaked before the parachute was deployed and so on this configuration, no additional protection is needed if the heat shield and aeroshell are retained after entry.

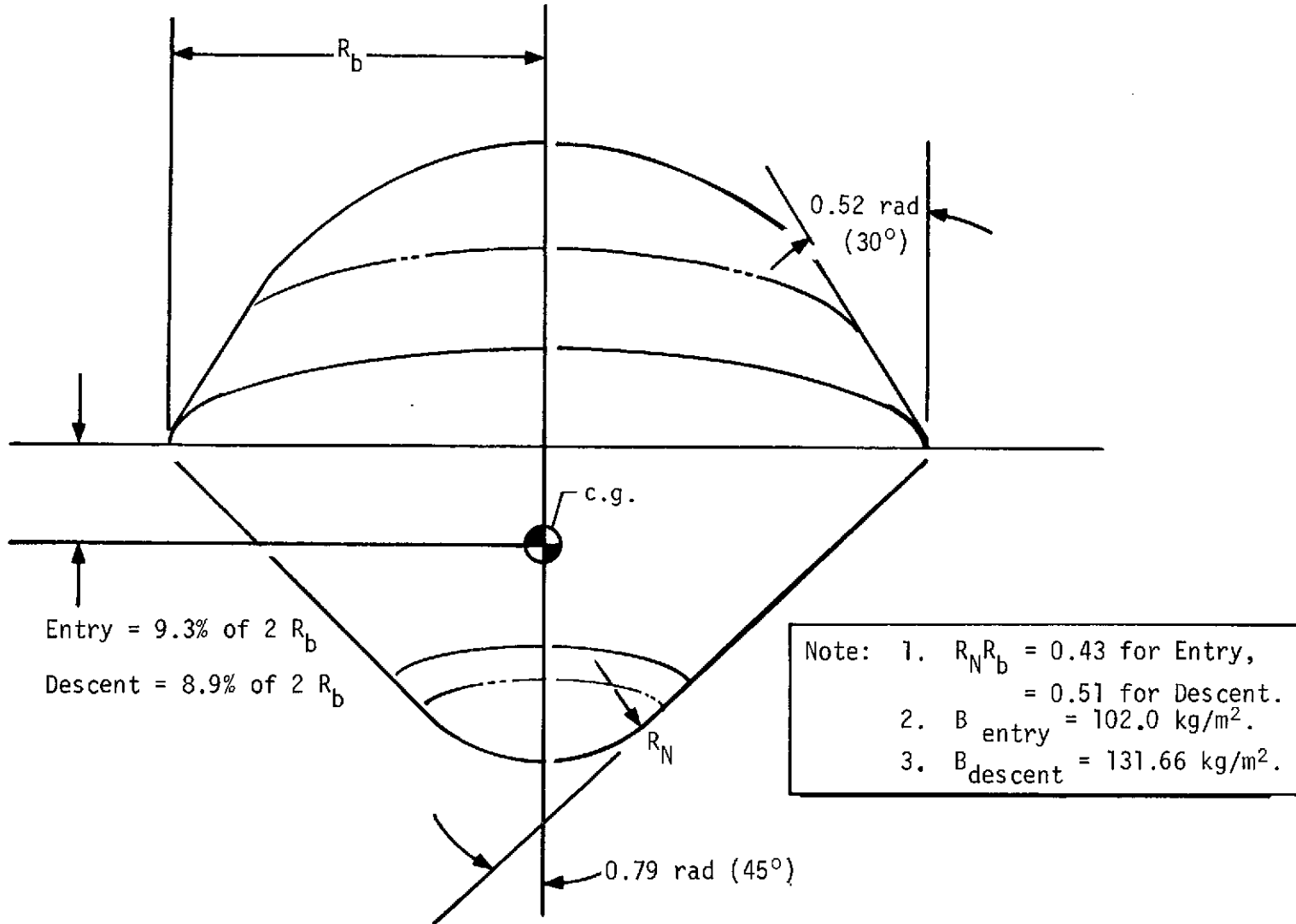


Figure 4.6-18 Alternate Configuration Deceleration System

#### 4.6.3.6 Thermal Control Subsystem (Alternate Configuration)

The thermal control subsystem maintains the temperatures within the probe at cruise at 278°K (40°F) by using 10 one watt RHUs. The multilayer insulation blanket is the same as that used for the baseline configuration. As before, 4.2 watts of excess heater power is conducted from the probe through the three support points to the probe/spacecraft interstage cone during the cruise phase. After the probe is released from the spacecraft, this excess energy warms the probe to the required entry temperature at the target planet.

A 2.5-cm-thick layer of foam insulation is applied to the internal surfaces of the probe to isolate the payload from the aeroshell and heat shield. A 1-cm layer of foam is also placed on the battery to eliminate free-convection cooling of the cells by the incoming atmospheric gas. Low-conductance phenolic washers thermally isolate the equipment deck from the support ring mounted on the aeroshell.

An argon gas pressurization system is activated immediately after entry to fill the probe with argon and delay the entry of atmospheric gas into the probe until the ambient pressure reaches  $2.5 \times 10^5 \text{ N/m}^2$  (2.5 bar). The argon gas enhances the insulation performance because the foam conductivity tracks that of the gas filling its structure.

Neon was selected for the baseline configuration to prevent gas from condensing in the insulation at the aeroshell. Neon condenses at 27°K (-411°F), whereas argon condenses at 87°K (-303°F). Since the spent heat shield remains on the aeroshell in this configuration, the aeroshell temperature drop during descent is minimized. Therefore, argon can be used as the fill gas; it is preferred because argon has only half the thermal conductivity of neon.

#### 4.6.4 Configuration Comparison (Nominal Atmosphere)

The configurations are compared in Table 4.6-8. Note that the baseline configuration uses a separable heat shield/aeroshell and a descent probe housed within the entry probe. This requires using separate structures for the forebody (aeroshell), base cover, and separation system. In comparison, the alternate configuration uses an integrated heat shield with a common structure for the entry and descent probes. This eliminates the need for separate structural assemblies release systems, and separation systems.

Table 4.6-8 Nominal Atmosphere Configuration Comparisons

	Baseline Configuration	Alternate Configuration
Weight of Entry Probe, kg (lb)	71.733 (158.15)	59.72 (130.67)
Weight of Descent Probe, kg (lb)	45.500 (100.32)	50.33 (110.97)
Entry Diameter, cm (in.)	90.40 (35.6)	82.30 (32.4)
Descent Diameter, cm (in.)	67.6 (26.60)	80.77 (31.8)
Entry c.g., % of Maximum Diameter	9.6	9.3
Descent c.g., % of Maximum Diameter	5.3	8.9
Weight of Structural kg (lb)	17.45 (38.46)	13.249 (29.21)
Weight of Forward Heat Shield, kg (lb)	15.204 (33.52)	12.660 (27.91)
Aeroshell	Separate	Integral
Base cover	Separate	Integral
Deceleration System	Aeroshell & Parachute	Aeroshell
Separation System	Parachute	Scientific Covers
Weight of Separation System, kg (lb)	4.77 (10.51)	2.06 (4.55)

All weights include a 15% contingency

Another major difference is that in the alternate design, the inlets to the science instruments are protected by individual covers that are deployed or jettisoned after entry, and do not depend on a parachute separation system. This is a significant advantage, since failure in the separation system or the aeroshell release system for the baseline probe could void the entire mission. The alternate design is simpler, and the failure of a release system would void only a portion of the scientific data acquired during the mission.

#### 4.6.5 Updated Alternate Configuration (Nominal Atmosphere)

The baseline and alternate configurations were based on preliminary PV data on science and electronic instruments. The alternate probe weight table has been updated to reflect the latest PV science and electronic instruments. The latest PV data were also used in the final configuration worst-case atmosphere probe for comparison purposes. This updating is shown in weight Table 4.6-9.

#### 4.6.6 Final Configuration Definition (Worst-Case Atmosphere)

The impact of the worst-case atmospheres on the probe is depicted in Table 4.6-10. Note that the worst-case atmosphere causes an increase in the descent time, which increases the power requirement and requires the use of a larger battery. Second, the increased g loading has major impact on the probe structure and heat shield requirements. The quartz nitrile phenolic previously used for the alternate configuration becomes too heavy. Therefore, carbon phenolic was used for the forward heat shield. The increased weight of the structure and heat shield areas also necessitated increasing the probe's maximum diameter to maintain the proper ballistic coefficients.

The final configuration heat shield/aeroshell structure protects the probe from the extreme heat pulse encountered during the planetary entry and provides an entry ballistic coefficient that is compatible with the science requirements. The aeroshell, afterbody, and radome are an integral part of the probe structure. The forward spherical section of the heat shield is a jettisonable cap that protects the mass spectrometer inlet and pressure gauge aperture from the entry environment. The nose cap is jettisoned by three pyro thrusters after entry, exposing the instrument inlets to the uncontaminated ambient atmosphere. The other science instruments, such as the temperature sensor and the nephelometer, are either deployed or uncovered after entry by mechanical systems. Once the scientific sensors are exposed the probe makes a ballistic descent through the planetary atmosphere to accomplish the scientific objectives.

Table 4.6-9 Updated Alternate Configuration Weight Breakdown

	Weight	
	kg	lb
<u>Science</u>		
Temperature Gauge	0.726	1.60
Pressure Transducer	0.454	1.00
Accelerometer	1.134	2.50
Neutral Mass Spectrometer Analyzer	9.072	20.00
Nephelometer	<u>0.499</u>	<u>1.10</u>
	11.884	26.20
<u>Power &amp; Power Conditioning</u>		
Power Control Unit	2.835	6.25
Entry Batteries	<u>5.008</u>	<u>11.04</u>
	7.843	17.29
<u>Cabling</u>		
Inner Probe	2.676	5.90
<u>Data Handling</u>		
Digital Telemetry Unit	1.814	4.00
Signal Conditioner	<u>0.136</u>	<u>0.30</u>
	1.950	4.30
<u>Communications</u>		
Probe Antenna	0.544	1.20
RF Transmitter	<u>1.134</u>	<u>2.50</u>
	1.678	3.70
<u>Pyrotechnics Subsystem</u>		
Pyro Squibs	0.091	0.20
<u>Structures &amp; Heat Shields</u>		
Probe Structure	8.437	18.60
Equipment Support Deck	3.992	8.80
Radome/Heat Shield (SLA-220)	0.839	1.85
Forward Heat Shield [5.72 kg (12.61 lb) ablated during entry]	11.009	24.27
Aft Heat Shield [ESA 3560 at 1.37 kg/m <sup>2</sup> (0.28 lb/ft <sup>2</sup> )]	0.562	1.24
	<u>24.839</u>	<u>54.76</u>
<u>Mechanisms</u>		
Nose Cap Thrusters	0.181	0.40
Vent Valve	0.476	1.05
Nephelometer Cover	0.517	1.14
Pin Pullers	<u>0.680</u>	<u>1.50</u>
	1.854	4.09
<u>Thermal</u>		
External Insulation Blanket (forward heat shield)	0.671	1.48
External Insulation Blanket (base cover)		
Probe Hull Insulation (internal)	0.998	2.20
Isotope Heaters	0.567	1.25
Environmental Tank & Argon	<u>0.544</u>	<u>1.20</u>
	2.780	6.13
TOTAL	55.595	122.57
15% Contingency	<u>8.341</u>	<u>18.39</u>
	63.936	140.96

Table 4.6-9 Concluded

	Weight	
	kg	lb
<u>Postentry Weight</u>		
Forward Heat Shield (ablated)	-5.720	-12.61
Aft Heat Shield (ablated)		
Forward Insulation Blanket	-0.671	-1.48
Aft Insulation Blanket		
	<u>-6.391</u>	<u>-14.09</u>
15% Contingency	<u>-0.959</u>	<u>-2.11</u>
Subtotal	-7.350	-16.20
TOTAL		
<u>63.936 - 7.350 = 56.586 kg</u>		
<u>(138.66 - 16.20 = 122.46 lb)</u>		
<u>Descent Weight</u>		
Nose Cap & Thrusters	-0.816	-1.80
Nephelometer Cover	<u>-0.363</u>	<u>-1.25</u>
	<u>-1.179</u>	<u>-3.05</u>
15% Contingency	<u>-0.177</u>	<u>-0.46</u>
Subtotal	-1.356	-3.51
TOTAL		
<u>56.586 - 1.356 = 55.230 kg</u>		
<u>(122.46 - 3.51 = 118.95 lb)</u>		



Table 4.6-10 Updated Alternate and Final Configurations Comparisons

	Up-dated Alternate Config. (Nominal Atmosphere)	Final Configuration (Worst-case Atmosphere)
Maximum Deceleration, m/sec <sup>2</sup> (g)	3660 (366)	5850 (585)
Weight of Entry Probe, kg (lb)	63.94 (140.96)	91.876 (202.56)
Weight of Descent Probe (Saturn), lb (kg)	55.23 (118.95)	72.295 (159.39)
Diameter of Entry Probe, cm (in.)	82.30 (32.4)	87.38 (34.4)
Diameter of Descent Probe, cm (in.)	80.77 (31.8)	84.94 (33.44)
Entry Probe c.g., % of Maximum Diameter	9.2	5.72
Descent Probe c.g., % of Maximum Diameter	8.9	6.90
Forward Heat Shield (Material)	Quartz Nitrile Phenolic	Carbon Phenolic
Weight of Structure, kg (lb)	14.293 (31.51)	22.8 (50.36)
Weight of Battery, kg (lb)	5.760 (12.70)	8.35 (18.40)

All weights include a 15% contingency

The entire probe is designed to withstand the entry heating and pressure loads encountered at Saturn and Uranus. For the missions considered in this report, the entry heating is most severe at Uranus and the most severe pressure loads occur at entry into Saturn. The mechanical and structural design for the probe is described in the following paragraphs.

#### 4.6.6.1 Configuration and General Arrangement

The configuration of the probe is shown in Figure 4.6-19. Table 4.6-11 shows the weight summary. The probe structure contains and protects all the science instruments and electrical and electronic equipment. Before entry, the probe has a diameter of 87.34 cm (34.4 in.) and a nose radius-to-base radius ( $R_N/R_B$ ) of 0.425. The aeroshell is a conical surface with a  $0.79 \text{ rad} (45^\circ)$  half-angle, and the afterbody consists of a truncated cone with a  $0.52 \text{ rad} (30^\circ)$  half angle faired into the spherical radome. At entry the probe weighs 91.96 kg (202.56 lb) and has a ballistic coefficient of  $142.6 \text{ kg/m}^2 (0.908 \text{ slug/ft}^2)$ . During descent, the probe has a maximum diameter of 84.94 cm (33.44 in.), weighs 72.36 kg (159.39 lb) for Saturn, and has a maximum diameter of 84.58 cm (33.3 in.), weighs 69.43 kg (152.93 lb) for Uranus. These reductions are due to the recession of the heat shield during entry. The ratio of nose-to-base radius changes to 0.49 after deployment of the nose cap. The descent ballistic coefficients for Saturn and Uranus are  $161.3 \text{ kg/m}^2 (1.03 \text{ slug/ft}^2)$  and  $160.0 \text{ kg/m}^2 (1.02 \text{ slug/ft}^2)$ .

The equipment within the probe is protected from the hostile cold environment of the planetary atmospheric by bonding a layer of low-density foam insulation to the interior of the probe shell. In addition, the equipment support deck is thermally isolated from the cold outer structure by a nonmetallic thermal barrier ring located between the equipment deck and the deck support ring. The inlet for the mass spectrometer and the aperture for the pressure gauge are located at the stagnation point of the aeroshell. They are protected during entry by a 25.4-cm (10 in.) diameter nose cap. These two penetrations in the nose of the aeroshell pass through a nonmetallic barrier reducing the thermal influence of the aeroshell on the science instrument inlets. The penetrations are also sealed to the thermal barrier to prevent internal argon gases from flowing into the mass spectrometer inlet and to prevent planetary atmospheric gases from reaching the probe's interior cavity. The nephelometer is also isolated from the probe's exterior structure by a nonmetallic viewing port to minimize internal heat losses. The temperature sensor is located near the periphery of the aeroshell and is extended through the forward heat shield after entry. The probe antenna is inside the radome, mounted on the aft bulkhead at the centerline of the probe.

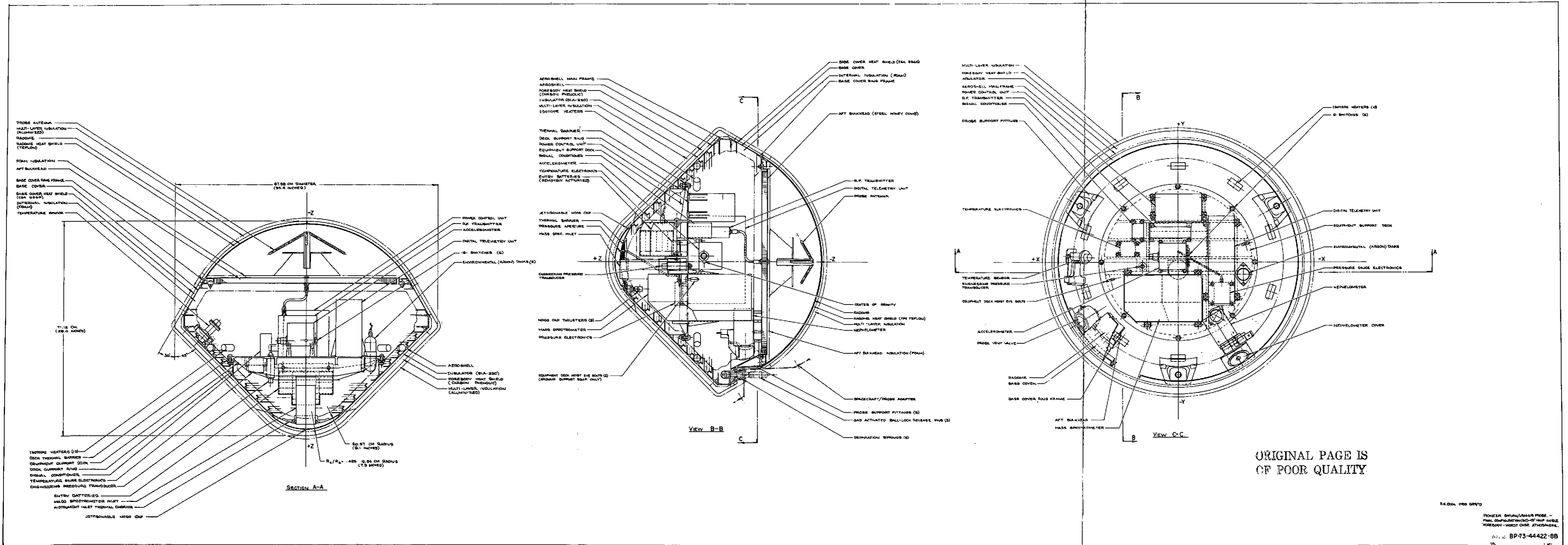
The forebody heat shield consists of carbon phenolic ablation material bonded to the SLA-220 insulator, which is bonded to the aeroshell. The insulator reduces the amount of entry heating conducted to the aeroshell, and permits the use of aluminum as the structural material. The afterbody heat shield has ESA-3560 bonded on the conical portion and Teflon on the radome. The Teflon provides RF transparency and protects the nonmetallic laminate against entry heating. During the cruise, coast, and entry phases of the mission, the probe is completely enclosed within a blanket of high-performance multilayer insulation for thermal control. Only the probe/spacecraft attachment and the electrical umbilical penetrate this insulation blanket. In our proposed design, the insulation blanket is permitted to remain on the probe during entry, at which time it should ablate away without excessive asymmetrical drag.

The aerodynamic stability of the probe is a function of the aerodynamic shape and the relationship of the c.g. to the probe's maximum diameter. Aerodynamic tests using a similar probe have already been performed in the NASA-Langley vertical spin tunnel and at the Ames Ballistic Range. The results of these tests show good stability from Mach 0 to Mach 2, and are depicted in Figure 4.6-15. The data shown in this figure are for the aerodynamic model of the PV small probe whose c.g. is 4% of the maximum diameter forward of the maximum diameter. The c.g. locations for the SU probe of 5.72% for the entry probe and 6.9% for the descent probe increase the stability compared to the PV small probe. PV and SU probes have the same aerodynamic shape.

#### 4.6.6.2 Structural Subsystem

The structural design is conventional in most aspects. The probe structure is vented, obviating the need for the structure to withstand the external atmospheric pressures, and avoiding a consequent weight penalty. To facilitate thermal control, the probe will be temporarily pressurized to approximately  $10^5$  N/m<sup>2</sup> (1 bar) with argon at entry.

The structural design of the probe is based on a 0.52 rad (30°) entry angle into Saturn which represents the most severe environment. For this particular entry, the peak deceleration is 5737 m/sec<sup>2</sup> (585 g) and the corresponding dynamic pressure acting on the aeroshell is  $7.3 \times 10^5$  N/m<sup>2</sup> (15,248 psf) at peak load. The structural design for the probe is shown in Figure 4.6-19. The basic structural elements are designed of aluminum alloy. The equipment support deck is an integrally rib-stiffened disc that is machined from a solid plate. With minor exceptions, all components are mounted on or suspended from this deck. In turn, the support deck rests directly on a circumferential



ORIGINAL PAGE IS  
OF POOR QUALITY

14-00000 000 000/13  
PIONEER ORION/ARSON PROBE -  
FINAL CONFIGURATION/50% HALF SCALE  
FOREBODY - WEST SIDE ATMO/SKIN  
REV. 10-67  
BP-73-44422-88

Figure 4.6-19 Pioneer SU Probe Final Configuration  
4.6-55 and 4.6-56

FOLDOUT FRAME

ORIGINAL PAGE IS  
OF POOR QUALITY

FOLDOUT FRAME

ORIGINAL PAGE IS  
OF POOR QUALITY

FOLDOUT FRAME

3

Table 4.6-11 Final Configuration Weight Breakdown

	Weight	
	kg	lb
<u>Science</u>		
Temperature Gauge	0.726	1.60
Pressure Transducer	0.454	1.00
Accelerometer	1.134	2.50
Neutral Mass Spectrometer Analyzer	9.072	20.00
Nephelometer	0.499	1.10
	<u>11.884</u>	<u>26.20</u>
<u>Power &amp; Power Conditioning</u>		
Power Control Unit	2.835	6.25
Entry Batteries	7.257	16.00
	<u>10.092</u>	<u>22.25</u>
<u>Cabling</u>		
Inner Probe	3.220	7.10
<u>Data Handling</u>		
Digital Telemetry Unit	1.814	4.00
Signal Conditioner	0.136	0.30
	<u>1.950</u>	<u>4.30</u>
<u>Communications</u>		
Probe Antenna	0.544	1.20
RF Transmitter	1.134	2.50
	<u>1.678</u>	<u>3.70</u>
<u>Pyrotechnics Subsystem</u>		
Pyro Squibs	0.091	0.20
<u>Structures &amp; Heat Shields</u>		
Probe Structure	13.878	30.595
Equipment Support Deck	5.833	12.86
Radome Heat shield (Teflon)	7.076	15.60
Nose Cap	0.150	0.33
Forward Heat Shield 9.72 kg (21.43 lb) ablated during entry	16.960	37.39
Aft Heat Shield ESA 3560 at 1.37 kg/m <sup>2</sup> (0.28 lb/ft <sup>2</sup> )	0.989	2.18
	<u>44.886</u>	<u>98.96</u>
<u>Mechanisms</u>		
Nose Cap Thrusters	0.181	0.40
Vent Valve	0.476	1.05
Nephelometer Cover	0.517	1.14
Pin Pullers	0.680	1.50
	<u>1.854</u>	<u>4.09</u>
<u>Thermal</u>		
External Insulation Blanket (forward heat shield)	1.417	3.26
External Insulation Blanket (base cover)	1.647	3.63
Probe Hull Insulation (internal)	0.567	1.25
Isotope Heaters	0.544	1.20
Environmental Tank & Argon	4.237	9.34
TOTAL	79.892	176.14
15% Contingency	11.984	26.42
	<u>91.876</u>	<u>202.56</u>

Table 4.6-11 Concluded

<u>Saturn</u>	Weight	
	kg	lb
<u>Postentry Weight</u>		
Forward Heat Shield (ablated)	-9.720	-21.43
Aft Heat Shield	-4.649	-10.25
Forward Insulation Blanket	-1.479	- 3.26
Aft Insulation Blanket		
	<u>-15.848</u>	<u>-34.94</u>
15% Contingency	- 2.377	- 5.24
Subtotal	<u>-18,225</u>	<u>-40.18</u>
TOTAL		
<u>91.876 - 18.225 = 73.651 kg</u>		
<u>(202.56 - 40.8 = 162.38 lb)</u>		
<u>Descent Weight</u>		
Nose Cap & Thrusters	-0.816	-1.80
Nephelometer Cover	-0.363	-0.80
	<u>-1.179</u>	<u>-2.60</u>
15% Contingency	-0.177	-0.39
Subtotal	<u>-1.356</u>	<u>-2.99</u>
TOTAL		
<u>73.651 - 1.356 = 72.295 kg</u>		
<u>(162.38 - 2.99 = 159.39 lb)</u>		
<u>Uranus</u>	Weight	
	kg	lb
<u>Postentry Weight</u>		
Forward Heat Shield (ablated)	-11.544	-25.45
Aft Heat Shield	- 5.375	-11.85
Forward Insulation Blanket	-1.479	- 3.26
Aft Insulation Blanket		
	<u>-18.398</u>	<u>-40.56</u>
15% Contingency	- 2.758	- 6.08
Subtotal	<u>-21.155</u>	<u>-46.64</u>
TOTAL		
<u>91.876 - 21.155 = 70.721 kg</u>		
<u>(202.56 - 46.64 = 155.92 lb)</u>		
<u>Descent Weight</u>		
Nose Cap & Thrusters	-0.816	-1.80
Nephelometer Cover	-0.363	-0.80
	<u>-1.179</u>	<u>-2.60</u>
15% Contingency	-0.177	-0.39
Subtotal	<u>-1.356</u>	<u>-2.99</u>
TOTAL		
<u>70.721 - 1.356 = 69.365 kg</u>		
<u>(155.92 - 2.99 = 152.93 lb)</u>		

deck support ring that is attached to the aeroshell. This support ring transfers deceleration loads from the equipment to the aeroshell. The remaining structural elements consist of conical aeroshell and a truncated conical afterbody with a flat aft honeycomb bulkhead.

The aeroshell is a Z-ring frame-stiffened monocoque structure with a machined peripheral ring. The deck support ring frame is fastened to the aeroshell at approximately the mid-diameter of the conical surface to distribute structural loads of the equipment. The radome is a 40.39-cm (15.9 in.) radius spherical segment fabricated from nonmetallic laminates. The area enclosed by the radome is vented to the ambient atmosphere for minimum structural weight. Detailed structural drawings of the final configuration are presented in Supplemental Document IR-73-2.

#### 4.6.6.3 Mechanisms Subsystem

The primary mechanisms are the probe/spacecraft support and separation mechanisms, the nose cap jettisoning system, the nephelometer cover and the temperature sensor deployment system and the probe vent valve system.

The probe separation mechanism is a three-point-support, gas-activated, ball-lock pin release system that has concentrically located coil springs on each pin to provide a positive separation velocity of .1 m/sec (.3 fps). These pins are common to the pins used on the Minuteman Program.

The nose cap jettisoning system is held in place by three pyro thrusters that are unsymmetrically located around the nose cap. When the pyros are activated, they release the nose cap and supply an asymmetrical separation force of approximately 3178 kg (7000 lbs), as shown in Figure 4.6-16.

The nephelometer cover is released by a G&H Technology Model 8003 nonexplosive pin-puller. The preloaded coil spring forces the entire cover assembly, which includes the separation spring and the retention link, to separate from the probe, as shown in Figure 4.6-17.

The temperature sensor is also activated by a Model 8003 nonexplosive pin-puller. This permits a preloaded coil spring to extend the unit into the airstream beyond the probe's boundary layer. The heat shield plug covering the temperature sensor is released and jettisoned at the same time the sensor is deployed, as shown in Figure 4.2-3.

The vent valve system consists of two valves designed to prevent differential pressures of over  $10^5$  N/m<sup>2</sup> (1 bar) across the probe structure. The external pressure venting valve is locked closed until after entry to seal the probe against the entry of hot gases, and is unlocked after entry. When the external pressure exceeds the internal pressure by  $10^5$  N/m<sup>2</sup> (1 bar) venting will occur. The internal pressure vent valve is a simple poppet valve. It vents internal pressure  $10^5$  N/m<sup>2</sup> greater than the external pressure. It is located in the aft bulkhead, and vents into the radome cavity, which is vented to the atmosphere.

#### 4.6.6.4 Mass Properties

The weight breakdown for the final probe configuration is presented in Table 4.6-11. Note that the weights for each subsystem are summed to establish the total weight of the probe. The last portion of the table shows the total weight of the probe at various phases during the mission.

#### 4.6.6.5 Deceleration Subsystem

The deceleration subsystem for the final configuration is based on aerodynamic drag. As shown in Figure 4.6-21, no deployable devices are required to stabilize the probe during entry or descent, or to control the descent rate through the planetary atmosphere.

Based on the analyses and tradeoffs discussed in Section 4.6.1.3, the heat shield for the final configuration was sized using the worst-case entry into the Uranus cool atmosphere and the worst-case entry into the Saturn warm atmosphere. The type of ablator material selected (carbon phenolic) was determined by the degree of ablation in the Uranus cool environment. The insulation material (SLA-220) was sized for the amount of heat soak in the Saturn warm environment.

The primary heat shield consists of 1.27-cm (0.50 in.) of carbon phenolic bonded to a 0.794-cm (0.3125 in.) thick insulator of phenolic honeycomb-reinforced SLA-220. This in turn, is bonded to the aeroshell. The heat shield is a constant thickness over the surface of the aeroshell.

The heat shield on the aft cover consists of 0.762-cm (0.30 in.) of Teflon over the radome and the same thickness of ESA-3560 over the remainder of the aft cover. Teflon replaced the SLA-220 used on previous configurations because of the detrimental charring characteristics of SLA-220 at the higher heating rates inherent in the worst-case atmospheres.



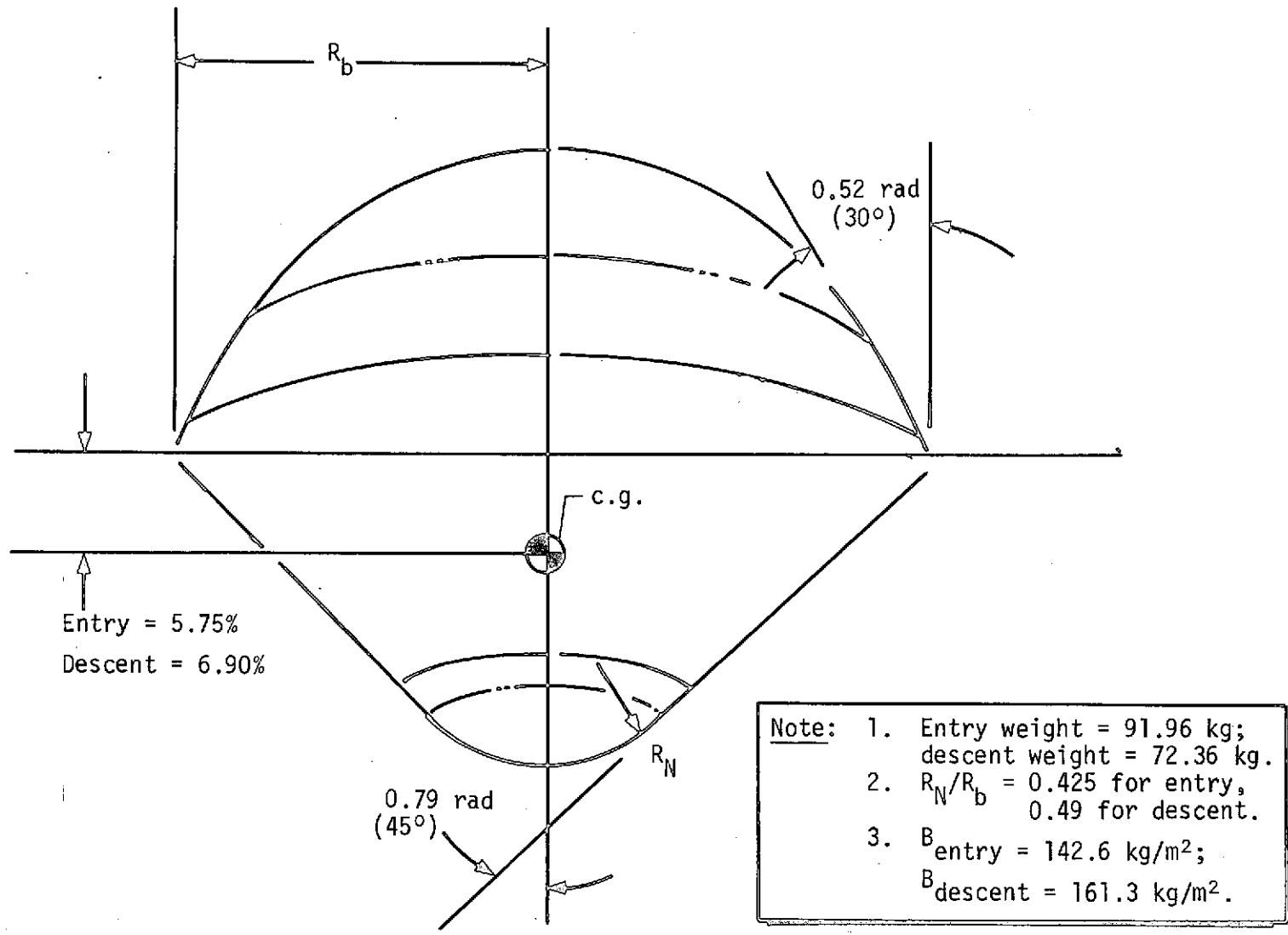


Figure 4.6-20 Final Configuration Probe Deceleration System

#### 4.6.6.6 Thermal Control Subsystem (Final Configuration)

Thermal control is provided as an integral part of the mechanical subsystem to ensure that all components will be within acceptable temperature limits during all phases of the mission. For the final probe configuration, the probe components must be isolated from the temperature extremes of the worst-case atmospheres. These extremes range from 47°K (-375°F) at upper altitudes in the Uranus cool atmosphere to 424°K (304°F) at  $10^6$  N/m<sup>2</sup> (10 bar) in the Saturn warm atmosphere.

Our analysis shows that the most critical thermal control problem during the mission is the high rate of heat loss to the Uranus cool atmosphere. Warm-atmosphere missions present no significant problem because the descent through the cool upper atmosphere conditions the probe for the warm environments at the lower altitudes. Our thermal control approach was to raise the temperature of the probe during the coast period to the target planet; this elevated entry temperature, raises the EOM temperatures of the components within the final probe configuration in the cool and nominal atmospheres.

The thermal control hardware is shown in Figure 4.6-21 and includes RHUs, multilayer insulation, low-density NOPCO foam insulation, low-conductivity thermal isolators, and an argon pressurization system. Ten RHUs, each dissipating one watt, are mounted on the aeroshell. These heaters maintain the desired temperatures during the cruise phase and, during coast, warm the probe to the desired entry temperature. The multilayer insulation consists of 21 layers of 1/4-mil, singly-aluminized Mylar covered with a outer layer of aluminized Kapton. A 2.5-cm layer of low-density NOPCO BX-250 foam insulation (density = 0.034 g/cm<sup>3</sup>) isolates the internal equipment from the cold aeroshell during the descent phase. A 1-cm layer protects the battery from free-convective heat transfer with the incoming atmospheric gas. The low-conductivity thermal standoffs uncouple the equipment deck from the support ring mounted on the aeroshell. The Argon from environmental gas bottles is bled into the probe after entry at a rate designed to prevent atmospheric gas from entering the probe until the probe reaches an ambient pressure of at least  $2.5 \times 10^5$  N/m<sup>2</sup> (2.5 bar). The Argon enhances the performance of the foam insulation because the conductivity of the foam closely parallels that of the gas filling its structure. Argon was selected since its thermal conductivity is an order of magnitude lower than that of the incoming atmospheric mixture of hydrogen and helium.

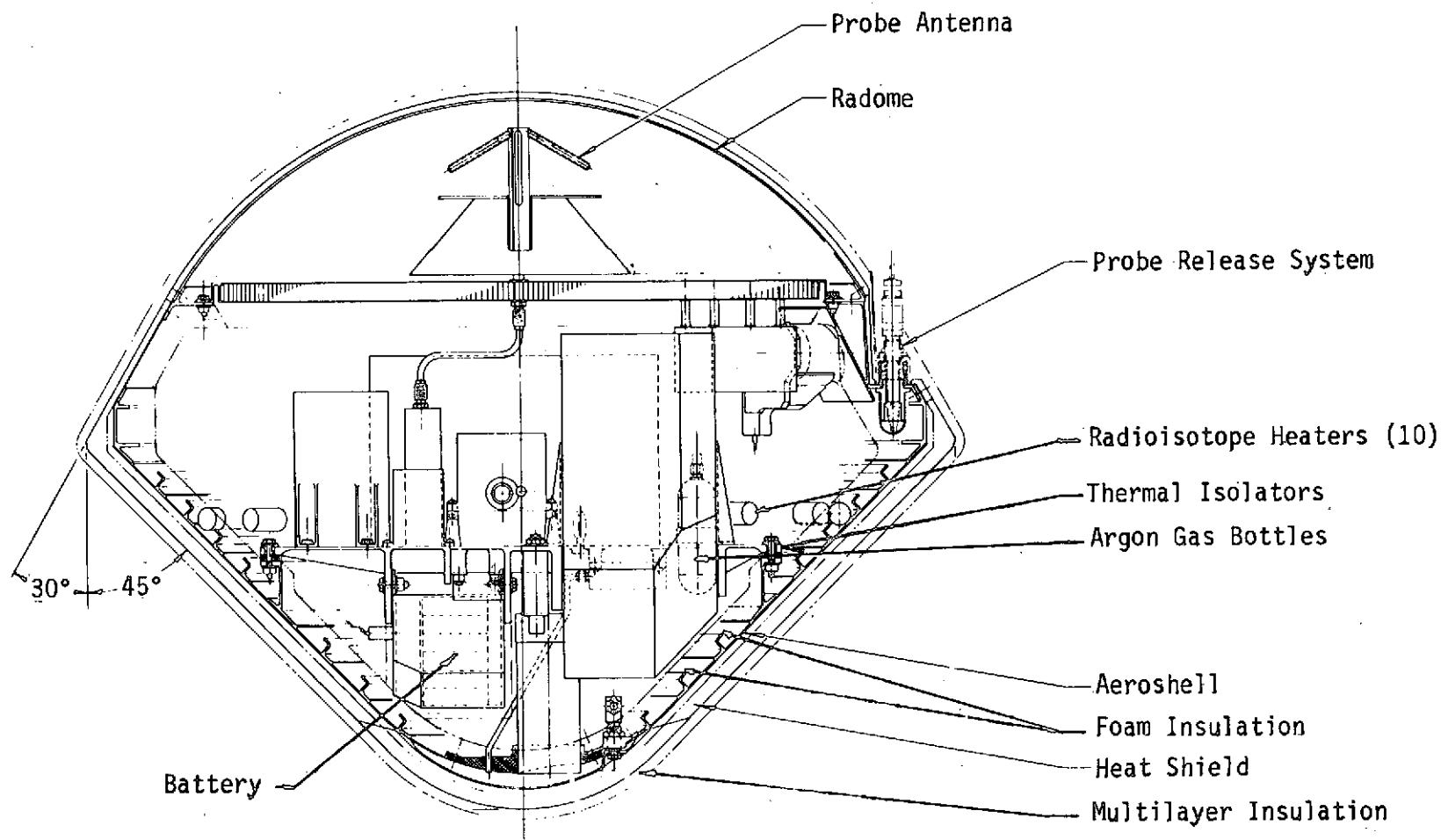


Figure 4.6-21 SU Common Probe Thermal Control Subsystem Hardware

## 5.0 Conclusions

## 5.0 CONCLUSIONS

This study shows that the basic concept of designing a scientific entry probe for the expected range of environments at Saturn or Uranus and making the probe compatible with the interface constraints of the Pioneer spacecraft is feasible for launches in the early 1980s. However, the most significant result of the study is that the amount of hardware commonality between that used in the Pioneer Venus (PV) program and that for the Saturn/Uranus (SU) probe was found to be approximately 85%. This means a SU program can be a low-cost program.

In many cases the SU probe requirements can be incorporated when designing the PV hardware, so both programs can use essentially the same equipment. In other cases--the existing PV read-only memories (ROMs) for example, which are used in several electronic components--the change only involves replacing the PV ROMs with different "off-the-shelf" units. To demonstrate the extent of the commonality between the PV and SU missions, the results of the aerodynamic stability test for the PV small probe is directly useable and the PV tooling for controlling the contour of the aeroshell can be used for both programs with minor modifications. Additional development studies should be conducted in several areas to improve the hardware definitions of our probe design. The recommended studies are tabulated below:

### 1. Heat Shield

The analysis of the Aerotherm heat shield, performed under Contract NAS2-7235 should be extended to include other half-angle cones, including 0.785 rad (45°), and should include experimental verification tests on samples of carbon phenolic and quartz nitrile phenolic in NASA/ARC's plasma-arc facility at the maximum capability.

### 2. Battery

Several approaches for remotely activating individual Ag-Zn battery cells should be designed, developed, and tested on actual models to demonstrate the activation hardware feasibility.

### 3. Nose Cap Jettisoning

Experimental verification tests should be conducted to evaluate: (a) the separation of the nose cap from the heat shield; (b) the effects of unsymmetrical thrust loading on the nose cap and on its relative trajectory to the probe; and (c) the performance of the pyrotechnic thrusters.

### 4. Thermal Control (Foam) Insulation

Experimental verification tests should be conducted on the NOPCO BX-250 foam insulation to evaluate: (a) its thermal conductivity and diffusion rates in a H<sub>2</sub>/He atmosphere; and (b) its basic mechanical properties.

### 5. Electronic Packaging for High Decelerations

Experimental verification tests should be conducted on a representative electronics package to evaluate packaging concepts that will withstand the high deceleration forces.

## 6.0 References

## 6.0 REFERENCES

- 4.1-1 W. M. Brubaker: *Astronaut Breath Analyzer, Final Report*. NASA CR 108384 (Contract NAS9-8371). July 1969.
- 4.2-1 *The Planet Saturn (1970) - NASA Space Vehicle Design Criteria (Environment)*. NASA SP-8091. June 1972.
- 4.2-2 *The Planets Uranus, Neptune and Pluto (1971) - NASA Space Vehicle Design Criteria (Environment)*. NASA SP-8103. November 1972.
- 4.2-3 *Statement of Work for System Definition Study for Saturn/Uranus Atmosphere Probe*. RFP 2-18541. NASA-Ames Research Center, August 1, 1972.
- 4.2-4 *Supplementary Requirements Document, Pioneer Venus Project, Specification PV-1006*. NASA-Ames Research Center, June 8, 1973.
- 4.2-5 R. S. Wiltshire: *Outer Planet Entry Probe System Study, Final Report*. JPL Contract 953311. Vol I-III, August 1972; Vol IV, January 1973. Martin Marietta Corporation, Denver, Colorado.
- 4.2-6 *Digital Accelerometer System (DAS) Design and Performance Characteristics*. D6349-927001. Bell Aerospace Company, Buffalo, New York, April 1972.
- 4.2-7 *Saturn/Uranus Atmospheric Entry Probe - System-Level Definition Study*. P72-44439-1. Martin Marietta Corporation, Denver, Colorado, September 1972.
- 4.3-1 NASA-Ames Research Center, TMX-2824, *Mission Planning for Pioneer Saturn/Uranus Atmospheric Probe Missions*, by B. L. Swenson, E. L. Tindle, L. H. Manning, dated November 16, 1972.
- 4.4-1 *Saturn/Uranus Atmospheric Entry Probe Mission - Spacecraft System Definition Study, Final Report*. 23267-6001-RU-00. TRW, Inc., Redondo Beach, California, July 15, 1973.
- 4.5-1 C. C. Korgel: *Modulation and Coding Techniques for Spacecraft and Planetary Probes*. IRAD Task 48744. Martin Marietta Corporation, Denver, Colorado, December 1973.
- 4.5-2 R. S. Wiltshire: *Outer Planet Entry Probe System Study*. Contract JPL 953311. Martin Marietta Corporation, Denver, Colorado, August 1972.



- 4.5-3 A. J. Viterbi: "Convolutional Codes and Their Performance in Communication Systems." *IEEE Transactions on Communication Technology*, Vol COM-19, No. 5, Part II, October 1971, pp 751-772.
- 4.5-4 J. A. Heller and I. M. Jacobs: "Viterbi Decoding for Satellite and Space Communication." *IEEE Transactions on Communication Technology*, Vol COM-19, No. 5, Part II, October 1971, pp 835-848.
- 4.5-5 D. W. Boyd: *Performance of FSK Systems with Large Uncertainty in the Carrier Frequency*. TM 3361-67-4. Jet Propulsion Laboratory, Pasadena, California, April 3, 1967.
- 4.5-6 S. Z. H. Taqvi: "Some Interesting Simulation Results of the Viterbi Decoder." *National Telemetry Conference 1971 Record*, p 240.
- 4.5-7 R. S. Wiltshire: *Systems-Level Study of a Nonsurvivable Jupiter Turbopause Probe*. MCR-72-91, Vol II (Contract NAS5-11445). Martin Marietta Corporation, Denver, Colorado, June 1972, pp X-1 through X-8.
- 4.5-8 D. C. Hogg and W. W. Mumford: "The Effective Noise Temperature of the Sky." *The Microwave Journal*, Vol 3, No. 3, March 1960, pp 80-84.
- 4.5-9 A. G. Smith: "Extraterrestrial Noise as a Factor in Space Communications." *Proc. IRE*, Vol 48, No. 4, April 1960, pp 593-599.
- 4.5-10 W. W. Mumford and E. H. Scheibe: *Noise Performance Factors in Communication Systems*. Horizon House - Microwave, Inc., Dedham, Massachusetts, 1968, pp 1-2.
- 4.5-11 R. E. Compton: *Spacecraft Receiver System Noise Temperature for the Pioneer Saturn/Uranus Mission*. Technical Note 73-44422-121. Martin Marietta Corporation, Denver, Colorado, April 1973.
- 4.5-12 E. Dyke: "Corrections and Coordination of Some Papers on Noise Temperature." *Proc. IRE*, Vol 49, No. 4, April 1961, pp 814-815.
- 4.5-13 T. S. Saad: *Microwave Engineers' Handbook*, Vol 2. Artech House, Inc., Dedham, Massachusetts, 1971, p 166.

6.0-2

- 4.5-14 H. C. Okean and P. P. Lombardo: "Noise Performance of M/W and mm-Wave Receivers." *The Microwave Journal*, Vol 16, No. 1, January 1973, pp 41-50.
- 4.5-15 *The Planet Saturn (1970) - NASA Space Vehicle Design Criteria (Environment)*. NASA SP-8091. June 1972.
- 4.5-16 *The Planets Uranus, Neptune, and Pluto (1971) - NASA Space Vehicle Design Criteria (Environment)*. NASA SP-8103. November 1972.
- 4.5-17 J. D. Kraus: *Radio Astronomy*. McGraw-Hill, Inc., New York, 1966, p 237.
- 4.5-18 A. R. Giddis: "Influence of External Noise on Antenna Temperature." *Microwaves*, Vol 3, No. 6, June 1964, pp 16-19.
- 4.5-19 R. F. Filipowsky and E. I. Muehldorf: *Space Communications Systems*. Prentice-Hall, Inc., Englewood Cliffs, New Jersey, 1965, pp 186-191.
- 4.5-20 D. A. DeWolf and G. S. Kaplan: *Investigation of Line-of-Sight Propagation in Dense Atmosphere: Phase III, Part I Final Report*. NASA CR-114416 (NASA Ames Research Center Contract NAS2-5310. RCS Laboratories, Princeton, New Jersey, November 1971, pp 5-11.
- 4.5-21 J. S. Hogan, S. I. Rasool, and T. Encrenaz: "The Thermal Structure of the Jovian Atmosphere." *Journal of the Atmosphere Sciences*, Vol 26, No. 5, Part 1, September 1969, pp 898-905.
- 4.5-22 M. B. McElroy: "The Ionospheres of the Major Planets." *Space Science Reviews*, Vol 14, No. 3/4, March/May 1973, pp 460-473.
- 4.5-23 R. C. Whitten and I. G. Poppoff: *Fundamentals of Aeronomy*, Wiley & Sons, Inc., New York, 1971, pp 282-326.
- 4.5-24 C. W. Allen: *Astrophysical Quantities*. The Athlone Press, London, 1955, pp 131-134.
- 4.5-25 K. Davies: *Ionospheric Radio Propagation*. Dover, New York, 1966, pp 339-341.

- 4.5-26 J. P. Liephart, et al: "Penetration of the Ionosphere by VLF Radio Signals - Results of the LOFTI I Experiment." *Proc. IRE*, Vol 50, No. 1, January 1962, pp 6-17.
- 4.5-27 A. Himy: *Development of a Heat-Sterilizabile 40-AH Sealed Silver-Zinc Cell*. NASA CR-1812. May 1971.

## Appendix

APPENDIX A

PRELIMINARY STRESS ANALYSIS

## APPENDIX A - PRELIMINARY STRESS ANALYSIS

### SATURN URANUS PROBE

A preliminary stress analysis was done to establish the size requirements of the major structural elements and confirm the feasibility and integrity of the design. The two conditions considered for the analysis were the maximum entry deceleration and atmospheric collapse pressure of one bar for the aft bulkhead. The booster launch environments result in very low load levels compared to the entry condition and designs only the local interface points.

For a final design additional analysis is recommended to assure integrity of all detail structural elements. Analysis is recommended in areas of:

- 1) Shock environment levels and allowables
- 2) Model structure to establish accurate internal loading - Equipment support beams and cylinder
- 3) Launch and entry acoustic environments
- 4) Determine mode shapes and frequencies of probe for dynamic and loads analysis
- 5) Computer analysis for aeroshell optimization
- 6) Thermal stress analysis

### Preliminary Stress Analysis

Margin of Safety Table

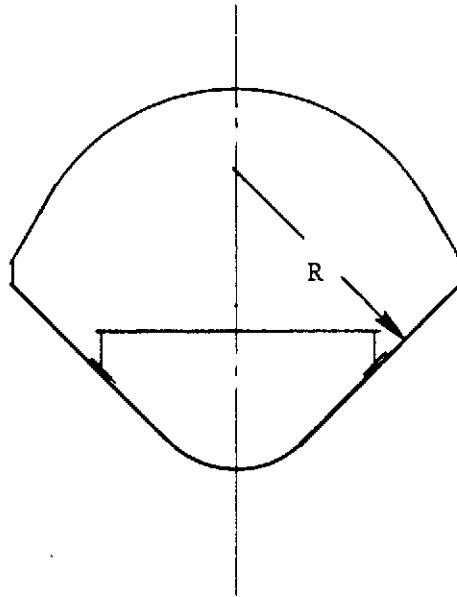
Part Name	Critical Condition	Failure Mode	M.S.
Aeroshell Forebody	Maximum Entry	General Instability	+1.22
Aeroshell Frame	Maximum Entry	Flange Crippling	+ .44
Aeroshell Skin	Maximum Entry	Buckling Between Fr.	+ .09
Base Cover Cone	Collapse Pressure	Buckling of Cone	+ .10
Aft Bulkhead	Collapse Pressure	Shear	+ .49
H/C Core			
Face Sheet	Collapse Pressure	Comp. Buckling	+1.20*
Support Ring	Collapse Pressure	Flange Bonding	+ .14**
Equip. Support Ribs	Maximum Entry	Rib Bonding	0
Antenna Arm	Maximum Entry	Bonding (weld)	+ .36
Antenna Petal	Maximum Entry	Bonding (weld)	+ .50

\* Designed by deflection

\*\* Many ribs analyzed and sized for 0 margin @ 60,000 psi

Design

Data



Peak Deceleration 585 g's Limit

Ultimate Design Factor 1.25

Outside Dia: 34.0 in.

Weight = 176 lbs.

15% Contingency = 26 lbs

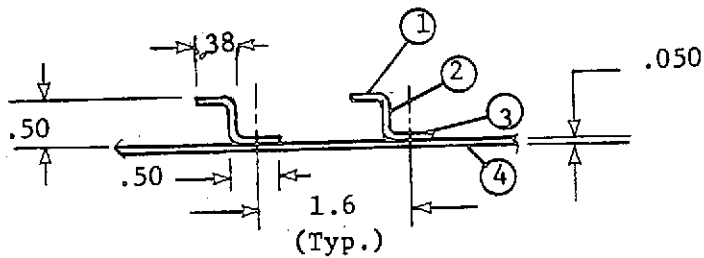
Weight Total = 202 lbs

$$\begin{aligned} \text{Average Pressure} &= \frac{202 (585) (1.25)}{17.0^2 \pi} \\ &= 163 \text{ p.s.i. ult.} \end{aligned}$$

Aeroshell Analysis

For R = 19 in. (approximately mid cone location)

$$\begin{aligned} \text{Hoop Load} &= PR = 163 (19) \\ &= 3100 \text{ lbs/in.} \end{aligned}$$



Section Properties

No.	a	y	ay	ay <sup>2</sup>	I <sub>o</sub>
1.	.34 x .040 = .0136	.50	.0068	.0034	-
2.	.50 x .040 = .0200	.30	.0060	.0018	.00042
3.	.46 x .040 = .0184	.07	.0013	.0001	-
4.	1.6 x .050 = .0800	.025	.0020	.0005	-
	.1320		.0161	.0058	.00042

$$\bar{y} = \frac{.0161}{.1320} = .122 \text{ in.}$$

$$I = .00042 + .0058 - .122 (.0161)$$

$$I = .0043 \text{ in.}^4$$

General Stability Check of Aeroshell

$$P_F = \frac{.736 E \bar{t}}{L R^{3/2}} \left[ \frac{12 I}{b_s \bar{t}} \right]^{3/4}$$

$$\bar{t} = \frac{.1320}{1.6} = .0825$$

$$b_s = 1.6$$

$$R = 19$$



$$P_F = \frac{.736 (10^7) (.0825)}{10 (19)^{3/2}} \left[ \frac{12 (.0043)}{1.6 (.0825)} \right]^{3/4}$$

$$= \underline{362 \text{ psi}} \text{ (failing pressure)}$$

$$\text{M.S.} = \frac{362}{163} - 1 = + \underline{1.22}$$

Check Frame Flange Crippling

$$b/t = \frac{.38}{.040} = 9.5$$

$$F_{cc} = 54,000 \text{ psi}$$

$$f_c = \frac{3100}{.0825} = \underline{37,600 \text{ psi}}$$

$$\text{M.S.} = \frac{54,000}{37,600} = \underline{+1.44}$$

Buckling Check of Cone Skin Between Frames

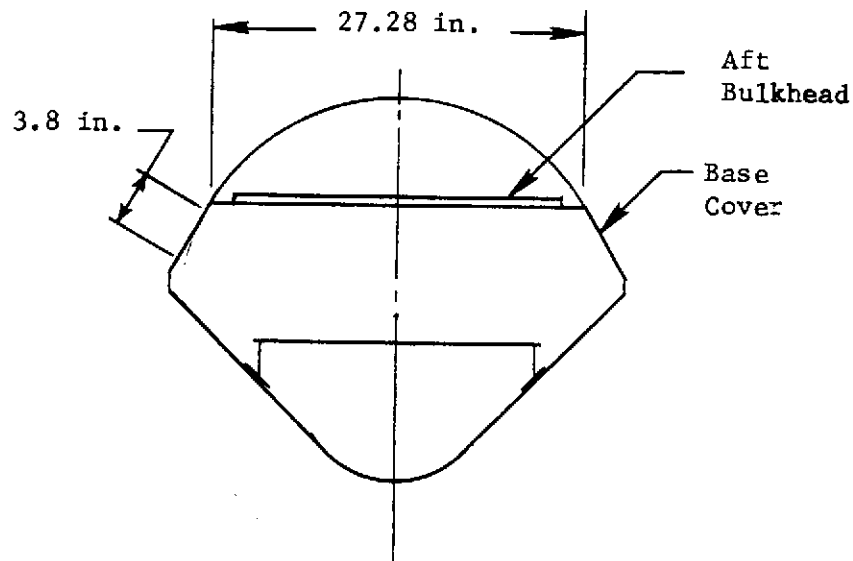
$$b/t = \frac{1.60}{.050} = 32$$

$$F_{cc} = 41,000 \text{ psi}$$

$$\text{M.S.} = \frac{41,000}{37,600} - 1$$

$$= \underline{+0.09}$$

Base Cover Analysis



Check the capability of aft end to take the 1 bar collapse pressure.

Try  $t = .050$  in cone for buckling

$$\frac{P_R}{t} = \frac{(14.7)(1.25)(16)}{.050} = \underline{5,900 \text{ psi}}$$

$$b/t = \frac{3.8}{.050} = 76$$

$$F_{cc} = 6500 \text{ psi}$$

$$\text{M.S.} = \frac{6500}{5900} - 1 = \underline{+.10}$$

### Aft Bulkhead Analysis

Pressure Load = 14.7 psi on flat plate

$$\text{Load} = \left(\frac{27.28}{2}\right)^2 \pi 14.7 = 8600 \text{ lbs limit} \\ = 10,750 \text{ lbs ult.}$$

Max. bending occurs at center of plate using Roark Case 1 Table X.

$$S = \frac{3w}{8\pi mt^2} (3m + 1) = \frac{3(10,750)}{8\pi\left(\frac{1}{3}\right)(1.0)^2} \left(3 \times \frac{1}{3} + 1\right) \\ = \underline{4,240 \text{ psi}} \quad \text{Based on } 1.0'' t$$

$$f_b = \frac{6M}{bt^2} = S \quad \text{For rectangular section}$$

$$M = \frac{S b t^2}{6} = \frac{(4240)(1.0)(1.0^2)}{6} \\ = 706 \text{ in.-lbs}$$

Now to determine required stress skin range required for this moment, using Stressskin Products Co. SDAM 100

Try cell height of .5 in. with 1/4" cell

Skin load from bending/in.

$$P = \frac{706}{.5} = 1412 \text{ lbs ultimate}$$

Local panel buckling design curve, Fig 3.2.4a PH15-7 M<sub>0</sub> (RH1125)

$$\text{Core } t_c = .0025 \text{ in.}$$

t	f <sub>c</sub> psi	F <sub>CR<sub>L</sub></sub> psi	M.S.
.010	141,200	121,000	-.14
.015	94,200	138,000	+.46
.020	70,600	144,000	+1.04

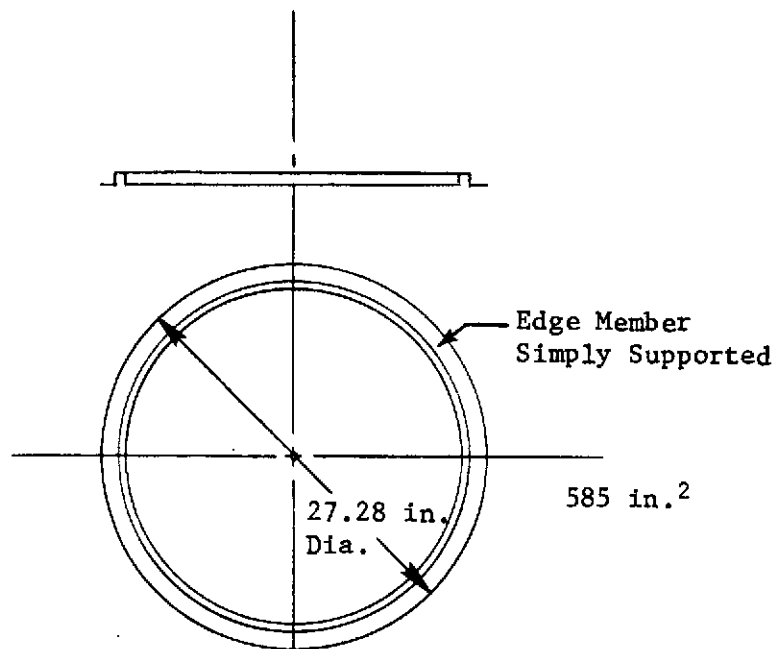
For .75 cell height

t	f <sub>c</sub>		
.015	62,800		-1.20

Check inertia loading on Honeycomb ranges

Antenna weight = 9.5 lbs

Panel weight = .035 (.277) = .0097 lbs/in.<sup>2</sup>



$$\begin{aligned} \text{Distributed Load} &= .0097 (690) (1.25) \left( \frac{27.28}{2} \right)^2 \pi \\ &= 4890 \text{ lbs ult.} \end{aligned}$$

$$\text{Antenna Load} = 2.5 (690) (1.25)$$

$$4'' \text{ Radius} = 2160 \text{ lbs ult.}$$

For antenna load (Case 3 Table X Roark)

$$\text{Max Stress} = \frac{3W}{2\pi mt^2} \left[ \frac{1}{2} (m-1) + (m+1) \log \frac{a}{r_o} - (m-1) \frac{r_o^2}{2a^2} \right]$$

$$\begin{aligned} r_o &= 4.0 & W &= 2160 \text{ lbs ult.} \\ a &= 13.64 & m &= 1/.3 \end{aligned}$$

$$\begin{aligned} S_{\text{max}} &= \frac{3(2160)}{2\pi(1/.3)(1.0^2)} \left[ \frac{1}{2} (1/.3-1) + (1/.3+1) \log \frac{13.64}{4} - \frac{(1-1)}{.3} \frac{4.0^2}{2(13.64)^2} \right] \\ &= 310 \left[ \frac{2.33}{2} + 4.33(1.23) - 2.33(.043) \right] \\ &= 310(6.39) = 1980 \text{ psi (based on 1" t)} \end{aligned}$$

$$M_c = \frac{S b t^2}{6} = \frac{1980(1.0)(1.0^2)}{6} = \underline{330 \text{ in. lbs}}$$

Distributed inertia load

$$M_d = 706 \left( \frac{10,750}{4240} \right) = \underline{179 \text{ in. lbs}}$$

$$\Sigma = 330 + 179 = \underline{509 \text{ in.-lbs ult. max.}}$$

This is not as critical as pressure loads which is 706 in.-lbs. ult.

Core check

$$\text{Shear} = \frac{10,750 \text{ lbs}}{27.28 \pi \text{ in.}} =$$

$$= 125.5 \text{ lbs/in.}$$

$$f_s = \frac{125.5}{.5} = \underline{251 \text{ psi (gross)}}$$

Fig. 2.3.1.4a SDAM-100

Core Density = 7.65 PCF

Depth = .5

$F'_s$  = 200 psi (transverse) (no good)

Try  $t_c$  = .0025

Core Density = 9.56 PCF

$F'_s$  = 270 psi (transverse)

$$\text{M.S.} = \frac{270}{251} - 1 = +.07 \text{ (not used)}$$

For depth of .75 in.

$$F_s = 250 \text{ psi}$$

$$f_s = \frac{125.5}{.75} = \underline{168 \text{ psi}}$$

$$\text{M.S.} = \frac{250}{168} - 1$$

$$= \underline{+.49}$$

### Aft Bulkhead Deflection Analysis

Properties of PH 15-7 MO

$$E_c = 30 \times 10^6 \text{ psi}$$

$$G = 11.0 \times 10^6 \text{ psi}$$

Look at deflections.

For .50 thick core .0025 in. .25 cell with .015 face sheet thickness

Based on Roark Table X Cond. 1

Bending deflection for face plate

$$y_{\max} = \frac{3W(m-1)(5m+1)a^2}{16\pi E m^2 t^3}$$

$$I_{.50} \text{ Plate} = \frac{(1.0)(.5^3)}{12} = .0104 \text{ in.}^4$$

$$I_{H/C} \text{ Panel} = 2 (.25)^2 (1 \times .015) = .001875$$

$$y_{\max} = \left( \frac{.0104}{.001875} \right) \left[ \frac{3(10,750)(2.33)(16.7)(13.64)^2}{16\pi 30 \times 10^6 \left( \frac{1}{.3} \right)^2 (.5^3)} \right]$$

$$= .62 \text{ in.}$$

For face  $t = .020$

$$y = .62 \left( \frac{.015}{.020} \right) = 0.465 \text{ in.}$$

Shear deflection



$$y = \frac{P_s L}{A_s G}$$

$$P_s = pA = p\pi x^2$$

$$L = x (\sin 45^\circ) = .707 x$$

$$A_s = (.5)(.0025(4)\pi(2x)) = .01 \pi x \text{ (core only)}$$

$$L = dx$$

$$G = 11.0 \times 10^6 \text{ psi}$$

$$y = \int \frac{p\pi x^2 dx}{.01\pi x G} = \frac{p}{.02 G} \int_0^{13.64} x dx$$

$$= \left[ \frac{18.4 x^2}{.01 (11.0 \times 10^6) (2)} \right]_0^{13.64} = \underline{.016 \text{ in.}}$$

Small compared to bending.

Check increasing core depth to .60 and .75 in.

Deflection is proportional to I using .015 t face sheet

$$I_{.60} = 2(.015)(1.0)(.30^2) = .0027 \text{ in.}^4$$

$$I_{.75} = 2(.015)(1.0)(.375^2) = .00422 \text{ in.}^4$$

$$y_{.60} = .62 \left( \frac{.001875}{.0027} \right) = .43 \text{ in.}$$

$$y_{.75} = .62 \left( \frac{.001875}{.00422} \right) = \underline{.276 \text{ in.}}$$

#### Aft Bulkhead Support Ring Analysis

Flange bending of support ring

Length of leg = 1.45 in.

$$\text{Load} = \frac{10,750 \text{ lbs}}{27.28 \pi} = 126 \text{ lb/in. ult. pressure loading}$$

Bending moment = 126 (1.3)

$$= \underline{164 \text{ in.-lbs}}$$

Material - 7075-T7351

$$F_{TU} = 62,000 \text{ psi short transverse}$$

Try  $t = .090$

$$f_b = \frac{6xM}{bt^2} = \frac{6(164)}{(1.0)(.090^2)}$$
$$= 121,000 \text{ psi (too high)}$$

$$F_b = 1.5 \times 62,000 = 93,000 \text{ psi}$$

Try  $t = .11$

$$F_b = \frac{6(164)}{(1.0)(.11)} = \underline{81,200 \text{ psi (o.k.)}}$$

Could be stepped down at outer edge.

$$M.S. = \frac{93,000}{81,200} = \underline{+1.14}$$

#### Equipment Support Deck Analysis

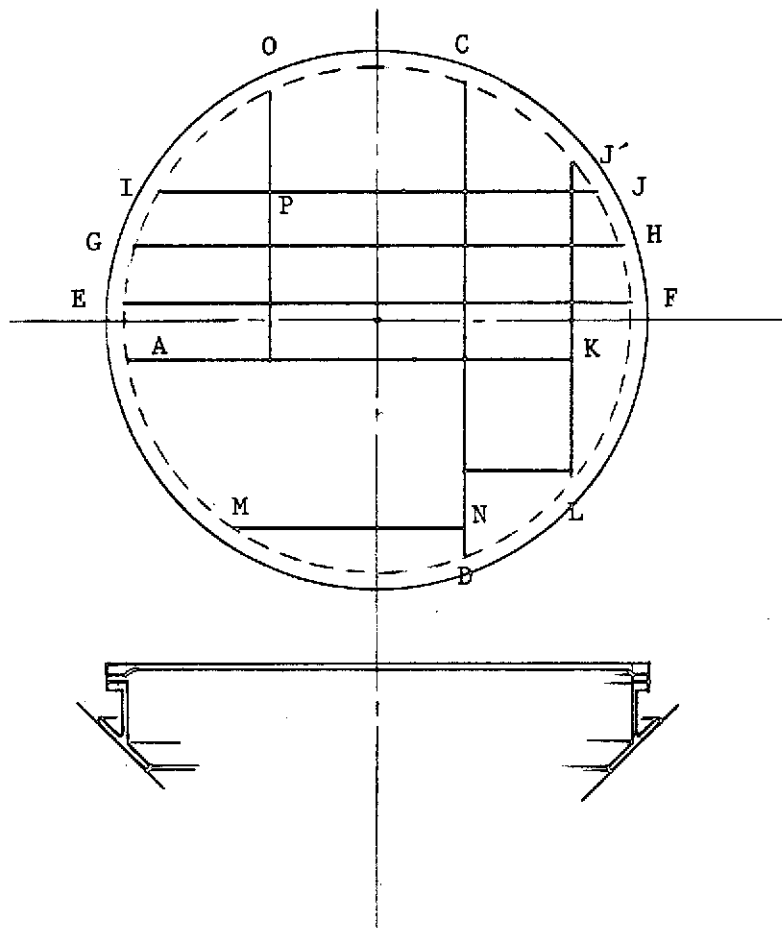
Check equipment support shelf for inertia loads due to maximum entry loads.

Equipment consists of:

	<u>Lbs</u>
Neutral mass spectrometer	20.0
Battery	16.0
Power Control Unit (PCU)	6.25
DTU	4.0
Accelerometer	2.5
Pressure Transducer	1.0
Environmental Tanks - 2 @ .6	1.2
Signal Conditioner	.3
Temp. Electronics	.7
Eng. Pressure Transducer	.3
Cabling	<u>7.1</u>
	59.7 lbs
Nephelometer on back plate	1.1 lb

For analysis of structure, the weight of structure is assumed to be 20% of the equipment weight, plus  $\frac{7.1}{52.6} = 13.5\%$  for

cabling.  $\Sigma = 33.5\%$ . Analysis is based on 720 g ult. instead of the current 585 x 1.25 - 730 g load. An unconservative analysis results in less than 2% error which was not updated at this time.



The equipment support beams were sized as rectangular sections to allow maximum room between beams for equipment. No stress analysis was done on the mockups of equipment for the entry inertia loading. This will be an additional task required if these will be subjected to the inertia loads of entry environment.

Plate thickness required to avoid compression buckling: (top plate of equipment platform)

For 60,000 psi stress

$b/t = 21$  both sides supp. Ref. NASA SAM Fig. C1.3.1-13

2.5 in. stiffener spacing

$$t_{\text{req'd}} = \frac{2.5}{21} = \underline{.119 \text{ in. (use .120 in.)}}$$

Shear at Point A on Beam A-K

$$R_1 = 6.25 (1.335) (720) = 6,000 \text{ lbs ult.}$$

$$\begin{aligned} \text{Area at end of beam} &= .32 \times (.40 + .25) \\ &= .21 \text{ in.}^2 \end{aligned}$$



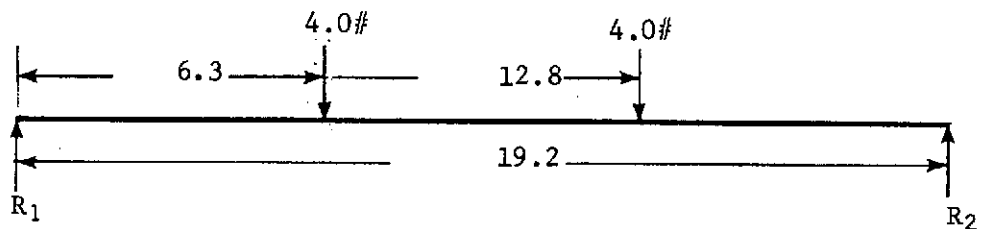
$$f_s = \frac{6000}{.21} = \underline{28,600 \text{ psi}} \quad (\text{o.k.})$$

$$F_s = 39,000 \text{ psi}$$

$$\text{M.S.} = \frac{39,000}{28,600} - 1 = \underline{+.36}$$

The battery box is assumed to carry its own load to the last attachment at the ends of the battery case to the support beam.

Beam E-F



$$R_2 = \frac{6.3(4.0) + 12.8(4.0)}{19.2} = 3.97 \text{ lb (use 4.0 lb)}$$

$$M = 6.3(4.0) = 25.2 \text{ in.-lbs}$$

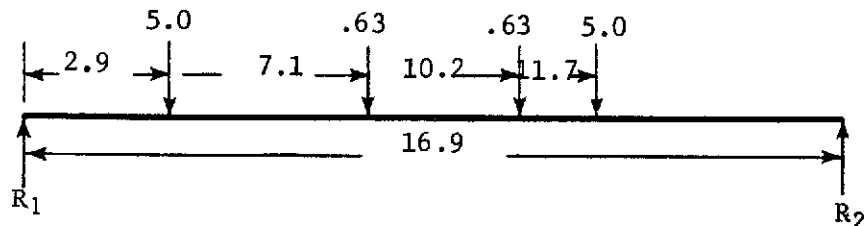
Include structure + wiring as 33.5% factor at the 720 g ult.

$$M = (25.2)(1.335)(720) = 24,200 \text{ in.-lbs}$$

For depth of 3.0 in.

$$\begin{aligned} \text{Width required} &= \frac{6(24,200)}{(3.0^2)(60,000)} \\ &= \underline{.27 \text{ in.}} \end{aligned}$$

Mass Spectrometer Beam A-K



1 g cond.

$$R_2 = \frac{2.9(5.0) + 7.1(.63) + 10.2(.63) + 11.7(5.0)}{16.9}$$

$$= 5.0 \text{ lbs}$$

$$R_1 = 6.25 \text{ lbs}$$

$$M_{\max} = 5.0(5.2) = 26.0 \text{ in.-lbs}$$

At 720 g's ult + 33.5% for wiring and structure

$$M_{\max} = 26.0(1.335)(720) \\ = 25,000 \text{ in.-lbs ult.}$$

For 2" deep rectangular section

$$t_{\text{req'd}} = \frac{6(25,000)}{2.0^2(60,000)} = .625 \text{ in.}$$

For depth of 2.5 in.

$$t_{\text{req'd}} = \frac{6(25,000)}{2.5^2(60,000)} = \underline{.40 \text{ in.}}$$

1.5 in. from  $R_1$

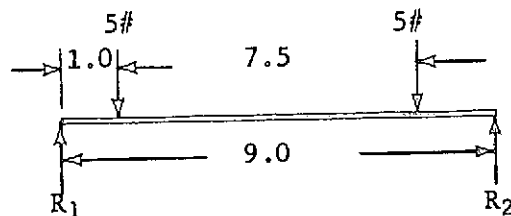
$$M = 6.25(1.5)(1.335)(720) = 9,000 \text{ in.-lbs ult.}$$

$$\text{Depth required} = \left[ \frac{9,000(6)}{.4(60,000)} \right]^{1/2} = \underline{1.5 \text{ in.}}$$

2.9 in. from  $R_1$

$$M = 6.25(2.9)(1.335)(720) = 17,400 \text{ in.-lbs ult.}$$

$$\text{Depth required} = \underline{2.1 \text{ in.}}$$



$$R_2 = \frac{1.0(5) + 7.5(5)}{9.0} = 4.7 \text{ lbs}$$

$$M_{\text{max}} = (4.7)(1.5) = 7.1 \text{ in.-lbs}$$

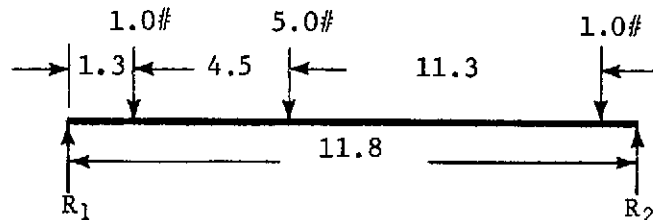
$$M = 7.1(1.335)(720) \\ = 6,800 \text{ in.-lbs ult.}$$

For depth of 1.5 in.

$$t_{\text{req'd}} = \frac{6(6800)}{1.5^2(60,000)} \\ = \underline{.30 \text{ in.}}$$

### Beam J'-L

1 g cond.



$$R_2 = \frac{1.3(1.0) + 4.5(5.0) + 11.3(1.0)}{11.8}$$

$$= 3.0 \text{ lbs.}$$

$$R_1 = 4.0 \text{ lbs.}$$

$$M_{\text{max}} = 4.5(4.0) - 3.2(1.0) \\ = 14.8 \text{ in.-lbs.}$$

$$M = 14.8(1.335)(720) \\ = 14,200 \text{ in.-lbs ult.}$$

For depth of 1.5

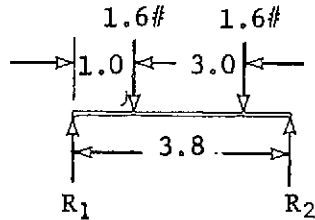
$$\text{Width required} = \frac{6(14,200)}{1.5^2(60,000)} \\ = .633 \text{ in.}$$

For 2.0 in. depth

$$\text{Width} = \frac{6(14,200)}{2.0^2(60,000)} \\ = \underline{.355 \text{ in. (use .36)}}$$

Beam O - P

1 g cond.



$$R_2 = \frac{1.6(1.0) + 1.6(3.0)}{3.8}$$

$$= 1.7 \text{ lbs}$$

$$R_1 = 1.5 \text{ lbs}$$

$$M_{\text{max}} = 1.5(1.0) = 1.5 \text{ in.-lbs}$$

$$M = 1.5(1.335)(720)$$

$$= 1440 \text{ in.-lbs ult.}$$

For 1.5 in. depth

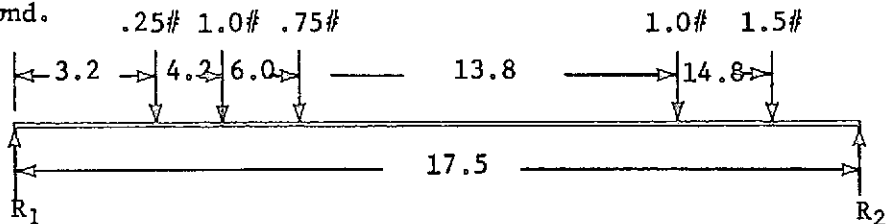
$$t_{\text{req'd}} = \frac{6(1440)}{1.5^2(40,000)}$$

$$= .096 \text{ in.}$$

For 1.0 in. depth use .25" t

Beam C - D

1 g cond.



$$R_2 = \frac{.25(3.2) + 1.0(4.2) + .75(6.0) + 1.0(13.8) + 1.5(14.8)}{17.5}$$

$$= 2.5 \text{ lbs}$$

$$M_{\text{max}} = 2.5(3.7) = 1.5(2.7)$$

$$= 5.2 \text{ in.-lbs}$$

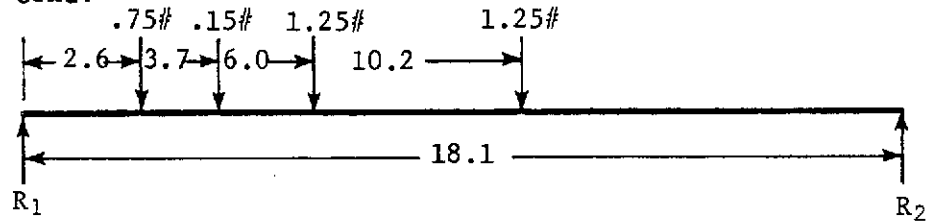
$$M = (5.2)(1.335)(720) = 5,000 \text{ in.-lbs ult.}$$

For depth of 1.5 in.

$$t_{\text{req'd}} = \frac{6(5000)}{1.5^2 (60,000)} = \underline{.27 \text{ in.}}$$

Beam G - H

1 g cond.



$$R_2 = \frac{2.6(.25) + 3.7(.15) + 6.0(1.25) + 10.2(1.25)}{18.1} = 1.24 \text{ lbs}$$

$$P_2 = 1.66 \text{ lbs}$$

$$M_{\text{max}} = 1.24(7.9) = 9.8 \text{ in.-lbs}$$

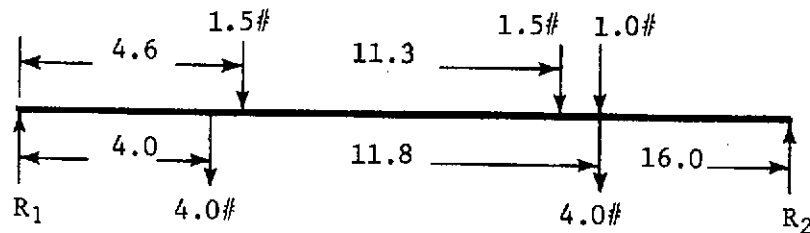
$$M = 9.8 (1.335)(720) = 9400 \text{ in.-lbs}$$

For 2.0 in. depth beam

$$t_{\text{req'd}} = \frac{6(9400)}{2.0^2 (50,000)} = \underline{.282 \text{ in.}}$$

Beam I - J

1 g cond.



$$R_2 = \frac{4.0(4.0) + 1.5(4.6) + 1.5(11.3) + 1.0(11.8) + 4.0(11.8)}{16.0}$$

$$= 6.2 \text{ lbs}$$

$$R_1 = 5.8 \text{ lbs}$$

$$M_{\text{max}} = 4.7(6.2) - (4+1)(.5)$$

$$= 26.6 \text{ in.-lbs}$$

$$M = 26.6(1.335)(720) = 25,600 \text{ in.-lbs ult.}$$

For 3.0 in. depth

$$t_{\text{req'd}} = \frac{6(25,600)}{3.0^2(60,000)} = .284 \text{ in. (Use .29 in.)}$$

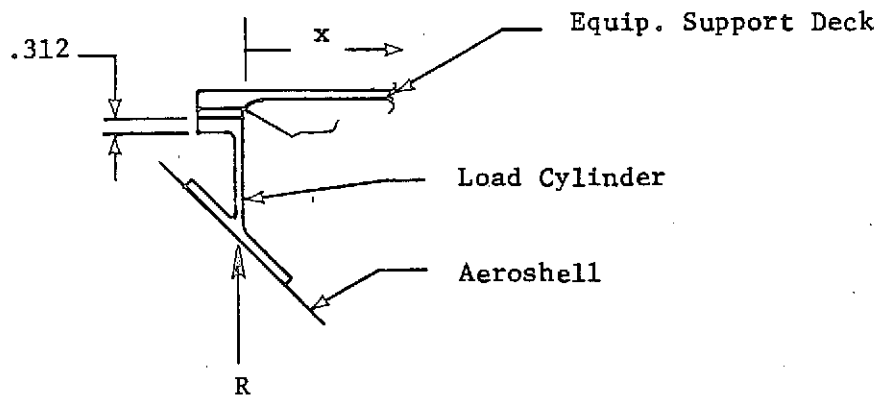
$$2 \text{ inches from Rt. End } M = 6.2(2.0)(1.335)(720) = 11,900 \text{ in.-lb}$$

$$\text{Req'd depth} = \left( \frac{6(11,900)}{(.29)(60,000)} \right)^{\frac{1}{2}} = \underline{2.02 \text{ in.}}$$

1 inch from end

$$\text{Req'd depth} = \left[ \frac{6(6,000)}{(.29)(60,000)} \right]^{\frac{1}{2}} = \underline{1.42 \text{ in.}}$$

Equipment Support Ring Analysis



Beam reaction at Point "A" for a 1 g load is 6.75 lbs.

At 720 g ult. load plus 33.5% for wiring harness

$$\text{Reaction is } 6.75(1.335)(720)$$

$$R = 6000 \text{ lbs}$$

Assume this is reacted locally at beam.

x	M	Req'd Depth for width = .40
1.0	6,000	1.22
2.0	12,000	1.73
2.9	17,400	2.08

Load cylinder check monocoque compression capability

$$\sigma_{cr} = \frac{K_c \pi^2 E}{12 (1-\nu^2)} \left( \frac{t}{L} \right)^2$$

$$Z = \frac{L^2}{rt} \sqrt{1-\nu^2}$$

$$L = 1.5 \text{ in.}$$

$$r = 9.5 \text{ in.}$$

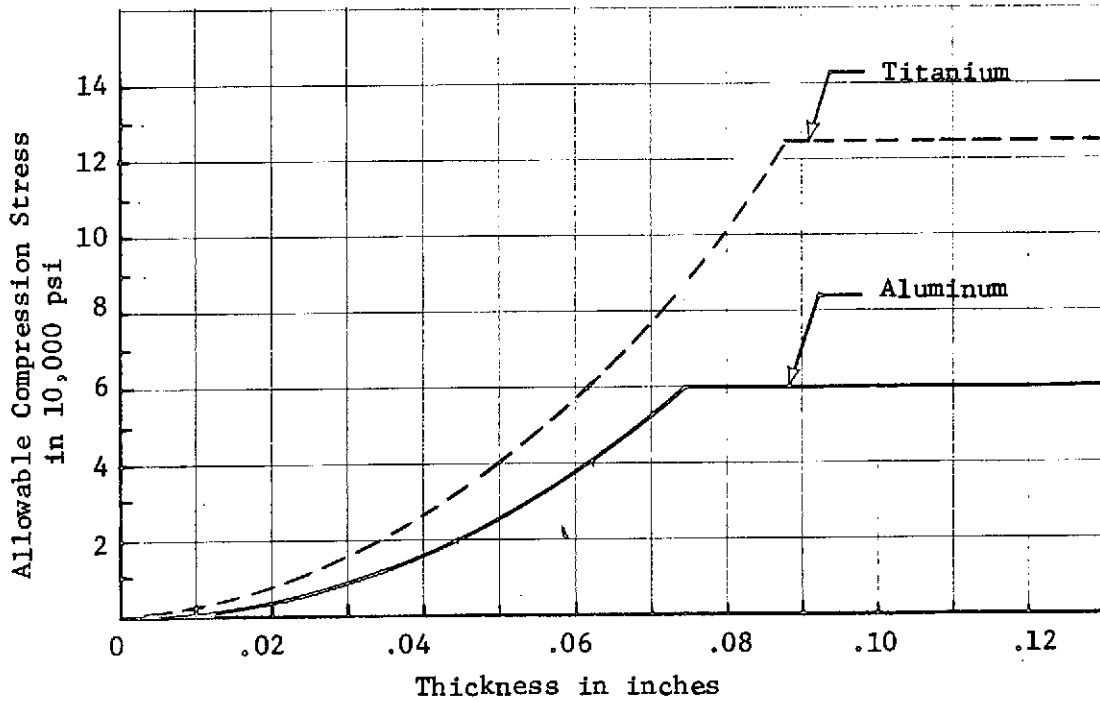
$$Z = \frac{1.5^2}{9.5t} \sqrt{1-.3^2} = \frac{.226}{t}$$

#### Aluminum

t	Z	r/t	K <sub>c</sub>	σ <sub>cr</sub>	P <sub>cr</sub>
.030	7.55	316	2.5	9,000	16,100
.060	3.77	158	2.5	36,000*	129,000
.100	2.26	95	2.5	100,000	596,000
.150	1.50	63	2.5	60,000*Yield	358,000
				225,000	625,000
				60,000 Yield	1700,000

#### Titanium

t	σ <sub>cr</sub>	P <sub>cr</sub>
.030	14,400	25,800
.060	57,700*	206,000
.100	160,000* 126,000	950,000/750,000
.150	360,000 126,000	1020,000/356,000



Equipment support loading on load cylinder is:

Point	1 g load	Ult. load
A	6.25 lbs	6,000 lbs ult.
C	2.5	
D	6.8	6,550 lbs
E	4.0	
F	4.0	
G	1.7	
H	1.2	
I	5.8	
J+J'	6.2+3.0 = 9.2	8,850 lbs
L	4.0	
M	4.7	
N	5.3	

Using Aluminum cylinder,

J + J' are assumed to apply the 8,850 lb load over 2.0 in. width of load cyl.

$$\text{Avg. Stress } Q_t = .10 = \frac{8850}{2(.10)} = \underline{44,200 \text{ psi}}$$

Allowable = 60,000 psi in compression



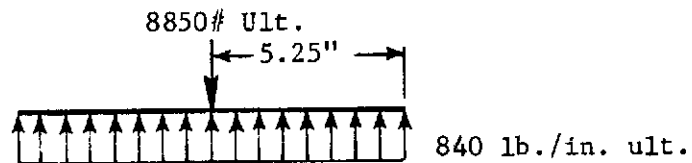
Look at bending of load cylinder

$$\text{Avg. load on cylinder from A/S} = \frac{70(720)}{19.5\pi} = 840 \text{ lb-in. ult.}$$

At J + J' load = 8850 lbs ult.

$$\text{Length of cylinder circumference required to react the 8850 lb load} = \frac{8850}{840} = 10.5 \text{ in.}$$

Approx. Moment



$$M = 4425 \left( \frac{5.25}{2} \right) = 11,600 \text{ in.-lbs ult.}$$

Cap load of cylinder = 11,600 in.-lb

Height = 1.8 in.

$$\frac{11,600}{1.8} = 6500 \text{ lbs ult.}$$

For .2 x .8 cap A = 16 in.

$$f_b = \frac{6500}{.16} = \underline{40,500 \text{ psi}} \quad (\text{o.k.})$$

At beam point support areas make cylinder thickness .10 in. for 1.0 in. width to carry comp. load. (2.0" @ J + J')

### Antenna

Check "petal" bending

Length = 2.64 inch

Base width = 1.7 inch

Assume t = .063 inch

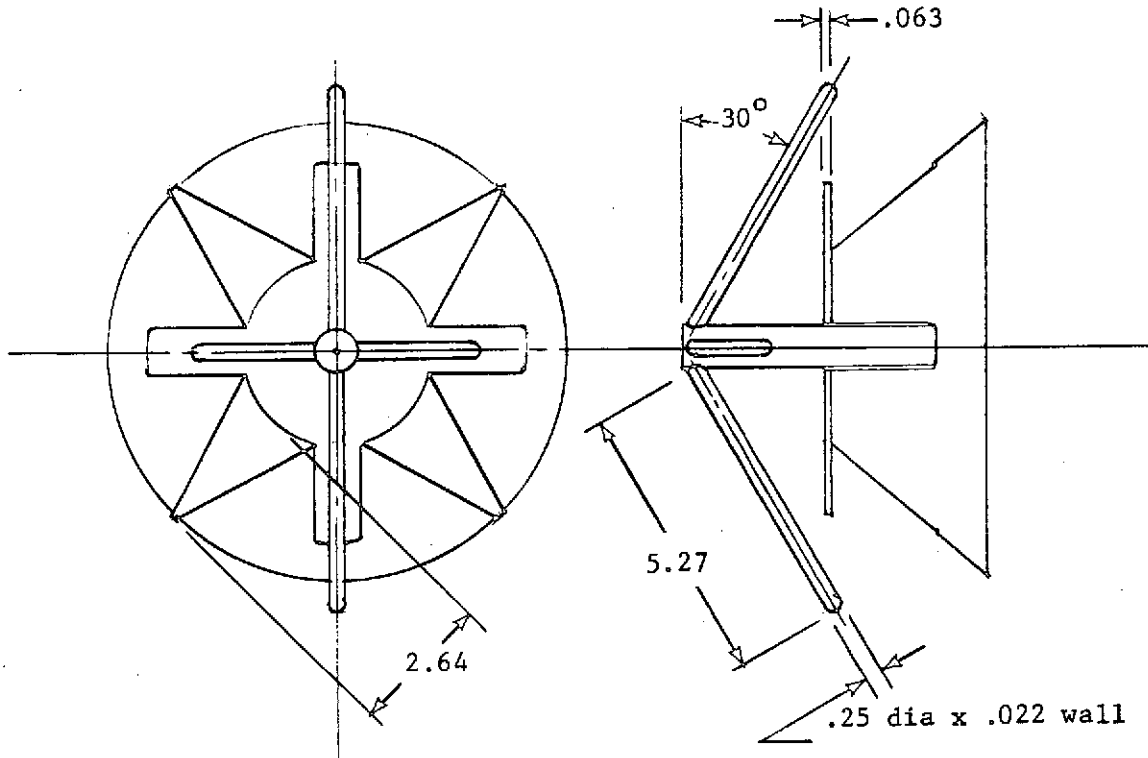
$$\begin{aligned} \text{Wt.} &= (1.7)(2.64) \left( \frac{1}{2} \right) (.063)(.10) \\ &= .0141 \text{ lb} \end{aligned}$$

$$\begin{aligned} M &= 720(.0141) \left( \frac{2.64}{3} \right) \\ &= 9.00 \text{ in.-lb} \end{aligned}$$

$$\begin{aligned} f_b &= \frac{6M}{bt^2} = \frac{6(9.00)}{(1.7)(.063^2)} \\ &= \underline{8,000 \text{ psi}} \quad (\text{o.k.}) \end{aligned}$$

$$F_{ty} = 12,000 \text{ psi (yield)}$$

$$\text{M.S.} = \frac{12,000}{8,000} = \underline{+1.50}$$



### Antenna Arm

Length - 5.27 in.

Aluminum 6061-T6 Tube

1/4 x .022 wall

$$A = .01576 \text{ in.}^2$$

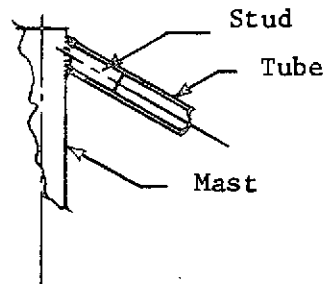
$$I = .000103 \text{ in.}^4$$

$$\text{Wt.} = .00156 \text{ lb.-in.}$$

$$\text{Cantilever Moment} = 5.27(.00156) \left( \frac{5.27}{2} \right) (.866)$$

$$\text{@ 1 g} \quad \quad \quad = .0187 \text{ in./lbs}$$

$$\text{@ 720 g's M} \quad \quad = 13.5 \text{ in.-lbs ult.}$$



For solid stud

$$I = .000192 \text{ in.}^4$$

$$f_b = \frac{M c}{I} = \frac{13.5(.125)}{.000192}$$

$$= \underline{8,800 \text{ psi}}$$

Weld all. 12,000 yield, 16,000 ult.

$$\text{M.S.} = \frac{12,000}{8800} - 1 = \underline{+.36}$$

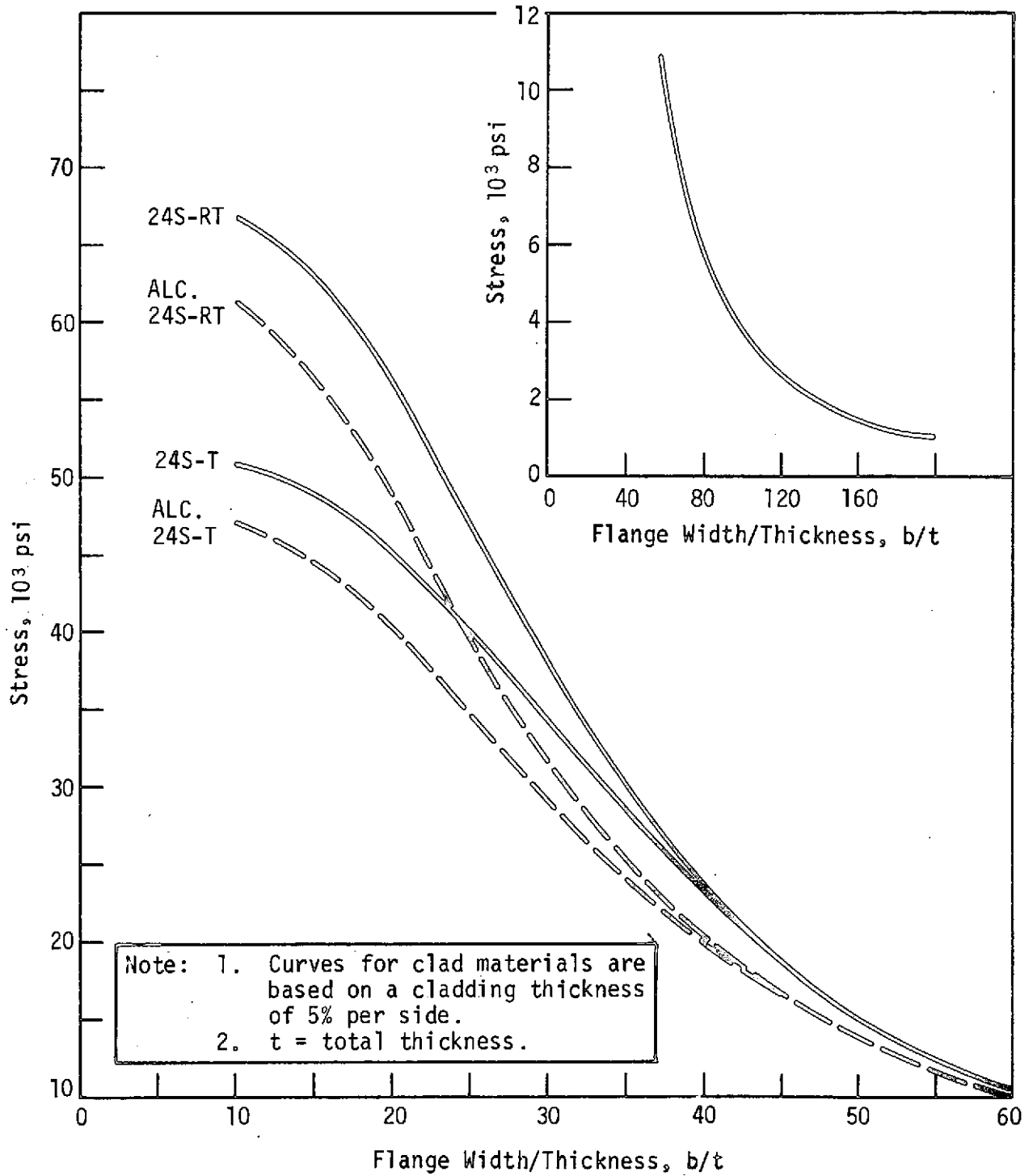
For Tube

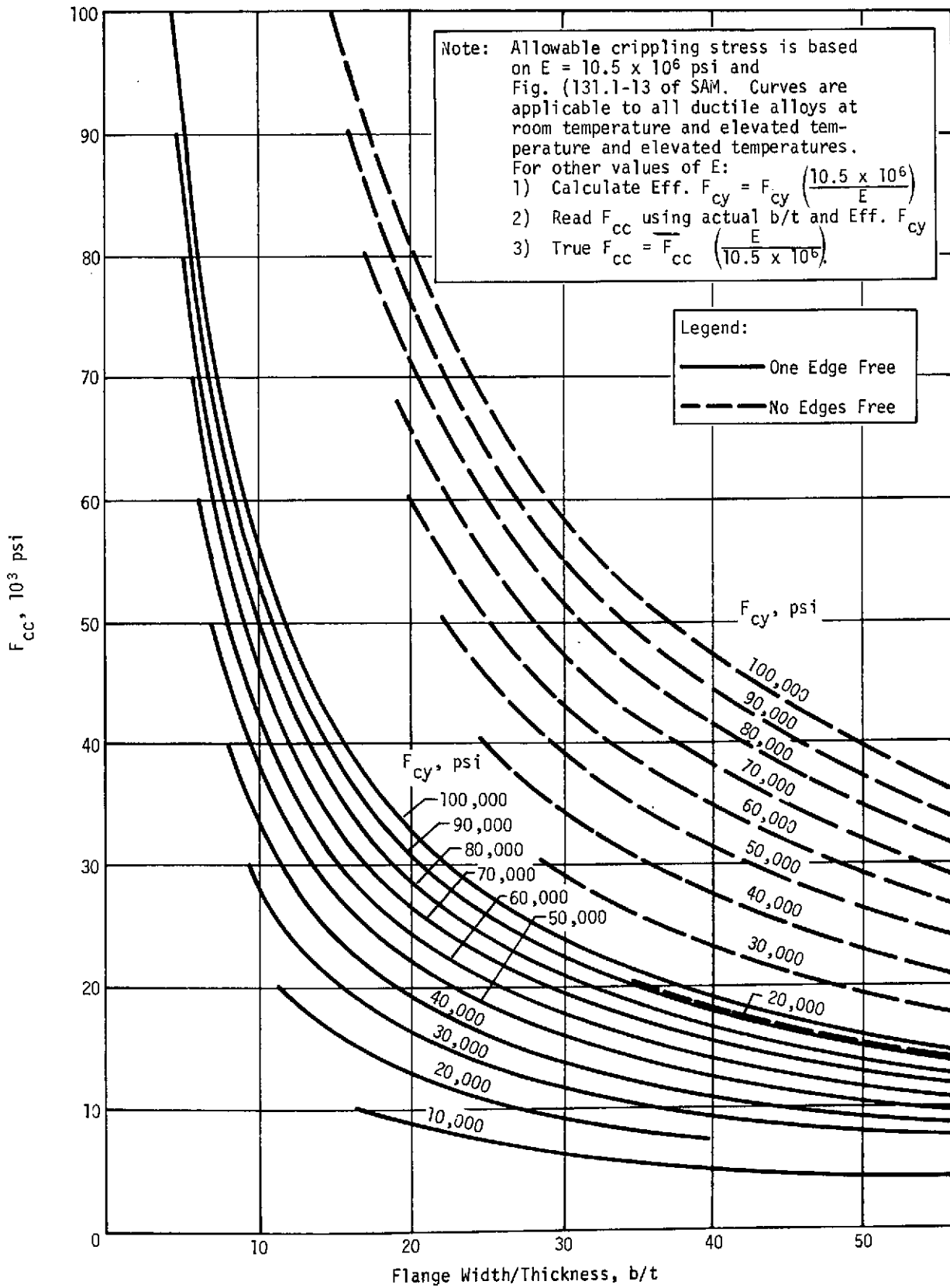
$$f_b = \frac{M c}{I} = \frac{(13.5)(.125)}{.000103}$$

$$= \underline{16,400 \text{ psi}}$$

$$\text{M.S.} = \frac{42,000}{16,000} - 1 = \underline{+1.62}$$

$F_{tu} = 42,000 \text{ psi}$  away from heat affected zone





APPENDIX B

HEAT SHIELD ANALYSIS

## APPENDIX B - HEAT SHIELD ANALYSIS

### HEATING DATA

The heating data for this study were derived from data obtained from Aerotherm Acurex Corporation (W. Nicolet, Program Manager of Aerotherm Project 7072, Saturn and Uranus Probe Study). The Aerotherm data comprise a large matrix of entry environments that consider all three atmospheres (warm, nominal, and cool) for both Saturn and Uranus, and various entry velocities, entry angles, ballistic coefficients, and sphere-cone radius ratios. All the Aerotherm data are based on a (60°) half angle sphere-cone or Apollo shape. Since none of the other available data for Saturn and Uranus probe missions fit the entry trajectories considered in this study, we modified the Aerotherm data to the trajectories defined for this study.

The modification consisted primarily of correcting the Aerotherm data to account for differences in the entry velocity (V), entry angle ( $\gamma$ ), ballistic coefficient (B), and nose radius (R). The variation in the half angle of the cone could not be corrected for, and the resulting effect is discussed in a subsequent section of this appendix.

The variation in the peak and total heating can be expressed as function of the variation of V,  $\gamma$ , B, and/or R, as shown below:

Convective heating

$$\dot{q}_{\max} = A \left( \frac{SB \sin \gamma}{R} \right)^{\frac{1}{2}} \left( \frac{V}{1000} \right)^3$$
$$Q_{\text{total}} = B \left( \frac{B}{S R \sin \gamma} \right)^{\frac{1}{2}} \left( \frac{V}{1000} \right)^2$$

Radiant Heating

$$\dot{q}_{\max} = R (SB \sin \gamma)^X V^3$$
$$Q_{\text{total}} = RB^X (S \sin \gamma)^Y V^2$$

where

A,B = constants  
S = scale height  
B = ballistic coefficient  
 $\gamma$  = entry angle  
V = entry velocity  
R = nose radius  
X,Y = exponents determined  
from Aerotherm data

The following example illustrates the modification of the Aerotherm stagnation heat fluxes for use in our analysis of the baseline configuration and our entry into the nominal Saturn atmosphere.

Table B-1 describes the baseline entry trajectory and the trajectory data obtained from Aerotherm. The heat flux curves were first modified and redrawn to account for the change in the entry angle. The  $\dot{q}_{\max}$  and  $Q_{\text{total}}$  corrections for the cold-wall (unblown) convective heat flux are as follows:

$$\dot{q}_{30^\circ} = (\sin 30/\sin 40)^{1/2} (6950) = 6130 \text{ Btu/ft}^2\text{-sec}$$

$$Q_{30^\circ} = (\sin 40/\sin 30)^{1/2} (46,000) = 52,150 \text{ Btu/ft}^2.$$

As with the Aerotherm data, the peak heating was assumed to occur at approximately 80% of the entry velocity. Using this assumption, a heat flux curve consistent with the Aerotherm data was drawn having the required  $Q_{\text{total}}$  for use in our analyses.

The resulting curve for entry into the Saturn nominal atmosphere is shown in Figure B-1. The remaining variables were accounted for by applying a multiplying factor to the heating curve shown in the figure. This multiplying factor is determined as

$$F_{\text{conv}} = \left(\frac{V_m}{V_a}\right)^3 \left(\frac{R_a}{R_m}\right)^{1/2} \left(\frac{B_m}{B_a}\right)^{1/2}$$
$$\left(\frac{29.17}{32}\right)^3 \left(\frac{20.5}{21.4}\right)^{1/2} \left(\frac{102}{140}\right)^{1/2} = 0.63$$



Table B-1 Baseline Trajectory Descriptions, Saturn Nominal

	Aerotherm 1	Aerotherm 2	Martin Marietta
$V_E$ , km/sec	32.0	32.0	29.17
$\gamma_E$ , rad (deg)	-0.26 (-15)	-0.70 (-40)	-0.52 (-30)
$R_N/R_B$	0.5	0.5	0.5
$\beta$ , gm/cm <sup>2</sup>	140	140	102
Cone Half Angle, rad (deg)	1.05 (60)	1.05 (60)	0.79 (45)
$R_N$ , cm	20.52	20.52	21.44
$q_{conv}$ , W/cm <sup>2</sup> (Btu/ft <sup>2</sup> -sec)	5000 (4400)	7898 (6950)	6966 (6130)
$Q_{conv}$ , J/cm <sup>2</sup> (btu/ft <sup>2</sup> )	81,250 (71,500)	52,272 (46,000)	59,261 (52,150)
$q_{rad}$ , W/cm <sup>2</sup> (btu/ft <sup>2</sup> -sec)	1108 (975)	3011 (2650)	3420 (2010)
$Q_{rad}$ , J/cm <sup>2</sup> (btu/ft <sup>2</sup> )	7500 (6600)	9773 (8600)	9080 (7990)

Modifying the radiant heat flux required defining the exponents X and Y. This was done using the trajectory heating data from Aerotherm. X was determined from the change in  $\dot{q}_{max}$  and Y was determined from the change in  $Q_{total}$  that resulted from changing in entry angle while holding V, R, and B constant. The resulting exponents are:

$$X = 1.1$$

$$Y = 0.29$$

Again, the cold-wall (unblown) radiant heat flux curves were first modified, as shown below, and then redrawn to account for the change in the entry angle.

$$\dot{q}_{30} = (\sin 30/\sin 40)^{1.1} (2650) = 2010 \text{ Btu/ft}^2\text{-sec}$$

$$Q_{total} = (\sin 30/\sin 40)^{0.29} (8600) = 7900 \text{ Btu/ft}^2$$

The resulting curve is shown in Figure B-2.

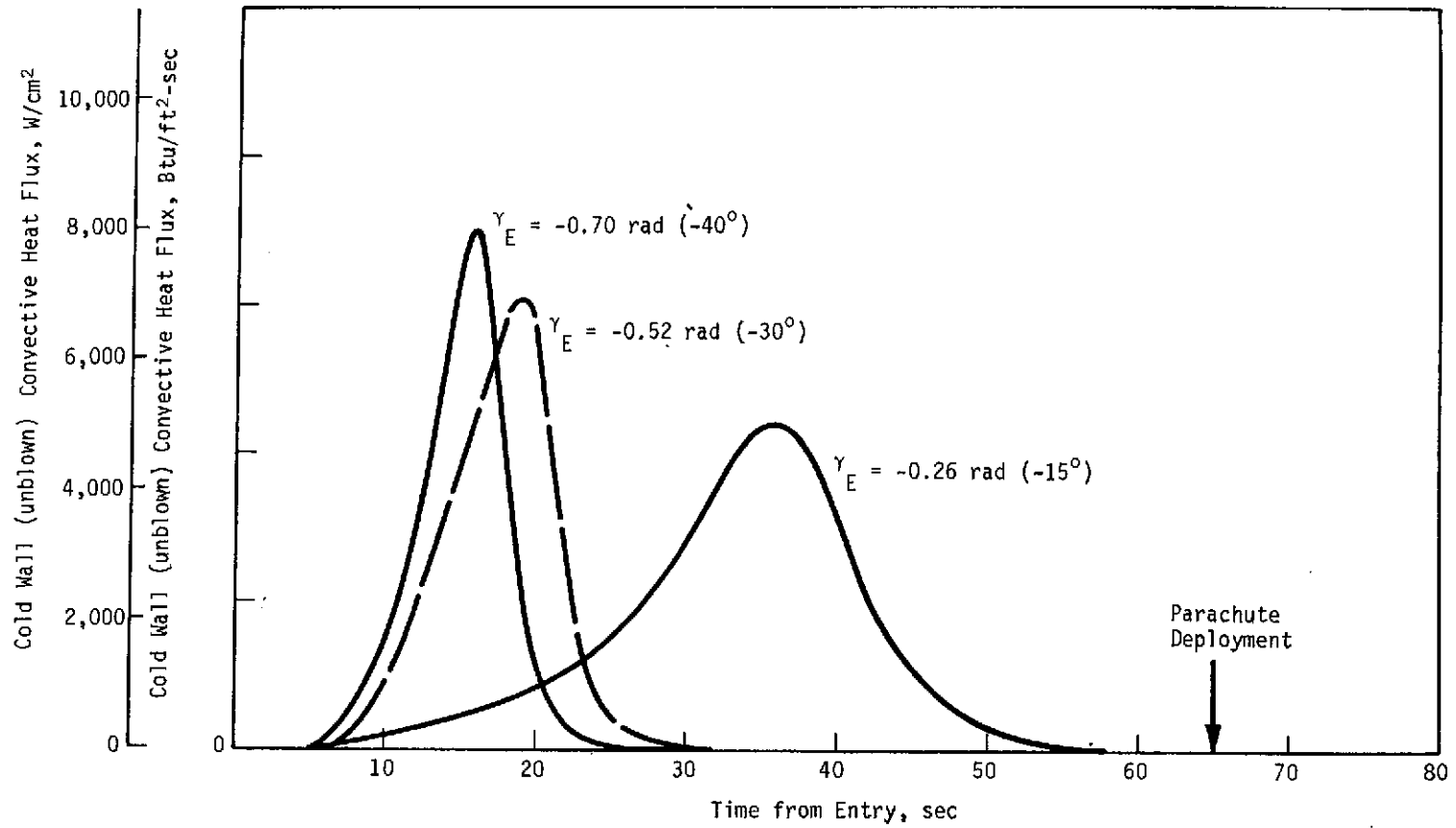


Figure B-1 Convective Heat Flux at Stagnation Point During Entry for Saturn Nominal Atmosphere

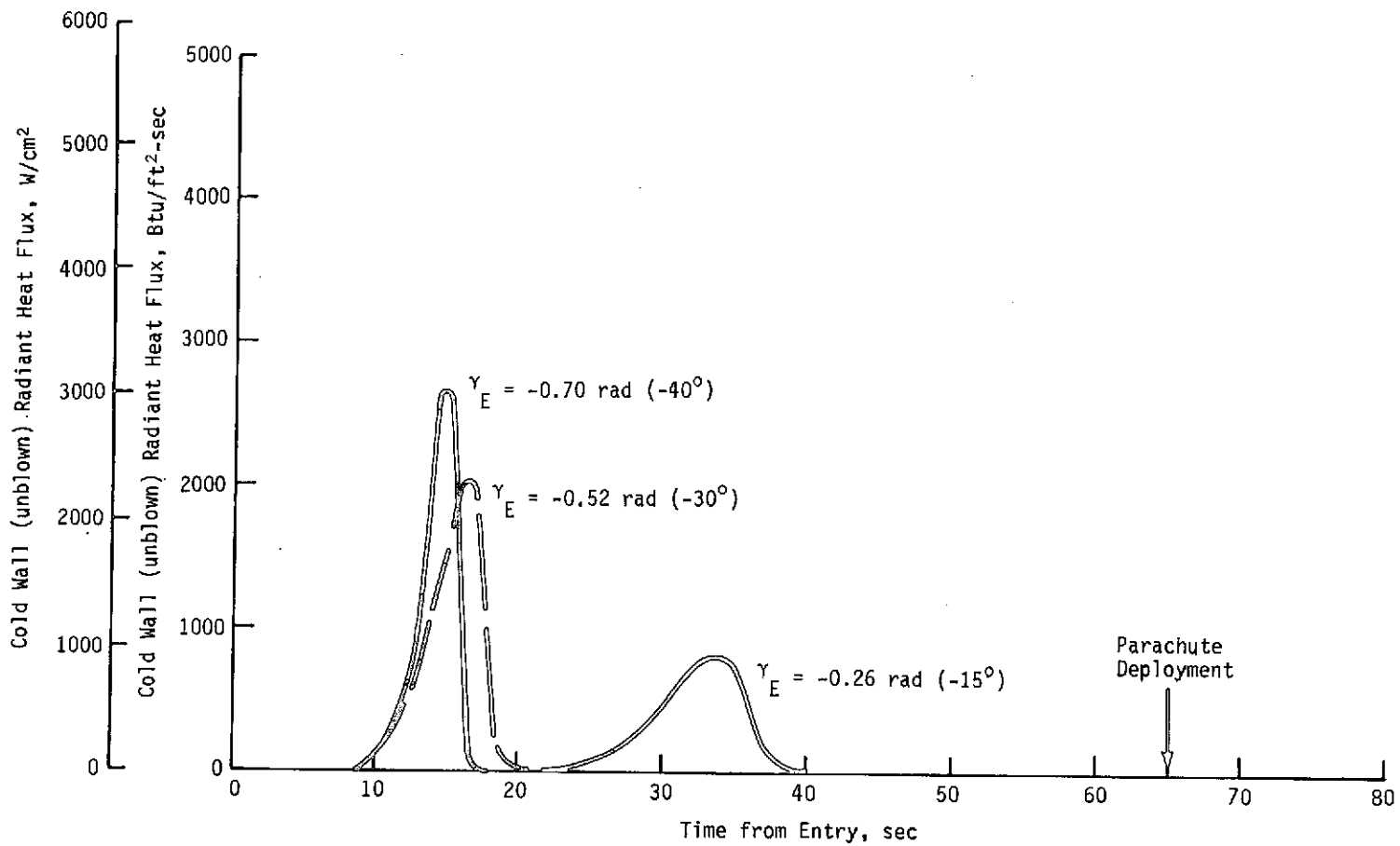


Figure B-2 Radiant Heat Flux at Stagnation Point During Entry for Saturn  
Nominal Atmosphere

The remaining variables gave the following multiplying factor:

$$F_{\text{rad}} = \left(\frac{V_m}{V_a}\right)^3 \left(\frac{R_m}{R_a}\right) \left(\frac{B_m}{B_a}\right)^{1.1}$$

$$= \left(\frac{29.17}{32}\right)^3 \left(\frac{21.4}{20.5}\right) \left(\frac{102}{140}\right)^{1.1} = 0.56$$

Note that the above corrections do not account for the difference in the cone angle between the Aerotherm data and that for the baseline configuration. The cone angle variation has no effect on stagnation heating, but does affect the heating on the remainder of the probe. The effect is highly dependent on the atmosphere being considered, but unfortunately, no direct correlation data are available for the Saturn or Uranus atmospheres. A comparison can be made, however, by using the data from Martin Marietta-sponsored Pioneer Venus studies. Figure B-3 illustrates the variation in the convective and radiant heating with a variation in the cone angle for

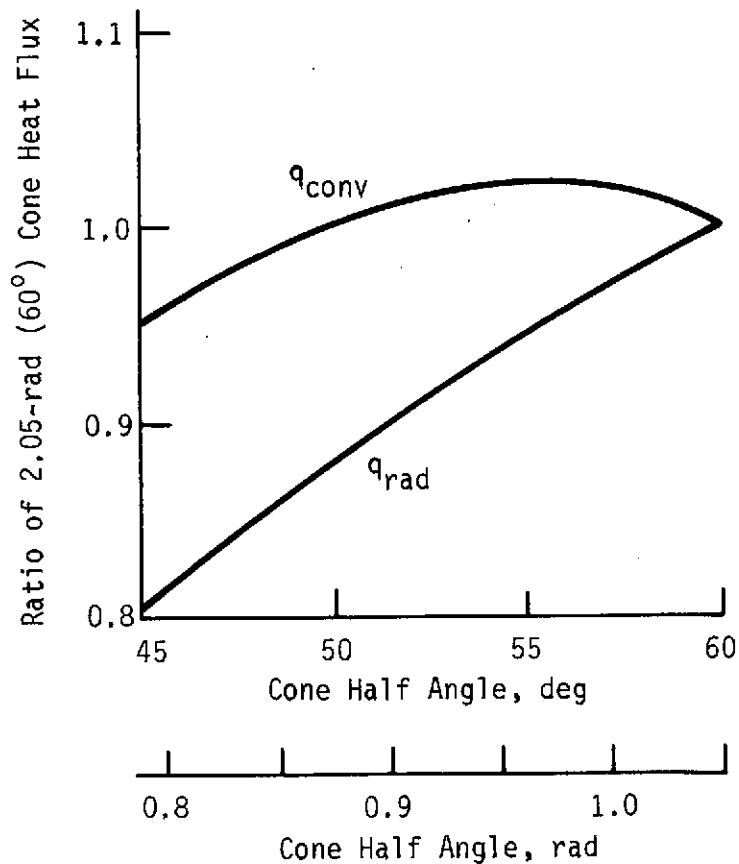


Figure B-3 Variation in Heat Flux with Change in Cone Angle

Pioneer Venus. The curves have been normalized to a 60° probe, and the shapes of the curves are believed to be typical for entry into a Saturn or Uranus atmosphere. Although the exact shape of the curves is not known, for Saturn or Uranus entry, the heating on the aft edge of the 45° probe used in this study should be less than that given for the 60° probe used in developing the Aerotherm data and using heat flux data uncorrected for the change in cone angle should give conservative results.

The corrections discussed above were made on all the heat flux data used in this study. Table B-2 compares the Aerotherm and Martin Marietta data for the various trajectories considered in this analysis. The table also shows the multiplying factors that were applied to the heat flux curves to correct them for change in entry angle.

#### ANALYTICAL APPROACH

All our analyses were conducted using the Martin Marietta Thermochemical Ablation Program (TCAP-III). The input for this program consists of temperature-dependent material and atmospheric data, as well as time-dependent trajectory data. The program incorporates blocking or blowing factors for correcting the convective and radiant heat flux, as well as hot-wall correction.

Most analyses were conducted on the aft point of the conical section of the probe aeroshell ( $0.05 R_B$  in from the aft edge). In all cases, the peak heating and total heat input were higher at the aft point than at the stagnation point, and therefore, the aft point defined the heat shield requirements.

The initial design criteria were as follows:

- 1) Peak structural temperature = 478°K;
- 2) Maximum weight = 13.6 kg (baseline configuration);
- 3) Use Pioneer Venus ablative material, if possible.

All models analyzed were one-dimensional models comprising ablative material, insulation (where applicable), and the aeroshell structure. The various materials were assumed to be bonded together and the backwall was assumed adiabatic.

#### BASELINE CONFIGURATION ANALYSIS

Heat shield analyses for the baseline and alternate con-

Table B-2 Trajectory Descriptions and Multiplying Factors

	Model		
	Aerotherm	Martin Marietta	Multiplying Factor
<b>Saturn Nominal</b>			
$V_E$ , km/sec	32	29.17	
$R_N/R_B$	0.5	0.5	$F_q = 0.63$
B, gm/cm <sup>2</sup>	140	102	$F_r = 0.56$
Cone Half Angle, rad (deg)	1.05 (60)	0.79 (45)	
$R_N$ , cm	20.52	21.44	
<b>Saturn Cool</b>			
$V_E$ , km/sec	32	29.17	
$R_N/R_B$	0.5	0.44	$F_q = 0.83$
B, gm/cm <sup>2</sup>	140	125.7	$F_r = 0.63$
Cone Half Angle, rad (deg)	1.05 (60)	0.79 (45)	
$R_N$ , cm	20.52	18.33	
<b>Saturn Warm</b>			
$V_E$ , km/sec	28.22	28.77	
$R_N/R_B$	0.5	0.425	$F_q = 1.0$
B, gm/cm <sup>2</sup>	149	142.6	$F_r = 1.0$
Cone Half Angle, rad (deg)	1.05 (60)	0.79 (45)	
$R_N$ , cm	20.52	17.89	
<b>Uranus Cool</b>			
$V_E$ , km/sec	25.2	25.06	
$R_N/R_B$	0.5	0.44	$F_q = 0.99$
B, gm/cm <sup>2</sup>	100	125.7	$F_r = 0.79$
Cone Half Angle, rad (deg)	1.05 (60)	0.79 (45)	
$R_N$ , cm	20.52	18.33	

figurations were conducted using the heat flux curves for entry into the Saturn nominal atmosphere (Figure B-4). This entry was defined, by Aerotherm, as the more severe of the entries into the Saturn and Uranus nominal atmospheres. Normal blocking curves developed by Martin Marietta (Figure B-5) were used to determine the convective heat flux. A condition of no blocking or magnification was assumed for the radiant heat flux.

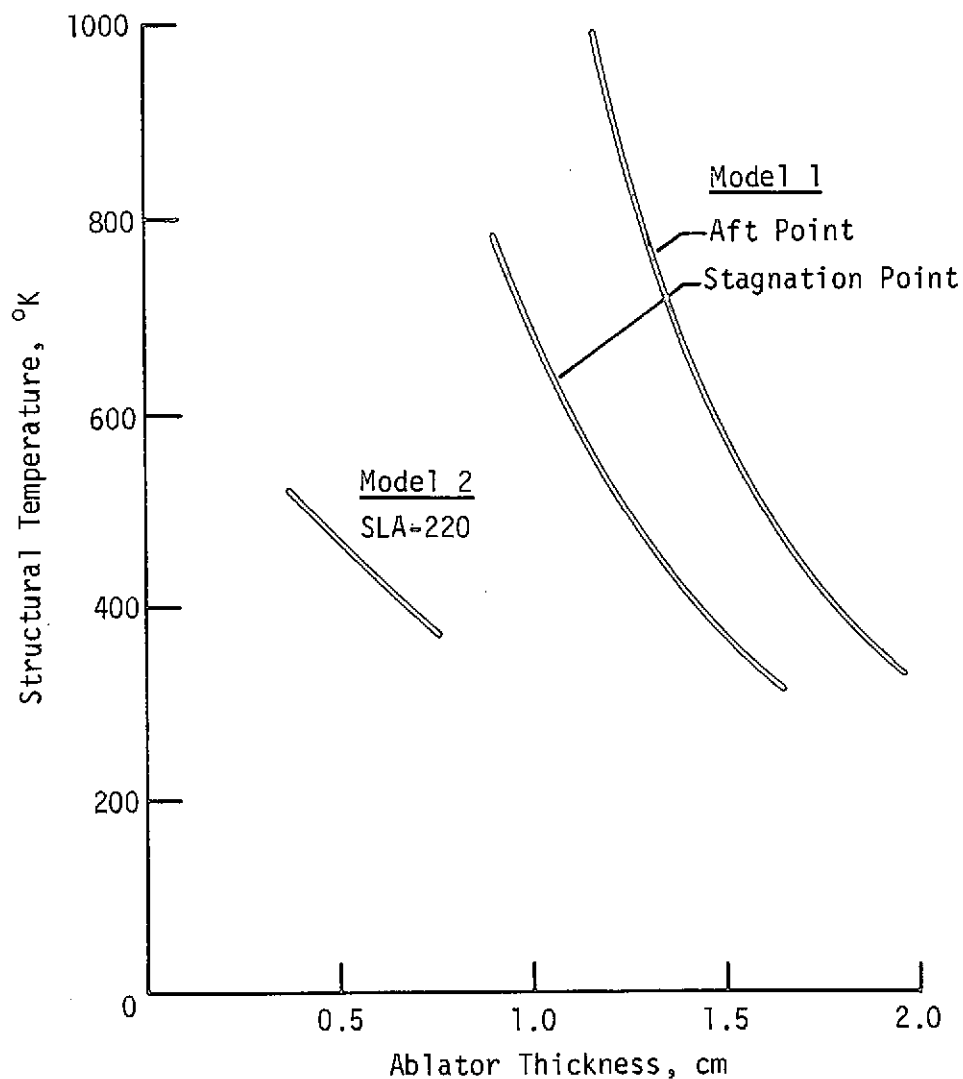
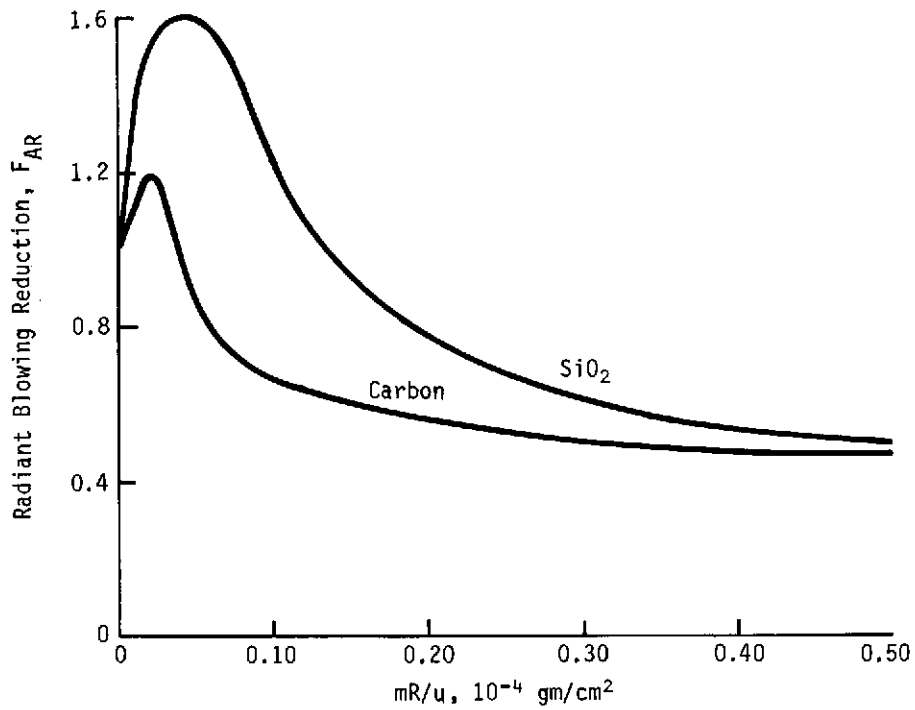
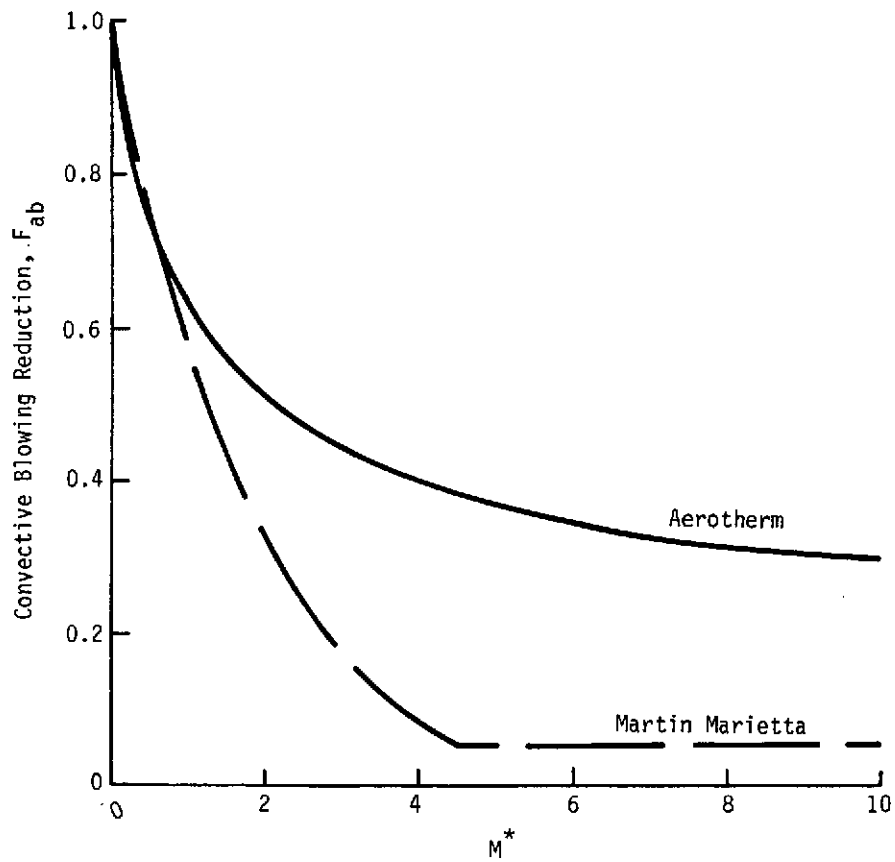


Figure B-4 Baseline Heat Shield Design Curves

Our initial analysis on the stagnation and aft points was based on the Pioneer Venus quartz nitrile phenolic ablator. Without specifying the required thickness of the ablator,



(a) Radiant Blowing Reduction vs  $mR/u$



(b) Convective Blowing Reduction vs  $M^*$



We determined the recession to be excessive and the ablative material was changed to a higher density, quartz nitrile phenolic. This material has a higher percentage of quartz cloth and improved recession characteristics. The results obtained with this material are shown in Figure B-6. The analysis indicated that the weight of the heat shield could be reduced by using an insulator between the ablator and the aeroshell structure. The insulator we used was SLA-220, which is a low-conductivity ablative material. The thickness of SLA-220 required is shown as a function of the structural temperature in the Model 2 curve of Figure B-6.

The heat shield defined for the baseline configuration consists of 0.794-cm layer of quartz nitrile phenolic bonded to a 0.457-cm honeycomb-reinforced sheet of SLA-220, which in turn, is bonded to the aeroshell structure.

#### FINAL CONFIGURATION ANALYSIS

The heat shield analysis for the final configuration was made considering the "worst case" entry environment. This consisted of using the Uranus cool-atmosphere entry to define the amount of quartz nitrile phenolic required and the Saturn warm-atmosphere entry to define the amount of SLA-220 insulation required. The analytical approach was changed in that the Aerotherm blocking curves (see Figure B-5) were used to define the convective and radiant heat inputs. Previously, a radiation blocking factor of 1.0 had been used in the analysis, using these curves reduces the radiant heat input. The convective heat input, however, increases dramatically.

The worst-case heat flux curves are compared with the baseline heating curves in Figure B-4 and B-7. Remember that these curves still need to be modified by using the multiplication factors given in Table B-2. Applying these factors reduces the entry heating curves for the nominal-atmosphere mission even more, relative to the other curves. The total heat input for the worst-case atmospheres is essentially twice that for the Saturn nominal-atmosphere entry (baseline).

Our initial analysis indicated that more than 2.54 cm (1.0 in.) of quartz nitrile phenolic would be required to adequately protect the aeroshell structure (Table B-3). At this point we decided to change the ablative material to carbon phenolic since its recession was small enough for a reasonable heat shield to be defined. The surface temperatures, recession, and structural temperatures for carbon phenolic during the Uranus cool entry are shown in Figure B-8.

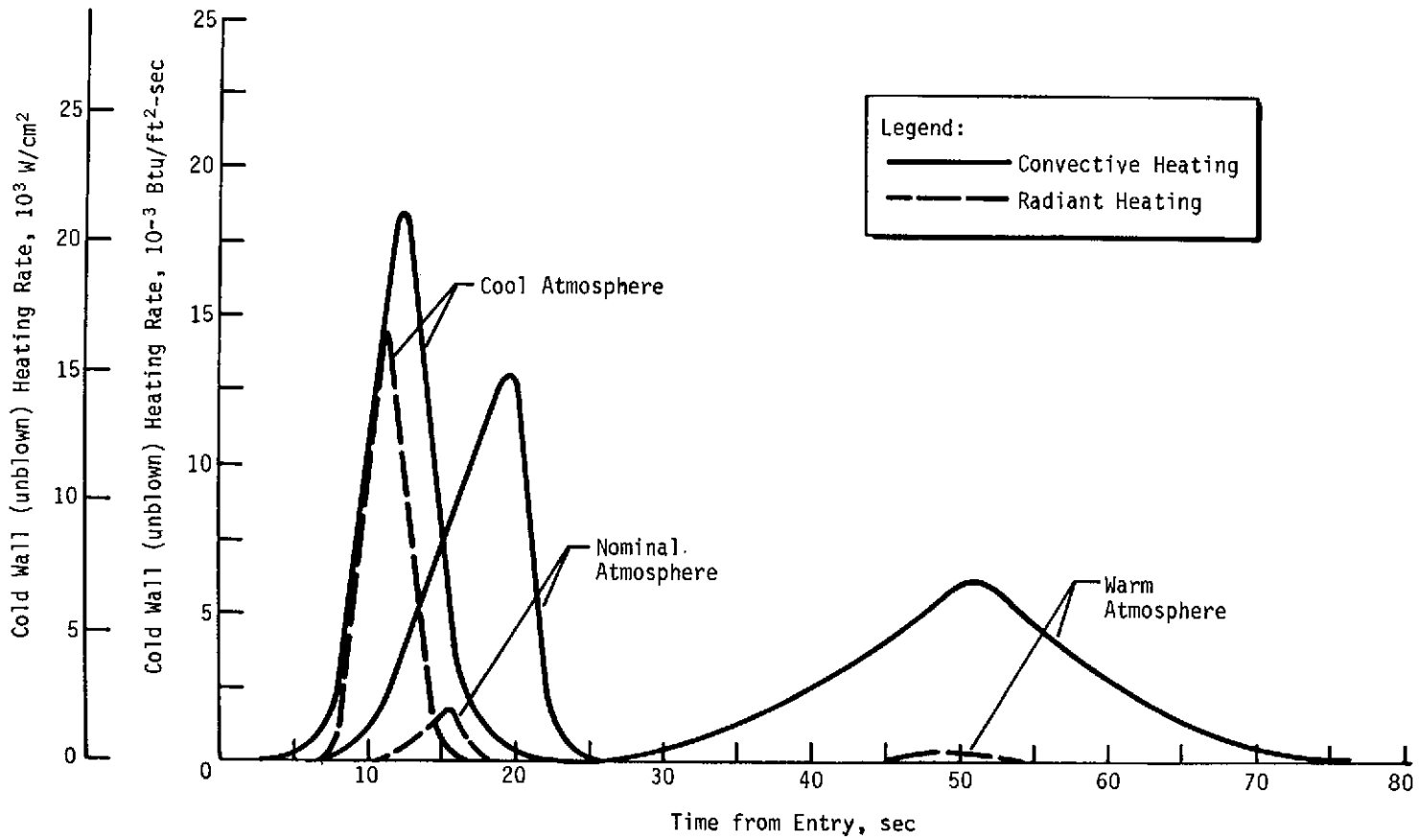


Figure B-6 Comparison of Aft Edge Heating Rates for Saturn Warm, Nominal and Cool Atmospheres

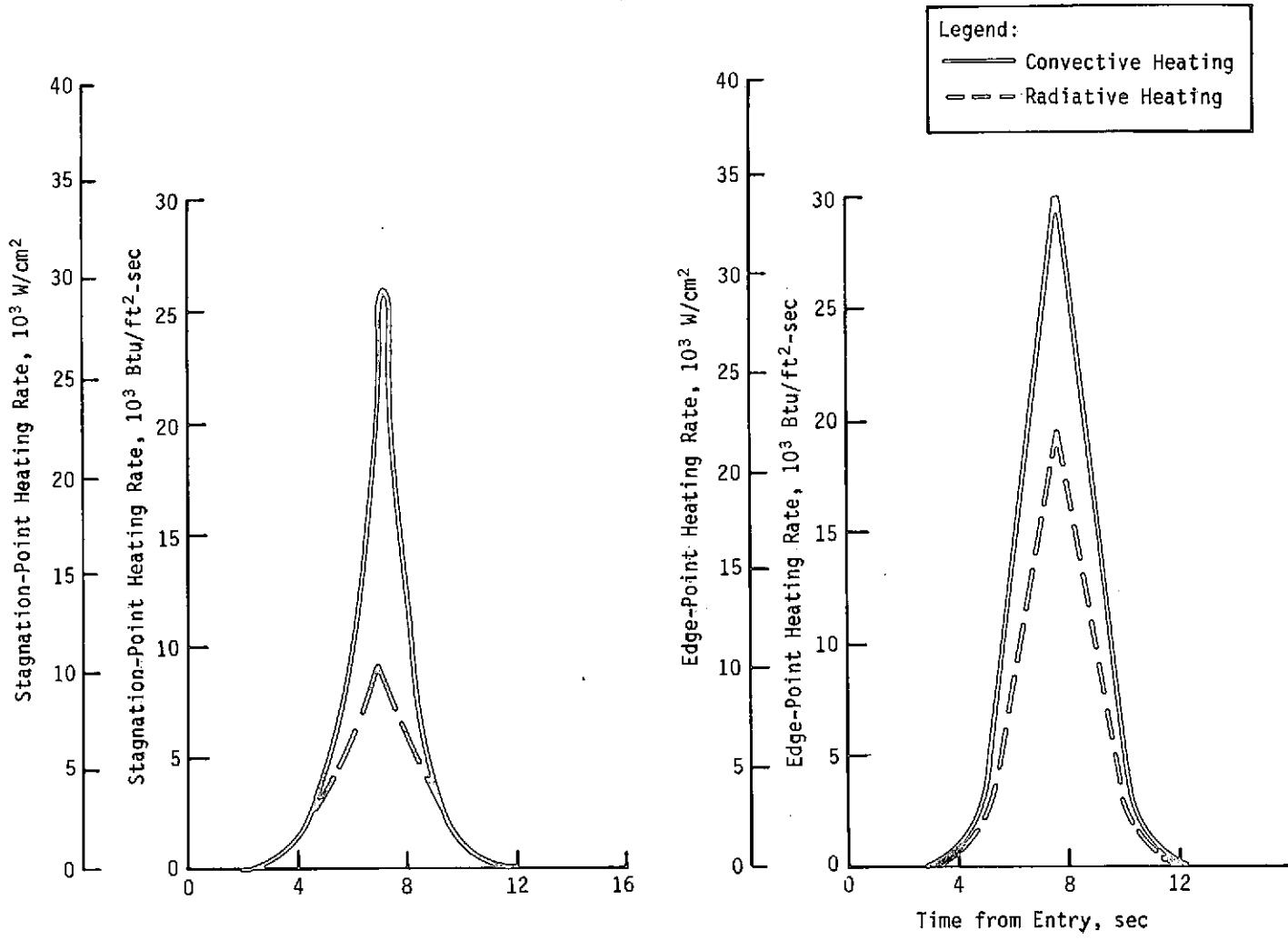


Figure B-7 Uranus Cool Heating Flux for -35° Entry

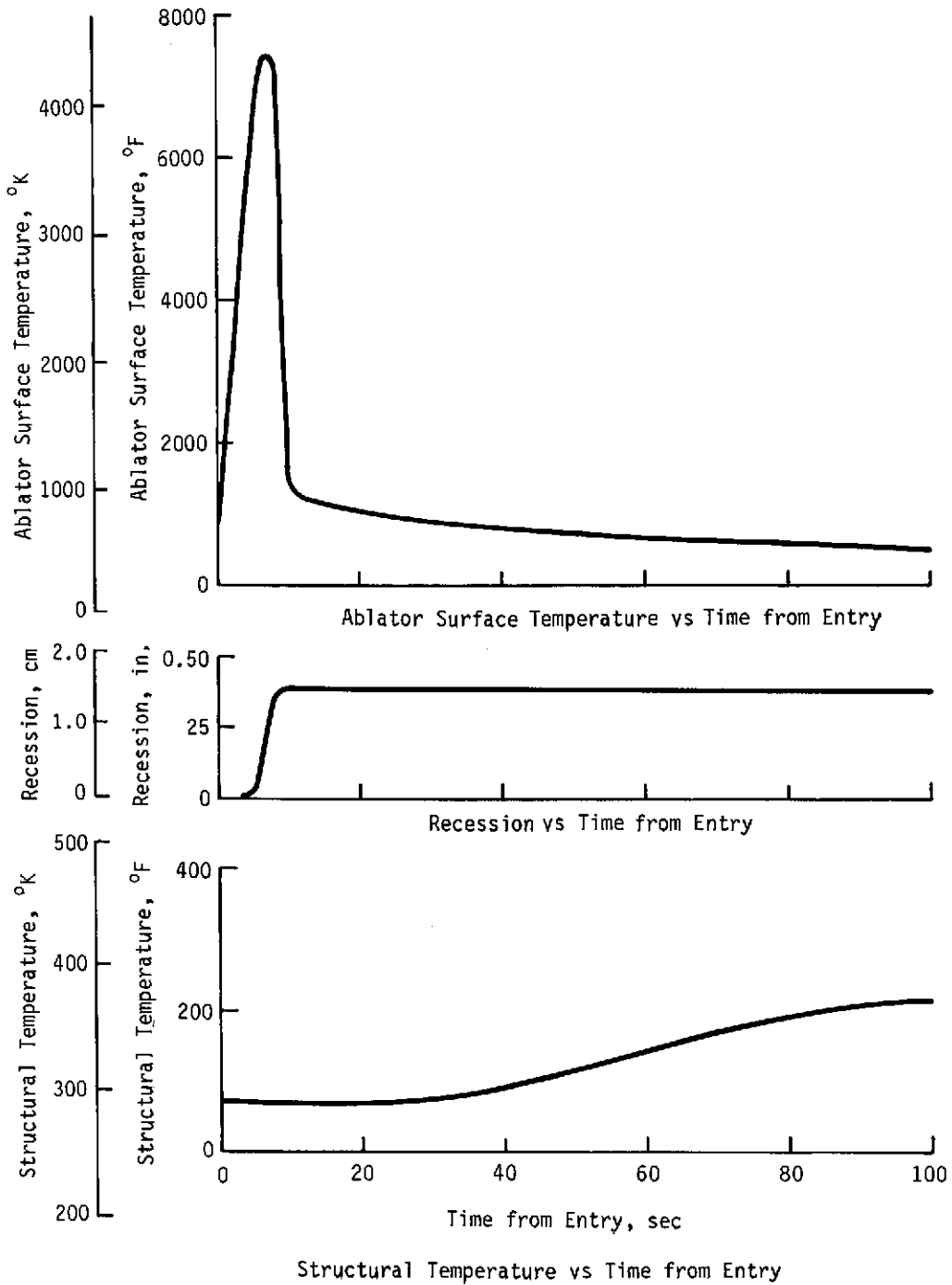


Figure B-8 Analytical Results - Final Configuration

The heat shield defined for the final probe configuration consists of 1.27 cm of carbon phenolic bonded to 0.794 cm of honeycomb-reinforced SLA-220, which in turn, is bonded to the aeroshell structure.

#### ANALYTICAL RESULTS

Our analytical results are summarized in Table B-3. The heat shields for the baseline and alternate configurations consist of 0.794 cm (0.3125 in.) of quartz nitrile phenolic and 0.457 cm (0.180 in.) of honeycomb-reinforced SLA-220. Note that the results for the final configuration using quartz nitrile phenolic are included to illustrate the material's high recession. This was considered an unacceptable design.

The heat shield for the final configuration consists of 1.27 cm (0.50 in.) of carbon phenolic over 0.794 cm (0.3125 in.) of honeycomb-reinforced SLA-220.

Table B-3 Analytical Results

Atmosphere	Entry Conditions			
	QNP, cm (in.)	C/P, cm (in.)	SLA-220, cm (in.)	Recession, cm (in.)
Saturn Nominal	0.794 (0.3125)		0.457 (0.180)	0.533 (0.21) <sup>*</sup>
Saturn Cool	2.54 (1.0)			2.134 (0.84) <sup>†</sup>
Uranus Cool	3.81 (1.5)		0.635 (0.25)	2.337 (0.92) <sup>†</sup>
Saturn Cool		1.27 (0.50)	0.794 (0.3125)	0.813 (0.32) <sup>†</sup>
Uranus Cool		1.27 (0.50)	0.794 (0.3125)	0.965 (0.38) <sup>†</sup>
Saturn Warm		1.27 (0.50)	0.794 (0.3125)	

\* Baseline configuration.  
† Final configuration.

APPENDIX C

THERMAL CONTROL ANALYSIS

## APPENDIX C -- THERMAL CONTROL

### CRUISE THERMAL ANALYSIS

A thermal analysis was conducted to determine the probe's steady-state temperature during the cruise phase of the Saturn Uranus missions. The desired nominal temperature for the probe during this phase was 277.6°K (40°F). A series of parametric runs were made to evaluate the sensitivity of this temperature to the following factors:

- 1) Variations in the amount of excess RHU power conducted from the probe to the spacecraft/probe interstage adapter through the probe support points;
- 2) Operating the Pioneer louvers between 225.4°K (0°F) and 305.4°K (90°F) (the louvers have a significant radiative view of the interstage adapter);
- 3) Varying the effective sink temperature of the spacecraft aft surface, which also has a significant view of the interstage adapter. Aft surface temperatures of 144.2°K (-200°F) and 199.8°K (-100°F) were assumed for the analysis.

Figure C-1 shows the configuration of the probe within the spacecraft during cruise. The model diagram shown in Figure C-2 was evaluated with Martin Marietta's MITAS thermal analyzer computer program to generate the probe temperature for limiting values of the above boundary conditions. Ten watts are continuously being dissipated in the probe by the RHU heaters.

The thermal conductance ( $k/\Delta x$ ) of the probe's multilayer insulation was evaluated as a function of the outer-layer temperature using the values given in Table C-1. The results from the parametric runs are presented in Figure C-3 for a spacecraft temperature of 144.2 K (-200°F).

Changing the spacecraft's temperature 199.8°K (-100°F) raised the probe temperature by 2.2 K (4°F), which meant that the probe was essentially uncoupled from the temperature excursions of the spacecraft's aft surface. Opening and closing the spacecraft louvers changed the probe temperature 7.5°K (13.4°F) which again is not a significant amount, especially since the louvers will probably be closed throughout most of the mission to maintain temperatures on the spacecraft above their lower limit.

The analysis showed that the probe temperature was highly dependent on the amount of heat transferred out of the probe through the support points and that this dependence was about 20°K/watt. The computed temperature of the interstage adapter



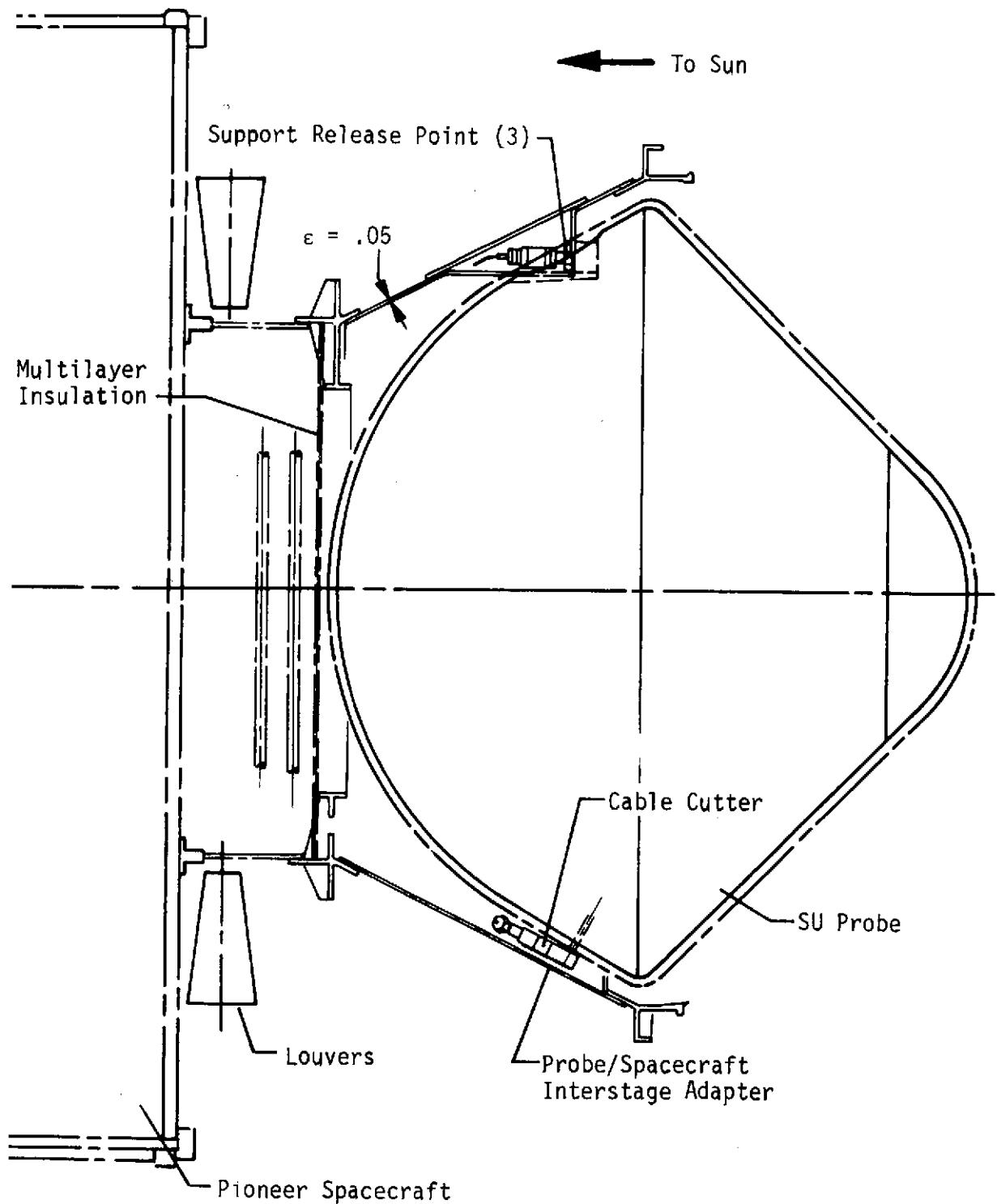


Figure C-1 Probe/Spacecraft Cruise Configuration, Final Probe Configuration

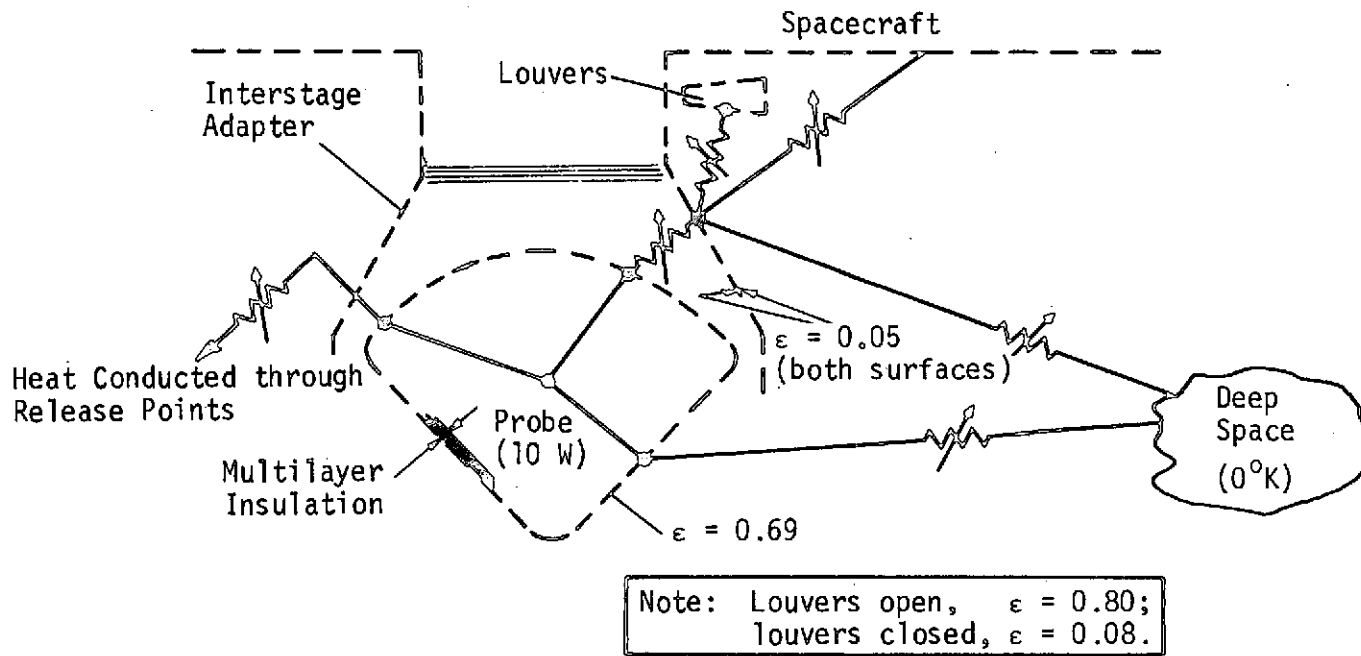


Figure C-2 Thermal Analysis Node Diagram, Probe on Spacecraft Configuration

Table C-1 Multilayer Insulation Conductance Versus Outer Layer Temperature

Temperature, °K (°F)	Conductance, W/m <sup>2</sup> - °K (Btu/hr-ft <sup>2</sup> - °F)
88.9 (-300)	0.0227 (0.004)
144.2 (-200)	0.0284 (0.005)
199.8 (-100)	0.0364 (0.0064)
255.4 (0)	0.0420 (0.0074)
310.9 (100)	0.0438 (0.0077)

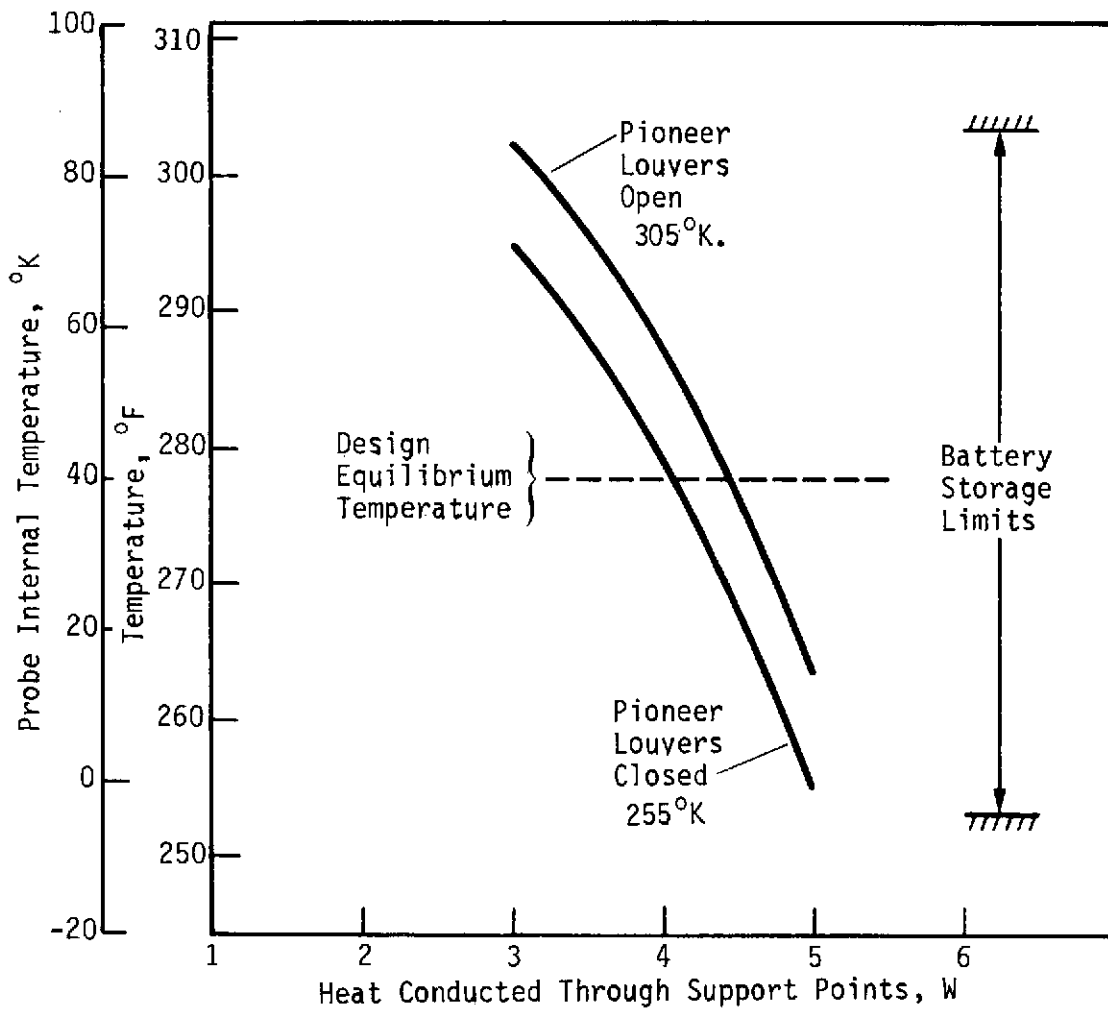


Figure C-3 Probe Internal Temperature Versus Heat Conduction Through Support Points During Cruise

ranged from 204.3°K (-92°F) to 160°K (-172°F) in the parametric with 4 watts conducted through the support points.

This fluctuation in the temperature of the interstage adapter points up the need to isolate the probe's heat rejection/conduction path from the adapter in order to achieve a stable operating condition. However, a full-scale thermal/vacuum test of the probe on the spacecraft cruise configuration would be required to verify the analysis.

#### COAST THERMAL ANALYSIS

During the coast portion of the mission (20.8 days at Uranus and 35.7 days at Saturn), the probe loses energy to the deep space environment. Internal temperatures will drop to unacceptable levels within a few days after the probe separates from the spacecraft unless additional energy is supplied to the probe. The temperature drop for the no-heating situation can be predicted using Schneider's temperature response curves\* for flat-plates. Figure C-4 depicts a plate cooling by radiation in a deep space environment. Since Chart 53 of Schneider's applies Figure C-5 (Figure C-5), the abscissa value is defined as

$$MF_o = \left( \frac{\sigma F_A F_\epsilon T_o}{\rho c \delta} \right) \theta, \quad (c-1)$$

where

M = radiation parameter

F<sub>o</sub> = Fourier number

σ = Stefan-Boltzman radiation constant = 5.67 x 10<sup>8</sup> w/m<sup>2</sup>-°K<sup>4</sup>

F<sub>A</sub> = radiation surface configuration factor = 1.0

F<sub>ε</sub> = radiation surface emissivity factor = 0.01

T<sub>o</sub> = initial plate temperature = 277.6°K (40°F)

ρ = plate density (see below)

c = plate specific heat = 0.464 W-h/g

δ = plate thickness (see below)

θ = time from start of cooling = 500 hr to Uranus, 836 hr to Saturn.

\* P. J. Schneider: *Temperature Response Charts*. J. Wiley and Sons, Inc. New York, 1963.

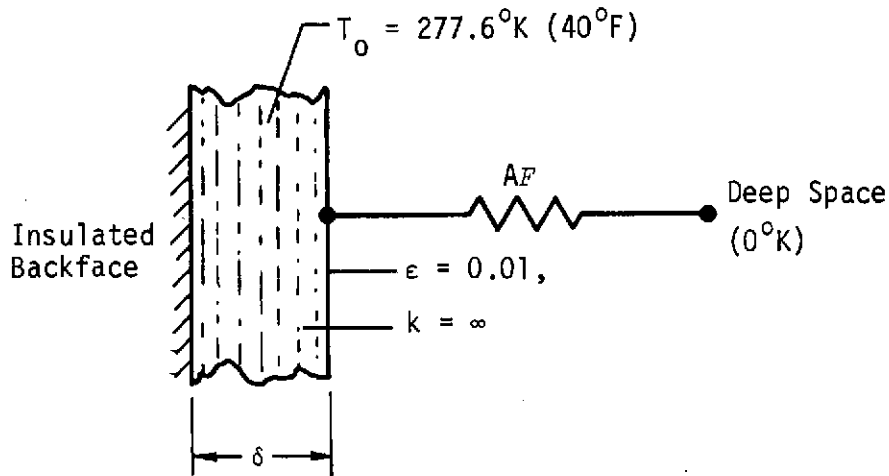


Figure C-4 Plate Analogy for Probe Cooldown after Spacecraft Separation

The produce of  $\rho\delta$  was determined from the ratio of the probe's mass to its external surface area:

$$\rho\delta = m/A_S$$

where

$m$  = probe mass = 93 kg

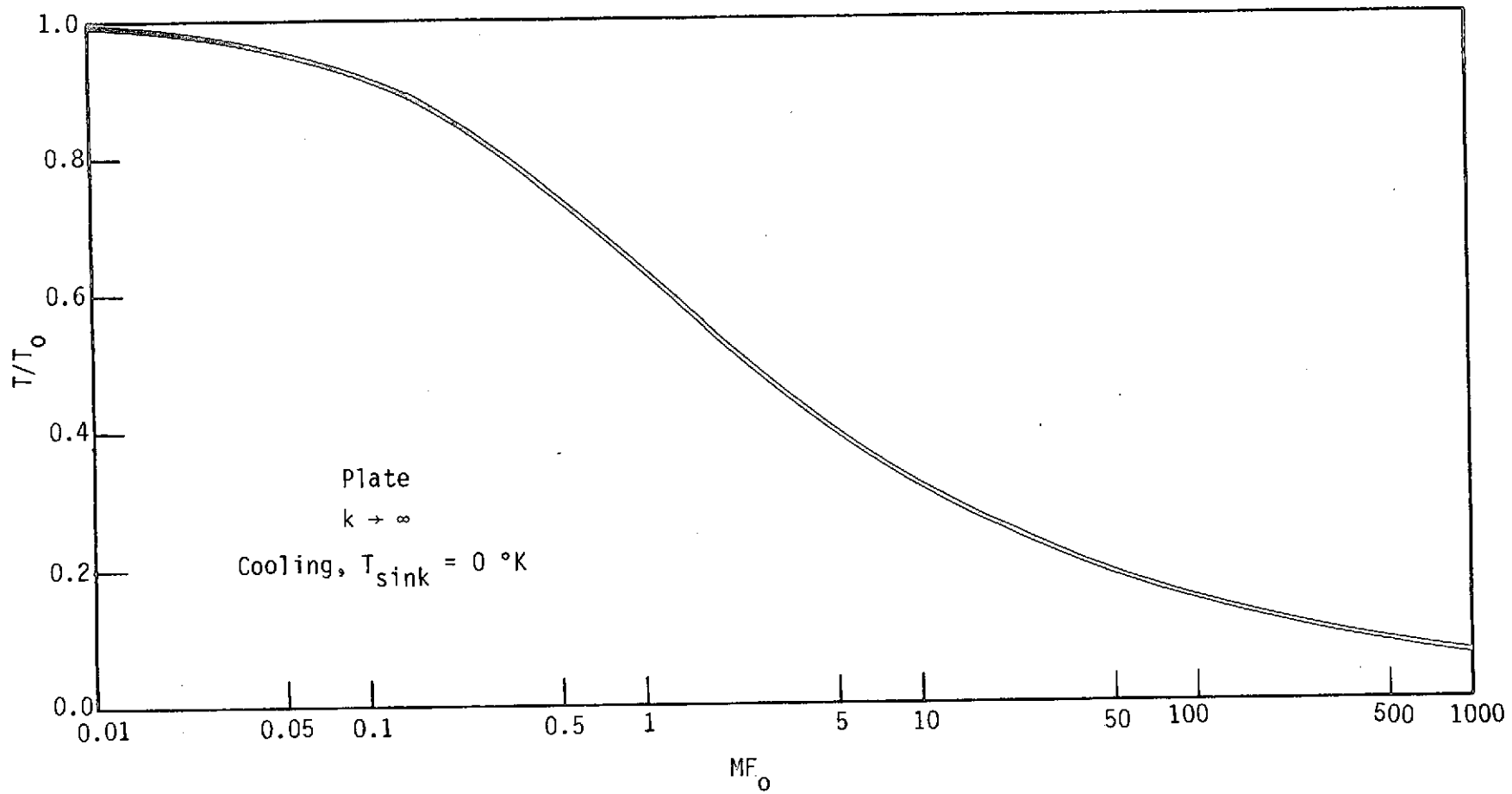
$A_S$  = probe external area = 1.65 m<sup>2</sup>.

Calculations were made with the probe's surface emissivity factor, set at 0.01, which is a reasonable design value for spacecraft multilayer insulations. The analysis was also run for effective emittance of 0.002 and 0.003 to see if a more advanced insulation system could minimize the temperature decay.

The above data were substituted in Eq (C-1) and the temperature response values were taken from Figure C-5. Figure C-6 shows the results as a plot of the probe's temperature after being released from the spacecraft. From the plot, it is evident that some form of heating must be supplied to maintain the components at an acceptable temperature during this coast phase.

With this in mind, we then used a transient thermal model of the probe to determine the amount of heating required. This computer model is shown in Figure C-7.

Parametric runs were made with the above network to determine the heater power required to heat the probe to the desired entry temperature of 297°K (75°F). The multilayer insulation was



C-7

Figure C-5 Schneider Chart 53 for a Plate Cooling by Radiation to  $T_{\text{sink}} = 0^\circ\text{K}$

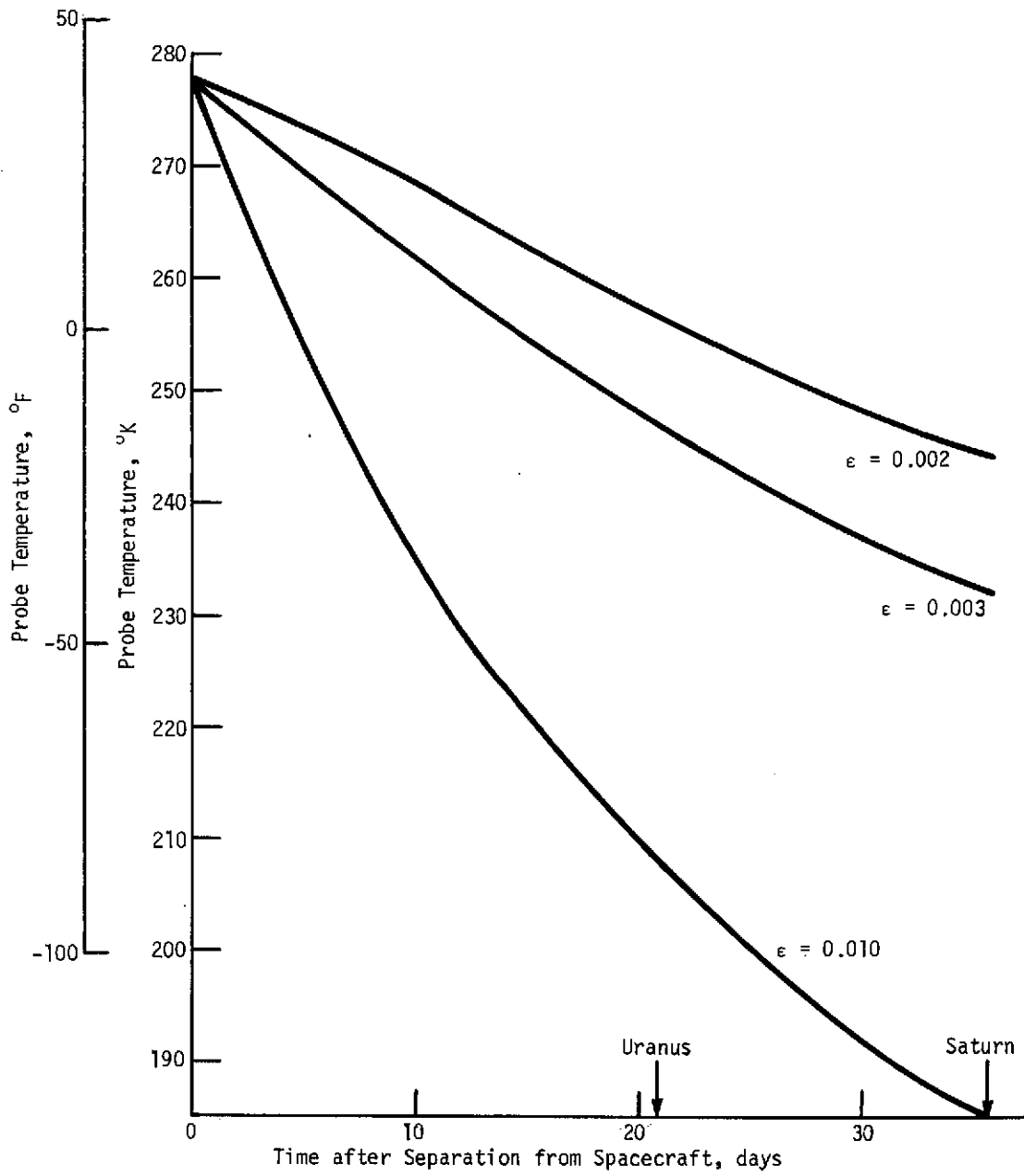
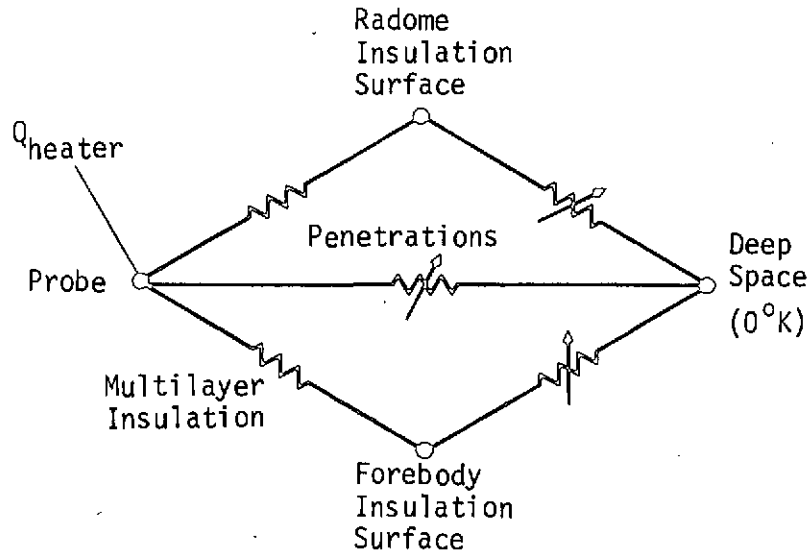


Figure C-6 Probe Cooldown after Spacecraft Separation, No Heaters Configuration



Note: Probe capacitance =  $21.3 \text{ W-hr/}^\circ\text{K}$ .

Figure C-7 Computer Simulation Network for Probe Coast Transient Analysis

modeled using the data in Table C-1 which corresponds to an effective emittance of 0.01. Results from the runs are plotted in Figure C-8.

An inspection of the temperatures plotted in this figure shows that the required heater power is 10 watts. This choice allows some heater margin, which can be rejected through a calibrated "thermal short" to achieve the  $297^\circ\text{K}$  entry temperature at the end of the coast phase. This adjustment would be during a thermal/vacuum test of the flight hardware to verify the thermal control design.

#### ATMOSPHERIC DESCENT THERMAL ANALYSIS

A 26-node finite-difference network (see Figure C-9) was used to predict the temperatures of the probe components during the atmospheric descent portion of the mission. The transmitter and battery were modeled in detail, but the science, power conditioning, and data handling components were lumped into one internal equipment mode. All significant heat-transfer modes were modeled, including convective exchange between the equipment and the atmospheric gas vented into the probe [the pressure inside the probe is maintained (1 bar) below atmospheric pressure by using a vent valve sized to open at a differential pressure of  $10^5 \text{ N/m}^2$  (1 bar)].



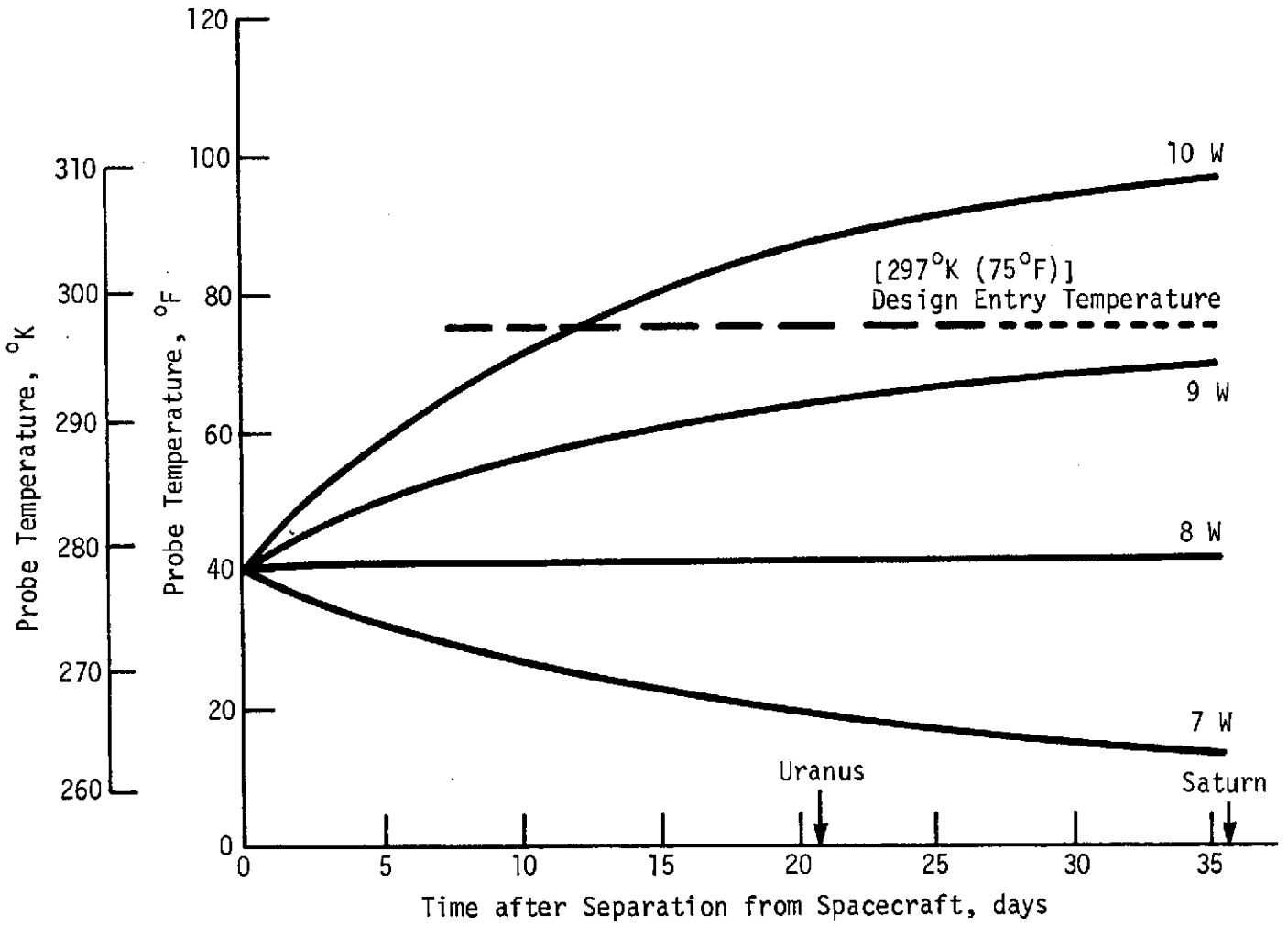


Figure C-8 Probe Coast Temperatures Versus Heater Power Levels

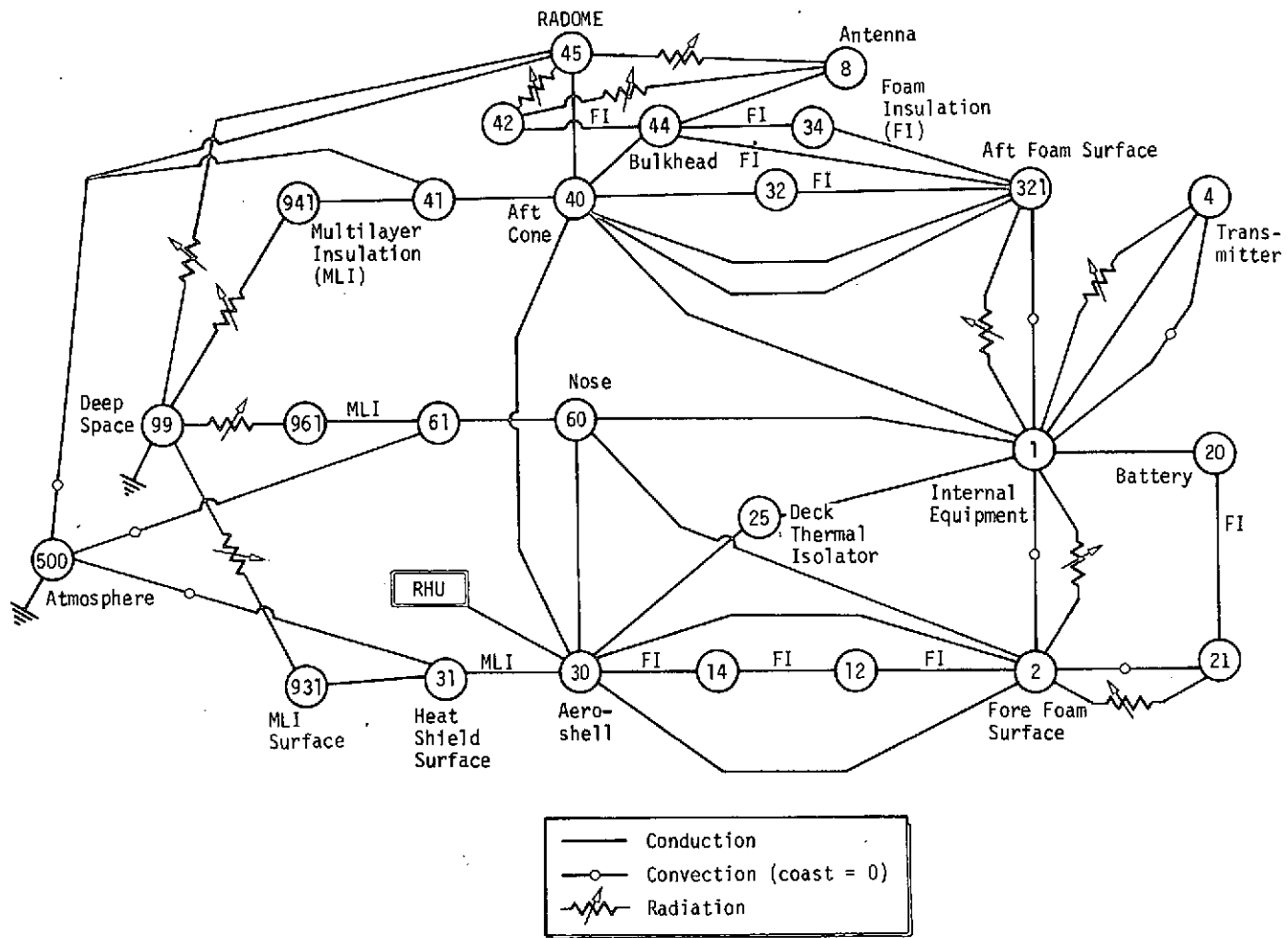


Figure C-9 Computer Simulation Network for SU Common Probe Atmospheric Descent Analysis

The expansion of this incoming atmospheric gas tends to cool the payload. This effect was accounted for in the computer analysis by using the following thermodynamic relationship:

$$\delta m_i h_i = du$$

where

$m_i$  = mass of incoming gas

$h_i$  = enthalpy of incoming gas

$u$  = internal energy of incoming gas.

The convective exchange between the probe and the planetary atmospheres was evaluated using the empirical relation for flow past a sphere:

$$h = \frac{k}{D} [2 + 0.6 Re^{\frac{1}{2}} Pr^{\frac{1}{2}}]$$

where

$h$  = heat transfer coefficient

$k$  = thermal conductivity of atmospheric gas

$D$  = probe maximum diameter

$Re$  = Reynolds number

$Pr$  = Prandtl number.

Natural convection inside the probe was accounted for with the following relation:

$$Nu_m = 0.59 (Gr Pr)^{\frac{1}{4}}; \quad 10^4 < Gr Pr < 10^9$$

where

$Nu_m$  = mean Nusselt number

$Gr$  = Grashof number.

The low-density foam insulation on the inner surfaces of the probe was evaluated by setting its thermal conductivity equal to the conductivity of the gas mixture filling its cells. However, the incoming atmospheric gas at Saturn or Uranus is a mixture of hydrogen and helium, both of which are highly conductive gases.

In his paper, Webb\* discusses this problem and plots the thermal conductivity of the gas and insulation. This plot is re-

---

\*C. Webb: *Thermal Control Subsystem Design of a Saturn/Uranus Atmospheric Entry Probe for Descent Missions to 20 bars.*  
AIAA Paper No. 73-770. 1973.

produced here as Figure C-10. Note that the thermal conductivity of the atmospheric constituents is an order of magnitude higher than that of the evaluated foam insulation. The plot also shows that the thermal conductivity of Argon gas is about the same order of magnitude as that of the foam.

The low thermal conductivity of Argon suggested that one possible thermal control approach is to fill the probe with Argon immediately after entry to enhance the effectiveness of the foam insulation. A fill pressure of  $1.5 \times 10^5 \text{ N/m}^2$  (1.5 bar) will delay the opening of the vent valve until the probe reaches an atmospheric pressure of  $2.5 \times 10^5 \text{ N/m}^2$  (2.5 bar) in the descent. This scheme was input to the analysis and computer runs were made to evaluate its effect on the probe heat losses during descent. Figure C-11 shows the results for the vented probe with and without the Argon gas system.

In determining the thermal conductivity of the gaseous mixture of Argon and He/H<sub>2</sub> during descent, we used the following relationship for nonpolar gases:

$$k_{\text{mix}} = \sum_{j=1}^n \frac{x_j k_j}{\sum_{j=1}^n x_j \phi_{ij}}$$

where

$x_i$  = the mole fractions

$k_i$  = the thermal conductivities of the pure components.

The coefficients,  $\phi_{ij}$ , are given by the relationship:

$$\phi_{ij} = \frac{1}{\sqrt{8}} \left( 1 + \frac{M_i}{M_j} \right)^{-\frac{1}{2}} \left[ 1 + \left( \frac{\mu_i}{\mu_j} \right)^{\frac{1}{2}} \left( \frac{M_j}{M_i} \right)^{\frac{1}{4}} \right]^2$$

where

$\mu$  = viscosity

$M$  = molecular weight.

Note that the heavier gases generally dominate the thermal conductivity of a gaseous mixture.

#### NEPHELOMETER WINDOW HEATER ANALYSIS

The nephelometer defined for the Saturn/Uranus probe has two small sapphire windows for atmospheric viewing ports. To keep these windows free from condensation during atmospheric de-

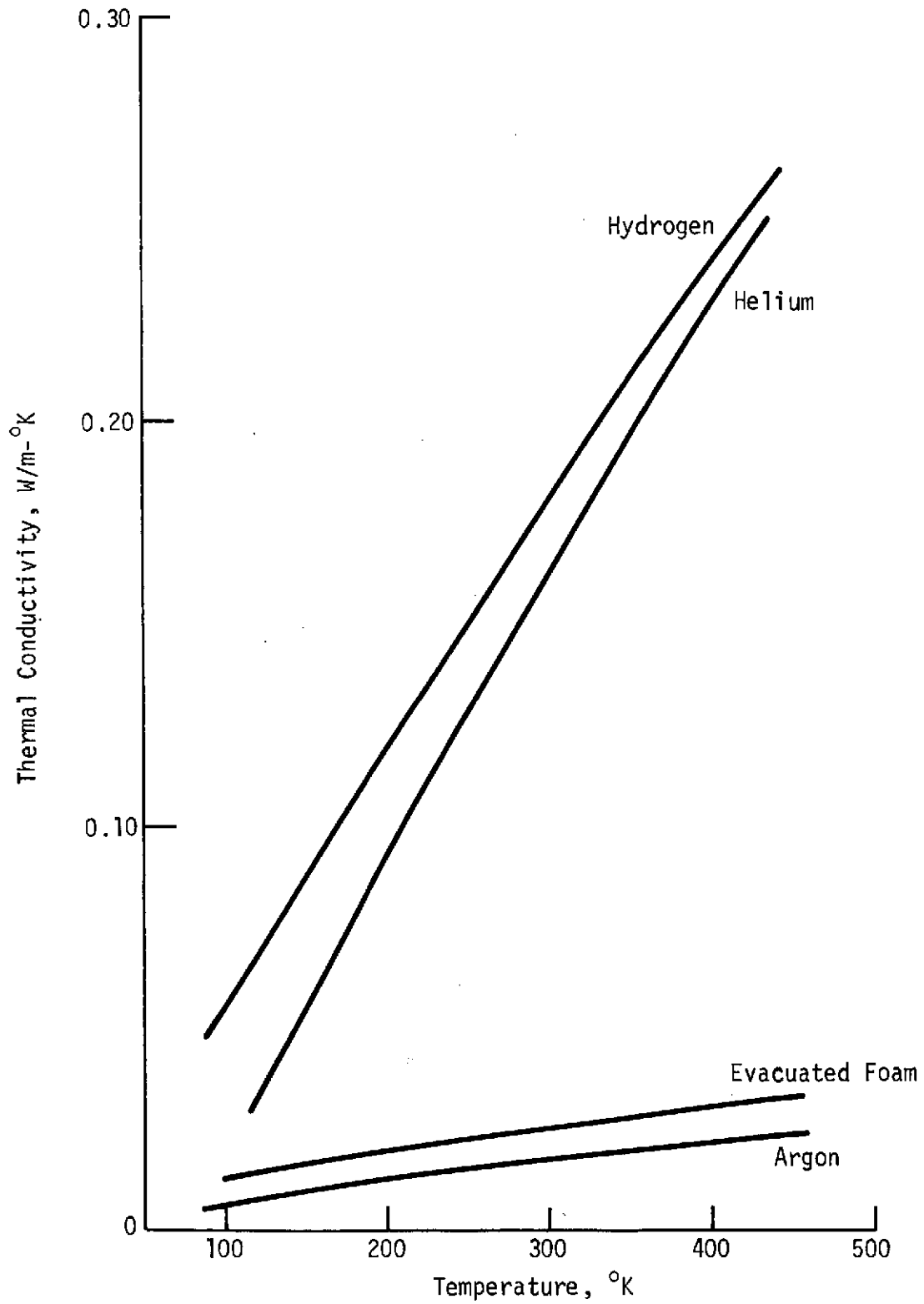


Figure C-10 Thermal Conductivity Versus Temperature for Hydrogen, Helium, Argon and an Evacuated Foam Insulation

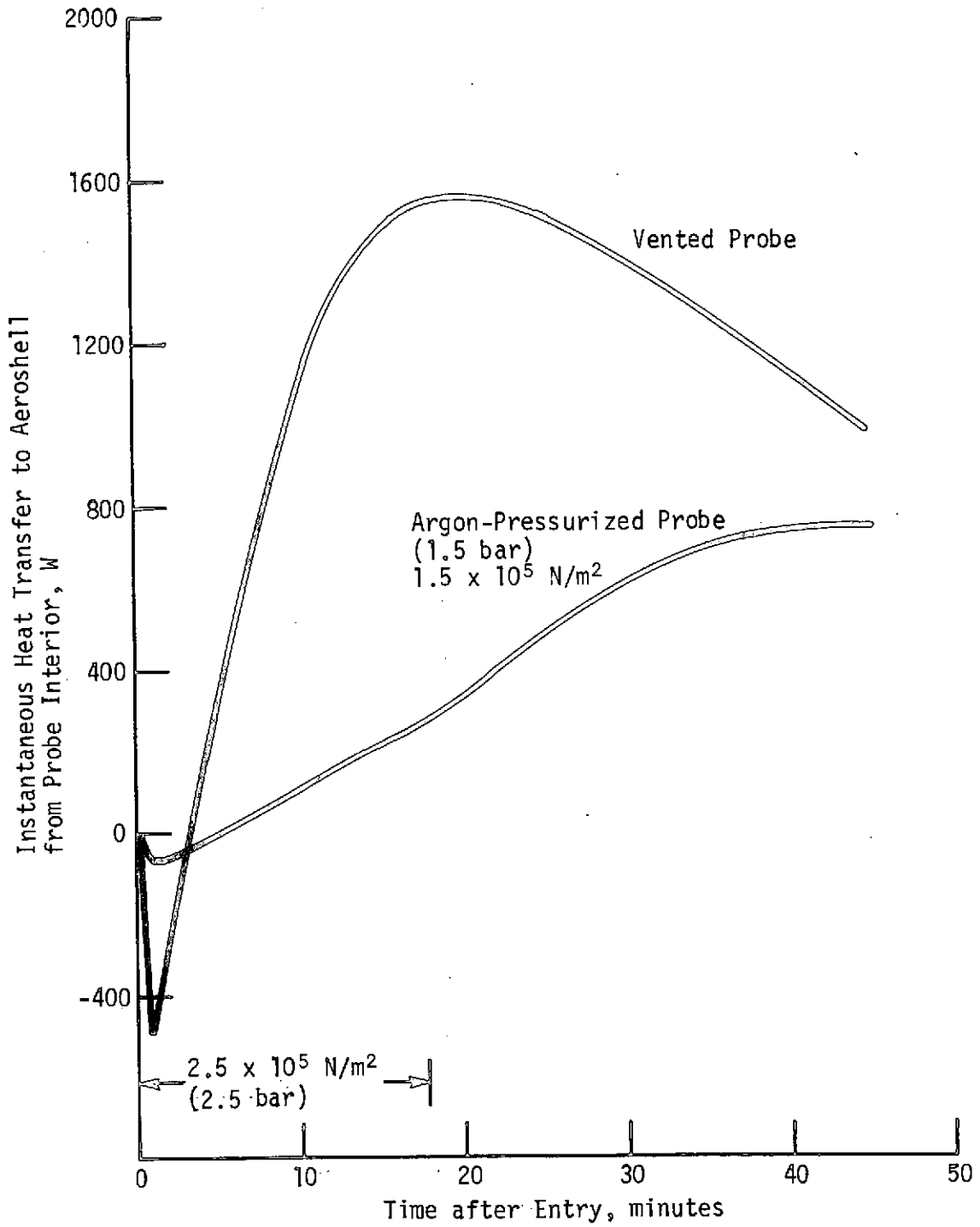


Figure C-11 Heat Loss Versus Time, Vented Probe and Argon Pressurized Probe, Uranus Nominal Atmosphere

scent, a small heater is located on the perimeter of the window and powered to a level that holds the temperature of the window  $10^{\circ}\text{K}$  above that of the local atmospheric gas. (This  $10^{\circ}\text{K}$  temperature difference is not a specified requirement, but is felt to contain adequate margin to ensure that no condensation will occur during the descent). The purpose of this analysis was to define the heater power required to maintain the  $10^{\circ}\text{K}$  temperature difference.

Figure C-12 shows the generalized window configuration that was analyzed in detail using the MITAS thermal analyzer. The heated window was separated from the instrument window by an insulated evacuated tube to minimize conduction losses from the window heater. Evacuating the tube eliminates free-convection and gas-conduction effects inside the tube.

The heater must be sized to offset the conduction and radiation losses down the tube, as well as the convection to the atmosphere from the exposed window surface. In addition, it must have adequate capacity to heat the window mass transiently to lead the atmospheric descent temperature profile by the required  $10^{\circ}\text{K}$ .

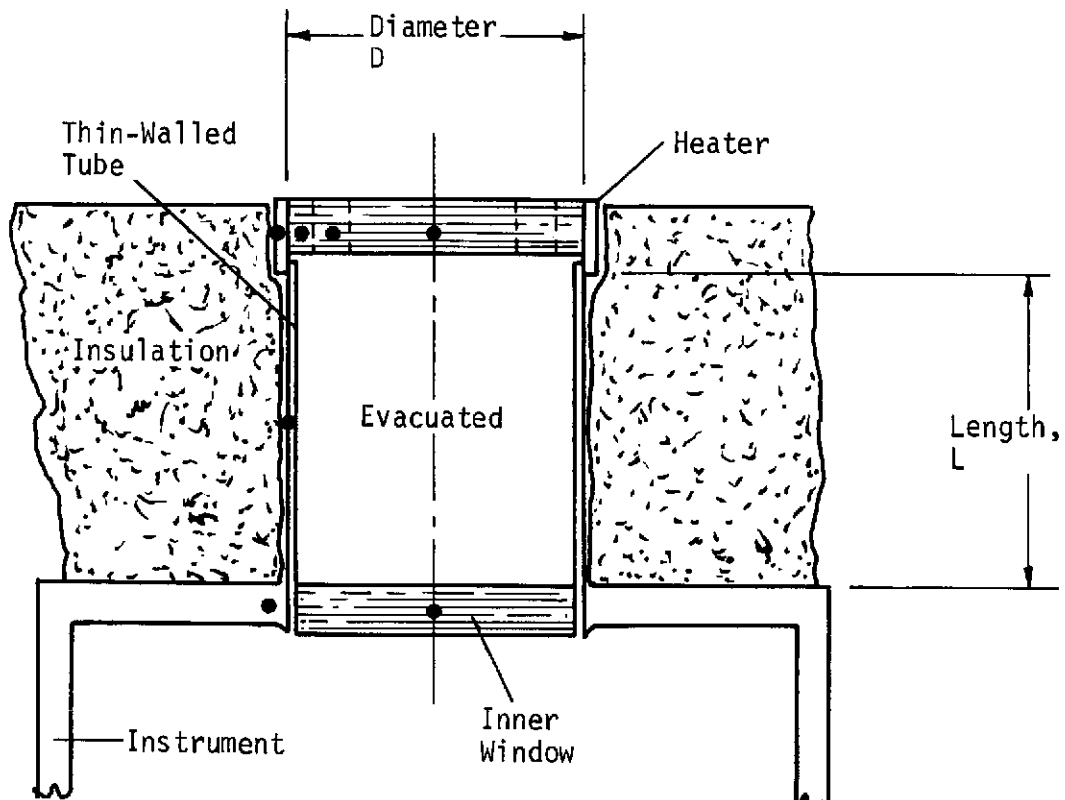


Figure C-12 Window Configuration for Heater Thermal Analysis

Our preliminary analysis showed that the Saturn warm atmosphere was the worst-case environment because the maximum heater power was required to satisfy the temperature requirement. The analysis also showed that the conduction in the tube away from the window was the significant heat loss that governed the size of the heater. Based on these results, we made a parametric study of various tube length to diameter ratios for a fixed tube wall thickness [0.51 mm (0.02 in.)] and a fixed window thickness [2.8 mm (0.112 in.)] using the Saturn warm atmosphere as the environment for all cases. The tube material was assumed to be Inconel, an alloy we have used successfully in assembling science windows for previous IRAD evaluation in Venusian environments\*.

The results of this parametric analysis are shown in Figure C-12. The heater power is plotted in terms of the window diameter because the radiative and convective losses from the window are dependent on the surface area of the window. The heat-transfer coefficient to the atmosphere was conservatively set at twice the value of the average heat transfer coefficient computed for the entire probe.

Figure C-13 shows that, for the Saturn/Uranus nephelometer and a tube length of 2.54 cm (1 in.) the required heater power would be 3.3 watts for a 1.91-cm (0.75 in.) diameter window, and 1.7 watts for a 1.14-cm (0.45 in.) diameter window.

Work performed under the above mentioned IRAD task has shown that predictions of window heater power based on an analysis similar to that described above correlate well with actual test results.

\*L. Wolfert: *Protection of Instruments against Ambient Environments*. Final Report, IRAD Task 48701. Martin Marietta Corporation, Denver, Colorado, November 1973.



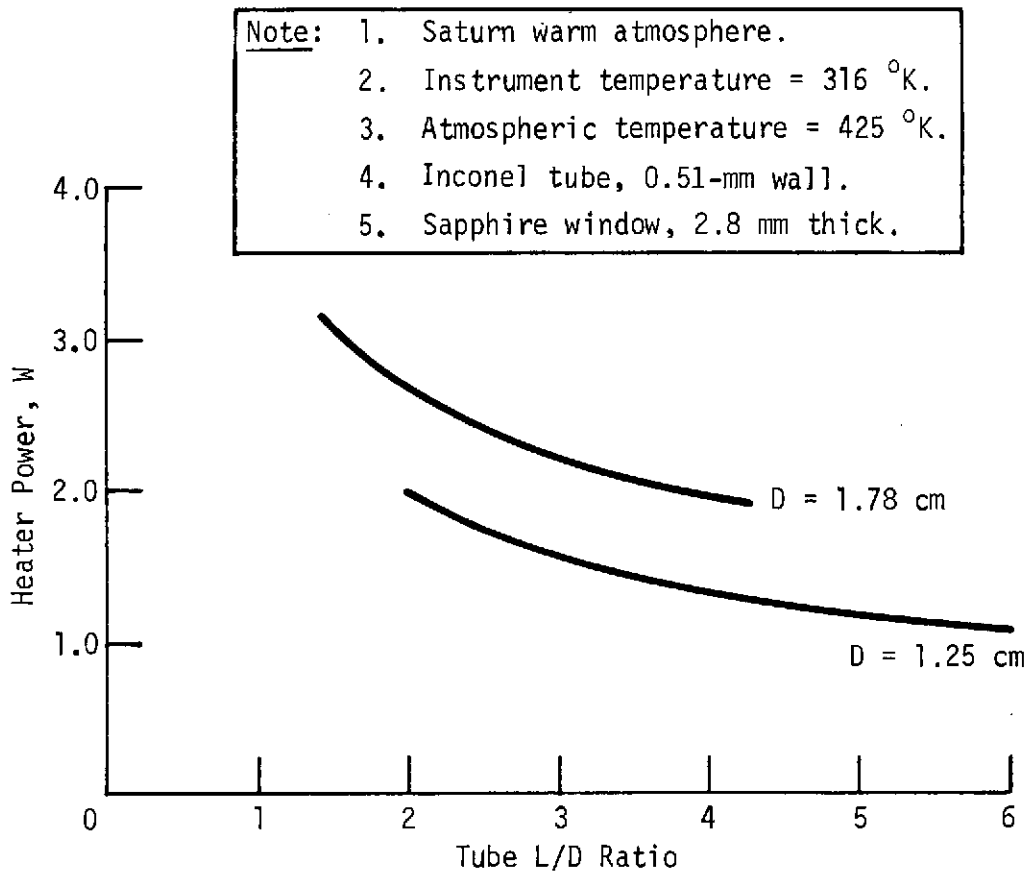


Figure C-13 Power Required to Heat Sapphire Window 10°K Above Saturn-Warm Atmosphere

APPENDIX D

ATC MASS SPECTROMETER INSTRUMENT DATA



Analog  
Technology  
Corporation

June 21, 1973

Mr. Ken Ledbetter  
Mail Stop 3001  
Martin Marietta Corporation  
Post Office Box No. 79  
Denver, Colorado

Dear Mr. Ledbetter:

I have just received an estimate of the size and volume of the electronics package (flight type) required to make our 2-inch quadrupole operable over the mass range from 1 through 40, with four mass increments per amu, as well as a few discreet mass settings. The estimated mass of the electronics package is 1.5 kilograms and the volume 1.2 liters. The vacuum system, including the ion pumps added, bring the mass of the entire package to an estimated 2.5 kilograms, and the volume to 1.5 liters.

If you have any further questions, please contact me or William Chiang, Vice President of Marketing.

Very truly yours,

ANALOG TECHNOLOGY CORPORATION

Wilson M. Brubaker  
Senior Staff Scientist

WMB/kit

D-1